

Durham E-Theses

Impact of crustal assimilation on the Lesser Antilles arc lava geochemistry

BEZARD, RACHEL,CHRISTINE

How to cite:

BEZARD, RACHEL,CHRISTINE (2014) *Impact of crustal assimilation on the Lesser Antilles arc lava geochemistry*, Durham theses, Durham University. Available at Durham E-Theses Online:
<http://etheses.dur.ac.uk/10763/>

Use policy

The full-text may be used and/or reproduced, and given to third parties in any format or medium, without prior permission or charge, for personal research or study, educational, or not-for-profit purposes provided that:

- a full bibliographic reference is made to the original source
- a [link](#) is made to the metadata record in Durham E-Theses
- the full-text is not changed in any way

The full-text must not be sold in any format or medium without the formal permission of the copyright holders.

Please consult the [full Durham E-Theses policy](#) for further details.

Academic Support Office, Durham University, University Office, Old Elvet, Durham DH1 3HP
e-mail: e-theses.admin@dur.ac.uk Tel: +44 0191 334 6107
<http://etheses.dur.ac.uk>

**Impact of crustal assimilation on the Lesser Antilles
arc lava geochemistry**

Rachel Christine Bezard

A thesis submitted for the degree of
Doctor of Philosophy (PhD) at Durham University

Department of Earth Sciences,
Durham University
2014

Abstract

Characterization of the mantle source of arc magmas using the composition of erupted lavas is only possible after the assessment of the effects of crustal assimilation. While the impact of crustal assimilation on continental arc lavas is commonly investigated, it is often ignored or debated in oceanic arcs. Nowhere has the debate been more acute than in the Lesser Antilles arc which is characterised by extreme ranges in geochemistry from typical oceanic arc to continental crust-like compositions. Given the oceanic provenance of the arc, these geochemical features can be inherited either from subducted sediments, or from crustal contamination by continental sediments intercalated in the arc crust. In this thesis, the problem is reassessed using a whole rock-to sub-grain scale trace element and isotopic (Sr-Nd-Hf-Pb-O isotopes) investigation of volcanic rocks from St Lucia Island, thought to encompass most of the arc's isotopic heterogeneities. In addition, an Os isotopic investigation of some of the most mafic and well constrained lavas from along the arc was performed.

New isotopic composition of St Lucia lavas confirm that the island covers most of the arc's compositional variations. Intra-crystal $^{87}\text{Sr}/^{86}\text{Sr}$ heterogeneities as well as the co-variation of lava radiogenic isotopes and trace elements with SiO_2 and mineral $\delta^{18}\text{O}$ suggest that crustal assimilation affected lavas as mafic as basaltic andesites and is responsible for the isotopic and trace element heterogeneities observed in the Island. The assimilant is thought to be a mix of detrital and organic sediments, likely to have been part of the sedimentary basin intruded by the arc. Assimilation of sediment is thought to occur in the middle crust of the arc and to be tightly linked with the production of silicic magmas.

Sr, Nd, Hf and Pb isotopic compositions of the lavas that avoided significant sediment assimilation suggest that no more than 2% of slab-derived sediment was added to the source of St Lucia magmas. However, an along arc $^{187}\text{Os}/^{188}\text{Os}$ investigation suggests that even the most mafic lavas, having escaped sediment assimilation, were modified on their way to the surface by assimilation of the igneous arc roots, possibly a plagioclase-rich cumulate. Care must therefore be applied before characterising the source using mafic lava compositions since this process is thought to modify the Os and Sr isotopes, as well as La/Sm and Sr/Th ratios. This suggests that, in the Lesser Antilles arc, very few lavas preserved their original mantle source characteristics.

Declaration

I, Rachel Christine Bezar, declare that this thesis, presented for the degree of Doctor of Philosophy at Durham University, is a result of my own original research. It is submitted simultaneously to both Durham and Macquarie Universities, following the cotutelle agreement rules.

The copyright of this thesis rests with the author. No quotation from it should be published without the author's prior written consent and information derived from it should be acknowledged.

Rachel Bezar

Sydney

April 2014

Acknowledgements

First and foremost, I would like to thank my two main supervisors Jon Davidson and Simon Turner for offering me the chance to work on this very exciting project and for supervising me over the last three years. They both have been very helpful, trustful, supportive, open minded and an important source of inspiration. I extend further thanks to Simon for cheerfully sending me to the Caribbean, to multiple conferences and to UCLA for lab work.

I am also grateful to my other supervisors, Colin Macpherson and Bruce Schaefer. They both gave me some very constructive comments and suggestions on some of the manuscripts and grant applications and were both very supportive. I must also thank the people I had the chance to collaborate with during this project: Adrian Boyce, Jan Linday, Axel Schmitt and David Selby. Adrian was very welcoming and helpful both during my visit at East Kilbride for O isotope analyses and during the related manuscript preparation. Jan has always been keen to collaborate. She showed me St Lucia geology for a few days, and kindly shared her sample collection and read the manuscript drafts I sent her. She has been very supportive. Axel offered me the chance to use the UCLA ion-probe and trained me for the sample preparation and analysis, which I am very grateful for. I thank Dave for collaborating, for our email discussions and for cheerfully accepting to read the versions of the manuscript I sent him.

I must thank Chris Ottley and Geoff Nowell for training me in the lab at Durham. They both gave me very rigorous training and encouraged me to be critical with every step of the protocols. I am very thankful for the time they spent with me in the lab. I am also very grateful to Norman Pearson and Peter Wieland from Macquarie. Norman gave me a lot of trust and encouragement and provided me with the space and material needed when I decided to set up a micro-Sr lab. Norm has been of great support and I cannot remember a time when he was not available to answer my questions or share my worries/successes. Peter also gave me a lot of trust and was very helpful in the lab. He really gave me the confidence to achieve a lot, and supported me in my downs with his famous “everything will be ok in the end”.

I would like to thank all the other people who assisted me in the lab: Terry Donelly and Alicia McDonald for their training during my visit at East Kilbride, Kevin Grant, Robert Rapp and William Powell for their help on the microprobe and LA-ICPMS and Felix Genske for his help and tips during the Os isotopes chemistry. I also would like to thank Jon Adams for always taking the time to answer my questions and taking the time to read a couple of chapters. I thank the rest of the U-series group for listening to my talks and participating to the related discussions.

Finally, I would like to thank my family and friends from France, Canada, the UK and Australia. I thank my parents Marinette and Serge, for unconditionally supporting me both emotionally and financially throughout my education. You gave me the inspiration and encouragement I needed and I dedicate this thesis to you. I thank my brother for being encouraging too, even if we live in very different parts of the world. I would like to thank James for being there during my ups and downs over the last two years and for keeping me sane! I think James has tried everything possible to relieve my stress and make the end of this PhD a fun ride. I thank my long-time friends from France, Julie and Audrey, for just being great friends and encouraging me! My friends from Canada, with a special wink to Steph and Emilie who have been there (on skype) to share my good news and frustrations. Emily also came to help me in St Lucia and was a fantastic field assistant! Finally I would like to thank the rest of my friends from both Durham and Macquarie for the fun times, especially Helen and Suzie and all the “rugby road” gang for all the fun nights to release the pressure over the last two years!

Contents

Abstract	i
Declaration	ii
Acknowledgements	iii
Contents	v
List of figures	xv
List of tables	xxiii

Chapter 1: Introduction

1.1 Subduction zones	2
1.2 Thesis organization and rationale	4

Chapter 2: Geological setting

2.1 Geodynamic evolution of the Caribbean plate and the development of the Lesser Antilles arc	12
2.1.1. The “pacific origin” model	13
2.1.2 The in situ/protocaribbean origin model	15
2.2 The Lesser Antilles subduction zone	18
2.2.1 The accretionary wedge and sediments on the subduction plate	19
2.2.1.1 Accretionary wedge	19
2.2.1.2 Nature of the subducted sediments	20
2.2.2 Forearc basin	24
2.2.3 The Lesser Antilles arc	25
2.2.3.1 Structure	25
2.2.3.2 The arc basement	25

2.2.3.3 Lava compositions	30
2.2.3.3.1. Lavas classification	30
2.2.3.3.2 The mantle source	34
2.2.3.3.3 Magma differentiation in the arc crust	39
2.2.4 St Lucia	44
2.2.4.1 Pre-SVC	45
2.2.4.2 SVC	46

Chapter 3: Assimilation of sediments embedded in the oceanic arc crust: myth or reality?

3.1 Introduction	55
3.2 Geological background	56
3.3 Methods	58
3.3.1 Whole rock Sr, Nd and Pb isotopes	58
3.3.2 $^{87}\text{Sr}/^{86}\text{Sr}$ in plagioclase	61
3.3.3 $\delta^{18}\text{O}$ in mineral separates	62
3.4 Results	63
3.5 Discussion	64
3.5.1 Intra-crustal magma contamination	64
3.5.2 Effect of contamination on whole rock compositions	67
3.5.3 Implications for other Lesser Antilles volcanoes and other arcs	72
3.6 Summary and conclusions	75

Chapter 4: Seeing through the effects of crust assimilation to assess the source composition beneath the southern Lesser Antilles arc

4.1 Introduction	79
4.2 Geological setting	81

4.2.1 Pre-Soufriere Volcanic complex	83
4.2.2 Soufriere Volcanic Complex	84
4.3 Sampling and analytical procedures	84
4.3.1 Samples	84
4.3.2 Trace elements	85
4.3.3 Hf isotopes	91
4.4 Results	91
4.4.1 Trace elements	91
4.4.2 Hf isotopes	93
4.5 Crustal assimilation control on magma compositions	93
4.5.1 Impact of crustal assimilation on $^{176}\text{Hf}/^{177}\text{Hf}$	93
4.5.2 Impact of crustal assimilation on trace elements	96
4.5.2.1 Determination of the fractionating assemblage using major elements	96
4.5.2.2 Impact of the fractionating assemblage on the trace element variations	100
4.5.2.2.1 Th/Th*	101
4.5.2.2.2 REE	101
4.6 Composition of the assimilant	104
4.6.1 Major and trace elements	104
4.6.2 Isotopic composition and rate of assimilation	105
4.6.2.1 The best fit for trace elements and isotope compositions of the assimilant	108
4.6.2.1.1 Sr, Nd, Hf and Pb concentrations of the assimilant	108
4.6.2.1.2 “Minimum” isotopic composition of the assimilant	108
4.6.2.1.3 Best fit for L/M-HREE and Ba/Th versus isotopes models	108
4.6.2.2 Comparison of the “minimum assimilant composition with the local sediments	110

4.7 The composition of the mantle source region beneath	
St Lucia	111
4.7.1 Crustal assimilation by Pre-SVC1 magmas?	112
4.7.2 Amount of sediment in the source	113
4.7.3 Comparison of St Lucia source to the rest of the arc	116
4.7.3.1 St Lucia and the north of the arc	118
4.7.3.2 St Lucia and the south of the arc	119
4.7.3.2.1 St Vincent	119
4.7.3.2.2 Martinique	121
4.7.3.2.3 Grenadine Islands	122
4.7.3.2.4 Grenada	123
4.7.3.2.5 Summary	123
4.8 Conclusions	124
 Chapter 5: Origin and evolution of silicic crust in oceanic arcs; an in situ study from St Lucia, Lesser Antilles	
5.1 Introduction	127
5.2 Geological background	128
5.3 Methods	131
5.3.1 Imaging and electron microprobe analysis	131
5.3.2 Trace elements	132
5.3.3 In-situ $^{87}\text{Sr}/^{86}\text{Sr}$ analysis of plagioclase	133
5.3.4 Zircon $\delta^{18}\text{O}$	135
5.4 Petrography	136
5.4.1 Pre-SVC	136
5.4.2 SVC	138
5.5 Mineral and groundmass major element data	141
5.5.1 Plagioclase	141
5.5.1.1 Pre-SVC1	141

5.5.1.2 Pre-SVC2	142
5.5.1.3 SVC	144
5.5.1.3.1 SVC1	144
5.5.1.3.2 SVC2,3	145
5.5.1.3.3 Groundmass of SVC1,2,3	145
5.5.2 Clinopyroxene phenocrysts	146
5.5.2.1 Pre-SVC	146
5.5.2.2 SVC	146
5.5.3 Orthopyroxene	146
5.5.3.1 Pre-SVC	146
5.5.3.2 SVC	146
5.5.4 Amphibole	147
5.5.5 Biotite	147
5.5.6 Groundmass	147
5.6 Mineral and Groundmass trace element data	149
5.6.1 Plagioclase	149
5.6.1.1 Pre-SVC1	149
5.6.1.2 Pre-SVC2	149
5.6.1.3 SVC	151
5.6.1.3.1 SVC	151
5.6.1.3.2 SVC2,3	151
5.6.2 Orthopyroxene	151
5.6.3 Clinopyroxene	152
5.6.4 Amphibole	153
5.6.5 Groundmass	154
5.6.5.1 Pre-SVC1	154
5.6.5.2 Pre-SVC2	154
5.6.5.3 SVC	154

5.7 Plagioclase and groundmass $^{87}\text{Sr}/^{86}\text{Sr}$ data	155
5.7.1 Pre-SVC1	155
5.7.2 Pre-SVC2	155
5.7.3 SVC	157
5.7.3.1 SVC1	157
5.7.3.2 SVC2,3	157
5.8 Zircon $\delta^{18}\text{O}$ data	158
5.9 Constraints on crystallisation conditions	161
5.9.1 Pressure and temperature	161
5.9.1.1 Pyroxene thermometer	161
5.9.1.2 Cumingtonite-orthopyroxene transition	162
5.9.1.3 Calcic amphibole thermobarometry	163
5.9.2 Oxygen fugacity	163
5.9.3 Melt- H_2O estimate	163
5.10 Processes controlling mineral major and trace element compositions	163
5.10.1 Ba and Sr concentrations in melt coexisting with Plagioclase	165
5.10.1.1 Suitability of the regression	165
5.10.1.2 Crystal chemical control	167
5.10.1.2.1 Sr	167
5.10.1.2.2 Ba	167
5.10.1.3 Diffusion	168
5.10.1.4 Change in melt composition during plagioclase growth	168
5.10.1.4.1 Pre-SVC1	169
5.10.1.4.2 Pre-SVC2	170
5.10.1.4.3 SVC1	173
5.10.1.4.4 SVC2,3	175
5.10.1.4.5 Summary of the crystallisation history of the	

Pre-SVC and SVC plagioclase	178
5.10.1.5 Change in melt composition before crystal growth	179
5.10.1.5.1 Pre-SVC2	180
5.10.1.5.2 SVC	180
5.10.2 La/Sm variations in plagioclase coexisting melt	181
5.10.3 Sr and Ba variations in amphibole and pyroxene coexisting melt	183
5.10.3.1 Pre-SVC1	183
5.10.3.2 SVC	184
5.11 Processes controlling $^{87}\text{Sr}/^{86}\text{Sr}$ and $\delta^{18}\text{O}$ mineral compositions	185
5.11.1 Process controlling $^{87}\text{Sr}/^{86}\text{Sr}$ variations between Pre-SVC1, Pre-SVC2 and SVC crystals	186
5.11.2 Process controlling crystal $^{87}\text{Sr}/^{86}\text{Sr}$ within Pre-SVC1, Pre-SVC2 and SVC groups	187
5.11.2.1 Pre-SVC1	187
5.11.2.2 Pre-SVC2	188
5.11.2.3 SVC	189
5.11.2.3.1 SVC1	189
5.11.2.3.2 SVC2,3	190
5.11.2.3.3 Summary	191
5.11.3 Processes controlling SVC mineral $\delta^{18}\text{O}$	191
5.12 Magmatic evolution of Pre-SVC and SVC	193
5.12.1 Pre-SVC1 lavas	193
5.12.2 Pre-SVC2	193
5.12.3 SVC	196
5.12.3.1 Decoupling of crustal assimilation and phenocryst crystallisation	196
5.12.3.2 Conditions and processes in the deep chamber	197

5.12.3.3 Conditions and processes in the shallow chamber	199
5.12.3.3.1 Same magma chamber for all SVC lavas	199
5.12.3.3.2 Depth and temperature of shallow storage	199
5.12.3.3.3 Recharge and mineral fractionation	200
5.12.3.3.4 Process triggering eruption	201
5.12.3.3.5 Focussing of the activity	202
5.12.4 Implications for the development and evolution of silicic complexes in mature arcs	203
5.13 Conclusions	204

Chapter 6: Lower crustal assimilation in oceanic arcs: insights from an osmium isotopic study of the Lesser Antilles

6.1 Introduction	207
6.2 Samples and analytical methods	208
6.2.1 Samples	208
6.2.2 Analytical methods	210
6.3 Results	214
6.4 Discussion	215
6.4.1 Crustal assimilation control on $^{187}\text{Os}/^{188}\text{Os}$	215
6.4.2 Source $^{187}\text{Os}/^{188}\text{Os}$	217
6.4.3 Characteristics and nature of the assimilant	219
6.4.3.1 Trace element and isotopic characteristics	219
6.4.3.2 Nature of the assimilant	220
6.4.3.3 Assimilation and fractional crystallisation (AFC) Modelling	221
6.4.4 Implications	223
6.4.4.1 The Lesser Antilles	223
6.4.4.2 Other arcs	225
6.5 Conclusions	226

Chapter 7: Conclusions and future work	
7.1 Introduction	230
7.2 Conclusions	230
7.2.1 Impact of sediment assimilation on the Lesser Antilles arc lava compositions	230
7.2.2 Conditions of sediment assimilation and development of a silicic complex	231
7.2.3 Impact of assimilation of the igneous arc roots on magma compositions	232
7.2.4 The arc mantle source composition	233
7.3 Future work	235
7.3.1 St Lucia	235
7.3.1.1 Plutonic enclaves	235
7.3.1.2 $^{187}\text{Os}/^{188}\text{Os}$ in SVC lavas	235
7.3.2 The rest of the arc	236
7.3.2.1 Detection of sediment assimilation in other islands	236
7.3.2.2 Detection of igneous arc root assimilation	236
7.3.3 Other arcs	237
References	239
Appendix A: Name, type and location of the samples Analysed	261
Appendix B: Supplementary data file of Chapter 3	265
Appendix C: Supplementary data file of Chapter 4	271
Appendix D: Supplementary data file of Chapter 5	289
Appendix E: Supplementary data file of Chapter 6	319
Appendix F: Detailed analytical techniques	323
Appendix G: All mineral major element data	359

List of figures

Chapter 1

- Fig. 1.1.** Schematic diagram of the subduction factory modified from Macdonald et al. (2000) and Tatsumi and Eggins (1995). 3

Chapter 2

- Fig. 2.1.** Structural map of the Caribbean area. Arrows indicate the drifting direction of the main plates. 12

- Fig. 2.2.** Two versions of the «pacific origin model» for the genesis and emplacement of the Caribbean plate. 14

- Fig. 2.3.** Paleogeographic reconstruction and kinematic evolution of the Caribbean Plate, from Late Jurassic to Tertiary. 16

- Fig. 2.4.** Bathymetric map of the Lesser Antilles arc region showing the islands of the Lesser Antilles arc, the trench-deformation front, the subduction trace, fracture zones, the main ridges, the Grenada and Tobago basins and the locations of Deep Sea Drilling Project (DSDP) hole 543/543A and hole 144. 18

- Fig. 2.5.** Sr and Nd isotopic composition of DSDP sites 144 and 543 and of Barbados Island sediments from Carpentier et al. (2009). 21

- Fig. 2.6.** Upper continental crust (UCC; McLennan, 2001) normalized trace element concentrations of the Lesser Antilles local sediment from Carpentier et al. (2009). 23

- Fig. 2.7.** $^{206}\text{Pb}/^{204}\text{Pb}$ ratio of DSDP sites 144 and 543 and the Barbados sediments against (a) $^{207}\text{Pb}/^{204}\text{Pb}$ ratio, (b) $^{208}\text{Pb}/^{204}\text{Pb}$ ratio and (c) $^{143}\text{Nd}/^{144}\text{Nd}$ ratio. 24

Fig. 2.8. Grenada and Tobago basins fault restoration (based on depth-converted seismic data) illustrating their common origin as a single Paleogene forearc basin.	27
Fig. 2.9. Map of the Cenozoic basins of the Venezuela and Los Llanos Basin of Columbia.	29
Fig. 2.10. Paleogeographic map of Eocene sediment dispersion system in northern South America.	29
Fig. 2.11. Sr and Nd isotopic compositions of the Lesser Antilles arc.	33
Fig. 2.12. Pb and Nd isotopic compositions of the lavas from the southern part of the Lesser Antilles arc compared with those of Site DSDP 144 sediments.	36
Fig. 2.13. $\delta^{18}\text{O}$ composition of the northern Lesser Antilles arc and of Martinique, representing the central islands, versus SiO_2 content.	42
Fig. 2.14. An overview of the mineral oxygen isotopic compositions versus location (latitude) in the arc.	43
Fig. 2.15. Geological map of St Lucia.	45
Fig. 2.16. Geological map of the SVC.	47
Fig. 2.17. Schematic model showing the different phases of magmatism leading to the formation of the SVC.	50

Chapter 3

Fig. 3.1. Bathymetric map of the Lesser Antilles arc showing the islands, the trench-deformation front, the main ridges, the Grenada and Tobago basins and the locations of Deep Sea Drilling Project (DSDP) hole 543/543A and hole 144.	56
---	----

Fig. 3.2. Whole rock compositions of St Lucia lavas.	61
Fig. 3.3. $^{87}\text{Sr}/^{86}\text{Sr}$ isotope ratios of twenty plagioclase phenocrysts showing isotopic disequilibrium among four of the most contaminated SVC lavas.	66
Fig. 3.4. $\delta^{18}\text{O}$ values of phenocrysts from SVC and Pre-SVC lavas (symbols as in Fig. 3.2).	67
Fig. 3.5. Correlation between mineral $\delta^{18}\text{O}$ and whole rock $^{87}\text{Sr}/^{86}\text{Sr}$ and SiO_2 (symbols as in Fig. 3.2).	69
Fig. 3.6. Variation of SiO_2 and CaO with MgO composition with the Pre-SVC and SVC lavas.	71
Fig. 3.7. Schematic model for the St Lucia magmatic plumbing system through time to explain the Pre-SVC and SVC whole rock and mineral isotopic compositions.	74
 Chapter 4	
Fig. 4.1. (a) Location of St Lucia on a bathymetric map of the Lesser Antilles arc area modified from Bezard et al. (2014).	80
Fig. 4.2. Comparison of Sr, Nd isotopic composition of St Lucia lavas to all the other lavas from the rest of the arc.	82
Fig. 4.3. Trace element composition of Pre-SVC1, Pre-SVC2 and SVC lavas.	92
Fig. 4.4. Sr, Nd, Hf, Pb isotopic composition of St Lucia lavas with AFC models.	94
Fig. 4.5. Hf, Nd, Sr, Pb isotopes and La/Sm and Th/Th^* vs. SiO_2 (wt.%) in St Lucia lavas.	95

Fig. 4.6. Major element variation of St Lucia lavas.	98
Fig. 4.7. CIPW norm composition of St Lucia in (a) the diopside-feldspar-hypersthene and in (b) quartz-feldspar-hypersthene systems. Paths to explain Pre-SVC and SVC rocks by differentiation from the most mafic Pre-SVC1 lava (basalt) are shown in (c) a 3D tetrahedral.	100
Fig. 4.8. Comparison of St Lucia lava composition with the schematic effect of mineral fractionation control on Dy/Dy* and Dy/Yb.	102
Fig. 4.9. Mixing models to constrain the amount of sediment involved in the source of Pre-SVC1 lavas.	114
Fig. 4.10. (a) MgO (wt.%), (b) La/Sm and (c) Ba/Th vs. $^{87}\text{Sr}/^{86}\text{Sr}$, $^{143}\text{Nd}/^{144}\text{Nd}$, $^{206}\text{Pb}/^{204}\text{Pb}$ of St Lucia lavas compared to both the north (top 4 figures of each panel) and the south of the arc (bottom 4 figures of each panel).	117
Fig. 4.11. Comparison of La/Sm, Ba/Th, $^{87}\text{Sr}/^{86}\text{Sr}$, $^{143}\text{Nd}/^{144}\text{Nd}$, $^{206}\text{Pb}/^{204}\text{Pb}$ of the most mafic samples analysed in each island along the arc.	120

Chapter 5

Fig. 5.1. (a) Geological setting of St Lucia. (b) Geological map of St Lucia divided into two main groups: Pre-Soufriere volcanic complex (Pre-SVC) and Soufriere Volcanic complex (SVC). (c) Geological map of the Soufriere area showing the name of all the extruded lava flows.	129
Fig. 5.2. Whole rock major element (a) and $^{87}\text{Sr}/^{86}\text{Sr}$ vs. $^{143}\text{Nd}/^{144}\text{Nd}$ isotopic compositions (b) of the different groups of Pre-SVC and SVC lavas.	131

Fig. 5.3. Representative modal proportions of St Lucia lavas phenocrysts.	137
Fig. 5.4. Representative photomicrographs of Pre-SVC and SVC lavas in plain light.	139
Fig. 5.5. U-Th/He eruption ages and U-Th and U-Pb zircon growth ages of the SVC lavas.	140
Fig. 5.6. Summary of textural and compositional characteristics of the different types of plagioclase found in (a) Pre-SVC1 and (b) Pre-SVC2 and SVC lavas.	143
Fig. 5.7. Representative SEM (a-e) and CL (f) images of some mineral textures in the SVC.	148
Fig. 5.8. Sr, Ba and La/Sm composition of the plagioclase from the different types of lava in St Lucia (a, c, e) and from the corresponding calculated melts (b, d, f).	150
Fig. 5.9. Compositional profiles in enstatite obtained for pyroxene along with the rare earth element pattern of the different zones of the crystals.	152
Fig. 5.10. Chondrite-normalised rare earth element composition of the two types of amphiboles found in the SVC.	153
Fig. 5.11. Summary of $^{87}\text{Sr}/^{86}\text{Sr}$ ratios in microdrilled zones of plagioclase crystals.	156
Fig. 5.12. Representative plagioclase compositional profiles for anorthite content, Ba and Sr concentrations, $^{87}\text{Sr}/^{86}\text{Sr}$ ratios and calculated melt Ba and Sr concentrations for (a, b, c) Pre-SVC1, (d, e, f) Pre-SVC2, (g, h, i) SVC1, (j, k, l) cummingtonite-bearing SVC2,3 and (m, n) orthopyroxene-bearing SVC2,3 lavas.	159

Fig. 5.13. Zircon $\delta^{18}\text{O}$ composition versus the corresponding U-Th and U-Pb growth ages.	162
Fig. 5.14. (a) Ba vs Sr concentrations and (b) Ba/Sr ratio vs La/Sm ratio of the calculated melt in equilibrium with plagioclase crystals.	166
Fig. 5.15. Schematic petrogenetic model for St Lucia lavas (not to scale).	195
 Chapter 6	
Fig. 6.1. Map of the Lesser Antilles arc with the location of selected lava samples (in black).	208
Fig. 6.2. $^{87}\text{Sr}/^{86}\text{Sr}$ vs. (a) $^{143}\text{Nd}/^{144}\text{Nd}$, (b) MgO (wt. %), (c) La/Sm, (d) Sr/Th of the lavas selected.	209
Fig. 6.3. Os (ppb) vs. $^{187}\text{Os}/^{188}\text{Os}$ of the lavas and subducting slab.	214
Fig. 6.4. Lavas Os (ppb) and MgO (wt. %) against $^{187}\text{Os}/^{188}\text{Os}$.	216
Fig. 6.5. Lavas (a) $^{87}\text{Sr}/^{86}\text{Sr}$, (b) La/Sm and (c) Sr/Th against $^{187}\text{Os}/^{188}\text{Os}$.	218
Fig. 6.6. Assimilation during Fractional Crystallisation (AFC) models of the $^{87}\text{Sr}/^{86}\text{Sr}$ (a, b), $^{187}\text{Os}/^{188}\text{Os}$ (a, c), Sr/Th (b) and La/Sm (c) Lesser Antilles primitive lavas using DePaolo (1981) equation.	223
Fig. 6.7. Schematic model for the Lesser Antilles plumbing system to explain the main factors influencing the compositional variations of the arc lavas.	224
Fig. 6.8. Comparison of the Lesser Antilles arc compositions with those of other arcs (continental and oceanic).	226

Chapter 7

Fig. 7.1. Cartoon illustrating the locus of both cumulate and sediment assimilation in the Lesser Antilles arc and their impact on some representative isotope and trace elements ratios.

234

List of tables

Chapter 2

Table 2.1. All ages of St Lucia rocks published in the literature.	51
---	----

Chapter 3

Table 3.1. St Lucia whole rock Sr-Nd-Pb isotopic compositions and the corresponding SiO ₂ and CaO content in wt. %.	59
---	----

Table 3.2. ⁸⁷ Sr/ ⁸⁶ Sr of single plagioclase grains separated from four of the most continental-like SVC hand samples.	63
--	----

Table 3.3. δ ¹⁸ O of single mineral separates from St Lucia along with the corresponding whole rock SiO ₂ (wt. %) and Sr isotopic composition.	64
---	----

Chapter 4

Table 4.1. Major and trace element contents and Sr-Nd-Pb-Hf isotopic compositions of St Lucia.	86
---	----

Table 4.2. Least square models to produce a residual melt with Pre-SVC1 andesite (SL-83-41; model #3), or SVC andesite (SL-83-17; models #1, 2) compositions from differentiation of Pre-SVC1 basalt (SL-83-44) and the corresponding Rayleigh fractionation models.	103
---	-----

Table 4.3. Mineral-melt distribution coefficients used for the Rayleigh fractionation and AFC models.	107
--	-----

Chapter 5

Table 5.1. Mineral and matrix $^{87}\text{Sr}/^{86}\text{Sr}$ ratios with the corresponding calculated trace element compositions.	134
---	-----

Table 5.2. Partition coefficients used.	187
--	-----

Chapter 6

Table 6.1. Composition of lavas and of altered basalt and sediments from the subducting slab.	210
--	-----

Table 6.2. AFC model parameters.	222
---	-----

Appendix A

Table A.1. List of St Lucia samples and their location	263
---	-----

Table A.2. List of the samples analysed for Os isotopes	264
--	-----

Appendix B

Table B.1. Details of the analyses of international standard solutions NBS981 obtained during Sr isotope analyses of St Lucia lavas on the MC-ICPMS at the Durham Geochemistry Centre (DGC) and at the Geochemical Analysis Unit (GAU) of Macquarie University.	267
--	-----

Table B.2. Details of the analyses of standard solutions obtained during Nd isotope analyses of St Lucia lavas.	268
--	-----

Table B.3. Details of the analyses of the international standard solution NBS981 obtained on the MC-ICPMS at DGC during Pb isotope analyses of St Lucia lavas.	269
---	-----

Table B.4. Details of the analyses of blanks and international standard solutions NBS981 obtained during Sr isotope analyses of single plagioclase crystals at DGC.	270
--	-----

Table B.5. Details of the analyses of international and in-house standards obtained during single mineral $\delta^{18}\text{O}$ analyses by laser-fluorination at East Kilbride (NERC facilities).	270
---	-----

Appendix C

Table C.1. Details of the analyses of the international standard solution JMC 475 obtained during $^{176}\text{Hf}/^{177}\text{Hf}$ analyses of St Lucia lavas by MC-ICPMS at DGC and by TIMS at the GAU.	273
--	-----

Table C.2. Details of the composition of international rock standards BHVO-1, BHVO-2, BIR-1, NBS 688, BCR-2, AGV-1 and W2 obtained during trace element analyses of St Lucia lavas at both DGC and the GAU.	274
--	-----

Table C.3. Assimilation during Fractional Crystallisation (AFC) models with assimilant “minimum” isotopic composition allowing to model the most extreme SVC lava compositions with ~15% fraction of melt remaining (F) in agreement with the least squares models.	277
--	-----

Table C.4. Assimilation during Fractional Crystallisation (AFC) models with assimilant “minimum” isotopic composition allowing to model the most extreme SVC lava compositions with ~ 55% fraction of melt remaining (F).	281
--	-----

Table C.5. Bulk sediment composition at DSDP sites 543 and 144 and Barbados and partition coefficients used to calculate sediment melt compositions.	285
---	-----

Table C.6. Composition of the most mafic lavas presented in Fig. 11.	286
---	-----

Appendix D

Table D.1. Details of the analyses of the international standard solutions NBS987 (8ng Sr) and micro-drilled NIST 611 and BCR2 glass standards during in situ Sr isotope analyses by microdrilling + TIMS at the GAU.	292
--	-----

Table D.2. Details of the Sr blank processed during the analyses of in-situ Sr isotopes by microdrilling + TIMS at the GAU.	292
--	-----

Table D.3. Details of the composition of the zircon standard 91500 obtained during the in-situ $\delta^{18}\text{O}$ zircon analyses performed at UCLA.	293
--	-----

Table D.4. Details of the BCR2-G compositions obtained during mineral analyses using LA-ICPMS at the GAU.	294
--	-----

Table D.5. Representative plagioclase major element composition obtained by electron microprobe.	295
---	-----

Table D.6. Representative clinopyroxene major element composition obtained by electron microprobe.	297
---	-----

Table D.7. Representative orthopyroxene major element composition obtained by electron microprobe.	298
---	-----

Table D.8. Representative amphibole major element composition obtained by electron microprobe.	298
---	-----

Table D.9. Representative biotite major element analyses obtained by electron microprobe.	299
--	-----

Table D.10. Matrix composition of St Lucia lavas obtained by EDS Zeiss EVO at the GAU.	299
---	-----

Table D.11. In-situ plagioclase major and trace element concentrations obtained for Pre-SVC1 basalt and rhyolite by LA-ICPMS at the GAU and the calculated Ba, Sr, La and Sm concentrations in the melt in equilibrium with the crystals.	300
Table D.12. In-situ plagioclase major and trace element concentrations obtained for Pre-SVC2 basaltic andesite and SVC1 andesite and dacite by LA-ICPMS at the GAU and the calculated Ba, Sr, La and Sm concentrations in the melt in equilibrium with the crystals.	304
Table D.13. In-situ plagioclase major and trace element concentrations obtained for orthopyroxene- and cummingtonite- bearing SVC2,3 dacites by LA-ICPMS at the GAU and the calculated Ba, Sr, La and Sm concentrations in the melt in equilibrium with the crystals.	308
Table D.14. In-situ pyroxene and amphibole major and trace element concentrations obtained for Pre-SVC and SVC lavas by LA-ICPMS at the GAU.	312
Table D.15. In-situ groundmass major and trace element concentrations obtained for Pre-SVC and SVC lavas by LA-ICPMS at the GAU.	313
Table D.16. In-situ zircon $\delta^{18}\text{O}$ compositions in St Lucia lavas obtained using the CAMECA ims 1270 at UCLA and the corresponding U-Th age from Schmitt et al. (2010).	315

Appendix E

Table E.1. Detail of the composition of the in-house solution standard JMC-2 and of the international rock standard WPR-1 obtained during the Os isotopic analyses of the Lesser Antilles lavas by N-TIMS.	321
---	-----

Appendix G

Table G.1. Plagioclase major element compositions obtained by electron microprobe.	361
Table G.2. Clinopyroxene major element compositions obtained by electron microprobe.	394
Table G.3. Orthopyroxene major element compositions obtained by electron microprobe.	396
Table G.4. Amphibole major element compositions obtained by electron microprobe.	401
Table G.5. Biotite major element compositions obtained by electron microprobe.	404
Table G.6. Ilmenite major element compositions obtained by electron microprobe.	405

Appendix H

Table H.1. Details of all the composition of the international rock standards W-2, BHVO-1 and AGV-1 analysed during the analysis of the trace element concentrations of single plagioclases.	409
Table H.2. Trace element concentrations of SVC single plagioclases analysed.	410

Chapter 1

Introduction

1.1 Subduction zones

Volcanic arcs are built from the magmas generated at subduction zones. The definition of a subduction zone is an area where a cold and dense lithospheric plate sinks into the Earth's mantle (Tatsumi and Eggins, 1995). The total length of subduction zones on earth equals 43 500 km (Von Huene and Scholl, 1991). Two kinds of subduction zones exist: the sub-continental subduction where an oceanic lithosphere sinks under a continental margin and the intra-oceanic subduction where one oceanic plate sinks beneath another. While sinking into the asthenosphere, the subducting oceanic slab dehydrates by prograde metamorphic reactions induced by the high mantle temperatures and releases fluids into the mantle wedge at around 120 km depth (Fig.1; e.g. Kessel et al., 2005). The resulting amphibole bearing mantle is thought to be dragged down by the convection caused by the subducting plate, leading to the break-down of hydrous phases at higher pressure. The aqueous fluids released by amphibole breakdown lead to partial melting of the mantle. The magmas produced then migrate upward due to higher buoyancy than the surrounding mantle. Decompression during ascent leads to an increase in melt fraction.

Arc lavas have geochemical features that are distinct from mid-ocean ridge basalt (MORB) or oceanic islands basalt (OIB). First, they have elevated water contents and oxidation states (Gill, 1981). But the most recognizable feature is the high abundance of large-ion lithophile elements (LILE; Cs, K, Rb, U, Ba, Sr) over the high field strength elements (HFSE; Th, Zr, Nb, Hf, Ta, Ti) and the light rare earth elements (LREE; Pearce and Peate, 1995). Although the basaltic slabs can undergo partial melting (Bédard, 1999), these chemical features are mainly inferred to be the consequence of the introduction of an *aqueous fluid component* and a *sediment component* into the mantle from the subducting slab. The *sediment component* is thought to be characterised by high LREE/HREE, Th/Nb and Th/Tb ratios (Elliot et al., 1997, Woodhead et al., 1998) and to vary in trace element and isotope composition according to the type of subducted sediment, with high $^{87}\text{Sr}/^{86}\text{Sr}$ ratios when continental sediments are subducted (Turner et al., 1996; Leat and Larter, 2003; Macpherson et al., 2003). The *aqueous fluid component* is produced by the dehydration of the basaltic slab and the dewatering of sediments (Leat and Larter, 2003).

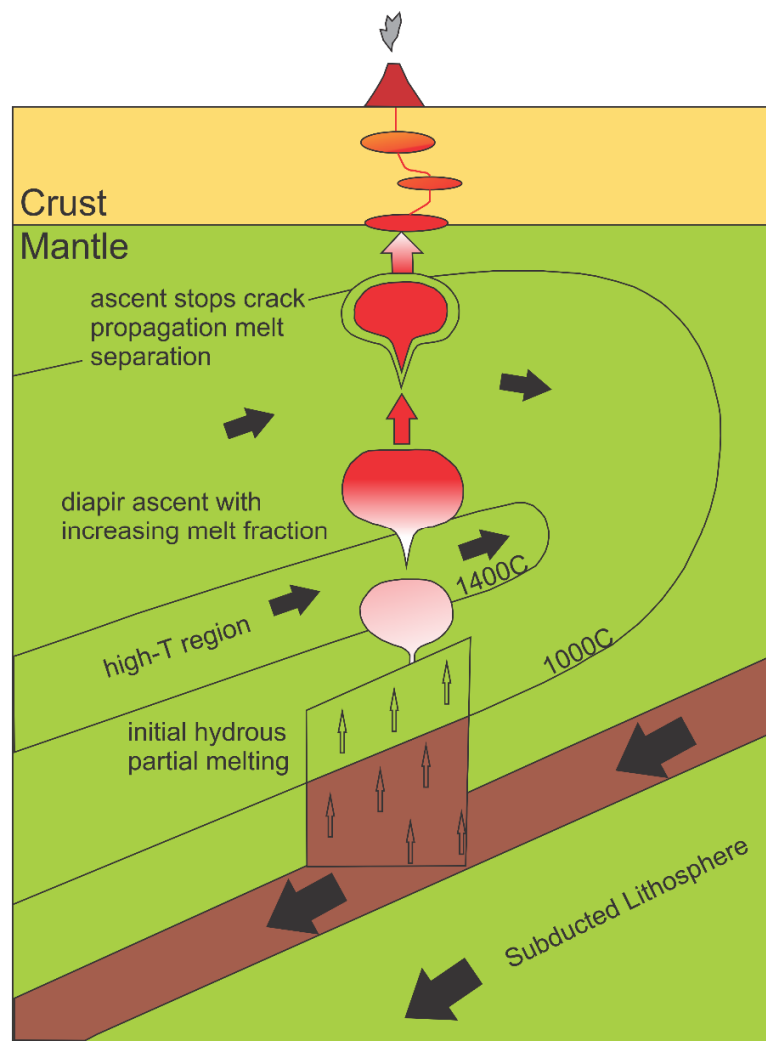


Fig. 1.1. Schematic diagram of the subduction factory modified from Macdonald et al. (2000) and Tatsumi and Eggins (1995). Open arrows indicate fluid while solid arrows indicate solid transport of material in the mantle wedge

It is thought to be enriched in elements that are very soluble in aqueous fluids (e.g., the LILE), and thus has high Ba/Th, Ba/Nb, B/Be and Cs/Rb ratios (Johnson and Plank, 1999).

Constraining the elemental budget contributed from fluid and sediment from the subducting slab that is recycled back to the arc crust through arc magmas is important in order to constrain the rate and processes of production and evolution of continental crust. Indeed, the major and trace element composition of continental crust is very similar to that of arc lavas, which suggests that subduction zones might be the locus of continental

crust production (Davidson and Arculus, 2006). The determination of crust recycling mass balance calculations at subduction zones is usually based on oceanic rather than continental arc lava compositions. This is because continental arcs magmas traverse a thick sialic crust before reaching the surface, during which significant contamination can modify their composition. On the other hand intra-oceanic arc magmas cross a thin oceanic lithosphere and should therefore more accurately reflect their source composition. However, crustal contamination of oceanic arc magmas has been shown to occur too (e.g. Macpherson et al., 1998). Yet most studies ignore the occurrence of this process and attribute all the crustal characteristics of these magmas to contributions from the subducting slab. Clearly, this neglect could compromise mass balance calculations. The systematic investigation and quantification of the potential impact of crustal assimilation should be a prerequisite to any source characterization based on arc lava compositions.

1.2 Thesis organization and rationale

The research conducted in this thesis is presented in Chapters 3, 4, 5 and 6 in the format of scientific papers. Each of these four chapters has a corresponding supplementary data file presented in the appendices. A summary of the main conclusions obtained in the four contributions is presented in Chapter 7. The broader rationale is presented below, followed by the specific objectives and author contributions for each chapter.

The aims of the research carried out for this thesis involved the investigation, characterization, and quantification of the effects of crustal assimilation on oceanic arc lava compositions. The occurrence of magma interaction with the crust is widely accepted in continental arcs but its importance is still highly debated in oceanic arcs. Addressing this issue is critical to accurately estimate budgets of crust recycling at subduction zones, which are mainly based in oceanic arc lava compositions.

Nowhere has the debate been more important than in the Lesser Antilles arc where the potential occurrence of crustal assimilation has been questioned for the last twenty years. The Lesser Antilles arc lavas display a wide range of trace element and isotopic compositions ranging from typical oceanic arcs to continental crust-like signatures. The occurrence of continental signatures in the arc lavas can be explained by either

incorporation of sediment in the mantle source, or assimilation during differentiation of the magma in the arc crust. Distinguishing between sediment incorporation in the mantle wedge and assimilation of sediments in the arc crust is not straightforward – the effects of mixing of sediment with mantle or with basalts are similar in most isotope-isotope spaces. Twenty years ago, using whole rock oxygen isotopes data across the arc, Davidson (1987) and Davidson and Harmons (1989) argued that the continental signature was mostly caused by arc crust assimilation. However, whole rock O isotopic compositions can be easily modified by weathering, and these interpretations have been questioned. Less than a decade later, Smith et al. (1996) and Thirlwall et al. (1996) showed the presence of crustal assimilation in lavas from the southern islands having “continental” compositions (Bequia and Grenada), this time using mineral oxygen isotopes and correlations between radiogenic isotopes and indices of differentiation. In 2002, Van Soest et al. confirmed the involvement of crustal assimilation using He, O and Sr isotope compositions in phenocryst separates (olivine and pyroxene) (Fig. 11) which are less susceptible to alteration than whole rock samples. However, in 2008, the debate was re-invigorated by the publication of new analyses of sediments from the subducted Atlantic plate (Carpentier et al., 2008). Up to that date, no sediments having radiogenic enough Pb isotope ratios to explain the Lesser Antilles arc lavas by sediment incorporation (either in the crust or in the source) had been found around the subduction zone region. In their publications, Carpentier et al. (2008; 2009) showed the existence of black shale in DSDP 144 located east of the Lesser Antilles, with compositions suitable to explain the arc lavas compositions by simple mixing in the mantle wedge. This interpretation was then supported by Labanieh et al. (2010; 2012) using trace elements and Sr Nd, Hf and Pb isotopic data from Martinique lavas, but subsequently refuted by Davidson and Wilson (2011), who argued that crustal assimilation is responsible for the “continental” signatures on Martinique.

In the light of lack of consensus regarding the occurrence of crustal assimilation in the Lesser Antilles arc, the geochemical composition of lavas from St Lucia Island, located in the central Lesser Antilles arc, was investigated here using a wide range of methods. Lavas from St Lucia were chosen for this study since a preliminary isotopic investigation showed that their compositions cover most of the range of isotopic variation in this arc or,

indeed, arcs in general. St Lucia therefore provides the locality of choice to constrain the mechanisms responsible for the isotopic variations observed along the arc. In addition, following the understanding gained from the study of St Lucia, the Os isotopic composition of the most mafic lavas from several islands from along the arc was investigated to assess models for along arc source variations.

Chapter 2 presents a review of the Lesser Antilles subduction zone. Models for the evolution of the Caribbean plate leading to the development of the Lesser Antilles arc are presented, followed by the structure and composition of the presently active arc.

Chapter 3 focuses on the detection of crustal assimilation in St Lucia lavas. In order to do this, whole rock $^{87}\text{Sr}/^{86}\text{Sr}$, $^{143}\text{Nd}/^{144}\text{Nd}$, $^{206}\text{Pb}/^{204}\text{Pb}$, $^{207}\text{Pb}/^{204}\text{Pb}$ and $^{208}\text{Pb}/^{204}\text{Pb}$ ratios along with mineral $^{87}\text{Sr}/^{86}\text{Sr}$ and $\delta^{18}\text{O}$ were analysed and interpreted in conjunction with major element concentrations in the corresponding samples from the literature. The study investigates the occurrence of sediment assimilation in lavas ranging from basalt to rhyolite and explores the control of assimilation on their isotopic compositions. The samples for this study were collected by Jon Davidson in 1983 or more recently by Jan Lindsay. For radiogenic isotopes, all sample preparation, laboratory work, data collection and evaluation were carried out by the author at either Durham or Macquarie Universities. For the $\delta^{18}\text{O}$ analyses, the author performed the mineral separation and preparation at Durham University as well as the O extraction by laser-fluorination at East Kilbride using NERC facilities. However, the extracted O (CO_2) was analysed by Alison McDonald on the mass spectrometer due to instrument breakdown during the authors visit. Geoff Nowell (Durham) and Peter Wieland (Macquarie) trained and supervised the author during the whole rock radiogenic isotope analysis, and Geoff Nowell trained the author during mineral Sr isotopic analysis. Adrian Boyce, Terry Donnelly and Alison McDonald trained and assisted the author during the O isotopes extraction. The chapter was written by the author with Prof. Jon Davidson, Prof. Simon Turner, Dr. Colin Macpherson, Dr. Adrian Boyce and Dr. Jan Lindsay providing editorial comments and suggestions. A version of this chapter is published in *Earth and Planetary Science Letters*. The supplementary data file corresponding to this chapter is presented in Appendix B.

Chapter 4 focuses on the understanding of the overall impact of sediment assimilation (shown to occur in Chapter 3) on the trace element and isotopic compositions of St Lucia lavas to determine the nature of the sediment and to thereby assess the source characteristics. This chapter presents new whole rock Hf isotope ratio and trace elements concentrations for St Lucia lavas. It uses this new data along with the whole rock Sr, Nd and Pb isotope data from Chapter 3 to fully constrain, model and quantify the impact of crustal assimilation on the lavas, and determine the nature of the assimilant. This allowed the subsequent analysis of the mantle source, including estimations of the amount of subduction slab components involved, and its comparison with source estimations for other islands. All sample preparation, laboratory work, data collection and evaluation were carried out by the author at Macquarie and Durham Universities. Geoff Nowell and Peter Wieland trained and supervised the author during Hf sample preparation and analysis and Chris Ottley trained the author during trace element sample preparation and analysis. The chapter was written by the author with Prof. Jon Davidson, Prof. Simon Turner, Dr. Colin Macpherson and Dr. Jan Lindsay providing editorial comments and suggestions. A version of this chapter has been submitted to *Journal of Petrology*. The supplementary data file corresponding to this chapter is presented in Appendix C.

Chapter 5 examines the processes responsible for the development and evolution of a silicic complex in a mature oceanic arc, using the Soufriere Volcanic Complex (SVC) on St Lucia as a case study. It includes detailed petrography for all of the St Lucia lava groups, in-situ major and trace element data for most of the observed phenocryst phases as well as in-situ $^{87}\text{Sr}/^{86}\text{Sr}$ data from plagioclase and in-situ $\delta^{18}\text{O}$ data from previously dated zircons. This study investigates the relative contribution of crystal fractionation versus crustal assimilation in the production and evolution of large amounts of silicic magmas. It also investigates the conditions of production of such magmas (depth, temperature) and the potential decoupling of the crystallisation of observed phenocryst assemblages and the production of silicic magma itself. Thin and thick polished sections were used for all in-situ analyses, excepting zircon $\delta^{18}\text{O}$, and were made by technicians from the Open University and Durham University. Sample preparation and analysis for major and trace elements as well as Sr isotopes were undertaken by the author at Macquarie University and the Australian National University (ANU). Assistance was

given by Peter Wieland (Macquarie) for in-situ $^{87}\text{Sr}/^{86}\text{Sr}$ while major element work was supervised by Kevin Grant (Macquarie) and Robert Rapp (ANU). Zircon had already been separated and mounted by Axel Schmitt at the University of California in Los Angeles (UCLA). The author polished the samples, imaged and analysed the zircon grains using the UCLA SEM and ion microprobe under the supervision of Axel Schmitt. The chapter was written by the author with Prof. Jon Davidson and Prof. Simon Turner providing editorial comments and suggestions. A version of this chapter will be submitted to *Journal of Petrology*. The supplementary data file corresponding to this chapter is presented in Appendix D. The latter includes some representative mineral major element compositions but given the important number of analyses, the full dataset is presented in a dedicated appendix: Appendix G.

Chapter 6 presents an Os isotopic investigation of some of the most mafic and well constrained lava samples from different islands along the Lesser Antilles arc, including St Lucia, and of sediments and altered basalt from the subducting slab. This investigation was done to test the ability of mafic lavas from along the arc to represent the full mantle source characteristics. It comprises a discussion of the relative control of the subducting slab composition versus crustal assimilation on the Os isotopic compositions of mafic lavas. Os isotopic signatures are then compared with lithophile isotope and trace element ratios to understand if these are controlled by similar processes. The lava compositions and the processes occurring in Lesser Antilles are then compared with those in other arcs. The lava samples came from collections of Simon Turner and Matthijs Van Soest and the sediment samples came from Jon Davidson's collection. All sample preparation and Os isotopic analysis of the arc lavas, the slab organic-poor sediment and slab altered basalt has been done by the author under the supervision of Bruce Schaefer at Macquarie University. The sample preparation and analysis of the organic-rich sediments from the slab has been done by David Selby at Durham University. The chapter was written by the author with Prof. Jon Davidson, Prof. Simon Turner, Dr. Bruce Schaefer and Dr. David Selby providing editorial comments and suggestions. A version of this chapter has been submitted to *Geochimica et Cosmochimica Acta*. The supplementary data file corresponding to this chapter is presented in Appendix E.

Chapter 7 synthesises the main conclusions outlined in the four previous chapters. Suggestions for future work are also presented.

Each of Chapters 3-6 comprises a condensed method section. Detailed protocols are presented in Appendix F.

Chapter 2

Geological setting

2.1 Geodynamic evolution of the Caribbean plate and the development of the Lesser Antilles arc

Knowledge of the evolution of the Caribbean plate is important to understand the origin of the development of the Lesser Antilles subduction zone and also to constrain the nature of the basement on which the arc has developed. The current Caribbean plate consists of an undeformed central area bounded by active margins (Fig. 2.1) (Giunta et al., 2006). The northern and southern margins consists of shear zones within Jurassic and Cretaceous deformed terranes. The Eastern and Western margins are convergent margins represented by the Central American Isthmus and the Lesser Antilles arcs.

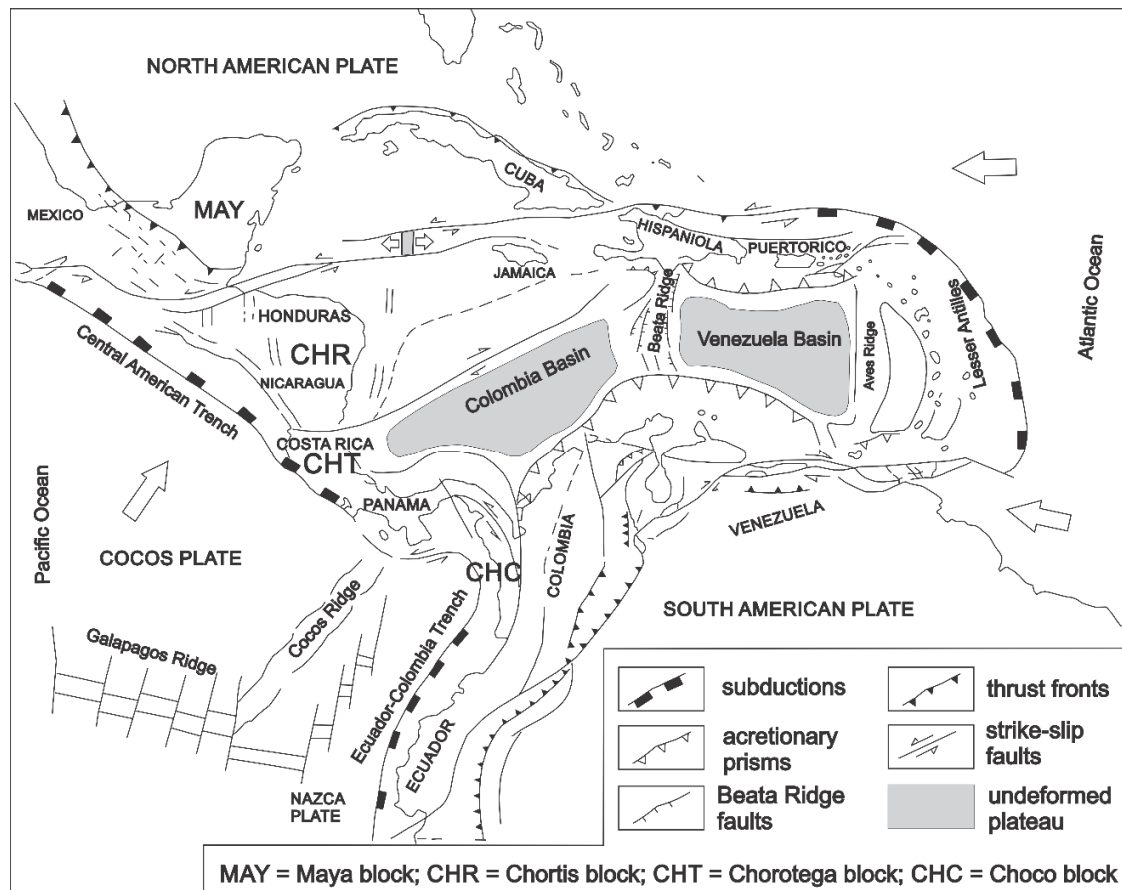


Fig. 2.1. Structural map of the Caribbean area. Arrows indicate the drifting direction of the main plates. Figure modified from Giunta et al. (2006).

Several models have been proposed for the geodynamic evolution of the Caribbean plate. They are all extremely complex and mostly differ in the cause and timing of events associated with the emplacement of the Caribbean plate into the basin between the North and South American plates (Kerr et al., 2003). The main discussion is about the location of the genesis of the Caribbean plate itself. Based on different plate origin ideas, two main geodynamic models exist and these are presented below as the “pacific origin” and the “in situ/proto Caribbean origin” models. In both models, it is accepted that the Caribbean plate is an oceanic plateau formed by hotspot activity. Both models also agree about the formation of the proto-Lesser Antilles arc, called the Aves ridge, by west dipping subduction and on the cause of the shift of activity from the Aves ridge to the present Lesser Antilles location, due to slab rollback.

2.1.1 The “pacific origin” model

The “pacific origin” model proposes that the Caribbean plate formed in the Pacific (Farallon plate) during the Jurassic and thickened above a hot spot at around 95-90 Ma (The Galapagos hot spot) to become an oceanic plateau which then drifted to the east between the American plates (Fig. 2.2a). During this eastward drift, it is thought to have entered and obstructed the trench of an eastward dipping subduction zone. This would have locked the subduction and reversed its polarity beneath the arc built during the subduction (“Great arc”; Kerr et al., 2003). Another version of this model (Fig. 2.2b) proposes that the subduction reversal occurred before the extrusion of the Caribbean plateau at the subduction area (Pindell, 1993), but the cause of the subduction reversal, which could be a seamount chain, is still unclear. In both cases, the Caribbean plate migrated eastward between the two American plates. The arc formed by the new west dipping subduction system is called the Aves ridge. During the Cenozoic, the opening of the Grenada inter- or back-arc basin separated the Aves ridge from the active volcanic zone where the Lesser Antilles developed. Most models propose that the cause of Grenada Basin opening was increased roll-back of the Atlantic slab which may have been caused by oblique collision of the island arc systems at the leading edge of the Caribbean Plate with the North and South American continents. The pre-existing arc (Aves Ridge) formed by west dipping subduction was rifted apart and the new Lesser Antilles subduction zone

initiated at ~50 Ma (Speed and Walker, 1991). The north of the Lesser Antilles arc is thought to be developed on the stretched crust of the Aves ridge (Wadge, 1986) while the central-south of the arc (south of Dominica) is thought to be intruded through the middle of the Aves ridge forearc basin, spitting it into the Grenada and the Tobago Basin (Speed and Walker, 1991; Aitken et al., 2011).

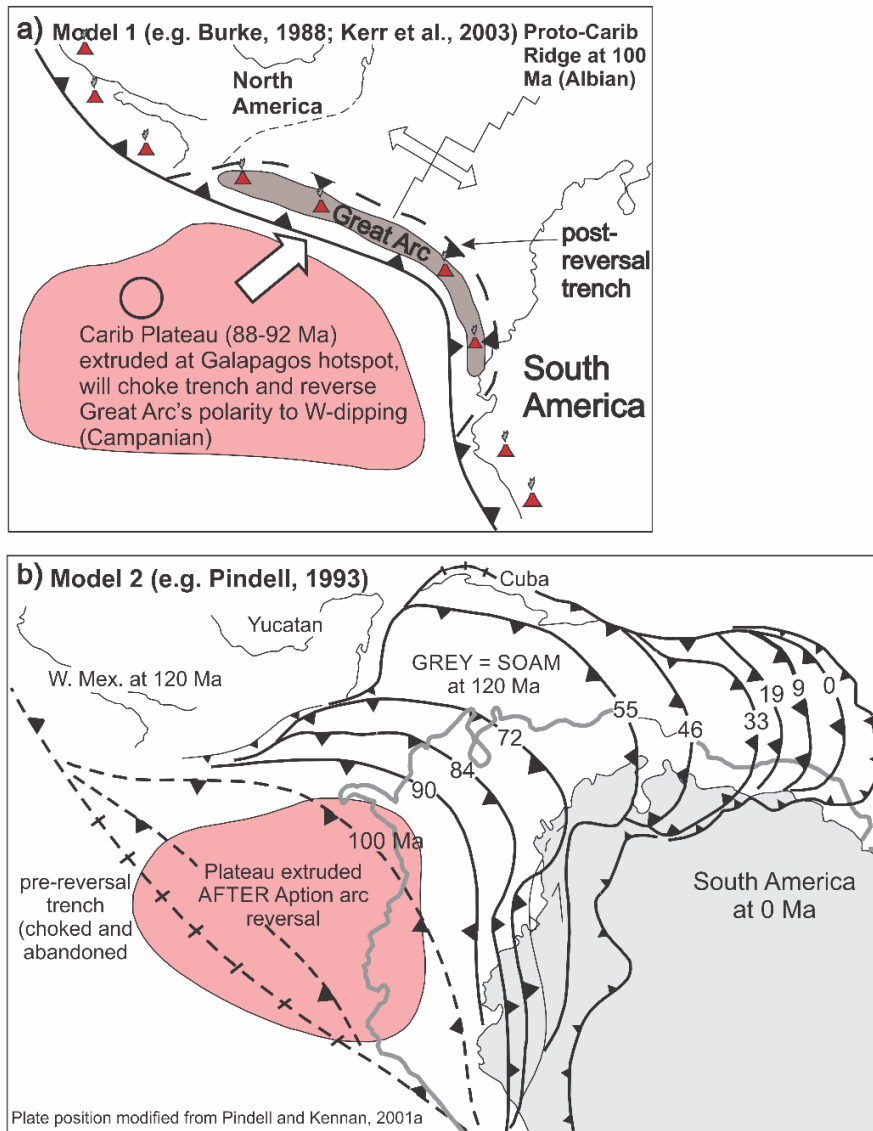


Fig. 2.2. Two versions of the «pacific origin model» for the genesis and emplacement of the Caribbean plate. In model (a) the Caribbean plateau is formed above a hotspot, drifts toward the subduction zone, obstructed the subduction zone and changes the slab polarity. In model (b) the reversal of polarity of the slab occurs before the extrusion of the plateau. SOAM = South America. Figure modified from Pindell et al. (2006).

2.1.2 The in situ/protocaribbean origin model

The “in situ” model proposes that the Caribbean plate formed in place between the diverging Americas. During the Jurassic, hot spot activity would have occurred during the opening of the proto-Caribbean Sea, producing the Caribbean plate and the separation of the two Americas. The Caribbean plate would then have drifted eastward due to slab rollback. One of the most recent versions of this model is presented by Giunta et al. (2006) (Fig. 2.3). It shows a complete paleogeographic reconstruction and kinematic evolution of the Caribbean plate from Late Jurassic to Tertiary. Giunta et al. (2006) propose that the history of the Caribbean plate can be separated into four major stages: (1) the Proto-Caribbean stage (2) the first Eo-Caribbean stage, (3) the second Eo-Caribbean stage and (4) the Caribbean stage.

The Proto-Caribbean stage (1) (Fig. 2.3a) would have taken place during the Late Jurassic-Early Cretaceous. During that stage, the Proto-Caribbean crust would have been generated between the South and North American plates in response to extensional forces related to the opening of the central Atlantic (Giunta et al., 2006). It would consist mostly of basaltic and gabbroic rocks of MORB affinity sometimes associated with picrites. According to this model, the Proto-Caribbean crust thickened considerably on its westernmost end during the end of the Cretaceous to become a typical oceanic plateau with rocks of OIB affinity (Beccaluva et al., 1999). The first Eo-Caribbean stage (2) (Fig. 2.3b) took place during the mid-Cretaceous. During that stage, the extensional setting turned into a compressive environment where intra-oceanic as well as sub-continental subduction occurred. This tectonic change was associated with the opening of the South Atlantic Ocean which led to westward and north-westward motion of the American plates. During this stage, tholeiitic and calc-alkaline arc magmatic rocks were generated as well as HP-LT metamorphic rocks at the Caribbean margins. The second Eo-Caribbean (3) (Fig. 2.3c) phase took place during the Late Cretaceous. The Caribbean plateau continued to move eastward relative to Americas, and the westward dipping subduction of the proto-Caribbean-Atlantic plate beneath the plateau led to the development of the Aves ridge magmatic arc system (Giunta et al., 2006). Oblique subduction under the plateau occurred at both the northern and southern boundaries of the plate leading to the genesis of tonalitic

arc rocks as well as HP-LT metamorphism. Finally, the Caribbean phase (4) (Fig. 2.3d), from Oligocene to present, corresponds to the collision of the North and the South American plates with the oceanic plateau. The collision was the result of eastward drifting of the Caribbean plate. At the same time, an eastward dipping subduction zone developed on its western margin and the Northern and Southern boundaries became two large shear zones. The eastward drift of the Caribbean plate, overriding the Atlantic lithosphere, lead to the development of the arc system of the Lesser Antilles and the Barbados accretionary prism (Giunta et al., 2006).

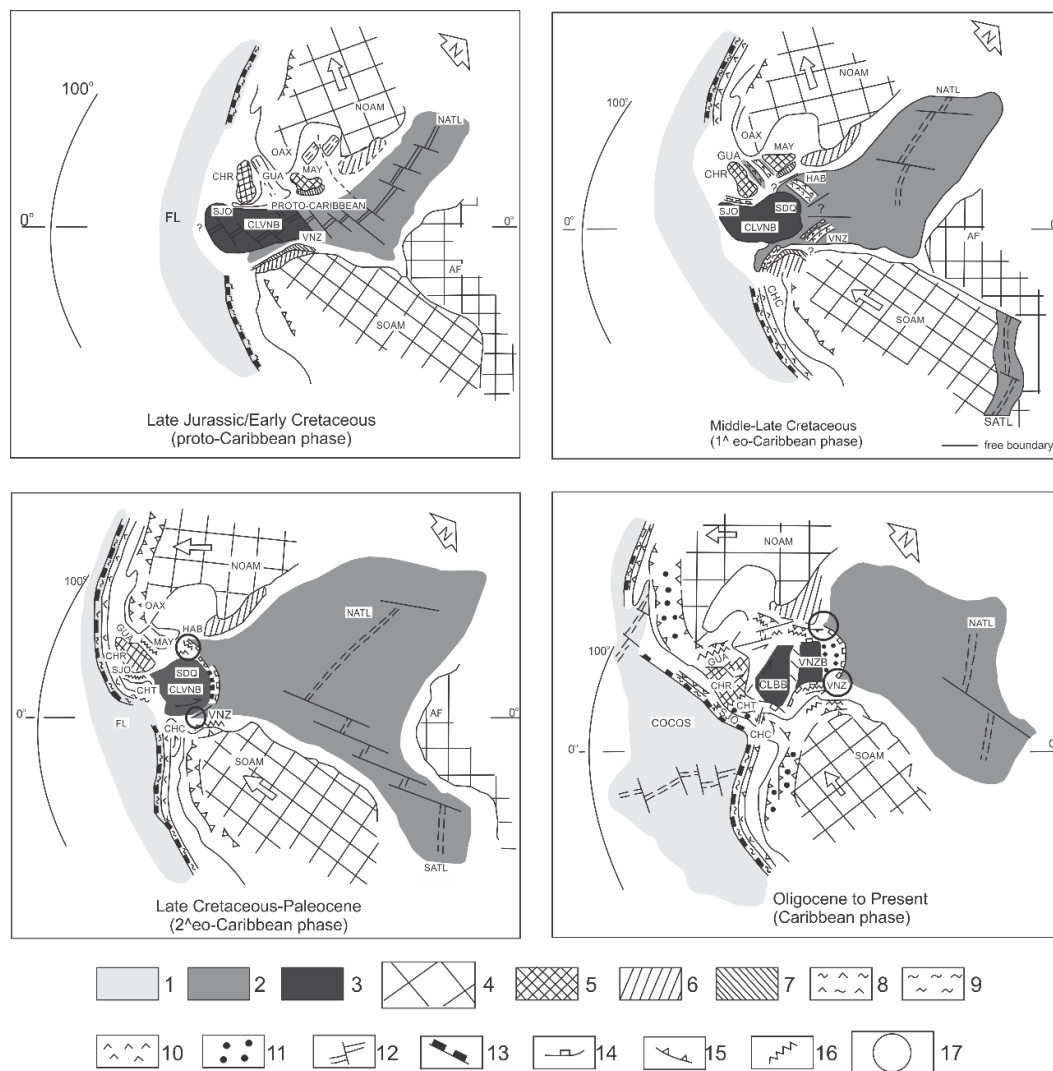


Fig. 2.3. Paleogeographic reconstruction and kinematic evolution of the Caribbean Plate, from Late Jurassic to Tertiary. Figure modified from Giunta et al. (2006). Numbers in legend: 1: Oceanic crust of the Farallon

Plate; 2: Proto-Caribbean-Atlantic oceanic crust; 3: Proto-Caribbean oceanic area undergoing crustal thickening; 4: North American, South American and African continental plates; 5: Minor continental blocks; 6: Continental margins; 7: Rifted continental margins; 8: Volcano-plutonic arc sequences; 9: Ophiolitic melanges; 10: Cretaceous arc volcanism of the Caribbean area; 11: Tonalitic magmatism and volcanic arcs; 12: Oceanic spreading centers; 13: Subductions of the Farallon-Pacific oceanic lithosphere; 14: Intra-oceanic subductions in the Caribbean area; 15: Main overthrust fronts; 16: Deformed and thrust belts, including suture zones, accretionary prisms, melanges and olistostromes; 17: Triple-junctions. Abbreviations: FL: Farallon; NOAM: North America; SOAM: South America; AF: Africa; NATL: Northern Atlantic; SATL: South Atlantic; OAX: Oaxaca; MAY: Maya; CHR: Chortis; CHT: Chorotega; CHC: Choco; SJO: Costa Rica; GUA: Guatemala; SDQ: Hispaniola; HAB: Cuba; VNZ: Venezuela; CLVNB: Colombia and Venezuela Basins; CLBB: Colombia Basin; VNZB: Venezuela Basin.

2.2 The Lesser Antilles subduction zone

The Lesser Antilles subduction zone results from the subduction of the Atlantic plate (also called American plate) beneath the Caribbean plate at a rate of 2-4 cm per year (Macdonald and Holcombe, 1978; McCann and Sykes, 1984). Similar to most intra-oceanic arc settings, the subduction zone (Fig. 2.4) is composed of an accretionary complex, a fore-arc region, an arc and a back-arc.

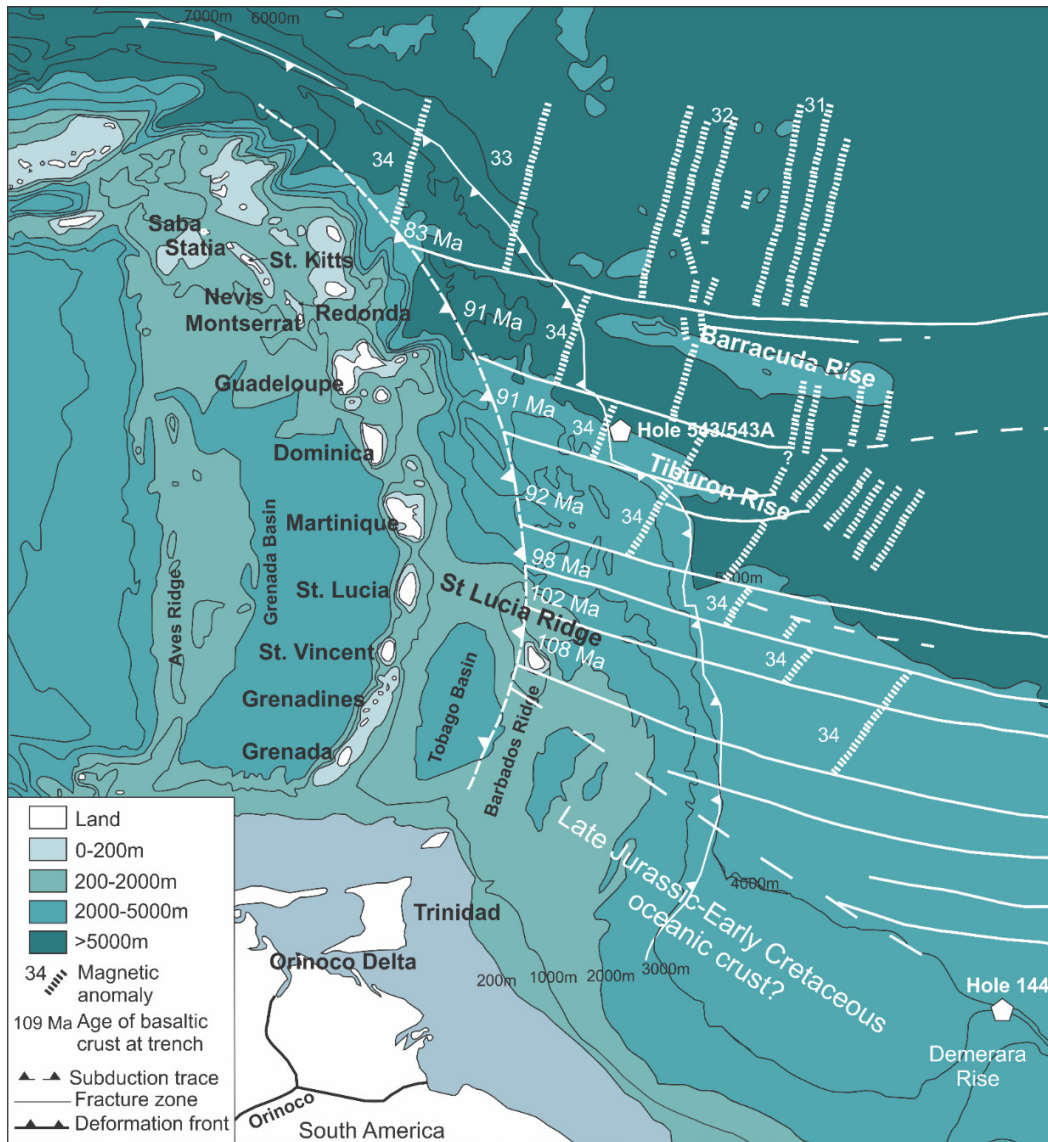


Fig. 2.4. Bathymetric map of the Lesser Antilles arc region showing the islands of the Lesser Antilles arc, the trench-deformation front, the subduction trace, fracture zones, the main ridges, the Grenada and Tobago basins and the locations of Deep Sea Drilling Project (DSDP) hole 543/543A and hole 144. The age of the

subducting slab is calculated using a Cretaceous half spreading rate of 2.2 cm/yr for the middle Atlantic ridge and the distance to the magnetic anomaly 34. Figure modified from Van Soest et al. (2002) and Carpentier et al. (2008).

2.2.1 The accretionary wedge and sediments on the subducting plate

2.2.1.1 Accretionary wedge

The accretionary wedge (Fig. 2.4) increases in size from the north to the south of the arc and reaches its maximum thickness of 20 km at Barbados Island. The large amount of sediment in the southern arc trench caused the overthrusting of the wedge onto the volcanic arc with the consequence that sediments are part of the arc basement in Grenada and the Grenadines (Torrini Jr. and Speed, 1989; Larue et al., 1991). The wedge is composed of sediments scrapped from the 0.7 to 4 km thick sediment pile on the American plate (Burke, 1988; Macdonald et al., 2000; Carpentier et al., 2008). The age of the American plate at the trench increases from ~83 Ma in the north to up to 105 Ma at the latitude of St Vincent, and may be as old as Late Jurassic south of St Vincent (Carpentier et al., 2008). The great thickness of the southern end of the accretionary wedge compared to its northern end is caused by its proximity to the deltas of the Orinoco and Amazon rivers, which transport sediments from the old South American continental crust (craton) to the front of the subduction zone and to some extent into the Caribbean Sea (Bowles and Fleischer, 1985). This north-south thickness change is accompanied by a change in sediment composition with the northern part of the wedge mainly comprised of pelagic sediments while the southern part is essentially composed of terrigenous turbidites (Westbrook et al., 1984). The presence of WNW-ESE aseismic ridges in the Lesser Antilles trench have been suggested to be a controlling factor for the morphology of the accretionary wedge as they seem to be responsible for stopping the transport of sediments to the northern part of the arc trench. The St Lucia ridge is the most efficient with the accretionary wedge displaying its greatest thickness just south of this while the trench is deeper in front of Martinique Island.

2.2.1.2 Nature of the subducted sediments

Geophysical studies (seismic reflection profiles) across the deformation front of the accretionary wedge showed the presence of a décollement surface within the sediment pile. Sediments above the décollement are thought to be overthrust and accumulated in the accretionary prism, while only sediments located beneath this interface can potentially be subducted (Biju-Duval et al., 1982; Moore et al., 1982; Westbrook et al., 1982; Westbrook and Smith, 1983). The knowledge of the nature of the subducted sediments is important to interpret the isotopic and chemical composition of the arc lavas. Indeed, variation in the composition of the subducted sediments has often been interpreted as the direct cause for the chemical and isotopic variations observed in lavas from along the arc (e.g. Labanieh et al., 2010).

The composition of the sediments entering the subduction zone has been characterised by several Deep Sea Drilling Projects (DSDP) and by analyses of the sediments at the Barbados Island. Amongst several others, two main drilling sites are thought to be representative of the subducted sediments: (1) DSDP 78A site 543 (Fig.2.4), located at the same latitude as Dominica, is thought to represent the sediments likely to be subducted beneath the northern part of the arc while (2) DSDP 14 site 144 (Fig. 2.4), located at the edge of the Guyana continental margin (Fig. 4), is thought to comprise the sediment pile being subducted beneath the southern part of the arc. Although the sequence at DSDP site 144 sediment is not located near the trench, sediments of similar age are thought to be subducted beneath the southern part of the arc.

(1) At DSDP 78A site 543, a sequence of 410 m of sediments and 44 m of basaltic Campanian (~80 Ma) basement has been cored. Above the 176 m décollement, the sequence is composed, from the top to bottom, of 10 m of ashy mud, 60 m of Pleistocene to upper Pliocene ashy nannofossil mud, which is transitional to a unit of Lower Pliocene to Lower Miocene mud and ashy mud. Beneath the 176 m décollement (Lower Miocene and older sequences), the sedimentary sequence is monotonous and mainly consists of pelagic clay and radiolarian clay (Biju-Duval et al., 1984) that is thought to have been deposited below the Carbonate Compensation Depth (CCD) (Hemleben and Troester, 1984). One unit, however, directly overlying the basaltic basement (unit 6), contains

carbonates and is thought to have been deposited above the CCD, in a ridge environment. Overall, sediments from site 543 have a similar trace element composition (Fig. 2.6) to Global Subducting Sediment (GLOSS; Plank and Langmuir, 1998) and Upper Continental Crust (UCC; McLennan, 2001) estimates, and no significant differences exist between lithological units (Carpentier et al., 2008). The Nd (Fig. 2.5) and Pb (Fig. 2.7) isotopic compositions of the sediments are similar in all units. The average sediment sequence has a Nd isotope ratio only slightly lower than GLOSS while Pb isotope ratios are higher than GLOSS (Carpentier et al., 2008). In terms of Sr isotopes (Fig. 2.5), no systematic variations can be observed through time, and most sediments are more radiogenic than the average UCC and GLOSS due to their origin from Achaean continental crust. $^{176}\text{Hf}/^{177}\text{Hf}$ ratios of site 543 sediments are more radiogenic than site 144, with the most radiogenic values observed at the top of the sequence due to the presence of ash in the sediment.

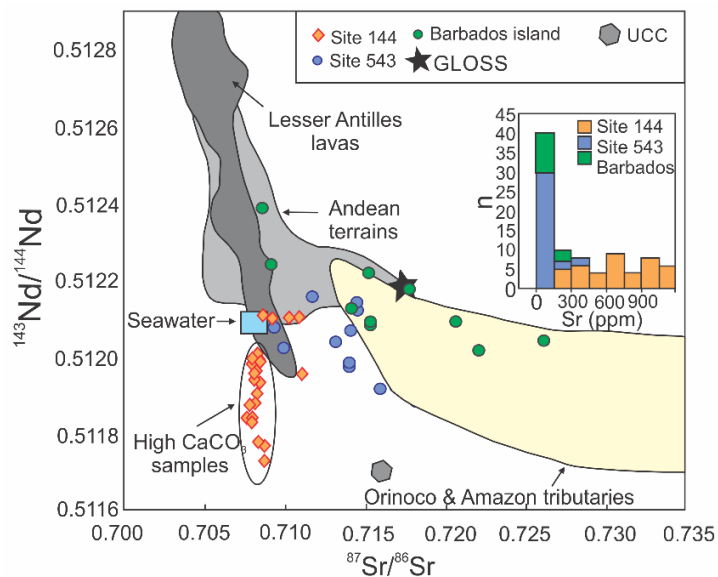


Fig. 2.5. Sr and Nd isotopic composition of DSDP sites 144 and 543 and of Barbados Island sediments from Carpentier et al. (2009). The inset shows the Sr concentrations of these sediments in a histogram. The Lesser Antilles arc lavas and the Andean terrains compositions from georock database (<http://georock.mpch-mainz.gwdg.de/georock/>), as well as the Orinoco and Amazon tributaries sediment composition from Allegre et al. (1996) and Parra et al. (1997) and the late Cretaceous to Miocene North Atlantic seawater compositions from Burton et al. (1997) and O’Nions et al. (1998) are also shown. UCC = average upper continental crust from Goldstein et al. (1984) and Goldstein and Jacobsen (1988); GLOSS is from Plank and Langmuir (1998). Figure modified from Carpentier et al. (2009).

(2) At DSDP site 144, a 350 m thick pile of sediments from the northern flank of the Demerara rise was sampled and classified into five distinct units. The oldest sediments are Early Cretaceous (around 115 Ma) and the youngest are Late Cretaceous to early Oligocene. As opposed to site 543, the sedimentary sequence is heterogeneous in composition. The oldest units (units 5-4) are composed of terrigenous claystone, siltstone and sandstone and contain variable amounts of carbonate. They are interpreted to be a syn-rift sequence linked to the opening of the Central Atlantic Ocean (Hayes et al., 1972; Carpentier et al., 2008). Unit 3 is dated between 96-84 Ma and is composed of laminated organic-rich shales called “black shales” intercalated with a few carbonate rich layers (25-80%). Finally, Unit 2 and 1 are composed of carbonate bearing (30-70%) grey marl and chalk ooze. The trace element compositions of site 144 sediments display significant variations (Fig. 2.6), mainly between Unit 3 comprising black shales, and the other units. Unit 3 has the lowest trace elements concentrations of site 144 sediments except for U, leading to a very high U/Pb of this unit. Globally, site 144 sediments have lower trace element concentrations than site 543 sediments and GLOSS, except for U, Ba and Sr (Carpentier et al., 2008). All units have Nd isotope ratios similar to site 543 sediments (Fig. 2.5). Variations are observed between units, with Units 5 and 4 having the highest $^{143}\text{Nd}/^{144}\text{Nd}$ and Unit 3 and the bottom half of unit 2 having the least radiogenic compositions of the site. Pb isotope ratios vary significantly through time (Fig. 2.7). Units 4 and 5 have $^{206-207-208}\text{Pb}/^{204}\text{Pb}$ isotope ratios similar to those of GLOSS while Unit 3 has extreme $^{206}\text{Pb}/^{204}\text{Pb}$ and $^{207}\text{Pb}/^{204}\text{Pb}$ ratios with intermediate $^{208}\text{Pb}/^{204}\text{Pb}$. Unit 2 has the highest $^{208}\text{Pb}/^{204}\text{Pb}$ but only slightly higher $^{207}\text{Pb}/^{204}\text{Pb}$, $^{206}\text{Pb}/^{204}\text{Pb}$ compared to Units 5 and 4. Hf isotope ratios do not show any systematic variations in the sequence and are less radiogenic than site 144 ratios.

Although the sediments of Barbados Island are part of the accretionary wedge, and are therefore unlikely to be subducted, similar sediments could have been introduced into the subduction zone. These sediments have been extensively studied since this is the only locality where the accretionary wedge outcrops and is easily accessible. Eighty five per cent of the sediments are Pleistocene reefs limestones. The remainder are tertiary marine sediments in the triangular north-east region of the island (Donovan et al., 2005). The tertiary sediments are composed of a folded sedimentary sequence divided into two

formations: (1) the Scotland Formation comprising Early to late Eocene (57-35 Ma) terrigenous sandstone and claystone and (2) the overlapping in age Mid Eocene to Miocene (45-15 Ma) Oceanic Formation composed of mudstone, marls, chalks and ash layers (Pudsey and Reading, 1982; Biju-Duval., 1985). Sediments from the Scotland Formation have similar $^{87}\text{Sr}/^{86}\text{Sr}$ ratios to site 543 sediments. On the other hand, sediments from the Oceanic Formation are much less radiogenic due to the presence of ash layers. The Scotland Formation shows lower $^{176}\text{Hf}/^{177}\text{Hf}$ isotopic ratio than sediment from the Oceanic formation, these two groups presenting the highest and lowest ratios found in the subducting plate.

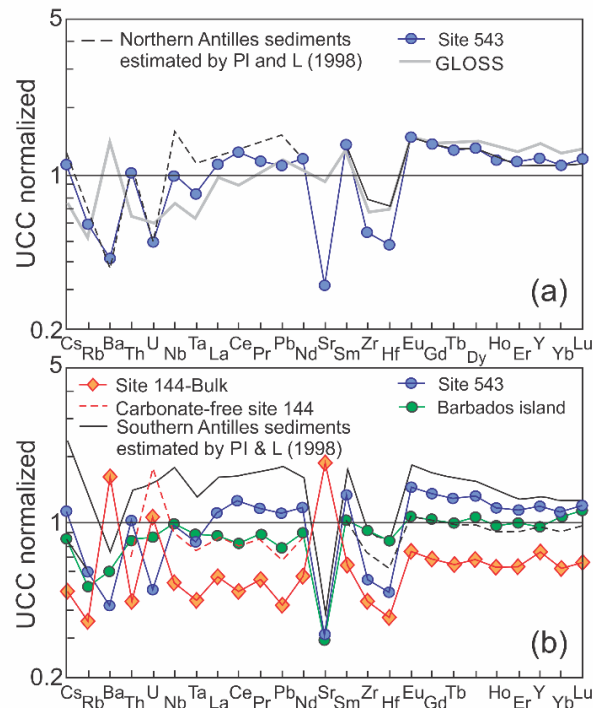


Fig. 2.6. Upper continental crust (UCC; McLennan, 2001) normalized trace element concentrations of the Lesser Antilles local sediment from Carpentier et al. (2009). (a) bulk DSDP site 543 sediment compared to GLOSS and the estimated Northern Antilles sediment composition of Plank and Langmuir (1998). (b) Bulk DSDP site 144 and Barbados average compositions compared to carbonate-free site 144, to Bulk DSDP site 543 and to the Southern Antilles sediments estimated by Plank and Langmuir (1998). Figure modified from Carpentier et al. (2009).

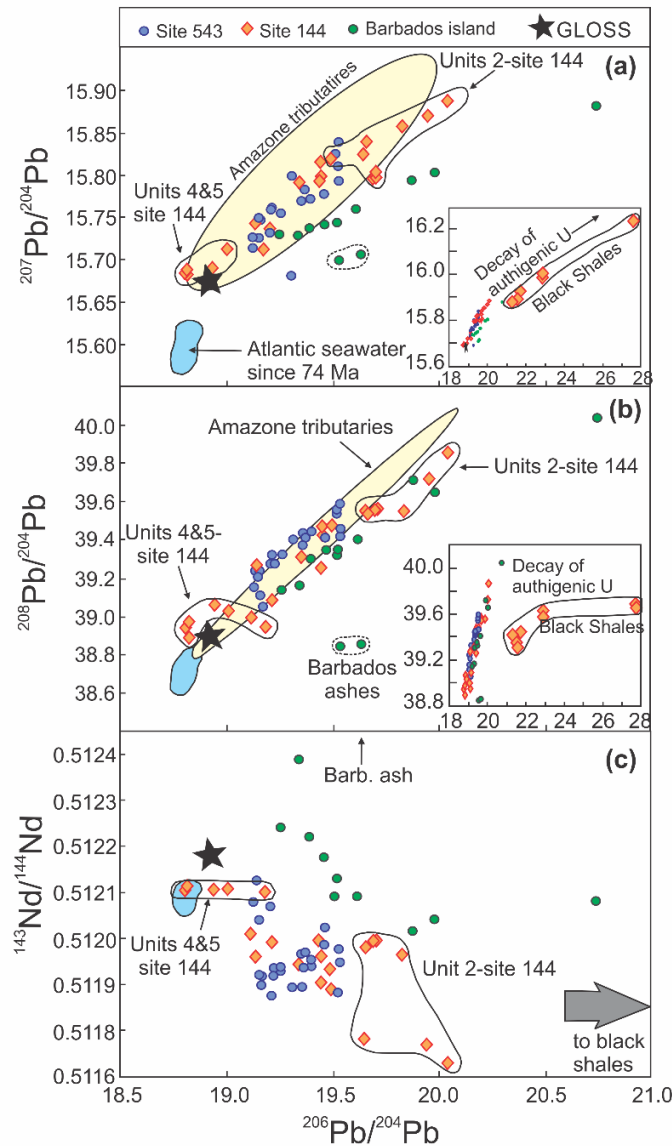


Fig. 2.7. $^{206}\text{Pb}/^{204}\text{Pb}$ ratio of DSDP sites 144 and 543 and the Barbados sediments against (a) $^{207}\text{Pb}/^{204}\text{Pb}$ ratio, (b) $^{208}\text{Pb}/^{204}\text{Pb}$ ratio and (c) $^{143}\text{Nd}/^{144}\text{Nd}$ ratio. Composition of the sediments from the Amazon Tributaries, of the Atlantic Sea water and of GLOSS are also shown. Same data source as in Fig. 2.5. Figure modified from Carpentier et al. (2008).

2.2.2 Forearc basin

The fore-arc zone is located to the east of the arc and to the west of the accretionary prism. It varies in width from 150 km in the north to 450 km in the south and varies also in depth with over 8km to the north to its disappearance in the south with the Barbados accretionary prism (Chase and Bunce, 1969). At the latitude of the Barbados accretionary wedge, the

forearc basin, called the Tobago Trough, is filled with a thick sedimentary pile (greater than 4 km). Recent geophysical studies suggests that most of the Tobago basin sediments are similar to those of the Grenada basin and were deposited in a same basin: the Aves Ridge forearc basin. It would have been separated from the Grenada basin during the intrusion of the Lesser Antilles arc (Aitken et al., 2011).

2.2.3 The Lesser Antilles arc

2.2.3.1 Structure

The Lesser Antilles arc itself is about 800 km long from Saba (north) to Grenada (south). It forms a single trend to the south but separates in two branches north of Martinique. The western branch has formed the active arc since the Early Miocene while the eastern branch was active during the Eocene to mid-Oligocene. The presently active arc can be divided in two segments based on the dipping angle of Benioff zone and the arc trend: (1) north of Martinique with an arc trend of N330° and a dipping angle of 60-50° for the Benioff zone, (2) from St Lucia to Grenada with an arc trend of N20° and a dip from 50-45° to vertical in the south of the segment (Wadge and Shepherd, 1984). Pleistocene to recent volcanism is also segmented. Three segments can be defined (Wadge and Shepherd, 1984): Saba-Montserrat, Guadeloupe-Martinique and St Lucia-Grenada, but the major break is between Martinique and St Lucia and correlates with the location of the kink in the Benioff Zone. The highest volume of volcanic product of the whole arc as well as the largest islands are located in and Guadeloupe, Dominica, Martinique and St Lucia.

2.2.3.2 The arc basement

Knowledge of the nature of the Lesser Antilles arc basement is important for the interpretation of the erupted lava compositions since assimilation of the arc crust during magma ascent/storage has been suggested as the factor responsible for the large isotopic and compositional range observed in the volcanic products along the arc (Davidson, 1987; Davidson and Harmon, 1989). Unfortunately, the arc basement seems to be very heterogeneous and poorly constrained. Two main geodynamic events have influenced the

basement composition: (a) slab rollback; and (b) the shift of the northern activity. In addition, (c) a geographical factor contributed to basement heterogeneity.

(a) The slab rollback and opening of the Aves Ridge forearc basin

Both the “pacific” and “in situ” geodynamic models presented in section 2.1 agree with the intrusion of the Lesser Antilles arc on the stretched Aves ridge arc or forearc crust, after a displacement of the volcanism east of the Aves Ridge (old arc; Aitken et al., 2011). A slab rollback is thought to be responsible for both this eastward shift of activity and the extensional regime of the overriding plate leading to the opening of the Grenada-Tobago forearc basin in the south and the stretching of the Aves ridge crust in the north, before the intrusion of the Lesser Antilles arc. Therefore, the north of the Lesser Antilles arc is thought to be entirely igneous since it was built upon the stretched crust of the Aves ridge (Wadge, 1986) while the basement in the central-south of the arc (South of Dominica) is thought to comprise some sedimentary sequences due to intrusion through the middle of the sediment-rich Aves ridge forearc basin, spitting it into the Grenada and the Tobago Basins (Davidson, 1987; Davidson and Harmon, 1989; Speed and Walker, 1991; Aitken et al., 2011). The nature of these sediments is important if they came into contact with magmas passing through the arc crust.

The Grenada and Tobago Basins sedimentary sequences comprise three megasequences (Fig. 2.8; Aitken et al., 2011). The first megasequence is thought to be Late Cretaceous to middle Eocene and made of deep-water, pelagic and volcanogenic shales and siltstones with some biogenic limestones in the lower part of the sequence (Ysaccis, 1997). The second megasequence is early to middle Miocene in age and comprises deep water turbidites topped by shallow water limestones. Finally megasequence 3 comprises sediments from late Miocene to recent which are pelagic with volcanogenic turbidites. Most sediments of Megasequence 1 and 2 and maybe the base of Megasequence 3 originated from the South American continent.

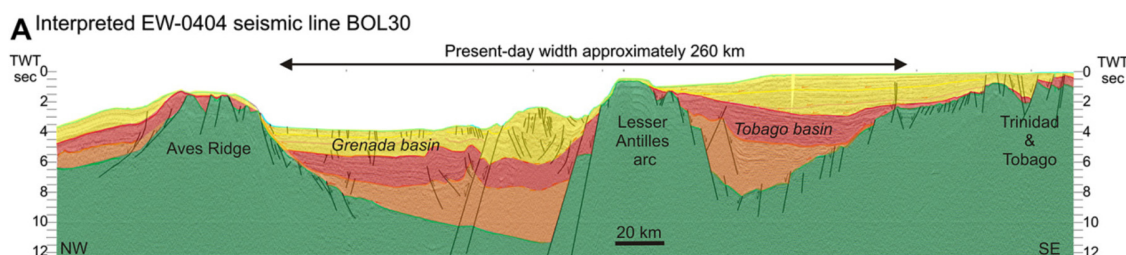


Fig. 2.8. Grenada and Tobago basins fault restoration (based on depth-converted seismic data) illustrating their common origin as a single Paleogene forearc basin. Figure from Aitken et al. (2011).

No published geochemical analyses are available for the Grenada and Tobago basin sediments, however, some geochemical characteristics can be inferred from their origin. The biogenic sediments present in Megasequence 1, are well known from industry wells for gas and oil, and are likely to contain high amounts of organic matter (Ysaccis, 1997). Such organic rich sediments tend to concentrate U and are likely to have very radiogenic $^{206}\text{Pb}/^{204}\text{Pb}$ and $^{207}\text{Pb}/^{204}\text{Pb}$ ratios after some time. Therefore, although younger, such sediment could share similar chemical and isotopic characteristics as the black shales found in DSDP site 144.

The remainder of the Grenada basin sediments are mainly terrigenous and were transported via the Proto-Orinoco River, which preceded the development of the Orinoco River that currently discharges large amounts of sediment into the arc trench. The current Orinoco River originates in the Guyana Highlands and then skirts the Guyana Shield by going north and then east until reaching the Atlantic Ocean in the south of Trinidad (Fig. 2.9; Diaz de Gamero, 1996). On its way, the river receives water and 99% of its sediment load from tributaries originating from the Eastern Cordillera of Columbia, la Merida Andes of Venezuela and the Caribbean system all of which were uplifted during the Neogene (Johnson et al., 1991; Diaz de Gamero, 1996). This current river configuration may have been similar since the Late Miocene. Before then, stratigraphic and microfauna evidence argue for the existence of a proto-Orinoco river from Middle Eocene to the Late Miocene. The proto-Orinoco river did not follow the same path as the Orinoco but was supplied from the same areas: the Guyana Highlands and the Columbian Andes. It flowed northward toward the current Maracaibo Basin (Fig. 2.10) before being forced, in the Late Miocene, to take a more E-W direction after uplift of the Eastern Cordillera of Colombia

and its extension in the Venezuela, the Merida Andes, marking the transition to the Orinoco River (Diaz de Gamero, 1996). Unlike the Orinoco River which transports almost exclusively Cordillera and Andes sediments with only 1% of its load coming from the Guyana shield, the proto-Orinoco river is thought to have transported a much larger amount of sediments from the Guyana shield (Cooper et al., 1996; Xie et al., 2010). The Guyana shield basement is almost entirely composed of igneous and metamorphic rocks from the Archaean to Phanerozoic (Goldstein et al., 1997 and references therein) while the central Cordillera of Columbia is composed of an igneous-metamorphic core with a sedimentary cover of Mesozoic age (Case et al., 1990). Hence, sediments derived from the Guyana shield have a very different composition and isotopic signature to the Andean sediments. This means the pre-Andean uplift (before late Oligocene) sediments transported by the proto-Orinoco River contained larger amount of terrigenous clastic sediments carrying extreme “continental” isotopic signatures (Cooper et al., 1995). This observation is important since more extreme isotopic signatures might be present in the Eocene and Oligocene sequences of the Grenada and Tobago basin, compared to the sediments currently found on the subducting plate and in the accretionary wedge. Indeed, the latter are thought to mostly derive from the Orinoco River. It was thought that some of oldest sediments on Barbados Island, some Eocene deep water sediments, may have been deposited by the submarine fans of the proto-Orinoco (Kasper and Larue, 1986; Pool and Barker, 1990). However, recent work (Xie et al., 2010) based on U-Pb ages of detrital zircons indicate that Eocene sediments from Barbados and Trinidad have a different source from the other proto-Orinoco deposits.

(b) Shift of northern activity

The second major event influencing the evolution of the arc basement is a 50 km shift of volcanic activity toward the west in the northern part of the subduction zone (from Martinique) during the Late Miocene. This shift is interpreted to result from the involvement of aseismic ridges in the trench (McCann and Sykes, 1984; Westbrook and McCann, 1990) and is responsible for the occurrence of volcanic products of different age in the north and the south of the arc. The basement of the southern islands comprise volcanic products as old as ~25 Ma, whereas the currently active northern islands only

started accreting 5.1 Ma ago. The different beginning of the current arc accretion may in turn be responsible for the north-south increase in basement thickness observed in the seismic data and gravity modelling going from 25-30 km around Montserrat (Maury et al., 1990; Sevilla et al., 2010) to 35-40 km around St Vincent (Maury et al., 1990).

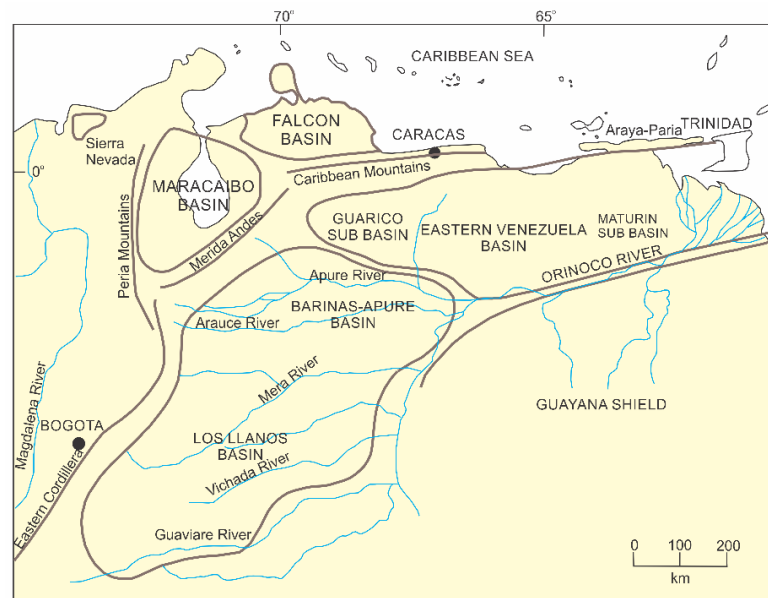


Fig. 2.9. Map of the Cenozoic basins of the Venezuela and Los Llanos Basin of Columbia. Figure modified from Diaz de Gamero et al. (1996).

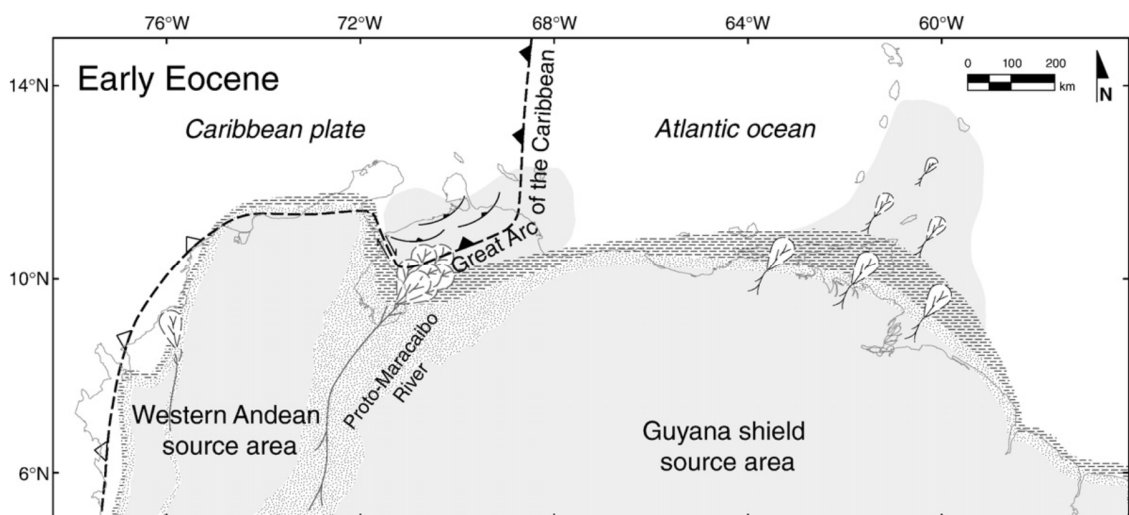


Fig. 2.10. Paleogeographic map of Eocene sediment dispersion system in northern South America. The location of the Proto-Orinoco River, here called the Proto-Maracaibo River system and of the Aves ridge arc, here called the Great Arc, are shown. Figure from Xie et al. (2010).

(c) Geographical factor

In addition to geodynamic control of the arc basement, a geographic factor is thought to play a role in the composition of the crust in the southern part of the arc. Indeed the proximity of the southern arc to the high flux of sediments from the South American continent is responsible for overthrusting of the accretionary wedge sediment onto the arc basement (Torrini Jr. And Speed, 1989). Sediments from the wedge can be observed in Grenada (Tufton Hall formation) where it consists of thick Upper Eocene folded flyschs (Tomblin, 1975). These sediments have lower $^{206}\text{Pb}/^{204}\text{Pb}$ than some of the Grenada lavas which suggests that they are not the cause of the continental signatures observed (see below), but the presence of other wedge sediments within the arc crust, with different composition, cannot be precluded.

2.2.3.3 Lava compositions

In 2000, Macdonald et al. published a review of the Lesser Antilles arc in which he discussed a large database of lava composition (273 rocks, 22 islands). Since then, several papers have been published that were mostly focussed on isotope analyses of the eruptive products (Van Soest et al., 2002; Gurenko et al., 2005; Lindsay et al., 2005; Toothill et al., 2007; Dufrane et al., 2009; Labanieh et al., 2010; Schmitt et al., 2010; Davidson and Wilson, 2011; Labanieh et al., 2012; Lindsay et al., 2013). This section reviews succinctly the published geochemical features of the lavas, their interpretation and their variations along the arc.

2.2.3.3.1 Lavas classification

The islands (Fig. 2.4) have been classified into groups based on the type of lava observed, their lava major and trace element compositions and their isotopic compositions.

Classifications based on rock types

Macdonald et al. (2000) separated the arc in three segments based on rock types. The northern segment, from Saba to Montserrat, is mainly andesitic although a few basalts and rhyolites have been erupted. The central segment, from Guadeloupe to St Lucia, also

comprises dominantly andesite but considerable basalts and dacites can be observed with minor rhyolites. Finally, the southern segment, from St Vincent to Grenada is dominated by mafic rocks with picritic basalts, ankaramitic basalts, basalt, basaltic andesite and andesite with the most mafic lavas found on Grenada being silica-undersaturated picrites (Macdonald et al., 2000).

Classification based on lava major and trace element chemistry

The arc lavas encompass the full range of existing major and trace element compositions in arcs. Brown et al. (1977) recognised 4 magmatic series: the low-K tholeiitic series, the medium-K series which consists of calc-alkaline rocks (Tatsumi and Eggins, 1995) and the Grenada C- and M- Grenada series. The C-series refers to ankaramitic basalts with high CaO content (compared to other series at a fixed MgO content) and that are highly clinopyroxene phyric (Thirlwall and Graham, 1984). The M-series are highly magnesian basalts with microphyric textures. An increasing spread in incompatible element abundances and ratios, as well as in the isotopic compositions, is observed in the sequence from the low-K basalts to the M-series basalts. Overall, M- and C- series basalts have higher Ba, LREE, Nb, Rb, Sr, Th and Zr, more radiogenic Sr and less radiogenic Nd than low K and medium K basalts but there is significant overlap. Brown et al. (1977) suggested that these 4 series occurred in different sections of the arc with the more tholeiitic rocks in the north, the calc alkaline lavas in the center and the alkaline series (C-M series) in the south. However, several subsequent studies have showed that, although this N-S compositional trend broadly exists, it is not strictly true in detail with the occurrence of both tholeiitic and calc-alkaline lavas in the north and central islands (Gun et al., 1974; Davidson and Wilson, 2011).

Macdonald et al. (2000) suggested that the Lesser Antilles rocks could also be separated into high-Ca and low-Ca groups. The high-Ca group includes the volcanic products from St Eustatius, St Kitts, Redonda, Guadeloupe, Dominica, Bequia and the so called C-series of Grenada. The low-Ca group comprises rocks from Saba, Montserrat, Martinique, St Vincent as well as the Grenada M-series rocks. The distinction between the high-Ca and low-Ca groups being clearest in the most mafic rocks ($\text{MgO} \leq 8 \text{ wt. \%}$), since the more

evolved compositions converge due to both fractional crystallisation and crustal contamination (Macdonald et al., 2000).

Based on trace element compositions, Macdonald et al. (2000) suggested the division of the islands into 3 groups with distinct geochemistry, which are slightly different from the segments defined by the rock types: (1) the northern island from Saba to Montserrat; (2) the central islands from Guadeloupe to Bequia and (3) the southern islands comprised of the Grenadines (except Bequia) and Grenada. Rocks from groups 1 and 2 have low Ce/Yb ratios whereas, group 3 lavas have high Ce/Yb, sometimes associated with a high Dy/Yb which has been interpreted to reflect a garnet bearing source or a source enriched in LREE by sediment addition. (Macdonald et al., 2000).

Classification based on isotope ratios

Based on Sr, Nd, Hf and Pb isotope ratios, the arc can be separated into a northern segment comprising islands from Saba to Dominica and a central-southern segment from Martinique to Grenada (e.g. Hawkesworth et al., 1993). Lavas from the north of the arc display “typical oceanic arc” composition similar to the Tonga, Mariana, South Sandwich and the Aleutian arcs (Fig. 2.11). They are characterised by a narrow range of Sr, Nd, Hf and Pb isotope compositions being only slightly different from mid-oceanic ridge basalts (MORBs). Lavas from the centre and south of the arc have more heterogeneous isotopic signatures ranging from “typical oceanic arc” to more “continental” compositions similar to the sediments observed on the subducting plate (Fig. 2.11). Lavas with “continental” isotopic signatures also have the highest L/M-HREE and LILE/HFSE (e.g. Ba/Th) ratios. The most extreme of these signatures are found on Martinique, St Lucia, Grenada and the Grenadine islands.

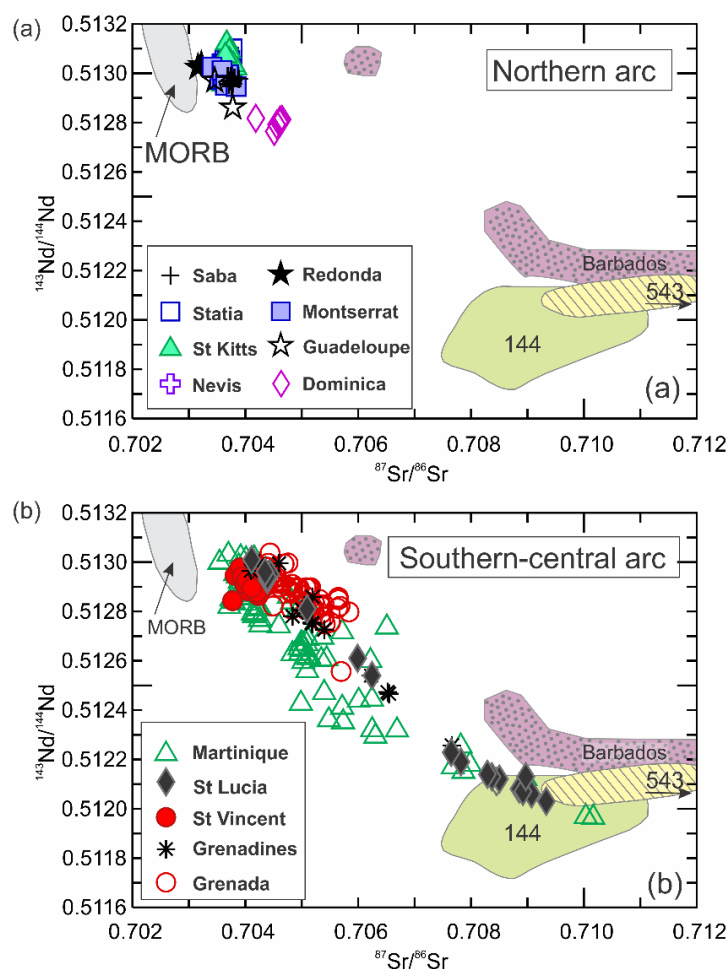


Fig. 2.11. Sr and Nd isotopic compositions of the Lesser Antilles arc. Data sources; Saba (Sherman, 1992; Van Soest, 2000; Dufrane et al. 2009), Statia (Davidson, 1984; Van Soest, 2002), St Kitts (Van Soest, 2000; Toothhill et al., 2007), Redonda (Davidson, 1984), Montserrat (Davidson, 1984; Van Soest, 2000), Guadeloupe (Van Soest, 2000); Dominica (Davidson, 1984), Martinique (Davidson, 1984; Van Soest et al., 2000; Labanieh et al., 2010;), St Lucia (Davidson, 1985; Vidal et al., 1991), St Vincent (Heat et al., 1998; Van Soest et al., 2000), Grenadines islands with Bequia (Smith et al., 1996), Ile de Caille (Van Soest, 2000) and Kick'em Jenny (Huang et al., 2011), and Grenada (Thirlwall and Graham, 1984; Thirlwall et al., 1996; Van Soest et al., 2000). MORB field is mid-Atlantic Ridge between 30°N and 30°S (data from PETDB: <http://petdb.org/science.jsp/>). 144 and 543 correspond to Atlantic sediments cored at the front of the trench at DSDP sites 144, 543. Barbados corresponds to sediments outcropping on Barbados. Sediment compositions are from Carpentier et al. (2008; 2009).

2.2.3.3.2 The mantle source

Slab contributions

Based on their major and trace element and isotopic compositions, lavas from the Lesser Antilles arc are commonly thought to derive from the partial melting of a depleted MORB mantle source (Turner et al., 1996; Heath et al., 1998) affected by (1) fluids from the altered basaltic crust and sediments from the subducted slab and (2) bulk sediment or sediment melt from the subducting slab. The relative contribution of these two components is the subject of much debate, especially for the islands erupting lavas with the “continental” signatures in the south of the arc (Fig. 2.11). Some authors attribute all trace element and isotopic signatures to source variations (White and Dupre 1986; Carpentier et al., 2008; Labanieh et al., 2010; 2012), while others attribute part of these to crustal assimilation during differentiation (Davidson, 1984; Thirlwall and Graham, 1984; Davidson, 1985; Davidson, 1987; Davidson and Harmon, 1989; Smith et al., 1996; Thirlwall et al., 1996; Van Soest et al., 2002; Davidson and Wilson, 2011).

Constraints on the source composition were first obtained in the late 70s and early 80s with the first combined trace element and isotopic studies by Hawkesworth et al. (1979), Hawkesworth and Powell (1980), Davidson (1983; 1984), Thirlwall and Graham (1984), White and Patchett (1984), Davidson (1985), White and Dupre (1986) and Davidson (1987). A second wave of publication occurred in the 90’s with Vidal et al. (1991), Turner et al. (1996), Smith et al. (1996), Thirlwall et al. (1996) and Heath et al. (1998) and more recently, a renewed interest occurred with fresh insights by Woodland et al. (2002), Lindsay et al. (2005), Toothill et al. (2007), Carpentier et al. (2008) Labanieh et al. (2010), Davidson and Wilson (2011) and Huang et al. (2011) and Labanieh et al. (2012).

In the 80’s, all contributions highlighted the role of both hydrous fluids and sediments from the slab to the source of the lavas. However, no precise estimates of the amounts of these components were made, with the exception of White and Patchett (1984) who estimated at least 1% of sediment and White and Dupre (1986) who estimated 3% or less of sediments in the source. In the 90s, most studies attempted to constrain the relative

contributions of fluid versus sediment in the source. We summarise below the budgets obtained in the different contributions from the 90s to recent.

Along arc studies- Using U-series, Sr, Nd and Pb isotope ratios in lavas from along the arc (Statia, St Kitts, Redonda, Martinique, St Lucia, St Vincent, Ile de Caille, Kick'em Jenny, Grenada), Turner et al. (1996) suggested that the mantle wedge was modified by (1) a fluid with low $^{87}\text{Sr}/^{86}\text{Sr}$ ratio, high U, Ba, Sr and K concentrations produced by the dehydration of the subducting oceanic crust and (2) by sediment and sediment melts from the slab having high Sr and Pb isotope ratios, low Nd isotope ratio and low Sr/Th ratio. Fluid input was thought to be similar along the arc, as well as the related degree of partial melting (10-15%) of the mantle. These authors suggested that the sediment contribution increases from ~ 2% in the north to ~ 15% in the south of the arc.

Similar sediment percentages were obtained by Carpentier et al. (2008), using new Pb and Nd isotope ratios of the local sediments and the whole range of compositions available for the Lesser Antilles arc on PETDB. These authors suggested that the Pb and Nd isotopic compositions in lavas from the north of the arc could be explained by addition of 1% of site DSDP 543 sediments to the mantle wedge, while up to 10% of site DSDP 144 sediments (Fig. 2.12) would be necessary to explain the compositions of lavas from the southern islands.

Using similar methods as Turner et al. (1996) in lavas from Saba, Montserrat, Guadeloupe and Grenada, Dufrane et al. (2009) agreed with the presence of slab-derived fluids but suggested significantly lower amounts of sediment for the source of the southern lavas with the addition of (1) around 5% of altered oceanic crust-derived fluids, and (2) between 0.2 and 2 % of bulk sediment addition or 0.4-2% of sediment melt to explain both the northern and southern lava compositions. These authors suggested that melts, instead of bulk sediments, are introduced in the mantle source of all lavas from Grenada and that both melts and bulk sediments contributed to the source of lavas from the north and the central arc. The lack of systematic behaviour was thought to be caused by a thermal structure whereby the upper portions of the subducted sediment pile lie close to their solidus beneath much of the arc.

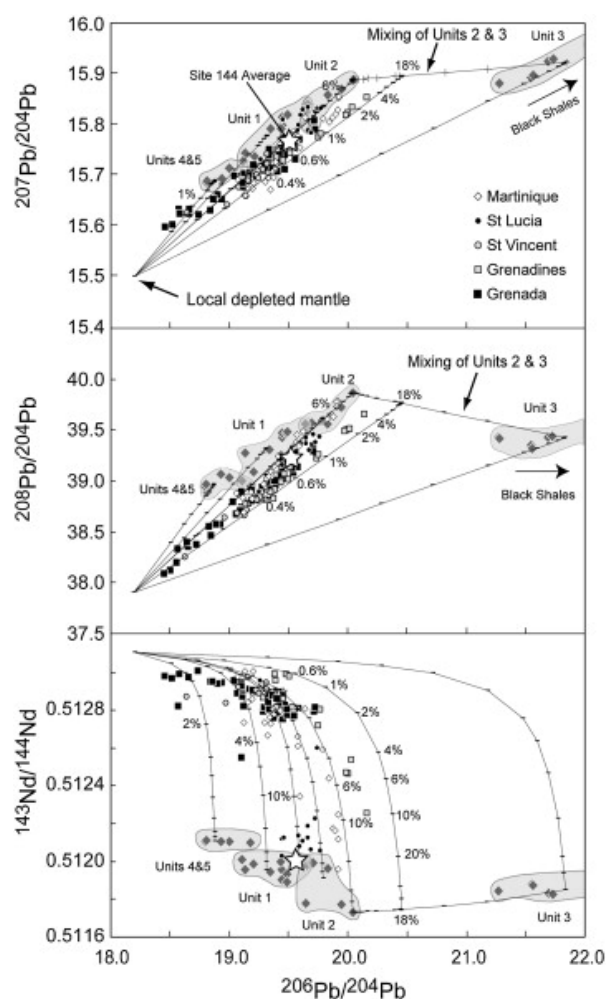


Fig. 2.12. Pb and Nd isotopic compositions of the lavas from the southern part of the Lesser Antilles are compared with those of Site DSDP 144 sediments. Data for samples from individual stratigraphic units are surrounded by a field. The solid lines represent mixing curves between local depleted mantle and site DSDP 144 sediments grouped by stratigraphic units. Ticks show the percentage of sediments in the mixture. Figure from Carpentier et al. (2008).

Individual islands studies- The involvement of sediment melts in the source of some of the Lesser Antilles magma was supported by Labanieh et al. (2010) who used Pb, Sr, Nd and Hf isotope ratios on lavas from Martinique island to suggest that the whole range of isotopic compositions observed in the island could be explained by 0.1-3% and 0.2-5% of sediments similar to those of site DSDP 144 in the source of the old (25 Ma-7.1 Ma) and recent volcanic rock (5 Ma-recent) respectively. These authors suggested that the introduction of an aseismic ridge into the trench at around 7 Ma corresponded to a change

in sediment composition toward slightly higher $^{208}\text{Pb}/^{204}\text{Pb}$. Since no fractionation occurs between Sr, Nd, Hf and Pb in the sediment component, the introduction of the crustal component by melt rather than by dehydration (fluid) was favoured. More recently Labanieh et al. (2012) used the trace element compositions of Martinique lavas to suggest that the mantle source of lavas with low La/Sm, also having high Ba/Th, U/Th and Nd and Hf isotopic signatures, were modified by slab dehydration fluids while the source of lavas with high La/Sm, also characterised by low Ba/Th, U/Th and Nd and Hf isotopic compositions, were modified by sediment melts. They suggested that lavas with high La/Sm ratios are dominantly present in the western part of the island due to a transition from aqueous fluid to hydrous melt transport of slab derived components occurring in the source beneath the middle of the island. However, Davidson and Wilson (2011), after removing the effect of differentiation, including crustal assimilation, suggested that the Sr, Nd, Pb isotope ratios of the Martinique lavas only require a source containing less than 1% sediment. This is similar to their estimates for the source beneath the Quill (Statia) located in the north of the arc. These authors highlighted the need of a hydrous fluid from the oceanic crust, in addition to the sediment contributions, to fully account for the trace element pattern of the lavas.

At St Lucia, using whole rock Sr, Nd, Hf and Pb isotopes, Vidal et al. (1991) suggested that the whole range of isotopic compositions observed could be explained by the involvement of more than 15% of sediment in the source, in addition to fluids from the dehydration of the sediment and oceanic crust.

For Grenada, after removing the effects of crustal assimilation and using Pb, Sr, Nd and O isotope geochemistry on M-, C- and MC- (transitional) series lavas, Thirlwall et al. (1996) suggested the involvement of (1) an hydrous fluid from altered subducted basaltic crust that enriched the mantle in Sr, Ba, U, K, Rb and LREE, (2) around 0.2% of sediment in the source of C-series lavas, and between 0.4-2% in the source of M and M-C lavas. Woodland et al. (2002), using PGE and Re-Os isotope ratios, suggested that ~ 2% of sediment were involved in the source of the Grenada picrites.

On Bequia, an island from the Grenadines, Smith et al. (1996) suggested that, after removing the effects of crustal assimilation, the mantle source here was enriched by 1-4%

of a subduction component comprising fluids and maybe minor silicic melts from the subducting slab.

Summary- In summary, while all studies agree on the involvement of less than 2% of sediment / sediment melt in the source of the northern island lavas, which display typical oceanic arc compositions, there is much less consensus for estimates of the magnitude of sediment contributions to the source of the lavas in the southern islands where estimates vary from less than 1% and 10% of sediments.

P-T-H₂O-fO₂ of the mantle during melting

Constraining the conditions during partial melting of the sub-arc mantle has been attempted using several methods based on lava/crystal compositions, and more recently by experiments. Studies mainly focussed on the two islands containing the most mafic lavas: St Vincent and Grenada. Indeed, such lavas are likely to represent primary magma characteristics, the latter being thought to be a silica-undersaturated picrite (Macdonald et al., 2000)

St Vincent- Heath et al. (1998) suggested that the most mafic lavas (high-MgO basalt) on St Vincent resulted from ~15% partial melting of a subduction-modified N-MORB source, and last equilibrated with the mantle at 50-60 km depth (~17 kbar) at temperatures around 1130°C and with fO₂ more oxidizing than FMQ + 1. An experimental study of the same high-MgO lavas from St Vincent was performed by Pichavant et al. (2002a). These authors suggested that the high-MgO lava, STV301, was formed by partial melting of a spinel lherzolitic mantle containing 0.3 wt.% of water with the primary magma having low amounts of water (~ 2 wt. %) and produced at temperatures of around 1230°C and pressures of around 13 kbar.

Grenada- In Grenada, picrites are thought to have been derived from ~10% partial melting at more than 65 km depth (around 100 km depth) (Arculus, 1973; Devine, 1995; Thirlwall et al., 1996). Woodland et al. (2002) suggested, based on PGE and Re-Os isotopic studies and the depletion in HREE of the picrites that the mantle source beneath Grenada lies within the garnet stability field.

2.2.3.3 Magma differentiation in the arc crust

Conditions of storage

Mineral thermometers and oxygen barometer- Several authors attempted to estimate magma temperatures using the coexisting Fe-Ti oxides method (D'Arco, 1982; Coulon et al., 1984; Smith and Roobol, 1990; Devine et al., 1998; Gurenko et al., 2005; Lindsay et al., 2005), the olivine spinel exchange geothermometer of Ballhauss et al., (1991) (Heath et al., 1998) as well as the two pyroxene thermometer of Lindsay (1983) (Barclay et al., 1998; Heath et al., 1998; Murphy et al., 1998; Lindsay et al., 2005; Toothill et al., 2007) in lava phenocrysts. Resulting temperatures for the different islands studied (St Eustatius, St Kitts, Montserrat, Dominica, Martinique, St Vincent) range between 1178°C-1132°C for basalts, between 970°C and 1100°C for basaltic andesites, and between 1000°C and 740°C for andesites and dacites. Conditions of storage can also be determined by the study of plutonic xenoliths found in the lavas. Many plutonic enclaves including cumulates, can be found on all islands except Nevis and Guadeloupe (Arculus and Will, 1980; Macdonald et al., 2000). Application of thermometry to these plutonic nodules gave temperature of crystallisation between 850-1050°C (Arculus and Will, 1980).

The oxygen fugacity (fO_2) has been determined for lavas from several islands using the coexisting oxides methods or the oxygen geobarometer of Ballhaus et al. (1991). Estimates of fO_2 in basalts from St Vincent range from NNO +0.7 to +3 (Heath et al., 1998). With the exception of Dominica with dacites ranging between FMQ+0.8 to +2 log units (Gurenko et al., 2005; Lindsay et al., 2005), most fO_2 estimates for andesites and dacites range from NNO +0.5 to NNO +2 with andesites and dacites from St Eustatius and Martinique ranging from NNO + 0.5 to NNO +2 (Macdonald et al., 2000), andesites from the Soufriere Hills volcano on Montserrat giving NNO +1 (Devine et al., 1998) and andesites from St Kitts giving ~ NNO + 1 (Toothill et al., 2007).

Phase equilibria barometry- Depths of magma chambers are likely to be different in every island due to the inferred heterogeneous nature and thickness of the basement. Due to the absence of reliable mineral barometers, pressures rely on phase equilibria studies. Heath et al. (1998) used experimentally determined sets of phase relationships to suggest that

the basalts of Soufriere on St Vincent were stored at around 15 kbar (~45 km) while basaltic andesites were produced at 10 kbar (30 km) and andesites at ~3 kbar (10 km).

H₂O content by RAMAN in glass inclusions- H₂O content of the magma during phenocryst crystallisation can be estimated by Raman spectroscopy, SIMS and FTIR in glass inclusions. H₂O contents in inclusions from dacitic pumices from Cabrits Dome on Dominica range between 1 and 6% (the lowest end of the range interpreted as degassing). H₂O contents in andesites from Mt. Pelee, Martinique, by Martel et al. (1998) line in the range 1.9-7.1 wt. %, and concentrations in andesites from Soufriere Hills Volcano in Montserrat are 4.3 ± 0.5 wt. % (Barclay et al., 1998).

Experimental Petrology: P-T-fO₂ and H₂O- A more robust approach to determine conditions during magma differentiation has been to combine petrologic observation with experimental results. Studies of this kind have been performed in Mt Pelée, on Martinique. Martel et al. (1998) and Pichavant et al. (2002b) determined the pressure and temperature of Mt Pelee andesites and basaltic andesite production. They suggested that the andesites were produced in a shallow, compositionally-zoned magma chamber at ~875-900°C, 2 ± 0.5 kbar, $\Delta\text{NNO} = +0.4-0.8$ and with a H₂O content of 5.3-6.3 wt. %. They argue that the mafic part of the chamber has a basaltic andesite composition produced at 4 kbar, 950-1025°C with melt H₂O concentrations ranging from 8.3 to 2.6 wt.% and is fed by basaltic liquids with $\leq 1050^\circ\text{C}$, high H₂O contents (>5-6 wt. %) and high fO₂ (between NNO +1 and +2 log units) while

Assemblages fractionated

Macdonald et al. (2000) suggested that, as a general rule, the Lesser Antilles primitive magmas fractionate olivine + clinopyroxene + plagioclase + spinel/titanomagnetite followed by clinopyroxene + plagioclase + orthopyroxene + titanomagnetite \pm amphibole.

Phenocryst assemblages appear to be quite variable. However, some authors point out that phenocryst assemblages do not necessarily represent the full assemblage fractionated during differentiation. It is the case in Mt Pelee (Martinique) and the Quill (St. Vincent) where cryptic amphibole fractionation impacted the differentiation trends of the lavas, yet it is

not observed in the phenocryst assemblage (Davidson and Wilson, 2011). Therefore, as highlighted by Macdonald et al. (2000), the understanding of the full range of phases fractionated may require a study of both phenocrysts and plutonic xenoliths (similar to Davidson and Wilson, 2011). Like the phenocryst assemblages, mineral assemblages of the plutonic nodules vary significantly and can comprise plagioclase, amphibole, clinopyroxene, orthopyroxene, olivine, magnetite, biotite, ilmenite, quartz and apatite (Arculus and Wills, 1980).

Crustal assimilation

While the major element compositions of the lavas from along the arc could be explained by a closed-system fractionation of the phenocryst/cumulate phases observed in the lavas/xenoliths, the analyses of the incompatible trace element concentrations and stable and radiogenic isotope ratios often suggest assimilation during crystal fractionation (AFC). The occurrence of crustal assimilation in the Lesser Antilles arc was first highlighted by Davidson (1984) and Thirlwall and Graham (1984). It was subsequently suggested by Davidson (1985; 1986; 1987), Davidson and Harmon (1989), Thirlwall et al (1996), Smith et al. (1996), Van Soest et al. (2002), Toothill et al. (2007) and Davidson and Wilson (2011). The assimilant is thought to be of sedimentary origin, and its interaction with the lavas is thought to be the most substantial in the southern part of the arc, in the islands where the most “continental” signatures can be observed in the lavas: Martinique, St Lucia and Grenada.

Davidson (1984; 1985; 1986; 1987) and Davidson and Harmon (1989) argued for the detection of crustal assimilation using $\delta^{18}\text{O}$ data from whole rock samples. While lavas from the northern islands showed values close to the mantle range, lavas from Martinique (Fig. 2.13) and St Lucia displayed compositions far above the mantle range. In addition, these authors noticed a clear correlation between increasing $\delta^{18}\text{O}$ and increasing $^{87}\text{Sr}/^{86}\text{Sr}$ or decreasing $^{143}\text{Nd}/^{144}\text{Nd}$. They argued that the shape of the related mixing curves could not be explained by sediment addition to the mantle source, and needed to be accounted for by crustal assimilation.

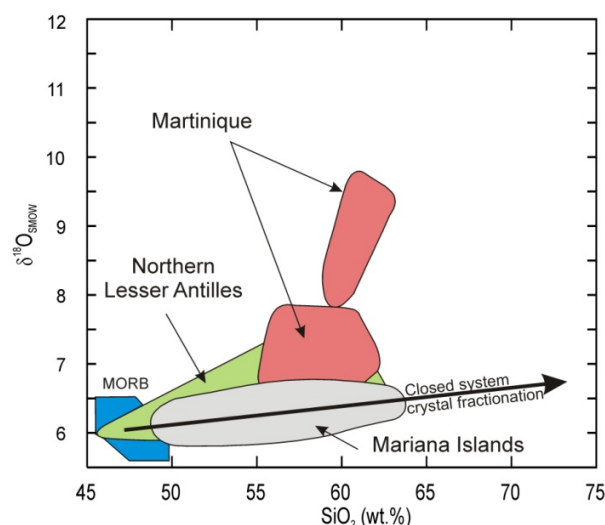


Fig. 2.13. $\delta^{18}\text{O}$ composition of the northern Lesser Antilles arc and of Martinique representing the central islands of the arc versus SiO_2 content (wt. %). Mariana Islands compositions are shown for comparison. Martinique compositions plot far from the closed system crystallisation trend indicating crustal contamination whereas Mariana simply display source modified compositions. Figure modified from Davidson and Harmon (1989).

Thirlwall and Graham (1984) came to the same conclusions for the Grenada C-series lavas, using whole rock trace elements and Sr, Nd, Pb isotope ratios. These authors noted an increase in $^{206}\text{Pb}/^{204}\text{Pb}$ and in Nd/Sr, Zr/Sm, Rb/Ba ratios with indices of differentiation (MgO). Subsequently, Thirlwall et al. (1996) showed that most lavas from both M- and C-series in Grenada, even the picrites, were affected by crustal assimilation on the basis of both mineral $\delta^{18}\text{O}$ (clinopyroxene, olivine and quartz) and whole rock Sr, Nd and Pb isotope data. The presence of quartz with up to $\delta^{18}\text{O} = 10\text{‰}$ in some intermediate lavas was seen as a clear argument for crustal assimilation. During the same year, crustal assimilation was also shown by Smith et al. (1996) to have occurred at Bequia (Grenadine Islands) where $^{87}\text{Sr}/^{86}\text{Sr}$, $^{143}\text{Nd}/^{144}\text{Nd}$ were shown to correlate with MgO in one of the suites (IDS) of samples, also corresponding to higher $\delta^{18}\text{O}$ in clinopyroxene.

In 2002, Van Soest et al. showed a regional control of crustal contamination using $^3\text{He}/^4\text{He}$ ratio and $\delta^{18}\text{O}$ (Fig. 2.14) in olivine and pyroxenes along with whole-rock Sr isotope ratios. Strong crustal contamination was shown to occur from Martinique to Grenada. In contrast, only a minor amount of crustal contamination is observed in the northern part of

the arc, from Guadeloupe to Saba, whereas Martinique seems to be transitional with the southern section.

More recently, work performed on glass inclusions in plagioclase and pyroxene in Dominica also supported shallow level assimilation of crustal rocks (Gurenko et al., 2005). Li and B concentrations and isotopic ratios vary considerably and imply the trapping of hybrid melts during assimilation of older volcanic rocks of the complex. On St Kitts, Toothill et al. (2007) showed that glass inclusions in phenocrysts are characterised by a positive correlation between Ba/La, La/Sm and $^{208}\text{Pb}/^{204}\text{Pb}$ and between $^{208}\text{Pb}/^{204}\text{Pb}$ and SiO_2 consistent with assimilation of < 10% of biogenic sediments (Toothill et al., 2007). Finally, Davidson and Wilson (2011) re-emphasized the occurrence of crustal assimilation for both Mt Pelee, Martinique, and the Quill, in Statia using coupled variations in trace elements and isotopes with differentiation.

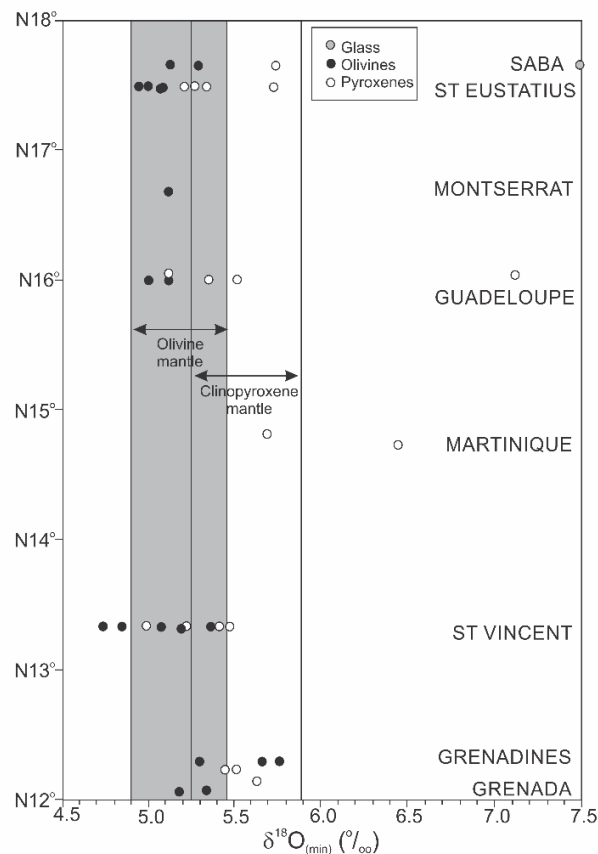


Fig. 2.14. An overview of the mineral oxygen isotopic compositions versus location (latitude) in the arc. Data are shown by island and mineral type. Also shown are two boxes for the range of olivine (gray box)

and clinopyroxene in equilibrium with mantle peridotites (Mattey et al., 1994). Figure modified from Van Soest et al. (2002).

2.2.4 St Lucia

St Lucia is located between Martinique and St Vincent and belongs to the central section of the arc. The first geological description of St Lucia was given by Tomblin (1964) and subsequently expanded by Westercamp and Tomblin (1979), Roobol et al. (1983), Wright et al. (1984), Wohletz et al. (1986). Current activity is only hydrothermal and is located within the Qualibou depression, a large sector collapse of around 10 km in diameter, in the south-west of the island, near Soufriere town (Lindsay et al., 2013). A compilation of all the eruption ages available for St Lucia lavas was done by Lindsay et al. (2013) and is presented in Table 2.1.

Based on age constraints, volcanic rocks of St Lucia can be separated in 3 groups in chronological order: (1) the eroded basalt and andesite centres, (2) the dissected andesite centres and related pyroclastic deposits and (3) the dominantly dacitic lava domes with block and ash flow deposits and dacitic-andesitic pumiceous pyroclastic flows (Fig.1; Lindsay, 2005). Volcanic rocks from both (2) and (3) were classified as being part of the Soufriere Volcanic Complex (SVC) by Lindsay et al. (2013). SVC lava flows are located in and around the Qualibou depression (Fig. 2.15). The origin of the Qualibou depression has long been debated. In 1980, Westercamp and Tomblin (1979) proposed an age of ~40 ka for the Qualibou depression formation based on K/Ar and ^{14}C dating and suggested its origin as a caldera collapse. The volcanic (explosive) origin of the depression was questioned by Roobol et al. (1983) and Wright et al. (1984) who argued for a gravity slide origin. Wohletz et al. (1986) tried to model in more detail the depression substructures. His work favoured an explosive origin for the caldera. Recently, based on pyroclastic rock compositions and ages, Lindsay et al. (2013) invoked a series of small volume explosive eruptions followed by sector collapse between 250 and 100 ka ago in order to explain the depression.

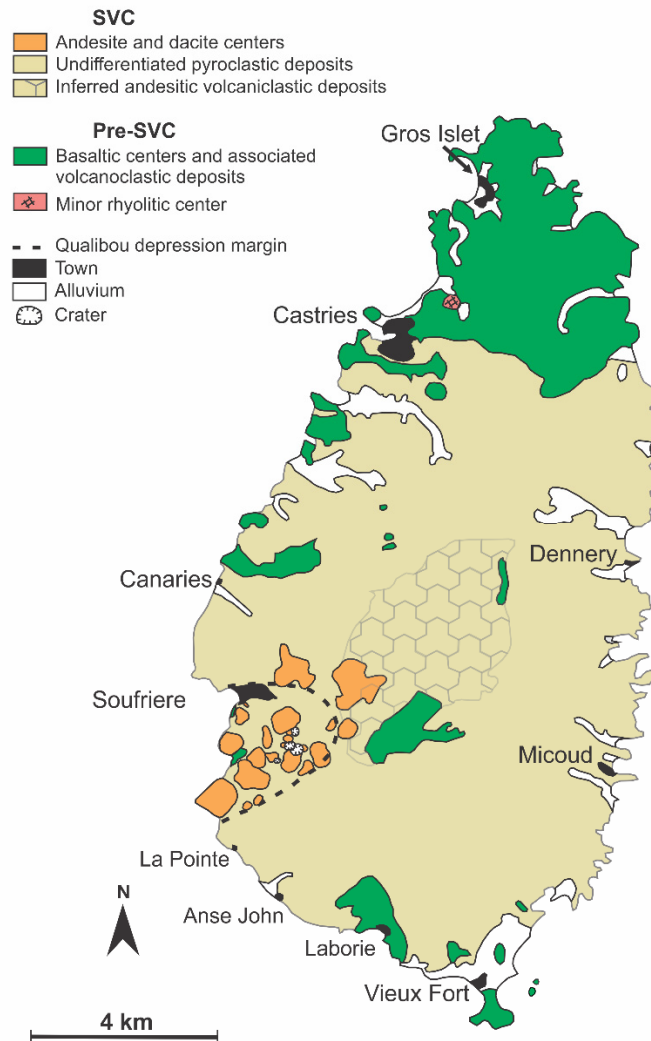


Fig. 2.15. Geological map of St Lucia. SVC = Soufriere Volcanic Complex units. Pre-SVC = Pre-Soufriere Volcanic Complex. Map modified from Lindsay (2005).

2.2.4.1 Pre-SVC

Volcanic rocks erupted before the SVC activity (Pre-SVC) consists mainly of eroded basalt, basaltic andesite and andesite centers, although a small rhyolite flow also occurs in the north of the island (Fig. 2.15). Pre-SVC lavas occur across the island, but are mostly buried by the volcanoclastic deposits from the most recent activity. They have been dated between 15-18 Ma and 3.13 Ma by Briden et al. (1979), Aquater, (1982) and Le-Guen De Kerneizon et al. (1983). Two Pre-SVC basaltic andesite flows, outcropping within the

Qualibou depression in the south-west of the island, were dated between 6.5 ± 0.6 Ma and 5.21 ± 0.15 Ma by Briden et al. (1979) and Aquater (1982) and more recently at 6.64 and 1.10 Ma, respectively, using the K-Ar method (Samper et al., 2008).

No detailed trace element study of the Pre-SVC lavas existed (before this thesis), with only one sample analysed for 6 trace element concentrations (Li, Rb, Sr, Y, Zr, Nb; isotope dilution) by Vidal et al. (1991) and 4 samples analysed for 9 elements (Ba, Cr, Ni, Rb, Sr, V, Y, Zn and Zr; XRF) by Lindsay et al. (2013). The samples analysed show that Pre-SVC lavas have higher Y and lower Ba, Rb, Sr and Zr concentrations compared to the SVC lavas. The first radiogenic isotope analyses of the Pre-SVC lavas were performed by Puskhar et al. (1973) (Sr isotopes on four lavas) followed by the analysis of six lavas (Sr, Nd) by Davidson (1985) two lavas (Sr and Nd isotopes) by White and Dupre (1986) and of one lava (Sr isotopes) by Vidal et al. (1991). $^{87}\text{Sr}/^{86}\text{Sr}$ and $^{143}\text{Nd}/^{144}\text{Nd}$ ratios obtained vary between 0.7035 and 0.7063 and between 0.51254 and 0.51301 respectively. $\delta^{18}\text{O}$ was analysed in six lavas by Davidson (1985) and ranged between 7.3 and 10.5 ‰ (after correction for differentiation). Puskhar et al. (1973), White and Dupre (1986) and Vidal (1991) suggested the production of the Pre-SVC lava isotopic signatures by addition of slab components to the mantle source, while Davidson (1985) suggested that part of the isotopic signature was due to sediment assimilation during magma differentiation, based on the high $\delta^{18}\text{O}$ data.

2.2.4.2. SVC

SVC units comprise dissected high-silica andesite and dacite centers with associated pyroclastic units (Fig. 2.16).

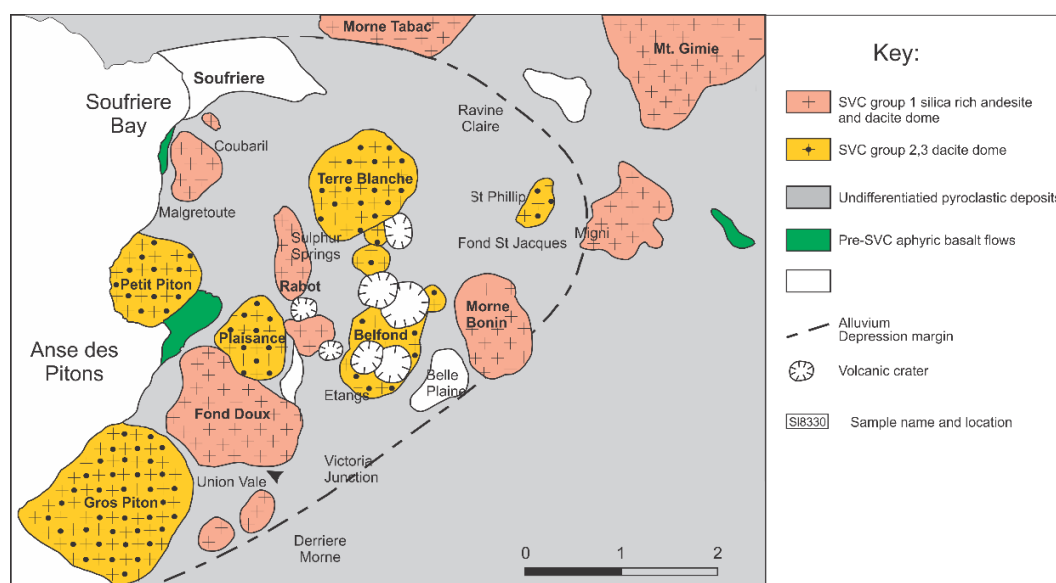


Fig. 2.16. Geological map of the SVC. Groups 1,2 and 3 refer to the 3 different eruption periods of the SVC. Modified from Lindsay et al. (2013).

Eruption ages

Based on (U-Th)/He eruption ages, (Schmitt et al., 2010; Lindsay et al., 2013), the activity in the SVC can be separated in three eruption periods:

-**Phase 1** ~3 Ma-250 ka: Emplacement of Micoud pyroclastic deposit (640 ka), of the silica rich andesites and dacites of the Mt Gimmie and Mt Tabac (~532 ka) stratovolcanoes, and deposition of the dacitic pyroclastic rocks and domes of Bellevue (264 ka) and Morne Bonin (273 ka).

-**Phase 2** ~105-50 ka: includes the eruption of Anse John quartz-poor pumice tuff (104 ka), Gros and Petit Piton domes (109 ka and 71 ka) and the Pointe Beach pumice (59 ka),

-**Phase 3** ~20 ka: eruption of Belfond tuff (20 ka) and the Belfond and Terre Blanche domes.

A major sector collapse resulting in the Qualibou depression occurred between phases 1 and 2 (~250 to 100 ka) and a period of eruptive quiescence (50-24 ka) occurred between phases 2 and 3. Recent activity only occurred in 1766, when a phreatic eruption, in the sulphur spring area and formed a 70 cm thinly bedded lithic ash blanket.

Mineralogy

Lavas from the SVC are highly porphyric (20-40% modal phenocryst) and have various phenocryst assemblages comprising plagioclase, orthopyroxene and some of the following phases: clinopyroxene, hornblende quartz, biotite, phlogopite and cummingtonite (Vidal et al., 1991; Lindsay et al., 2013). Lindsay et al. (2013) provided a petrological description of the SVC pyroclastic deposits and of lavas from phase 3. They pointed out that volcanic rocks from phase 1 had different mineralogical assemblages than rocks from phases 2 and 3. Pyroclastic deposits from phase 1 have less and smaller phenocrysts than equivalent rocks from phases 2 and 3. The former mainly comprise orthopyroxene and plagioclase, have no biotite and less quartz than phases 2 and 3 products. Pyroclastic rocks from phases 2 and 3 contain plagioclase, orthopyroxene, biotite, quartz and can contain cummingtonite. Hornblende can be found in minor amounts in phase 1 and in various amounts in phases 2 and 3. Lavas from phases 2 and 3 contain more quartz, plagioclase and amphibole but less biotite than their pyroclastic equivalents. Magnetite and other spinels are almost absent in all eruption phases. Plutonic xenoliths found in the SVC lavas present the same phases as the lavas, with similar to higher modal abundances of mafic phases.

Geochemistry

SVC lavas and pyroclastic rocks are medium-K calc-alkaline with SiO₂ comprised between 61.6 and 67.7 wt. % (volatile-free; Lindsay et al., 2013). Silica systematically correlates negatively with MgO, TiO₂, FeO and CaO suggesting that fractional crystallisation was a dominant factor in producing the observed compositional variations (Lindsay et al., 2013). Trace element analyses of the SVC lavas were presented by Vidal et al. (1991) and Lindsay et al. (2010). In both studies, data suggest that all the SVC lavas share similar trace element compositions and are characterised by higher L/M-HREE ratios and higher Rb, Ba, Th and Pb concentrations compared to the rest of the northern and central islands of the arc such as Dominica, Martinique and St Vincent. The “continental” isotopic composition of the SVC lavas was first highlighted by the

publication of elevated $^{87}\text{Sr}/^{86}\text{Sr}$ ratios comprised between 0.7079 and 0.7092 ($n = 3$) by Puskhar et al. (1973; $n = 3$). It was later confirmed by Davidson (1985) who analysed Sr, Nd and Pb isotopes in two lavas ($^{87}\text{Sr}/^{86}\text{Sr} = 0.70765$ and 0.70897 ; $^{143}\text{Nd}/^{144}\text{Nd} = 0.51213$ and 0.51223 ; $^{206}\text{Pb}/^{204}\text{Pb} = 19.574$ and 19.726 ; $^{207}\text{Pb}/^{204}\text{Pb} = 15.786$ and 15.823 ; $^{208}\text{Pb}/^{204}\text{Pb} = 39.45$ and 39.336) and by Donnelly et al. (1991; $^{87}\text{Sr}/^{86}\text{Sr} = 0.7084$ and 0.7087 ; $n = 2$) and Vidal et al. (1991; $^{87}\text{Sr}/^{86}\text{Sr} = 0.70782 - 0.70933$ ($n = 9$); $^{143}\text{Nd}/^{144}\text{Nd} = 0.51203 - 0.51219$ ($n = 9$); $^{206}\text{Pb}/^{204}\text{Pb} = 19.445 - 19.773$ ($n = 8$); $^{207}\text{Pb}/^{204}\text{Pb} = 15.776 - 15.833$ ($n = 8$); $^{208}\text{Pb}/^{204}\text{Pb} = 39.140 - 39.439$ ($n = 8$); $^{176}\text{Hf}/^{177}\text{Hf} = 0.28237 - 0.28256$ ($n = 4$)). Davidson et al. (1985) also analysed the $\delta^{18}\text{O}$ composition from two SVC lavas, and showed that those were characterised by ratios well above the mantle range (8.2 and 9.7‰; after correction for differentiation). Puskhar et al. (1973), Donnelly et al. (1991) and Vidal et al. (1991) suggested that the continental isotopic signature of the SVC lavas were due to the introduction of large amounts of subducted sediments in the mantle, while Davidson et al. (1985) proposed the involvement of sediment assimilation during magma differentiation, like for all other lavas of the arc with high $\delta^{18}\text{O}$ values.

Current magmatic model

From (U-Th)/He eruption ages and U-Th and U-Pb zircon ages, Schmitt et al. (2010) proposed an evolutionary model for the SVC (Fig. 2.17). This model invokes episodic thermal and mechanical reactivation of a complex of mid-crustal plutons of intermediate composition under the Qualibou depression. The source of the heat necessary for reheating remains unconstrained but was suggested to be the result of mafic magma underplating beneath the plutonic complex. The model is based on several observations: (1) zircon crystallisation ages predate volcanism, and this is more obvious for phases 2 and 3 than for phase 1; (2) zircon crystallisation age distributions are not distinguishable between plutonic inclusions and their host lava; (3) zircons record discontinuous crystallisation episodes; and (4) the age distribution of zircon growth in lavas and pyroclastic deposits from different eruption periods and that are spatially separated share strong similarities.

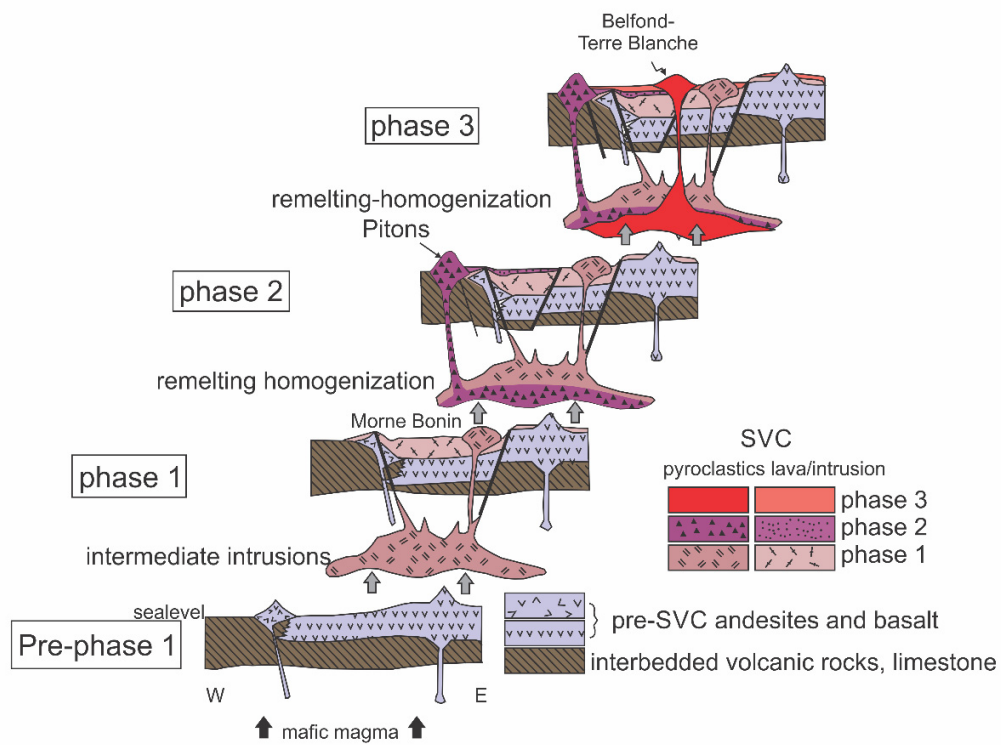


Fig. 2.17. Schematic model showing the different phases of magmatism leading to the formation of the SVC. Figure modified from Schmitt et al. (2010).

Table 2.1. All ages of St Lucia rocks published in the literature. Table from Lindsay et al. (2013).

Description	Location	Age + Error	Original ¹⁴ C age (uncalibrated)	Method	Reference
Lava domes					
Belfond dome	Sand & ballast quarry	13.6 ± 0.4 ka		(U-Th)/He	Schmitt et al. (2010)
Belfond dome	Belfond	3.30 ± 0.24 Ma*		K-Ar	Le Guen de Kerneizon et al. (1983)
Belfond dome	Etangs	5.30 ± 0.39 Ma*		K-Ar	Le Guen de Kerneizon et al. (1983)
Terre Blanche dome	NE flank of dome	3 ± 3 ka		K-Ar	Samper et al. (2008)
Terre Blanche dome	Eastern slope of dome	15.3 ± 0.4 ka		(U-Th)/He	Schmitt et al. (2010)
Morne Bonin dome	Western slope of dome	273 ± 15 ka		(U-Th)/He	Schmitt et al. (2010)
Morne Bonin dome		0.91 ± 0.08 Ma*		K-Ar	Le Guen de Kerneizon et al. (1983)
Gros Piton	SW flank	77 ± 2 ka		K-Ar	Samper et al. (2008)
Gros Piton	Northern flank	71.1 ± 3ka		(U-Th)/He	Schmitt et al. (2010)
Gros Piton		0.23 ± 0.1 Ma		K-Ar	Aquater (1982)
Gros Piton		0.29 ± 0.1 Ma		K-Ar	Aquater (1982)
Petit Piton	NW flank	0.26 ± 0.04 Ma		K-Ar	Briden et al. (1979)
Petit Piton	NW flank	95 ± 2 ka		K-Ar	Samper et al. (2008)
Petit Piton	Northern flank	109 ± 4 ka		(U-Th)/He	Schmitt et al. (2010)
Pyroclastic flow deposits					
Belfond Pyroclastic flow deposit	Saltibus	24,002 ± 1,351 Cal yBP	20,000 ± 1,100	C14	Wright et al. (1984)
Belfond Pyroclastic flow deposit	Near Migny	20,700 ± 700		(U-Th)/He	Schmitt et al. (2010)
Belfond Pyroclastic flow deposit	Near Choiseul	25,153 ± 686 Cal yBP	21,000 ± 500	C14	Wright et al. (1984)
Belfond Pyroclastic flow deposit	Near Migny	21,000 +/- 1,200		(U-Th)/He	Schmitt et al. (2010)
Belfond Pyroclastic flow deposit	Quiesse Reserve	25,775 ± 890 Cal yBP	21,440 ± 640	C14	Roobol et al. (1983)
Belfond Pyroclastic flow deposit	Anse Noir	26,926 ± 699 Cal yBP	22,380 ± 420	C14	Wright et al. (1984)
Belfond Pyroclastic flow deposit	East of Laborie	27,726 ± 428 Cal yBP	23,170 ± 180	C14	Lindsay et al. (2002)
Belfond Pyroclastic flow deposit	Durandeau	28,381 ± 309 Cal yBP	23,500 ± 140	C14	Smith & Roobol (written comm)
Belfond Pyroclastic flow deposit	Near Choiseul	27,623 ± 491 Cal yBP	23,080 ± 280	C14	Wright et al. (1984)
Belfond Pyroclastic flow deposit	North of Millet	28,979 ± 407 Cal yBP	24,210 ± 150	C14	Lindsay et al. (2002)
Belfond Pyroclastic flow deposit	Venus Estate	29,319 ± 595 Cal yBP	24,520 ± 340	C14	Smith & Roobol (written comm)
Belfond Pyroclastic flow deposit	Durandeau - Millet	30,218 ± 812 Cal yBP	25,300 ± 700	C14	Wright et al. (1984)
Belfond Pyroclastic flow deposit	Ravine Poisson	33,399 ± 923 Cal yBP	29,100 ± 1,100	C14	Wright et al. (1984)
Choiseul Tuff	Saltibus	38,732 ± 1,981 Cal yBP	34,200 ± 1670	C14	Wright et al. (1984)
Choiseul Tuff	East end of Choiseul beach	39,776 ± 816 Cal yBP	34,500 ± 350	C14	Lindsay et al. (2002)
Choiseul Tuff	Choiseul	43,269 ± 1,061	39,050 ± 1,500	C14	Tomblin (1964)
Choiseul Tuff	South of Saltibus		>32,840	C14	Wright et al. (1984)
Choiseul Tuff	Near Micoud	0.87 ± 0.07 Ma*		K-Ar	Le Guen de Kerneizon et al. (1983)
"La Pointe" flow deposit	Sth end La Pointe beach	59.8 ± 2.1 ka		(U-Th)/He	Schmitt et al. (2010)
"Anse John" flow deposit	Anse John Beach	104 ± 4 ka		(U-Th)/He	Schmitt et al. (2010)
"Bellevue" flow deposit	Road cut near Dugard	264 ± 8 ka		(U-Th)/He	Schmitt et al. (2010)
"Micoud" flow deposit	Quarry in Micoud	640 ± 19 ka		(U-Th)/He	Lindsay et al. (2013)
Choiseul Tuff	East end of Choiseul beach	515 ± 19 ka		(U-Th)/He	Lindsay et al. (2013)
Mafic lavas within depression					
Basalt lava flow	Jalousie	1.10 ± 0.02 Ma		K-Ar	Samper et al. (2008)
Basalt lava	Jalousie	6.1 ± 0.6 Ma		K-Ar	Aquater (1982)
Basalt lava	Jalousie	6.5 ± 0.6 Ma		K-Ar	Aquater (1982)
Basalt lava	Malgretoute	5.61 ± 0.25 Ma		K-Ar	Briden et al. (1979)
Basalt lava flow	Malgretoute	6.64 ± 0.12 Ma		K-Ar	Samper et al. (2008)
Andesitic-basaltic centres and deposits around depression					
Morne Tabac	Southwestern flank	532 ± 21 ka		(U-Th)/He	Lindsay et al. (2013)
Mt. Gimie		0.9 ± 0.8 Ma		K-Ar	Aquater (1982)
Mt. Gimie		1.7 ± 0.2 Ma		K-Ar	Westerncamp and Tomblin (1979)
Basalt lava	Anse Galet	2.02 ± 0.08 Ma		K-Ar	Aquater (1982)
Andesite lava	Derriere Dos	2.8 ± 0.14 Ma		K-Ar	Le Guen de Kerneizon et al. (1983)
Andesite lava flow	Migny	3.13 ± 0.16 Ma		K-Ar	Le Guen de Kerneizon et al. (1983)
Mt. Gimie?	Near Migny	3.3 ± 0.16 Ma		K-Ar	Le Guen de Kerneizon et al. (1983)
Basalt lava	Savannes	5.21 ± 0.15 Ma		K-Ar	Briden et al. (1979)
Basaltic andesite lava flow	Dennerly	5.52 ± 0.27 Ma		K-Ar	Le Guen de Kerneizon et al. (1983)
Altered andesite pumice	Dennerly	5.7 ± 0.28 Ma		K-Ar	Le Guen de Kerneizon et al. (1983)
Andesite lava flow	Laborie (Gomier?)	7.10 ± 0.36 Ma		K-Ar	Le Guen de Kerneizon et al. (1983)
Andesite dome	Beausejour	7.30 ± 0.36 Ma		K-Ar	Le Guen de Kerneizon et al. (1983)
Andesite dike	Moule a Chique	8.15 ± 0.40 Ma		K-Ar	Le Guen de Kerneizon et al. (1983)
Andesite dome	St. Urbain	8.66 ± 0.43 Ma		K-Ar	Le Guen de Kerneizon et al. (1983)
Andesite lava flow	de Mailly	10.12 ± 0.50 Ma		K-Ar	Le Guen de Kerneizon et al. (1983)

Note that C14 ages here are calibrated using CalPal-Online (<http://www.calpal.de>); * geologically unrealistic ages, probably related to excess Ar.

Chapter 3

Assimilation of sediments embedded in the oceanic arc crust: myth or reality?

A version of this chapter is published in *Earth and Planetary Science Letters* co-authored by Jon Davidson, Simon Turner, Colin Macpherson, Jan Lindsay and Adrian Boyce. It will be referred to as Bezard et al. (2014) in the next chapters.

The supplementary data file of this chapter is presented in Appendix B.

Abstract

Arc magmas are commonly assumed to form by melting of sub-arc mantle that has been variably enriched by a component from the subducted slab. Although most magmas that reach the surface are not primitive, the impact of assimilation of the arc crust is often ignored with the consequence that trace element and isotopic compositions are commonly attributed only to varying contributions from different components present in the mantle. This jeopardises the integrity of mass balance recycling calculations. Here we use Sr and O isotope data in minerals from a suite of volcanic rocks from St Lucia, Lesser Antilles arc, to show that assimilation of oceanic arc basement can be significant. Analysis of $^{87}\text{Sr}/^{86}\text{Sr}$ in single plagioclase phenocrysts from four Soufrière Volcanic Complex (SVC; St Lucia) hand samples with similar composition ($^{87}\text{Sr}/^{86}\text{Sr} = 0.7089\text{--}0.7091$) reveals crystal isotopic heterogeneity among hand samples ranging from 0.7083 to 0.7094 with up to 0.0008 difference within a single hand sample. $\delta^{18}\text{O}$ measurements in the SVC crystals show extreme variation beyond the mantle range with +7.5 to +11.1‰ for plagioclase ($n = 19$), +10.6 to +11.8‰ for quartz ($n = 10$), +9.4 to +9.8‰ for amphibole ($n = 2$) and +9 to +9.5‰ for pyroxene ($n = 3$) while older lavas (Pre-Soufrière Volcanic complex), with less radiogenic whole rock Sr composition ($^{87}\text{Sr}/^{86}\text{Sr} = 0.7041\text{--}0.7062$) display values closer to mantle range: +6.4 to +7.9‰ for plagioclase ($n=4$) and +6 to +6.8‰ for pyroxene ($n = 5$). We argue that the $^{87}\text{Sr}/^{86}\text{Sr}$ isotope disequilibrium and extreme $\delta^{18}\text{O}$ values provide compelling evidence for assimilation of material located within the arc crust. Positive correlations between mineral $\delta^{18}\text{O}$ and whole rock $^{87}\text{Sr}/^{86}\text{Sr}$, $^{143}\text{Nd}/^{144}\text{Nd}$ and $^{206,207,208}\text{Pb}/^{204}\text{Pb}$ shows that assimilation seems to be responsible not only for the isotopic heterogeneity observed in St Lucia but also in the whole Lesser Antilles since St Lucia encompasses almost the whole-arc range of isotopic compositions. This highlights the need for detailed mineral-scale investigation of oceanic arc suites to quantify assimilation that could otherwise lead to misinterpretation of source composition and subduction processes.

3.1 Introduction

A key question in oceanic arc geochemistry concerns the relative contributions of subducting slab and intra-crustal material in the chemical and isotopic characteristics of lavas. Oceanic arc magmas are generated by partial melting of the mantle wedge modified by H₂O-rich fluids and melts from the subducting slab (Tatsumi and Eggins, 1995) and subsequently ascend through the arc crust before eruption. Lavas erupted at oceanic arcs rarely have major element compositions in equilibrium with mantle peridotite (Annen et al., 2006) which suggests that the magmas experienced differentiation during storage within or at the base of the arc crust. Depending on the nature of the arc basement, such magmas may interact with igneous or metasedimentary wall rocks during differentiation. Distinguishing between sediment addition to the mantle wedge and assimilation of metasediments located in the arc crust is not straightforward on the basis of whole rock compositions alone— the effects of mixing sediment into the mantle wedge or with basaltic melts in the crust are similar in most radiogenic isotope-isotope spaces.

In order to investigate the role of crustal assimilation in oceanic arcs we selected a suite of rocks from the Lesser Antilles arc where, despite the absence of continental basement, whole rock isotope ratios of arc lavas can be very “continental”. As a result, the case has long been made both for crustal assimilation (e.g. Thirlwall and Graham, 1984; Davidson, 1987; Davidson and Harmon, 1989; Smith et al., 1996; Thirlwall et al., 1996; Van Soest et al., 2002), and incorporation of sediment or sediment melt into the mantle wedge (e.g. White and Dupré, 1986; Carpentier et al., 2008; 2009; Labanieh et al., 2010; 2012). Our suite of samples, from the island of St Lucia, encompasses almost the entire range of whole rock isotopic compositions observed in the Lesser Antilles, ranging from values close to typical intra-oceanic arc rocks to those resembling continental crust (e.g. $^{87}\text{Sr}/^{86}\text{Sr}$, $^{143}\text{Nd}/^{144}\text{Nd}$ and $^{206}\text{Pb}/^{204}\text{Pb}$ ranging from 0.70411-0.70906, 0.51210-0.51298 and 19.291-19.797 respectively). $^{87}\text{Sr}/^{86}\text{Sr}$ and $\delta^{18}\text{O}$ analyses of individual minerals separated from lavas with extreme crust-like whole rock isotopic composition from the Soufriere Volcanic Complex (SVC), demonstrate the importance of open system behaviour on oceanic arc magmatism and challenge our understanding of magma differentiation in oceanic arcs.

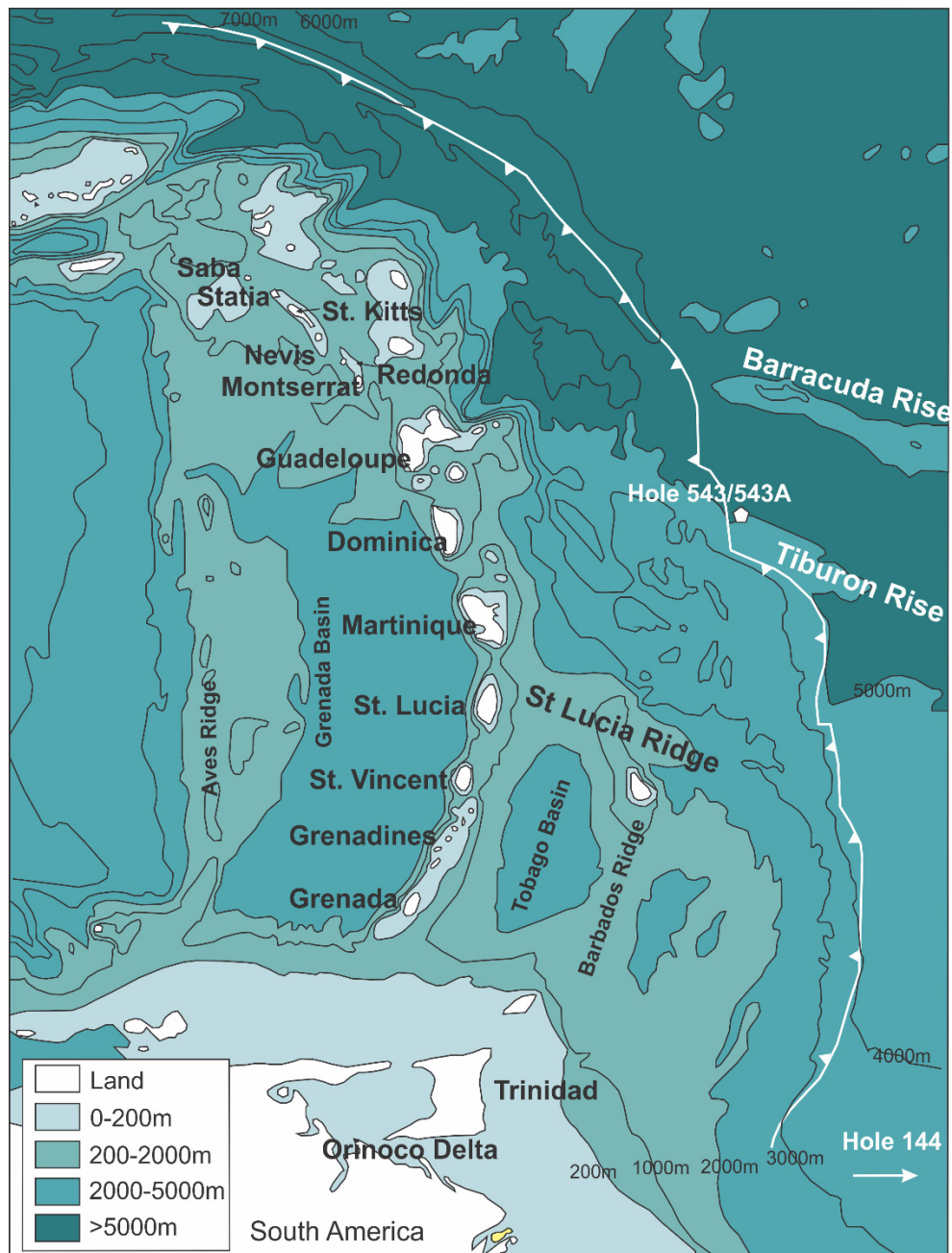


Fig. 3.1. Bathymetric map of the Lesser Antilles arc showing the islands, the trench-deformation front, the main ridges, the Grenada and Tobago basins and the locations of Deep Sea Drilling Project (DSDP) hole 543/543A and hole 144. Figure modified from Van Soest et al. (2002).

3.2 Geological background

The Lesser Antilles arc (Fig. 3.1) formed as a result of subduction of the North American Plate under the Caribbean Plate. Its lavas have typical oceanic arc compositions in the northern section but unusually heterogeneous isotopic signatures in the central and southern part of the arc where both typical intra-oceanic arc and very

continental crust-like signatures are observed (e.g. Macdonald et al., 2000; Fig. 3.2). Two main processes have been proposed to explain these extreme compositions: (1) incorporation of sediment into the mantle source or (2) significant assimilation of sediment-rich arc crust. While a high sediment input to the source could be explained by the presence of abundant sediment in the southern Antilles Trench, due to discharge from the Orinoco and Amazon rivers (e.g. Carpentier et al., 2008; 2009), assimilation of sediment in the arc crust is also possible because the central-southern Lesser Antilles arc is thought to have developed above the thick forearc basin of the (now extinct) Aves Ridge Arc, splitting it into the Grenada and the Tobago basins (Fig. 3.1; Aitken et al., 2011). Sediments entering the subduction zone are chemically and isotopically well constrained by analyses from DSDP Sites 144 and 543 (Fig. 3.1; White and Dupré, 1986; Carpentier et al., 2008; 2009). In contrast, the nature of the basement of the Southern Lesser Antilles arc is still poorly known. While the detrital sediments from the South American craton, which dominate the sequences on both the subducting and the overriding plates, were often targeted in the past to explain the high $^{87}\text{Sr}/^{86}\text{Sr}$ and low $^{143}\text{Nd}/^{144}\text{Nd}$ ratios of the lavas, they fail to explain their very radiogenic Pb signatures. Recently, analyses of Mesozoic black shales sampled at DSDP site 144 showed that these sediments have sufficiently radiogenic Pb to account for the compositions of the lavas from the southern arc (Carpentier et al., 2009). Because such radiogenic Pb has not yet been reported from the sediments of the Grenada and Tobago basins, sediment addition to the source alone has been suggested to explain the whole range of isotopic data in the southern arc lavas (Carpentier et al., 2008; 2009; Labanieh et al., 2010). However, it cannot be ruled out that such sediments exist within the basement of the southern arc since biogenic rich limestones have been reported in the overriding plate, in the Late Cretaceous to Oligocene sequences of the Carupano Basin (Ysaccis, 1997).

St Lucia is an island in the central-southern part of the arc (Fig. 3.1). The lavas from this single island encompass almost the whole range of isotopic variation observed in the arc making it the perfect location to study the influence of crustal components (Fig. 3.2). The more continental crust-like compositions are found in andesites (3Ma to ca. 250 ka) and dacites (100 ka to present) of the Soufriere Volcanic Complex (SVC), while more mantle-like compositions are observed in the more mafic Pre-SVC lavas dominated by basalt, basaltic andesite and andesite (18 Ma to 1.1 Ma; Briden et al.,

1979; De Kerneison et al., 1983; Samper et al., 2008; Schmitt et al., 2010; Lindsay et al., 2013).

3.3 Methods

3.3.1 Whole rock Sr, Nd and Pb isotopes

Except for 7 samples in which Sr and Nd isotope ratios were measured at the Geochemical Analysis Unit at Macquarie University (Aus), whole rock powders were analysed at the Arthur Holmes Isotope Geology Laboratory (AHIGL) which is part of Durham Geochemistry Centre (DGC) at Durham University (UK). At both institutes, 0.1g of sample powder was dissolved in Teflon distilled 29M HF and 16M HNO₃.

At Durham, Pb and Sr were separated from the sample solution using Sr-spec resin columns. Nd was collected from the same Sr-spec column before being passed through a cation column where it was collected as part of a total REE cut after elution of Hf, Rb and Ba. Samples were analysed for their $^{87}\text{Sr}/^{86}\text{Sr}$, $^{143}\text{Nd}/^{144}\text{Nd}$ and $^{206}\text{Pb}/^{204}\text{Pb}$, $^{207}\text{Pb}/^{204}\text{Pb}$ and $^{208}\text{Pb}/^{204}\text{Pb}$ compositions by plasma ionisation multicollector mass spectrometry (PIMMS) using a Thermo Scientific Neptune instrument. During the $^{87}\text{Sr}/^{86}\text{Sr}$ and $^{143}\text{Nd}/^{144}\text{Nd}$ analytical sessions, instrument performance was monitored by analysis of NBS987 Sr standard and an in house J&M Nd standard and within-run instrument mass fractionation was corrected using an exponential law and the normalising value of $^{88}\text{Sr}/^{86}\text{Sr} = 8.375209$ and $^{146}\text{Nd}/^{145}\text{Nd} = 2.079143$, respectively (equivalent to $^{86}\text{Sr}/^{88}\text{Sr} = 0.1194$ and $^{146}\text{Nd}/^{144}\text{Nd} = 0.7219$). Since Nd was analysed as part of a total REE cut, the data required an algebraic correction for Sm interference on Nd based on the approach of Nowell and Parrish (2001). The accuracy of this correction was monitored by analysis of Sm-doped J&M, with a Sm/Nd ratio of ~0.25. The average $^{87}\text{Sr}/^{86}\text{Sr}$ for NBS987 was 0.710272 ± 0.000020 (2sd; n = 14) and the average $^{143}\text{Nd}/^{144}\text{Nd}$ for both pure and Sm-doped J&M was 0.511105 ± 0.00002 (2sd; n = 15) (detail in supplementary data file, Appendix B). $^{87}\text{Sr}/^{86}\text{Sr}$ ratios are reported relative to NBS987 standard value of 0.71024 (Thirlwall, 1991) and $^{143}\text{Nd}/^{144}\text{Nd}$ is reported relative to a J&M standard value of 0.511110 which is equivalent to a La Jolla value of 0.511862 (Royse et al., 1998). The $^{87}\text{Sr}/^{86}\text{Sr}$ and $^{143}\text{Nd}/^{144}\text{Nd}$ ratios of the two international rock standards BHVO-1 and BIR-1 were 0.703463 and 0.512989 and 0.703115 and 0.513073 respectively. The accuracy of the

Sm correction on the $^{143}\text{Nd}/^{144}\text{Nd}$ ratio is illustrated by the analysis of BHVO-1, which after Sm correction is identical to the ratio of 0.512986 ± 0.000009 (2sd; $n = 19$) that Weis et al. (2005) obtained by thermal ionisation mass spectrometry (TIMS).

Table 3.1. St Lucia whole rock Sr-Nd-Pb isotopic compositions and the corresponding SiO_2 and CaO content in wt. %. SiO_2 and CaO concentrations are from Davidson (1987) and Lindsay et al. (2013), and normalised to 100% volatile free.

Durham University							
Sample name	$^{143}\text{Nd}/^{144}\text{Nd}$	$^{87}\text{Sr}/^{86}\text{Sr}$	$^{206}\text{Pb}/^{204}\text{Pb}$	$^{207}\text{Pb}/^{204}\text{Pb}$	$^{208}\text{Pb}/^{204}\text{Pb}$	SiO_2	CaO
SL8303	0.512261	0.707542	19.728	15.826	39.438	64	5.79
SL8308	0.512161	0.708925	19.721	15.830	39.457	66.9	5.36
SL8312	0.512147	0.708914	-	-	-	66.7	5.29
SL8315	0.512169	0.708346	19.760	15.837	39.467	62.1	6.89
SL8316	0.512161	0.70843	19.737	15.833	39.466	64.1	6.28
SL8317	0.512106	0.709056	19.797	15.845	39.489	61.5	6.73
SL8319	0.51218	0.708412	19.748	15.837	39.479	65.5	5.62
SL8324	0.512215	0.708237	19.730	15.828	39.446	65.7	5.61
SL8325	0.512946	0.704394	19.291	15.748	38.930	55.8	7.41
SL8344	0.512957	0.704132	19.341	15.747	39.110	51.8	11.02
SL-JL-22	0.512178	0.708402	19.753	15.832	39.471	63.6	6.45
SL-JL-23	0.512111	0.708801	19.779	15.836	39.479	63.9	6.06
SL-JL-24	0.512101	0.709049	19.770	15.834	39.484	67.1	5.27
SL-JL-33	0.512177	0.708511	19.759	15.832	39.473	67.1	5.31
SL-JL-51	0.512108	0.708946	19.766	15.834	39.484	66.4	5.57
SL-JL-57	0.51214	0.708672	19.773	15.840	39.489	66.3	5.42
SL-JL-61	0.512096	0.709063	19.782	15.846	39.528	67.5	5.32
SL-JL-79	0.512187	0.708313	-	-	-	65.6	5.45
SL-JL-83	0.512194	0.708202	19.758	15.835	39.483	66.5	5.55
SL-JL-84	0.512209	0.708313	-	-	-	64.3	6.26
Macquarie University							
Sample name	$^{143}\text{Nd}/^{144}\text{Nd}$	$^{87}\text{Sr}/^{86}\text{Sr}$	$^{206}\text{Pb}/^{204}\text{Pb}$	$^{207}\text{Pb}/^{204}\text{Pb}$	$^{208}\text{Pb}/^{204}\text{Pb}$	SiO_2	CaO
SL8326	0.512505	0.706219	-	-	-	53.5	10.24
SL8339	0.51258	0.706106	-	-	-	57.4	8.53
SL8341	0.512958	0.704354	-	-	-	61.4	6.09
SL8342	0.512983	0.704174	-	-	-	50.9	11.68
SL8345	0.512975	0.704109	-	-	-	71.9	2.37
SL-JL-1	0.512143	0.708393	19.757	15.838	39.489	65.4	5.25
SL-JL-2	0.512091	0.708504	-	-	-	62.8	6.41

Following chemistry, the Pb fractions were taken up in 1 ml of 3% HNO_3 . The Pb concentration of the aliquots was analysed before isotopic measurements, in order to calculate the appropriate amount of Tl spike to add to obtain a Pb/Tl ratio of ~ 12 . This

minimises the tail from ^{205}Tl onto ^{204}Pb and from ^{206}Pb onto ^{204}Tl . During isotopic measurements, the samples were introduced into the Neptune using an ESI PFA50 nebuliser and a cyclonic spray-chamber. The normal H skimmer cone was used. Sensitivity for Pb on the Neptune using such setup is typically around 100 V total Pb ppm^{-1} at an uptake rate of $90 \mu\text{m min}^{-1}$. Pb mass bias was corrected externally using the $^{205}\text{Tl}/^{203}\text{Tl}$ ratio of the spike and an exponential law. The $^{205}\text{Tl}/^{203}\text{Tl}$ used for correction was determined for each analytical session by minimising the difference in offset between the session average Pb ratios and the Galer (1997) triple spike Pb isotope values. The Tl isotope ratio was calculated to yield the best fit to all the Pb isotope ratios of Galer (1997) simultaneously. During the analytical sessions, the NBS981 standard solution was analysed regularly ($n = 16$). The average ratios were: $^{206}\text{Pb}/^{204}\text{Pb} = 16.941 \pm 0.0024$ (2 sd), $^{207}\text{Pb}/^{204}\text{Pb} = 15.497 \pm 0.0012$ (2 sd), $^{208}\text{Pb}/^{204}\text{Pb} = 36.715 \pm 0.0039$ (2 sd) (detail in supplementary data file, Appendix B). Furthermore, a total procedural BHVO-1 was analysed. The $^{206}\text{Pb}/^{204}\text{Pb}$, $^{207}\text{Pb}/^{204}\text{Pb}$, $^{208}\text{Pb}/^{204}\text{Pb}$ ratios obtained were 18.687, 15.568 and 38.342, respectively which is in good agreement with the GEOREM accepted value ($^{206}\text{Pb}/^{204}\text{Pb} = 18.692 \pm 0.008$ (2 sd); $^{207}\text{Pb}/^{204}\text{Pb} = 15.572 \pm 0.006$ (2 sd); $^{208}\text{Pb}/^{204}\text{Pb} = 38.355 \pm 0.022$ (2 sd)).

At Macquarie, Sr was separated from the sample solution using Biorad AG50W-X8 resin and Nd was collected after separation from Ba and LREE using Eichrom[®] Ln.spec resin columns following the method of Pin et al. (1997). $^{87}\text{Sr}/^{86}\text{Sr}$ and $^{143}\text{Nd}/^{144}\text{Nd}$ ratios were measured by TIMS using a Thermo-Fisher Triton instrument. During the analytical session, instrument performance was monitored by analyses of Sr standards NBS987 and Nd standard JMC321 and mass bias was corrected as in Durham. The average $^{87}\text{Sr}/^{86}\text{Sr}$ for NBS987 was 0.710220 ± 0.000022 (2sd, $n = 4$) and the average $^{143}\text{Nd}/^{144}\text{Nd}$ for JMC321 was 0.511123 ± 0.000006 (2sd; $n = 3$) (detail in supplementary data file, Appendix B). $^{87}\text{Sr}/^{86}\text{Sr}$ and $^{143}\text{Nd}/^{144}\text{Nd}$ were not reported relative to a literature value. During the course of this study, analyses of processed international BHVO-2 standard yielded average $^{87}\text{Sr}/^{86}\text{Sr}$ and $^{143}\text{Nd}/^{144}\text{Nd}$ ratios of was 0.703469 ± 0.000012 (2sd; $n = 4$) and 0.512976 ± 0.000012 (2sd; $n = 4$), respectively.

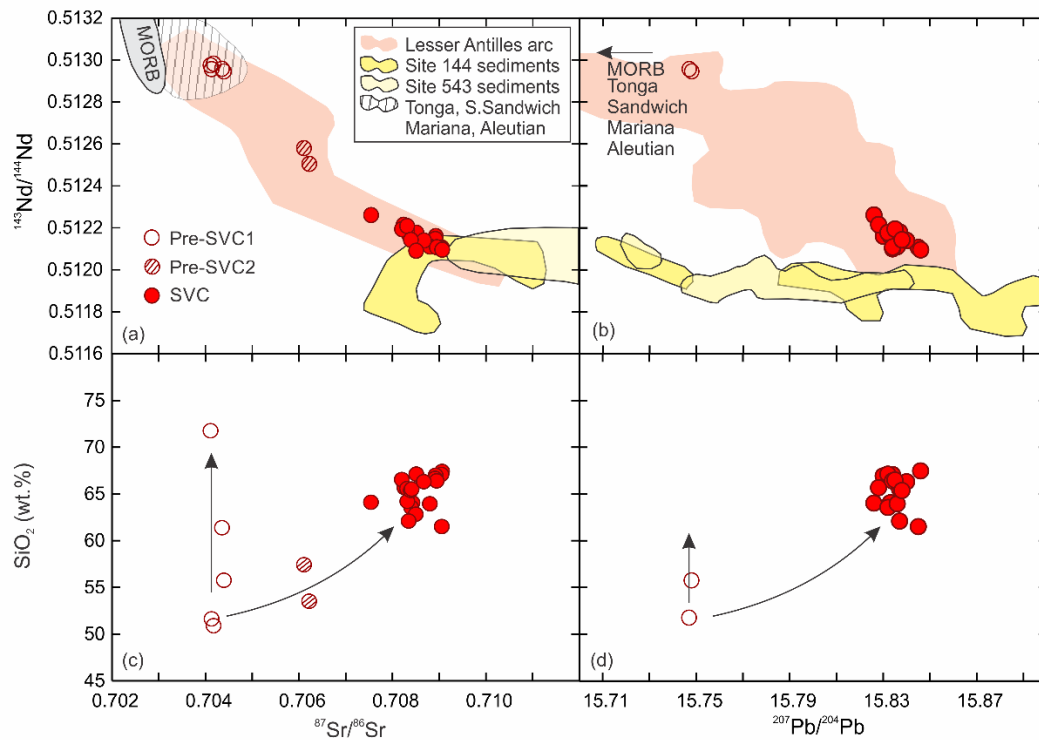


Fig. 3.2. Whole rock compositions of St Lucia lavas. (a) Sr and Nd and (b) Pb and Nd isotopic diversity. St Lucia data show a similar range to most of the Lesser Antilles arc, ranging between typical oceanic arc compositions and Atlantic sediments cored at the front of the trench (DSDP sites 144 and 543; Carpentier et al., 2008, 2009). SVC = Soufriere Volcanic Complex. Pre-SVC lavas with typical oceanic arc compositions, called Pre-SVC1, are shown by open circles and lavas with the most radiogenic compositions, called Pre-SVC2, are represented by striped circles. The SVC lavas are shown by solid red circles. (c) $^{87}\text{Sr}/^{86}\text{Sr}$ and (d) $^{207}\text{Pb}/^{204}\text{Pb}$ vs. SiO_2 (wt. %) of St Lucia lavas showing the two trends observed. SiO_2 and Sr-Nd-Pb isotopic compositions are provided in the Table 3.1. Tonga, South Sandwich, Mariana and Aleutian compositions from Georock database: <http://georoc.mpch-mainz.gwdg.de/georoc/>. MORB field is mid-Atlantic Ridge between 30°N and 30°S (data from PETDB: <http://petdb.org/science.jsp/>) and the Lesser Antilles arc field represents data from other islands: Grenada from Thirlwall and Graham (1984); Soufrière, St Vincent from Heath et al. (1998); Dominica and Martinique from Davidson (1986, 1987) and Davidson and Wilson (2011); Mt Misery, St Kitts from Toothill et al. (2007), The Quill, Statia from Davidson and Wilson (2011); Saba from Sherman (1992).

3.3.2 $^{87}\text{Sr}/^{86}\text{Sr}$ in plagioclase

Four of the most continental-like lavas from St Lucia (SVC), ranging from andesitic to dacitic in composition and with very similar whole rock radiogenic isotope signatures, were chosen for in-depth isotopic study. Sr isotope ratios were determined for five single plagioclase crystals from each lava. The crystals were carefully hand-

picked from lightly crushed hand specimens using a binocular microscope. Grains were selected for being free of both inclusions and adhering glass. Each grain, containing at least 60 ng Sr, was individually digested in Romil Upa grade HNO₃ and HF. Sr was separated using Sr-spec resin columns and ⁸⁷Sr/⁸⁶Sr was measured by TIMS using the Thermo Fisher Triton at Durham University. During the TIMS analyses, the average ⁸⁷Sr/⁸⁶Sr ratio for NBS987 obtained on 12ng of Sr was 0.710243 ± 0.000009 (2sd, n = 3). This is in excellent agreement with the value reported by Thirlwall (1991) of 0.710248 ± 0.000023 (2sd, n = 427). Two total procedure blanks contained 18 and 32 pg of Sr which represent 0.03 and 0.05% of the lowest sample Sr concentration analysed and are therefore negligible. The detail of both NBS 987 and blank values are reported in the supplementary data file (Appendix B).

3.3.3 δ¹⁸O in mineral separates

Samples ranging from typical oceanic arc lavas to the most continental-like composition were selected for individual mineral oxygen isotope extraction by laser-fluorination. Minerals separates were hand-picked from lightly crushed hand specimens under a binocular microscope, avoiding any inclusions or glass adhering to the grains. Oxygen was extracted from 0.9-3.7 mg of separate using a total laser fluorination system based on the method of Sharp (1990), at the Scottish Universities Environmental Research Centre (SUERC). All fluorinations resulted in 100% release of O₂ from mineral lattice. This oxygen was converted to CO₂ and analysed on a VG Optima mass spectrometer. Oxygen isotope (δ¹⁸O) values are reported as per mil (‰) deviations relative to Vienna Standard Mean Ocean Water (V-SMOW). Samples were analysed during two periods. During the first period (March 2012) 31 unknowns were analysed along with the international and in-house standards UWG2 and SES and GP147. The average δ¹⁸O values obtained for UWG2 (garnet, +5.7‰ ± 0.2 (2sd), n = 11), SES (quartz, +10.4‰ ± 0.6 (2sd), n = 10) and GP147 (garnet, +7.2‰ ± 0.4 (2sd), n = 3) are in very good agreement with their accepted values of +5.8‰ (Valley et al., 1995), +10.2‰ and +7.2‰ (Mattey and Macpherson, 1996), respectively. The internal SES standard has been run many hundreds of time over the past 20 years in SUERC, and is well calibrated against UWG2, NBS 28 and NBS 30, as well as GP147. Twelve unknowns were analysed during the second period of study (November 2012) when the average δ¹⁸O values for UWG2, SES and GP147 were +5.9‰ ± 0.2 (2 sd, n = 2),

+10.2‰ ± 0.3 (2 sd, n = 6), +7.15‰ ± 0.4 (2 sd, n = 2) respectively. The detail of all standards analysed is presented in the supplementary data file (Appendix B).

3.4 Results

Whole rock Sr, Nd and Pb isotope ratios are given in Table 3.1. Plagioclase Sr isotopes and mineral $\delta^{18}\text{O}$ data are presented in Tables 3.2 and 3.3 respectively.

Table 3.2. $^{87}\text{Sr}/^{86}\text{Sr}$ of single plagioclase grains separated from four of the most continental-like SVC hand samples. Whole rock SiO_2 (wt. %) and $^{87}\text{Sr}/^{86}\text{Sr}$ are also shown (see Table 3.1 for references).

Sample name	$^{87}\text{Sr}/^{86}\text{Sr}$	2 SE	Whole rock $^{87}\text{Sr}/^{86}\text{Sr}$	Whole rock SiO_2
SL8317PI1	0.709377	0.000010	0.709056	61.5
SL8317PI2	0.709107	0.000009		
SL8317PI3	0.708974	0.000013		
SL8317PI4	0.709071	0.000009		
SL8317PI5	0.709050	0.000008		
SL-JL-24PI6	0.708482	0.000006	0.709049	67.1
SL-JL-24PI7	0.708646	0.000005		
SL-JL-24PI8	0.708478	0.000010		
SL-JL-24PI9	0.708311	0.000007		
SL-JL-24PI10	0.709143	0.000009		
SL-JL-51PI11	0.708538	0.000007	0.708946	66.4
SL-JL-51PI12	0.708501	0.000010		
SL-JL-51PI13	0.708426	0.000007		
SL-JL-51PI14	0.708400	0.000007		
SL-JL-51PI15	0.708669	0.000005		
SL-JL-61PI16	0.708352	0.000008	0.709063	67.5
SL-JL-61PI17	0.708739	0.000006		
SL-JL-61PI18	0.708901	0.000007		
SL-JL-61PI19	0.708627	0.000007		
SL-JL-61PI20	0.708691	0.000006		

Whole rock $^{87}\text{Sr}/^{86}\text{Sr}$ and $^{143}\text{Nd}/^{144}\text{Nd}$ ratios range between 0.70411 and 0.70622 and 0.51251 and 0.51298, respectively, in the Pre-SVC samples and from 0.70754 to 0.70906 and 0.51210 to 0.51226, respectively, in the SVC samples (Fig. 3.2a). Whole rock $^{206}\text{Pb}/^{204}\text{Pb}$, $^{207}\text{Pb}/^{204}\text{Pb}$ and $^{208}\text{Pb}/^{204}\text{Pb}$ ratios were analysed in selected samples with the highest and the lowest $^{87}\text{Sr}/^{86}\text{Sr}$ isotope ratios, to verify coupling with other isotopic systems. Pb isotope ratios vary from 19.291 to 19.341 for $^{206}\text{Pb}/^{204}\text{Pb}$, from 15.747 to 15.748 for $^{207}\text{Pb}/^{204}\text{Pb}$ (Fig. 3.2b) and from 38.96 to 39.11 for $^{208}\text{Pb}/^{204}\text{Pb}$ in the Pre-SVC lavas analysed. In the SVC lavas, ratios vary from 19.721 to 19.797 for $^{206}\text{Pb}/^{204}\text{Pb}$, from 15.826 to 15.846 for $^{207}\text{Pb}/^{204}\text{Pb}$ and from 39.438-39.528 for $^{208}\text{Pb}/^{204}\text{Pb}$. Plagioclase crystals from the SVC have heterogeneous $^{87}\text{Sr}/^{86}\text{Sr}$ ratios (Fig. 3.3) ranging between 0.7083 and 0.7094 with variations of up to 0.00083 among crystals from a single lava (SL-JL-51). In the Pre-SVC, plagioclase and pyroxene $\delta^{18}\text{O}$ vary from + 6.4 to +7.9‰ and from +6 to +6.8‰ respectively (Fig. 3.4). In the SVC,

mineral $\delta^{18}\text{O}$ are higher and vary from +7.5 to +10.9‰ for plagioclase, from +10.6 to +11.8‰ for quartz, from +9.4 to +9.8‰ for amphibole and +9 to +9.5‰ for pyroxene.

Table 3.3. $\delta^{18}\text{O}$ of single mineral separates from St Lucia along with the corresponding whole rock SiO_2 (wt. %) and Sr isotopic composition. WR = whole rock. SiO_2 content from Davidson (1987) and Lindsay et al. (2013) and normalised to 100% volatile free.

Sample name	Kind of mineral	Group	$\delta^{18}\text{O}_{\text{V-SMOW}} (\text{‰})$	WR SiO_2	WR $^{87}\text{Sr}/^{86}\text{Sr}$
8308PI	Plagioclase	SVC	10.6	66.9	0.708925
8312PI	Plagioclase	SVC	10.4	66.7	0.708914
8316PI	Plagioclase	SVC	10.4	64.1	0.70843
8317PI	Plagioclase	SVC	10.9	61.5	0.709056
8317PI	Plagioclase	SVC	9.9	61.5	0.709056
8319PI	Plagioclase	SVC	10.1	65.5	0.708412
8324PI	Plagioclase	SVC	9.9	65.7	0.708237
8325PI	Plagioclase	Pre-SVC1	6.4	55.8	0.704394
8326PI1	Plagioclase	Pre-SVC2	7.3	53.5	0.706219
8326PI2	Plagioclase	Pre-SVC2	7.9	53.5	0.706219
8344PI	Plagioclase	Pre-SVC1	6.6	51.8	0.704132
JL01PI	Plagioclase	SVC	10.1	65.4	0.708393
JL02PI	Plagioclase	SVC	7.5	62.8	0.708504
JL22PI	Plagioclase	SVC	11.1	63.6	0.708402
JL23PI	Plagioclase	SVC	10.8	63.9	0.708801
JL24PI	Plagioclase	SVC	10.8	67.1	0.709049
JL33PI	Plagioclase	SVC	10.2	67.1	0.708511
JL51PI	Plagioclase	SVC	10.9	66.4	0.708946
JL57PI	Plagioclase	SVC	10.1	66.3	0.708672
JL61PI	Plagioclase	SVC	10.9	67.5	0.709063
JL83PI	Plagioclase	SVC	10.5	66.5	0.708202
JL84PI	Plagioclase	SVC	10.0	64.3	0.708313
JL79PI	Plagioclase	SVC	10.0	65.6	0.708313
8303Qz	Quartz	SVC	11.2	64.0	0.707542
JL01Qz	Quartz	SVC	11.3	65.4	0.708393
JL02Qz	Quartz	SVC	11.4	62.8	0.708504
JL22Qz	Quartz	SVC	11.3	63.6	0.708402
JL23Qz	Quartz	SVC	10.9	63.9	0.708801
JL24Qz	Quartz	SVC	11.4	67.1	0.709049
JL33Qz	Quartz	SVC	11.1	67.1	0.708511
JL51Qz	Quartz	SVC	11.3	66.4	0.708946
JL57Qz	Quartz	SVC	10.6	66.3	0.708672
JL61Qz	Quartz	SVC	11.8	67.5	0.709063
8324Opx	Orthopyroxene	SVC	9	65.7	0.708237
8326Py1	Clinopyroxene	Pre-SVC2	6.8	53.5	0.706219
8326Py2	Clinopyroxene	Pre-SVC2	6.4	53.5	0.706219
8344Py1	Clinopyroxene	Pre-SVC1	6.0	51.8	0.704132
8344Py2	Clinopyroxene	Pre-SVC1	6.2	51.8	0.704132
8344Py3	Clinopyroxene	Pre-SVC1	6.3	51.8	0.704132
JL57Opx	Orthopyroxene	SVC	9.5	66.3	0.708672
JL79Opx	Orthopyroxene	SVC	9.1	65.6	0.708313
8308Am	Amphibole	SVC	9.8	66.9	0.708925
JL33Am	Amphibole	SVC	9.4	67.1	0.708511

3.5 Discussion

3.5.1 Intra-crustal magma contamination

The unusually radiogenic composition of some lavas from the Lesser Antilles arc has been explored by many authors using whole rock samples, and explained through models invoking either sediment incorporation into the source (e.g. Labanieh et al., 2010) or assimilation during fractional crystallisation (AFC; e.g. Davidson, 1987).

Discriminating between these two processes using only whole rock isotopes is difficult mainly due to uncertainties in determining the precise composition of the endmembers. Correlations between whole rock isotopes and indexes of differentiation such as SiO₂ or MgO are however useful in detecting isotopic changes during differentiation and have been employed by several authors to argue for AFC in Grenada (Thirlwall et al., 1996), the Grenadine Islands (Smith et al., 1996) and Martinique (Davidson, 1987; Davidson and Wilson, 2011). In St Lucia, two distinct trends are observed (Fig. 3.2c): the first one, comprising only some Pre-SVC samples (Pre-SVC1), shows an absence of covariation between radiogenic isotopes and SiO₂ or MgO while the second trend, comprising the remaining Pre-SVC (Pre-SVC2) and the SVC lavas, displays progressive increase in Sr and decrease in Nd isotope ratios with increasing SiO₂ and decreasing MgO. Pb isotope ratios were not analysed for all St Lucia lavas but variations in the Pre-SVC1 and SVC lavas are consistent with those defined by Sr and Nd isotopes (Fig. 3.2d). While the first (“vertical”) trend can be explained by simple differentiation of a mafic mantle-derived magma, the second trend requires a different/additional process. If this latter trend were to reflect a source process, this would require either (1) the production of silicic SVC magmas in the mantle or (2) their derivation by differentiation of more mafic melts from a mantle source where a common factor controls both the amount of sediment melt/sediment derived fluids added to the source and the future extent of magma differentiation. The first hypothesis cannot be reconciled with the low MgO content of silicic SVC lavas compositions (MgO = 1.1-2.7 wt.%) since andesitic to dacitic magma generated either by mantle melting or by reaction between ascending slab-derived silicic melts and mantle peridotite typically have elevated MgO contents (Grove et al., 2003; Yogodzinsky and Kelemen, 1998). The second hypothesis, involving a coincidental process, is equally very hard to conceive. It is, however, directly testable. Since magmatic differentiation has negligible effect on radiogenic isotopic ratios, the amount of sediment incorporated into the magma during its genesis in the mantle should be reflected in the ⁸⁷Sr/⁸⁶Sr of all its components. Therefore, once separated from its source, a magma that has remained a closed system should demonstrate negligible ⁸⁷Sr/⁸⁶Sr variation between the melt and all phenocrysts. Furthermore, the Sr isotope ratio of the phenocrysts would also be observed for the whole rock. Conversely, isotopic disequilibrium between different phases in a rock or between different crystals of the same phase would require that open system behaviour

occurred. Therefore, the variation in $^{87}\text{Sr}/^{86}\text{Sr}$ ratios within single samples is a hallmark for open system behaviour (Davidson et al., 2007).

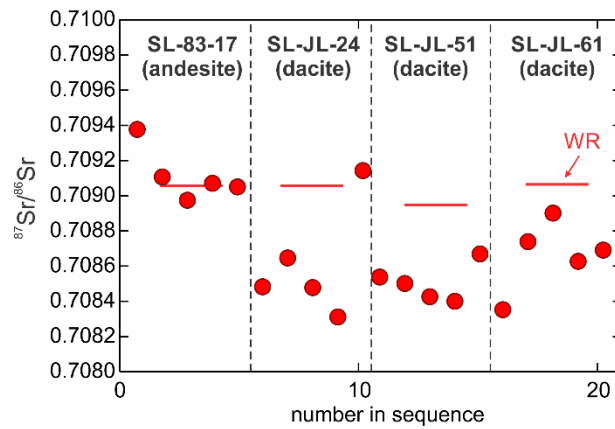


Fig. 3.3. $^{87}\text{Sr}/^{86}\text{Sr}$ isotope ratios of twenty plagioclase phenocrysts showing isotopic disequilibrium among four of the most contaminated SVC lavas. The whole rock value for each lava is shown as a horizontal line. For all data, 2 standard errors (SE) are < 0.000014 which is smaller than the symbol size. Data are presented in Table 3.2.

Despite their similar whole rock Sr isotopic ratios, the $^{87}\text{Sr}/^{86}\text{Sr}$ ratios of crystals from the four SVC samples vary substantially amongst and within hand specimens (Table 3.2; Fig. 3.3). Such disequilibrium cannot be explained by incorporation of sediment in the source, and must instead be accounted for by an open system process, such as crustal assimilation during crystallisation.

Most of the plagioclase crystals analysed have lower $^{87}\text{Sr}/^{86}\text{Sr}$ than their respective whole rock values. This indicates that at least part of the volume of each of those plagioclase crystals grew in a magma with less radiogenic Sr than now represented by the matrix. The zoned nature of the crystals requires an igneous origin but does not allow discrimination between phenocrysts which grew from a magma changing in $^{87}\text{Sr}/^{86}\text{Sr}$ composition and xenocrysts which were remobilized during re-melting of plutonic rocks. The latter option was preferred by Schmitt et al. (2010) to explain variation in core to rim U-Th zircon ages obtained in the SVC lavas.

3.5.2. Effect of contamination on whole rock compositions

In order to confirm that crustal assimilation is largely responsible for the radiogenic whole rock isotopic signatures observed in St Lucia, the mineral $\delta^{18}\text{O}$ study was performed. Although the $\delta^{18}\text{O}$ of crustal-derived material ($> +10\text{‰}$) is much higher than the mantle range ($+5.5\text{‰} \pm 0.2$), 80% of the $\delta^{18}\text{O}$ values of any given phase in oceanic arc lavas fall within $\pm 0.2\text{‰}$ of the average value for that phase in upper mantle peridotites and MORBs (Mattey et al., 1994; Eiler et al., 2000). Because the concentration of oxygen in the mantle and the crust is similar, a large input of crustal derived fluids and/or sediments would be necessary to modify the mantle signature (James, 1981). Thus, O isotopes provide a powerful tool to discriminate between addition of sediments to the mantle source from assimilation of sediments in the arc crust, the latter being a much more efficient way of modifying the mantle-derived $\delta^{18}\text{O}$ value of the magma (e.g. Macpherson et al., 1998). Previous oxygen isotopic analyses performed on olivine and pyroxene phenocrysts from the Lesser Antilles showed the existence of values greater than the mantle range and that these correlate with whole rock radiogenic isotopes, suggesting crustal assimilation (Smith et al., 1996; Thirlwall et al., 1996; Van Soest et al., 2002). However, although higher, the excess relative to the range of mantle $\delta^{18}\text{O}$ values was small, with only up to $+1\text{‰}$ excess for olivine and up to $+0.6\text{‰}$ for pyroxene with the exception of one pyroxene, which was $+1.6\text{‰}$ and two quartz crystals which were $+3.83\text{‰}$ and $+4.37\text{‰}$ higher than the mantle range.

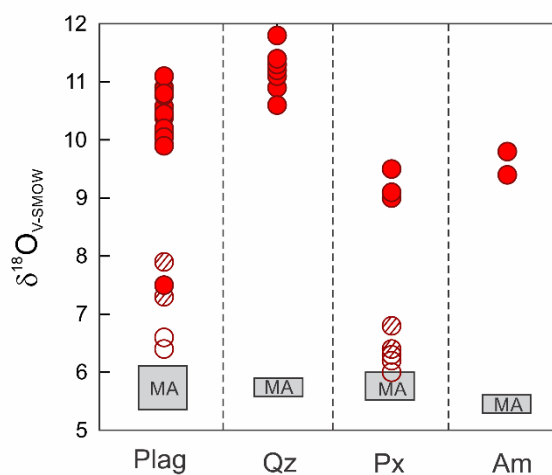


Fig. 3.4. $\delta^{18}\text{O}$ values of phenocrysts from SVC and Pre-SVC lavas (symbols as in Fig. 3.2). Plag = plagioclase; Qz = quartz, Py = pyroxene; Am = amphibole and MA = mantle range. Mantle ranges are from Bindeman and Valley (2002) for Quartz (from differentiation of mantle derived magma), Chazot

et al. (1997) for pyroxene and amphibole and Eiler et al. (2000) for plagioclase (defined using crystals from samples with SiO₂ similar to Pre-SVC mafic lavas). 2 sd reproducibility error of the O isotope technique was typically $\pm 0.4\text{‰}$ (see section 3.3).

In this study, 93% of the 44 mineral analyses lie outside their respective mantle ranges and the SVC displays extreme $\delta^{18}\text{O}$ values never observed before in oceanic arcs lacking known continental basement (Fig. 3.4). Moreover, a strong positive correlation is observed between the mineral $\delta^{18}\text{O}$ and the whole rock radiogenic isotopes (Fig. 3.5) with the highest $\delta^{18}\text{O}$ values found in SVC lavas with very radiogenic whole rock $^{87}\text{Sr}/^{86}\text{Sr}$ and $^{206,207,208}\text{Pb}/^{204}\text{Pb}$ ratios (and unradiogenic $^{143}\text{Nd}/^{144}\text{Nd}$ ratios). Although the SVC products have more differentiated compositions than the pre-SVC samples, the maximum effect of closed system differentiation on $\delta^{18}\text{O}$ is typically very small: $+0.3$ to $+0.4\text{‰}$ (Macpherson and Matthey, 1998; Bindeman et al., 2004). Thus, even after correction for this effect, the SVC mineral $\delta^{18}\text{O}$ range lies well beyond the mantle range. The mean anorthite (An) content of SVC plagioclase is slightly lower than that of the pre-SVC crystals. However, since the difference is small (mean An of 68% (ranging from 65% to 71%) and of 59% (ranging from 54% to 68%) respectively for SVC andesite and dacite vs. mean An of 80% (70% - 90%) for Pre-SVC basaltic andesite and basalt) the related increase in $\delta^{18}\text{O}$ in the SVC plagioclase is thought to be negligible. This is confirmed by the fact that phenocrysts from SVC lavas with different SiO₂ (high-silica andesites and dacites: 60.5-67.5 wt. %) possess similar $\delta^{18}\text{O}$ values. SVC plagioclase-quartz pairs (from the same hand sample) have $\Delta_{\text{plag-qtz}}$ (where $\Delta_{i-j} = \delta^{18}\text{O}_i - \delta^{18}\text{O}_j$) between -0.1 to -1.21‰ ($n = 8$; with $n = 5$ higher than -0.7‰) except for one pair where $\Delta_{\text{plag-qtz}} = -3.9\text{‰}$. Andesitic-dacitic temperatures ($T^\circ = 800\text{-}1000^\circ\text{C}$) typically produce $\Delta_{\text{plag-qtz}}$ between -0.84 and -1.45‰ (e.g. using the Chiba et al. (1989) fractionation coefficients and considering a large range of anorthite content between An₄₀ and An₇₀). Therefore, most $\Delta_{\text{plag-qtz}}$ are higher than equilibrium. SVC plagioclase-pyroxene pairs display fractionation of $\Delta_{\text{plag-py}}$ between $+0.60$ and $+0.95\text{‰}$ ($n = 3$) which are similar to that expected from equilibrium fractionation at andesitic-dacitic temperatures ($\Delta_{\text{plag-py}} = +0.66$ to $+1.21\text{‰}$ at $T^\circ = 800\text{-}1000^\circ\text{C}$ and An₄₀₋₇₀). Therefore, both pyroxene and plagioclase are likely to have crystallised in equilibrium from a similar magma. The lowest $\delta^{18}\text{O}$ values are observed in Pre-SVC1 lavas, which have low whole rock $^{87}\text{Sr}/^{86}\text{Sr}$ and Pb isotope ratios (SL-83-25, 44). In

these samples, $\delta^{18}\text{O}_{\text{plag}}$ values are higher than the mantle range, whereas the $\delta^{18}\text{O}_{\text{px}}$ values overlap the upper end of the mantle range. However, plagioclase-pyroxene pairs ($\Delta_{\text{plag-py}}$ from +0.3 to +0.6‰) are close to oxygen isotopic equilibrium at basaltic to basaltic andesite temperatures ($\Delta_{\text{plag-py}} = +0.35\text{‰}$ to $+0.51\text{‰}$ at $T^\circ = 1100\text{--}1200^\circ\text{C}$ and An₉₉₋₈₀ using Chiba et al.'s (1989) equation). Thus, it is difficult, in these samples, to differentiate between small error on the mantle mineral range of composition and the impact of small amounts of crustal assimilation during plagioclase crystallisation. Pre-SVC2 lavas, that have the highest whole rock $^{87}\text{Sr}/^{86}\text{Sr}$ ratios (SL-83-26; $^{87}\text{Sr}/^{86}\text{Sr} = 0.706219$; basaltic andesite) of the Pre-SVC group, also display higher $\delta^{18}\text{O}_{\text{plag}}$ than $\delta^{18}\text{O}_{\text{px}}$. However, $\Delta_{\text{plag-py}}$ varies between +0.5‰ to +1.5‰. Such values are too high to be explained simply by equilibrium fractionation. We believe that the high $\Delta_{\text{plag-py}}$ values result from the addition of a crustal component late in the differentiation sequence when plagioclase formed a larger component of the crystallising assemblage. This provides further support for an origin through crustal assimilation rather than sediment addition to the source. In this case, plagioclase provides a more sensitive record of crustal assimilation than the mafic phases. This may be important when targeting minerals for oxygen isotopic analysis in settings where more subtle changes in $\delta^{18}\text{O}$ are anticipated, due to smaller isotopic contrasts between magma and the crust into which it is emplaced.

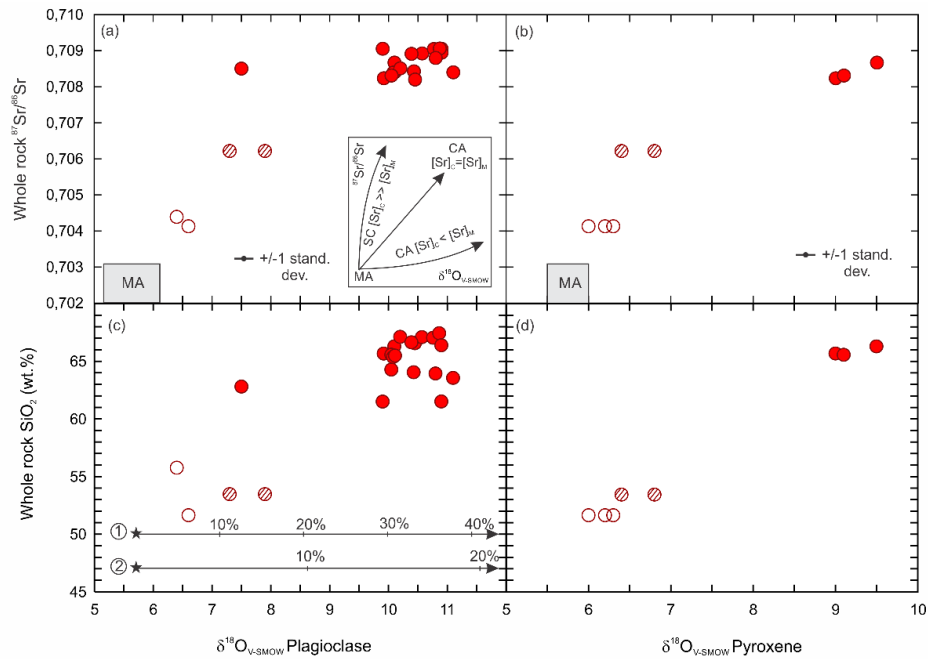


Fig. 3.5 Correlation between mineral $\delta^{18}\text{O}$ and whole rock $^{87}\text{Sr}/^{86}\text{Sr}$ and SiO_2 (symbols as in Fig. 3.2). (a, b) plagioclase and pyroxene $\delta^{18}\text{O}$ vs. whole rock $^{87}\text{Sr}/^{86}\text{Sr}$. (c,d) plagioclase and pyroxene $\delta^{18}\text{O}$ vs.

whole rock SiO_2 . Mixing models between mantle ($\delta^{18}\text{O} = +5.7\text{‰}$) and sediment with $\delta^{18}\text{O}$ of $+20\text{‰}$ (1) and $+35\text{‰}$ (2) are also shown. Oxygen concentration is assumed to be the same for both the mantle and the sediment in the model. MA = MORB mantle range with $\delta^{18}\text{O}$ from Eiler et al. (2000) and $^{87}\text{Sr}/^{86}\text{Sr}$ from mid-Atlantic Ridge between 30°N and 30°S (data from PETDB: <http://petdb.org/science.jsp/>). In the schematic inset $[\text{Sr}]_C$ is the Sr concentration in sediment and $[\text{Sr}]_M$ is the Sr concentration in the mantle during source contamination (SC) and in the melt during crustal assimilation (CA).

A simple mixing model (Fig. 3.5) between a typical mantle composition and a sediment having the highest $\delta^{18}\text{O}$ reported ($+35\text{‰}$; Bindeman, 2008) shows that a minimum of 10-20% of sediment would be required to be added to the mantle or a mantle derived magma in order to explain the SVC mineral $\delta^{18}\text{O}$ data. However, we know from DSDP 78A site 543 and DSDP 14 site 144 that sediments subducted at the Lesser Antilles trench comprise a mixture of pelagic clay, radiolarian clay, terrigenous claystone siltstone and sandstones (30% carbonate on average; Carpentier et al., 2008). Thus, the bulk sediment would possess an average $\delta^{18}\text{O}$ closer to the composition of site 543 pelagic clays of $+20\text{‰}$ (Davidson, 1987). In this more realistic case, addition of 20-40 % sediment would be required to generate the range of SVC $\delta^{18}\text{O}$ values and addition of 10-20% sediment could reproduce the Pre-SVC sample with the most elevated $\delta^{18}\text{O}_{\text{plag}}$ ($+7.3$ to $+7.9\text{‰}$ in SL-83-26; Fig. 3.5c). Introducing such large amounts of sediments to the mantle wedge should also modify the major element composition of the primitive magmas, such that increasing sediment incorporation (i.e. increasing mineral $\delta^{18}\text{O}$ and $^{87}\text{Sr}/^{86}\text{Sr}$) should correlate with an increase of SiO_2 (clay, sand) or CaO (carbonate) of the melt. As discussed in section 3.5.1., the SVC lavas cannot have been directly produced in the mantle since their MgO is too low. If the SVC lavas resulted from differentiation of a primary magma produced in the mantle by mixing with substantial amounts of sediment melt, the resulting suite of lava would likely have a higher SiO_2 or CaO content than a suite derived from Pre-SVC_{1,2} primitive magmas at a given MgO content (different differentiation trends). However, SVC and Pre-SVC_{1,2} lavas share similar (although scattered) differentiation trend (Fig. 3.6), and therefore back project toward a similar primitive magma. Hence, it seems unlikely that the SVC and Pre-SVC lavas were derived from very different mantle sources. Instead, the single trend of differentiation recorded by major elements in all St Lucia lavas is consistent with variable assimilation of crustal material. This is because, during differentiation, major element

compositions are largely controlled by phase equilibria and, to a lesser extent, by the nature of the sediment assimilated, the latter likely to be derived from the erosion of upper continental crust with a similar composition to the felsic differentiates of the Pre-SVC lavas (Fig. 3.6). Therefore, the strong correlation between $\delta^{18}\text{O}$ and whole rock Sr isotopes indicate that assimilation is the major factor controlling the whole rock radiogenic isotope ratios observed in the St Lucia lavas (Fig. 3.7). For both plagioclase and pyroxene, the correlation is slightly convex-up, suggesting that the magma had a slightly lower Sr content than the material it assimilated (c.f. inset to Fig. 3.5). More importantly, the plagioclase $\delta^{18}\text{O}$ values are displaced further from the mantle field than is the case for pyroxene in Pre-SVC samples, requiring a larger proportion of assimilant than required for the pyroxenes. Quartz is only found in the SVC lavas where no correlation between $\delta^{18}\text{O}_{\text{qz}}$ and whole rock $^{87}\text{Sr}/^{86}\text{Sr}$ is observed. The slight disequilibrium between quartz and plagioclase (low $\Delta_{\text{plag-qtz}}$) indicates that quartz crystallised in a magma with slightly lower $\delta^{18}\text{O}$ than the plagioclase.

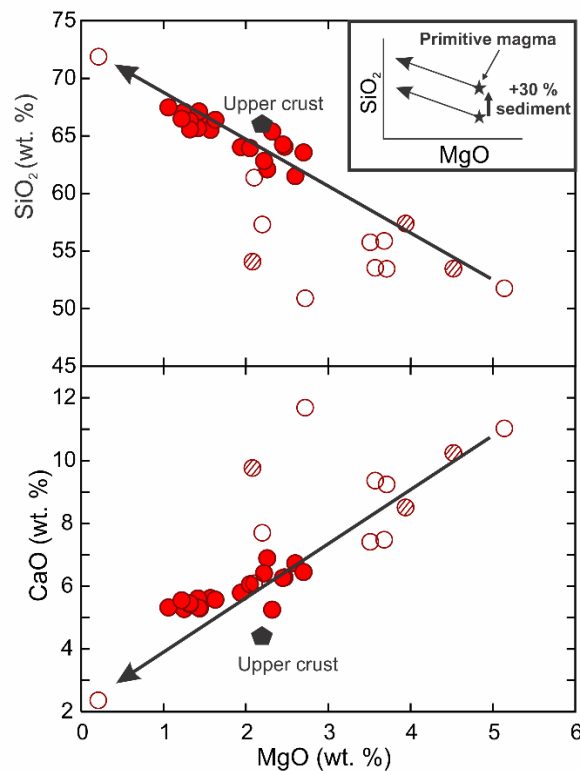


Fig. 3.6. Variation of SiO_2 and CaO with MgO composition with the Pre-SVC and SVC lavas. Upper continental crust composition is from Rudnick and Fountain (1995). The schematic inset illustrates the impact of incorporation of large amounts of terrigenous sediment into the mantle source on primitive magma compositions. The same concept can be applied to CaO versus MgO , for large amounts of carbonate rich sediment.

3.5.3 Implications for other Lesser Antilles volcanoes and other arcs

The crystal $^{87}\text{Sr}/^{86}\text{Sr}$ data show that lavas with extreme whole rock compositions underwent assimilation of crustal material in an open system supporting previous work by Thirlwall and Graham (1984), Davidson (1987), Davidson and Harmon (1989) Smith et al. (1996), Thirlwall et al. (1996), and Van Soest et al. (2002). The extreme $\delta^{18}\text{O}$ signature observed in lavas with the most continental Sr, Nd and Pb isotope ratios (SVC) confirms late assimilation of arc crust as the cause of these variations and shows that the amount of material assimilated is not trivial ($>20\%$). More importantly, crustal assimilation did not only affect the andesites and dacites, but also substantially (10-20% assimilation) modified the composition of a basaltic andesite (Pre-SVC2) with similar SiO_2 and MgO contents to the most mafic lava of the island. Therefore, in St Lucia, the use of the most mafic lavas erupted on the island to constrain the source characteristics is compromised since some of them have clearly interacted with the crust. Similar problems may affect other Lesser Antilles islands and other oceanic arcs where basaltic andesites with $\text{MgO} \sim 4 \text{ wt. } \%$, or even more differentiated lavas, have been used studies to constrain the source composition. For example Labanieh et al. (2010) suggested that isotopic ratios in lavas from Martinique with up to $\sim 70 \text{ wt. } \%$ SiO_2 ($\text{MgO} \sim 0.23$) faithfully reflect the source composition. Likewise, Carpentier et al. (2008) modeled all the published data for Lesser Antilles lavas by sediment addition to the source, without taking into account the degree of differentiation of the lavas.

Because St Lucia lavas encompass Sr, Nd and Pb isotopic range almost as great as the whole Lesser Antilles arc it follows that much of the isotopic heterogeneity observed in the rest of the arc could also reflect variable crustal assimilation. Sediment present in the Lesser Antilles arc crust is likely to originate from the closest continental mass: South America. It has very “continental” $^{87}\text{Sr}/^{86}\text{Sr}$, $^{143}\text{Nd}/^{144}\text{Nd}$ and $^{206,207,208}\text{Pb}/^{204}\text{Pb}$ ratios (e.g. Carpentier et al., 2008). Sediments with such signatures were found on the edge of the north east part of South America (site 144 sediment; Carpentier et al., 2008; 2009) and their presence on the subducting plate was used as a strong argument for incorporation of sediment in the mantle source as being the cause for the extreme isotopic compositions of the arc lavas. However, our data show that most of the arc lava isotopic variations are generated by contamination in the arc crust. Therefore,

subduction of material resembling site 144 sediments is not *required* to explain the extreme Sr, Nd, Pb and O isotopic signatures of the Lesser Antilles arc lavas.

It is important to stress that this does not preclude incorporation of subducted sediment into the source of the lavas having an impact on the whole rock isotopic ratios. Indeed, mineral $\delta^{18}\text{O}$ compositions of the Pre-SVC1 lavas (SL-83-44; SL-83-25) are very close to mantle values which indicate that, if crustal assimilation affected these lavas, it would be in very low amounts. Yet, although their Sr and Nd isotope ratio overlap typical oceanic arc compositions, their Pb isotope ratios are slightly more radiogenic (Fig. 3.2b). This not only suggests the involvement of sediment in the source but also that these are slightly more abundant or more radiogenic than sediments present in the source of most “typical” oceanic arcs. However, Sr, Nd and Pb isotope compositions of the Pre-SVC1 lavas remain very close to typical oceanic composition spectrum, and we suggest that subducted material is not a major factor in causing large isotopic heterogeneity in Lesser Antilles arc lavas.

The extreme contamination observed in at least some of the Lesser Antilles lavas may reflect the unique presence of sediment in the arc crust that, in turn, reflects a specific geodynamic context (Aitken et al., 2011). However, similar assimilation of sediments and/or altered crust in lower amounts and/or different composition may occur in other oceanic arcs and has already been suggested to explain compositions observed in the offshore Taupo Volcanic zone in New Zealand (Macpherson et al., 1998). Eiler et al. (2000) estimated that although most oceanic arc minerals (olivine, plagioclase, glass, biotite) fall within the mantle range in $\delta^{18}\text{O}$, around 20% of the data are slightly higher by up to 0.43‰. These ‘out of mantle range’ phases come from samples with higher whole rock Sr isotope ratios, which is also what we observe on St Lucia. Because the displacement from the mantle range is not substantial, these data have been interpreted to reflect sediment incorporation into the mantle wedge. However, all these higher $\delta^{18}\text{O}$ ratios were observed in mafic minerals (primarily olivine). At St Lucia, in the least contaminated rocks, plagioclase reveals assimilation more clearly than pyroxene, probably because it crystallised over a greater range of magmatic evolution, persisting to the most differentiated stages. Hence, comparing olivine and pyroxene $\delta^{18}\text{O}$ values with whole rock $^{87}\text{Sr}/^{86}\text{Sr}$ may be a less effective means to detect small amounts of assimilation than the use of plagioclase $\delta^{18}\text{O}$ data.

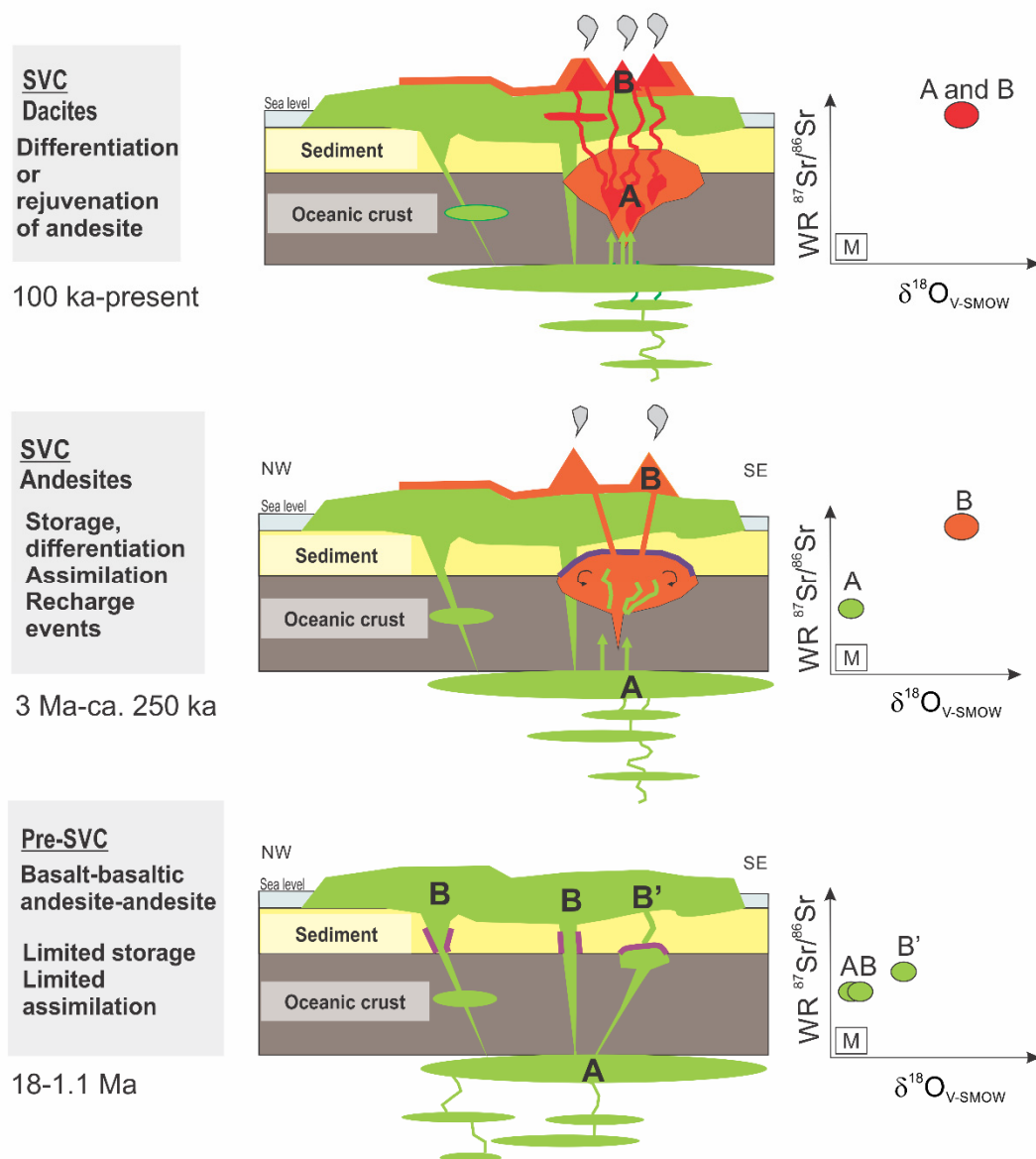


Fig. 3.7. Schematic model for the St Lucia magmatic plumbing system through time to explain the Pre-SVC and SVC whole rock and mineral isotopic compositions. The bottom panel illustrates the storage, intrusion and eruption of the Pre-SVC lavas. The magma storage is limited and/or occurs mostly in the mantle and in the oceanic crust: assimilation of sediment (purple) is limited. The middle panel illustrates the development of a large SVC andesitic complex at shallower depth where active assimilation of sediment takes place. Finally, the upper panel illustrates the evolution of the SVC dacite from the andesite. Minimal or no assimilation occurs at this stage.

3.6 Summary and conclusions

Our new single plagioclase Sr isotopic data and mineral $\delta^{18}\text{O}$ data show that crustal assimilation was important in magma evolution at St Lucia. Correlations of mineral $\delta^{18}\text{O}$ values with whole rock Sr isotopic composition shows that assimilation controls most of the Sr, Nd and Pb isotopic variation in St Lucia lavas. Isotopic variation at St. Lucia replicates most of the range for the whole Lesser Antilles arc, therefore we suggest that up to 20-40% assimilation could be responsible for the unusual diversity of isotopic compositions observed along the arc. Assimilation of such large volumes of sediment within the Lesser Antilles crust may be related to a specific geographic and geodynamic setting. However, similar crustal assimilation could take place in other oceanic arcs where a lack of geochemical contrast between assimilated sediments and the magma and/or the lower amounts of sediments assimilated may make it more challenging to track.

Chapter 4

Seeing through the effects of crust assimilation to assess the source composition beneath the southern Lesser Antilles arc

A version of this chapter has been submitted to *Journal of Petrology* co-authored by Simon Turner, Jon Davidson, Colin Macpherson and Jan Lindsay.

The supplementary data file of this chapter is presented in Appendix C.

Abstract

Assessing the impact of crustal assimilation on the composition of oceanic arc lavas is important if source composition is to be correctly interpreted. This is particularly the case in the Lesser Antilles where lavas encompass a very large range in radiogenic isotope ratios. Here we present new $^{176}\text{Hf}/^{177}\text{Hf}$ and trace element data for a suite of samples from St Lucia, in the southern Lesser Antilles arc, where assimilation of sediments located within the arc crust has been shown to significantly impact Sr-Nd-Pb isotope compositions. We show that a high rate of assimilation ($r = 0.8$) of crustal material is responsible for the co-variation of Th/Th^* , La/Sm , $^{87}\text{Sr}/^{86}\text{Sr}$, $^{206}/^{207}/^{208}\text{Pb}/^{204}\text{Pb}$, $^{143}\text{Nd}/^{144}\text{Nd}$ and $^{176}\text{Hf}/^{177}\text{Hf}$ toward extreme “continental” compositions. Lavas that escaped assimilation have a typical oceanic arc signature and provide the best reflection of source characteristics. They display similar Ba/Th, La/Sm and Nd isotopic composition but slightly more radiogenic Sr and Pb than lavas further north in the arc. Calculations indicate that addition of less than 2 % of the local subducting sediments in the mantle can explain these compositions; this estimate is similar to those previously obtained for the northern arc. Therefore, after removal of the effects of crustal assimilation, St Lucia lavas have only slightly more radiogenic Pb and Sr signatures compared to the northern islands and this can be attributed to differences in the isotopic composition of the subducting sediment rather than greater sediment input, as has been previously proposed. Comparison of St Lucia with the other southern Lesser Antilles islands suggests similar source compositions exist beneath Martinique, St Vincent and maybe Bequia, while a more “continental” source might characterize Ile de Caille, Kick'em Jenny and Grenada.

4.1 Introduction

Global arc studies have shown that oceanic arcs can be divided into two groups based on their trace element and isotope compositions (Hawkesworth et al., 1993). The first group comprises Tonga, Mariana, South Sandwich and the Aleutian arcs which are characterised by compositions often termed “typical oceanic arcs” that have a narrow range of Sr, Nd, Hf and Pb isotope compositions that differ only slightly from mid-oceanic ridge basalts (MORBs). Oceanic arcs from the second group (Java, Banda, Philippines) have more heterogeneous and “continental” isotopic compositions (higher Sr and Pb isotope ratios with lower Nd and Hf isotopic compositions) but also higher light versus middle and heavy rare-earth elements ratios (L/M-HREE) and lower ratios of large-ion lithophile elements versus high field strength elements (LILE/HFSE; e.g. Ba/Th), similar to continental arcs (Hawkesworth et al., 1993). Understanding the origin of the “continental” signature observed in some oceanic arcs is important to assess the crust production and recycling at subduction zones (Davidson and Arculus, 2006).

The Lesser Antilles arc (Fig. 4.1) is a well-known example of an oceanic arc which has a “continental” signature (White and Dupre, 1986; Davidson, 1987; Macdonald et al., 2000; Fig. 4.2). Lavas with “continental” trace element and Sr, Nd, Hf and Pb isotope compositions are restricted to islands from the central-southern segments of the arc, while the northern islands display “typical oceanic arc” compositions. The continental signature observed in some of the lavas from the southern arc, could be explained by the involvement of greater amounts of sediment, or sediment with a more “continental” signature from the subducting slab in the mantle wedge beneath the southern islands compared to their northern neighbours (White and Dupre, 1986; Labanieh et al., 2010; 2012). However, crustal assimilation has been shown to be significant in Martinique and St Lucia which are the two islands displaying the largest isotopic heterogeneities. Therefore, the interpretation of mantle source compositions requires a detailed understanding of the impact of crustal assimilation on both isotope and trace element compositions of the magmas. Such an exercise has been performed for Martinique, where Davidson and Wilson (2011) stripped off the effects of crustal assimilation and other differentiation processes by back-extrapolating major and trace element and isotope differentiation trends to a SiO₂ composition likely to characterize

the primary magmas of the suite ($\text{SiO}_2 = 48 \text{ wt. } \%$). They extended their comparative studies to other islands and proposed that the mantle source beneath Martinique and St Vincent, both from the southern arc, is not very different from the source of the northern islands magmas. This suggests that the north-south trace element and isotopic variations would be almost entirely produced by crustal assimilation.

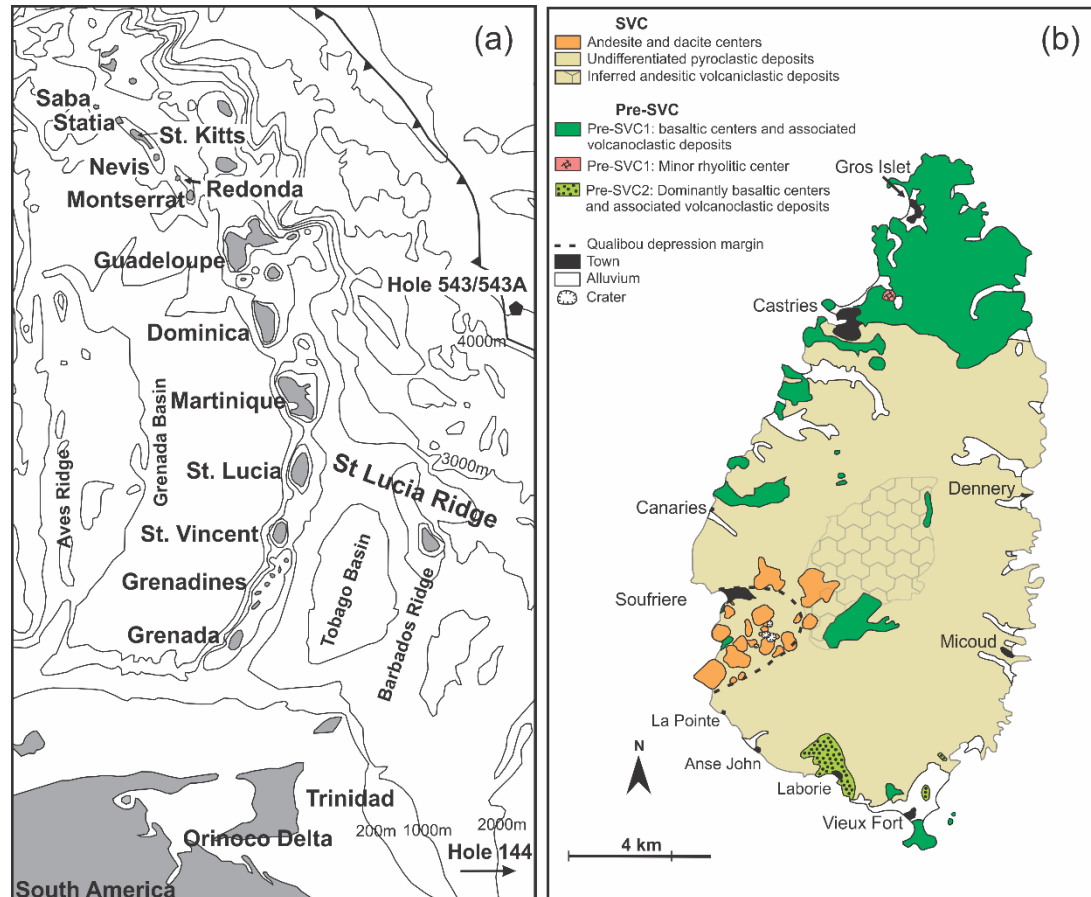


Fig. 4.1. (a) Location of St Lucia on a bathymetric map of the Lesser Antilles arc area modified from Bezard et al. (2014). The location all the islands of the arc, of the Grenada and Tobago basins, as well as The Barbados and St Lucia ridges and the DSDP sites 543 and 144 are also shown (b) geological map of St Lucia modified from Lindsay et al. (2013).

In order to test this hypothesis, we performed a detailed study of lavas from St Lucia. Here, the filtering of crustal assimilation cannot be performed using the back extrapolation method of Davidson and Wilson (2011), because differentiation trends are harder to establish. However, in St Lucia, very good constraints on which lavas are affected by crustal assimilation are available from a study of $\delta^{18}\text{O}$ in phenocrysts (Bezard et al., 2014). This allows comparison of the compositions of lavas that are significantly affected by crustal assimilation and those that are negligibly affected in

order to isolate which elements and isotopes were modified by crustal assimilation. This exercise was carried out for Sr, Pb and Nd isotopes by Bezard et al. (2014), and is extended here to Hf isotopes and trace element compositions to constrain the overall impact of assimilation, the composition of the assimilant and to compare the mantle source characteristics beneath St Lucia with other Lesser Antilles islands.

4.2 Geological setting

The 800 km long Lesser Antilles arc (Fig. 4.1a) results from subduction of the North American Plate under the Caribbean Plate (Fig. 4.1a). The arc was initiated in the late Oligocene (Germa et al., 2011) and is still currently active. It exhibits major geochemical and isotopic differences from north to south. Northern islands are characterised by tholeiitic and calc-alkaline volcanic rocks with very limited isotope and trace element variations (e.g. Sr-Nd isotopes). In contrast, the central and southern sections of the arc have erupted a wider range of magma types, extending to alkaline lavas. These central-southern magmas are characterised by large isotope and trace element variations, ranging from compositions similar to those of the northern islands to compositions more similar to continental crust (Fig. 4.2). This geographic variation has been suggested to reflect physical variations of the arc system (e.g. Van Soest et al., 2000). The first major along-arc difference is the nature of the basement. While the basement in the north is thought to be entirely igneous (intruded through the extended crust of the extinct Cretaceous arc called the Aves ridge; Wadge, 1986), the basement in the central-south of the arc (South of Dominica) is thought to comprise sediments. In this region, magmas intruded through the middle of the Aves ridge sediment-rich forearc basin, splitting it into the Grenada Basin and the Tobago Basin (Speed and Walker, 1991; Aitken et al., 2011). Furthermore, the age of the Lesser Antilles volcanic sequences vary from north to south. the southern islands (Martinique to Grenada) comprise volcanic products as old as ~25 Ma, whereas volcanism in the northern islands only commenced 5.1 Ma ago, due to a westward shift in activity from the now-extinct eastern branch (Eocene to mid-Oligocene) of the arc toward its current position (McCann and Sykes, 1984; Bouysse and Westercamp, 1990). Finally, the amount and the nature of sediment in the trench varies systematically along the arc. While the trench is clearly defined by negative topography in the north, it is entirely filled with sediment in the south, with a well-defined accretionary wedge cropping out

above sea level (at the island of Barbados). This is due to the proximity of the southern arc to extremely high discharges of sediment from South America into the Orinoco and Amazon River deltas (Burke, 1988). This proximity is also reflected in a more terrigenous or “continental” composition of the sediment than in the north (Carpentier et al., 2008).

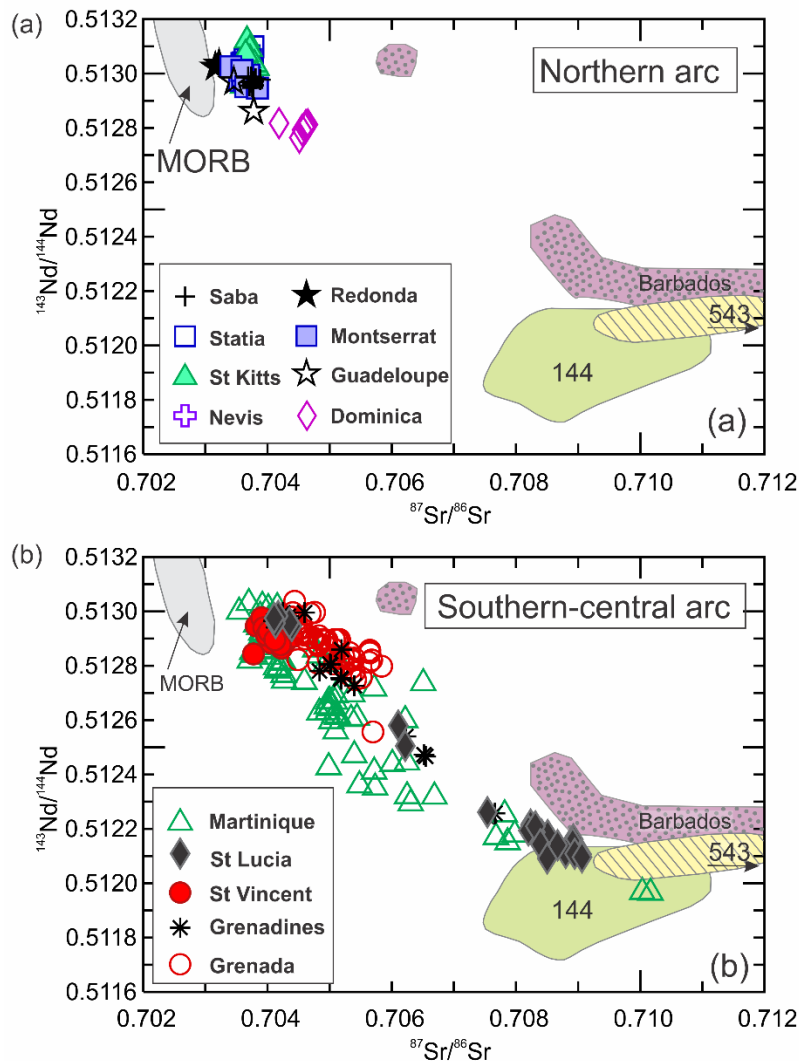


Fig. 4.2. Comparison of Sr, Nd isotopic composition of St Lucia lavas to lavas from the rest of the arc. St Lucia compositions cover most of the arc variations. Data sources; Saba (Sherman, 1992; Van Soest, 2000; Dufrane et al. 2009), Statia (Davidson, 1984; Van Soest, 2000), St Kitts (Van Soest, 2000; Toothhill et al., 2007), Redonda (Davidson, 1984), Montserrat (Davidson, 1984; Van Soest, 2000), Guadeloupe (Van Soest, 2000); Dominica (Davidson, 1984), Martinique (Davidson, 1984; Van Soest, 2000; Labanieh et al., 2010), St Lucia (Bezard et al., 2014), St Vincent (Heat et al., 1998; Van Soest, 2000), Grenadine with Bequia (Smith et al., 1996), Ile de Caille (Turner et al., 1996; Van Soest, 2000) and Kick'em Jenny (Huang et al., 2011), and Grenada (Thirlwall and Graham, 1984; Thirlwall et al., 1996; Van Soest, 2000). MORB field is mid-Atlantic Ridge between 30°N and 30°S (data from PETDB: <http://petdb.org/science.jsp/>). 144 and 543 correspond to Atlantic sediments cored at the front of the

trench at DSDP sites 144, 543 and Barbados corresponds to sediments outcropping on Barbados (Carpentier et al., 2008, 2009).

St Lucia is located between Martinique and St Vincent (Fig. 4.1a) and belongs to the central section of the arc as defined by Macdonald et al. (2000). Current activity is focused within the Qualibou depression (Fig. 4.1b), a large sector collapse in the south-west of the island (Lindsay et al., 2013). St Lucia rocks can be separated into two main groups based on age constraints.

4.2.1. Pre-Soufrière Volcanic Complex

The first and oldest group, termed the Pre-Soufrière Volcanic Complex (Pre-SVC) consists dominantly of eroded basalt, basaltic andesite and andesite centers, with only one rhyolite flow. Rocks in this group are present across the island (Fig. 4.1b) and have been dated by K-Ar to between 15-18 Ma and 3.13 Ma by Briden et al. (1979), Aquater, (1982) and De Kerneizon et al. (1983). Two Pre-SVC basaltic andesite flows, cropping out in the Qualibou depression, in the south-west of the island were dated by K-Ar to between 6.5 ± 0.6 Ma and 5.21 ± 0.15 Ma by Briden et al. (1979) and Aquater (1982) and more recently at 6.64 and 1.10 Ma respectively (Samper et al., 2008). Pre-SVC lavas can be separated into two subgroups on the basis of their Sr-Nd isotopic signatures (Bezard et al., 2014). The first, and main, subgroup (Pre-SVC1) has typical oceanic arc signatures in terms of $^{87}\text{Sr}/^{86}\text{Sr}$ and $^{143}\text{Nd}/^{144}\text{Nd}$ (0.70411-0.70439 and 0.51295-0.51298 respectively). Pre-SVC1 lavas also have Pb isotopes close to typical oceanic arc signatures ($^{206}\text{Pb}/^{204}\text{Pb}$, $^{207}\text{Pb}/^{204}\text{Pb}$ and $^{208}\text{Pb}/^{204}\text{Pb}$ range from 19.291-19.341, 15.747-15.748, 38.96-39.11 respectively). According to mineral $\delta^{18}\text{O}$, this group is thought to be minimally affected by assimilation of the arc crust (Bezard et al., 2014). The second subgroup (Pre-SVC2) has more “continental” Sr-Nd isotopic compositions (0.70611-0.70622 and 0.51251-0.51258, respectively; Pb isotopes were not analysed) which vary with indexes of differentiation such as SiO_2 and with mineral $\delta^{18}\text{O}$ values which indicates larger contributions of assimilated sediment within the arc crust.

4.2.2 Soufriere Volcanic Complex

The second, younger group of volcanic rocks on the island is the Soufriere Volcanic Complex (SVC). It comprises dissected high-silica andesite and dacite centers with associated volcanoclastic units (Fig. 4.1b) dated between 3 Ma to Recent. Lindsay et al. (2013) separated the activity of the SVC into three different periods. The first period of eruption occurred between 3 Ma and ca. 250 Ka and produced the andesitic stratovolcanoes of the SVC as well as andesitic to dacitic pyroclastic deposits. This was followed by a major sector collapse between 250-100 Ka resulting in the Qualibou depression and uncovering the SVC basement made of mafic Pre-SVC units. Finally, dacitic domes and pyroclastic deposits were emplaced in the region of the depression during two main eruptive periods: 100-50 Ka and 20 Ka-present.

The SVC plumbing system was investigated by Schmitt et al. (2010) who proposed an evolutionary model based on U-Th and (U-Th)/He zircon ages. Their results indicated episodic thermal and mechanical rejuvenation within a complex of a long-lived intermediate mid-crustal plutons under the Qualibou depression. Compared to Pre-SVC lavas, SVC volcanic rocks display extreme Sr-Pb-Nd isotopic compositions displaced toward continental crust, with high Sr-Pb ($^{87}\text{Sr}/^{86}\text{Sr} = 0.70754\text{-}0.70906$; $^{206}\text{Pb}/^{204}\text{Pb} = 19.721\text{-}19.797$, $^{207}\text{Pb}/^{204}\text{Pb} = 15.826\text{-}15.846$, $^{208}\text{Pb}/^{204}\text{Pb} = 39.438\text{-}39.528$) and low Nd isotopic ratios (0.51210-0.51226; Bezard et al., 2014). This shift to continental signatures, correlates with an increase in SiO_2 and is associated with high $\delta^{18}\text{O}$ values in phenocrysts, supporting sediment assimilation (Bezard et al., 2014).

4.3 Sampling and analytical procedures

4.3.1 Samples

A total of 32 lava and pumice samples from St Lucia were selected to encompass the whole range of major element compositions in both the Pre-SVC (basalt to rhyolite) and the SVC (high silica andesite to dacite). These were analysed for their trace elements and 26 were selected for Hf isotope analyses. All the samples have been previously analysed for major elements (Davidson., 1984; Lindsay et al., 2013) and Sr-Nd-Pb isotopes (Bezard et al., 2014). Furthermore, 2 samples previously analysed

for trace elements (Lindsay et al., 2013) by LA-ICPMS were re-analysed to maintain an internally consistent dataset. For both trace element and Hf isotopes, all samples were split and weathered surfaces were discarded before crushing and milling.

4.3.2 Trace elements

30 samples were analysed at Durham University and 2 samples analysed at the Geochemical Analysis Unit (GAU) at Macquarie University.

At both Durham and Macquarie, samples were analysed twice: once on crushed powder and once on fused glass to obtain Zr, Hf, U and Ti concentrations in zircon-bearing rocks. At Durham trace elements were analysed in solution by inductively coupled plasma mass spectrometry (ICP-MS) using the Thermo Scientific X-Series Element 2 instrument using the technique described by Ottley et al. (2003). In all zircon-bearing felsic samples, rock powders were also fused with Lithium tetraborate flux and subsequently crushed and analysed again in solution. At Macquarie, rock powders were analysed in solution using an Agilent 7500 Series ICP-MS instrument. As in Durham, the rock powders were fused with Lithium tetraborate flux to obtain Zr, Hf and Ti concentrations. Fused disks were analysed using a NewWave UP-213 laser ablation system linked to an Agilent 7700 Series ICP-MS system. Ablation of the samples was performed in a helium-filled chamber using a frequency of 5 Hz and an ablation spot size of 50 μm or a line 240 μm long. CaO from XRF analyses was used as an internal standard. At both Durham and Macquarie Universities, the reproducibility was checked by analysing three replicates of the same sample in each batch. Standard deviation between the three replicates of each batch was less than 3% for all elements presented. The inter-lab reproducibility of the data was verified by analysing BHVO-1 or BHVO-2 (which are identical for the elements presented, except for Pb) in every batch of sample (results are provided in the Supplementary file, Appendix C). Differences between our measured BHVO-1 concentrations in every batch and the Georem preferred values (<http://georem.mpch-mainz.gwdg.de>) are less than 5% for all elements presented.

Table 4.1. Major and trace element contents and Sr-Nd-Pb-Hf isotopic compositions of St Lucia.

Group:	SVC	SVC	SVC	SVC	SVC	SVC	SVC
Sample:	SL-83-03	SL-83-08	SL-83-12	SL-83-15	SL-83-16	SL-83-17	SL-83-19
SiO ₂	64.02	66.93	66.65	62.10	64.05	61.51	65.52
TiO ₂	0.49	0.42	0.43	0.55	0.50	0.61	0.39
Al ₂ O ₃	17.77	16.97	16.96	17.91	17.29	18.07	17.20
FeO tot	4.67	3.54	3.72	5.13	4.32	5.32	3.88
MnO	0.13	0.12	0.12	0.17	0.13	0.14	0.12
MgO	1.94	1.43	1.44	2.26	2.47	2.60	1.57
CaO	5.79	5.36	5.29	6.89	6.28	6.73	5.62
Na ₂ O	3.13	3.07	3.18	2.85	2.92	2.71	3.44
K ₂ O	1.42	1.67	1.68	1.44	1.46	1.57	1.73
P ₂ O ₅	0.11	0.10	0.11	0.12	0.10	0.14	0.10
LOI	1.75	1.19	1.23	3.45	0.16	1.66	0.37
Ti	4600	4110	4031	4952	4745	5573	3665
V	65	21	19	32	48	36	23
Ga	17.65	17.66	17.66	17.40	16.78	17.78	17.12
Rb	66.99	78.00	77.68	60.30	59.45	70.72	75.32
Sr	325	313	314	298	296	310	319
Y	20.14	16.28	16.22	16.40	17.59	17.68	16.36
Zr	110	128	129	117	111	128	113
Nb	5.39	7.38	7.22	5.17	6.28	6.81	5.80
Ba	440	515	514	411	425	425	470
La	18.66	21.78	22.38	16.94	17.90	19.29	19.41
Ce	33.93	41.55	44.18	33.08	34.91	37.33	37.25
Pr	4.35	4.85	5.27	3.96	4.22	4.55	4.34
Nd	16.38	17.49	18.68	14.45	15.63	16.61	15.69
Sm	3.21	3.37	3.48	3.00	3.19	3.36	2.97
Eu	0.91	0.88	0.88	0.86	0.85	0.90	0.83
Gd	3.19	3.07	3.09	2.88	3.02	3.16	2.83
Tb	0.50	0.47	0.47	0.46	0.49	0.48	0.42
Dy	2.82	2.51	2.54	2.52	2.66	2.72	2.39
Ho	0.60	0.51	0.51	0.52	0.54	0.57	0.50
Er	1.76	1.46	1.46	1.52	1.57	1.60	1.45
Tm	0.27	0.24	0.23	0.24	0.25	0.26	0.24
Yb	1.78	1.57	1.51	1.55	1.63	1.71	1.59
Lu	0.30	0.26	0.27	0.26	0.27	0.29	0.28
Hf	2.89	3.32	3.42	2.98	2.87	3.14	2.94
Ta	0.39	0.55	0.60	0.36	0.48	0.47	0.48
Pb	12.12	15.93	15.28	10.81	12.28	16.50	15.40
Th	5.69	7.19	7.27	5.29	5.66	6.11	6.45
U	2.04	2.70	2.63	1.86	1.99	2.12	2.37
La/Sm	5.81	6.46	6.44	5.66	5.62	5.74	6.53
Th/Th*	0.90	0.90	0.93	0.90	0.92	0.96	0.91
¹⁴³ Nd/ ¹⁴⁴ Nd	0.512261	0.512161	0.512147	0.512169	0.512161	0.512106	0.512180
⁸⁷ Sr/ ⁸⁶ Sr	0.707542	0.708925	0.708914	0.708346	0.70843	0.709056	0.7084115
²⁰⁶ Pb/ ²⁰⁴ Pb	19.728	19.721		19.760	19.737	19.797	19.748
²⁰⁷ Pb/ ²⁰⁴ Pb	15.826	15.830		15.837	15.833	15.845	15.837
²⁰⁸ Pb/ ²⁰⁴ Pb	39.438	39.457		39.467	39.466	39.489	39.479
¹⁷⁶ Hf/ ¹⁷⁷ Hf	0.282603	0.282452		0.282535	0.282527	0.282419	0.282476

Major element concentrations are from Davidson (1987) and Lindsay et al. (2013). Sr, Nd and Pb isotope ratios are from Bezard et al. (2014).

Table 4.1. (continued).

Group:	SVC	SVC	SVC	SVC	SVC	SVC	SVC
Sample:	SL-83-24	SL-JL-22	SL-JL-23	SL-JL-24	SL-JL-33	SL-JL-51	SL-JL-57
SiO ₂	65.67	63.56	63.94	67.08	67.12	66.39	66.30
TiO ₂	0.43	0.52	0.57	0.38	0.38	0.44	0.42
Al ₂ O ₃	17.02	17.83	18.51	17.36	17.07	17.14	18.04
FeO tot	4.02	4.20	4.26	3.34	3.39	3.75	3.84
MnO	0.12	0.10	0.09	0.09	0.09	0.10	0.09
MgO	1.42	2.70	2.05	1.25	1.43	1.63	1.32
CaO	5.61	6.45	6.06	5.27	5.31	5.57	5.42
Na ₂ O	3.48	3.06	2.89	3.31	3.40	3.12	3.04
K ₂ O	1.66	1.46	1.48	1.79	1.69	1.74	1.44
P ₂ O ₅	0.11	0.13	0.15	0.13	0.12	0.12	0.08
LOI	0.90	0.40	1.28	1.51	1.58	0.71	1.99
Ti	3920	5227	5482	3576	3646	4120	3125
V	23	44	26	8	12	22	11
Ga	16.21	16.69	17.77	16.32	16.56	16.78	17.07
Rb	67.02	59.32	63.65	73.44	73.80	77.38	69.52
Sr	287	298	309	303	292	295	299
Y	13.56	16.86	16.74	15.00	14.79	16.51	15.21
Zr	108	115	126	118	117	125	113
Nb	5.56	6.44	6.67	6.66	5.92	7.43	6.13
Ba	436	431	424	448	421	510	489
La	18.60	18.76	20.91	21.47	25.98	24.47	19.98
Ce	34.11	34.23	37.44	39.41	41.57	39.26	38.24
Pr	3.97	4.12	4.66	4.56	4.90	4.62	4.65
Nd	14.43	15.16	17.23	16.57	17.33	16.86	16.90
Sm	2.70	3.07	3.38	3.05	3.18	3.28	3.19
Eu	0.76	0.84	0.93	0.82	0.80	0.80	0.85
Gd	2.52	2.91	3.26	2.78	2.76	3.01	2.91
Tb	0.38	0.45	0.48	0.42	0.40	0.44	0.43
Dy	2.09	2.56	2.63	2.28	2.21	2.44	2.28
Ho	0.43	0.54	0.54	0.47	0.44	0.50	0.46
Er	1.25	1.54	1.53	1.34	1.30	1.42	1.30
Tm	0.21	0.25	0.24	0.22	0.21	0.23	0.21
Yb	1.34	1.60	1.55	1.45	1.41	1.50	1.33
Lu	0.22	0.28	0.25	0.25	0.24	0.25	0.22
Hf	2.83	2.94	3.23	3.07	2.99	3.17	2.91
Ta	0.45	0.46	0.45	0.49	0.45	0.55	0.43
Pb	12.46	12.21	11.58	14.45	14.41	14.35	13.05
Th	5.82	5.70	5.49	6.50	7.14	6.82	6.22
U	2.23	2.02	1.96	2.47	2.51	2.53	2.09
La/Sm	6.88	6.12	6.19	7.03	8.16	7.46	6.26
Th/Th*	0.87	0.91	0.90	0.91	1.01	0.89	0.93
¹⁴³ Nd/ ¹⁴⁴ Nd	0.512215	0.512178	0.512111	0.512101	0.512177	0.512108	0.512140
⁸⁷ Sr/ ⁸⁶ Sr	0.708237	0.708402	0.708801	0.709049	0.708511	0.708946	0.708672
²⁰⁶ Pb/ ²⁰⁴ Pb	19.730	19.753	19.779	19.770	19.759	19.766	19.773
²⁰⁷ Pb/ ²⁰⁴ Pb	15.828	15.832	15.836	15.834	15.832	15.834	15.840
²⁰⁸ Pb/ ²⁰⁴ Pb	39.446	39.471	39.479	39.484	39.473	39.484	39.489
¹⁷⁶ Hf/ ¹⁷⁷ Hf	0.282554	0.282475	0.282455	0.282427	0.282485	0.282462	0.282460

Major element concentrations are from Davidson (1987) and Lindsay et al. (2013). Sr, Nd and Pb isotope ratios are from Bezard et al. (2014).

Table 4.1. (continued).

Group:	SVC	SVC	SVC	SVC	SVC	SVC	Pre-SVC1
Sample:	SL-JL-61	SL-JL-79	SL-JL-83	SL-JL-84	SL-JL-1	SL-JL-2	SL-83-23
SiO ₂	67.47	65.57	66.49	64.25	65.37	62.82	53.55
TiO ₂	0.36	0.39	0.41	0.45	0.46	0.57	1.26
Al ₂ O ₃	17.27	17.20	17.31	17.38	17.60	18.66	17.84
FeO tot	3.44	4.33	3.86	4.24	4.07	4.81	9.24
MnO	0.08	0.11	0.10	0.10	0.10	0.11	0.17
MgO	1.06	1.32	1.22	2.45	2.32	2.22	3.57
CaO	5.32	5.45	5.55	6.26	5.25	6.41	9.36
Na ₂ O	3.13	3.77	3.24	3.15	3.01	2.80	3.10
K ₂ O	1.76	1.74	1.70	1.60	1.68	1.47	0.73
P ₂ O ₅	0.11	0.12	0.11	0.11	0.12	0.14	0.16
LOI	1.29	1.60	0.14	0.46	1.48	1.25	1.59
Ti	3325	3389	4366	3782	2922	3706	11690
V	7	11	43	20	45	45	292
Ga	16.63	16.15	16.58	17.22	17.83	18.73	17.22
Rb	73.58	71.65	70.73	73.49	68.47	63.51	13.49
Sr	309	296	298	315	251	288	193
Y	14.94	13.09	15.33	16.08	15.71	19.51	30.26
Zr	115	115	104	110	140	145	105
Nb	6.34	5.62	5.44	5.82	6.02	6.12	3.00
Ba	454	454	430	476	472	436	163
La	21.54	19.82	18.27	19.17	19.59	20.51	5.74
Ce	37.81	34.82	33.80	38.97	38.63	38.00	14.38
Pr	4.53	4.08	4.11	4.51	4.49	4.86	2.44
Nd	16.20	14.60	14.86	16.43	15.55	17.20	12.12
Sm	2.96	2.74	2.88	3.03	3.03	3.44	3.55
Eu	0.83	0.78	0.78	0.80	0.92	1.04	1.12
Gd	2.69	2.46	2.71	2.82	2.78	3.30	4.44
Tb	0.40	0.37	0.41	0.42			0.79
Dy	2.23	2.03	2.27	2.29	2.44	2.93	5.08
Ho	0.46	0.41	0.46	0.48	0.51	0.62	1.09
Er	1.32	1.17	1.33	1.37	1.46	1.76	3.06
Tm	0.22	0.19	0.22	0.22			0.53
Yb	1.42	1.26	1.47	1.44	1.47	1.70	3.21
Lu	0.24	0.20	0.24	0.25	0.23	0.26	0.53
Hf	2.96	2.87	2.66	2.75	3.78	3.90	2.86
Ta	0.48	0.42	0.41	0.41	0.46	0.41	0.23
Pb	14.28	13.24	11.59	13.51	15.42	12.19	4.13
Th	6.44	6.01	5.87	6.64	8.19	7.04	1.28
U	2.47	2.24	2.01	2.20	2.70	2.14	0.63
La/Sm	7.27	7.24	6.35	6.33	6.47	5.95	1.62
Th/Th*	0.89	0.88	0.94	0.97	1.06	1.08	0.60
¹⁴³ Nd/ ¹⁴⁴ Nd	0.512096	0.512187	0.512194	0.512209	0.512143	0.512091	
⁸⁷ Sr/ ⁸⁶ Sr	0.709063	0.708313	0.708202	0.708313	0.708393	0.708504	
²⁰⁶ Pb/ ²⁰⁴ Pb	19.782		19.758		19.757		
²⁰⁷ Pb/ ²⁰⁴ Pb	15.846		15.835		15.838		
²⁰⁸ Pb/ ²⁰⁴ Pb	39.528		39.483		39.489		
¹⁷⁶ Hf/ ¹⁷⁷ Hf	0.282376	0.282373	0.282560	0.282530	0.282546	0.2825189	

Major element concentrations are from Davidson (1987) and Lindsay et al. (2013). Sr, Nd and Pb isotope ratios are from Bezard et al. (2014).

Table 4.1. (continued).

Group:	Pre-SVC1	Pre-SVC2	Pre-SVC1	Pre-SVC1	Pre-SVC2	Pre-SVC2	Pre-SVC1
Sample:	SL-83-25	SL-83-26	SL-83-30	SL-83-32	SL-83-38	SL-83-39	SL-83-40
SiO ₂	55.76	53.47	55.88	57.31	54.08	57.39	53.46
TiO ₂	1.52	0.76	1.15	0.64	0.68	0.70	0.77
Al ₂ O ₃	15.12	18.35	15.38	18.99	21.91	17.08	19.19
FeO tot	10.73	8.13	11.04	8.04	6.58	7.27	8.93
MnO	0.20	0.20	0.22	0.25	0.16	0.18	0.20
MgO	3.51	4.52	3.68	2.20	2.08	3.94	3.71
CaO	7.41	10.24	7.48	7.70	9.76	8.53	9.24
Na ₂ O	3.36	2.76	3.22	3.45	3.16	2.64	2.96
K ₂ O	1.00	0.59	0.58	0.34	0.77	1.38	0.46
P ₂ O ₅	0.21	0.08	0.14	0.18	0.08	0.07	0.08
LOI	3.49	0.33	2.22	2.47	1.00	1.24	0.76
Ti	13800	6999	10280	5959	6186	6388	7212
V	348	235	296	52	132	198	198
Ga	17.20	15.63	16.39	17.15	16.89	15.40	16.94
Rb	15.85	34.63	11.05	5.71	25.06	48.58	12.94
Sr	190	195	173	238	238	174	205
Y	38.72	19.69	28.38	24.36	18.15	22.28	19.92
Zr	134	72	81	81	67	96	54
Nb	3.85	2.06	1.96	2.87	1.74	2.42	1.68
Ba	226	211	150	100	199	283	129
La	7.24	7.05	4.58	5.02	6.00	8.22	3.95
Ce	18.14	14.58	11.58	13.02	12.81	17.14	9.51
Pr	3.05	2.06	2.01	2.26	1.87	2.43	1.60
Nd	15.23	9.08	10.37	11.45	8.55	10.70	7.80
Sm	4.46	2.38	3.21	3.25	2.36	2.71	2.31
Eu	1.32	0.78	1.12	1.22	0.87	0.80	0.88
Gd	5.63	2.92	4.11	3.76	2.95	3.43	2.91
Tb	1.01	0.52	0.75	0.65	0.51	0.59	0.53
Dy	6.38	3.34	4.84	4.11	3.27	3.70	3.41
Ho	1.38	0.70	1.05	0.89	0.69	0.79	0.74
Er	3.87	1.98	2.93	2.51	1.90	2.20	2.05
Tm	0.65	0.33	0.49	0.43	0.33	0.39	0.34
Yb	4.02	2.08	2.99	2.80	2.04	2.35	2.17
Lu	0.64	0.34	0.49	0.47	0.32	0.38	0.35
Hf	3.65	2.03	2.28	2.16	1.89	2.63	1.59
Ta	0.29	0.15	0.16	0.20	0.14	0.18	0.13
Pb	5.05	4.89	6.19	3.54	3.60	6.55	2.62
Th	1.71	2.41	0.94	0.72	2.11	3.32	0.96
U	0.86	0.88	0.52	0.39	0.79	1.30	0.44
La/Sm	1.63	2.97	1.42	1.55	2.54	3.04	1.71
Th/Th*	0.58	0.84	0.51	0.55	0.80	0.82	0.61
¹⁴³ Nd/ ¹⁴⁴ Nd	0.512946	0.512505				0.512580	
⁸⁷ Sr/ ⁸⁶ Sr	0.704394	0.706219				0.706106	
²⁰⁶ Pb/ ²⁰⁴ Pb	19.291						
²⁰⁷ Pb/ ²⁰⁴ Pb	15.748						
²⁰⁸ Pb/ ²⁰⁴ Pb	38.930						
¹⁷⁶ Hf/ ¹⁷⁷ Hf	0.283027	0.282755				0.2828024	

Major element concentrations are from Davidson (1987) and Lindsay et al. (2013). Sr, Nd and Pb isotope ratios are from Bezard et al. (2014).

Table 4.1. (continued).

Group	Pre-SVC1	Pre-SVC1	Pre-SVC1	Pre-SVC1
Sample:	SL-83-41	SL-83-42	SL-83-44	SL-83-45
SiO ₂	61.38	50.90	51.77	71.88
TiO ₂	0.53	0.76	0.78	0.28
Al ₂ O ₃	16.62	22.11	18.87	13.44
FeO tot	7.66	7.75	8.41	4.23
MnO	0.22	0.20	0.18	0.17
MgO	2.10	2.72	5.14	0.21
CaO	6.09	11.68	11.02	2.37
Na ₂ O	3.71	2.51	2.47	4.97
K ₂ O	0.68	0.43	0.34	1.92
P ₂ O ₅	0.15	0.08	0.09	0.05
LOI	1.99	1.43	0.95	2.49
Ti	4887	6973	6974	2507
V	52	207	236	<1
Ga	15.42	16.67	15.46	17.28
Rb	20.94	10.00	7.71	45.21
Sr	228	221	178	103
Y	21.67	16.92	17.63	57.63
Zr	65	44	49	209
Nb	2.58	1.20	1.11	4.71
Ba	157	79	80	324
La	5.54	2.80	3.34	12.32
Ce	13.63	7.10	8.08	29.38
Pr	2.25	1.25	1.36	4.93
Nd	10.91	6.44	6.75	23.56
Sm	2.94	1.98	2.03	6.62
Eu	1.01	0.79	0.74	1.39
Gd	3.38	2.58	2.57	7.89
Tb	0.58	0.46	0.46	1.44
Dy	3.64	2.99	2.98	9.34
Ho	0.77	0.64	0.65	2.01
Er	2.17	1.79	1.80	5.76
Tm	0.38	0.30	0.30	1.01
Yb	2.40	1.81	1.92	6.32
Lu	0.40	0.29	0.31	1.03
Hf	1.85	1.30	1.41	6.02
Ta	0.19	0.11	0.11	0.36
Pb	3.50	1.67	2.31	6.39
Th	0.78	0.49	0.70	3.30
U	0.44	0.27	0.28	2.01
La/Sm	1.88	1.41	1.65	1.86
Th/Th*	0.45	0.52	0.71	0.59
¹⁴³ Nd/ ¹⁴⁴ Nd	0.512958	0.512983	0.512957	0.512975
⁸⁷ Sr/ ⁸⁶ Sr	0.704354	0.704174	0.704132	0.704109
²⁰⁶ Pb/ ²⁰⁴ Pb			19.341	
²⁰⁷ Pb/ ²⁰⁴ Pb			15.747	
²⁰⁸ Pb/ ²⁰⁴ Pb			39.110	
¹⁷⁶ Hf/ ¹⁷⁷ Hf	0.2830812	0.2830317	0.283116	0.2831556

Major element concentrations are from Davidson (1987) and Lindsay et al. (2013). Sr, Nd and Pb isotope ratios are from Bezard et al. (2014).

4.3.3 Hf isotopes

For Hf isotopes, 20 samples were analysed by plasma ionisation multicollector mass spectrometry (PIMMS) using the Thermo Scientific Neptune instrument at Durham and 6 samples were analysed using the same method but using a Nu plasma instrument at Macquarie. At both Durham and Macquarie, the measurements were made in static-collection mode and mass bias was corrected using a $^{179}\text{Hf}/^{177}\text{Hf}$ ratio of 0.7325 and an exponential law. At Durham, 10 JMC475 solutions were analysed during the analytical session (Details are presented in the supplementary data file, Appendix C). The average $^{176}\text{Hf}/^{177}\text{Hf}$ was 0.282144 ± 0.000006 (2sd). $^{176}\text{Hf}/^{177}\text{Hf}$ ratios are reported relative to the JMC475 standard value of 0.282160 (Nowell et al., 1998). The $^{176}\text{Hf}/^{177}\text{Hf}$ ratios of the two international rock standards BIR-1 and BHVO-1 analysed were 0.283239 and 0.283105, respectively. At Macquarie, 4 JMC475 solutions were analysed during the analytical session. The average was 0.282162 ± 0.000017 (2sd) which is in very good agreement with the accepted value. The $^{176}\text{Hf}/^{177}\text{Hf}$ of BHVO-1 was 0.2831074, which is in excellent agreement with Weiss et al. (2007) (0.283106 ± 12 ; 2sd) and with the BHVO-1 composition obtained in Durham which demonstrates the excellent inter-lab reproducibility.

4.4 Results

New trace element and Hf isotope data are presented in Table 4.1 along with the corresponding major elements (Davidson, 1987; Lindsay et al., 2013) and Sr, Nd and Pb isotope ratios (Bezard et al., 2014).

4.4.1 Trace elements

Pre-SVC and SVC lavas display classic arc trace element signatures with enrichment in LILE and depletion of HFSE relative to the REE. However, in detail, distinctions exist, not only between the Pre-SVC and SVC lavas, but also between the Pre-SVC1 and Pre-SVC2 samples (Fig. 4.3). When normalised to chondrite, Pre-SVC1 lavas (Fig. 4.3a, b) display negative Th anomalies with $\text{Th}/\text{Th}^* (\text{Th}_\text{N} / ((\text{Ba}_\text{N} + \text{U}_\text{N})/2))$ between 0.45-0.71, variable Ba/Th ratios (98-200) and a flat REE pattern with La/Sm, La/Yb, Dy/Dy* ($= (\text{Dy}_\text{N}) / (\text{La}_\text{N}^{(4/13)} * \text{Yb}_\text{N}^{(9/13)})$) and Dy/Yb ranging between 1.4-19, 1.5-2.3, 0.87-1.07 and 1.47-1.65 respectively. Compared to Pre-SVC1, Pre-SVC2 (Fig.

4.3c and d) lavas have slightly higher Th/Th^* (0.80-0.84) lower Ba/Th (85-95) and slightly enriched LREE/M-HREE with La/Sm , La/Yb , Dy/Dy^* and Dy/Yb ranging between 2.5-3, 2.9-3.5, 0.79-0.85 and 1.58-1.6, respectively. Samples from the SVC (Fig. 4.3e, f) plot within a very narrow compositional range. They have negligible Th anomaly ($\text{Th}/\text{Th}^*=0.87\text{-}1.08$), low Ba/Th (58-79) and a REE pattern highly enriched in LREE compared with M-HREE, with La/Sm , La/Yb , Dy/Dy^* and Dy/Yb between 5.6-8.2, 10.5-18.4, 0.47-0.59, 1.51-1.72, respectively.

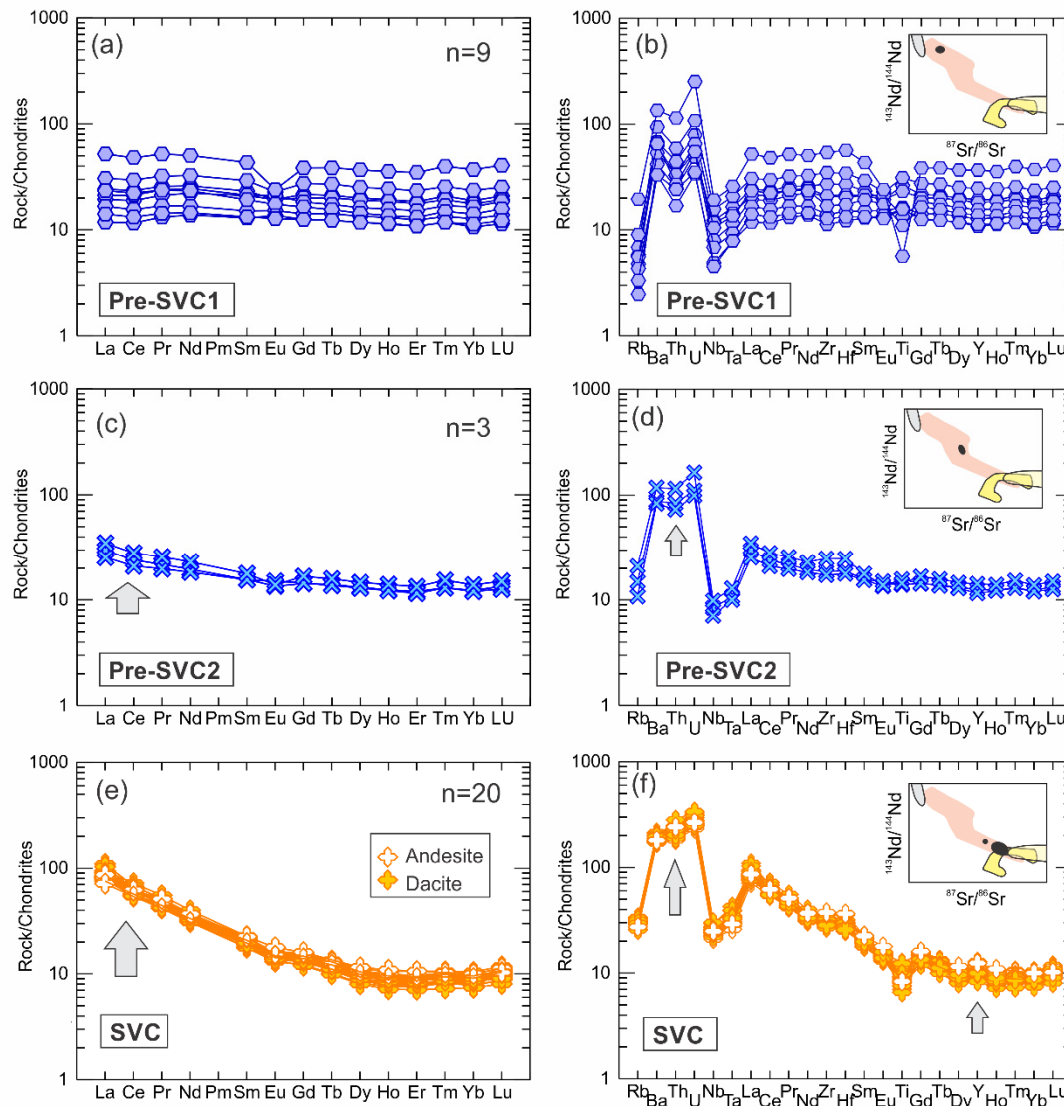


Fig. 4.3. Trace element composition of Pre-SVC1, Pre-SVC2 and SVC lavas. Rare earth element (a, c, e) and multi-element (b, d, f) diagrams show concentrations normalised to chondrite C1 of Sun and McDonough (1989). Insets show the position of the Pre-SVC1, 2 and SVC Sr-Nd isotopic composition compared to MORB; sediments from sites DSDP 543 and 144 and arc field shown in Fig. 4.2.

4.4.2 Hf isotopes

Hf isotope ratios (Fig. 4.4b) also differ between the three groups defined by the Sr-Nd-Pb isotopes (Fig. 4.4a). Pre-SVC1 samples have typical oceanic arc isotopic signatures with $^{176}\text{Hf}/^{177}\text{Hf}$ ranging between 0.283027 and 0.283156. Pre-SVC2 lavas extend toward some more radiogenic signatures with $^{176}\text{Hf}/^{177}\text{Hf}$ ranging between 0.282755 and 0.282802. Finally, all the SVC samples have very radiogenic signatures with $^{176}\text{Hf}/^{177}\text{Hf}$ between 0.282419 and 0.282603.

4.5 Crustal assimilation control on magma compositions

4.5.1 Impact of crustal assimilation on $^{176}\text{Hf}/^{177}\text{Hf}$

Two principal factors are capable of producing variations in the isotopic compositions of arc magmas: (1) variation in the nature and amount of the subducted slab component(s) added to the source and (2) changes in the amount of crustal material assimilation. Bezard et al. (2014) showed that on St Lucia, Sr-Pb-Nd isotope variations correlate with indices of differentiation and also with a clear departure from the mantle range of phenocryst $\delta^{18}\text{O}$ values providing unequivocal evidence for crustal assimilation. Given that Hf isotopes correlate with Nd, Sr and Pb isotopes, they should then also be controlled by assimilation and their variations should also correlate with an index of differentiation. This is confirmed when Hf isotopes are plotted against SiO_2 (Fig. 4.5a) revealing similar trends to that shown by $^{143}\text{Nd}/^{144}\text{Nd}$ versus SiO_2 (Fig. 4.5b). Pre-SVC1 shows negligible variation in $^{176}\text{Hf}/^{177}\text{Hf}$ trend while Pre-SVC2 and SVC lavas show a clear negative correlation. Since the two trends back project toward a similar end member, the two groups seem to share a similar primitive/parental magma, as suggested by Sr-Nd isotopes. The Pre-SVC1 trend, shows no correlation between radiogenic isotope compositions and indices of differentiation which suggests closed system fractional crystallisation, while the positive correlation formed by SVC and Pre-SVC2 samples argues for assimilation during differentiation.

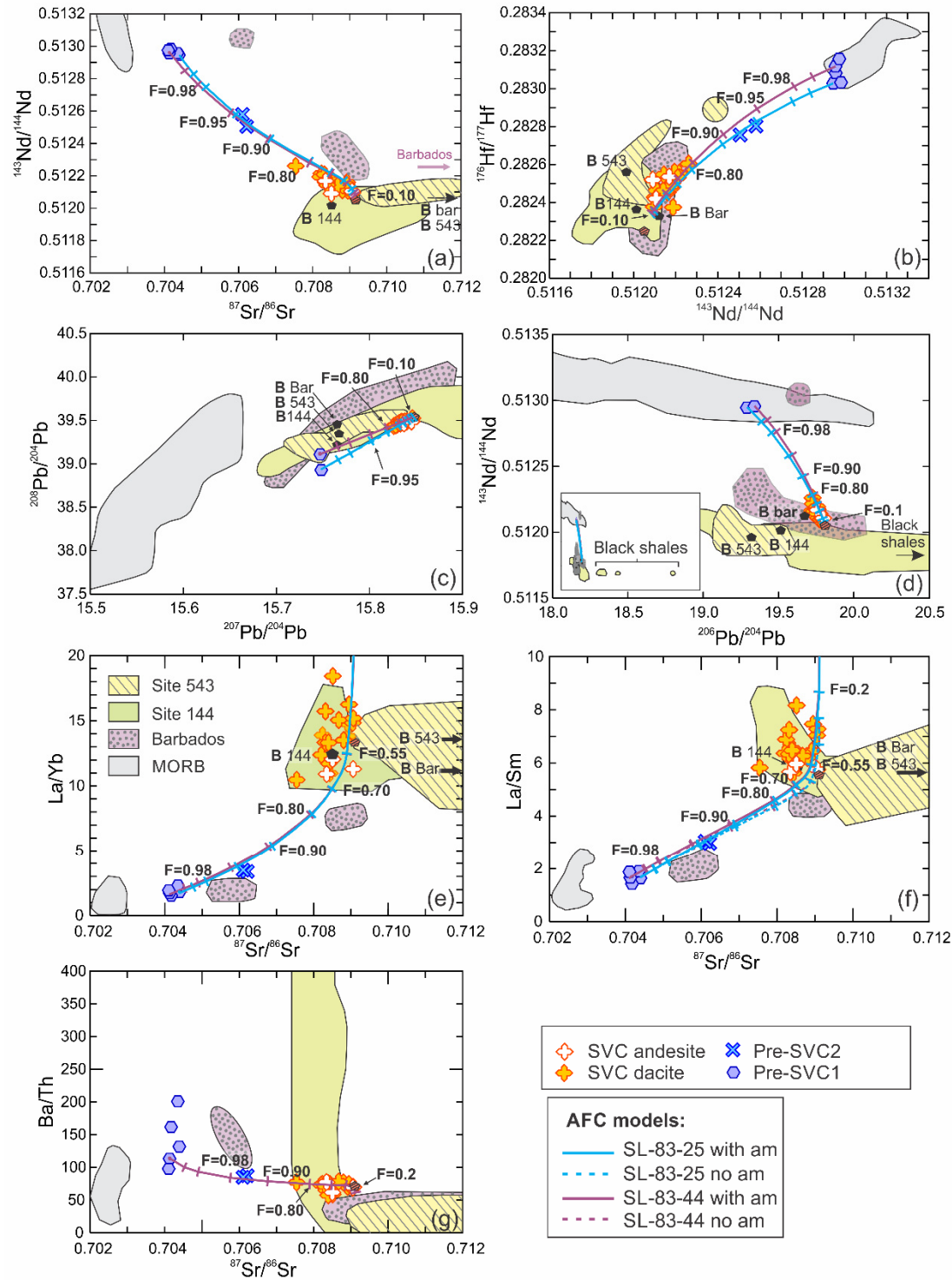


Fig. 4.4. Sr, Nd, Hf, Pb isotopic composition of St Lucia lavas with AFC models. See text for description of parameters used. Full model parameters and data are presented in supplementary data file (Appendix C). SL-83-25 with am = AFC model using SL-83-25 isotopic composition and least square model #2. SL-83-25 no am = AFC model using SL-83-25 isotopic composition and least square model #1. SL-83-44 with am/no am models use the isotopic composition of SL-83-44 lava. F = amount of residual melt. MORB, local sediment fields as well as the bulk sediment of each locality) are also shown (data source as in Fig. 4.2). B Bar, B 543 and B 144 = the bulk sediment composition of Barbados, DSDP site 543

and DSDP site 144 respectively. Red and black striped pentagons represent the assimilant composition. The inset in panel (d) shows the very radiogenic Pb composition of the black shales from DSDP site 144, making them unlikely to be the assimilant.

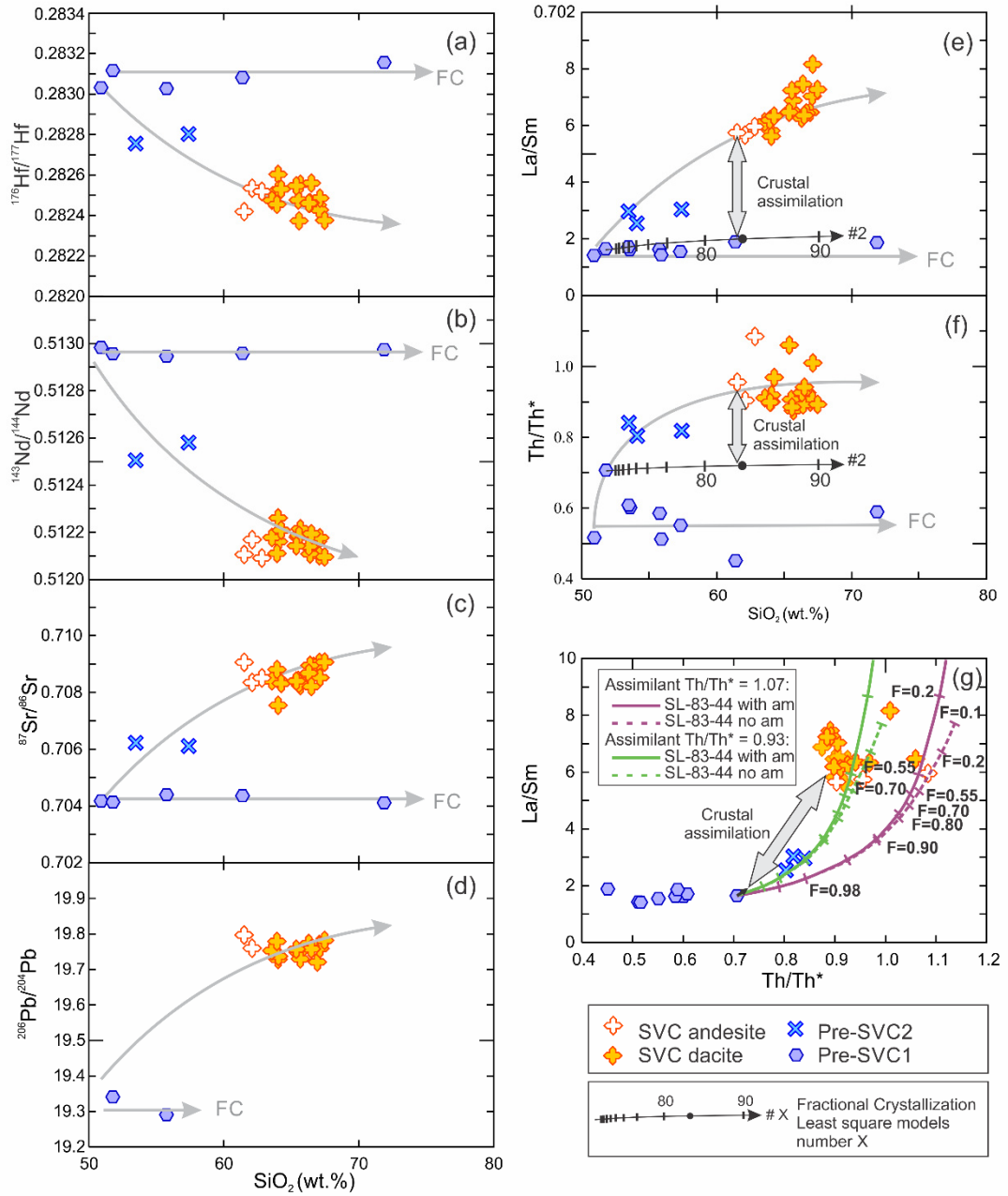


Fig. 4.5. Hf, Nd, Sr, Pb isotopes and La/Sm and Th/Th* vs. SiO_2 (wt. %) in St Lucia lavas. Pre-SVC2 and SVC composition vary exactly the same way in all the proxies with increasing SiO_2 (wt. %) while Pre-SVC1 lava compositions remain similar in isotope and trace element ratios during differentiation. Sr, Nd and Pb isotope ratios are from Bezard et al. (2014). Impact on La/Sm and Th/Th* of mineral fractionation of assemblages obtained by least square models is presented in e and f. Tick marks on the arrows represent the amount of fractionation and the black dot on each arrow represent the percentage of phases fractionated for the best fit. Impact of AFC on La/Sm and Th/Th* is presented in g where tick marks correspond to the amount of melt remaining (see text and supplementary data file in Appendix C for model parameters).

4.5.2 Impact of crustal assimilation on trace elements

The main trace element variations observed amongst the St Lucia lavas are tightly linked with the isotopic variations shown to result from crustal assimilation and may therefore be controlled by the same process. Indeed, similarly to radiogenic isotopes, no La/Sm and Th/Th* variation exist with increasing SiO₂ in Pre-SVC1 lavas, while Pre-SVC2 and SVC lavas form a trend toward higher Th/Th* and La/Sm with increasing SiO₂, similar to the isotope ratios (Fig. 4.5e, f). However, unlike radiogenic isotopes, trace elements are affected by mineral fractionation. Therefore, the increases in La/Sm and Th/Th* observed in St Lucia lavas, which are tightly linked with the assimilation event, do not necessarily reflect the composition of the assimilant and might instead (or in part) be produced by a change in the fractionating mineral assemblage. For example, a change in the fractionating assemblage could be caused by a change in water content of the magma produced by the dehydration of the assimilant during its incorporation. In order to constrain the impact of assimilation on the trace element variations observed between Pre-SVC1, Pre-SVC2 and SVC lavas, the effects related to fractional crystallisation need to be quantified first. To do so, determination and quantification of the phases involved in fractionation of the Pre-SVC1 basalt liquid to produce the SVC lavas was undertaken using major element concentrations. A Pre-SVC1 basalt (SL-83-44) was chosen as a starting composition since this represent the most mafic end-member on the island and both the trends formed by Pre-SVC1 and by Pre-SVC2 and SVC back project toward this composition. Using partition coefficients, we subsequently model La/Sm and Th/Th* variations due to mineral fractionation and then compare these with the observed SVC compositions.

4.5.2.1 Determination of the fractionating assemblage using major elements

In the absence of crustal assimilation, the major element compositions of volcanic rocks are only controlled by the composition of the primitive magma and the phases removed by crystal fractionation. In a case where crustal assimilation is significant and the assimilant has a distinct major element composition to the lavas, the differentiation trend might show a clear change at the onset of assimilation.

When plotted on an AFM diagram (Fig. 4.6a), all of the Pre-SVC1 samples plot in the tholeiitic field (Irvine and Baragar (1971) boundary) while the SVC samples all belong to the calc-alkaline field and Pre-SVC2 lavas plot at the boundary between the two or in the calc-alkaline field. Therefore, samples that suffered from increasing assimilation were progressively displaced toward the calc-alkaline field. Such an observation is consistent with experiments of Grove et al. (1982) which show that assimilation of crustal material can produce a calc-alkaline trend from tholeiites. However, when major element oxide variations are plotted against SiO₂ (Fig. 4.6b-g), no significant change in the differentiation trends between Pre-SVC and SVC samples are observed. In the Pre-SVC samples, most major element oxides show a general linear trend from basalt to rhyolite, although some scatter exists in the data. The absence of inflections indicates that there was no sudden major modal abundance changes in the fractionating assemblages, nor sudden addition of assimilant with a very distinct composition. The SVC compositional trends are linear and overlap with the Pre-SVC trends for CaO, TiO₂, MgO and K₂O, however, the SVC have slightly higher Al₂O₃ and lower FeO_T. This slight difference might be either due to a change in the phases of the fractionating assemblage and/or in the amount of the phases fractionated or due to assimilation.

For all St Lucia samples, > 93% of CIPW normative minerals plot in the quartz-feldspar-orthopyroxene-clinopyroxene tetrahedral system and all Pre-SVC and SVC samples could have been differentiated from the most mafic Pre-SVC sample (SL-83-44) by fractionation of clinopyroxene + orthopyroxene + plagioclase (Fig. 4.7). SVC samples follow the Pre-SVC cotectic and Pre-SVC and SVC andesites have very similar normative compositions. Although CIPW norms represent a dry system, the results are in very good agreement with the mineralogical assemblages observed in thin section. All the Pre-SVC lavas phenocryst assemblages comprise plagioclase, clinopyroxene, orthopyroxene with minor ilmenite and resorbed olivine. The SVC andesite phenocryst assemblages are mainly comprised of plagioclase, orthopyroxene with minor resorbed quartz. Finally, in the SVC dacites contain some or all of the phases plagioclase, orthopyroxene or cummingtonite, quartz, biotite and hornblende microphenocrysts. Plutonic inclusions found in some of the SVC lavas have the same mineral assemblage as their host lavas but in different modes.

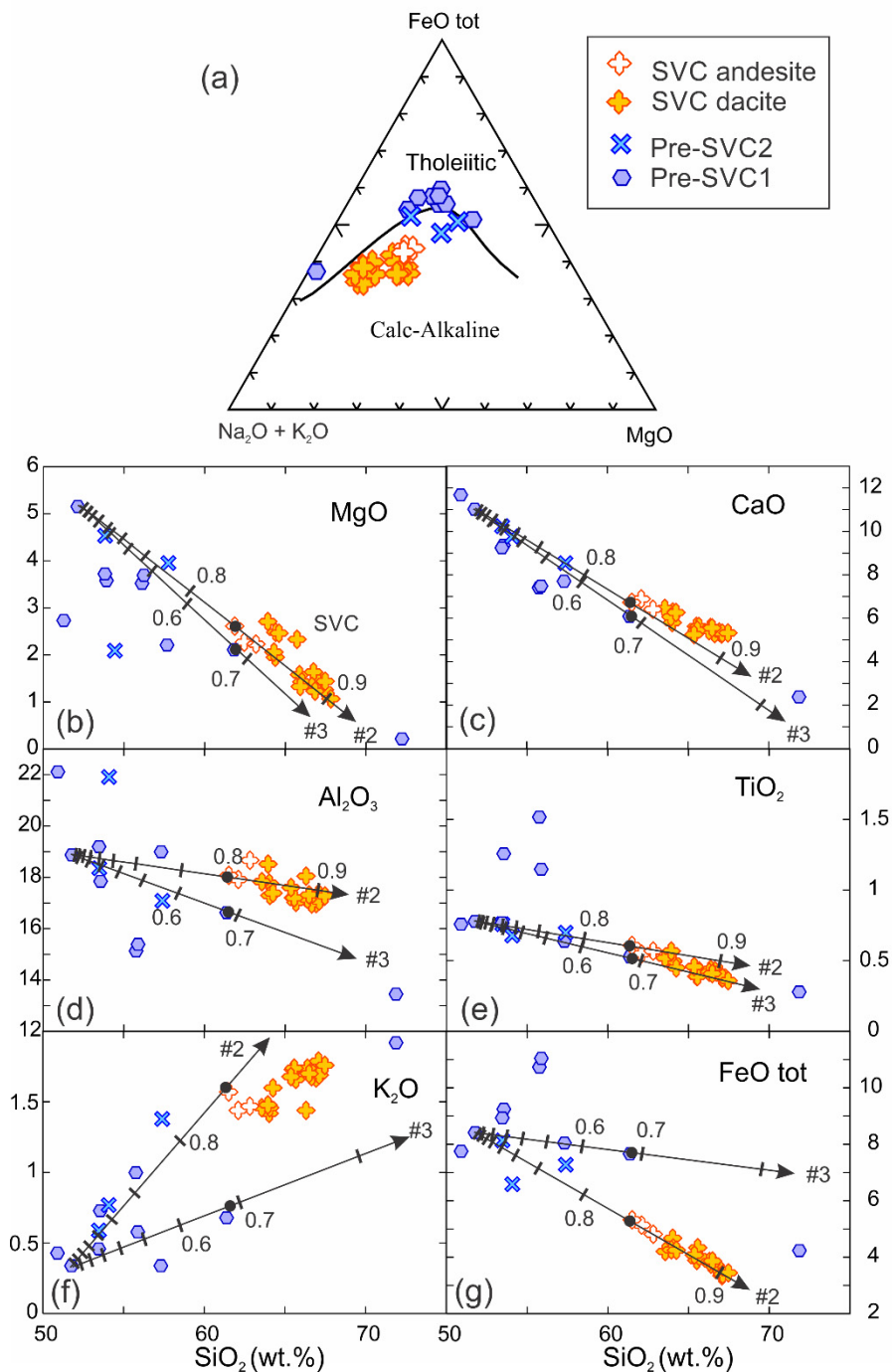


Fig. 4.6. Major element variation of St Lucia lavas. (a) AFM diagram with dividing line from Irvine and Baragar (1971) (b) MgO, (c) CaO, (d) Al₂O₃, (e) TiO₂, (f) K₂O and (g) FeO_{tot} variations are plotted against SiO₂ and. Least square models #2 and #3 are also presented (#1 is not shown here but is similar to #2). Tick marks on the arrows represent the amount of fractionation and the black dot on each arrow represent the amount of phases fractionated for the best fit of the least square models.

In order to further test whether the Pre-SVC1 and SVC andesites can both be produced by fractionation of similar phases from the most mafic Pre-SVC1 lava and to constrain the modal abundances of such phases, least-squares modelling using an Excel-based version of XTLFRAC (Stormer and Nicholls, 1978) was performed. The most mafic Pre-SVC1 lava (SL-83-44) was used as a starting composition, and high-silica andesite (with similar SiO_2) from both the Pre-SVC and the SVC groups for the resultant magmas. For the possible fractionating assemblages, combinations of all different phase compositions found in both the Pre-SVC mafic-andesitic samples and the SVC andesitic mineral assemblages (and in both lavas and xenoliths) were explored. Since amphibole is not present in either the Pre-SVC or SVC andesites, the composition of high-Ca and low-Ca hornblende micro-phenocrysts found in some SVC dacites and in the plutonic xenoliths were used. In the model, combinations of 9 major elements oxides and 4 phases were used.

The least squares models are presented in Fig. 4.6b-g. A very good fit of $\sum R^2 = 0.05$ was obtained by fractionating the observed plagioclase + clinopyroxene + orthopyroxene + ilmenite assemblage for the Pre-SVC andesite (Table 4.2 model #3). Using the same phenocryst assemblage, but with orthopyroxene having slightly lower MgO and plagioclase with lower anorthite, a very good $\sum R^2$ was obtained for the SVC andesite ($\sum R^2 = 0.03$) (Table 4.2, model #1).

No least squares solution that involves fractionation of amphibole (using either the SVC dacite or granitoid amphibole composition) or olivine produced a residual melt with the Pre-SVC andesite composition. For the SVC andesite, a good fit for an amphibole-bearing assemblage, however, it only involved fractionation of less than 1% of amphibole (Table 4.2, model #2). The fits were not improved when phase compositions from the plutonic xenolith assemblages were used.

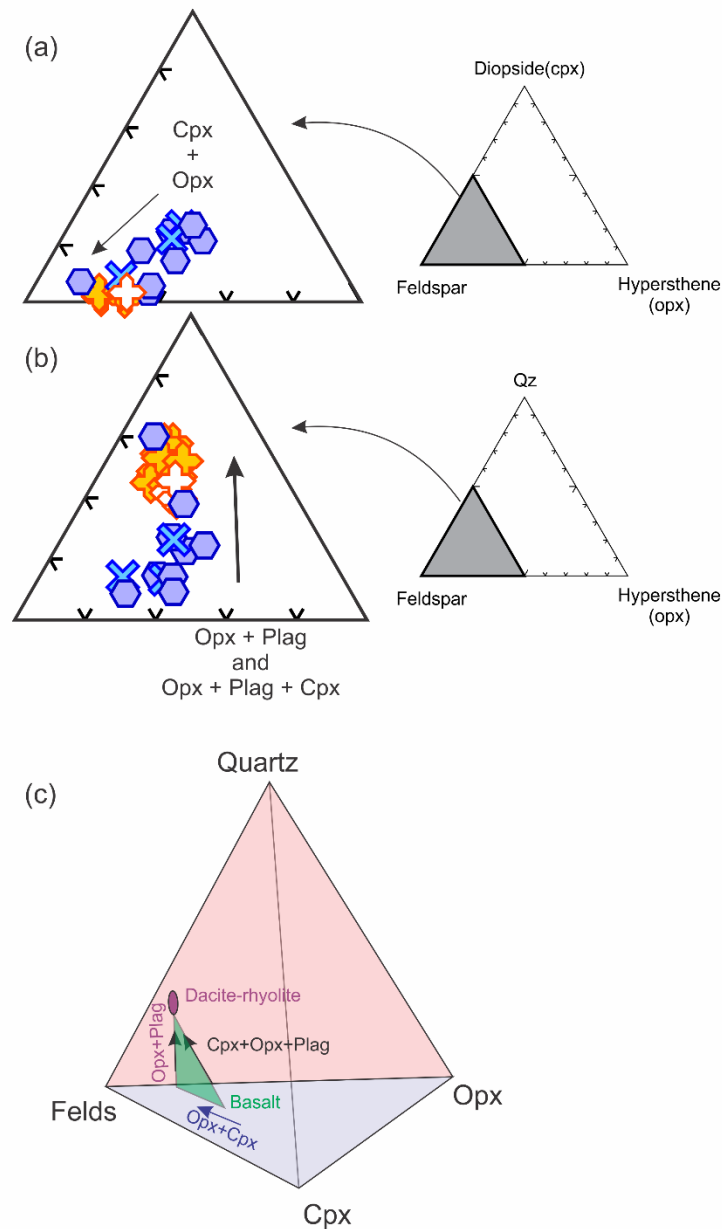


Fig. 4.7. CIPW norm composition of St Lucia in (a) the diopside-feldspar-hypersthene and in (b) quartz-feldspar-hypersthene systems. Paths to explain Pre-SVC and SVC rocks by differentiation from the most mafic Pre-SVC1 lava (basalt) are shown in (c) a 3D tetrahedral. Symbols as in Fig. 4.6.

4.5.2.2 Impact of the fractionating assemblage on the trace element variations

Using the partition coefficients presented in Table 4.3 and the Rayleigh fractionation equation, the impact of fractionation of the least squares model assemblages on Th/Th* and the REE ratios of the lavas was calculated. Results are presented in Table 4.2.

4.5.2.2.1 Th/Th*

The results show that none of the fractionating assemblages obtained from the least squares models can produce a significant increase in Th/Th* (Fig. 4.5f). Residual melts from least square models #1 and #2 have a Th/Th* ratio of 0.72, while the residual melt from model #3 has a ratio of 0.71. Therefore, Th/Th* ratios of all residual melts are very similar or identical to the starting melt composition (SL-83-44; Th/Th* = 0.71), and indicate that Th/Th* remains almost constant during fractionation. The Th/Th* ratios obtained are far lower than the ratio observed in the SVC andesite of 0.96, suggesting that the difference needs to be accounted for by crustal assimilation. Because the reduction of the Th anomaly in the Pre-SVC2 and the SVC lavas relative to Pre-SVC1 lavas is due to an increase in Th instead of a decrease in Ba and U (Fig. 4.3), we argue that the assimilant possessed higher Th/Ba and Th/U ratios than the Pre-SVC1 lavas.

Ba/Th is often used to constrain the amount of fluid versus sediment from the subducting slab in the mantle wedge source. On St Lucia, the increase in Th reduces the Ba/Th ratio of the Pre-SVC2 and SVC volcanic rocks by 16-25% and 32-39% respectively. We therefore suggest that a correlation between Th/Th* and SiO₂ should be precluded before using a proxy such as Ba/Th for source characterisation. Pre-SVC1 samples do not show any correlation of Th anomaly with SiO₂, therefore, the large range of Ba/Th should represent source variations, if no other cryptic assimilation has occurred.

4.5.2.2.2 REE

As noted by Davidson et al. (2007), during magma differentiation, fractionation of olivine and plagioclase does not significantly affect the L/M-HREE ratio. Although pyroxene fractionation can increase the L/M-HREE of the lava slightly, amphibole and garnet fractionation produce larger changes in this ratio.

The fractionating assemblages obtained from least squares modelling provide no suggestion of garnet fractionation during differentiation from Pre-SVC1 basalt to Pre-SVC1 or SVC andesites, which leaves only pyroxene and amphibole fractionation capable of increasing the L/M-HREE ratios. The absence of garnet fractionation is confirmed by the lower Dy/Dy* ratio of the SVC lavas compared to Pre-SVC1 basalt

(Fig. 4.8). Indeed, garnet preferentially incorporates HREE followed by MREE and LREE while amphibole and pyroxene preferentially incorporate MREE followed by HREE and LREE. Fig. 4.8 shows that Dy/Yb and Dy/Dy^* of the most mafic Pre-SVC1 lava (SL-83-44) is chondritic, therefore, any garnet fractionation during differentiation of such magma would produce lavas with $Dy/Dy^* > 1$. However, Dy/Dy^* is < 1 for Pre-SVC2 and SVC lavas, which indicates that fractionation of garnet from the more primitive St Lucia basalt is very unlikely to be involved in their genesis (Fig. 4.8).

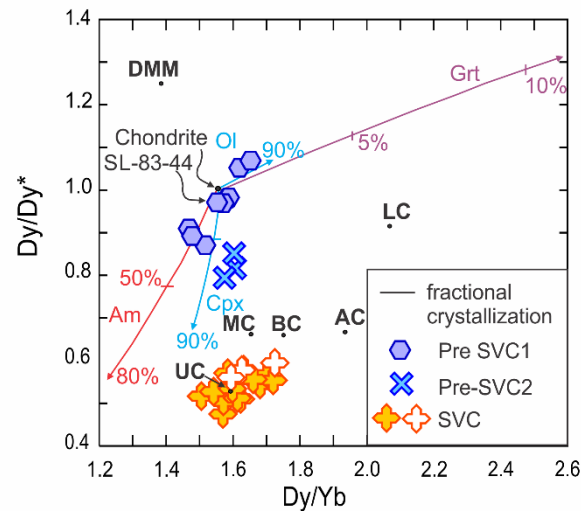


Fig. 4.8. Comparison of St Lucia lava composition with the schematic effect of mineral fractionation control on Dy/Dy^* and Dy/Yb . Vectors (arrows) and partition coefficients used are taken from Davidson et al. (2013) and represent fractionation of amphibole, clinopyroxene, olivine and garnet. Vectors start at a chondritic liquid composition and amount of fractionation is indicated in percentages. UC = upper crust, MC = middle crust, BC = bulk crust and LC = lower crust from Rudnick and Fountain (1995). DMM = Depleted MORB mantle from Workman and Hart (2005). Symbols as in Fig. 4.6.

As for Th/Th^* , fractionation of the least squares model mineral assemblages obtained for the production of Pre-SVC1 andesites (SL-83-41; $La/Sm = 1.9$; $La/Yb = 2.3$) and SVC andesites (SL-83-17; $La/Sm = 5.7$; $La/Yb = 11.3$) from the differentiation of Pre-SVC1 basalt (SL-83-44; $La/Sm = 1.65$; $La/Yb = 1.74$) did not result in any significant increase in La/Sm in the residual melt (Fig. 4.5e). Indeed, results show that fractionation of assemblages #1 and #3, which are amphibole-free, produced a residual melt with L/M-HREE similar to the observed Pre-SVC1 andesitic ratios (SL-83-41; $La/Yb = 2.30$; $La/Sm = 1.90$) with La/Yb and La/Sm of 2.19-2.31 and 1.82-1.90 respectively. Fractionation of the amphibole-bearing assemblage (0.9% hornblende; #2), also yields low La/Yb or La/Sm (2.29 and 2.02; Fig. 4.5e). These low L/M-HREE

ratios indicate that the increase in La/Sm (and La/Yb) observed in the SVC lavas cannot be due to mineral fractionation but rather reflects the characteristics of the assimilant.

Table 4.2. Least square models to produce a residual melt with Pre-SVC1 andesite (SL-83-41; model #3), or SVC andesite (SL-83-17; models #1, 2) compositions from differentiation of Pre-SVC1 basalt (SL-83-44) and the corresponding Rayleigh fractionation models.

#1	Init. mag.	Final mag.	Phase analyses (normalized to 100%)			
	SL-83-44	SL-83-17	Plag1	Opx1	Ilm1	Cpx1
SiO ₂	52.35	61.96	49.77	50.29	0.00	60.94
TiO ₂	0.78	0.62	0.04	0.11	53.01	0.44
Al ₂ O ₃	19.08	18.21	31.5	0.59	0.12	5.02
FeOt	8.51	5.36	0.79	27.71	45.51	4.51
MgO	5.20	2.62	0.10	20.45	1.27	0.12
CaO	11.14	6.78	13.32	0.84	0.02	28.76
Na ₂ O	2.50	2.73	3.98	0.01	0.00	0.21
K ₂ O	0.34	1.58	0.14	0.00	0.01	0.00
P ₂ O ₅	0.09	0.14	0.35	0.00	0.07	0.00
Total	100	100	100	100	100.0	100
$\Sigma(R^2)$	Res. Melt (%)		Phase (in % relative to initial magma)			
0.03	14.27		50.13	23.02	1.10	11.48

#2	Init. mag.	Final mag.	Phase analyses (normalized to 100%)				
	SL-83-44	SL-83-17	Plag1	Opx1	Ilm1	Cpx1	Am1
SiO ₂	52.35	61.96	49.77	50.29	0	60.94	42.24
TiO ₂	0.78	0.62	0.04	0.11	53.01	0.44	1.85
Al ₂ O ₃	19.08	18.21	31.5	0.59	0.12	5.02	15.45
FeOt	8.51	5.36	0.79	27.71	45.51	4.51	8.63
MgO	5.2	2.62	0.1	20.45	1.27	0.12	16.53
CaO	11.14	6.78	13.32	0.84	0.02	28.76	12.77
Na ₂ O	2.5	2.73	3.98	0.01	0	0.21	2.08
K ₂ O	0.34	1.58	0.14	0	0.01	0	0.45
P ₂ O ₅	0.09	0.14	0.35	0	0.07	0	0
	100	100	100	100	100	100	100
$\Sigma(R^2)$	Res. Melt (%)		Phase (in % relative to initial magma)				
0.02	14.96		49.28	22.44	1.11	11.31	0.90

Table 4.2. (continued).

#3	Init. mag.	Final mag.	Phase analyses (normalized to 100%)			
	SL-83-44	SL-83-41	Plag2	Cpx2	Opx2	Ilm2
SiO ₂	52.35	62.04	49.88	51.2	50.77	0.27
TiO ₂	0.78	0.54	0.04	0.37	0.41	16.14
Al ₂ O ₃	19.08	16.8	30.86	3.25	1.36	2.15
FeOt	8.51	7.75	0.83	6.82	21.71	80.52
MgO	5.20	2.12	0.11	16.56	23.45	0.78
CaO	11.14	6.16	14.47	21.6	2.29	0.12
Na ₂ O	2.50	3.75	3.39	0.2	0.01	0.01
K ₂ O	0.34	0.69	0.10	0.00	0.00	0.01
P ₂ O ₅	0.09	0.15	0.32	0.00	0.00	0.00
Total	100	100	100	100	100	100
$\Sigma(R^2)$	Res. Melt (%)		Phase (in % relative to initial magma)			
0.05	31.27		42.65	12.85	9.94	3.29

Rayleigh fractionation model:			
	La/Yb	La/Sm	Th/Th*
SL-83-44	1.74	1.65	0.71
SL-83-17	11.31	5.74	0.96
SL-83-41	2.31	1.88	0.45
#1 res. Melt	2.31	1.82	0.72
#2 res. Melt	2.29	2.02	0.72
#3 res. Melt	2.19	1.90	0.71

4.6 Composition of the assimilant

4.6.1 Major and trace elements

The limited differences in major element compositions between Pre-SVC and SVC can be easily accounted for by fractional crystallisation alone. This indicates that, if significant crustal assimilation occurred in the SVC, addition of the assimilant must have had a similar effect on major element compositions lavas as removal of the crystallising assemblage. Terrigenous sediments derived from continental crust could have appropriate compositions since they are andesitic on average. Many of the local sediments fulfill such criteria. This is true of the pelagic and radiolarian clays drilled on the subducting plate at Site DSDP site 543 and for the terrigenous claystones and sandstones from Barbados sediments, both of which originate from the South

American craton (Carpentier et al., 2009). Contamination by carbonate-rich sediments, such as the grey marl and chalk ooze (unit 1 and 2; Mean CaO = 30 wt. %) or the black shales (unit 3; Mean CaO = 33 wt. %) intersected at DSDP site 144, seems less likely since their assimilation should produce a shift in the differentiation trend of CaO in the Pre-SVC2 and SVC volcanic rocks compared to Pre-SVC1 lavas, which is not observed (Fig. 4.6). Alternatively, it could be argued that the effect on CaO of assimilation of such sediment could be buffered by fractionation of large quantities of calcic magmatic phases such as plagioclase and clinopyroxene.

Local sediments having the assimilant trace element features are abundant since high La/Yb or La/Sm ratios and high Th/Ba and Th/U relative to Pre-SVC1 lavas characterise sediments from both DSDP sites 543, 144 and from the Scotland formation of Barbados (not the Oceanic formation which comprises tephra) (Carpentier et al., 2008; 2009).

4.6.2 Isotopic composition and rate of assimilation

AFC modelling performed in the 1980's and 1990's to explain the extreme isotope signatures of the Lesser Antilles lavas, highlighted the need for the assimilant to have very radiogenic Pb, but failed to find local sediment with such composition (e.g. Thirlwall et al., 1996). The local sediments are mainly terrigenous, and it was suggested that biogenic (organic-rich) sediments, which typically have more radiogenic Pb, would be necessary to explain the lava isotopic compositions (Thirlwall et al., 1996). Recently, Carpentier et al. (2008; 2009) presented new isotopic data for local sediments including those from Barbados, DSDP site 543 and DSDP site 144. At the latter site, black shales (present only in unit 3) with extremely radiogenic Pb were encountered (e.g. Carpentier et al., 2008; 2009) and could possibly represent the "missing endmember".

We calculated the "minimum" isotopic composition, i.e. the composition with the lowest Sr and Pb isotope ratios and highest Nd and Hf isotope ratios, necessary for any assimilant that would be able to explain Pre-SVC2 and SVC signatures using reasonable parameters. This was then compared to the composition of the local sediments to assess the most likely relative contribution of terrigenous versus biogenic sediment (such as black shales). We used the AFC equation of De Paolo (1981), in

which several parameters must be accounted for: (1) the initial magma composition, (2) the fractionating assemblage, (3) the fraction of melt remaining, “F”, (4) the partition coefficients, the (5) trace element and (6) isotopic composition of the assimilant and (7) the assimilation / crystallisation ratio, “r”. Given that reasonable assumptions can be made for the first five factors, we can constrain the “minimum” isotopic composition of the assimilant (6) and the rate of assimilation (7).

In the following sections we describe each fixed parameter before presenting the best fit:

(1) Initial magma composition

As in the least squares models, and for the same reasons, the most mafic Pre-SVC1 lava (SL-83-44) was used for the initial magma composition for trace elements. For the isotopic composition, we again used SL-83-44, along with SL-83-25 to cover most of the range of isotopic compositions observed in the Pre-SVC1 samples.

(2) Fractionating assemblage

The assemblages produced by the two best least square models obtained for SVC andesite were used (models #1 and 2; Table 4.2).

(3) Fraction of melt remaining

We ensured that the amount of fractionating assemblage, and therefore the amount of melt remaining, was constant in every isotope-isotope space modelled. We used phase assemblages obtained by least square models #1 and #2, which leads to $F = 15\%$. However, the SVC lavas display some isotopic variation, with andesite overlapping dacite compositions, precluding the modelling of all SVC lavas by the same amount of fractionation. Although the isotopic variations could have been produced by small changes to other parameters, such as a slightly heterogeneous assimilant composition, different rate of assimilation or different modal abundances in the phases fractionated; for simplicity all the data were modeled using only one set of parameters. Therefore, we made sure that the most extreme lava composition of the SVC (highest Sr and Pb isotope ratios and lowest Nd and Hf isotope ratios) plotted at $F \sim 15\%$ ($\sim 85\%$ fractionation, as suggested by the least square models) in all isotopic systems.

(4) The partition coefficients

We used the compilation of partition coefficients (k_{ds}) presented in Table 4.3.

Table 4.3. Mineral-melt distribution coefficients used for the Rayleigh fractionation and AFC models.

	Plag	Cpx	Opx	Ilm	Hbl
La	0.035	0.105	0.002	0.098	0.544
Nd	0.018	0.287	0.030	0.140	1.340
Sm	0.013	0.477	0.050	0.150	1.804
Yb	0.016	0.601	0.340	0.170	1.642
Hf	0.009	0.121	0.010	0.380	1.534
Sr	1.670	0.070	0.040	0.010	0.480
Pb	0.36	0.0102	0.0013	0.01	0.1
Ba	0.29	0.001	0.011	0.00034	0.16
U	0.25	0.01	0.0046	0.0082	0.004
Th	0.25	0.012	0.0012	0.00055	0.004

Distribution coefficients were compiled from Arth (1976), Paster et al. (1974), Dostal (1983), Fujimaki et al. (1984), Green et al. (1989), McKenzie and O’Nions (1991), Salters and Longhi (1991), Zack and Brumm (1998), Aigner-torres et al. (2007) and set to 0.01 where not available and known to be insignificant. Plag = Plagioclase, Cpx = clinopyroxene, Opx = orthopyroxene, Ilm = ilmenite; Hbl = hornblende.

(5) Trace element composition of the assimilant

As discussed in the previous section, the assimilant displays higher La/Sm ratio and Th concentration than the Pre-SVC1 lavas. Such characteristics can be found in all local sediments that have been analysed (Carpentier et al., 2008), except the Oceanic Formation in Barbados, which contains ash layers. Because the magmas erupting in the southern arc are thought to have intruded through the Aves Ridge forearc basin, any sediments from the Grenada and Tobago basins could represent the assimilant. These two basins accumulated up to 14 km of sedimentation that started in the Paleogene. Sequences deposited before the Lesser Antilles magmatism were all mainly derived from the South American continent, with only minor amounts from the Aves Ridge (Aitken et al., 2011 and references therein). Because no published trace element compositions exist for the Grenada and Tobago sediments, we used published compositions of the sediments located on the subducting slab near the trench since they were shown to derive dominantly from the Amazon tributary draining the Guyana and Brazilian cratons (Allegre et al., 1996). We tried 4 different options for trace element concentrations: (a) the bulk composition of site 144 (mainly biogenic), (b) the bulk composition of site 543 sediment (mainly terrigenous), (c) the bulk composition of the Scotland Formation of Barbados (terrigenous) and (d) a mix of 50 % each of bulk compositions of sediments from DSDP sites 543 and 144.

4.6.2.1 The best fit for trace elements and isotope compositions of the assimilant

4.6.2.1.1 Sr, Nd, Hf and Pb concentrations of the assimilant

No good fit to the isotopic trends was obtained using the bulk trace element composition of sediments from the three different sites (a, b, c); mainly due to Sr/Nd being either too low, or too high, suggesting that the assimilant cannot be pure terrigenous or biogenic sediment. However, a 50-50% mix of site 144 and site 543 sediments (d), results in Sr/Nd, Hf/Nd and Nd/Pb ratios (~20, ~0.15, ~1.75, respectively) that can explain the trends observed in these different isotope-isotope diagrams (Fig. 4.4a). This mixed sediment has Sr, Nd, Hf and Pb concentrations of 382 ppm, 22.7 ppm, 2.5 ppm, 13.0 ppm, respectively.

4.6.2.1.2 “Minimum” isotopic composition of the assimilant

Taking into account all the previous parameters (See supplementary data file in appendix C for all parameters and AFC model data), the “minimum” composition permissible for the assimilant is: $^{87}\text{Sr}/^{86}\text{Sr} = 0.7091$, $^{143}\text{Nd}/^{144}\text{Nd} = 0.51205$, $^{176}\text{Hf}/^{177}\text{Hf} = 0.28227$, $^{206}\text{Pb}/^{204}\text{Pb} = 19.81$, $^{207}\text{Pb}/^{204}\text{Pb} = 15.85$, $^{208}\text{Pb}/^{204}\text{Pb} = 39.54$ (Fig. 4.4a-d). The presence of amphibole (<1%) in the fractionating assemblage results in insignificant changes in the modeled trends on the isotope-isotope diagrams. The use of SL-83-25 as a starting composition results in a better fit than using SL-83-44. This ‘minimum’ isotopic composition of the assimilant to explain the Pre-SVC2 and SVC lava compositions requires that $r = 0.8$. This rate of assimilation is considered reasonable since assimilant incorporation processes such as reactive bulk assimilation can explain $r \geq 1$ (Beard et al., 2005). Given that all the parameters used in this model are reasonable, we suggest that the modeled “minimum” composition for the assimilant is realistic.

4.6.2.1.3 Best fit for L/M-HREE and Ba/Th versus isotopes models

Given that the variations in lava isotopic compositions are correlated with variations in REE patterns and LILE/HFSE, we verified that the 50-50% mix of site 144 and site 543 sediments, having ideal Sr, Nd, Hf and Pb concentrations to model the isotopic variations in St Lucia lavas, also had suitable REE and Ba, Th and U concentrations

to explain the high La/Yb and La/Sm ratios of the lavas (Fig. 4.4e,f) and the observed Ba/Th and Th/Th* ratios using the same other model parameters. This mixed sediment has La, Sm and Yb concentrations of 25.16 ppm, 4.47 ppm and 1.90 ppm, with La/Sm and La/Yb ratios of 5.6 and 13.2 and Ba and Th concentrations of 562 ppm and 7.8 ppm, respectively.

REE

The increase in La/Yb and La/Sm ratios observed from Pre-SVC1 to Pre-SVC2 lavas are very well reproduced by the model with no change in parameters. The La/Yb and La/Sm ratios of SVC lavas can also be modeled very well, however, more residual melt than the amount fixed in the isotope-isotope models ($F \sim 15\%$) is needed to explain the SVC lavas. This can be observed in Fig. 4.4e and f which shows that using both amphibole-bearing and amphibole-free assemblages, the La/Yb composition of the SVC andesites plot between $F = 70-55\%$ which corresponds to 30-45% fractionation, and the SVC andesites La/Sm ratios plot between $F = 70-20\%$ ($F = 70-55\%$ for amphibole-bearing assemblage and $F = 55-20\%$ for the amphibole-free assemblage).

This F discrepancy could be argued to be due to the use of La/Sm and La/Yb assimilant values that are too high. However, a decrease of these ratios to unreasonable values ($\text{La/Yb} = 5.3$; $\text{La/Sm} \leq 4.24$) would be necessary in order to explain alone the SVC andesites compositions with $F \sim 15\%$. Indeed, no local sediment would have low enough La/Yb and La/Sm while having $^{87}\text{Sr}/^{86}\text{Sr}$ radiogenic enough (Fig. 4.4e) to explain the lava compositions. Therefore, we suggest that the F discrepancy in the L/M-HREE versus isotope ratio model may result from the interplay of both (1) values of La/Sm and La/Yb that are slightly too high in the assimilant used and (2) an overestimation of the amount of fractionation obtained by the major element least squares models which may instead be comprised between 55 and 75% ($F = 45-25\%$). The overestimation of the amount of fractionation could easily be explained by the fact that the system is open, and may be caused by the impact of both recharge events and of assimilation on the major element composition of the SVC lavas. The impact of this potential overestimation of F on the modeled “minimum” assimilant composition from the isotope data is nevertheless insignificant. Indeed, using $F \sim 55\%$ instead of $F \sim 15\%$ to model the most extreme SVC signature in the isotope-isotope

models yields a very similar minimum assimilant isotopic composition: $^{87}\text{Sr}/^{86}\text{Sr}=0.7093$, $^{143}\text{Nd}/^{144}\text{Nd}=0.5120$, $^{176}\text{Hf}/^{177}\text{Hf}=0.28220$, $^{206}\text{Pb}/^{204}\text{Pb}=19.83$, $^{207}\text{Pb}/^{204}\text{Pb}=15.85$, $^{208}\text{Pb}/^{204}\text{Pb}=39.54$ (see supplementary file, Appendix C).

Ba/Th

In a similar way to La/Sm and La/Yb, the SVC Ba/Th ratios were modeled successfully, but with $F > 20\%$ (Fig. 4.4g) which supports the inference of an overestimation of fractionation from the REE. However, unlike for the REE, the choice of a sediment with slightly higher Ba/Th ratio compared to the composition of the mix used is possible and could cancel the small F discrepancy. A sediment with a slightly higher Ba/Th (~83 instead of 72 for the mix) would be consistent with the Th/Th* necessary to model Pre-SVC2 and SVC lavas. Indeed, using the Ba, Th and U content of the 50-50% mix of site 144 and site 543 manages to successfully reproduce the Th/Th* ratio increase between Pre-SVC1 and SVC, as shown in Fig. 4.5g. However, for the model path to go through Pre-SVC2 lavas, the sediment assimilated needs to have a slightly lower Th/Th* (0.93) than the mix of 50% B543 + 50% B144 sediment used (1.07; Fig. 4.5g).

4.6.2.2 Comparison of the “minimum” assimilant composition with the local sediments

The modeled isotopic composition of the assimilant overlaps unit 1 and 2 of DSDP site 144 sediments in terms of Sr, Nd and Pb isotopes but is also not very different from site 543 and Barbados sediment compositions (Fig. 4.4). In terms of Hf isotope ratio, the assimilant plots amongst the less radiogenic compositions of Barbados and unit 1 and 2 of site 144 sediments. Black shales such as those present in unit 3 of DSDP site 144, and which display the most radiogenic Pb isotopic composition known in the Caribbean area, are not required in the St Lucia basement to explain SVC lava isotopic compositions. In fact, although our modeled assimilant represents the “minimum” composition which means the assimilant could be more radiogenic, assimilation of black shales seems very unlikely. This is because black shales all display $^{206}\text{Pb}/^{204}\text{Pb} > 21$ which can hardly be reached by a model that goes through the SVC lavas. It is particularly obvious on the $^{143}\text{Nd}/^{144}\text{Nd}$ vs. $^{206}\text{Pb}/^{204}\text{Pb}$ diagram presented in Fig. 4.4d. Furthermore, the black shales have higher $^{176}\text{Hf}/^{177}\text{Hf}$ ratios

than some SVC lavas (> 0.2824), which argues against their likelihood of representing the assimilant. Carbonate-rich sediment similar to Unit 1 and 2 of site 144 could fit with the isotopic composition of our assimilant. However, as mentioned earlier, these sediments have a mean CaO of ~ 30 wt. % and significant plagioclase fractionation would be needed to offset the related CaO increase in the lavas during assimilation. Furthermore, the trace element composition of such sediments is not suitable because the Sr/Nd ratio is too high (Mean Units 1 and 2 sediment Sr/Nd = 62 while Sr/Nd needed in the model is ~ 20). Terrigenous sediments from DSDP 543 and Barbados have isotopic compositions very close to the modelled assimilant. However, like site 144 unit 1-2 sediments, their trace element composition is not suitable for modelling St Lucia lavas because Sr/Nd (~ 4) is too low. We therefore suggest that the assimilant is more likely to be a mix of terrigenous and biogenic sediment, since this would fulfil all the characteristics of the assimilant, both in terms of major, trace elements and isotopes. Such an interpretation would be in agreement with the heterogeneous composition of the sequences found in the Grenada and Tobago basins, through which the arc magmas are thought to have intruded. Indeed the basin sequences comprise deep-water turbidite, pelagic and volcanogenic shales and siltstone, with some biogenic limestone in the deeper parts (Aitken et al., 2011).

4.7 The composition of the mantle source region beneath St Lucia

Due to the continental signature of the lavas, the mantle source under the south of the arc has long been suspected to comprise more sediment than in the north of the arc and/or sediment with more “continental” isotopic composition (White and Dupre, 1986; Carpentier et al., 2008). However, Bezard et al. (2014) showed that in St Lucia, lavas with Sr, Nd and Pb isotopic compositions more continental than those of “typical oceanic arc” are in fact produced by assimilation of continent-derived sediment. So are the lava Hf isotopic compositions, as discussed in section 4.5.1. Therefore, the source beneath St Lucia may in fact be similar to that beneath the northern islands. Below, we analyse St Lucia source characteristics and compare these with the rest of the arc.

4.7.1 Crustal assimilation by Pre-SVC1 magmas?

The absence of a correlation between SiO₂ and radiogenic isotopes, Ba/Th and L/M-HREE in the Pre-SVC1 lava compositions suggest that they avoided substantial sediment assimilation from basalt to rhyolite differentiation, and could therefore have preserved St Lucia source characteristics. However, their low MgO indicates that they evolved from a more mafic precursor. Therefore, the possibility of cryptic assimilation, either during the basalt differentiation from the primary magma and/or between basalt and rhyolite differentiation, should be considered. Methods to investigate assimilation of crust during the production of Pre-SVC1 basalt are limited. Bezard et al. (2014) shown that $\delta^{18}\text{O}$ values of pyroxene and plagioclase phenocrysts from Pre-SVC1 basalt lie at the upper-hand of, or slightly above their mantle ranges. This suggests that these crystals recorded very limited amount of sediment assimilation. Such low amounts are unlikely to have had substantial effects on the whole rock isotopic composition (Bezard et al., 2014).

Pre-SVC1 samples display nearly flat REE patterns (normalised), a large range of Ba/Th, and a very narrow range of Sr, Nd, Hf and Pb isotope ratios. However, in detail, while $^{143}\text{Nd}/^{144}\text{Nd}$ and $^{207}\text{Pb}/^{204}\text{Pb}$ isotope compositions are nearly identical in the different samples, some variation can be observed for $^{87}\text{Sr}/^{86}\text{Sr}$, $^{177}\text{Hf}/^{176}\text{Hf}$, $^{208}\text{Pb}/^{204}\text{Pb}$ and $^{206}\text{Pb}/^{204}\text{Pb}$ ratios (Fig. 4.4). These variations do not follow the same trajectory as the SVC and Pre-SVC2 AFC trend, and cannot be explain by assimilation of any local sediments. Instead, they could either be explained by variations in the composition of sediment subducted into the mantle source, or by very limited amounts of intra-crustal assimilation of an igneous component. It is not possible to discriminate between these two processes using the radiogenic isotopes and the mineral $\delta^{18}\text{O}$ data available. Indeed, the very limited radiogenic isotope variation in Pre-SVC1 group and the absence of correlation between these variations and SiO₂ does not preclude sporadic assimilation, or assimilation of material with SiO₂ contents resembling the magma. In addition, no constraints can be obtained from Pre-SVC1 mineral $\delta^{18}\text{O}$ data since they were mainly analysed in crystals from a single lava (SL-83-44) (with only one plagioclase analysed in another lava) precluding the comparison of mineral $\delta^{18}\text{O}$ between Pre-SVC lavas with different radiogenic isotope signature. It is also possible that the assimilant could have a same $\delta^{18}\text{O}$ composition as mantle-derived magmas.

4.7.2 Amount of sediment in the source

Constraining the source characteristics of the primitive St Lucia magmas, such as the amount and the isotopic composition of slab-derived material added to the mantle, is not straightforward. This arises because the range of isotopic variation in Pre-SVC1 lavas is very limited and, as discussed above, the small isotopic variations observed amongst Pre-SVC1 samples cannot be used as a trend since they may in fact be due to crustal assimilation. With no compositional trend, determination of the isotopic composition of the source is problematic. However, the maximum amount of sediment involved can be estimated using mixing models and published compositions of the subducting slab units.

Slab components in the lava source region could be inherited from (1) fluids or melts from the subducting sediments and/or (2) fluids or melts from the subducted basaltic oceanic crust. White et al. (1985) found that the isotopic composition of DSDP site 543 basalt, on the subducting plate had a typical MORB composition (e.g. $^{87}\text{Sr}/^{86}\text{Sr} = 0.7030\text{--}0.7033$). This means that fluids/melts derived from basalt dehydration/melting should have a negligible impact upon the isotopic composition of the mantle wedge. Hence, only the subducted sediments would possibly affect the mantle isotopic signature. Given the very restricted composition of the Pre-SVC1 lavas, our only option to determine the maximum amount of sediment involved is to use the “least crustal” isotopic composition of the local sediment and their trace element compositions, in a mixing model passing through the mean Pre-SVC1 lavas using the depleted mantle (Workman and Hart (2005) for trace element and White et al. (1985) for isotopic compositions) as a starting composition.

Three local sedimentary sequences that represent possible subducted sediments are: the DSDP site 543 sediments, site 144 sediments and sediments similar to those preserved on Barbados (although the latter was accreted, similar sediment could also have been subducted). These three sedimentary sequences not only display large ranges in Sr-Nd-Hf-Pb isotope composition, they also display large differences in trace element concentrations and ratios (Carpentier et al., 2008; 2009). The greatest difference is seen in very high Sr and low Nd, Hf and Pb concentrations in site 144 sediments compared to site 543 and Barbados. Such high Sr produces Sr/Nd, Sr/Hf and Sr/Pb ratios up to 15 times higher than at site 543 and Barbados, while there are

insignificant differences in Nd/Hf, Nd/Pb and Hf/Pb ratios between all three sets of sediments. Because elemental concentrations and ratios strongly influence the shape of mixing curves, we performed two models using extreme concentrations and elemental ratios to encompass the whole range of local sediment composition variations.

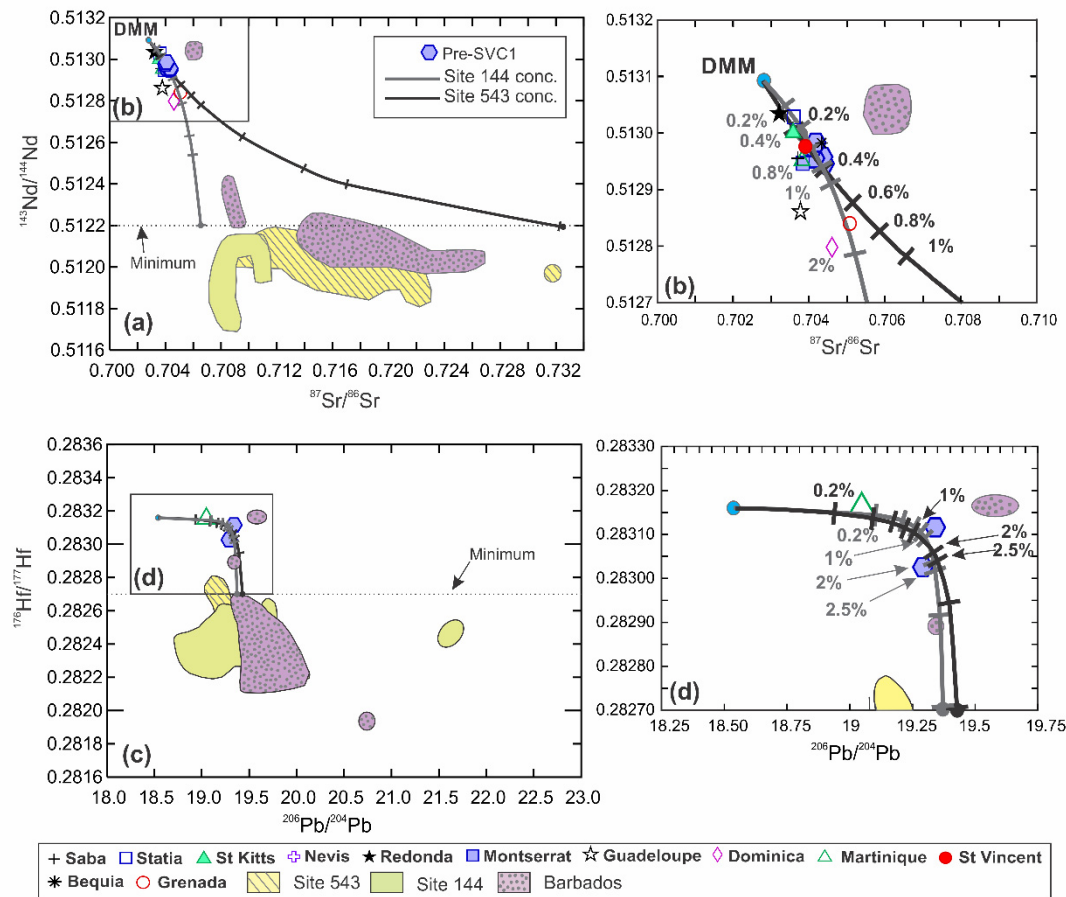


Fig. 4.9. Mixing models to constrain the amount of sediment involved in the source of Pre-SVC1 lavas. Site 144 conc. = model in which Sr, Nd, Hf and Pb concentrations of the bulk of site 144 compositions were used. Site 543 conc. = model in which Sr and Nd concentrations in the bulk site 543 compositions were used. $^{143}\text{Nd}/^{144}\text{Nd}$ and $^{176}\text{Hf}/^{177}\text{Hf}$ were fixed at 0.5122 and 0.2827 which are the least crustal composition found in most local sediments. The most mafic lava of every island of the arc as well as all the local sediment composition are also shown for comparison (same reference as in Fig.4.2). DMM = depleted MORB mantle (DMM) (same data source as in Fig. 4.8).

In the first model, we used the trace element compositions of the bulk site 144 (B144) sediments, which has the highest Sr concentrations and the highest Sr/Nd ratio with the lowest Pb concentration and a low Pb/Hf ratio (3.4) similar to the lowest bulk value corresponding to Barbados (2.7). In the second model we used the trace element

compositions of the bulk site 543 (B543) sediment which has the lowest Sr concentration and Sr/Th ratio and the highest Pb and Pb/Hf ratios (6.7). Bulk sediment concentrations at each DSDP site were used to represent the average of the whole subducting pile. We present the models in both the Sr-Nd and the Hf-²⁰⁶Pb isotope diagrams (Fig. 4.9) in which we fixed the highest realistic Nd and Hf isotope compositions of the local sediment to $^{143}\text{Nd}/^{144}\text{Nd} = 0.5122$ and $^{176}\text{Hf}/^{177}\text{Hf} = 0.2827$. These values correspond to the highest Nd and Hf isotope compositions amongst the local sediment having similar to or more radiogenic Sr and Pb isotopic compositions than the lavas (Barbados sediment containing ash layers, are not considered since unlikely to be subducted given that such layer would be at the top of the sedimentary sequence). The models were constrained to pass through the mean composition of the Pre-SVC1 lavas and the Sr and Pb isotopic compositions of the sediment end-member was constrained to realistic isotopic compositions, i.e. plotting in the field of composition of the local sediments. The position of Pre-SVC1 samples on the two modeled curves of each diagram constrains the maximum amount of sediment involved in the source of the lavas for the whole spectrum of Sr and Pb concentrations and Sr/Nd and Pb/Hf ratios of the local sediments at these fixed Nd and Hf isotopic composition. Decreasing $^{143}\text{Nd}/^{144}\text{Nd}$ and $^{176}\text{Hf}/^{177}\text{Hf}$ of the sediment used in the model toward more crustal compositions, while still permitting the model to pass through Pre-SVC1 lava compositions, will decrease the amount of sediment necessary to explain Pre-SVC compositions. Hence, we can be confident that our models constrain the maximum possible amount of local sediment in the source.

The best fit obtained using B144 Sr and Nd concentrations involves between 0.6-0.8% of sediment in the source of Pre-SVC1 lavas; using site 543 sediment composition requires 0.2-0.4% of sediment in the source. Using Hf and Pb concentrations from either B144 or B543 implicates between 1 and 2% of sediments in the source (the higher “maximum” value obtained using Pb/Hf compared to Sr/Nd is due to the smaller isotopic difference between the least “continental” local sediments and the DMM). Therefore, even taking into account the large variations in trace element composition of the local sediments, the amount of sediment needed in the source does not exceed 2%. Such a low amount of sediment in the mantle wedge source is similar to amounts estimated for the north of the arc (1% by Carpentier et al. (2008); <1% by Davidson and Wilson (2011) for Statia; ~2% by Turner et al., (1996)), as well as for

Martinique (<1%; Davidson and Wilson, 2011), Grenada (0.2-2%; Thirlwall et al., 1996) and the whole arc (0.2-2% bulk sediment addition for the Lesser Antilles source by DuFrane et al., 2009).

Our models involve incorporation of bulk sediments in the mantle. However, some authors have suggested that sediment melts, rather than bulk sediments, may be involved in the source of some lavas from arc (DuFrane et al., 2009; Labanieh et al., 2012). Sr/Nd and Pb/Hf ratios are different in sediment melts from the bulk sediments, due to the presence of residual phases during melting. We calculated the melt Sr/Nd and Pb/Hf of B144 and B543 sediments using partition coefficients from Johnson and Plank (1999) and Hermann and Rubatto (2009) (see supplementary data file, Appendix C). Results show that the melts display lower Sr/Nd (0.55 for B543 melt and 6.73 for B144 melt) and lower Pb/Hf ratios (2.94 for B543melt and 1.48 for B144 melt) than the bulk sediments. These lower ratios require less sediment melt in the source to explain Pre-SVC1 lavas, compared to bulk sediments, with a maximum of $\leq 1\%$ sediment melt in both Sr-Nd and Pb-Hf systems. This confirms a maximum of 2% sediment in the source of St Lucia magmas.

4.7.3 Comparison of St Lucia source to the rest of the arc

Although small amounts of cryptic assimilation may have affected Pre-SVC1 lavas, these represent the lavas with the composition closest to that of the source beneath St Lucia. Their very small range in Sr-Nd-Hf-Pb isotope ratios allow us to compare the possible range of composition of the source of St Lucia magmas, with the source of the magmas beneath the other islands.

In order to compare St Lucia source (Pre-SVC1) compositions with the rest of the arc, we plotted in Fig. 4.10 $^{87}\text{Sr}/^{86}\text{Sr}$, $^{143}\text{Nd}/^{144}\text{Nd}$ and $^{206}\text{Pb}/^{204}\text{Pb}$ against MgO, La/Sm and Ba/Th for all Lesser Antilles samples available in the literature. In addition, we selected the most mafic lava composition available from each island and plotted them on Figs. 4.9 and 4.11.

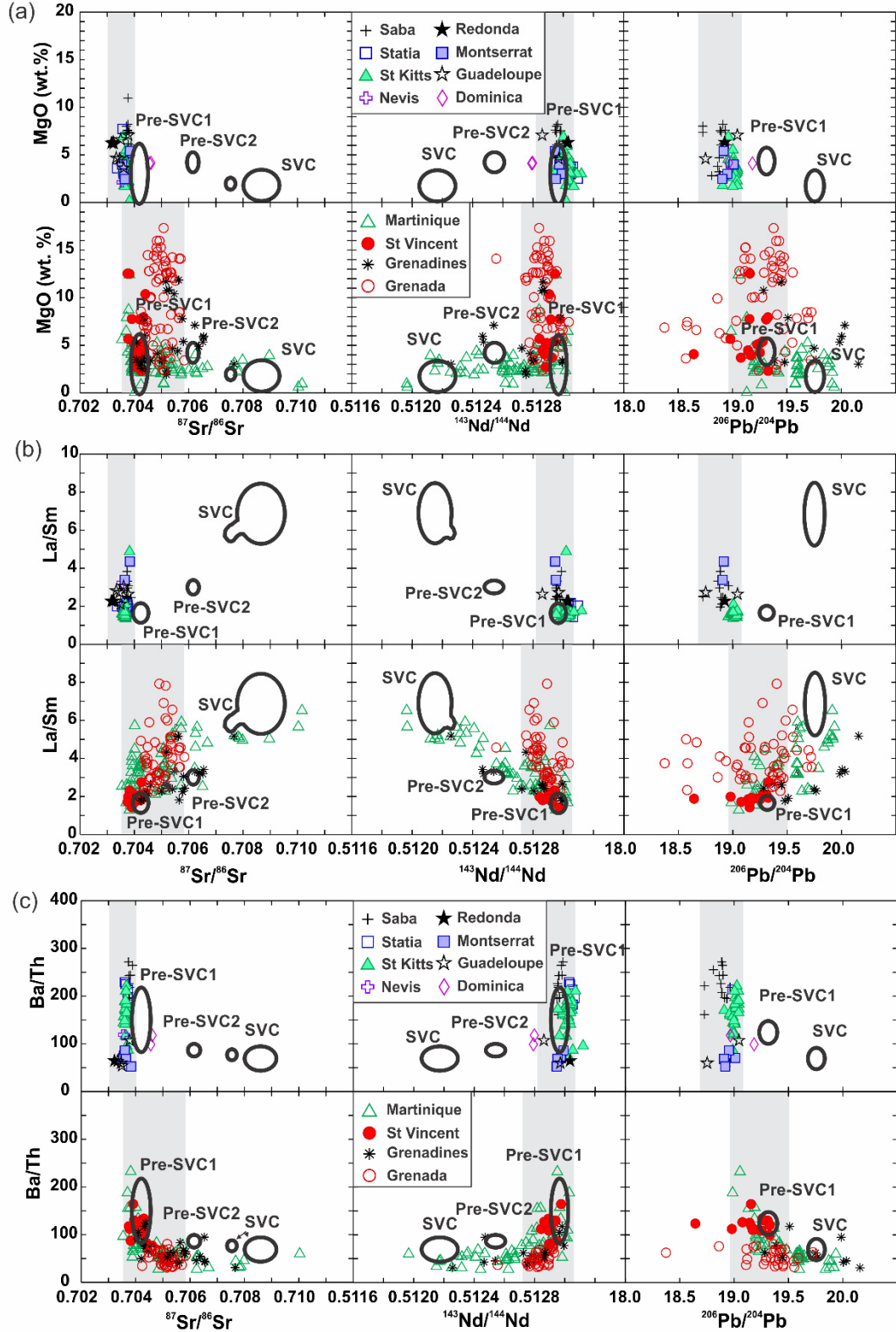


Fig. 4.10. (a) MgO (wt.%), (b) La/Sm and (c) Ba/Th vs. $^{87}\text{Sr}/^{86}\text{Sr}$, $^{143}\text{Nd}/^{144}\text{Nd}$, $^{206}\text{Pb}/^{204}\text{Pb}$ of St Lucia lavas compared to both the north (top 4 figures of each panel) and the south of the arc (bottom 4 figures of each panel). Grey field in all diagrams indicates the isotopic composition of the most primitive samples in the different islands of the northern and southern arc. Same data source as in Fig. 4.2 for Lesser Antilles lavas.

4.7.3.1 St Lucia and the north of the arc

The source composition beneath the northern islands can be estimated based on the compositions of the most mafic lavas. As with Pre-SVC1 lavas, it cannot be precluded that limited or cryptic assimilation occurred in these lavas. However, the isotopic composition of the most mafic lava found in the northern islands is very close to the primitive magma composition estimated by extrapolation of lava compositions to 48% SiO₂ by Davidson and Wilson (2011), which suggests that they represent a good approximation of the source (Fig. 4.11). This is due to the very limited isotopic range of the lavas from each northern island, even over a wide range of SiO₂ (e.g. The Quill $^{87}\text{Sr}/^{86}\text{Sr} = 0.703545\text{--}0.703794$ for SiO₂ between 53.4–61.4 wt. %), which suggests that the impact of crustal assimilation was limited here.

In terms of radiogenic isotopes, Pre-SVC1 $^{143}\text{Nd}/^{144}\text{Nd}$ compositions overlap with the field for the northern islands (Fig. 4.10). $^{87}\text{Sr}/^{88}\text{Sr}$ isotope compositions are only slightly more radiogenic than all northern islands except Dominica (Fig. 4.10). The only significant difference between St Lucia and the northern islands is observed in Pb isotopes, where Pre-SVC1 are clearly more radiogenic than all lavas in the northern islands (Fig. 4.10). In terms of La/Sm ratio, the northern islands display a large variation (Fig. 4.10b). However, unlike the Pre-SVC2 and SVC lavas, no correlation can be observed between La/Sm and radiogenic isotopes, which precludes this variation being controlled by assimilation of a crustal component like that of St Lucia. The highest La/Sm ratio (>2) is found in the most differentiated samples, suggesting the increase in La/Sm ratio is controlled by mineral (amphibole) fractionation. Pre-SVC1 La/Sm ratios overlap with those of the mafic northern islands lavas (Fig. 4.11), which indicates similar REE compositions and/or partial melting conditions for their primitive magmas. Furthermore, Ba/Th ratios of Pre-SVC1 lavas also overlap with the northern island compositions and span a similar range as on St Kitts (Fig. 4.10c).

In summary, based on the composition of the most mafic lavas, the source beneath the northern islands would have similar La/Sm, Ba/Th, $^{143}\text{Nd}/^{144}\text{Nd}$, but slightly less radiogenic $^{87}\text{Sr}/^{88}\text{Sr}$ and less radiogenic $^{206,207,208}\text{Pb}/^{204}\text{Pb}$ than that inferred for St Lucia (Fig. 4.11). The similar range of Ba/Th ratios argues for a similar fluid/sediment ratio beneath the northern islands and St Lucia. Their similar La/Sm ratios indicate that the sediment composition and the process of incorporation (melt vs. bulk

sediment) do not change substantially from north to south. The similar Nd isotopic composition are also consistent with a similar amount of sediment in the source. Finally, the higher isotope ratios of St Lucia Pre-SVC1 lavas could be explained by sediment with more radiogenic Sr and Pb in the source of St Lucia than in the north of the arc. We prefer this to the alternative argument that the more radiogenic Sr and Pb isotope ratios were produced by very small amount of sediment assimilation, where only Pb and Sr isotopes were sensitive to assimilation, due to larger differences in concentration of these elements between the magma and the assimilant than for Nd. While this would be consistent with the mineral $\delta^{18}\text{O}$ data plotting close to the upper hand of the mantle range, it is not supported by the differences in Sr, Pb and Nd concentrations observed between Pre-SVC1 basalt and the inferred composition of the assimilated sediment. Indeed, the modeled sediment assimilated (similar to 50-50% mix of site 144 and site 543) has ~3.2 times more Nd than Pre-SVC1 basalt. Although this concentration difference is slightly lower than the ratio for Pb (~5 times), it is higher than that for Sr (~2.2 times). Yet, we do not observe the greater displacement of $^{143}\text{Nd}/^{144}\text{Nd}$ than $^{87}\text{Sr}/^{86}\text{Sr}$ that would be anticipated for assimilation of sediment by a primary melt with isotopic composition similar to the northern islands. Therefore, we suggest that the Sr isotopic difference between St Lucia and the northern islands and, at least part of the Pb isotopic contrast are not due to sediment assimilation and are, rather, explained by more radiogenic subducted sediment in the mantle beneath St Lucia.

4.7.3.2 St Lucia and the south of the arc

In the next sections, we compare St Lucia to each southern island separately.

4.7.3.2.1 St Vincent

Although located in the south of the arc, St Vincent shares compositional similarities with the northern islands (Fig. 4.10). Recent oxygen isotope measurements performed on minerals from upper crustal cumulates overlap or plot very close to the mantle range precluding any significant crustal assimilation (Tollan et al., 2012). St Vincent lavas have a range of Sr and Nd isotope compositions that overlap both the northern islands and St Lucia compositions (Fig. 4.10). $^{208}\text{Pb}/^{204}\text{Pb}$ ratios of most St Vincent

samples overlap those of the northern islands (not shown). Their $^{207,206}\text{Pb}/^{204}\text{Pb}$ ratios overlap the northern islands but some slightly more radiogenic compositions exist. $^{207}\text{Pb}/^{204}\text{Pb}$ ratios do not overlap Pre-SVC1 samples while the most radiogenic $^{206}\text{Pb}/^{204}\text{Pb}$ ratios do. In terms of La/Sm and Ba/Th, St Vincent lavas overlap the compositions of the northern islands and Pre-SVC1 samples (Fig. 4.10b.c; Fig. 4.11). No clear correlation can be observed between radiogenic isotopes and La/Sm, precluding significant assimilation of sediment.

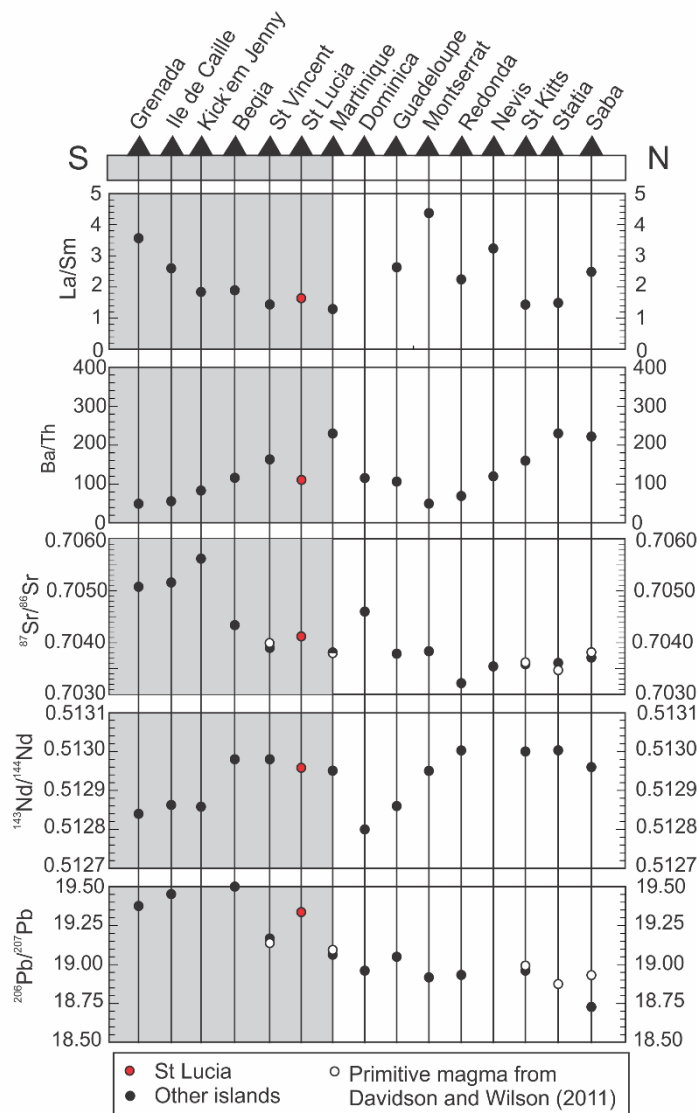


Fig. 4.11. Comparison of La/Sm, Ba/Th, $^{87}\text{Sr}/^{86}\text{Sr}$, $^{143}\text{Nd}/^{144}\text{Nd}$, $^{206}\text{Pb}/^{204}\text{Pb}$ of the most mafic samples analysed in each island along the arc. Primitive magma isotopic compositions from Davidson and Wilson (2011) is also shown for comparison. The grey section of the diagrams represent the central-southern section of the arc. Same data source as in Fig. 4.2. Full compositions and names of the mafic samples used are presented in the supplementary data file (Appendix C).

4.7.3.2.2 Martinique

Martinique is the Lesser Antilles Island over which there has been the most intense debate over “source contamination” versus “crustal assimilation” to explain the extreme isotopic compositions (Davidson, 1987; Davidson and Harmon, 1989; Labanieh et al., 2010; 2012). As on St Lucia, the lavas display co-variation of Sr, Nd, Hf, Pb, Ba/Th and of La/Sm even after correction for amphibole fractionation (Labanieh et al., 2012). Although some volcanoes show a clear correlation of these isotopic and trace element ratios with SiO₂ or MgO (Davidson and Wilson, 2011) and some whole rock $\delta^{18}\text{O}$ ratios are much higher than the mantle range, assimilation during differentiation has been rejected by some authors (Labanieh et al., 2010; 2012). The rationale for this is (1) the $r > 0.5$ necessary to explain the lavas compositions was considered unreasonably high, (2) the published whole rock $\delta^{18}\text{O}$ were thought to be modified by alteration (Labanieh et al., 2010) and (3) the mineral $\delta^{18}\text{O}$ data presented in Davidson and Wilson (2011) for Mt Pelee was close to the mantle range. However, in St Lucia where crustal assimilation is clearly the factor producing the “continental” signature, our models show that $r > 0.5$ is necessary. Such a high rate of assimilation (and $r > 1$) can be produced by some recent assimilation models (Beard et al., 2005) whereby bulk assimilation of crust is driven by reactions during melting, limiting the energy necessary for the process to occur. In addition, $\delta^{18}\text{O}$ mineral data published in Davidson and Wilson (2011) come from samples with some of the less radiogenic Sr and Pb compositions on the island (Mt Pelee). These are similar to Pre-SVC1 lavas in terms of their radiogenic isotopes, and so cannot be used to preclude assimilation in the more “continental” samples on the island. Finally, Martinique lavas with the highest MgO, and, therefore, those least likely to have suffered from crustal assimilation, have Sr-Nd isotope ratios that overlap with the northern islands and only slightly more radiogenic Pb toward those of Pre-SVC1 lavas. They also have low La/Sm similar to the most mafic lavas of the northern islands and to St Lucia Pre-SVC1 compositions (Figs. 4.9-4.11). Therefore, we suggest that all Martinique lavas with “continental” isotopic compositions reflect crustal assimilation of sediments similar to those inferred to be present in the crust of St Lucia. Thus the source beneath Martinique may be similar to that of St Lucia or the northern islands.

4.7.3.2.3 Grenadine Islands

Most of the isotopic data available for the Grenadine islands are from Bequia with only a few from Ile de Caille and Kick'em Jenny. In Bequia, Smith et al. (1996) highlighted the occurrence of crustal assimilation and separated the samples into a IDS (Isotopically Diverse Suite) which experienced assimilation and IHS (Isotopically homogeneous suite) which did not. Smith et al. (1996) used mineral oxygen isotope data and a correlation between radiogenic isotopes and MgO, to show that crustal assimilation of 10-55% of sediment from the Guyana shield affected the IDS samples. The IHS samples, which comprise the most mafic lavas of the island, overlap the northern islands and Pre-SVC lavas in terms of $^{143}\text{Nd}/^{144}\text{Nd}$ and overlap Pre-SVC1 lavas in terms of Sr and Pb isotopes (Fig. 4.10). They also have low La/Sm and variable Ba/Th ratios. IDS samples, however, display more radiogenic compositions, correlating with an increase in La/Sm and a decrease in Ba/Th similar to the trends observed on St Lucia and Martinique. The four samples from Ile de Caille, for which Sr (4 samples) and Nd (3 samples) and Pb (2 samples) isotopic compositions are available, display high MgO (~10.4-10.8 wt. %). These lavas display more crustal Sr and Nd isotope ratios, higher La/Sm and lower Ba/Th ratios than Pre-SVC1 lavas. The two lavas analysed for Pb isotopes show compositions similar to more radiogenic than Pre-SVC1 lavas. The most differentiated lava has the highest $^{87}\text{Sr}/^{86}\text{Sr}$ and La/Sm ratios and the lowest Ba/Th ratio. However, given the very small number of samples it is hard to confidently suggest crustal assimilation of sediment. In the case of Kick'em Jenny, six samples were analysed for trace elements, $^{87}\text{Sr}/^{86}\text{Sr}$ and U-series isotopes and were shown to be affected by crustal assimilation (Huang et al., 2011). Ba/Th ratios are low and overlap SVC compositions. La/Sm ratios display a wide range of composition overlapping with Pre-SVC1, Pre-SVC2 and higher values, but the most mafic samples display a ratio similar to Pre-SVC1 (Fig. 4.11). $^{87}\text{Sr}/^{86}\text{Sr}$ are more radiogenic than Pre-SVC1 lavas and one of the most differentiated lavas overlaps with Pre-SVC2 compositions. No clear correlation can be observed between MgO (4.39-11.85) and $^{87}\text{Sr}/^{86}\text{Sr}$, however, Ba/Th and La/Sm ratios correlate negatively, with the lowest Ba/Th ratio corresponding to the highest La/Sm. The highest La/Sm, in turn, corresponds to the lava with the lowest MgO. Such observations suggests that assimilation of sediment might be involved in the magmatic evolution at Kick'em Jenny, but a more detailed study would be required to verify this.

4.7.3.2.4 Grenada

Grenada has two major suites of magma type: the M- and the C- series (Thirlwall et al., 1996) that both overlap the northern islands and Pre-SVC1 in terms of Nd isotopic compositions, but have more radiogenic Sr (Fig. 4.10). They display a large range of Pb isotope ratios, overlapping both the northern islands and Pre-SVC1 compositions. In terms of La/Sm, all the samples, even the most mafic, have higher La/Sm compared with any other islands in the arc (Figs. 4.10, 4.11). Ba/Th ratios are very low with a maximum of 66. Crustal assimilation has been shown to affect the Grenada lavas, with the most “continental” isotopic signatures corresponding to the most differentiated samples (Thirlwall et al., 1996). In each suite, the most “continental” lavas have the highest La/Sm ratios as a general feature, however, data are scattered. The most mafic sample, a picrite with MgO=17.3 (wt. %), has a La/Sm ratio of 3.6, higher $^{87}\text{Sr}/^{88}\text{Sr}$ (0.70508) and slightly lower $^{143}\text{Nd}/^{144}\text{Nd}$ than the northern islands with Pb isotopes plotting between the northern islands and St Lucia.

4.7.3.2.5 Summary

In summary, except for Grenada, Ile de Caille and Kick'em Jenny (not shown), the most mafic lavas from all the islands in the Lesser Antilles arc have compositions overlapping in terms of Nd isotopes, La/Sm and Ba/Th ratios (Fig. 4.11). Sr and Pb isotope compositions tend to be slightly more radiogenic in the south of the arc, although some samples from both Martinique and St Vincent have ratios overlapping the Northern arc. Therefore, we suggest that a similar slab-derived fluid /sediment ratio characterises the source along the Lesser Antilles arc and that the variations in isotopic signatures amongst the most mafic lavas along the arc largely reflect different isotope compositions of the sediment in the source. The presence of sediment with more radiogenic Sr and Pb in the source of the southern islands compared to the north of the arc has been suggested in the past (e.g. Carpentier et al., 2008). However, previous estimates of the nature and composition of these sediments were made using the whole Lesser Antilles arc lava dataset, without taking into account the degree of differentiation of the lavas or crustal assimilation. Here we show that isotopic variations in the most mafic lavas are restricted compared to the variations observed when lavas of all degrees of differentiation are selected. Therefore, previous estimates

of the nature and isotopic composition of the subducted sediments, based on the whole Lesser Antilles arc lavas dataset, are biased and need to be reassessed. These studies include that of Carpentier et al. (2008) who suggested the need of subducted sediment with extreme Pb isotopic compositions such as those found in site 144 sediments, to explain the southern islands lava compositions.

4.8 Conclusions

Lavas with continental isotopic compositions observed in St Lucia are produced by high rates of assimilation of sediment in the arc crust, which are responsible for the co-variation of Sr, Nd, Hf and Pb isotope ratios, L/M-HREE and Th/Th* with SiO₂. The sediment assimilated is likely to be a mix of biogenic and terrigenous sediments originating from the South American continent. Some lavas escaped significant crustal assimilation, these have signatures close to “typical oceanic arc” isotopic signatures with similar Ba/Th, La/Sm, Nd isotope ratios to the northern islands mafic lavas but slightly more radiogenic Sr and Pb isotopes. Such lavas can be produced by the addition in the source of less than 2% of sediment with more radiogenic Sr and Pb than the sediments involved in the source of the northern islands. A comparison of St Lucia with other islands from the south of the arc suggests that the source of Martinique, St Vincent and Bequia magmas is similar to St Lucia. Only Grenada, Ile de Caille and Kick'em Jenny could have a source containing large amounts of, or more radiogenic, sediment. Martinique and Grenada, which along with St Lucia are the two other islands with extreme isotopic compositions, display a similar co-variation of Sr, Nd, Hf and Pb isotope ratios, Ba/Th and L/M-HREE to that observed in St Lucia lavas affected by crustal assimilation. We suggest that assimilation is the only process responsible for the extreme isotopic compositions observed in the arc and that, except for Grenada, Ile de Caille and maybe Kick'em Jenny, the amount of sediment present in the source of the north and the south of the arc is similar. The more radiogenic Sr and Pb signatures observed in the southern lavas are instead explained by a more radiogenic sediment.

Chapter 5

Origin and evolution of silicic crust in oceanic arcs; an in situ study from St Lucia, Lesser Antilles

A version of this chapter will be submitted to *Journal of Petrology* co-authored by Simon Turner, Jon Davidson, Axel Schmitt and Jan Lindsay.

The supplementary data file of this chapter is presented in Appendix D.

Abstract

Processes linked with the genesis, evolution and eruption of silicic complexes in arcs are still poorly constrained. Of particular interest are the depth of magma production, the relative contribution of crystal fractionation versus crustal partial melting, and the timescales involved. The Soufriere Volcanic Complex (SVC) on St Lucia is one of the largest silicic centres in the Lesser Antilles arc. Here we present the results of a detailed mineral study, including in-situ Sr isotopes in plagioclase and in-situ $\delta^{18}\text{O}$ in dated zircons, of both SVC and Pre-SVC lavas in order to place constraints on the processes intrinsic to the development and evolution of the silicic complex. Our data suggest that the production of silicic magma in the SVC occurs in two stages. The first stage involves differentiation of mafic magma by crustal assimilation and mineral fractionation in the middle-lower crust of the arc to produce magmas with intermediate compositions. These intermediate magmas are water rich (~7 wt. %) and have high $^{87}\text{Sr}/^{86}\text{Sr}$, Ba, Sr and La/Sm (~5) compared to Pre-SVC lavas. Near constant trace element and isotopic compositions throughout the SVC lifespan indicate that the same process was persistent over the last 600 ka. In the second stage, the intermediate magmas are transferred to a shallower and more differentiated chamber (~ 6 km depth). During ascent, any crystals or xenocrysts residual from stage one in the deeper chamber become fully resorbed and the magma crystallises hornblende microphenocrysts, followed by anorthite-rich plagioclase close to or at the water saturation depth. During mixing in the shallow chamber, plagioclase from the recharging magma are partially resorbed. So are the crystals in equilibrium with the resident differentiated magma. The recharge event triggers chamber wide convection. Mixing is thought to trigger eruption of the silicic complex.

5.1 Introduction

Whilst important for the evolution of the andesitic continental crust, our understanding of the genesis and evolution of silicic magma bodies in continental and mature oceanic arcs remains limited. Models for silicic magma production include crystallisation of mantle derived mafic magma in either the upper (Pichavant et al., 2002) or lower crust (Prouteau and Scaillet, 2003), partial melting of previously emplaced igneous rocks (Jackson et al., 2003), mixing of mafic magma with partial melts of metasediment present in the arc crust (Druitt et al., 1999) or assimilation of igneous rocks and/or metasediments by mafic magma either by sensible heat (from cooling) and/or by latent heat from fractional crystallisation (DePaolo, 1981). These processes could occur separately or be combined, as in the “hot zone” model proposed by Annen et al. (2006), where partial crystallisation of basalt sills in the lower crust produces both residual silicic melts and anatectic melts from partial melting of pre-existing crustal rocks. Determination of the depth at which andesite-dacite production occurs is not straightforward. While most andesite-dacite phenocryst assemblages suggest crystallisation at low pressure and temperature, the lack of large volumes of mafic cumulate in the upper crust may argue against significant differentiation at shallow depth (Muntener et al., 2001). Instead, there may be a decoupling of phenocryst fractionation occurring at shallow depth, and andesite-dacite liquid production itself taking place in a deeper chamber. In this case, popular processes for the triggering of segregation and ascent of felsic magmas produced in the middle-lower crust include compaction of partially molten rock (McKenzie, 1985) or the injection of recharge magma which could force silicic magma to ascend along pre-existing or initiated fractures (e.g diking; Brown, 2007). High water contents can aid ascent and lead to resorption of crystals and xenocrysts due to heating of the magma during decompression (Annen et al., 2006). Conditions and processes involved in shallow magma chambers prior to eruption include magma mixing or mingling between hot recharge magma and cooler silicic resident magma as well as extensive crystal fractionation due to the decompression and degassing.

This study presents detailed petrography and mineral chemistry for lavas from St Lucia island, in the Lesser Antilles arc, where volcanism transitioned from mainly mafic to silicic around 3 Ma ago (Lindsay et al., 2013). We use petrographic

observations along with in-situ mineral $\delta^{18}\text{O}$, $^{87}\text{Sr}/^{86}\text{Sr}$, major and trace elements in representative lavas to assess (1) the role of deep versus shallow differentiation and the role of crustal assimilation in the genesis of the silicic magmas and (2) the relative roles of cooling, reheating and magma mixing on the evolution and lifetime of the SVC.

5.2 Geological background

St Lucia is located in the southern section of the Lesser Antilles arc, between Martinique and St Vincent islands (Fig. 5.1a). On St Lucia, two groups of lavas can be separated, both in terms of composition and age. The oldest group is termed the Pre-Soufriere Volcanic complex (Pre-SVC) (Bezard et al., 2014). Pre-SVC lavas are present across the island (Fig. 5.1b). They are mainly mafic (Fig. 5.2a) but display compositions ranging from basalt to rhyolite, dated between 18 and 1.1 Ma. The second and younger group of lavas is the Soufriere Volcanic complex (SVC). Lavas from this group are silica-rich andesites and dacites (62-67 wt. % SiO_2 ; Fig. 5.2a) that were extruded from 3 Ma to recent in the south-western part of the island (Fig. 5.1c), in and around a large depression called the Qualibou depression. The associated volcanoclastic rocks cover most of the central and southern part of the island (Fig. 5.1b, c).

Using $\delta^{18}\text{O}$ and $^{87}\text{Sr}/^{86}\text{Sr}$ data from hand-picked minerals, Bezard et al. (2014), showed that most St Lucia lavas were affected by crustal assimilation of sediment intercalated within the arc crust. The SVC lavas are the most affected by crustal assimilation, and display “continental” isotopic compositions with $^{87}\text{Sr}/^{86}\text{Sr}$ and $^{143}\text{Nd}/^{144}\text{Nd}$ of 0.70411-0.70439 and 0.51295-0.51298, respectively (Fig. 5.2b). In contrast, Pre-SVC lavas were much less affected by assimilation and have more typical oceanic arc signatures (Pre-SVC1; Fig. 5.2b) (whole-rock $^{87}\text{Sr}/^{86}\text{Sr}$ and $^{143}\text{Nd}/^{144}\text{Nd}$ between 0.70411-0.70439 and 0.51295-0.51298, respectively), except for a few lavas located in the south-east of the island, which display more “continental” signatures with transitional isotopic compositions between SVC and Pre-SVC1 (Pre-SVC2; Fig. 5.2b; $^{87}\text{Sr}/^{86}\text{Sr}$ and $^{143}\text{Nd}/^{144}\text{Nd}$ of 0.70611-0.70622 and 0.51251-0.51258 respectively). In chapter 4, it was shown that on St Lucia, variations in lava whole rock Hf and Pb isotopes, rare earth element composition (L/M-HREE) and in $\text{Th}/\text{Th}^*(\text{Th}_{\text{CN}}/((\text{Ba}_{\text{CN}} + \text{U}_{\text{CN}})/2))$ were

all also controlled by crustal assimilation of sediment. The latter is inferred to have Sr, Nd, Hf and Pb isotopic composition similar to the local sediments as well high La/Sm ratio (~ 6) and high Th concentrations.

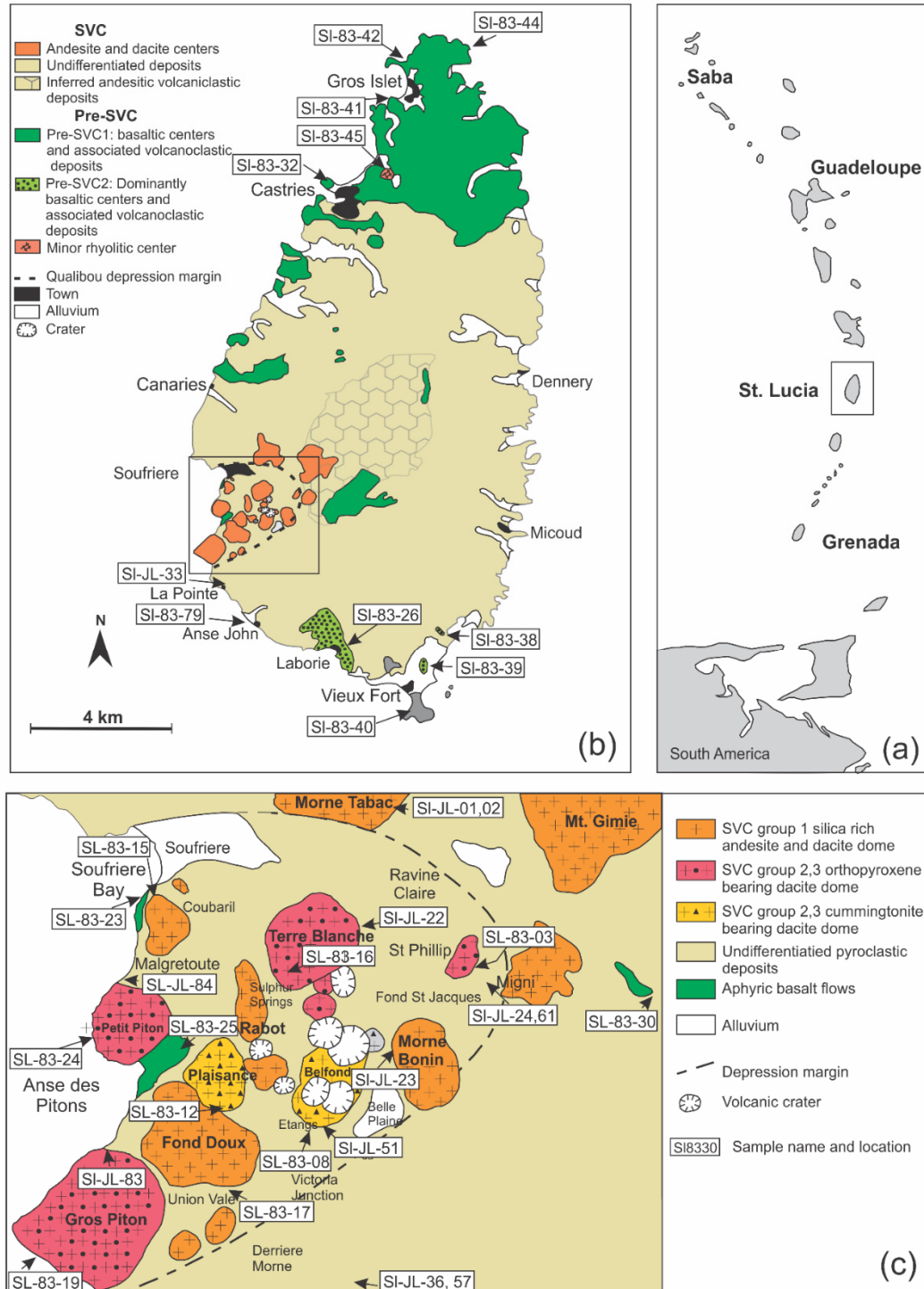


Fig. 5.1. (a) Geological setting of St Lucia. (b) Geological map of St Lucia divided into two main groups: Pre-Soufriere volcanic complex (Pre-SVC) and Soufriere Volcanic complex (SVC). (c) Geological map of the Soufriere area showing the name of all the extruded lava flows. Location of

samples discussed in this contribution are presented in (b) and (c). Figure modified from Bezard et al. (2014).

Based on (U-Th)/He eruption ages, (Schmitt et al., 2010; Lindsay et al., 2013), the activity in the SVC can be separated in three eruption periods:

-Phase 1 ~640-250 ka: Emplacement of Micoud pyroclastic deposit (640 ka), of the silica-rich andesites and dacites of the Mt Gimmie and Mt Tabac (~532 ka) stratovolcanoes, and deposition of the dacitic pyroclastic rocks and domes of Bellevue (264 ka) and Morne Bonin (273 ka).

-Phase 2 ~105-50 ka: includes the eruption of Anse John quartz-poor pumice tuff (104 ka), Gros and Petit Piton domes (109 ka and 71 ka) and the Pointe Beach pumice (59 ka),

-Phase 3 ~20 ka: eruption of Belfond tuff (20 ka) and the Belfond and Terre Blanche domes.

A major sector collapse resulting in the Qualibou depression occurred between phase 1 and 2 and a period of eruptive quiescence occurred between phase 2 and 3.

From (U-Th)/He eruption ages and U-Th zircon ages, Schmitt et al. (2010) proposed an evolutionary model for the SVC. This model invokes episodic re-melting within a complex of mid-crustal plutons of intermediate composition under the Qualibou depression. The source of the heat necessary for re-melting remains unconstrained but was suggested to be due to mafic magma underplating beneath the plutonic complex. The model is based on several observations: (1) zircon crystallisation ages predate volcanism, and this is more obvious for phases 2 and 3 than for phase 1; (2) zircon crystallisation age distributions are not distinguishable between plutonic inclusions and their host lava; (3) zircons record discontinuous crystallisation episodes; and (4) the age distribution of zircon growth in lavas and pyroclastic deposits from different eruption periods and that are spatially separated share strong similarities.

In this contribution, the existing evolutionary model proposed for the SVC is tested and the development of silicic magmatism on St Lucia is further constrained using a detailed petrographic, chemical and isotopic investigation of the different groups of eruptive products. In the following sections, SVC lavas were subdivided into SVC1,2 and 3 referring to the 3 main phases of eruption of the silicic complex. Here the term “phenocryst” is used to refer to the size of the crystal (typically with diameter > 600 µm) and has no genetic meaning.

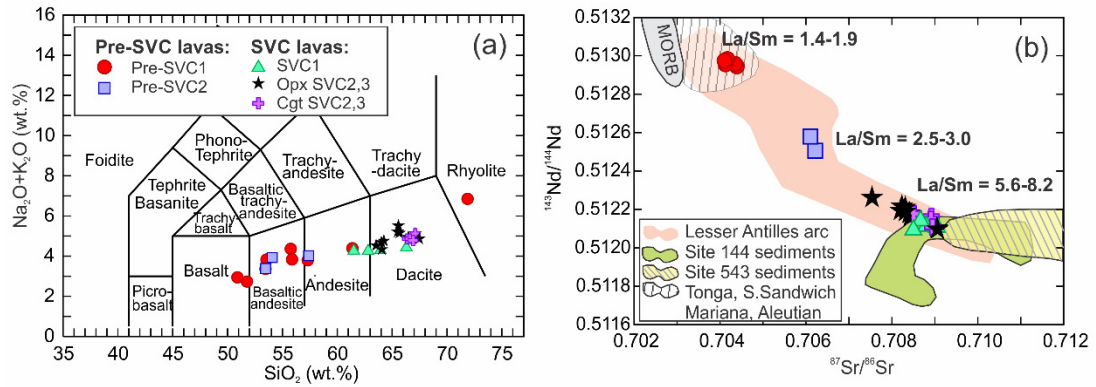


Fig. 5.2. Whole rock major element (a) and $^{87}\text{Sr}/^{86}\text{Sr}$ vs. $^{143}\text{Nd}/^{144}\text{Nd}$ isotopic compositions (b) of the different groups of Pre-SVC and SVC lavas. Figure modified from Chapter 4.

5.3 Methods

For this study, we performed petrographic analyses on 30 thin (30 μm) and 24 thick polished (100 μm) sections of samples covering the different groups of eruptive products (Pre-SVC1,2 and SVC1,2,3). The location for each sample analysed is shown on Fig. 5.1. Twelve thick sections were chosen for SEM imaging and electron microprobe major element analysis. Based on the combined SEM and EMP data, eight and six thick sections, respectively, were selected for in-situ trace element analysis by laser-ICP MS and in-situ $^{87}\text{Sr}/^{86}\text{Sr}$ by microdrilling-TIMS analyses. In-situ $\delta^{18}\text{O}$ measurements in zircons separated from ten SVC lavas and mounted in indium and aluminium mounts were also performed. The zircons selected had been previously dated by the U-Th and U-Pb methods (Schmitt et al., 2010).

5.3.1 Imaging and electron microprobe analysis

Over 200 back-scattered electron images were collected on thick sections of representative samples using a Zeiss EVO MA15 scanning electron microscope at the Geochemical Analysis Unit (GAU), Macquarie University, with an accelerating voltage of 15 kV. Brightness and contrast were varied to accentuate the textures. A few images of the thick sections were also obtained by cathodoluminescence with a fixed voltage of 15 kV and variable current. Imaging of zircon mounts was performed at the University of California in Los Angeles (UCLA) using a LEO 1430 VP Scanning Electron Microscope (SEM) and similar analytical conditions.

Mineral major element analyses were completed using a CAMECA SX100 electron microprobe either at Macquarie University or at the Australian National University (ANU) with an accelerating voltage of 15 kV, a 20 nA beam current and a beam diameter of 1-2 μm . Calibration at Macquarie was based on the following standards: orthoclase (K), wollastonite (Ca, Si), albite (Na), hematite (Fe), kyanite (Al), chromium (Cr), rutile (Ti), olivine (Mg). At ANU, the following standards were used: albite (Na), K412 glass (Mg, Al, Fe), chromite (Cr), rhodonite (Mn), Sanidine (K), rutile (Ti), P on #375 glass.

Major element compositions of the lava groundmasses were determined using an energy dispersive spectrometer (X-max Oxford Instruments) attached to the Zeiss EVO scanning electron microscope at operating conditions of 20 kV and 8-10 nA, at GAU. The instrument (spectrum) was calibrated using a thin pure copper grid attached to each section analysed.

5.3.2 Trace elements

In-situ trace element concentrations were determined using a New Wave UP-213 laser ablation system linked to an Agilent 7700 Series ICP-MS system at the GAU, Macquarie University. Ablation of the samples was performed in a helium chamber using a frequency of 5 Hz and an ablation size of 55 μm for single spots or a line of 120 μm long and 30 μm wide when rastering was needed. Concentrations and detection limits were obtained using GLITTER software (<http://www.glitter-gemoc.com/>). The instrument was calibrated using the NIST610 glass standard and the CaO (wt. %) concentration obtained from the electron microprobe was used as an internal standard for each analysis. The BCR-2 standard was analysed at least at the beginning and the end of each analytical session. Results for BCR-2 are presented in the Supplementary data file (Appendix D). Differences between our measured BCR-2 concentrations in every batch and the Georem preferred values are less than 5% for all elements presented. Given the presence of melt inclusions in most crystals and in order to ensure data quality, incompatible trace elements in the mineral analysed were carefully checked and all abnormal data (e.g. unreasonable enrichment in elements incompatible in plagioclase) were discarded. Furthermore, every LA-ICPMS analysis included major elements allowing comparison with the major element obtained by electron microprobe, and the calculation of the structural formula for every spot.

5.3.3 In-situ $^{87}\text{Sr}/^{86}\text{Sr}$ analysis of plagioclase

In-situ $^{87}\text{Sr}/^{86}\text{Sr}$ analyses were performed by microdrilling thick sections (100 μm) followed by measurements by Thermal Ionization Mass Spectrometry (TIMS). Two crystals from the most mafic Pre-SVC1 lavas (basalt SL-83-44), three crystals from the most mafic Pre-SVC2 (basaltic andesite SL-83-26) as well as 7 crystals from the SVC lavas (one from SL-JL-02 and one from SL-JL-23, three from SL-JL-51 and two from SL-JL-83) were selected for analysis. Groundmass from the corresponding lavas was also analysed. Before microdrilling, electron microprobe traverses and trace element analyses were performed across all the selected crystals. Microsampling was performed at the GAU, Macquarie University, using a Merchantek[®] micromill, following the method developed by Charlier et al. (2006). Microdrilling of the sample was performed in a drop of MQ water and collected using a micropipette, then placed in a Teflon Savillex beaker and dried before being digested in HF and HNO₃. Sr separation was carried out using ~ 70 μl of pre-washed Sr-Spec resin and samples were analysed using a Finnigan Triton TIMS instrument in static collection mode. Correction for within-run mass fractionation was done using an exponential law and the normalising value of $^{86}\text{Sr}/^{88}\text{Sr} = 0.1194$. Sr samples were run unspiked since the young age (< 20 Ma) and low Rb/Sr (0.44-0.02) of St Lucia lavas precluded the need of isotopic dilution to age correct the measured ratios. Rb was monitored and burned off the filament during slow heating prior to analysis. During the analytical session instrument performance was monitored by analyses of Sr standard NBS987. The average $^{87}\text{Sr}/^{86}\text{Sr}$ ratio for NBS987 obtained on 8 ng Sr was 0.710237 ± 0.000021 (2sd; n = 8). This is in very good agreement with the value reported by Thirlwall (1991) of 0.710248 ± 0.000023 (2sd, n = 427). During the course of this study, analyses of microdrilled international glass standards NIST611 and BCR-2G (~ 20 ng Sr loads) were carried out and the average $^{87}\text{Sr}/^{86}\text{Sr}$ was 0.70965 ± 0.000037 (2sd; n = 4) and 0.705026 ± 0.000030 (2sd; n = 4) respectively. BCR-2G values are identical to values determined for large loads of Sr (> 100 ng Sr) by Mahoney et al. (2003) of 0.705024 ± 0.000010 (2sd). Three total procedure blanks contained 22, 33 and 7 pg of Sr which represent 0.22, 0.33 and 0.07 % of the smallest Sr sample analysed (10 ng) and are therefore negligible. The details of NBS987, NIST611, BCR-2G and blanks data are presented in the supplementary data file (Appendix D).

Table 5.1. Mineral and matrix $^{87}\text{Sr}/^{86}\text{Sr}$ ratios with the corresponding calculated trace element compositions.

	$^{87}\text{Sr}/^{86}\text{Sr}$	Std error	Sequ.	TE analysis #	La/Sm	Sr	Ba	An*
Pre-SVC1 basalt (WR $^{87}\text{Sr}/^{86}\text{Sr} = 0.704132$)								
44-3-2A	0.704270	0.000007	A	47+48	4.9	291.7	9.4	0.90
44-3-2A	0.704196	0.000007	B	58	4.4	267.5	8.3	0.92
44-3-2B	0.704145	0.000008	C	49	n.a	263.9	7.4	0.86
44-3-2B	0.704191	0.000006	D	50+59	3.0	245.1	10.9	0.78
44-3-1A	0.704125	0.000007	A	55	n.a	271.6	8.1	0.91
44-3-1B	0.704126	0.000019	B		n.a	n.a	n.a	n.a
44-3-1C	0.704110	0.000009	C	56	n.a	268.0	9.2	0.90
44-3-M	0.704255	0.000008	M		n.a	n.a	n.a	n.a
Pre-SVC2 basaltic andesite (WR $^{87}\text{Sr}/^{86}\text{Sr} = 0.706219$)								
26-6-1A	0.705773	0.000006	A	11	n.a	285.2	12.4	0.94
26-2-1A	0.706164	0.000007	A	6	8.3	343.2	26.0	0.88
26-2-1B	0.706093	0.000007	B	7	6.2	342.1	52.1	0.75
26-2-1A	0.706101	0.000006	C	8+9	7.9	380.2	58.5	0.73
26-2-1C	0.706267	0.000006	D	10	11.3	369.5	67.6	0.68
26-C6-1A	0.706136	0.000006	A	12	6.1	366.4	38.2	0.84
26-C6-1B	0.706295	0.000013	B		n.a	n.a	n.a	n.a
83-26-M	0.706384	0.000008	M		7.1	n.a	367	n.a
26-C6-M(v2)	0.706374	0.000007	M(V2)		7.1	n.a	75	n.a
SVC1 andesite, dacite (WR $^{87}\text{Sr}/^{86}\text{Sr} = 0.70850$)								
02-C4-1A	0.708442	0.000009	A		n.a	n.a	n.a	n.a
02-C4-1B	0.708386	0.000010	B	13	20.9	645.3	162.5	0.56
02-C4-1C	0.708490	0.000005	C		n.a	n.a	n.a	n.a
JL02 M	0.708548	0.000008	M		n.a	n.a	n.a	n.a
23-4-1A	0.708955	0.000007	A	22	15.0	633.9	31.1	0.92
23-4-1B	0.708870	0.000007	B	23+69	16.7	728.3	209.3	0.59
JL23M	0.708820	0.000015	M		6.4	162	725	n.a

Trace element analysis of the bulk zone microdrilled was obtained by LA-ICPMS. When the microdrilled surface overlapped two zones with distinct trace element composition, the bulk trace element composition was calculated consequently using the composition of the two zones and the percentage of it. The trace element analysis number (#) correspond to the data number in the supplementary data file. An* = Anorthite content of the microdrilled zone that was calculated using the major element profile obtained by EMP. WR = whole rock; sequ. = sequence from core to rim except M = matrix; Opx = orthopyroxene; Cgt = cummingtonite.

Table 5.1. (continued).

	$^{87}\text{Sr}/^{86}\text{Sr}$	Std error	Sequ.	TE analysis #	La/Sm	Sr	Ba	An*
Opx-bearing SVC2,3 (WR $^{87}\text{Sr}/^{86}\text{Sr} = 0.708202$)								
83-5-1A	0.708761	0.000008	A	37	24.4	739.7	130.6	0.54
83-5-1B	0.708655	0.000007	B		n.a	n.a	n.a	
83-5-1C	0.708761	0.000007	C	77	20.9	590.1	91.5	0.61
83-1-1A	0.708312	0.000007	A	34+35+75	23.4	774.1	149.8	0.60
83-1-1B	0.708491	0.000006	B	36+76	28.5	725.6	171.7	0.52
83-1-1B v2	0.708478	0.000005	B v2	36+76	28.5	725.6	171.7	0.52
JL83M	0.708124	0.000010	M		7.1	75.0	367.0	n.a
Cgt-bearing SVC2,3 (WR $^{87}\text{Sr}/^{86}\text{Sr} = 0.708946$)								
JL51-C3-1A	0.708454	0.000007	A	24+25+70	26.7	729.5	119.8	0.60
JL51-C3-1B	0.708420	0.000006	B	26	28.0	668.1	117.4	0.55
JL51-C3-1C	0.708501	0.000005	C	27	19.8	739.4	120.6	0.64
JL51-C3-1D	0.708605	0.000006	D	28	25.3	675.4	132.5	0.53
JL51-C4-1A	0.708327	0.000007	A	29+30	30.4	642.9	126.7	0.48
JL51-C4-1B	0.708963	0.000007	B	31+71	28.0	730.7	155.2	0.50
JL51-C5-1A	0.709238	0.000008	A	32	14.5	663.6	40.0	0.83
JL51-M	0.709140	0.000008	M		n.a	n.a	n.a	n.a

Trace element analysis of the bulk zone microdrilled was obtained by LA-ICPMS. When the microdrilled surface overlapped two zones with distinct trace element composition, the bulk trace element composition was calculated consequently using the composition of the two zones and the percentage of it. The trace element analysis numbers (#) correspond to the data numbers in the supplementary data file. An* = Anorthite content of the microdrilled zone that was calculated using the major element profile obtained by EMP. WR = whole rock; sequ. = sequence from core to rim except M = matrix; Opx = orthopyroxene; Cgt = cummingtonite.

5.3.4 Zircon $\delta^{18}\text{O}$

Oxygen isotope ratios in SVC zircons were analysed using the CAMECA ims 1270 high-resolution ion microprobe at UCLA using multi-collection analysis as described in Trail et al. (2007). Oxygen isotope ($\delta^{18}\text{O}$) values are reported in the standard per mil (‰) notation relative to the Vienna Standard Mean Ocean Water (V-SMOW). Standard AS3 ($\delta^{18}\text{O}_{\text{VSMOW}} = 5.34\text{‰}$; Trail et al., 2007) was analysed several times ($n = 80$) at the beginning, during and at the end of each analytical session to determine instrumental mass fractionation. The accuracy of the measurements was confirmed by replicate analysis of the in house zircon standard 91500 ($\delta^{18}\text{O} = 9.78 \pm 0.37$ (2 sd; $n = 10$). The details of the standard compositions are presented in the supplementary data file (Appendix D).

5.4 Petrography

Representative modal analyses for each lava group are presented in Fig. 5.3.

5.4.1 Pre-SVC

Pre-SVC1 basalts (Fig. 5.4a) are porphyritic to glomeroporphyritic (30-35% phenocrysts). Their phenocryst assemblage is dominated by plagioclase (89-90%) resorbed olivine (5-8%) and clinopyroxene (2-4%) with minor orthopyroxene (1%) and microphenocrysts of ilmenite (1%). Plagioclase occurs as subhedral laths or as anhedral grains in aggregates. They are lightly zoned and contain angular melt inclusions. Clinopyroxene is also subhedral and contains rounded oxide inclusions. Olivine is pseudomorphosed by serpentine and low grade amphibole. The groundmass is composed of plagioclase, clinopyroxene, ilmenite and orthopyroxene.

Pre-SVC1 basaltic andesite textures vary from almost aphyric, trachytic or porphyritic to glomeroporphyritic while Pre-SVC2 basaltic andesites (Fig. 5.4b) are porphyritic to glomeroporphyritic. In Pre-SVC1,2 lavas with porphyritic to glomeroporphyritic textures, plagioclase is always the dominant phase (59-89%) followed by clinopyroxene (10-20%) and orthopyroxene (6-20%; Fig. 5.3). Rare replaced olivine can be observed (1-2%). Plagioclase is zoned and inclusion-rich. Pyroxene is subhedral to euhedral. In some samples, clinopyroxene forms a corona around orthopyroxene (SL-83-26) or just a thin overgrowth (SL-83-38, 40). The groundmass comprises glass, plagioclase, clinopyroxene, orthopyroxene and ilmenite. In lavas with trachytic texture, clinopyroxene dominates the assemblage (69%) and plagioclase constitutes only 30% along with 1% of pseudomorphosed olivine.

Pre-SVC1,2 andesites are all porphyritic (35-40% phenocrysts). Plagioclase (70-78%) is the most abundant phase. Orthopyroxene (12-15%) occurs along with clinopyroxene (8-15%) or alone in which case it is more abundant (27%). Ilmenite microphenocrysts occur as a minor phase (2-3%).

Finally, Pre-SVC1 rhyolite is almost aphyric with only 4% phenocrysts. The main phases are plagioclase (70%), orthopyroxene (15%) and clinopyroxene (15%). Ophitic textures can be observed. Plagioclase often forms in aggregate with pyroxene. The groundmass is comprised of plagioclase, clinopyroxene and ilmenite.

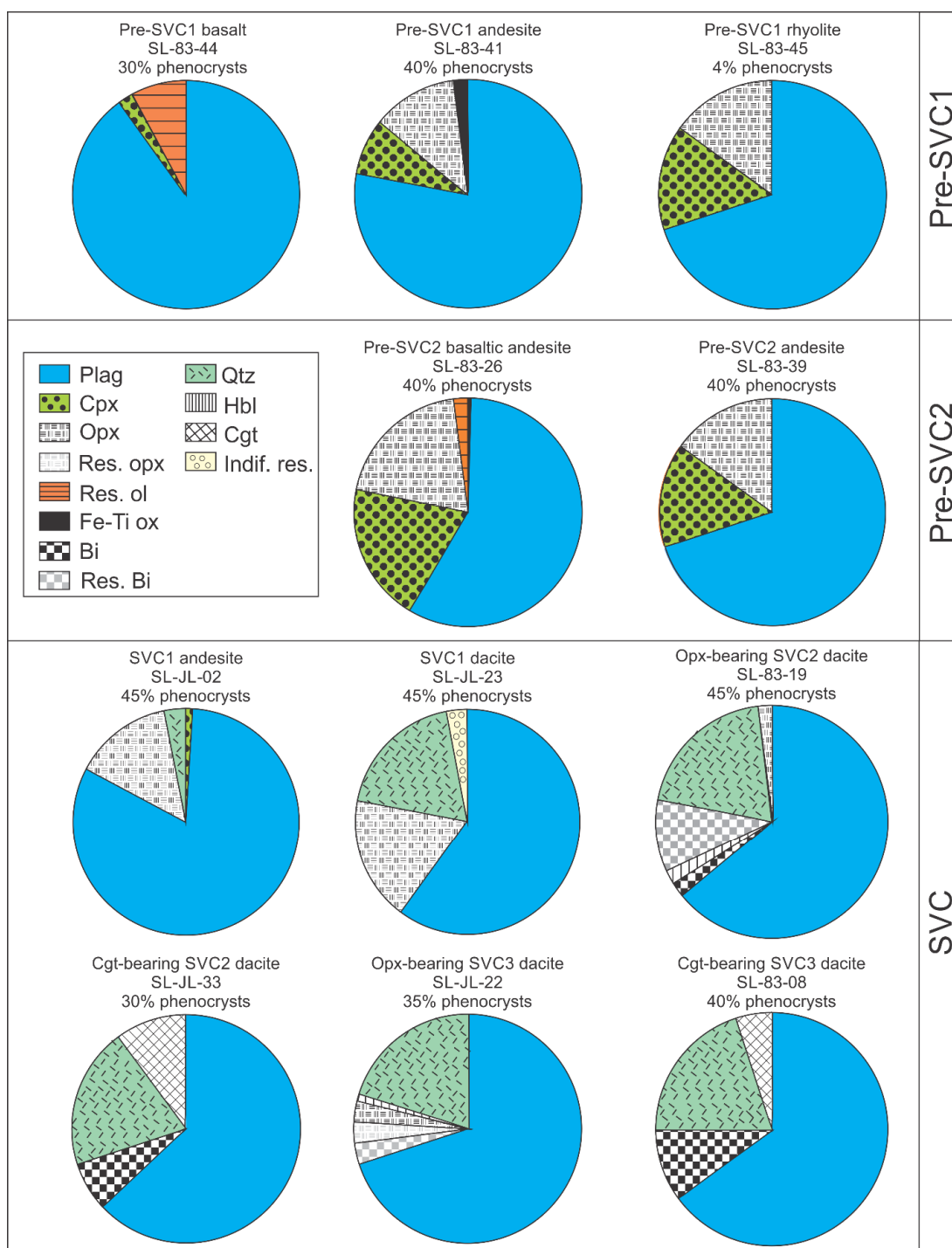


Fig. 5.3. Representative modal proportions of St Lucia lavas phenocrysts. Plag = plagioclase; Cpx = clinopyroxene; Opx = orthopyroxene; Res. opx = resorbed orthopyroxene; Res. ol = resorbed olivine; Fe-Ti oxide = iron-titanium oxide; Bi = biotite; Res. Bi = resorbed biotite; Qtz = quartz; Hbl = hornblende; Cgt = cummingtonite; Indif. Res. = indifferntiated resorbed phase.

5.4.2 SVC

SVC1 (3 Ma-250 ka; Fig. 5.5) andesite and dacite lavas (Figs. 5.1 and 5.2a) are porphyritic (15-45% phenocrysts; Fig. 5.4c). The main phenocryst phases in the andesites are plagioclase (79-82%) and orthopyroxene (15%). Andesites also contain 1-3% phenocrysts of quartz and 1% of micro-phenocrysts of clinopyroxene. The dacites have lower plagioclase (45-60%) and higher quartz modal abundances (19-40%) than the andesites, but a similar amount of orthopyroxene. In both andesites and dacites, quartz is zoned and displays corroded gulfs and melt inclusions. Orthopyroxene is automorphic to subautomorphic and displays ilmenite inclusions that are usually parallel to the growth pattern. Plagioclase is rich in melt inclusions. Andesite and dacite groundmasses comprise mainly plagioclase and variable amounts of pyroxene ilmenite and quartz.

SVC2 (100-50 ka; Fig. 5.5) dacites (Fig. 5.2a) are also porphyritic (20-45% phenocrysts). For all volcanic products except the youngest (Lapointe pyroclastic flow), the main phenocryst phases are inclusion-bearing plagioclase (37-67%), euhedral or rounded quartz (15-48%) and rounded to subhedral inclusion-bearing orthopyroxene (10-20%) (Fig. 5.4e). In samples from Gros Piton, orthopyroxene in equilibrium (0-2%) is rare and they typically have resorbed texture (10%). Euhedral microphenocrysts of hornblende are present in all samples, except the Lapointe pyroclastic flow. They occur in variable proportions (2-10%) and are rimmed by oxides. Rare microphenocrysts of clinopyroxene can also be found in hornblende-bearing samples. The highest proportion of hornblende is found in the Gros Piton lavas. All samples display minor amounts of brown biotite (2-7%). Biotite typically contains inclusions of melt, ilmenite, zircon and plagioclase and is rimmed by oxides. Sometimes, biotite is totally replaced by black oxides. The groundmass is comprised of variable amounts of plagioclase, orthopyroxene, hornblende, ilmenite, quartz and biotite. The Lapointe pyroclastic flow (SL-JL-33), which is the youngest volcanic product of group 2 (59.8 ka; Fig. 5.5), has a different phenocryst assemblage compared to the rest of the group 2 lavas with 63% plagioclase, 35% quartz, 15% cummingtonite and 5% biotite. Both brown biotite and brown cummingtonite occur as large phenocrysts that appear to be in equilibrium and contain ilmenite inclusions (Fig. 5.4d, f). Plagioclase and quartz are both zoned. The groundmass assemblage is similar to the phenocryst assemblage.

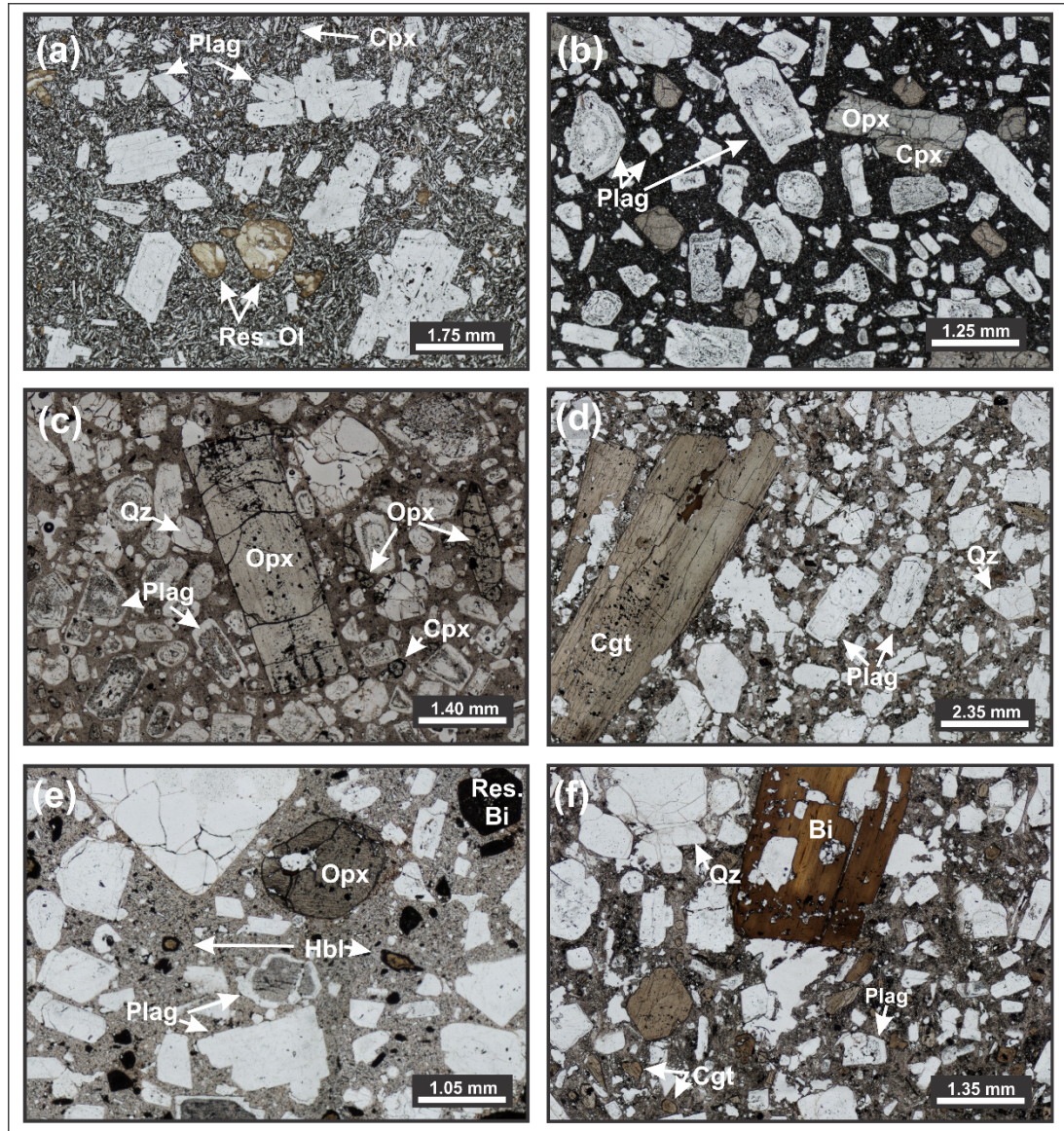


Fig. 5.4. Representative photomicrographs of Pre-SVC and SVC lavas in plain light. (a) Pre-SVC1 basalt; (b) Pre-SVC2 basaltic andesite; (c) SVC1 dacite; (d) Cummingtonite-bearing SVC2,3 dacites; (e) Orthopyroxene-bearing SVC2,3 dacite also displaying hornblende microphenocrysts and resorbed biotite; (f) Large biotite crystal in cummingtonite-bearing SVC 2, 3 dacite. Res Ol = resorbed olivine; Cpx = clinopyroxene; Plag = plagioclase; Opx = orthopyroxene; Qz = quartz; Bi = biotite; Hbl = hornblende; Cgt = cummingtonite.

Finally, SVC3 (~20 ka-present) dacites are porphyritic (20-40% phenocrysts) and characterised by larger quartz phenocrysts than found in the group 2 lavas and higher abundances of brown biotite. Once again, the older products (20.7 ka-15.3 ka; Fig. 5.5) contain orthopyroxene while the most recent products (13.6 ka) are cummingtonite-bearing. The Terre Blanche dacite dome (SL-83-16; SL-JL-22; 15.3

ka) and the oldest Belfond pyroclastic flow (SL-JL-61; SL-JL-24; 20.7-21 ka) contain 3-13% of orthopyroxene while the Belfond dacite lavas contain 5-15% of microphenocrysts of cummingtonite. In all samples, plagioclase is still the main phenocryst phase (43-70%) followed by quartz (15-40%) and biotite (1-7%). In orthopyroxene-bearing dacites, microphenocrysts of hornblende can be observed (1%; Terre Blanche dacite). In such cases, orthopyroxene can display resorbed textures with a rim of hornblende and biotite is present in small amounts (1%) and is mainly resorbed. When no microphenocrysts of hornblende are present, both orthopyroxene and cummingtonite-bearing lavas have high percentages of biotite with texture similar to group 2 (5-10%; Belfond dacite dome and pyroclastic flow). The groundmass comprises variable amounts of plagioclase, orthopyroxene or cummingtonite, biotite quartz and ilmenite.

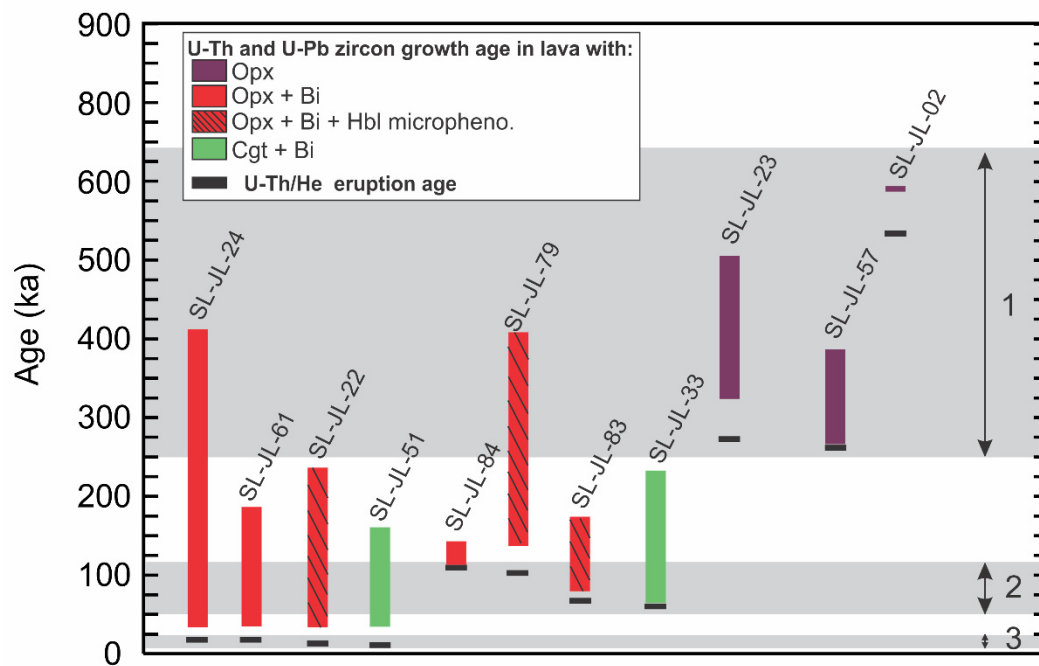


Fig. 5.5. U-Th/He eruption ages and U-Th and U-Pb zircon growth ages of the SVC lavas. All ages are from Schmitt et al. (2010) and Lindsay et al. (2013) and the three corresponding eruption periods are highlighted in grey. Opx = lava with only orthopyroxene (SVC1); Opx + Bi = lava with both orthopyroxene and biotite; Opx + Bi + Hbl = lava with orthopyroxene, biotite and hornblende. Cgt = lava with cummingtonite and biotite. The youngest lava of both eruption periods 2 and 3 contain cummingtonite.

5.5 Mineral and groundmass major element data

Representative major element compositions for plagioclase, clinopyroxene, orthopyroxene, amphibole, biotite and groundmass are presented in the supplementary data file (Appendix D). All mineral major element compositions with full structural formulas are presented in Appendix G.

5.5.1 Plagioclase

We concentrated on phenocrysts with diameter > 400 μm and performed SEM imaging and major element profiles across crystals with a step distance of $\sim 25 \mu\text{m}$. In the Pre-SVC1 group, we focussed on SL-83-44 (basalt), SL-83-25 (basaltic andesite) and SL-83-45 (rhyolite). SL-83-44 and SL-83-25 represent lavas with the most and the least “continental” isotopic signature, respectively out of the Pre-SVC1 samples, and SL-83-44 and SL-83-45 are the least and the most differentiated sample of the group, respectively. In the Pre-SVC2 group the most mafic sample (SL-83-26; basaltic andesite) was analysed. In the SVC, two SVC1 andesites (SL-JL-02 and SL-83-17) and a dacite (SL-JL-23) were selected and finally, in SVC2 and 3 groups both orthopyroxene- and cummingtonite-bearing samples were analysed: SL-JL-83 (SVC2; orthopyroxene-bearing dacite), SL-83-03 (SVC2-3; orthopyroxene-bearing dacite), SL-83-08 (SVC3; cummingtonite-bearing dacite) and SL-JL-51 (SVC3; cummingtonite-bearing dacite). A summary of all the plagioclase textures and major element compositions described below is presented in Fig. 5.6.

5.5.1.1 Pre-SVC1

In the Pre-SVC1 basalt, plagioclases are automorphic to subautomorphic with a mean anorthite content of An_{88} (1 sd = 6; $n = 89$). Phenocrysts typically contain an anorthite rich core ($\text{An}_{\sim 90}$) and are zoned. A few crystals are inclusion-poor and normally zoned, but most crystals have one or two melt inclusion-bearing zones in their core or in the mantle which displays a heterogeneous texture, involving low anorthite (An_{85}) and high anorthite (An_{90}) plagioclase, as illustrated in Fig. 5.6a. Such zones are preceded by a decrease in anorthite leading to a $\sim 10 \mu\text{m}$ large inclusion-free $\text{An}_{\sim 86}$ zone. The very outer rim always displays a low anorthite content of $\text{An}_{\sim 65}$ similar to the plagioclase in the groundmass. Pre-SVC1 basaltic andesites have plagioclase with a

mean anorthite content of 74 (1sd = 8; n = 40). With a few exceptions, the crystals are generally inclusion-free. They display a general decrease in anorthite from core (An₈₀) to rim (An₅₈) punctuated by reverse zoning in the mantle of most crystals with corresponding fluctuations in anorthite of around An₁₀ (Fig. 5.6). Finally, plagioclases in Pre-SVC1 rhyolite are inclusion-poor and lightly zoned. Anorthite content variations are not significant and range between An₃₁ and An₄₀. The crystals display either normal or reverse zoning. A mild oscillatory zoning can also be observed.

5.5.1.2 Pre-SVC2

Pre-SVC2 basaltic andesite plagioclases have a similar mean anorthite content to the Pre-SVC1 basaltic andesites (An₇₉; 1sd = 9; n = 118). However, the crystals are more inclusion-rich, and display more important disequilibrium textures. They can be grouped within four representative types in terms of texture and major element composition illustrated in Fig. 5.6b. Type 1 is dominant in the samples. It consists of a melt inclusion- and anorthite-rich core (An₈₅) resorbed and replaced by more sodic plagioclase producing a “sieved” texture (Fig. 5.7c). The mantle and rim are more sodic (An₇₀) than the average core and have a fine wavy oscillatory texture. The wavy oscillatory texture is characterised by the crystallisation and resorption of micrometer-scale anorthite-rich plagioclase subzones. A variation in Type 1 crystal textures is the presence of an inclusion-free core (An₈₀) before the sieved texture. Type 2 (Fig. 5.6b) crystals have an anorthite-rich (An₉₀) and inclusion-poor core, surrounded by a more sodic mantle and rim dominated by inclusion-free zones with a wavy oscillatory texture (Fig. 5.7e) that also comprises inclusion-rich zones. The inclusion-rich zones grew after a major dissolution surface and are either homogeneous and anorthite-rich (An₈₀) or display a “flame texture” consisting in an intimate intergrowth of anorthite-rich and more sodic plagioclase (Fig. 5.7d). In the latter case, the flame texture is typically followed by the growth of a more homogeneous anorthite-rich zone. Type 3 (Fig. 5.6) is similar to Type 2 but differs in the presence of small inclusions in the anorthite-rich core (An₈₂). Finally, Type 4 crystals contain small rounded unorganised melt inclusions, are very homogeneous and have consistently high anorthite contents (An₉₅) from core to rim.

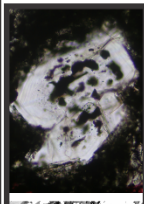
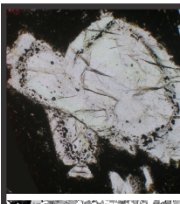
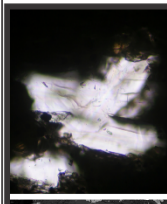
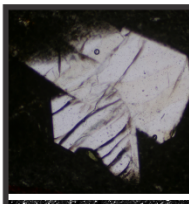
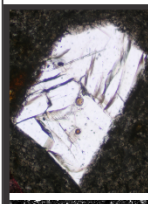
(a) Pre-SVC1	Host rock	Major element	Core	Mantle-rim	Interpretation
	Basalt	Core: inclusion-rich, heterogeneous An-rich Rim: separated from core by a dissolution surface. An-poor, inclusion-free, normal zoning	An ₈₅₋₉₀	An ₄₅	Crystallized in a shallow and heterogeneous reservoir where inclusion-rich zones grew during mixing of two batches of magma of slightly different degrees of differentiation
			Sr ~210; Ba ~100	Sr ~120-140 ; Ba ~70	
	Basalt	Core: inclusion-free, homogeneous texture, An-rich Mantle: alternance of inclusion-free large zones cut by inclusion-rich zones with 'flame' textures and An-rich Rim: Inclusion-free, normal zoning, An-poor	An ₉₀	Mantle with incl. An ₈₅	Crystallized in shallow and heterogeneous reservoir. The core crystallized in a slightly more mafic recharging magma than the mantle. Inclusion rich zones crystallized during movement in a slightly more differentiated zone of the chamber.
			Sr ~210-240; Ba ~80-90	Rim An ₈₀ Sr ~200; Ba ~90	
	Basaltic andesite	Core: inclusion-free, homogeneous texture and An-rich Mantle-rim: alternating An-poor and An-rich euhedral zones Rim: Inclusion-free, low anorthite	An ₈₀	Low-An zones An ₆₀₋₇₀	Crystallized in a shallow reservoir, just before the matrix. Anorthite-rich zones in the mantle were produced by growth in hotter and/or a more mafic part of the magma chamber (no trace element).
			n.a.	High-An zones An ₈₀ n.a.	
	Rhyolite	Core: inclusion-free Rim: inclusion-free, inverse zoning	An ₃₀	An ₄₀	Crystallized in homogeneous rhyolitic magma chamber. Light variation in degree of differentiation of the magma created the light inverse zoning.
			Sr ~60 ; Ba ~210	Sr ~70; Ba~140	
	Rhyolite	Core: inclusion-free Rim: inclusion-free, normal zoning	An ₄₀	An ₃₀	Crystallized in homogeneous rhyolitic magma chamber.
			Sr ~70 Ba~210	Sr ~70; Ba~180	

Fig. 5.6. Summary of textural and compositional characteristics of the different types of plagioclase found in (a) Pre-SVC1 and (b) Pre-SVC2 and SVC lavas. Sr and Ba concentrations presented are for the calculated melt in equilibrium with plagioclase and are expressed in ppm.

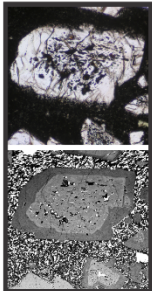
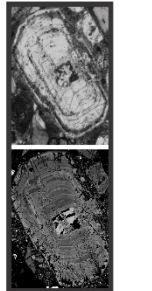
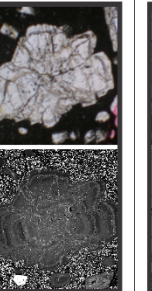
(b) Pre-SVC2 and SVC	Host rock	Texture	Core	Mantle-rim	Interpretation
	Pre-SVC2 basaltic andesite & andesite SVC1 andesite and dacite	Type 1 Core: inclusion-rich in which An-rich plagioclase is resorbed and replaced by anorthite poor plagioclase channels. Rim: separated from core by resorption surface. Inclusion -free, wavy oscillatory zoning	Pre-SVC2: An ₄₀₋₆₀ ; SVC1: An ₄₀₋₆₀ Pre-SVC2: Sr ~ 240; Ba ~ 300 SVC1: n.a.	Pre-SVC2: An ₄₀₋₆₀ ; SVC1: An ₄₀₋₆₀ Pre-SVC2: Sr ~ 150-160; Ba ~ 240-290 SVC1: Sr ~ 170; Ba ~ 570	Anorthite rich core crystallized in a more primitive magma than the rim. Resorption was caused by physical and chemical changes at the arrival of the crystal in the more differentiated magma during a recharge event. The wavy oscillatory texture was formed during convection in the hybrid magma after/during recharge event.
		Type 2 Core: An-rich, inclusion-poor, homogeneous or lightly oscillatory zoned Mantle-rim: separated from core by resorption surface. Mainly inclusion-free low-An with wavy oscillatory zoning but can contain inclusion-rich zones with flame textures.	Pre-SVC2: An ₆₅₋₉₀ ; SVC1: An ₆₀₋₉₀ ; Cgt-SVC2,3: An ₆₀₋₉₀ Ba ~ 240 SVC1: Sr ~ 390-490; Ba ~ 510-770 Cgt-SVC2,3: Sr ~ 390-430; Ba ~ 450-570	Pre-SVC2: An ₄₀₋₆₀ ; SVC1: An ₆₀₋₉₀ Cgt-SVC2,3: An ₆₀₋₉₀ Ba ~ 160-210; Ba ~ 290-320 SVC1: Sr ~ 140-250; Ba ~ 470-1040 ppm Cgt-SVC2,3: Sr ~ 160-250; Ba ~ 360-590	
	Pre-SVC2 basaltic andesite & andesite SVC1 andesite & dacite	Type 3 Core: inclusion rich (angular inclusions) and An-rich with oscillatory texture. Mantle-rim: mainly An-poor and inclusion-free with wavy oscillatory zoning, but can contain inclusion-rich zones with flame textures.	Pre-SVC2: An ₄₀ SVC1: An ₄₀ Pre-SVC2: n.a. SVC1: n.a.	Pre-SVC2: An ₇₀₋₈₀ SVC1: An ₇₀₋₇₀ Pre-SVC2: Sr ~ 190-220; Ba ~ 280-300 SVC1: n.a.	The wavy oscillatory texture formed during convection in a hybride magma following a recharge event. The inclusion-rich mantle zones result from the contact of the crystal with a more primitive magma from a recharge event.
		Type 4 Core-mantle-rim: An-rich with homogeneous texture and unorganised small inclusions	Pre-SVC2: ~An ₆₅ SVC1: n.a. Pre-SVC2: Sr ~ 240; Ba ~ 140	Pre-SVC2: ~An ₆₅ SVC1: n.a. Pre-SVC2: Sr ~ 240; Ba ~ 140 SVC1: n.a.	
	SVC1 andesite & dacite Opx-Cgt- SVC2,3 dacite	Type 5 Core-mantle: An-poor core partially or entirely resorbed and replaced by An-rich plagioclase. Resorption zone is inclusion rich with a flame texture. Rim: inclusion-free, An-poor wavy-oscillatory zoned	SVC1: ~An ₅₀₋₆₀ Opx-SVC2,3: ~An ₅₀ Cgt-SVC2,3: ~An ₅₀ SVC1: Sr ~ 180; Ba ~ 630-750 Opx-SVC2,3: Sr ~ 162-190; Ba ~ 420-550 Cgt-SVC2,3: Sr ~ 130-140; Ba ~ 330-350	Mantle (An-rich zone): Rim: SVC1: An ₇₀₋₈₀ ; Opx-SVC2,3: An ₇₀ ; Cgt-SVC2,3: An ₇₀ ; Mantle-Rim (An-poor): SVC1: Sr ~ 290 Ba ~ 800 Opx-SVC2,3: Sr ~ 300-340 Ba ~ 670-780 Cgt-SVC2,3: Sr ~ 240 Ba ~ 740 SVC1: ~An ₆₀₋₇₀ Opx-SVC2,3: An ₄₅₋₆₅ Cgt-SVC2,3: An ₄₅₋₆₅ SVC1: n.a. Opx-SVC2,3: n.a. Cgt-SVC2,3: Sr ~ 140-190 Ba ~ 310-540	The core grew in a very differentiated magma that was subsequently recharged by a hotter and more primitive magma. The wavy oscillatory texture formed during convection in a hybride magma following /during the recharge event.
		Type 6 Core: homogeneous and An-poor. Rim: separated from core by inclusion-rich resorption surface, inclusion-free, wavy oscillatory zoning	SVC1: ~An ₆₀ Opx-SVC2,3: An ₆₀ Cgt-SVC2,3: An ₄₅₋₆₅ SVC1: n.a. Opx-SVC2,3: n.a. Cgt-SVC2,3: Sr ~ 120-150; Ba ~ 290-350	SVC1: ~An ₆₀₋₇₀ Opx-SVC2,3: An ₄₅₋₆₅ Cgt-SVC2,3: An ₄₅₋₆₅ SVC1: n.a. Opx-SVC2,3: n.a. Cgt-SVC2,3: Sr ~ 140-190 Ba ~ 310-540	

Fig. 5.6. (continued).

5.5.1.3 SVC

5.5.1.3.1 SVC1

Plagioclases in SVC1 have the highest anorthite content of all the SVC crystals with a mean of An₆₈ in both andesites (1sd = 10; n = 208) and low-silica dacites (1sd = 12; n = 92). The textures are very complex and record several resorption events in some

instances. All the crystal types observed in Pre-SVC2 basaltic andesites (excluding Type 4) can be found in SVC1 crystals. However, although the anorthite-rich cores or zones of Types 1, 2, 3 and 4 crystals have a similar composition as in Pre-SVC2 (An_{80-90}), the sodic zones (of Types 1, 2 and 3 crystals) have lower anorthite content in SVC1 lavas ($An_{\sim 65}$ in the Pre-SVC2 vs. $An_{\sim 55}$ in the SVC1)). In addition, two new crystal types are observed: Types 5 and 6. Type 5 (Fig. 5.6) crystals exhibit very patchy cores with ‘flame’ textures formed by the resorption of sodic cores ($An_{\sim 0.6}$) subsequently filled by anorthite-rich channels ($An_{\sim 80}$; Fig. 5.7d)). Channel-rich zones also contain a high proportion of inclusions. The mantles display wavy-oscillatory zoning which can comprise small anorthite-rich resorbed zones with a sieved texture (Fig. 5.7e). Finally, Type 6 is an inclusion-poor crystal with a low anorthite content (mean $An_{\sim 55}$). The core is sodic and homogeneous ($An_{\sim 50}$) and surrounded by a mantle-rim with wavy oscillatory zoning ($An_{\sim 50-70}$).

5.5.1.3.2 SVC2,3

In SVC2 and 3, the orthopyroxene-bearing dacites only contain plagioclase with textures of Types 5 and 6 and have an average anorthite content of An_{59} (1sd = 10; n = 166; SL-83-03 and SL-JL-83). Plagioclase in cumingtonite-bearing samples (SL-83-08 and SL-JL-51) have textures of Types 2, 5 and 6 and display a slightly lower anorthite content with a mean of An_{56} (1sd = 8; n = 264).

5.5.1.3.3 Groundmass of SVC1,2,3

In SVC1, plagioclase in the groundmass has $\sim An_{60-70}$. In SVC2 and 3, plagioclase microlites in the groundmass of orthopyroxene-bearing samples are very enriched in anorthite with the core of a microlite having $\sim An_{90}$ and a rim of An_{85} (in SL-JL-83). On the other hand, plagioclase microlites in cumingtonite-bearing lava matrices is either consistently sodic with $\sim An_{50-60}$ or have an anorthite-rich core (e.g. An_{86}) and sodic rim (e.g. An_{60}).

5.5.2 Clinopyroxene phenocrysts

5.5.2.1 Pre-SVC

In Pre-SVC1 basalt (lava $Mg\# = 72$), clinopyroxene (En_{46-51} , Wo_{35-44} , Fs_{9-14}) are slightly zoned and vary from endiopside to augite. $Mg\#$ varies between 83 and 93, Al_2O_3 and TiO_2 contents range from 2.1 to 3.6 (wt. %) and 0.23 to 0.37 (wt. %) respectively. In pre-SVC1 rhyolite ($Mg\# = 0.17$), clinopyroxene (En_{18} , Wo_{40-41} , Fs_{39-40}) is homogeneous ferroaugite. It has an $Mg\#$ between 31-33 and Al_2O_3 and TiO_2 contents between 1-1.65 (wt. %) and 0.31-0.50 (wt. %) respectively.

Clinopyroxene in Pre-SVC2 basaltic andesite (lava $Mg\# = 70$) consists of zoned augite (En_{41-43} , Wo_{37-43} , Fs_{13-20}) with $Mg\#$ between 67 and 77 and Al_2O_3 and TiO_2 contents ranging between 1.1 and 2.5 (wt. %) and 0.30-0.59 (wt. %).

5.5.2.2 SVC

In SVC1 andesites (whole rock $Mg\# = 49-67$), a rare clinopyroxene microphenocryst is diopside (En_{42} , Wo_{49} , Fs_9 ; $Mg\# = 88$). In SVC2,3 orthopyroxene-bearing dacites (lava $Mg\# = 39-64$), zoned augite (En_{43-47} , Wo_{46-48} , Fs_{5-9} and $Mg\# = 87-94$) microphenocrysts have been found.

5.5.3 Orthopyroxene

5.5.3.1 Pre-SVC

Pre-SVC1 basalts do not contain any orthopyroxene. Pre-SVC2 basaltic andesites ($Mg\# = 70$) contain magnesium rich hypersthene (En_{62} , Wo_4 , Fs_{32-33}) with a $Mg\#$ of 66.

5.5.3.2 SVC

In SVC1 lavas, orthopyroxene in both the andesites and dacites are similar in composition and consist of slightly zoned hypersthene (En_{43-57} , Wo_{1-11} , Fs_{40-50} ; $Mg\# = 49-61$). SVC2,3 dacites also contain zoned hypersthene similar to SVC1 lavas in their texture but with higher iron contents (En_{39-47} , Wo_{1-3} , Fs_{49-58} ; $Mg\# = 39-52$).

5.5.4. Amphibole

Amphibole is restricted to SVC2,3 lavas in which both calcic and Mg-Fe-Mn-Li amphiboles are observed. Calcic amphiboles occur as microphenocrysts in the orthopyroxene-bearing samples while Mg-Fe-Mn-Li amphibole phenocrysts occur in assemblages where orthopyroxene is absent.

According to the Leake et al. (1997, 2004) classification, calcic amphibole is magnesio-hastingsite, magnesio-hornblende and tschermakite. Two groups of composition are observed. The first group consists of magnesio-hastingsite and tschermakite (Leake et al., 1997, 2004) which have high Al^T (1.93-2.5) and Ti (0.17-0.22 apfu) with low Si/Al (2.3-3), moderate Mg# ($100 * Mg / (Mg + Fe^{tot})$) of 66-79, but very high minimum Mg# ($100 * Mg / (Mg + Fe^{2+})$) of 73-95 due to a high Fe^{3+}/FeO^{tot} . The second group consists of magnesio-hornblende and tschermakite which display low Al^T (1.65-1.86) and Ti (0.15-0.17 apfu) with high Si/Al (3.3-5.4) and low Mg# and Mg# of 41-64 and 41-68. In both groups, amphibole type can vary from dark brown to light brown or greenish brown and can be zoned with either a magnesio-hornblende core surrounded by a tschermakititic rim or a tschermakititic core surrounded by a magnesio-hastingsite rim.

The Mg-Fe-Mn-Li amphibole is cummingtonite with Mg# 46-55. It has Ti and Al^{tot} between 0.03 and 0.06 (apfu) and between 0.34 and 0.60 (apfu) respectively.

5.5.5 Biotite

Biotite is found only in SVC2 and 3 dacites. Its Mg# varies between 37 and 44.

5.5.6 Groundmass

Pre-SVC1 basalts have a basaltic andesite groundmass ($SiO_2 = 55.2$ wt. %) while Pre-SVC1 basaltic andesite have an andesitic groundmass ($SiO_2 = 60.7$ wt. %). Pre-SVC1 rhyolites have a rhyolitic groundmass ($SiO_2 = 74.3$ wt. %) very close to the whole-rock composition ($SiO_2 = 72.2$ wt. %), consistent with a low abundance of phenocrysts. In the Pre-SVC2, the basaltic andesite has an andesitic groundmass. The difference in silica content between whole rock and groundmass is more significant for Pre-SVC2 (+5.4 wt. %) than for Pre-SVC1 basaltic andesite (+4.3 wt. %), which

could be explained by the lower percentage of phenocrysts in Pre-SVC1 basaltic andesites.

In the SVC, both andesites and dacites have a rhyolitic groundmass ($\text{SiO}_2 = 73.5\text{--}77.9$ wt. %), except for one dacite with a silica-rich dacitic groundmass ($\text{SiO}_2 = 71$ wt. %) which displays the smallest difference between whole rock and groundmass SiO_2 content of the SVC (+6.6 wt. %). The latter also corresponds to the lava with the least “continental” isotopic composition amongst the SVC. The two SVC andesites (SVC1) have a groundmass with extremely high silica content ($\text{SiO}_2 = 73.5$ wt. % and 77.9 wt. %) and have the most significant whole-rock-groundmass increase in SiO_2 (+13 wt. % and +14 wt. % respectively).

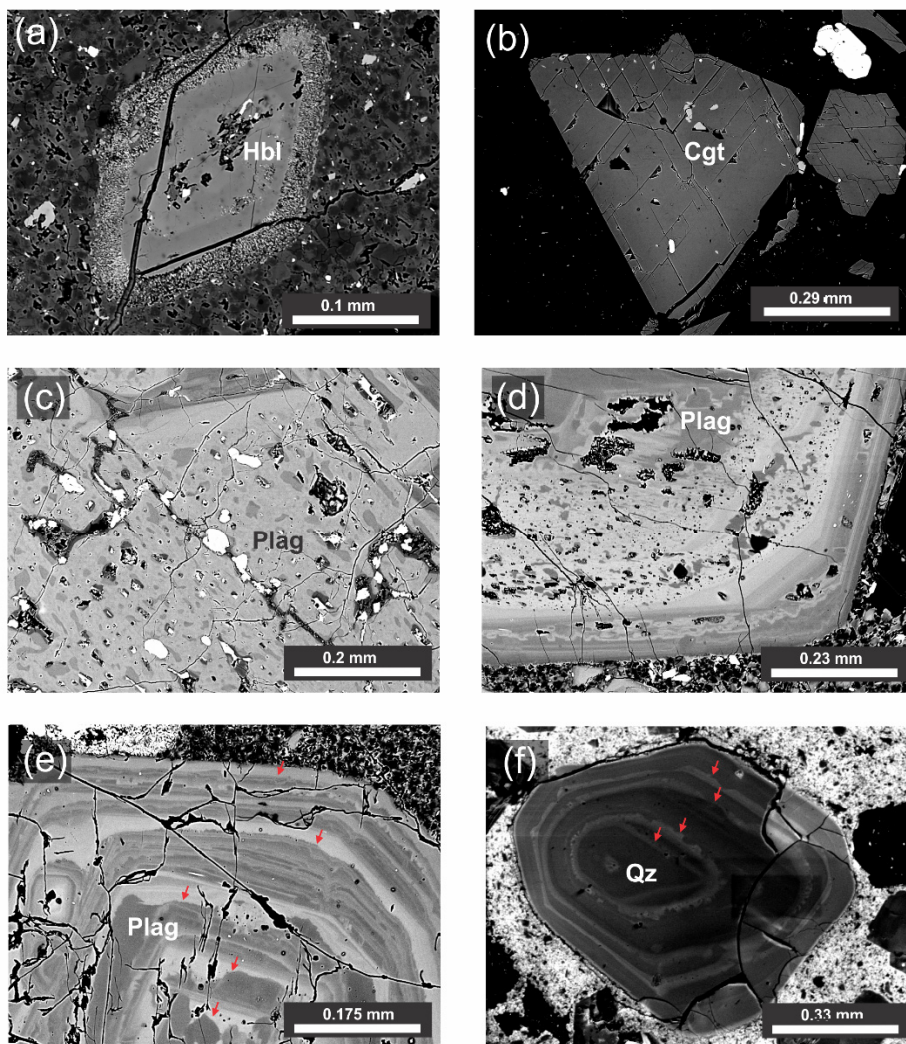


Fig. 5.7. Representative SEM (a-e) and CL (f) images of some mineral textures in the SVC. (a) microphenocryst of zoned hornblende from orthopyroxene-bearing SVC2,3 lavas; (b) homogeneous phenocryst of cummingtonite from SVC2,3 lavas; (c) sponge texture of Type 1 plagioclase core

characterized by anorthite-rich plagioclase resorbed and replaced by more sodic plagioclase; (d) Sponge and flame texture around Type 5 crystal core followed by a sodic rim with wavy-oscillatory zoning. Sodic core is resorbed and followed by the growth of anorthite-rich plagioclase; (e) Type 5 crystal mantle presenting sodic zones with wavy oscillatory zoning separated by major dissolution surfaces from narrow anorthite-rich zones. Major dissolution surfaces are highlighted with red arrows; (f) Wavy oscillatory zoning in quartz. Major dissolution surfaces are highlighted with a red arrows. Hbl = hornblende; Cgt = cummingtonite; Plag = plagioclase; Qz = quartz.

5.6 Mineral and groundmass trace element data

All the phenocryst and groundmass trace element concentrations are given in the supplementary data file (Appendix D).

5.6.1 Plagioclase

Only Ba, Sr and Rare Earth Element (REE) analyses are discussed here and presented in Fig. 5.8.

5.6.1.1 Pre-SVC1

In Pre-SVC1 basalt (SL-83-44), plagioclase REE concentrations are very low, and HREE of most samples are below the detection limit. The L-MREE pattern is relatively flat ($\text{La/Sm} = 2.4\text{-}5.1$; Fig. 5.8e) and Sr and Ba abundances are very low ($\text{Sr} = 243\text{-}303$ ppm; $\text{Ba} = 7\text{-}18$ ppm; Fig. 5.8a, c). In the rhyolite (SL-83-45), plagioclase displays higher La/Sm ratios and much higher Sr and Ba concentrations than Pre-SVC1 basalt ($\text{La/Sm} = 5.5\text{-}13.1$; $\text{Sr} = 422\text{-}457$ ppm; $\text{Ba} = 106\text{-}151$ ppm; Fig. 5.8a, c, e).

5.6.1.2 Pre-SVC2

In Pre-SVC2 basaltic andesite (SL-83-26), plagioclase La/Sm ratios ($5.7\text{-}16.1$) overlap those from the Pre-SVC1 rhyolites whereas Sr and Ba concentrations overlap Pre-SVC1 basalt plagioclase values ($\text{Sr} = 285\text{-}385$ ppm; $\text{Ba} = 12\text{-}68$ ppm).

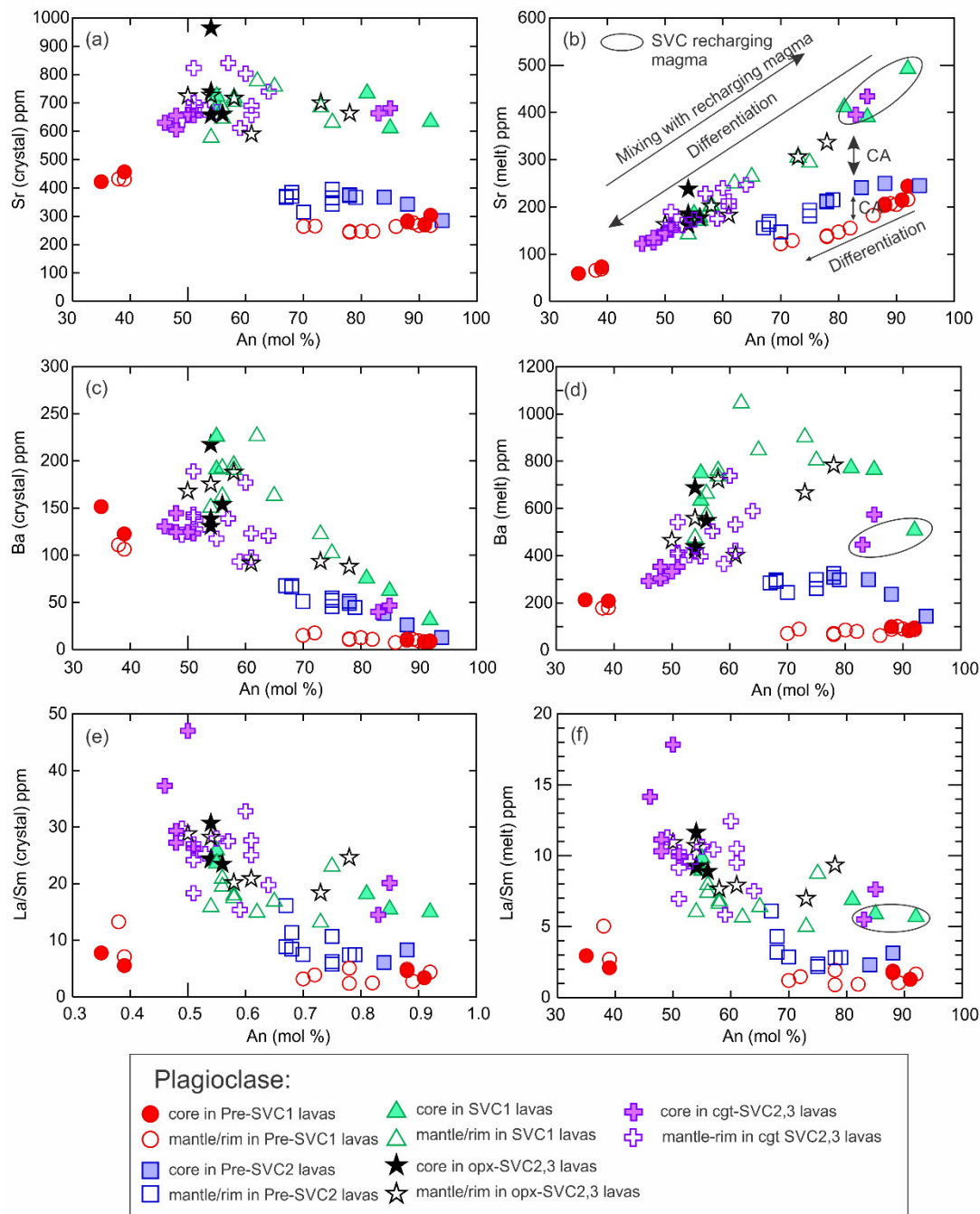


Fig. 5.8. Sr, Ba and La/Sm compositions of the plagioclases from the different types of lava in St Lucia (a, c, e) and from the corresponding calculated melts (b, d, f). Sr and Ba in melts in equilibrium with plagioclase were calculated using Blundy and Wood (1991) equation and a temperature of 1000°C for plagioclase from mafic rocks and 800°C for plagioclase from intermediate and felsic lavas. La/Sm ratio in melts in equilibrium with plagioclase was calculated using partition coefficients presented in Table 5.2. For all data, the error is equal or smaller than the symbol size. Opx-SVC2,3 lavas = orthopyroxene bearing SVC2,3 lavas. Cgt-SVC2,3 lavas = cummingtonite-bearing SVC2,3 lavas.

5.6.1.3 SVC

5.6.1.3.1 SVC1

Both SVC1 andesite and dacite plagioclases have similar trace element compositions with La/Sm ratios between 13.1 ppm and 25.9 ppm and Sr and Ba content ranging from 611 ppm to 777 ppm and from 31 ppm to 226 ppm, respectively. Most La/Sm ratios and Ba concentrations are higher than Pre-SVC1,2 lavas although they overlap with their highest value. Sr content is significantly higher than Pre-SVC1,2 lavas, by up to 200 ppm.

5.6.1.3.2 SVC2,3

SVC2,3 orthopyroxene-bearing dacites have plagioclase with La/Sm ratios of 18-30, and Sr and Ba concentrations of 590-964 ppm and 91-218 ppm respectively while cummingtonite-bearing dacites have plagioclase with La/Sm ratios of 14.5-47, Sr contents of 606-841 ppm and Ba concentrations between 40 ppm and 189 ppm.

5.6.2 Orthopyroxene

The trace element composition of the core, the mantle and the rim of a representative zoned SVC hypersthene crystal were analysed (Fig. 5.9a). All analyses have a clear negative europium anomaly ($Eu/Eu^* = Eu_{CN} / ((Sm_{CN}^{0.5}) * (Gd_{CN}^{0.5}))$). The variation in amplitude of the anomaly correlates with the enstatite variations of the crystals: both Eu/Eu^* and enstatite content increases from the core ($Eu/Eu^* = 0.06$; En_{50-53}) to the mantle ($Eu/Eu^* = 0.22$; En_{52-57}), and subsequently decreases toward the rim ($Eu/Eu^* = 0.12$; En_{47-52}). Intra-crystal variations in L/M-HREE ratios are also correlated with the enstatite content. The core exhibits the highest La/Yb (1.29) and Dy/Yb (0.71) of the crystal. The mantle (higher enstatite content) is characterised by a significant decrease in L-MREE ($La/Yb = 0.05$; $Dy/Yb = 0.48$) compared to the core. Finally, the rim (lowest enstatite content) has a higher La/Yb ratio than the mantle ($La/Yb = 0.43$) and higher Dy/Yb ratio, similar to the core ($Dy/Yb = 0.75$). The mantle is also depleted in Ba and Sr concentrations ($Ba = 0.09$ ppm; $Sr = 0.16$ ppm) compared to the core and the rim (core: $Ba = 0.18$ and $Sr = 1.11$ ppm; rim: $Ba = 0.16$ and $Sr = 1.32$ ppm).

5.6.3 Clinopyroxene

The trace element compositions of the core and the rim of a clinopyroxene crystal (Fig. 5.9b) from the most mafic sample of Pre-SVC1 (SL-83-44) and of one of the rare clinopyroxene microphenocrysts (Fig. 5.9c) in the SVC1 dacite (SL-JL-83) were analysed. In both instances, no europium anomaly was observed. In the crystal from Pre-SVC basalt, the bulk core and the bulk rim analysed have similar enstatite contents. The core has similar but slightly higher La/Yb and Dy/Yb ratios (crystal cores are 0.20 and 1.94, respectively) than the rim (La/Yb and Dy/Yb of 0.16 and 1.68, respectively). The Ba and Sr content are also slightly higher in the core (0.11 and 12.2 ppm respectively) than in the rim (0.05-10.5 ppm). On the other hand, in the SVC dacite, the clinopyroxene has lower La/Yb and Dy/Yb ratios in the core (0.24 and 2.04 respectively) than in the rim (0.43 and 2.34 respectively), correlating with a decrease in the enstatite content from Ens_{46-48} in the core to Ens_{46-43} in the rim. The Ba and Sr contents appear similar in the core (0.08 ppm and 19.7 ppm respectively) and in the rim (less than 0.05 ppm and 19 ppm respectively).

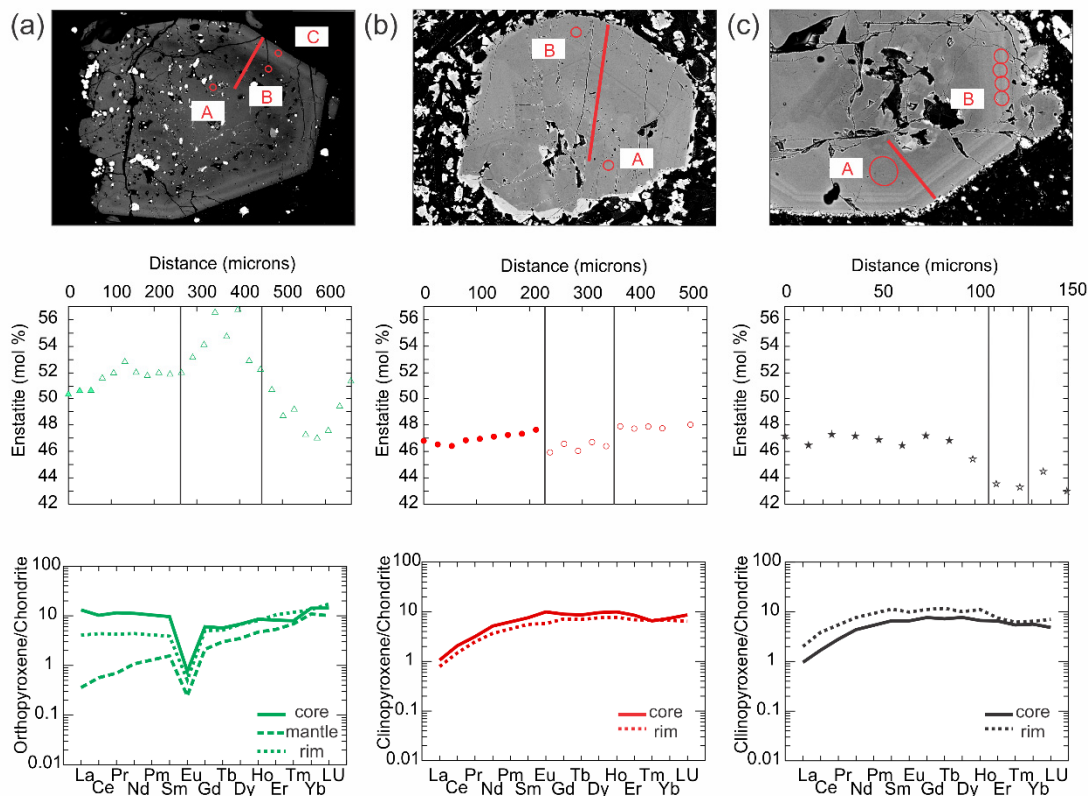


Fig. 5.9. Compositional profiles in enstatite obtained for pyroxene along with the rare earth element pattern of the different zones of the crystals. Emplacement of the major element profiles is shown by the red line and emplacement of trace element analyses are shown by red circles on the SEM images. (a) Orthopyroxene phenocryst from SVC1 dacite (SL-JL-23). (b) Clinopyroxene phenocryst from Pre-

SVC1 basalt (SL-83-44). (c) Clinopyroxene microphenocryst from orthopyroxene-bearing SVC2,3 dacite (SL-JL-83). Symbols on the enstatite profiles are the same as in Fig. 5.10.

5.6.4 Amphibole

Trace element compositions of a most calcic and aluminium-rich SVC hornblende (the most primitive), and of a cummingtonite were investigated (Fig. 5.10). The two amphibole types have very different trace element composition. The magnesio-hastingsite (from SL-JL-83 dacite) shows relatively mild MREE enrichment compared to L-HREE with La/Yb and Dy/Yb ratios of 0.95 and 2.06 respectively, and no europium anomaly. On the other hand, cummingtonite is very depleted in LREE with La/Yb and Dy/Yb ratios of 0.06-0.09 and 1.07-1.15 respectively, but also has a europium negative anomaly ($\text{Eu}/\text{Eu}^* = 0.35$) larger than orthopyroxene. The Ba and Sr concentrations are almost a hundred times higher in the magnesio-hastingsite (80 ppm Ba, 166.8 ppm Sr) compared to the cummingtonite (0.5-1.13 ppm Ba; 3.8-3.9 ppm Sr).

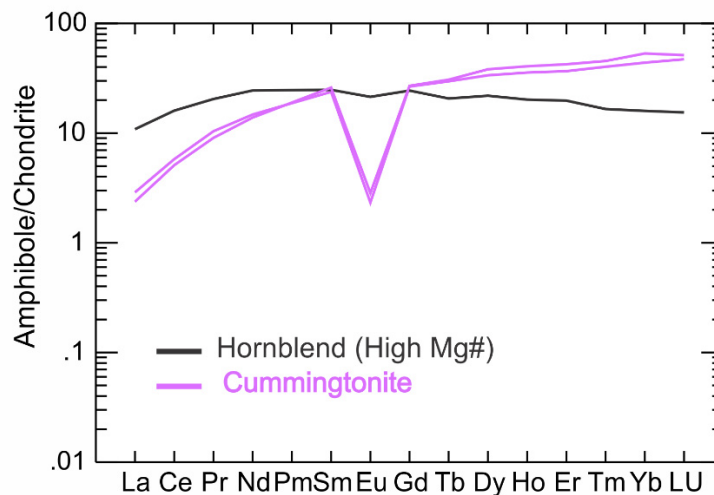


Fig. 5.10. Chondrite-normalised rare earth element composition of the two types of amphiboles found in the SVC. In pink is the composition of a cummingtonite and in black is the composition of the core of a high Mg## hornblende microphenocryst.

5.6.5 Groundmass

5.6.5.1 Pre-SVC1

Groundmasses from the Pre-SVC1 basalt (SL-83-44), basaltic andesite (SL-83-25) and rhyolite (SL-83-45) all have La/Sm ratios between 1.5 and 2 which is very similar to the corresponding whole rock ratio (1.6-1.9; Chapter 4). Ba and Sr concentrations in the basalt and basaltic andesite groundmasses range between 128 ppm and 235 ppm and between 159 ppm and 210 ppm, respectively, which are also very similar to the whole rock concentrations (Ba = 80-226 ppm; Sr = 178-190 ppm). Rhyolite Ba (164 ppm) and Sr (46 ppm) concentrations in the groundmass are much lower than their whole-rock values (Ba = 324 ppm and Sr = 103 ppm).

5.6.5.2 Pre-SVC2

The mean groundmass of Pre-SVC2 basaltic andesite has a La/Sm ratio of 3.0 and a Ba content of 214 ppm, which is very similar to the whole-rock values (La/Sm = 3; Ba = 211 ppm). However, the groundmass Sr content (143 ppm) is lower than in the whole rock (195 ppm Sr).

5.6.5.3 SVC

In the SVC1 lavas (SL-JL-23) two zones of groundmass from the same sample yielded different compositions. Both have La/Sm ratios (5.5 and 7.3) comparable to the whole rock (6.2) however, Ba and Sr concentrations of the two zones differ greatly with Ba content ranging between 343 ppm and 1108 ppm and Sr content ranging between 149-174 ppm. Comparison of groundmass Ba concentration with the whole-rock is therefore difficult. However, both zones analysed have a lower Sr content than the whole rock (Sr = 309 ppm).

The groundmass of orthopyroxene-bearing SVC2 lava (SL-JL-83) has a La/Sm ratio (7.1) similar to but slightly higher than, the whole rock (6.4). Ba (367 ppm) and Sr (75 ppm) contents of the groundmass are higher and lower than the whole rock, respectively (Ba = 430 ppm and Sr = 298 ppm in the whole rock).

5.7 Plagioclase and groundmass $^{87}\text{Sr}/^{86}\text{Sr}$ data

All the plagioclase and groundmass $^{87}\text{Sr}/^{86}\text{Sr}$ ratios are presented in Table 5.1 and in Fig. 5.11. $^{87}\text{Sr}/^{86}\text{Sr}$ variations can be compared with variations in texture and major and trace elements concentrations in Fig. 5.12.

5.7.1 Pre-SVC1

In Pre-SVC1 basalt (SL-83-44), the groundmass $^{87}\text{Sr}/^{86}\text{Sr}$ is 0.70426 which is more radiogenic than the whole-rock ($^{87}\text{Sr}/^{86}\text{Sr} = 0.70413$) (Fig. 5.11a, b). Core to rim $^{87}\text{Sr}/^{86}\text{Sr}$ profiles were performed in two representative crystals with similar zoning patterns (Fig. 5.12a, b) but different size. The crystals both have an inclusion-free core surrounded by a mantle containing an inclusion-rich zone and a clear outer rim. Both crystals analysed have an isotopic composition very close to the whole-rock and the groundmass ratios. The smaller crystal (~800 microns) displays a homogeneous signature from core to rim ($^{87}\text{Sr}/^{86}\text{Sr} = 0.70411$ -0.70413) which is similar to the whole-rock isotopic composition. In contrast, the larger phenocryst displays isotopic variation with the core ($^{87}\text{Sr}/^{86}\text{Sr} = 0.70427$) being more radiogenic than the rest of the crystal and the groundmass. The crystal isotopic composition then decreases toward the inclusion-rich zone ($^{87}\text{Sr}/^{86}\text{Sr} = 0.70415$) of the mantle where the least radiogenic composition is found. A slight increase can be observed at the rim ($^{87}\text{Sr}/^{86}\text{Sr} = 0.70419$) (The very outer rim of around 20 μm could not be analysed).

5.7.2 Pre-SVC2

In Pre-SVC2, the groundmass $^{87}\text{Sr}/^{86}\text{Sr}$ was analysed twice, in two different zones of the same thin section and yielding values of 0.70637 and 0.70638 which indicate isotopic equilibrium of the groundmass at the centimetre-scale (Fig. 5.11a, c). It also indicates that the groundmass has more radiogenic Sr than the whole rock ($^{87}\text{Sr}/^{86}\text{Sr} = 0.70622$). $^{87}\text{Sr}/^{86}\text{Sr}$ was determined in Type 1, 2 and 4 crystals (Fig. 5.11a, c). Type 1 (Fig. 5.12f) inclusion-rich core (A in Figs. 5.11c and 5.12f) has $^{87}\text{Sr}/^{86}\text{Sr}$ of 0.70614 while the oscillatory-zoned mantle-rim (B) has more radiogenic $^{87}\text{Sr}/^{86}\text{Sr}$ of 0.70630. Type 2 (Figs. 5.11c and 5.12d) inclusion-poor core (A) is less radiogenic than the whole rock with a $^{87}\text{Sr}/^{86}\text{Sr}$ ratio of 0.70616. The surrounding inclusion-rich zones (B and C) are less radiogenic than the core with $^{87}\text{Sr}/^{86}\text{Sr}$ of 0.70609 (B) and 0.70610 (C).

respectively. They are followed by a more radiogenic inclusion-free outer rim (D) with $^{87}\text{Sr}/^{86}\text{Sr} = 0.70627$, similar to Type 1 crystals. Finally, the Type 4 crystal (Figs. 5.11c and Fig. 5.12e) has the least radiogenic signature in this sample with $^{87}\text{Sr}/^{86}\text{Sr} = 0.70577$. Such a composition is very distinct from the whole-rock and the groundmass composition.

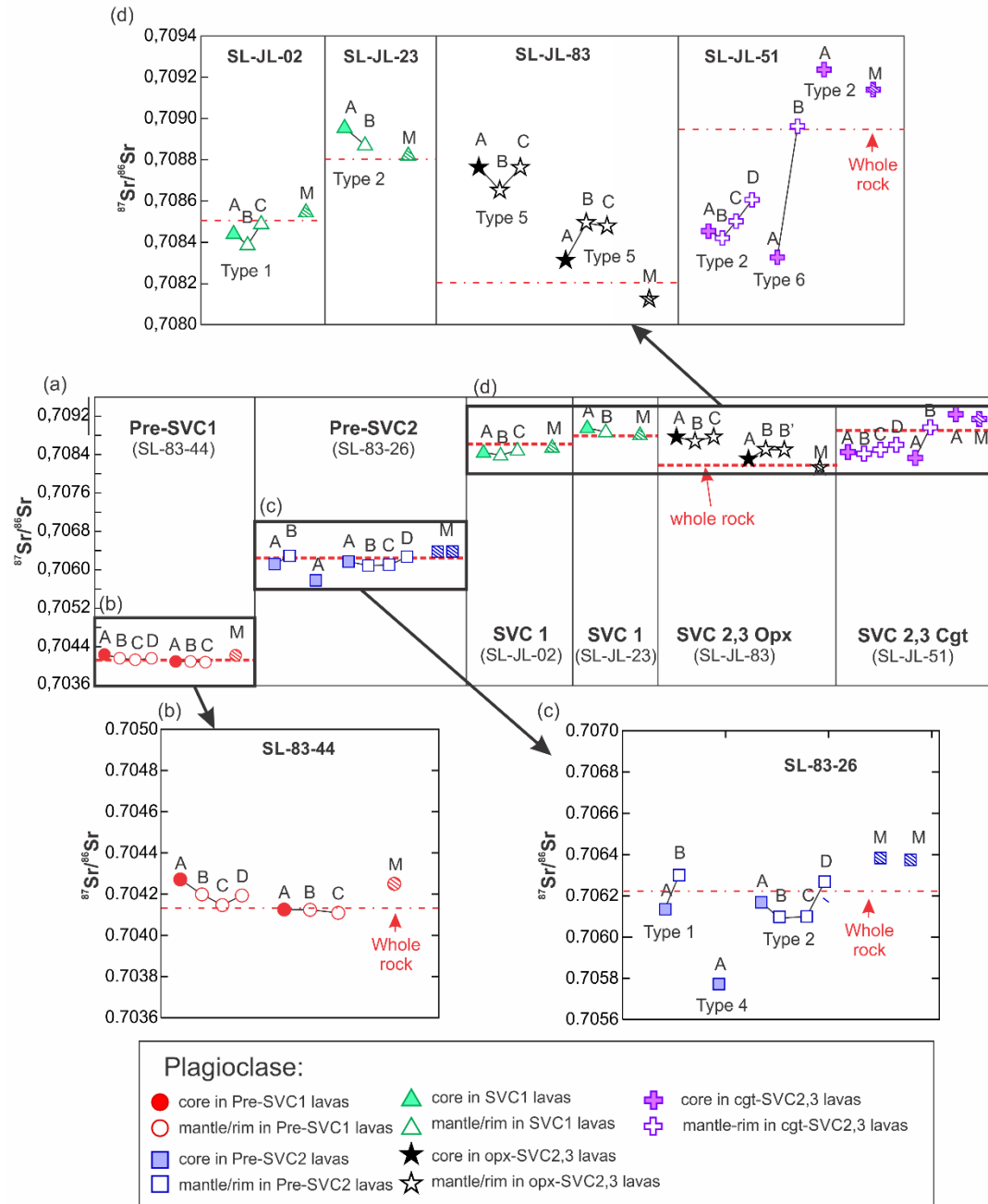


Fig. 5.11. Summary of $^{87}\text{Sr}/^{86}\text{Sr}$ ratios in microdrilled zones of plagioclase crystals. ABCD = profile from core to rim; M = groundmass; B' is a repeat analysis of B. For all data, 2 standard error (2 SE) is smaller than 0.00003 which represent half of the symbol size. The whole rock $^{87}\text{Sr}/^{86}\text{Sr}$ is also shown for each lava. Opx-SVC2,3 lavas = orthopyroxene bearing SVC2,3 lavas. Cgt-SVC2,3 lavas = cummingtonite-bearing SVC2,3 lavas.

5.7.3 SVC

5.7.3.1 SVC1

The Sr isotopic compositions of SVC1 groundmass are only slightly more radiogenic than the whole-rock compositions (with $^{87}\text{Sr}/^{86}\text{Sr}$ of 0.70855 in andesite and $^{87}\text{Sr}/^{86}\text{Sr}$ of 0.70882 in dacite (c.f. whole-rock andesite and dacite $^{87}\text{Sr}/^{86}\text{Sr} = 0.70850$ and 0.70880, respectively; Fig. 5.11d). Type 1 (Figs. 5.11d and 5.12g) inclusion-rich core (A) has $^{87}\text{Sr}/^{86}\text{Sr}$ of 0.70844, which is less radiogenic than the whole rock and the groundmass but is more radiogenic than the surrounding anorthite-poor and inclusion-free zone (B) with $^{87}\text{Sr}/^{86}\text{Sr}$ of 0.70839. The mantle-rim (C) of the crystal is more radiogenic with $^{87}\text{Sr}/^{86}\text{Sr}$ of 0.70849 which is similar to the whole rock composition. Type 2 inclusion-free core (A in Figs. 5.11d and 5.12h) has $^{87}\text{Sr}/^{86}\text{Sr}$ of 0.70896 which is more radiogenic than the rest of the crystal, the groundmass and the whole rock. The surrounding zone (B) comprising resorbed low anorthite material with oscillatory zoning, cross-cut by anorthite-rich channels has a $^{87}\text{Sr}/^{86}\text{Sr}$ ratio of 0.70887, which is lower than the core, but higher than the whole rock and the groundmass composition.

5.7.3.2 SVC2,3

The $^{87}\text{Sr}/^{86}\text{Sr}$ compositions of a sample with orthopyroxene (SL-JL-83, SVC2) and a sample with cummingtonite (SL-JL-51, SVC3) were investigated. Unlike in SVC1, where the groundmass composition is very close to the whole rock $^{87}\text{Sr}/^{86}\text{Sr}$, the groundmass of the cummingtonite-bearing lava is much more radiogenic than the whole rock (Figs. 5.11d and 5.12j) with a $^{87}\text{Sr}/^{86}\text{Sr}$ ratio of 0.70914. On the other hand, the groundmass of the orthopyroxene-bearing lava has $^{87}\text{Sr}/^{86}\text{Sr}$ of 0.70812 which is less radiogenic than the whole rock and the groundmass. In the orthopyroxene-bearing sample, $^{87}\text{Sr}/^{86}\text{Sr}$ variations within 2 crystals of Type 5 were investigated. The first phenocryst (Figs. 5.11d and 5.12n) exhibits an inclusion-rich core (A) with $^{87}\text{Sr}/^{86}\text{Sr} = 0.70849$ which is significantly less radiogenic than the oscillatory-zoned mantle-rim (B) having a $^{87}\text{Sr}/^{86}\text{Sr}$ ratio of 0.70849. In the second phenocryst (Fig. 5.11d and 5.12m), the inclusion and anorthite-poor core (A) has $^{87}\text{Sr}/^{86}\text{Sr}$ of 0.70876 while the surrounding inclusion-rich mantle (B) is less radiogenic with $^{87}\text{Sr}/^{86}\text{Sr} = 0.70865$. Finally, the oscillatory-zoned outer rim (C) has the same $^{87}\text{Sr}/^{86}\text{Sr}$ composition as the core ($^{87}\text{Sr}/^{86}\text{Sr} = 0.70876$). It is clear in Type 5 phenocrysts that the resorbed inclusion-rich zone is less radiogenic than inclusion-poor parts of the crystal. In the

cummingtonite-bearing sample, we analysed phenocrysts of Types 2 and 6 and a microphenocryst of Type 2. In the Type 2 phenocryst (Fig. 5.11d and 5.12l), the core (A) which is anorthite-rich and oscillatory-zoned, has a $^{87}\text{Sr}/^{86}\text{Sr}$ ratio of 0.70845. It is surrounded by an inclusion-poor zone (B) with similarly low $^{87}\text{Sr}/^{86}\text{Sr}$ of 0.70842. The youngest zones comprising an inclusion-rich zone rimmed by an oscillatory-zoned margin show an increase in radiogenic Sr toward the rim (C: $^{87}\text{Sr}/^{86}\text{Sr}$ = 0.70850; D: $^{87}\text{Sr}/^{86}\text{Sr}$ = 0.70861). The Type 2 microphenocryst (Figs. 5.11d and 5.12k) is the most radiogenic crystal analysed from the SVC. Due to its small size only its high anorthite core composition could be analysed. It has $^{87}\text{Sr}/^{86}\text{Sr}$ of 0.70924, which is more radiogenic than the groundmass. The Type 6 (Fig. 5.12j) inclusion-poor and low anorthite core (A) is very unradiogenic compared to the whole rock and the groundmass with $^{87}\text{Sr}/^{86}\text{Sr}$ = 0.70833. Surrounding the core is plagioclase with oscillatory zoning (B) which is significantly more radiogenic ($^{87}\text{Sr}/^{86}\text{Sr}$ = 0.70896) and similar to the Sr isotopic composition of the whole-rock.

5.8 Zircon $\delta^{18}\text{O}$ data

The oxygen isotopic composition of 143 zircon zones aged from 27 to 605 ka was investigated to detect potential $\delta^{18}\text{O}$ variation through time. All the data are available in the supplementary data file (Appendix D) and plotted on Fig. 5.13. Results show that zircon $\delta^{18}\text{O}$ from all ages and from both lavas and plutonic xenoliths range between 7.0 and 9.4 ‰ except for one zircon of 61 ka which displays $\delta^{18}\text{O}$ of 5.6‰. The latter data was retained in the dataset since the CL image of the ablated zircon did not show any evidence of inclusions. However, one analysis out of 143 is not statistically significant and all other values are well above the composition of zircons in equilibrium with the mantle range of 5.3 ± 0.3 ‰ (Valley et al., 2003). Although the scatter in $\delta^{18}\text{O}$ seems to increase through time, this might simply be an artefact of the number of data ($n = 14$, $n = 29$, $n = 99$ in groups 1, 2 and 3, respectively) and in general the mean isotopic composition of SVC zircons is relatively constant over the last 605 ka.

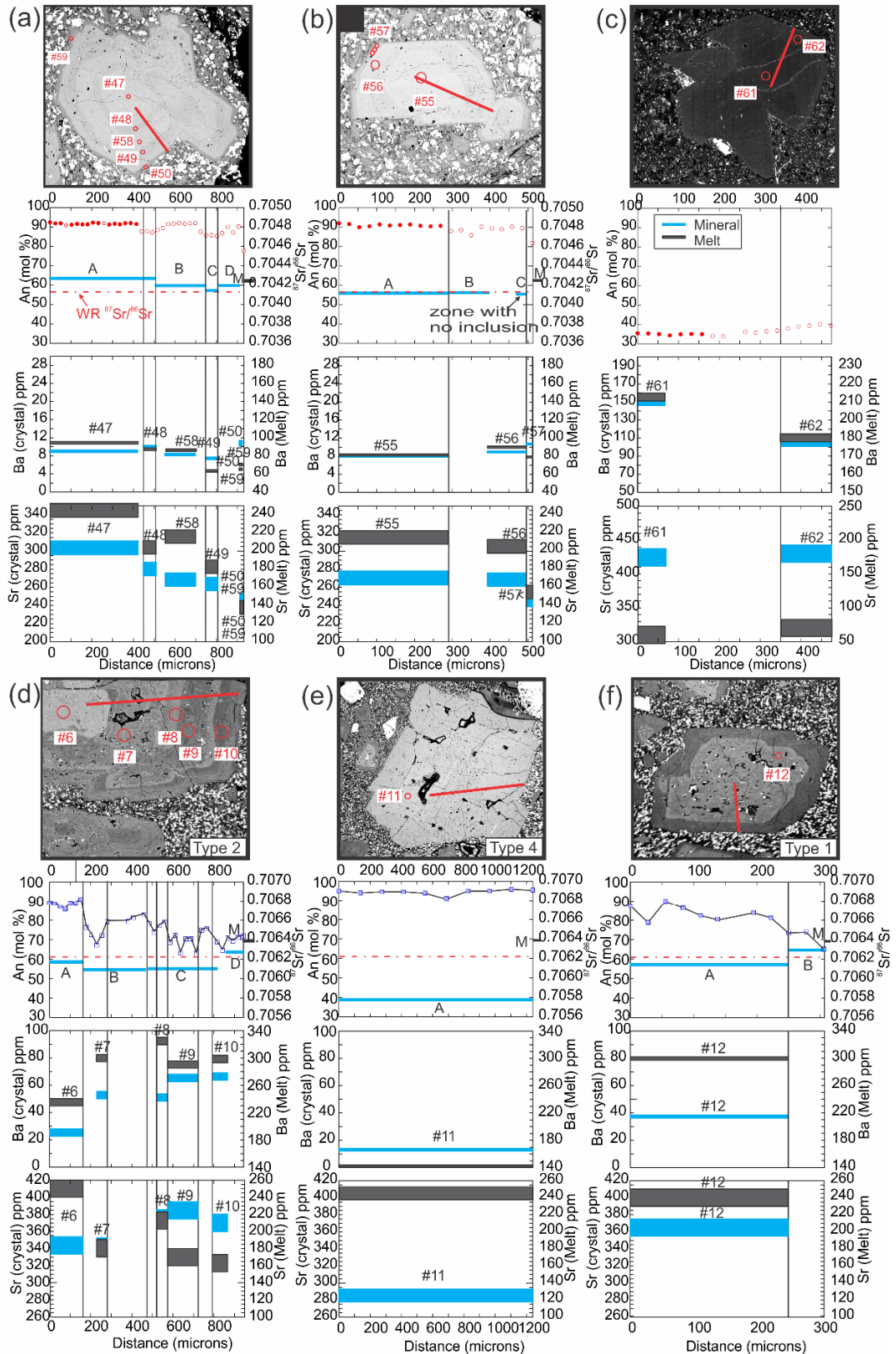


Fig. 5.12. Representative plagioclase compositional profiles for anorthite content, Ba and Sr concentrations, $^{87}\text{Sr}/^{86}\text{Sr}$ ratios and calculated melt Ba and Sr concentrations for (a, b, c) Pre-SVC1, (d, e, f) Pre-SVC2, (g, h, i) SVC1, (j, k, l) cummingtonite-bearing SVC2,3, and (m, n) orthopyroxene-bearing SVC2,3 lavas. Location of the analysis in the crystal is indicated on the corresponding SEM

image with the red line corresponding to the anorthite content profile while the red circles corresponds to the laser spot ablated for trace elements. The number associated correspond to the number of the analyses in the supplementary data file. Symbols for the profiles in anorthite are the same as in Fig. 5.10. For trace elements concentrations and $^{87}\text{Sr}/^{86}\text{Sr}$: blue and grey boxes correspond to crystal and calculated melt compositions respectively. For all data, 2 standard error is the size of the box or smaller. Whole rock $^{87}\text{Sr}/^{86}\text{Sr}$ ratio from for the corresponding crystals is taken from Bezard et al. (2014) and represented by a discontinued red line.

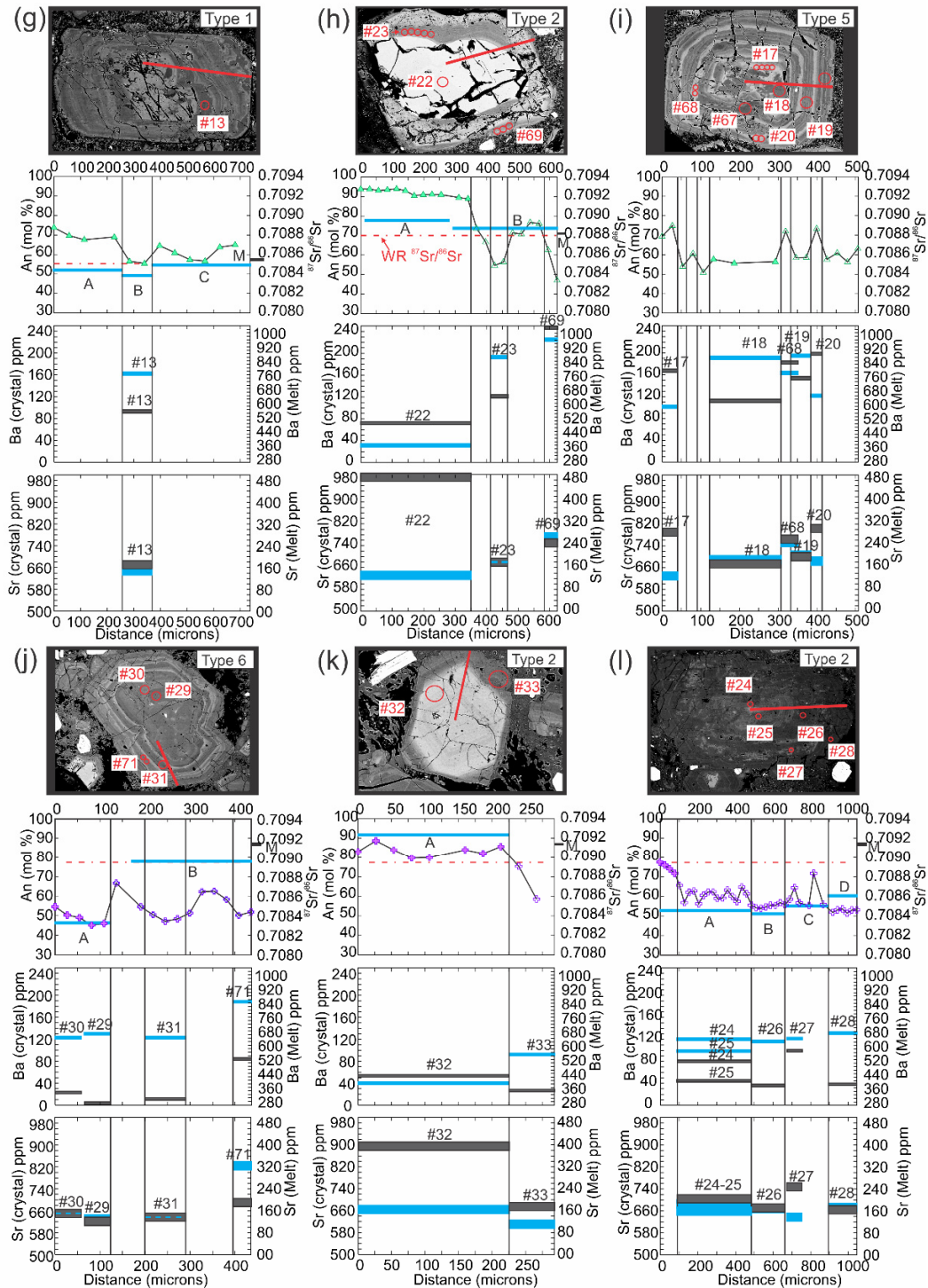


Fig. 5.12. (continued).

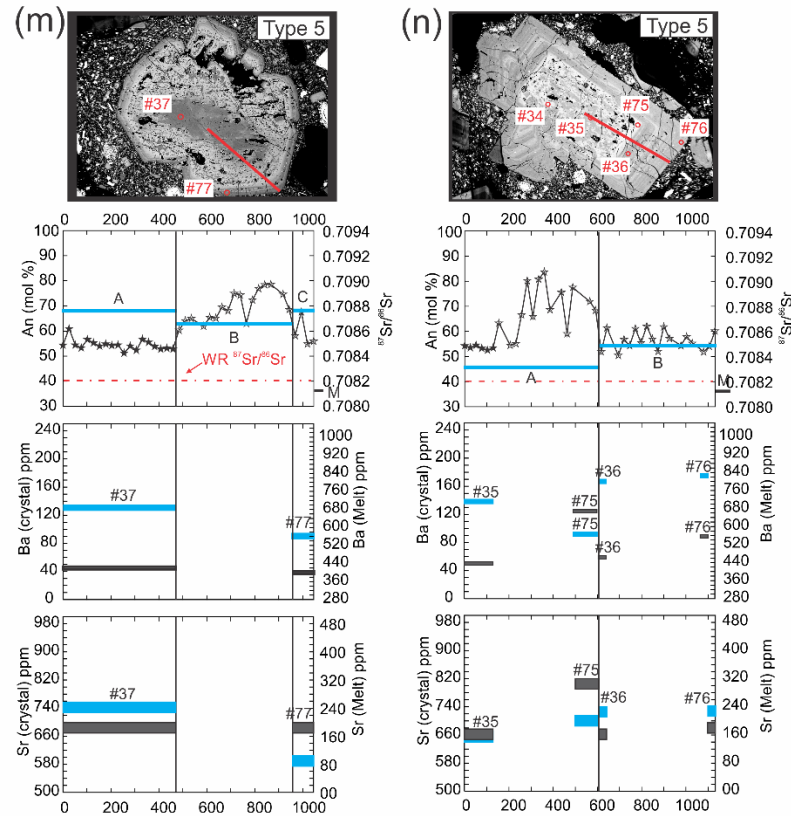


Fig. 5.12. (continued).

5.9 Constraints on crystallisation conditions

5.9.1 Pressure and temperature

5.9.1.1 Pyroxene thermometer

Magmatic temperatures were estimated using the single clinopyroxene thermometer of Nimis and Taylor (2000) at 5 kbar. In Pre-SVC1 basalt, a profile from core to rim in a clinopyroxene indicate variations from 1194°C to 928°C while 2 pyroxenes from its groundmass indicate similar temperatures to the upper limit of the phenocryst range with temperatures between 1211°C and 1125°C. In the Pre-SVC1 rhyolite, the pyroxene compositions indicate low temperatures of crystallisation (886-893°C). Pre-SVC2 basaltic andesite pyroxene crystallised between 1041°C and 864°C. In the SVC, clinopyroxene microphenocrysts found in SVC1 lavas crystallised at 1046°C and 834°C, respectively. Finally, one microphenocryst found in an SVC2,3 lava crystallised at 962°C.

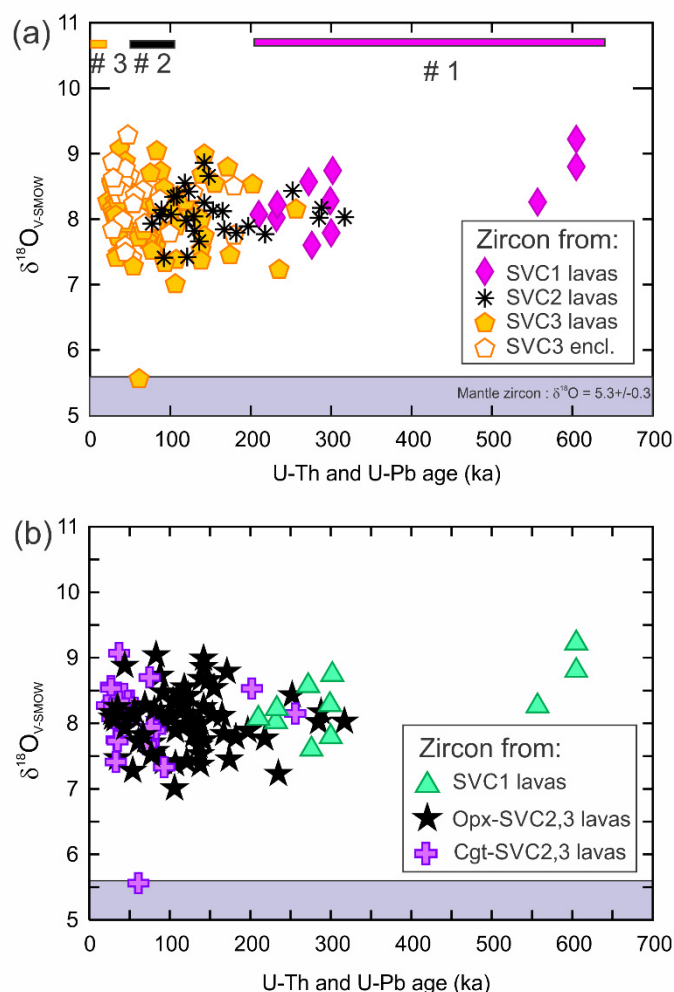


Fig. 5.13. Zircon $\delta^{18}\text{O}$ composition versus the corresponding U-Th and U-Pb growth ages. Growth ages and eruption periods (1, 2, 3) are from Schmitt et al. (2010) and Lindsay et al. (2013). In (a) symbols represent zircons from SVC lavas or enclaves from different eruption periods. In (b), symbols represent zircons from SVC lavas with different mineralogy with SVC1 = SVC lavas from eruption period 1 comprising only orthopyroxene; Opx-SVC2,3 = orthopyroxene-bearing SVC2 and 3 lavas and Cgt-SVC2,3 = cummingtonite-bearing SVC2 and 3 lavas. 2 sd reproducibility error of the O isotope technique was typically of $\pm 0.4\%$ during these analyses (see method section).

5.9.1.2 Cummingtonite-orthopyroxene transition

In SVC2,3, the presence of cummingtonite in the assemblage can be used as an index of pressure and temperature of the magma. Indeed, the experimental study of Geschwind and Rutherford (1992) showed that cummingtonite was constrained to conditions between 2-3 kbar and 790°C in silicic volcanic rocks. An increase in temperature from 790° to 810°C produces the breakdown of cummingtonite and the nucleation of orthopyroxene. Therefore, SVC group 2 and 3 lavas containing

cummingtonite were likely stored at temperatures $< 800^{\circ}\text{C}$ and under 2-3 kbars while the orthopyroxene-bearing lavas were stored at $\geq 800^{\circ}\text{C}$.

5.9.1.3 Calcic amphibole thermobarometry

An estimation of the temperature and pressure of crystallisation of the microphenocrysts of calcic amphibole from SVC2,3 lavas was performed using the equation of Ridolfi et al. (2010). The results suggest the existence of two different depths/temperatures of crystallisation. The first group corresponds to the high Mg# amphiboles which crystallised at $1044\text{-}1016 \pm 22^{\circ}\text{C}$ and $5.8\text{-}7.2 \pm 0.8$ kbar (20-26 km depth) while the second group, with low Mg#, crystallised at $814\text{-}844 \pm 22^{\circ}\text{C}$ and $1.1\text{-}2.1 \pm 0.5$ kbar ($\sim 4\text{-}8$ km depth).

5.9.2 Oxygen fugacity

The oxygen fugacity in the magma in equilibrium with the high and low Mg# amphiboles was estimated using the method of Ridolfi et al. (2010) based on the correlation between Mg content and oxygen fugacity. Values of $\log(f\text{O}_2)$ for the high Mg# amphibole melt range between -8.0 to -8.4 (NNO+1.4 to NNO+1.5). Low Mg# amphibole from the SVC indicate $\log(f\text{O}_2)$ ranging from -11.1 to -13.4 (NNO+0 to NNO+1.9). The less oxidising conditions were obtained in the amphibole with the lowest pressure which could have grown during the degassing of the sample.

5.9.3 Melt-H₂O estimate

An estimation of the magma water content based on amphibole composition can be determined using formulation from Ridolfi et al. (2010). H₂O in melt in which high Mg# amphiboles grew is 7.6-8 wt. % H₂O, whereas low Mg# amphibole grew in a melt with 5.4-7.5 wt. % H₂O.

5.10 Processes controlling mineral major and trace element compositions

The major element zoning observed in plagioclase, quartz and pyroxene phenocrysts, and the occurrence of major dissolution textures in all St Lucia lavas but the Pre-SVC1

rhyolite, suggest that magmatic evolution of St Lucia lavas is relatively complex. Constraining the magmatic processes responsible for major and trace element compositional changes in the phenocrysts is not straightforward. Indeed, even in closed systems, several processes such as cooling, crystallisation, crystal fractionation, convection of the magma and degassing will change magma composition and therefore influence crystal compositions and textures (Druit and Bacon 1989; Marsh, 1989; Cashman, 1992). In open systems, additional processes need to be considered such as magma mixing, magma mingling, thermal equilibration and crustal assimilation (Bacon, 1986; Bacon et al., 1989).

An approach combining plagioclase phenocryst textures, with major and trace element compositions affords a potential means to discriminate between these different processes (e.g. Blundy and Shimizu, 1991; Berlo et al., 2007, Ginibre and Davidson, in press). Plagioclase offers the best opportunity to constrain magmatic processes since (1) it is present in all St Lucia lavas; (2) it is stable in a large range of magma composition, water content, pressure and temperature, allowing a full record of magma differentiation; and (3) its slow Si-Al interdiffusion allows conservation of primary textures and compositions (Grove et al., 1984). The major element composition and texture of plagioclase is controlled by intensive and kinetic parameters such as pressure (Nelson and Montana, 1992), temperature, growth rate (Lofgren, 1980), magma composition and H₂O content (Lofgren, 1980; Nelson and Montana, 1992; Nakamura and Shimakita, 1998; Hammer and Rutherford, 2002). In the following sections, we calculate trace element composition for melts in equilibrium with the different plagioclase zones to attempt to discriminate between plagioclase compositional changes related to variations in intensive parameters from changes due to variations in magma composition during the growth of the phenocrysts. This allows us to assess the origin of the changes in magma composition occurring both before and during phenocryst fractionation, and their relationship with the factors of development and sustainability of the silicic complex. The composition of the melt in equilibrium with the hornblende microphenocrysts found in the SVC were also calculated to constrain the depth of such changes, and of the pyroxenes to investigate their growth conditions.

5.10.1 Ba and Sr concentrations in melt coexisting with plagioclase

Like in every mineral, trace element concentrations in plagioclase are controlled by the partition coefficients between crystal and melt, intracrystal diffusion and kinetic processes. Therefore, to determine the coexisting melt composition during crystal growth, the effect of the partition coefficients needs to be removed, and diffusion and kinetic processes need to be taken into account. We focussed on Ba and Sr since they are the most abundant trace elements in plagioclase and their partitioning between plagioclase and melt is better understood than for any other trace element. We used equations from Blundy and Wood (1991) ($RT \ln D_{\text{Sr}} = 26,800 - 26700X_{\text{An}}$; $RT \ln D_{\text{Ba}} = 10,200 - 38200X_{\text{An}}$) that were derived from experimental and natural samples to estimate Sr and Ba partition coefficients in plagioclase based on their dependence on the temperature and the anorthite content. We used temperatures derived from the geothermometry above: 1000°C for the Pre-SVC basalt and basaltic andesite and 800°C for Pre-SVC rhyolite and all SVC lavas (calculations allow an error of $\pm 100^\circ\text{C}$ on the temperature estimate). The calculated Ba and Sr melt concentrations are plotted against anorthite content on Fig. 5.8b, d and against each other on Fig. 5.14a. Melt Ba and Sr compositions in profiles from representative crystals from each lava groups of St Lucia are presented in Fig. 5.12 in which they are compared to major elements, $^{87}\text{Sr}/^{86}\text{Sr}$ and measured Ba and Sr concentrations of the crystals.

5.10.1.1 Suitability of the regression

Given that crystals can record large changes in magma composition during their growth, the calculated equilibrium melt compositions are not expected to be exactly the same as the whole-rock, the latter being the reflection of the whole crystal cargo along with uncrystallised melt. In all St Lucia lavas, the differences between the calculated melt Ba and Sr concentrations and the whole-rock compositions are limited, and not systematically higher or lower than the whole-rock compositions (Fig. 5.14a). This provides confidence in the suitability of the Blundy and Wood (1991) regressions for our set of samples. The use of alternative equations from Bindeman et al. (1998) does not modify significantly the calculated melt compositions, or the trends. Absolute values will still be considered with caution in the following paragraphs, and interpretations will be based on general trends and relative variations within crystals.

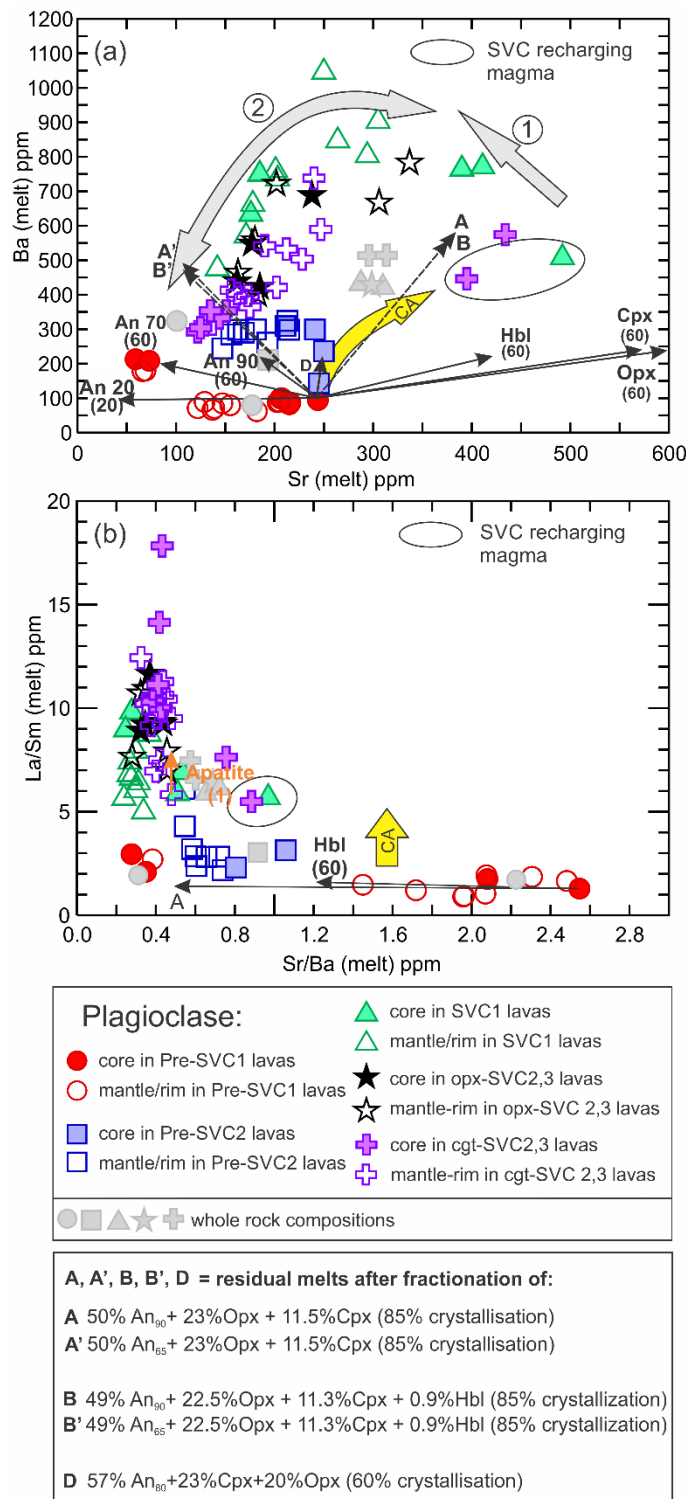


Fig. 5.14. (a) Ba vs Sr concentrations and (b) Ba/Sr ratio vs La/Sm ratio of the calculated melt in equilibrium with plagioclase crystals. Thin arrows show the change in composition of the melt after fractionation of plagioclase crystals of different anorthite content (An) and clinopyroxene (Cpx), orthopyroxene (Opx) and hornblende (Hbl) from the most primitive plagioclase melt of Pre-SVC1 lavas. The percentage of single phase fractionated is indicated under the name of the phase. A' and B' correspond to the residual melt after fractionation of the assemblage necessary to produce whole rock major element composition of SVC1 andesites from Pre-SVC1 basalt according to least squares models

(see Chapter 4). A, B, only differ from A' and B' by the anorthite content of plagioclase fractionated. D refers to the residual melt to produce Pre-SVC2 basalt from Pre-SVC1's most primitive melt. Arrow 1 indicate the evolution of the composition of the recharging magma during fractionation of anorthite-rich plagioclase before or during its arrival at the shallow magma chamber. Arrow 2 indicate the direction of a mixing line between the recharging melt after fractionation of anorthite-rich plagioclase, and the more differentiated magma (low Ba and Sr concentrations) of the shallow chamber. CA = impact of crustal assimilation. Plagioclase partition coefficients are calculated using equations from Blundy and Wood (1991). Partition coefficients for other minerals are presented in Table 5.2.

5.10.1.2 Crystal chemical control

5.10.1.2.1 Sr

When plotted against the anorthite content (Fig. 5.8b), calculated melt Sr from all St Lucia groups of rock form positive trends where, in each group, the highest anorthite contents correspond to the highest Sr values. Pre-SVC1 and SVC calculated melts have the lowest and the highest Sr concentrations, respectively at a fixed anorthite content. Such positive trends are not observed when measured Sr compositions (Fig. 5.8a) are plotted against anorthite content. The divergence between the trends formed by calculated melt Sr and the trends characterizing the measured plagioclase concentrations needs to be accounted for by the impact of crystal-chemical control (anorthite content) on the measured Sr values. The use of calculated melt values rather than measured concentrations in the crystal is therefore necessary to observe changes in Sr concentration due to magmatic processes.

5.10.1.2.2 Ba

Unlike for Sr, calculated melt-Ba variations with the anorthite content of crystals from different groups of St Lucia lavas do not form parallel trends (Fig. 5.8d). In Pre-SVC1 basalts, both calculated melt-Ba (Fig. 5.8d) and measured crystal Ba content (Fig. 5.8c) form a flat trend, which indicate very limited influence of the anorthite content on the partition coefficient. On the other hand, the negative trend formed by Pre-SVC2 and SVC measured Ba concentrations is not observed in the calculated melt-Ba data which argues for an important crystal chemical control on the Ba partition coefficients of the corresponding plagioclases.

5.10.1.3 Diffusion

The SVC is a long-lived magmatic system (Schmitt et al., 2010, Linsday et al., 2013) in which trace element diffusion in plagioclase crystal needs to be considered. If important Ba and Sr diffusion occurred, measured variations across the crystals, and consequently the derived calculated melt compositions, may not represent the real spectrum of magma compositional variations during plagioclase growth (Ginibre et al., 2002). Indeed, for a labradorite composition, typical of SVC plagioclases, at 776°C and 1075°C, the diffusivity D is between 9.92×10^{-17} and 5.98×10^{-14} cm²/s (Cherniak and Watson, 1994). Given that plagioclase growth rate in natural melt varies from 10^{-8} to 10^{-12} cm/s (Cashman, 1990; Davidson and Tepley, 1997), Sr diffusion and plagioclase growth rate are in similar order of magnitude. Sr diffuses faster than Ba (Cherniak, 1999) in plagioclase, therefore, if total diffusive equilibration occurred, calculated Sr melt concentrations would be homogeneous through the crystals while a few Ba melt concentration variations would remain measurable. However, in both Pre-SVC and SVC crystal cores and mantles, large changes in Sr are preserved across major dissolution surfaces not larger than 50-150 microns. Such observation indicates that complete diffusive equilibration did not occur at such scales, and that diffusion did not affect significantly the core-mantle of the crystals which may only have been slightly smoothed. Partial diffusive equilibration, affecting only small scale compositional heterogeneities, such as in the fine oscillatory textures, could have taken place. However, we did not perform high-resolution trace element profiles across the crystals and rather focused in major resorption surfaces linked to major changes in composition. Therefore, the potential occurrence of small-scale equilibrium concentration profiles does not affect our interpretations. Since Ba diffuses slower than Sr (Cherniak, 1999), it cannot have been significantly affected by diffusion either.

5.10.1.4 Changes in melt composition during plagioclase growth

Intracrystal variations in trace elements that are not due to chemical control or diffusion need to be accounted for by a change in melt composition or kinetic processes during crystal growth (Singer et al., 1995; Ginibre et al., 2002). Kinetic processes can be differentiated from melt compositional variations by monitoring the relative behaviour of compatible versus incompatible elements in plagioclase. The

coupling of Ba and Sr variations in the crystals and the anorthite content can help to differentiate between different magmatic processes such as fractional crystallisation and recharge events. Below, we discuss the calculated Ba and Sr melt concentrations variations associated with crystal textures. A summary of the melt compositions and interpretations for each crystal types is presented in Fig. 5.6.

5.10.1.4.1 Pre-SVC1

In the basalt analysed, the core of zoned crystals grew in a melt with higher Sr but similar Ba concentrations to the mantle-rim (Fig. 5.14a). The lowest calculated melt-Sr recorded from core-to-rim, also corresponds to the lowest anorthite content (Fig. 5.8b), which is consistent with progressive magma differentiation where plagioclase dominates the fractionating assemblage. The absence of Ba increase recorded in melts from core-to-rim in the plagioclase crystals indicate the absence of major pyroxene or amphibole crystallisation during crystallisation of the plagioclase (see Fig. 5.14a). It also precludes the crystallisation of anorthite-rich plagioclase that would also slightly increase the Ba concentration of the melt. Using the core in equilibrium with the most Sr-rich calculated melt as a starting composition, and partition coefficients calculated using the Blundy and Wood (1991) equation, the crystallisation of around 12 % of An₂₀ plagioclase could explain the lowest Sr values observed in the mantle-rims.

In detail, the core-to-rim decrease in melt-Sr and anorthite is not smooth (Fig. 5.12a, b) and this suggests that processes other than simple progressive plagioclase fractionation occurred during crystal growth. Indeed, all the phenocrysts analysed display minor dissolution surfaces followed by inclusion-rich zones corresponding to a decrease in anorthite content of around An₅. In the largest phenocryst analysed, the decrease in anorthite is accompanied by a drop in melt-Sr concentrations of 35-40 ppm (Fig. 5.12a). Variations in both major and trace elements observed at the inclusion-rich zones cannot be explained simply by physical changes to the magma (P-T-H₂O) since unreasonable fluctuations of temperature of more than 300°C would be necessary to account for the change in Sr concentrations of the melt. The abrupt decrease in anorthite contents and the small width of the zones argue against their growth in a magma affected by in-situ crystallisation. The constant or lower Mg content associated with the decrease in melt-Sr and anorthite (see supplementary file for Mg concentrations) argues against kinetic control over melt-Sr variations, such as

those occurring at crystal boundary layers during rapid growth (Ginibre et al., 2002). Therefore, the decrease in melt-Sr at inclusion-rich zones of the large phenocrysts needs to be accounted for by a change in magma composition. We propose that such change could be related to transport into a slightly more differentiated zone of the magma or could have been produced by magma mixing with a slightly more differentiated melt. In the smaller phenocrysts, the decrease in anorthite content and in melt-Sr concentrations in the inclusion-rich zones is more subtle (e.g. Fig. 5.12b) and the small decrease in melt-Sr concentrations is accompanied by an increase in Mg content of the crystal. This suggests that the slight Sr decrease might be due to a kinetic process instead of a variation in the magma composition.

In the Pre-SVC1 rhyolite, where no major dissolution surfaces can be observed in plagioclase, variations in anorthite and melt Sr and Ba content are limited (Fig. 5.12c). Whether located in the core or in the rim, the more anorthite-rich zones of the crystals grew in a melt with slightly higher Sr concentrations than the zones with lower anorthite content. Ba varies independently from anorthite or Sr concentrations and displays a clear decrease from the core to the rim of the crystal. Such a decrease is also observed with K content and could therefore indicate the beginning of fractionation of very small amounts of a K rich phase such as biotite or potassic feldspar between the growth of the core and the rim of the crystals, although the latter phase is not present in the phenocryst assemblage. The absence of resorption textures and the very limited difference in composition between the different zones of the crystals argue for their growth during limited movements in parts of a magma chamber displaying only slight variations in degree of differentiation. Pre-SVC1 rhyolite plagioclase-melts can successfully be produced from the most primitive Pre-SVC1 basalt melt (Fig. 5.14a) after around 60% of crystallisation of An₇₀ (using calculated partition coefficients from Blundy and Wood (1991)).

5.10.1.4.2 Pre-SVC2

In the Pre-SVC2 basaltic andesite, as in Pre-SVC1 basalt, crystal cores (anorthite-rich) crystallised in a melt with higher Sr concentrations than the mantle-rim but with similar to lower Ba concentrations (Figs. 5.6, 5.8b, d and 5.14a). Variations in Ba concentrations are greater than in the Pre-SVC1 basalt plagioclase-melts. Amongst the crystal cores, melt Ba content increases with decreasing anorthite content (from ~An₉₅

to $\sim\text{An}_{85}$; Fig. 5.8d), while melt Ba is relatively constant in all mantles and rims (from $\sim\text{An}_{85}$ to $\sim\text{An}_{67}$). Mantle zones with intermediate anorthite content grew in a melt with intermediate Sr values between those of the core and rim (Fig. 5.8b).

The large unzoned and subeuhedral Type 4 crystal analysed (Fig. 5.12e), which has the highest anorthite content of Pre-SVC2 lavas grew in a melt overlapping the Sr compositions recorded by the Pre-SVC1 cores and only has slightly higher Ba values (Fig. 5.14a). Such melt-Ba concentration is lower than concentrations recorded by the rest of the Pre-SVC2 crystal which suggests that Type 4 crystals crystallised in a different magma and were incorporated as antecrysts into the lava during ascent or emplacement of the magma. This is also supported by the absence of a rim in major element equilibrium with the groundmass. Type 1, 2 and 4 crystals all display a core that grew in a melt rich in Sr.

In Type 2 crystals (e.g. Fig. 5.12d), the transition between the inclusion-free and anorthite-rich core and the inclusion-rich mantle zone with a “flame texture” is characterised by an important dissolution surface accompanied by a large drop in melt-Sr of up to ~ 70 ppm. Such a large decrease cannot be attributed to a simple variation in magmatic temperature since a decrease of more than 300°C would need to occur, which is unreasonable. Therefore, these trace element variations need to be accounted for, either by a change in composition of the magma, or by a kinetic control over Sr concentrations due to rapid growth after resorption of the core of the crystal (Bottinga et al., 1996). The coupling between the decrease of a compatible element concentration such as Sr, with an increase in incompatible elements such as Ba and Mg in the calculated melt could support a kinetic control over the trace element composition after the resorption surface. The fast growth would also be consistent with the presence of large amounts of inclusions in the zone subsequent to the resorption surface. However, most of the rest of the crystal mantle-rim has similarly low melt-Sr, high melt-Ba, and high Mg, K and Fe concentrations, yet it displays variable textures comprising an inclusion-free uniform zone, as well as inclusion-free oscillatory zoning. Because the mantle displays different textures, it is unlikely that the whole mantle rim of the crystal crystallised at a fast rate. It is therefore proposed that the decrease in Sr and increase in incompatible elements records a change in magma composition rather than invoking kinetic factors. In this scenario, the core would have crystallised from a melt containing around ~ 250 ppm Sr whereas the mantle rim of the

crystal would have crystallised from a melt with around ~170 ppm Sr. Because the decrease in Sr is accompanied by a resorption surface and an important decrease in anorthite content, we suggest that Type 2 crystal cores crystallised in a more primitive magma than the mantle, and was resorbed upon its contact with a more differentiated melt, possibly during a recharge event. The flame texture of the mantle would therefore have grown right after mixing with the more differentiated magma. Although limited compared to the core-mantle transition, the rest of the mantle of Type 2 crystal shows chemical variations linked with specific textures of the subzones (Fig. 5.12d). Anorthite-rich narrow zones located directly after inclusion-rich portions of the mantle display clear increase in melt-Sr and Ba (Fig. 5.12d) compared to the surrounding zones. This increase is once again hard to explain by a change of temperature or by kinetic factors, and the anorthite-rich zones need to have crystallised in a melt more enriched in Sr and Ba than the most sodic zones of the crystal. Sodic zones occur after each anorthite-rich zone of the mantle and display a wavy oscillatory texture. Such textures, characterised by the crystallisation and resorption of micrometer-scale anorthite-rich plagioclase subzones, are typically considered to crystallise in a melt that underwent frequent and rhythmic variations in temperature and H₂O content, due to chamber wide convection (Ginibre et al., 2002). We suggest that the wavy oscillatory texture characterizing the sodic part of the crystal is related to the entrainment of the crystals into chamber-wide convection in a heterogeneous chamber following, or during, a recharge event. Anorthite-rich zones would then correspond to the contact of the crystal with more primitive recharging melt.

In Type 1 crystals, the core comprises a mix of resorbed anorthite-rich core and sodic channels (Fig. 5.12f). Calculated melt compositions have slightly lower and higher Sr and Ba concentrations, respectively, compared to the core of Type 2 crystals core-melts (Figs. 5.6 and 5.12f) while the sodic mantle-rim, as in Type 2 sodic zones, grew in a melt with low Sr. The anorthite-rich nature of the core before resorption, and its growth in a melt with relatively similar Sr-concentrations to Type 2 crystal core suggests that both crystallised in the same recharge magma, while Type 1 rims crystallised after mixing with a more differentiated magma. The inclusion-rich nature of Type 1 cores compared to Type 2 may be related to larger change in temperature or water content during its arrival in the chamber. For example, crystals from a recharge magma would experience a higher drop of temperature upon mixing with resident

magma than crystals brought into the system during the end of a recharge event, since the magma chamber would have by then increased in temperature. As for Type 1 crystals, the sodic mantle display a wavy oscillatory texture, which could have been produced by convection in the magmatic chamber triggered by the recharge event.

5.10.1.4.3 SVC1

Similar to Pre-SVC1 and 2, the highest melt Sr concentrations calculated for SVC1 plagioclase are recorded by anorthite-rich crystal cores and correspond to variable Ba values (Fig. 5.8b, d). These cores, found in Type 2 phenocrysts such as the one illustrated in Fig. 5.12h (diameter > 600 microns) and microphenocrysts (diameter \leq 600 microns), were affected by partial resorption (dissolution surface) followed by the crystallisation of more sodic and (wavy) oscillatory zoned plagioclase from a melt with low Sr concentrations and variable Ba content (e.g. Figs. 5.6 and 5.12h). This decrease in anorthite content, accompanied by significant changes in trace element concentrations beyond the dissolution surface, cannot be explained simply by a change in physical conditions in the magma chamber. Furthermore, Mg concentrations (incompatible element) decrease with Sr content which argues against the involvement of kinetic processes. Therefore, the decrease in Sr concentration observed at the resorption surface is due to an abrupt change in magma composition. Given that (1) andesite-dacite differentiation typically decreases the Sr content of the magma and (2) anorthite-rich plagioclase consistently have high Sr concentrations while sodic mantles have significantly lower Sr content, we suggest that Type 2 cores grew in a more primitive magma than the mantles. The dissolution surface at the core-mantle interface would therefore correspond to a recharge event. Although all Type 2 crystal-cores analysed (three) grew in a melt with high Sr and Ba concentrations, they are not identical in composition (Fig. 5.14a). The core with the highest anorthite content and the most homogeneous texture grew in a melt with higher Sr and lower Ba than the other two. The high anorthite content of this crystal suggests that the corresponding melt Ba and Sr compositions are the most representative of the primitive magma composition recharging the chamber. In this case, we suggest that the composition of the melts of the two other cores could be explained by fractionation of small amounts of anorthite-rich plagioclase (similar to the crystal with the highest anorthite content) occurring in the recharging magma, before the cores crystallised. Fractionation of

anorthite-rich plagioclase would increase Ba and decrease Sr in the recharging magma. Melts in equilibrium with Type 2 sodic mantles have variable Ba content and we suggest that this is due to variable mineral assemblages fractionated in the magma chamber between recharge events. For example, although absent from the phenocryst assemblage of SVC1 lavas, fractionation of small amounts of biotite could decrease the Ba concentration of the magma, while fractionation of pyroxene, amphibole and anorthite-rich plagioclase would increase the Ba content of the melt. Finally, as for Pre-SVC2, the sodic zones have wavy oscillatory texture, which suggests convection of the crystal in the magma chamber after the recharge event.

In Type 1 crystals (e.g. Fig. 5.12g), no trace element composition could be obtained for the core due to the abundance of inclusions, however, the sodic plagioclase that grew during/right after the resorption surface between the core and the mantle, is from a melt with the same composition as the oscillatory zoned mantle-rim of Type 2 sodic plagioclase. We therefore interpret Type 1 crystals texture and composition by a similar process as for Type 2, where, the anorthite rich cores from a recharge magma is injected in a more differentiated magma triggering core resorption and magma convection. However, in the case of Type 1 crystals, as for Pre-SVC2 Type 1 plagioclases, the anorthite-rich core would have been resorbed more significantly at its arrival in the magma chamber, producing the pervasively channelled “sponge” texture.

In Type 5 crystals (e.g. Fig. 5.12i), sodic cores and sodic oscillatory mantle zones all grew in a melt with similar composition to Type 1 and 2 sodic mantles. Type 5 cores are highly resorbed and replaced by anorthite-rich zones/channels. Similar, but less dramatic, major resorption textures followed by anorthite-rich plagioclase growth can be observed within the crystal mantle. All anorthite-rich zones/channels growing after major dissolution surfaces in Type 5 crystals grew in a melt with slightly lower Sr and slightly higher Ba content than anorthite-rich zones in Type 2 crystals, (Fig. 5.12h, i). No increase in incompatible elements such as Mg accompanies the increase in melt-Sr, discounting any kinetic effect. Based on these compositional constraints, we suggest that Type 5 crystals represent phenocrysts that started crystallising in a differentiated magma chamber, subsequently recharged by a more primitive magma. We suggest that the arrival in the chamber of a more primitive magma produced the partial resorption of the existing sodic crystals, followed by crystallisation of

anorthite-rich zones in equilibrium with the recharging melt and finally by the convection of the crystal responsible for the wavy oscillatory zoning. The cause of the slightly higher Ba and lower Sr concentrations in the primitive melt in equilibrium with the anorthite-rich zones compared to the Type 2 core-melts could be explained by early fractionation of small amounts of anorthite-rich plagioclase within the recharging melt, (e.g. due to decompression) which would produce its slight increase in Ba and decrease in Sr. The presence of at least 3 major resorption events recorded in a same crystal indicate that several pulses of the recharge affected the chamber. The occurrence of a microphenocryst with a high An-Sr-Ba core and only a thin rim in equilibrium with the rhyolitic groundmass (~100 μm) indicates that recharge events were still occurring close to the time of eruption.

Therefore, all crystals of SVC1 record the recharge of a magma chamber by a more primitive magma. Whether the more differentiated magma represents the residual melt from differentiation of a magma similar to the recharge melt (i.e. Type 2 anorthite-rich core melt) is hard to constrain since the initial differentiation of the magma is not recorded in the crystals analysed.

5.10.1.4.4 SVC2, 3

SVC2,3 with orthopyroxene

Unlike for SVC1 lavas in which most crystals have anorthite-rich cores, plagioclase in SVC2,3 orthopyroxene-bearing samples are mainly of Type 5 and 6 and have sodic cores grown in a melt with low Sr and Ba concentrations. These cores are dominantly partially resorbed (Type 5; Fig. 5.12m, n) and surrounded by anorthite-rich plagioclase with high melt Ba and Sr concentrations, similar to the rare Type 5 crystals in SVC1. The anorthite-rich plagioclase is itself surrounded by a sodic oscillatory zoned mantle-rim grown in a melt with similar melt Ba and Sr concentrations to the sodic core. The sodic resorbed core of Type 5 crystals as well as sodic oscillatory zoned mantle-rim all grew in a melt with similar to slightly lower Sr concentration as the melt in equilibrium with the SVC1 sodic zones with a similar large range of Ba. The anorthite-rich plagioclase that crystallised after resorption of the sodic cores, filling the channels, crystallised from a melt with slightly lower Sr values than the anorthite-rich zones of SVC1 but with similar Ba concentrations (Figs. 5.6 and 5.12m, n). The slighty

lower Sr concentrations of the calculated melt compared to the melt in equilibrium with SVC1 anorthite-rich zones could either be due to the sampling of a bit of sodic plagioclase by the laser spot, or due to the fact that the anorthite-rich plagioclase zones crystallised from a melt that already mixed with the more differentiated magma. Once again, the shift in melt Ba and Sr concentrations between the resorbed sodic core and the anorthite-rich plagioclase cannot be explained by a change in physical conditions but rather reflect crystallisation from two melts with different composition. Therefore, we propose that the trend formed by orthopyroxene-bearing SVC2 crystal-melts reflects a recharge event where, similarly to SVC1, a magma chamber with low Sr and Ba concentrations was being recharged by a more primitive melt with high Sr and Ba concentrations, producing the resorption of sodic plagioclase followed by anorthite-rich crystal growth. The scarce presence of Type 1, 2 and 3 crystals may indicate different conditions in the magma chamber during the recharge event compared to SVC1 (e.g. a lower magma temperature). Since orthopyroxene bearing SVC2,3 crystals grew in a melt where the trace element composition of both the recharging magma and of the more differentiated magma is similar to SVC1, both lavas seem to have been produced in the same magma chamber.

SVC2,3 with cummingtonite

In cummingtonite-bearing lavas, as in orthopyroxene-bearing samples, sodic cores of Type 5 crystals also crystallised in a melt with low Sr and Ba values. They were resorbed and surrounded by anorthite-rich plagioclase grown in a melt with high Sr and Ba concentrations. Type 6 sodic cores (e.g. Fig. 5.12j) grew in a melt with low Sr and Ba abundances separated by a major dissolution surface from a wavy oscillatory-zoned mantle (e.g. Fig. 5.12j). Type 5 and 6 cores tend to be more sodic and clearly have lower melt Sr and Ba than SVC1 and SVC2,3 orthopyroxene-bearing sodic plagioclase (Fig. 5.6). The sodic zones of the mantle and rims display similar to higher melt Sr and Ba than the sodic cores. The variation in trace elements recorded in the crystals cannot be explained by a simple change in temperature and needs to be accounted for by growth in a magma that was evolving in composition. Like Type 5 crystals in orthopyroxene-bearing SVC2,3 lavas, we suggest that Type 5 and 6 sodic crystal cores crystallised in a magma chamber with low Ba and Sr concentrations being recharged by more primitive magma with high Sr and Ba contents. The lower Sr and

Ba abundances in the melt in which sodic cores crystallised compared to other SVC groups suggest that these crystals resided in a more differentiated magma. More differentiated magmas tend to be cooler, which is consistent with the crystallisation of cummingtonite. In addition, compared to SVC1 orthopyroxene-bearing SVC2 and SVC1 crystals, cummingtonite-bearing lava plagioclases have thinner and less abundant anorthite rich zones, which suggests a more limited contact of the phenocrysts with the recharge magma. Such observations could be consistent with the magma being stored in a cooler part of the magma chamber, more distant to the bottom of the chamber where the recharge magma is injected.

A rare Type 2 phenocryst from a cummingtonite bearing SVC2,3 lava (Fig. 5.12l) comprises a small resorbed anorthite-rich core surrounded by wavy oscillatory texture, itself surrounded by an unzoned sodic zone. The unzoned sodic zone is subsequently resorbed and replaced by anorthite-rich plagioclase (“flame texture”) followed by oscillatory texture. The resorbed core could not be analysed. However, in the rest of the phenocryst, the two zones with the highest anorthite content (i.e., the oscillatory zoned and the anorthite-rich plagioclase with a flame texture grown after resorption of the sodic plagioclase) grew in melts with the highest Ba and Sr concentrations compared to the rest of the crystal. The unzoned sodic part of the mantle, and the sodic oscillatory-zoned rim both grew in a melt with similar and low Ba and Sr concentrations. Mixes of anorthite-rich and sodic plagioclase analysed in the inclusion-rich zones displaying “flame textures” possess intermediate melt compositions between the melts of the sodic and anorthite-rich zones of SVC group 1. We suggest that the Type 2 phenocryst recorded the effects of two recharge events. The anorthite rich-core would come from a first batch of recharging magma. It would have resorbed at its arrival in the differentiated magma and subsequently be entrained into convection, producing the wavy oscillatory texture. The following unzoned sodic zone of the crystal suggests the absence of convection and we suggest that the resorption of this sodic zone is produced by another recharge event, the latter generating a second period of convection for the crystal (wavy oscillatory zoning).

Type 2 microphenocrysts (~500 microns; Fig. 5.12k) with anorthite-rich and inclusion-poor euhedral cores grew in a melt with similar Sr content as SVC1 anorthite-rich zones. They have only slightly lower Ba concentrations and suggest the occurrence of a recharge event close to the time of eruption. The cores are surrounded

by very sodic plagioclase with low Sr and Ba concentrations. The sharp decrease in anorthite and trace element composition is not linked with a resorption texture. The very primitive composition of the core-melt and the very differentiated composition of the rim-melt once again suggests that Type 2 microphenocryst cores crystallised in a recharge magma while the thin rim (~25 μm) crystallised in the magma chamber following the recharge event and shortly before eruption. Microphenocrysts cores have the highest anorthite content out of all the crystals analysed in the cummingtonite-bearing SVC2,3 lavas and they grew in a melt with Ba and Sr concentrations similar to the most primitive SVC1 lavas. This indicates that the recharging magma maintained a similar trace element composition over 600 ka.

5.10.1.4.5 Summary of the crystallisation history of Pre-SVC and SVC Plagioclase

All but the Pre-SVC1 rhyolite evolved in an open system:

- In Pre-SVC1 basalts, early growth of plagioclase crystals occurred in a Sr-rich and Ba-poor melt. It was followed by mantle and rim growth in a heterogeneous and slightly more differentiated magma with lower Sr content. The decrease in magma Sr was probably produced by small amounts of sodic plagioclase fractionation.
- Pre-SVC1 rhyolite plagioclase crystals grew in a homogeneous magma chamber characterised by only very small variations in composition due to slight differences in the degrees of differentiation of the magma.
- Pre-SVC2 Type 1, 2 and 3 crystals grew during a recharge event. They started growing in a recharge magma with higher Ba content compared to Pre-SVC1 crystals. These cores were thereafter partially resorbed, followed by the growth of the mantle in a more differentiated Sr-poor magma with variable Ba content. Subsequently, the mantle of the crystals recorded up to two other recharge events (mixing with more primitive magma in the resident more differentiated chamber), each followed by chamber wide convection in the magma chamber. On the way to the surface, the magma incorporated Type 4 crystals, probably from the wallrock.

- In the SVC, all crystals but Type 4 recorded the effects of at least one mixing event of primitive magma in a more differentiated magma chamber. Type 1, 2 and 3 plagioclase cores grew in the primitive recharge melt characterised by higher Sr and Ba concentrations than any calculated Pre-SVC1 and Pre-SVC2 melts. The crystal cores were subsequently resorbed during mixing of the recharge magma with a more differentiated magma with lower Sr and Ba concentrations in which the mantle of the crystals grew. During the growth of the mantle up to two other recharge events affected the chamber. The primitive recharge melt maintained a similar trace element composition over the last 600 ka. Each recharge event was followed by chamber-wide crystal convections producing wavy oscillatory zoning. Early growth of Type 5 and 6 crystals occurred in the differentiated magma chamber and was followed by resorption during mixing with a primitive recharge magma. Resorption was followed by chamber wide convection of the crystals. The differentiated magma chamber composition, between recharge events, seems to have become progressively more differentiated (lower Sr and Ba contents) through the SVC existence.

5.10.1.5 Change in melt composition before crystal growth

It is clear that the recharge magma in the SVC and Pre-SVC2 chambers had different Ba and Sr concentrations to the most primitive Pre-SVC1 lava. This is demonstrated in Fig. 5.8b and d by the difference in concentrations, especially for Sr, observed between the Pre-SVC1 and Pre-SVC2 melts and between Pre-SVC2 and SVC melts at a fixed anorthite content. The three different groups of lava composition therefore either (1) had different parental magmas; or (2) had similar parental magmas that had undergone different extents of fractionation; or (3) had similar parental magmas that suffered from different extents of crustal assimilation. The first hypothesis is considered unlikely since it was shown in Chapters 3 and 4 that all the St Lucia lavas seem to have differentiated from a similar magma with a composition analogous to Pre-SVC1 basalt. Therefore, the difference in Ba and Sr compositions in the lavas needs to be accounted for by either mineral fractionation only, or by the interplay of mineral fractionation and crustal assimilation. Sediment assimilation has been shown to clearly control REE and Th/Th* variations between Pre-SVC1, Pre-SVC2 and SVC lavas (Chapter 4). Although the SVC lavas have higher Ba and Sr than the other

groups, the impact of assimilation on the concentrations in these elements was not obvious using whole rock compositions only since, unlike for La/Sm, Th/Th* and isotopes, no clear variation of Sr and Ba concentrations with SiO₂ could be observed between Pre-SVC1 and Pre-SVC2 and SVC lavas (Pre-SVC2 and Pre-SVC1 lavas have overlapping Ba and Sr concentrations at similar SiO₂). Below is discussed the potential impact of sediment assimilation on Sr and Ba, using the calculated melt compositions.

5.10.1.5.1 Pre-SVC2

Discrimination between different extents of fractionation or the involvement of crustal assimilation in the production of Pre-SVC2 primitive melt from Pre-SVC1's most primitive melt using trace element data is not straightforward. Indeed Pre-SVC2 crystal core-melt compositions could be produced either by fractionation (of at least 60% of an assemblage of anorthite-rich plagioclase with pyroxene from Pre-SVC1's most primitive melt, e.g. 60% crystallisation of an assemblage containing 57% An₈₀ plagioclase + 23% clinopyroxene + 20% orthopyroxene; Fig. 5.14a model D) or assimilation of a Sr-rich assimilant.

5.10.1.5.2 SVC

The most primitive calculated melt from the SVC plagioclases (the recharging magma composition) has much higher Sr and Ba concentrations than any Pre-SVC1,2 calculated melt (Fig. 5.14a). Therefore, if SVC primitive melt was produced by differentiation from Pre-SVC1's most primitive melt, significant anorthite-rich plagioclase in addition to pyroxene or amphibole would need to be fractionated in order to increase both the Sr and the Ba contents of the melt (Fig. 5.14a). In Chapter 4, least squares models were used to show that the whole rock major element composition of SVC1 lavas could be derived from Pre-SVC1's most mafic lava by 85% fractionation of an assemblage comprised of 50% plagioclase (~An₆₅), 23% orthopyroxene and 11.5% clinopyroxene. To test whether fractionation of such assemblage could also explain the Ba and Sr concentrations in the primitive SVC melt, we calculated the Ba and Sr concentrations of the residual melt after fractionation of this assemblage, using partition coefficients from Blundy and Shimizu (1991). Results show that this model does not produce a residual melt with Ba and Sr concentrations

high enough to simulate the primitive SVC1 melt (A' and B' in Fig. 5.14a). The Sr and Ba concentrations in the primitive SVC melt could only be achieved by fractionation involving much more calcic plagioclase ($\geq \text{An}_{90}$) (A and B in Fig. 5.14a). However, fractionation of such an assemblage would produce a very differentiated residual melt composition, depleted for example in CaO. Subsequent crystallisation of this residual melt would be unlikely to yield anorthite-rich plagioclase, even if the water content in the magma was high. Thus, this is inconsistent with the anorthite-rich nature of the SVC crystals that grew in the most primitive SVC melt. We therefore suggest that simple fractional crystallisation of the most mafic Pre-SVC1 magma is not responsible for the parental SVC magmas, and propose instead that crustal assimilation is responsible for Sr and Ba enrichment between the Pre-SVC and SVC stages.

5.10.2 La/Sm variations in plagioclase coexisting melt

As mentioned in the previous section, the increase in La/Sm ratios observed between Pre-SVC1, Pre-SVC2 and SVC1 whole rock lavas was shown to be mostly controlled by sediment assimilation in Chapter 4. Here, we calculated the La/Sm ratios of melts in equilibrium with Pre-SVC and SVC plagioclase (Fig. 5.14b), using the partition coefficients given in Table 5.2, to bring additional constraints on this process. Since La and Sm partition coefficients can be affected by melt composition, temperature and anorthite content of the crystal, we used $D_{\text{La/Sm}}$ rather than absolute D_{La} and D_{Sm} values themselves to cancel these effects, since very little relative change of the La partition coefficient compared to Sm coefficient occurs with major element variation of the magma (between basalt and rhyolite) or the crystal (between anorthite-rich and anorthite-poor crystals) (e.g. plagioclase $D_{\text{La/Sm}}$ from Fujimaki et al. (1984) for basaltic andesites is only ~ 1.6 times higher than $D_{\text{La/Sm}}$ from Nash and Crecraft (1985) for rhyolite). Diffusion is unlikely to have affected La and Sm concentrations in plagioclase since the rate of this process is slower for REE than for Sr (Cherniak, 2003).

The calculated melt La/Sm ratios from Pre-SVC1 basalt crystals (Fig. 5.8f) are all similarly low from core-to-rim. Pre-SVC1 rhyolite melts are not significantly higher in La/Sm (~ 2 times) than Pre-SVC1 basalt melts, illustrating the negligible impact of magma and crystal major element variations on La/Sm. Melt La/Sm ratios calculated

from Pre-SVC2 crystals (Fig. 5.8f) are heterogeneous and vary from Pre-SVC1 rhyolite melt compositions to higher values and finally, SVC melts have La/Sm ratios similar to the highest ratios for Pre-SVC2 melts or higher with La/Sm comprised between 5.0-17.8. Extreme La/Sm compositions occur in melts from cummingtonite-bearing SVC2,3 lavas. The most primitive SVC melt compositions in terms of Ba and Sr, display some of the lowest La/Sm ratios amongst the SVC. When calculated melt La/Sm ratios are plotted against calculated melt Ba/Sr ratios (Fig. 5.14b), data form a hyperbolic trend where high melt Sr/Ba ratios have low La/Sm ratios, and high melt La/Sm have low melt Sr/Ba ratios.

Like for Ba and Sr concentrations, although more subtle, melt La/Sm ratios are higher in Pre-SVC2 than in Pre-SVC1 and higher in the SVC than in Pre-SVC2 at a fixed anorthite content (Fig. 5.8f). This suggest that the primitive melt of each group had different ratios. On Fig. 5.14 is shown the effect of fractionation from Pre-SVC1 primitive melt of the mineral assemblage “A” (see Fig. 5.14 for assemblage composition) comprising very anorthite-rich (An_{90}) plagioclase necessary to produce Ba and Sr compositions similar to SVC primitive melts. Fractionation of large amounts of hornblende and pyroxene was also modelled since these preferentially incorporate middle rare earth elements (high L/MREE) (Fig. 5.14b). As expected, the results show that no individual phase or phase assemblage could produce a residual melt with La/Sm higher than the Pre-SVC1 rhyolite. Fractionation of an accessory phase such as apatite, could increase the La/Sm ratio. However, the effect of trace amounts of apatite crystallisation, even in differentiated melts, seems very limited, as illustrated by the low La/Sm of Pre-SVC rhyolite, and should therefore not have affected the SVC melt either. In addition, crystallisation of 1% apatite, which is unlikely since the P content of most SVC plagioclase overlap the P content of Pre-SVC plagioclase, increases La/Sm by only 2. Pre SVC2 melt La/Sm ratios cannot be explained by mineral fractionation from Pre-SVC1 primitive melt either. Indeed, these melts overlap or are only slightly higher than Pre-SVC1 rhyolite melts, but the mafic nature of Pre-SVC2 precludes significant fractionation of accessory phases from Pre-SVC1 basalt. In addition the fractionation of assemblage “D” (described in Fig. 5.14), modelling successfully the Ba and Sr concentrations of Pre-SVC2, does not increase the La/Sm of the melt enough to reach Pre-SVC2 core values.

This confirms the conclusions obtained in Chapter 4 that crustal assimilation did produce an increase of La/Sm in the magmas, since the variations observed from Pre-SVC1 to Pre-SVC2 and SVC primitive melts cannot be due to fractional crystallisation. However, the primitive SVC melt (recharging melt) have some of the lowest melt La/Sm ratios of the SVC while the highest La/Sm ratios are found in the melts with the most evolved Ba and Sr compositions (and lower An content). This observation strongly suggests that the whole rock La/Sm variations within the SVC lava group itself is not due to variations in the recharge magma composition through time, but is instead due to a process linked with the differentiation of the SVC magmas during plagioclase phenocryst growth.

5.10.3 Sr and Ba variations in amphibole and pyroxene coexisting melt

Since the increase in plagioclase melt Ba and Sr concentrations and La/Sm ratio observed between Pre-SVC1 and SVC lavas seems to be caused by crustal assimilation, any mafic phases growing after the crustal assimilation event should have grown in a melt with similarly high concentrations and ratio, while concentrations similar to Pre-SVC1 lavas would indicate that the phases crystallised before assimilation. In order to constrain at which depth crustal assimilation could have occurred, we calculated the Ba and Sr content of the melt in equilibrium with the high Mg# hornblende (using the partition coefficients given in Table 5.2) for which barometric calculation indicated crystallisation in the middle to lower crust depth. We also calculated the melt Ba and Sr composition in equilibrium with Pre-SVC1 clinopyroxene, clinopyroxene microphenocrysts and orthopyroxene phenocrysts from the SVC, to verify if all SVC phenocrysts crystallised in the shallow chamber, like plagioclase. Unlike for plagioclase, no equations to remove the effect of the chemical control on the partition coefficient has been developed for pyroxene and amphibole, and calculated melts need to be interpreted with care.

5.10.3.1 Pre-SVC1

In the Pre-SVC1 basalt, clinopyroxene phenocryst core grew in a melt with ~180 ppm Sr and ~50 ppm Ba and the rim grew in a melt with ~160 ppm Sr and ~20 ppm Ba. Given the very low partition coefficient of Ba and Sr, the error on calculated melt composition can be important. However, the melt concentrations in Sr and Ba are very

different from that observed in the SVC, and are instead consistent with the melt compositions calculated from Sr and Ba plagioclase of Pre-SVC1 samples.

5.10.3.2 SVC

The high-Mg# hornblende microphenocryst analysed in the orthopyroxene bearing SVC2,3 dacite grew in a melt with ~420 ppm of Sr and ~890 ppm of Ba. Although the partition coefficients may be underestimated, this calculation indicates that the melt in which the high-pressure amphibole grew was already enriched in Ba and Sr compared to Pre-SVC magmas. This is consistent with their growth in the SVC recharge melt and constrains the minimum depth at which crustal assimilation occurred: in the middle crust.

On the other hand, a rare zoned high Mg# clinopyroxene microphenocryst found in SVC has a core that crystallised from a melt with ~290 ppm Sr and ~30 ppm Ba and a rim that crystallised in a melt with ~280 ppm Sr (measured barium beneath detection limit). Therefore, the melt Ba and Sr composition as well as the high Sr/Ba ratio are consistent with the melt composition estimated using Pre-SVC1 plagioclases and the microphenocryst must be a xenocryst from Pre-SVC1 units. The slightly higher Sr concentration of the calculated melt for that crystal than for Pre-SVC1 clinopyroxene is consistent with its higher Mg#.

Finally, the core, mantle and rim of a large orthopyroxene phenocryst in SVC1 grew in melts with very low Sr and Ba concentrations: ~10-70 ppm Sr and ~10-20 ppm Ba. These values are much lower than any melt composition calculated from the Pre-SVC and SVC crystals, even in the most differentiated lavas. The very low calculated concentrations may therefore be due to the inadequacy of partition coefficients to the SVC system. This is supported by the fact that a melt with such low Ba and Sr concentrations would be rhyolitic and crystallise orthopyroxene with very low Mg# which is inconsistent with the moderate Mg# of the crystal overlapping whole rock SVC Mg#. This suggests that the orthopyroxene is more likely to have crystallised in the same chamber as the SVC plagioclase phenocrysts which is consistent with the $\delta^{18}\text{O}$ composition of all orthopyroxene crystals analysed by Bezard et al., (2014) which were far above the mantle range. A striking observation in the orthopyroxene composition is the change in La/Sm ratio and Sr and Ba concentrations related to the

zoning of the crystal. Clearly, the core with the La/Sm ratio of ~ 2 is resorbed and followed by the growth of an enstatite-rich zone (having higher Mg#, higher Al and Ca contents) with low La/Sm ratio (~ 0.35) low Sr and Ba (Sr = 0.2 ppm, Ba = 0.09 ppm). The mantle is surrounded by an oscillatory-zoned rim with lower enstatite content, and higher La/Sm ratio Sr and Ba concentrations. Such a zoning pattern is similar to Type 5 plagioclase phenocrysts where the crystal cores are resorbed during a recharge event and starts convecting. However, the recharging magma is inferred to have high Ba and Sr concentrations from plagioclase-melt calculations, therefore an increase in such elements should correspond with the enstatite-rich pyroxene, which is not the case. The control of the variations in trace elements of the different zones is unlikely to be due to the chemical (major element) control on the partition coefficient since the zone with high enstatite displays similar to slightly higher Ca content compared to the core and the rim of the crystals, which should result in similar to slightly higher Ba and Sr concentrations in the crystal, unlike what observed. The only plausible interpretation of the low Ba and Sr and low L/M-HREE of the enstatite-rich zone is that it was competing with other phases for such elements during or slightly after the recharge event. It is likely that plagioclase fractionated very rapidly at the onset of the recharge event, which would significantly reduce the La/Sm ratio and Ba and Sr concentrations of the remaining magma.

5.11 Processes controlling $^{87}\text{Sr}/^{86}\text{Sr}$ and $\delta^{18}\text{O}$ mineral compositions

The Sr isotopic disequilibrium observed between and within crystals of each of the St Lucia lavas analysed indicates that magmas from all groups evolved in an open system (Fig. 5.11a, b, c, d). In the following sections, we discuss the isotopic differences observed within and between plagioclase from Pre-SVC1, Pre-SVC2 and SVC groups and their relationship with the plagioclase-melt trace element variations. We subsequently look into detail into the processes responsible for the isotopic heterogeneities observed within each group.

5.11.1 Process controlling $^{87}\text{Sr}/^{86}\text{Sr}$ variations between Pre-SVC1, Pre-SVC2 and SVC crystals

The significant increase in $^{87}\text{Sr}/^{86}\text{Sr}$ observed between crystals from the three lava groups (Fig. 5.11a) is consistent with that observed in the whole-rock compositions and is interpreted to reflect increasing extents of assimilation of sediment by the magmas (Bezard et al., 2014). Although some small variations exist, the $^{87}\text{Sr}/^{86}\text{Sr}$ ratios of plagioclase from within each group are similar, and intermediate isotopic compositions between groups are not observed. Given that plagioclase-melt trace element concentrations in both Pre-SVC2 and SVC lavas indicate the occurrence of recharge events, the absence of intermediate isotopic compositions between the three lava groups suggests that assimilation occurred deeper than the chamber in which plagioclase phenocrysts crystallised (i.e. in the chamber from where the recharging melt was derived). Indeed, if crustal assimilation and phenocryst fractionation occurred in the same chamber, it would have to be in a two-layer system, where magma was effectively assimilating wallrock in the deeper zone and recharging the more differentiated upper layer only before eruption. However, in this case, plagioclase fractionation would likely occur in both layers, due to their similar depth. And the plagioclase fractionated in the deeper layer of the chamber would likely record the assimilation event during growth and present some intermediate isotopic compositions between Pre-SVC1 and Pre-SVC2 or SVC. The mixing of the magma from the deep-zone with the differentiated magma of the upper zone of the chamber should subsequently transport these plagioclase with intermediate isotopic compositions in the erupted lavas, which is not observed. In addition, this layered magma chamber model is inconsistent with the presence in the SVC lavas of high pressure hornblende microphenocrysts that grew in a recharge magma already affected by crustal assimilation, as indicated by their trace elements compositions. Instead, crustal assimilation is likely to have occurred in a different chamber from the locus of phenocrysts fractionation, located in the lower-middle crust as indicated by the composition of the hornblende microphenocrysts. Such a scenario can much more easily explain the absence of plagioclase zones having recorded the assimilation event, either by crystal dissolution during ascent between the two reservoir, by absence of plagioclase crystallisation at high depth, or by segregation of the crystals in the first chamber. In addition, the similar $^{87}\text{Sr}/^{86}\text{Sr}$ ratios of all SVC crystals is consistent with

the relatively constant Ba and Sr composition observed in the recharging melt through the SVC lifetime which argues for similar processes generating the recharge melt.

Table 5.2. Partition coefficients used.

Mineral	Plagioclase	Orthopyroxene	Clinopyroxene	Hornblend
D Ba	calc.	0.011	0.0023	0.09
Source	Blundy and Wood (1991)	McKay and Weill (1977)	Green et al. (1989)	Gill (1981)
D Sr	calc.	0.018	0.067	0.4
Source	Blundy and Wood (1991)	McKay and Weill (1977)	Green et al. (1989)	Green and Pearson (1985)
D La	0.035	0.002	0.105	0.544
Source	Fujimaki et al. (1984)	McKenzie and O'Nions 1991	Fujimaki et al. (1984)	Fujimaki et al. (1984)
D Sm	0.013	0.05	0.477	1.804
Source	Fujimaki et al. (1984)	Arth (1976)	Fujimaki et al. (1984)	Fujimaki et al. (1984)

5.11.2 Process controlling crystal $^{87}\text{Sr}/^{86}\text{Sr}$ within Pre-SVC1, Pre-SVC2 and SVC groups

5.11.2.1 Pre-SVC1

Although the Pre-SVC1 basalt analysed has whole-rock isotopic signatures typical of oceanic arc lavas, some small $^{87}\text{Sr}/^{86}\text{Sr}$ variations are observed within and amongst crystals and between crystals and the groundmass (Fig. 5.11a, b). While the smaller phenocrysts (Fig. 5.12b) display a homogeneous $^{87}\text{Sr}/^{86}\text{Sr}$ from core to rim, the Sr isotopic composition of the largest phenocryst (Fig. 5.12a) decreases from the core to the zone just before the rim. Its outer rim displays an increase in $^{87}\text{Sr}/^{86}\text{Sr}$ toward the groundmass composition. The groundmass composition is similar to that of the core of the crystal. The inclusion-rich zone of the large crystal analysed has the lowest $^{87}\text{Sr}/^{86}\text{Sr}$ which is similar to the isotopic composition of the whole-rock and the smaller phenocryst. In the previous section we showed, using plagioclase-melt trace elements that this inclusion-rich zone crystallised in a more differentiated melt than the surrounding crystal zones. If the isotopic variations recorded by the crystals were produced by crustal assimilation during plagioclase fractionation, then the most differentiated melt should have the highest $^{87}\text{Sr}/^{86}\text{Sr}$ ratio, which is the opposite of what we observe. We therefore suggest that the small isotopic variations observed in the crystals result from mixing with a recharge magma that is slightly more radiogenic than the resident magma. The large phenocryst core grew in the recharge magma. Mixing of the slightly more radiogenic recharging melt with the magma in the chamber created a hybrid isotopic composition in some zones of the chamber, while other parts

of it remained unaffected where the smaller phenocrysts grew. Movement of the large phenocryst through the low $^{87}\text{Sr}/^{86}\text{Sr}$ and slightly more differentiated zones of the chamber produced the resorption of the crystal and growth of its inclusion-rich zones. A second recharge event with similar composition could have triggered the eruption of the lava since the groundmass has an intermediate $^{87}\text{Sr}/^{86}\text{Sr}$ ratio between the core and the mantle of the large phenocryst. The origin of the small isotopic variations between different batches of Pre-SVC1 magma might either be due to limited assimilation of sediment during the ascent of some of the magma batches toward a shallower reservoir, or to isotopic heterogeneities produced in the source of the magma. However, Bezard et al. (2014) showed that $\delta^{18}\text{O}$ of Pre-SVC1 plagioclase were slightly higher than the mantle range arguing for some small crustal interaction with the magma. We therefore suggest that crustal assimilation is responsible for the very small isotopic variations observed in the Pre-SVC1 crystals.

5.11.2.2 Pre-SVC2

In Pre-SVC2 plagioclase, Sr isotopic heterogeneities are greater than in Pre-SVC1 basalt crystals. The Type 2 phenocryst analysed (Fig. 5.12d) has a core (zone A) that is more radiogenic than its mantle (zones B and C) but less radiogenic than the outer rim of the crystal. The Type 1 phenocryst core (Fig. 5.12f) is also less radiogenic than the sodic outer-rim while the groundmass is more radiogenic than any other zone of the crystals. The increase in $^{87}\text{Sr}/^{86}\text{Sr}$, in the outer rim of the Type 1 and 2 crystals, toward more radiogenic composition without reaching the groundmass composition indicates the growth of the phenocrysts mantle-rim in a magma that was evolving in composition rather than the re-entrainment of cumulus plagioclase since the latter would be expected to have a rim with $^{87}\text{Sr}/^{86}\text{Sr}$ in equilibrium with the groundmass. Such an increase in $^{87}\text{Sr}/^{86}\text{Sr}$ in the crystal sodic rim and in the groundmass prior to eruption could either be linked with small assimilation of the walls of the magma chamber or by mixing with a more radiogenic recharge magma. However, the correlation between $^{87}\text{Sr}/^{86}\text{Sr}$ variations and resorption textures favours the second hypothesis. Indeed, the growth of the radiogenic sodic mantle-rim directly after resorption (clear in Type 1 crystals) indicates an absence of plagioclase growth between the resorption of the crystal and the growth of its radiogenic rim. In addition, high phenocryst contents of the Pre-SVC2 lavas (35-40%) implies an elevated

viscosity rendering assimilation very difficult to occur. We therefore suggest that the outer-rim increase in $^{87}\text{Sr}/^{86}\text{Sr}$ toward more radiogenic compositions occurred after a recharge event by slightly more radiogenic magma, during convection and hybridization of the magma. The Type 4 crystal (Fig. 5.12e), on the other hand, is much less radiogenic than the rest of the crystals. The difference in its isotopic composition compared to the rest of the samples is consistent with the xenocrystic origin deduced from textural and major and trace element evidences. The similar signature obtained from the two groundmass samples indicates isotopic equilibrium of the groundmass at the centimetre scale.

5.11.2.3 SVC

5.11.2.3.1 SVC1

The isotopic compositions of the SVC1 groundmasses are almost identical to their respective whole rock values (Fig. 5.11d) which indicates that most phenocrysts must have a similar isotopic composition to the groundmass and that therefore, no significant change in isotopic composition occurred between the beginning of plagioclase fractionation and eruption. However, subtle changes were recorded in the crystals that correspond to specific textural features. First, resorbed anorthite-rich cores from both Type 1 and 2 plagioclase (Fig. 5.12g, h) tend to be more radiogenic than the anorthite-poor plagioclase that crystallised straight after resorption, even when the groundmass is more radiogenic than the crystal. Second, the outer mantle-rim with low-anorthite content and wavy oscillatory texture displays an increase or a decrease in $^{87}\text{Sr}/^{86}\text{Sr}$ toward the groundmass composition (similar to Pre-SVC2 crystals). We therefore suggest that these two observations can be explained if the anorthite-rich crystal cores were introduced by a recharge event and became partially resorbed in the more differentiated/cooler resident magma, which was of slightly different isotopic composition. The recharge event would have progressively changed the magma chamber composition and produced convection responsible for the wavy oscillatory texture of the crystals recording the progressive change in isotopic composition of the magma. This is consistent with the plagioclase-melt Ba and Sr compositions which indicate crystallisation of the anorthite-rich cores in a more primitive melt (higher Ba and Sr) than the oscillatory zones.

5.11.2.3.2 SVC2,3

The amplitude of the small isotopic variations observed in SVC1 are exacerbated in SVC2,3. The cummingtonite-bearing sample seems to have recorded the same process as in SVC1 but resulting in different textures. Whether the core of the phenocryst is uniform and sodic (Type 6; Fig. 5.12j) or has a more complicated texture (Type 2; Fig. 5.12l), the last main resorption texture/surface is followed by a zone with wavy oscillatory zoning having $^{87}\text{Sr}/^{86}\text{Sr}$ displaced toward the groundmass composition. The resorption texture is either a resorption surface with limited small inclusions, or a “flame” texture. Similar to SVC1, such textures indicate that, the isotopic variations in the crystals were produced by the arrival of a recharge magma of only slightly different composition to that resident in the SVC magma chamber. The recharge event produced the resorption of the existing sodic phenocryst followed by either limited growth of an anorthite-rich plagioclase and an oscillatory zoned mantle-rim due to convection during crystallisation or simply an oscillatory-zoned mantle-rim. Such an interpretation is supported by the isotopic composition of the Type 2 microphenocryst (Fig. 5.12k) which is more radiogenic than the groundmass. Indeed, the high calculated Ba and Sr concentrations in the melt in equilibrium with this crystal, as well as the very small size of the crystal indicate that it crystallised from the last recharge magma of the SVC chamber before eruption. Its mixing with the less radiogenic resident magma in which the core of Type 6 and Type 2 phenocryst crystals grew (Fig. 5.11), would produce a magma with hybrid isotopic composition between the two, which is what is recorded in the $^{87}\text{Sr}/^{86}\text{Sr}$ ratio of the rim of the Type 6 and Type 2 crystals.

In the orthopyroxene-bearing sample, partial resorption of the sodic core of the Type 5 crystal (Fig. 5.12m, n) and the subsequent growth of anorthite-rich plagioclase with a less radiogenic composition, is consistent with recharge by a less radiogenic magma, similar to the groundmass. However, although the growth of anorthite-rich plagioclase is followed by a mantle/rim with oscillatory texture, (as in SVC1 and in cummingtonite-bearing SVC2,3), the $^{87}\text{Sr}/^{86}\text{Sr}$ of the rim does not decrease toward the lower $^{87}\text{Sr}/^{86}\text{Sr}$ ratio of the groundmass (Fig. 5.12m, n). This observation suggests that the mantle-rim of the crystals did not grow in a melt affected by the recharge event that transported the crystals to the surface. We suggest that, like Pre-SVC2 and other SVC crystals, the phenocrysts of the orthopyroxene-bearing sample also recorded a

recharge event, but that the recharge melt did not efficiently mix in the chamber. The recharge event, of lower isotopic composition than the crystals, produced resorption of the sodic phenocrysts and the crystallisation of anorthite-rich crystal in a hybrid melt before convection transferred the crystal into an isotopically different zone of the chamber. We infer that this zone had not at the time been influenced by the recharge event, and yielded the slightly different isotopic composition to the wavy oscillatory-zoned mantle-rim. We suggest that there was insufficient time to homogenise the whole chamber after the mixing with the recharging melt. The crystals were then brought to the surface in a magma influenced by the same or a second recharge event of similar isotopic composition to the first.

5.11.2.3.3 Summary

As inferred for Pre-SVC2, assimilation occurred early and before phenocryst fractionation in the SVC plumbing system. Small isotopic heterogeneities recorded in the crystals reflect hybridisation of the magma in the shallow chamber by different recharge events, each of them having slightly different $^{87}\text{Sr}/^{86}\text{Sr}$ ratios. During each recharge event, phenocryst or microphenocryst cores that crystallised in the recharge magma, prior to the mixing event, were resorbed and subsequently entrained into chamber-wide convection movements in the new hybrid magma with the corresponding new isotopic composition (zones with wavy-oscillatory textures). Phenocrysts present in the magma chamber (sodic) prior to recharge were also partially resorbed, sometimes followed by growth of anorthite-rich plagioclase with a flame texture before starting convecting vigorously while growing (oscillatory texture) in the hybrid melt.

5.11.3 Processes controlling SVC mineral $\delta^{18}\text{O}$

Like for in-situ $^{87}\text{Sr}/^{86}\text{Sr}$, although some variation exists (Fig. 5.13), the mean zircon $\delta^{18}\text{O}$ of lavas from each eruption period of the SVC is similar (Period 1: $\delta^{18}\text{O} = +8.4$ ‰; Period 2: $\delta^{18}\text{O} = +8.0$ ‰; Period 3: $\delta^{18}\text{O} = +8.2$ ‰). The mean $\delta^{18}\text{O}$ is also independent of the mineralogy since similar for both orthopyroxene- and cummingtonite-bearing SVC2,3 lavas (orthopyroxene-bearing SVC2,3: $\delta^{18}\text{O} = +8.1$ ‰; cummingtonite-bearing SVC2,3: $\delta^{18}\text{O} = +8.0$ ‰). Finally, zircons from plutonic

enclaves found in SVC3 lavas have compositions overlapping those from the lavas (Fig. 5.13a; mean $\delta^{18}\text{O} = 8.2\text{‰}$). The very similar mean $\delta^{18}\text{O}$ observed in the zircons through time suggests a relatively constant isotopic composition of the magma through the SVC lifespan. However, as highlighted by Schmitt et al. (2010), the SVC zircons have long residence times whereby cores are typically 100-300 kyr older than the rim. Therefore, zircon could have undergone isotopic equilibration. In this case, the homogeneous mean $\delta^{18}\text{O}$ could be due to volume diffusion of O in the zircon through time, which would have homogenised potential extreme (low or high) signatures.

Both experiments and natural systems show that diffusion rates increase with $P_{\text{H}_2\text{O}}$ (Watson and Cherniak, 1997 and Zheng and Fu, 1998). However, the rate of diffusion in zircon at a given temperature is still controversial (Valley et al., 2003) and experimentally determined oxygen diffusion rates are higher than those estimated from natural samples. To estimate whether SVC zircons could have experienced diffusive equilibration, we determined the maximum zircon surface affected by diffusion using the fastest experimentally determined diffusion rates (Zheng and Fu, 1998). The calculations suggest that, at 900°C , diffusion should only have affected $187\text{ }\mu\text{m}^2$ after 600 kyr. Given that the SVC zircon size is typically around $6000\text{ }\mu\text{m}^2$ and that 900°C is an overestimation of the magmatic temperature, diffusion should not have affected more than 30% of the crystal. Therefore, the homogeneous mean signature recorded by the zircons should not be due to diffusion, but instead reflect the absence of major fluctuations in isotopic composition of the magma through time. The high $\delta^{18}\text{O}$ of the SVC zircon is in agreement with the $\delta^{18}\text{O}$ values obtained by Bezard et al. (2014) in other minerals of the lavas which indicate a large amount of crustal assimilation of metasediment during magma differentiation. It is also consistent with the high $^{87}\text{Sr}/^{86}\text{Sr}$ ratios of the SVC plagioclase. Given that both textures, trace elements and $^{87}\text{Sr}/^{86}\text{Sr}$ composition of the plagioclase phenocrysts suggest that the SVC chamber was affected by recharge events, the relatively high isotopic signature of all the SVC zircons needs to be explained by the recharge magma having previously experienced crustal assimilation. This suggests that crustal assimilation occurred in a deeper reservoir than the locus of phenocrysts growth and is consistent with both plagioclase trace element and $^{87}\text{Sr}/^{86}\text{Sr}$. Finally, the $\delta^{18}\text{O}$ variations amongst zircons, consistent with the small $^{87}\text{Sr}/^{86}\text{Sr}$ variations observed within and amongst plagioclase

crystals from the SVC, suggests a slightly distinct signature of the different recharge events affecting the shallow chamber.

5.12 Magmatic evolution of Pre-SVC and SVC

A schematic model for the magmatic evolution of Pre-SVC1,2 and SVC lavas is illustrated in Fig. 5.15.

5.12.1 Pre-SVC1 lavas

Pre-SVC1 basalts were last stored in the magma chamber where all plagioclase crystallisation occurred. Since the Pre-SVC1 basalt is not primitive, the absence of olivine or pyroxene fractionation recorded in the core-to-rim plagioclase-melt compositions indicates that the fractionation of such phases occurred before plagioclase, probably in a deeper magma chamber. In the shallow chamber, both textural, trace element and $^{87}\text{Sr}/^{86}\text{Sr}$ evidence suggests that crystals were exposed to changing conditions, in a slightly heterogeneous magma chamber. Heterogeneities are likely to have been produced by mixing of different batches of magma, variably affected by small amounts of assimilation.

The Pre-SVC1 rhyolite does not display any textural or chemical indication of open-system processes. Trace element composition of plagioclase-melts indicate that the rhyolite could have been generated by significant fractionation of plagioclase from a Pre-SVC1 basalt. The resultant melt was subsequently stored in a relatively homogeneous magma chamber during which sodic plagioclase crystallised.

We suggest that the limited impact of crustal assimilation on the Pre-SVC1 lavas, which are mainly mafic, might be due to the ascent of small volumes of magma reaching the surface rapidly using pre-existing crustal weak zones (Fig. 5.15). This would be consistent with the spread of Pre-SVC1 activity across the island.

5.12.2 Pre-SVC2

The crystal textures and compositions in the Pre-SVC2 lavas indicate their growth in a magma chamber undergoing frequent recharge by more primitive magma. The absence of evidence for progressive assimilation in the plagioclase phenocrysts argues

that crustal assimilation occurred in a deeper chamber, where the recharge magmas were produced. Small isotopic and chemical variations in the crystals corroborate textural evidence for recharge events. However, because the crystal heterogeneities are limited, we infer that all of recharge magmas had undergone similar amounts of assimilation. This indicates a process capable of buffering the amount of assimilation before ascent toward the shallow chamber.

During ascent toward the shallow magma chamber, anorthite-rich plagioclase crystals crystallised in the recharge magma. These were subsequently partially resorbed during the mixing between the recharge magma and the more differentiated magma resident in the shallow chamber. Sodic plagioclase present in the magma chamber prior to recharge suffered from partial resorption sometimes followed by a small anorthite-rich zone when growth following resorption occurred close to the recharge locus of the chamber. The recharge event resulted in increased convection in the cool chamber, and all crystals grew a mantle-rim with wavy oscillatory texture in equilibrium with the hybrid and heterogeneous magma.

Unlike Pre-SVC1 magmas, we suggest that Pre-SVC2 magmas were stored in the middle crust in contact with metasedimentary wall-rocks prior to ascending to a shallow reservoir where phenocryst fractionation occurred. Such additional storage in the middle crust, could be due to the absence of pre-existing structures to promote a fast ascent to the surface and to a more significant volume of magma preventing the magma from freezing, and allowing it to reach the surface. Given that all Pre-SVC2 lavas are located in the same area in the south of the island, local conditions of the crust might be responsible for halting the magma in the middle crust. We suggest that the mafic to intermediate nature of the Pre-SVC2 lavas and their lower extents of assimilation (lower $^{87}\text{Sr}/^{86}\text{Sr}$, and lower Sr and Ba in plagioclase-melt) reflect a shorter residence time in the middle crust than the SVC magmas.

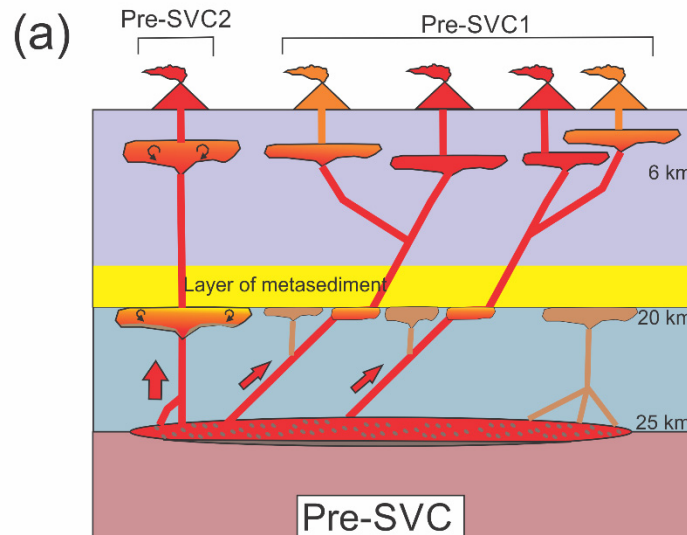


Fig. 5.15. Schematic petrogenetic model for St Lucia lavas (not to scale). (a) Model for evolution of Pre-SVC1 and Pre-SVC2 lavas. Pre-SVC1 lavas fractionated pyroxene and olivine in a storage at the base of the crust, ascended through pre-existing weakness zones of the crust, escaped major assimilation, and were stored in a shallow chamber close to water saturation depth where plagioclase phenocrysts crystallised. Pre-SVC2 lavas probably fractionated pyroxene and olivine at the base of the crust, but were subsequently stored in the middle crust at the interface between a metasedimentary layer and lower crust. Crustal assimilation occurred at such depth and the resulting magma then ascended toward the shallow chamber where the lava phenocrysts crystallisation occurred. Although Pre-SVC2 lavas are more mafic (basaltic-andesite to andesite) than in the SVC (high-silica andesite-dacite), processes occurring during crystal fractionation in the shallow chamber are similar to the SVC. (b) In the SVC, like Pre-SVC2 lavas, magma probably started crystallising in a storage at the base of the crust, and then ascended to the middle crust interface between the metasediment layer and the mafic crust. High flux of mafic magma from the chamber at base of the crust allowed the elevation of the local geotherm and the development of a large magma chamber. In this chamber crustal assimilation of the metasediment was important and accompanied by fractionation. The resulting magma was andesitic, had high amounts of water and ascended toward a shallow reservoir. During the ascent, existing crystals or xenocrysts were dissolved due to the overheating of the magma, but hornblende microphenocrysts crystallised, followed by crystallisation of anorthite-rich plagioclase due to depression and decrease in water solubility. Recharging magma arrival at shallow depth, close to water saturation, caused more anorthite-rich plagioclase crystallisation. At such depth the recharging magma started mixing with the magma in a shallow chamber. During the mixing, both crystals in equilibrium with the recharging melt (anorthite-rich) and with the cool and differentiated magma (sodic) were affected by partial resorption. In the sodic crystals, partial resorption can be followed by a short growth of anorthite rich plagioclase. All crystals are then entrained into the convection produced by the recharge event, during which the mantle-rim of the crystals grew a wavy oscillatory zoned rim. Mixing is thought to have triggered eruption.

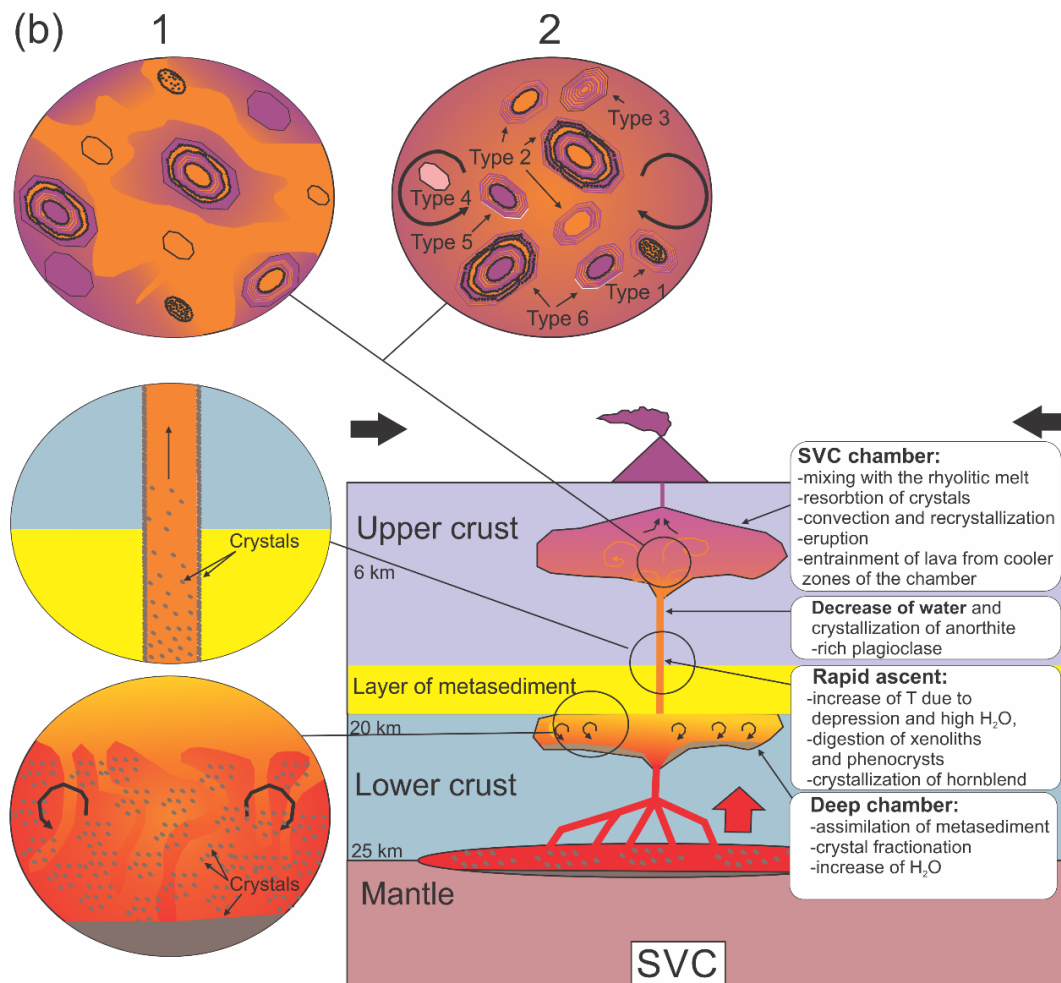


Fig. 5.15. (continued).

5.12.3 SVC

5.12.3.1 Decoupling of crustal assimilation and phenocryst crystallisation

The decoupling of crustal assimilation and phenocryst crystallisation in the SVC magmas (two different magma chambers) is supported by (1) the absence of intermediate $^{87}\text{Sr}/^{86}\text{Sr}$ isotopic compositions between Pre-SVC1 and SVC plagioclase, which indicates that assimilation did not occur during plagioclase growth, nor in a different layer of a same chamber; (2) the absence of mantle-like $\delta^{18}\text{O}$ in zircons from SVC1,2,3 lavas which indicates that assimilation did not occur during zircon crystallisation over the last 600 ka; and (3) the growth of the high-pressure hornblende from a melt with similar Ba and Sr composition to the SVC plagioclase. The latter also having very radiogenic $^{87}\text{Sr}/^{86}\text{Sr}$ ratios which suggests that the recharge magma had already experienced crustal assimilation. We therefore suggest that assimilation

occurred in a deeper chamber than the chamber where phenocryst crystallisation occurred.

5.12.3.2 Conditions and processes in the deep chamber

The absence of metasedimentary xenoliths or antecrystals from the deep chamber in the lavas renders difficult the constraint of the conditions during crustal assimilation in any detail. One clue comes from the composition of the crystals that grew within the recharge magma(s). High Mg# hornblende microphenocrysts found in SVC2,3 lavas indicate a mid- to lower- crustal depth and a magmatic temperature of around 1000°C of the recharge magma. Hornblende major element composition (High Mg^{##}, low Cr₂O₃ and NiO) indicates an andesitic rather than basaltic nature of the recharge magma. This is supported by the absence of enclaves with quench textures in the SVC lavas, the latter usually occurring during mixing of two magmas with large temperature contrasts. It is also consistent with the large amounts of assimilation required by the mineral ⁸⁷Sr/⁸⁶Sr and $\delta^{18}\text{O}$ ratios which are hard to conceive without a magma change toward more felsic compositions. Indeed, both assimilation by latent heat of crystallisation and assimilation by melting of the metasediment by sensible heat, would produce an increase in SiO₂, either by important fractionation or by mixing with a felsic melt. Bezard et al. (2014) show that all St Lucia whole rock trace element and isotope compositions back project toward the Pre-SVC1 basalt compositions. We therefore suggest that the middle-crust magma chamber was recharged by a more primitive magma similar to Pre-SVC1 basalt that subsequently became modified by crustal assimilation. The basaltic nature of the recharge melt is necessary to supply the heat source needed for the development of a long-lived (here at least 600 kyr) magma chamber in the middle to lower crust (Annen and Sparks, 2002). Crustal assimilation increased the Ba, Sr, La/Sm, ⁸⁷Sr/⁸⁶Sr and $\delta^{18}\text{O}$ of the magma. The latter also had high oxygen fugacity (NNO+1.4 to +1.5) and was very hydrous with H₂O = 7.6-8 wt. %, as indicated by the composition of the high Mg# hornblende microphenocrysts. Given that average H₂O contents of arc basalts are around 4 wt. % (Plank et al., 2013), the high water content of the inferred magma needs to be produced either by significant crystal fractionation, or by assimilation of water-rich material. The high water content of the magma might have facilitated the ascent of the magma toward the surface (Annen et al., 2006) and caused the dissolution of crystal or xenoliths present in the

magma during ascent due to overheating. Hornblende microphenocrysts and anorthite-rich plagioclase crystallised in the water-rich magma during ascent to the shallow chamber. Small isotopic variations between batches of magma recorded in zircon ($\delta^{18}\text{O}$) and plagioclase ($^{87}\text{Sr}/^{86}\text{Sr}$) compositions of the SVC argue for slight variations in the amount of assimilation or in the composition of the assimilant throughout SVC time. However, in general, isotopic composition of all SVC plagioclases ($^{87}\text{Sr}/^{86}\text{Sr}$) and zircons ($\delta^{18}\text{O}$) are similar which indicates that magma extraction from the deep reservoir is always triggered after a similar amount of assimilation. The process of assimilation remains hard to constrain. The hot zone model proposed by Annen et al. (2006) could be considered. It hypothesises that magmas intruding as sills at the interface between igneous crust and metasedimentary-rich upper crust (1) partially crystallise leaving a residual andesitic melt enriched in H_2O ; and (2) lead to partial melting of surrounding country rocks (in our case inferred to be metasediments). The constant isotopic signature observed in the SVC over the last 600 kyr could then be explained by a low rate of magma intrusion into the hot zone, since it can lead to an almost constant ratio of residual melt/partial melt through time (Annen et al., 2006). In this case, the phases fractionated during differentiation of the magma would primarily be pyroxene since lava Dy/Dy^* and Dy/Yb relationships preclude any amphibole or garnet fractionation (see Chapter 4).

However, the textures and in-situ $^{87}\text{Sr}/^{86}\text{Sr}$ data indicate that crustal assimilation occurred via a similar process in both SVC and Pre-SVC2 lavas and, unlike in the SVC, lavas as mafic as basaltic andesites are found in the Pre-SVC2 group which indicates that assimilation is not necessarily coupled with silicic magma production. Because the coupling of the two latter processes are necessary in the hot zone model, the model cannot account for Pre-SVC2 lavas, and another process of crust assimilation needs to be considered. The $^{87}\text{Sr}/^{86}\text{Sr}$ ratios of the SVC and Pre-SVC2 whole-rocks form a positive correlation against SiO_2 which indicates that the extent of crustal assimilation is either proportional to crystal fractionation or that it is proportional to the amount of incorporation of felsic metasediment. The incorporation of metasediment, without drastic differentiation (production of silicic magma), can be done by bulk melting if the temperature of the magma is $>1000^\circ\text{C}$. At lower temperature, metasediment incorporation could have occurred by dehydration-melting as proposed by Beard et al. (2005). In their model, amphibole and/or biotite + quartz

+ plagioclase from a metasediment reacts with the magma to produce orthopyroxene and/or clinopyroxene + calcic plagioclase + oxides + hydrous melt. Such a process allows a high rate of assimilation/crystal fractionation since it consumes less energy than melting the metasediment and could very well explain the mafic to andesitic nature of Pre-SVC2 lavas. It could also be viable to explain the SVC lavas, as the SiO_2 of the lava could be proportional to the amount of crust incorporated. If assimilation of metasediment liberated a lot of water in the chamber, the latter could have been controlling the periodicity of ascent of the magma to the upper chamber. Because the amount of water would be proportional to the amount of metasediment assimilated, a constant rate of assimilation/magma could then be achieved.

5.12.3.3 Conditions and processes in the shallow chamber

5.12.3.3.1 Same magma chamber for all SVC lavas

The similar $\delta^{18}\text{O}$, $^{87}\text{Sr}/^{86}\text{Sr}$ and trace element compositions of the SVC phenocrysts suggests that all SVC lavas crystallised in the same shallow magmatic chamber, which supports the interpretation of Schmitt et al. (2010) based on correlations between growth pulses of zircons from different eruption ages.

5.12.3.3.2 Depth and temperature of shallow storage

Based on published cummingtonite stability conditions (2-3 kbar and 800-850°C) and thermobarometric calculations on the low-Mg# hornblende microphenocrysts present in the orthopyroxene-bearing SVC2,3 lavas (814-844°C and 1.14-2.12 kbar), we suggest that the shallow SVC chamber is located at less than 10 km depth. Temperature is heterogeneous in the chamber and varies from less than 800°C in the cummingtonite-bearing part of the chamber to 800-840°C in the orthopyroxene-bearing part of the chamber before and during eruption of SVC2,3 lavas. Although no thermobarometric estimations exist for the shallow storage conditions of SVC1 lava, the absence of biotite in the lavas indicates slightly higher temperatures than for SVC2,3 magma. The change in mineralogy observed from SVC1 to SVC2,3 lavas indicate that the magma chamber is progressively cooling since the onset of the SVC.

5.12.3.3.3 Recharge and mineral fractionation

Textures of all types of plagioclase crystals except Type 4 were produced as a result of mixing of a more primitive magma in a shallow chamber during recharge events. The more primitive nature of the recharge magma is indicated by its higher Ba and Sr concentrations and higher Sr/Ba ratio. Before reaching the shallow chamber, anorthite-rich plagioclase (Type 1 and 2 cores) and hornblende microphenocrysts crystallised in the recharging magma. The stalling of the magma at shallow depths might be due to an increase of viscosity in response to plagioclase fractionation close to or at the water saturated liquidus (~6 km depth). Fractionation produced a rhyolitic groundmass, even in the SVC1 andesites. During the recharge events, mixing of the primitive magma in the more differentiated chamber led to partial resorption of its anorthite-rich crystals (Type 1, 2 cores) due to the differences in composition, temperature and volatile content of the magma. The difference in temperature and in water content between the recharging magma and the shallow chamber was recorded by the composition of the high and low Mg# amphiboles, respectively. The injection of the more primitive and hotter magma into the shallow chamber also led the partial resorption of the resident sodic plagioclase (Type 5 and 6 cores), and sometimes orthopyroxene and biotite crystals in equilibrium with the more differentiated magma. When the sodic crystals were in contact with the recharge magma, the resorption texture was followed by crystallisation of anorthite-rich plagioclase with trace element and isotopic compositions similar to the recharge melt (Type 5). Recharge events triggered chamber-wide convection and heterogeneities in the magma chamber. Chamber wide convection in the heterogeneous chamber is responsible for the wavy oscillatory zoning observed in all plagioclase mantle-rims grown (Types 1, 2, 3, 5, 6) after the partial resorption of both the anorthite-rich and the sodic crystals (or after the anorthite-rich overgrowth following sodic core resorption if observed). Orthopyroxene that grew after partial resorption consists of a more enstatite-rich zone followed by an oscillatory rim, similarly to plagioclase. In cummingtonite-bearing lavas, very limited anorthite-rich zones grew after partial resorption of sodic crystal cores, and the occurrence of large crystals of unresorbed cummingtonite suggest that the magma was not in the “hot part” of the magma chamber where the recharging magma is injected. This is consistent with the lower Ba and Sr of the melt in which sodic plagioclase from these samples crystallised compared to other SVC lavas.

Indeed, such compositions indicate a very differentiated melt, which did not experience much mixing with more primitive magma. In addition, the extrusion of the cumingtonite-bearing lavas at the end of SVC2 and SVC3 eruption periods suggest that such lavas may have come from a cooler zone of the magma chamber forced to erupt by physical entrainment following the eruption of large amounts of magma. The presence of a large number of plutonic enclaves in the SVC lavas, with similar mineralogy and with zircons sharing similar growth age and $\delta^{18}\text{O}$ to the lavas, indicate that these are subsolidus equivalents of the SVC magma. Therefore, parts of the magma chamber were even cooler than the cumingtonite-bearing lavas.

5.12.3.3.4 Process triggering eruption

Recharge events seem to have closely preceded the eruption of the lavas, it is particularly obvious in the cumingtonite-bearing lavas where a sodic rim of less than 50 μm surrounds a microphenocryst in equilibrium with the recharge melt. We therefore suggest that recharge events triggered all SVC eruptions by reactivating the cool and differentiated shallow magma chamber. The period of incubation between the onset of the recharge events and eruption seems to be much longer than in the case where mafic magma mix with a rhyolitic melt. Indeed, in the latter case, narrow rims of less than 50 μm typically grow between the resorption texture and eruption (e.g. Kent et al., 2010), whereas in the SVC crystals, although a few crystals show a narrow rim, a wavy oscillatory-zoned rim of up to 200-300 μm in width can be observed. This may be the consequence of the more differentiated and cooler nature of the recharge melt compared to a mafic magma. Such a difference in the recharging melt characteristics will lead to less efficient reactivation of the cool and viscous shallow chamber, but still lead to eruption. The time lag between the beginning of recharge events and eruption could have become progressively longer from SVC1 to SVC3 because of the more differentiated and cooler state of the shallow chamber. This would be in agreement with the fact that the growth of zircon rims during or just before the two last eruption periods (SVC2, 3) is scarcer than for SVC1 period during which the growth of zircon rims preceding volcanism by up to 10-20 kyr (Schmitt et al., 2010). Indeed, zircon growth is inhibited above 800°C and important recharge events (~1000°C according to hornblende thermometry) probably increase the temperature of the magma chamber to slightly greater than 800°C. Therefore, in SVC1, since the

zircons grew until close to the time of eruption, the time between recharge and eruption was very short while in SVC2,3, the cessation of growth 10-20 kyr before eruption indicate a long time gap between the first recharge and eruption. Eruption of the cummingtonite-bearing lavas at the end of SVC2 and SVC3 periods is also linked with the recharge event, and resorption textures as well as the wavy oscillatory textures which attest to convection of the crystals in a hybrid melt before eruption, indicate the impact of the mixing with recharge melt. However, their lower temperature indicates that they were more likely to be erupted by entrainment following the eruption of the orthopyroxene-bearing lavas.

5.12.3.3.5 Focussing of the activity

The SVC lavas erupted only in the south-west of the island, and no other volcanic centre was simultaneously active (Lindsay et al., 2013). The transition between the spread of the activity to the focussed magmatism in the south western part of the island is clearly linked with the transition between mainly mafic eruptive products to the development of the SVC silicic complex. The large amounts of magma erupted and the constant crustal assimilation rate through 600 ka indicate a long-lived plumbing system and we suggest that the development of the SVC was possible due to a significant and regular input of magma from the mantle. Indeed, as highlighted by Annen et al. (2006), the development of a magma chamber in the middle or lower crust requires a regular input of magma to increase the local temperature enough to avoid the freezing of the magma.

The presence of a metasedimentary layer in the middle to lower crust is probably another major factor in the development of the complex, since it would produce a major rheological interface, similar to a transition between lower and upper crust in continental arcs, affecting the ascent of the magma. In such context, if no pre-existing weakness zones (e.g. faults) are present to facilitate the ascent of mafic magma to the surface, magmas would tend to accumulate at this boundary, producing increasing heat, development of a magma chamber, differentiation and assimilation of the wall rocks.

5.12.4 Implications for development and evolution of silicic complexes in mature arcs

This study indicates that the development of a silicic complex in St Lucia results from a combination of processes rather than a single one as suggested by Annen et al. (2006). The need for the production of andesitic magma in the arc middle-lower crust instead of in a shallow reservoir was highlighted by Annen et al. (2006) for several localities such as Mount Mazama in the Cascades. The assimilation of sialic material in the genesis of the andesitic magma at depth is observed for several continental arcs (e.g. Hildreth and Moorbath, 1988) but has never been shown to occur in oceanic arcs before. The crystallisation of all the phenocrysts present in the lavas, dominated by plagioclase, close to and in the shallow magma chamber at around 200 MPa supports the decoupling of silicic magma production from the lava phenocryst crystallisation as suggested by Annen et al. (2006). The very similar amounts of assimilation by all recharging magma batches before magma extraction toward the shallow chamber suggests that the factor triggering the ascent may be intrinsic to the assimilant composition. The occurrence of lower amounts of assimilation on some basaltic andesite from Pre-SVC2 indicate that the production of silicic magma in the deep crust is not necessary to result in crust assimilation, but instead that the development of silicic magma may be partly due to increasing assimilation. Although mixing has long been recognised to occur in andesitic and dacitic magma bodies and to be responsible for the different crystal populations and textures observed in such rock, most cases involve mixing of basalt and basaltic andesites with rhyolite (Kent et al., 2000) and mixing between andesitic and rhyolitic magma is less common. Finally, the SVC lavas have major, trace element and isotopic composition very similar to the upper and middle continental crust (see Chapter 4). This suggests that the processes involved in the production of silicic magmas in mature oceanic arcs such as the Lesser Antilles may be viable to generate new silicic continental crust.

5.13 Conclusions

The integration of petrographic observations, mineral major and trace elements, plagioclase in situ $^{87}\text{Sr}/^{86}\text{Sr}$ and zircon in situ $\delta^{18}\text{O}$ in lavas erupted before and during the existence of the Soufriere volcanic complex in St Lucia indicate the production of silicic lavas occurred in an open system comprising at least two magma chambers. The difference in isotopic and trace element composition between the SVC and the older and more mafic Pre-SVC1 lavas result from their storage in the middle-lower crust in contact with a metasedimentary layer. Crustal assimilation and crystal fractionation occurred to produce andesitic magma with high water content and oxygen fugacity and a similar composition over the silicic complex existence. The andesitic magmas were then transferred to a shallow chamber where, except for a few crystals that crystallised during the ascent, the phenocrysts observed in the lavas crystallised. The mixing of the recharging andesite with the cooler and more differentiated magma of the shallow chamber is responsible for all the major resorption textures observed in the phenocrysts. It is also thought to have triggered the SVC silicic eruptions.

Chapter 6

Lower crustal assimilation in oceanic arcs: insights from an osmium isotopic study of the Lesser Antilles

A version of this chapter has been submitted to *Geochimica et Cosmochimica Acta* co-authored by Bruce Schaefer, Simon Turner, Jon Davidson and David Selby.

The supplementary data file of this chapter is presented in Appendix E.

Abstract

We present whole rock $^{187}\text{Os}/^{188}\text{Os}$ data for the most mafic lavas along the Lesser Antilles arc ($\text{MgO} = 5\text{-}17$ wt. %) and for the subducting basalt and sediments. $^{187}\text{Os}/^{188}\text{Os}$ ratios vary from 0.127-0.202 in the arc lavas. Inverse correlations between $^{187}\text{Os}/^{188}\text{Os}$ and Os concentrations and between $^{187}\text{Os}/^{188}\text{Os}$ and indices of differentiation such as MgO suggests that assimilation, rather than source variation, is responsible for the range of Os isotopic variation observed. $^{87}\text{Sr}/^{86}\text{Sr}$, La/Sm and Sr/Th are also modified by assimilation since they all correlate with $^{187}\text{Os}/^{188}\text{Os}$. The assimilant is inferred to have a MORB-like $^{87}\text{Sr}/^{86}\text{Sr}$ with high Sr (>700), low L/M-HREE ($\text{La}/\text{Sm} < 1.6$; $\text{La}/\text{Yb} < 1.7$) and $^{187}\text{Os}/^{188}\text{Os} > 0.2$. Such compositional features are likely to correspond to an early-arc plagioclase rich cumulate. Given that assimilation affects lavas that were last stored at more than 5 kbar, assimilation must occur in the middle-lower crust.

Only a high MgO picrite from Grenada escaped assimilation ($\text{MgO} = 17\%$ wt. %) and could reflect mantle source composition. It has a very radiogenic $^{87}\text{Sr}/^{86}\text{Sr}$ (0.705) but a $^{187}\text{Os}/^{188}\text{Os}$ ratio that overlaps the mantle range (0.127). $^{187}\text{Os}/^{188}\text{Os}$ and $^{87}\text{Sr}/^{88}\text{Sr}$ ratios of the sediments and an altered basalt from the subducting slab vary from 0.18-3.52 and 0.708-0.714. We therefore suggest that, unlike Sr, no Os from the slab was transferred to the parental magmas. Os may be either retained in the mantle wedge or even returned to the deep mantle in the subducting slab.

6.1 Introduction

Understanding the behaviour of siderophile elements such as Os in subduction zones is important for both scientific and economic reasons. Whether Os stays in the subducting slab, is transferred to residual phases of the upper mantle, or is recycled back to the crust via the magma needs to be constrained in order to (1) better estimate the crust-mantle fluxes of siderophile elements throughout Earth evolution; (2) constrain its application as a powerful isotope tracer to understand subduction processes; and (3) understand the formation of precious metal ore-bodies.

In this context, the origin of radiogenic $^{187}\text{Os}/^{188}\text{Os}$ ratios within arc lavas, compared to the depleted upper mantle (DMM), has been debated for more than a decade (Borg et al., 2000; Alves et al., 2002; Chesley et al., 2002; Richter et al., 2002). While the enrichment in radiogenic Os could be due to contamination of the mantle wedge by slab derived fluids/melts (e.g. Borg et al., 2000; Alves et al., 2002), it could also be caused by assimilation of arc crust during the magma ascent (Richter et al., 2002), or both (Suzuki et al., 2011). Arguments for crustal assimilation include (1) a negative correlation between $^{187}\text{Os}/^{188}\text{Os}$ and Os that is observed in most arcs lavas (Chesley et al., 2002; Richter et al., 2002); (2) experimental evidence (Xiong and Wood, 1999; 2000) coupled with observed low Re content of primitive arc basalts that suggest that Os is very unlikely to be transported in the mantle wedge since slab derived-fluids capable of carrying Os would carry several order of magnitude more Re than Os (Richter et al., 2002); and (3) the very unradiogenic $^{187}\text{Os}/^{188}\text{Os}$ of some mantle xenoliths from the Japan and Izu Bonin arcs (Parkinson et al., 1998; Senda et al., 2007) which suggest the absence of enrichment in radiogenic Os of the mantle wedge. On the other hand, a slab origin for radiogenic Os in arc lavas is supported by the radiogenic signature of some mantle xenoliths from Cascades, Japan, New Ireland and Kamchatka arcs (Brandon et al., 1996; McInnes et al., 1999; Widom et al., 2003). Such an origin is also consistent with the trend to more radiogenic $^{187}\text{Os}/^{188}\text{Os}$ with decreasing Cr# and increasing Fe^{3+} in Cr-spinels from the Izu Bonin arc which suggests an increase in mobility of slab derived Os during an arc lifetime due to a progressive change in oxidation state of the mantle (Suzuki et al., 2011).

The Lesser Antilles arc (Fig. 6.1) is an excellent natural laboratory to investigate the mobility of Os in subduction zones since: (1) very primitive lavas such as picrites with

MgO = 17.4 (wt. %) can be sampled; (2) large amounts of Os should be subducted in the southern part of the subduction zone where the slab contains organic-rich sediments (black shales) that are typically highly enriched in Os and have very radiogenic isotopic signatures; and (3) the arc lavas and the subducting slab sediment/basalts are both very well constrained in terms of major, trace elements and radiogenic isotopes. Accordingly, we have analysed the most mafic and well constrained lavas from along the arc, as well as representative sediments and altered basalt from the subducting slab.

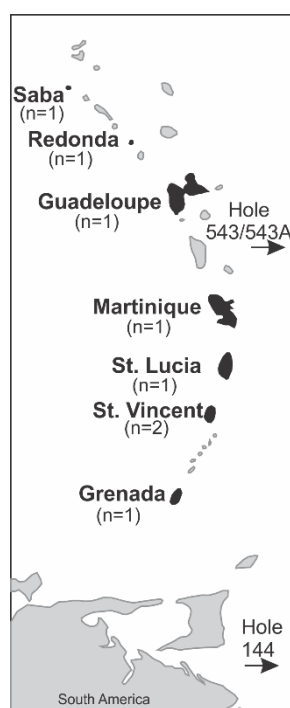


Fig. 6.1. Map of the Lesser Antilles arc with the location of selected lava samples (in black). One sample from each island (except St. Vincent, $n = 2$) was analysed. See Table 6.1 for sample identification. The latitude of DSDP sites 543/543A and 144 is also indicated.

6.2 Samples and analytical methods

6.2.1 Samples

We selected the most mafic lava samples (MgO = 5-17 wt. %) available from 7 different islands along the Lesser Antilles arc ($n = 8$), as well as an altered basalt ($n = 1$; DSDP site 543), organic-poor sediment ($n = 1$; DSDP site 543) and organic-rich black shales ($n = 11$; Unit 3-5 DSDP site 144) from the subducting American Plate (Table 6.1). The organic-poor sediment analysed consists of early Miocene clay with

minor ash (Biju-Duval et al., 1984). The organic-rich sediments selected record sedimentation preceding (Unit-5-4; Late-Aptian to lower Cenomanian; Carpentier et al., 2008) and contemporaneous (Unit-3; Lower Turonian to Santonian) with the oceanic anoxic event 2 (OAE2; 93.5 My e.g. Turgeon and Creaser, 2008). Samples from Unit 5 consist of quartzose carbonaceous clay or mudstone while unit 4 sample is marl. Finally samples from Unit 3 are zeolitic calcareous carbonaceous black shale (Hayes et al., 1972).

By selecting the most mafic lavas, we attempted to minimise the effects of crustal assimilation by continent-derived sediment present in the arc crust. Such sediment is responsible for the extreme isotopic compositions observed in the central-southern parts of the arc (e.g. Davidson, 1987; Bezard et al., 2014). All lavas (Fig. 6.2) and sediments have previously been analysed for major, trace elements and Sr-Nd isotopes (Davidson, 1984; Davidson, 1986; Heat et al., 1998; Van Soest, 2000; Dufrane et al., 2009; see Table 6.1). The most primitive lava sampled, which is also the most primitive lava in the arc, is a picrite from Grenada (MgO = 17.4 wt. %). Out of the samples selected, it displays the highest Light on Middle Rare Earth Element ratio (L/M-HREE), the lowest Sr/Th and the most radiogenic Sr isotopic composition (Sr/Th = 123; $^{87}\text{Sr}/^{86}\text{Sr} = 0.7051$; Fig. 6.2). Such features characterise all Grenada primitive lavas when compared to basaltic lavas from other islands of the arc (Macdonald et al., 2000). St Vincent contains very mafic lavas (MgO = 12.6 wt. %) with the most primitive lavas from the remaining islands having MgO contents that range from 5.1 to 8.7 (wt. %). All of the lavas selected are 1 Ma old or younger with the exception of the St Lucia lava flow which is dated at 11 Ma (Table 6.1).

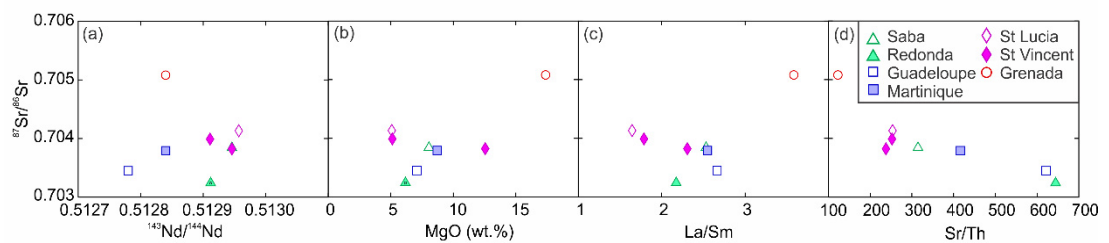


Fig. 6.2. $^{87}\text{Sr}/^{86}\text{Sr}$ vs. (a) $^{143}\text{Nd}/^{144}\text{Nd}$, (b) MgO (wt. %), (c) La/Sm and (d) Sr/Th of the lavas selected. Data presented in Table 6.1.

6.2.2 Analytical methods

All samples, except the organic-rich sediments, were analysed for Os and $^{187}\text{Os}/^{188}\text{Os}$ at the Geochemical Analysis Unit (GAU) at Macquarie University. The organic-rich sediments were analysed for Re, Os and isotope compositions ($^{187}\text{Re}/^{188}\text{Os}$; $^{187}\text{Os}/^{188}\text{Os}$) at the TOTAL Laboratory for Source Rock Geochronology and Geochemistry which is part of the Durham Geochemistry Centre (DGC) at Durham University.

Table 6.1. Composition of lavas and of altered basalt and sediments from the subducting slab.

	Os (ppb)	2 SE	$^{187}\text{Os}/^{188}\text{Os}$	2 SE	$^{187}\text{Re}/^{188}\text{Os}$	2 SE	Re (ppb)
Lavas							
Saba-LAS1 ^a	0.028	0.0001	0.181	0.00024	—	—	—
Redonda-R8204 ^a	0.005	0.00006	0.202	0.00053	—	—	—
Guadeloupe-GUAD510 ^a	0.033	0.00038	0.192	0.00032	—	—	—
Martinique-M8328 ^a	0.044	0.0002	0.188	0.00033	—	—	—
St Lucia-SL8344 ^a	0.006	0.00001	0.169	0.00039	—	—	—
St Vincent-STV301 ^a	0.161	0.00098	0.145	0.00024	—	—	—
St Vincent-STV324 ^a	0.018	0.00004	0.169	0.00025	—	—	—
Grenada-LAG4 ^a	0.362	0.00116	0.127	0.00007	—	—	—
ALT. BASALT ^a	0.01	0.00018	0.466	0.00141	—	—	—
Sediment							
78A-543-17-3-120-124 ^b	11.154	0.42354	0.185	0.00041	—	—	—
14-144Z-4-2 interval 60-64 ^c	0.478	0.00259	3.523	0.0164	1493.9	7.5	102.77
14-144Z-4-2 interval 143-146 ^c	0.602	0.00261	3.341	0.0105	1424.9	6.2	125.37
14-144Z-4-3 interval 31-33 ^c	0.534	0.00194	1.913	0.006	754.5	3.3	67.82
14-144Z-4-3 interval 100-103 ^c	0.484	0.00195	1.746	0.007	580.2	2.7	48.07
14-144Z-5-1 interval 5-6 ^c	0.231	0.00131	0.682	0.0081	177.7	1.7	7.93
14-144Z-5-1 interval 143-143 ^c	0.186	0.00202	0.718	0.0204	164	3.4	5.89
14-144Z-7-1 interval 136-137 ^c	0.116	0.00115	0.335	0.0096	32.3	0.7	0.76
14-144Z-7-1 interval 123-124 ^c	34.48	0.33892	0.344	0.0098	121.7	2.5	846.63
14-144Z-8-3 interval 136-137 ^c	0.093	0.00053	0.321	0.0049	16.7	0.7	0.32
14-144A-5-1 interval 123-124 ^c	0.101	0.00079	1.334	0.0189	388.7	4.5	7.03
14-144A-6-1 interval 70-110 ^c	0.941	0.003	1.844	0.0047	720.9	2.8	114.99

^a Os, $^{187}\text{Os}/^{188}\text{Os}$, Re analysed at Macquarie University and all other data/information are from Van Soest (2000) (LAS1; LAG4), Davidson (1984;1986) (R8204; M8328); Bezard et al. (2014) and Chapter 4 (SL8344); Dufrane et al. (2009) (GUAD510) and Heat et al. (1998) (STV301; STV 324). Ages of Lava flows were taken from the following sources: Saba (Dufrane et al. 2009); Redonda (Baker, 1984); Guadeloupe (Dufrane et al., 2009); Martinique, Carbet Complex (Germa et al. (2011); St Lucia, Anse Galet (Le Guen de Kerneizon et al. (1983) ; St Vincent (Heath et al. (1998) ; Grenada (Dufrane, 2009).

^b Organic poor sediment: Os, $^{187}\text{Os}/^{188}\text{Os}$, Re analysed at Macquarie University and all other data/information are from Davidson (1987).

^c Organic rich sediment: Os, $^{187}\text{Os}/^{188}\text{Os}$, Re analysed at Durham University all the other data/information are from Carpentier et al. (2008).

^d Initial Os isotopic ratio were calculated using the ages presented in the table, from Carpentier et al. (2008).

Note: Unit name and lithology (=Lith) Unit number refer to the name and numbering used in Carpentier et al. (2008).

Table 6.1. (continued).

	Age (ka)	$^{187}\text{Os}/^{188}\text{Os}$ initial ^d	MgO (wt. %)	Mg#	Sr (ppm)	La (ppm)	Sm (ppm)
Lavas							
Saba-LAS1 ^a	<10		8.05	0.82	321	5.8	2.29
Redonda-R8204 ^a	1000		6.17	0.74	493	4	1.84
Guadeloupe-GUAD510 ^a	500		7.08	0.76	261	3.7	1.4
Martinique-M8328 ^a	<1000		8.71	0.83	358	5.2	2.04
St Lucia-SL8344 ^a	11400		5.08	0.69	177	3.3	2.03
St Vincent-STV301 ^a	180		12.55	0.86	202	5.7	2.47
St Vincent-STV324 ^a	<3.6		5.12	0.74	236	4.9	2.72
Grenada-LAG4 ^a	<10		17.38	0.89	296	9.3	2.6
ALT. BASALT ^a	—				—	—	3.36*
Sediment							
78A-543-17-3-120-124 ^b	16000	—	2.91	—	83	23.5	4.83
14-144Z-4-2 interval 60-64 ^c	93000	1.21	0.71	—	570	6.5	0.97
14-144Z-4-2 interval 143-146 ^c	93000	1.13	0.71	—	570	6.5	0.97
14-144Z-4-3 interval 31-33 ^c	93000	0.74	0.71	—	570	6.5	0.97
14-144Z-4-3 interval 100-103 ^c	93000	0.85	0.71	—	570	6.5	0.97
14-144Z-5-1 interval 5-6 ^c	98000	0.39	1.26	—	446	22.5	4.2
14-144Z-5-1 interval 143-143 ^c	98000	0.45	1.26	—	446	22.5	4.2
14-144Z-7-1 interval 136-137 ^c	106000	0.28	2.03	—	270	28.8	5.4
14-144Z-7-1 interval 123-124 ^c	106000	0.13	2.03	—	270	28.8	5.4
14-144Z-8-3 interval 136-137 ^c	113000	0.29	2.26	—	349	29.4	5.5
14-144A-5-1 interval 123-124 ^c	85000	0.78	0.79	—	750	10.4	1.46
14-144A-6-1 interval 70-110 ^c	89000	0.77	0.66	—	681	11.5	1.56

^a Os, $^{187}\text{Os}/^{188}\text{Os}$, Re analysed at Macquarie University and all other data/information are from Van Soest (2000) (LAS1; LAG4), Davidson (1984;1986) (R8204; M8328); Bezard et al. (2014) and Chapter 4 (SL8344); Dufrane et al. (2009) (GUAD510) and Heat et al. (1998) (STV301; STV 324). Ages of Lava flows were taken from the following sources: Saba (Dufrane et al. 2009); Redonda (Baker, 1984); Guadeloupe (Dufrane et al., 2009); Martinique, Carbet Complex (Germa et al. (2011); St Lucia, Anse Galet (Le Guen de Kerneizon et al. (1983); St Vincent (Heath et al. (1998); Grenada (Dufrane, 2009).

^b Organic poor sediment: Os, $^{187}\text{Os}/^{188}\text{Os}$, Re analysed at Macquarie University and all other data/information are from Davidson (1987).

^c Organic rich sediment: Os, $^{187}\text{Os}/^{188}\text{Os}$, Re analysed at Durham University all the other data/information are from Carpentier et al. (2008).

^d Initial Os isotopic ratio were calculated using the ages presented in the table, from Carpentier et al. (2008).

Note: Unit name and lithology (=Lith) Unit number refer to the name and numbering used in Carpentier et al. (2008).

At Macquarie, whole rock powders (2-5g) were spiked for Os and digested using carius tubes in inverse *aqua-regia* using double Teflon distilled reagents at 220°C for 3 days. Given the young age of the samples, no age correction on the $^{187}\text{Os}/^{188}\text{Os}$ ratio was necessary and Re was not analysed. Os was separated by solvent extraction following the method of Cohen and Waters (1996) and was analysed by N-TIMS on a Thermo-Finnigan Triton mass spectrometer at Macquarie University in dynamic mode. All data were blank corrected using the total procedural blank (TPB) processed with the samples analysed. TPB was 6.30 pg Os with an $^{187}\text{Os}/^{188}\text{Os}$ ratio of 0.1821 (n = 1). This corresponds to corrections of 0-12% except for the two lavas with the

Table 6.1. (continued).

	Yb (ppm)	Th (ppm)	$^{87}\text{Sr}/^{86}\text{Sr}$	$^{143}\text{Nd}/^{144}\text{Nd}$	Unit name	Unit #	depth (m)
Lavas							
Saba-LAS1 ^a	1.83	1.02	0.70384	0.51295	—	—	—
Redonda-R8204 ^a	1.51	0.77	0.70324	0.51291	—	—	—
Guadeloupe-GUAD510 ^a	1.12	0.42	0.70345	0.51278	—	—	—
Martinique-M8328 ^a	1.75	0.86	0.70379	0.51284	—	—	—
St Lucia-SL8344 ^a	1.92	0.7	0.70413	0.51296	—	—	—
St Vincent-STV301 ^a	1.74	0.85	0.70382	0.51295	—	—	—
St Vincent-STV324 ^a	2.43	0.94	0.70399	0.51291	—	—	—
Grenada-LAG4 ^a	1.52	2.41	0.70508	0.51284	—	—	—
ALT. BASALT ^a	3.07*	—	0.70304*	—	—	—	—
Sediment							
78A-543-17-3-120-124 ^b	2.4	8.69	0.71408	0.51207	543 18 4W 15-17	3	155
14-144Z-4-2 interval 60-64 ^c	0.56	1.45	0.70781	0.51188	144 4 2W 60-64	3	215
14-144Z-4-2 interval 143-146 ^c	0.56	1.45	0.70781	0.51188	144 4 2W 60-64	3	215
14-144Z-4-3 interval 31-33 ^c	0.56	1.45	0.70781	0.51188	144 4 2W 60-64	3	215
14-144Z-4-3 interval 100-103 ^c	0.56	1.45	0.70781	0.51188	144 4 2W 60-64	3	215
14-144Z-5-1 interval 5-6 ^c	1.95	6.39	0.70856	0.51211	144 5 1W 123-125	4	265
14-144Z-5-1 interval 143-143 ^c	1.95	6.39	0.70856	0.51211	144 5 1W 123-125	4	265
14-144Z-7-1 interval 136-137 ^c	2.52	8.42	0.71083	0.51211	144 7 1W 80-82	5	299
14-144Z-7-1 interval 123-124 ^c	2.52	8.42	0.71083	0.51211	144 7 1W 80-82	5	299
14-144Z-8-3 interval 136-137 ^c	2.49	8.19	0.71029	0.5121	144 8 3W 130-135	5	328
14-144A-5-1 interval 123-124 ^c	0.98	2.31	0.70787	0.51184	144A 5 1W 119-124	3	181
14-144A-6-1 interval 70-110 ^c	0.89	2.16	0.70788	0.51183	144A 6 1W 90-93	3	190

^a Os, $^{187}\text{Os}/^{188}\text{Os}$, Re analysed at Macquarie University and all other data/information are from Van Soest (2000) (LAS1; LAG4), Davidson (1984;1986) (R8204; M8328); Bezard et al. (2014) and Chapter 4 (SL8344); Dufrane et al. (2009) (GUAD510) and Heat et al. (1998) (STV301; STV 324). Ages of Lava flows were taken from the following sources: Saba (Dufrane et al. 2009); Redonda (Baker, 1984); Guadeloupe (Dufrane et al., 2009); Martinique, Carbet Complex (Germa et al. (2011); St Lucia, Anse Galet (Le Guen de Kerneizon et al. (1983); St Vincent (Heath et al. (1998); Grenada (Dufrane, 2009).

^b Organic poor sediment: Os, $^{187}\text{Os}/^{188}\text{Os}$, Re analysed at Macquarie University and all other data/information are from Davidson (1987).

^c Organic rich sediment: Os, $^{187}\text{Os}/^{188}\text{Os}$, Re analysed at Durham University all the other data/information are from Carpentier et al. (2008).

^d Initial Os isotopic ratio were calculated using the ages presented in the table, from Carpentier et al. (2008).

Note: Unit name and lithology (=Lith) Unit number refer to the name and numbering used in Carpentier et al. (2008).

lowest abundances where these corrections amounted to 21 and 25%. During the analytical session, instrument performance was monitored by analysis of Os in-house solution standard JMC-2. $^{187}\text{Os}/^{188}\text{Os}$ for 5 ng loads in dynamic collection mode was 0.18311 ± 0.00016 (2sd; n = 4) which is in good agreement with the long term running means of 5ng JMC-2 in dynamic mode of 0.18294 ± 0.00070 (2sd; n = 17 since 2006). The average $^{187}\text{Os}/^{188}\text{Os}$ ratio of the WPR-1 international rock standard was 0.1451 ± 0.0013 (2sd; n = 4) with concentrations of $17.19 \text{ ppb} \pm 0.71$ (2sd; n = 4) which is in good agreement with the accepted values (Cohen and Waters, 1996; $^{187}\text{Os}/^{188}\text{Os} =$

0.14543 ± 0.00018 (2sd) and Os = $16.06 \text{ ppb} \pm 0.8$ (2sd)). The detail of both JMC-2 and WPR-1 compositions is presented in the supplementary data file (Appendix E).

At Durham, the organic-rich whole rock powders were also analysed by isotope-dilution negative thermal ionization mass spectrometry. Prior to being powdered, all the samples were polished to remove any minor drill marks. Samples were powdered in a Zr dish. A dried sample weight of $\geq 30 \text{ g}$ was powdered in order to homogenise the Re and Os within the sample (Kendall et al., 2009). The Re-Os analysis was conducted using Carius tube digestion in a 0.25 g/g CrO_3 4N H_2SO_4 reagent at 220°C for 48hrs with the Re and Os isolated from the acid medium using solvent extraction, micro-distillation and anion chromatography methodology (Selby and Creaser, 2003). In brief, $\sim 0.5 \text{ g}$ of sample powder was loaded in a Carius tube with a known amount of mixed tracer solution $^{190}\text{Os} + ^{185}\text{Re}$, with 8 ml of $\text{CrO}_3\text{-H}_2\text{SO}_4$ solution. The sealed Carius tubes were then placed in an oven at 220°C for 48 hrs. Osmium was isolated and purified using solvent extraction (CHCl_3) and microdistillation methods. Anion chromatography was used to purify the Re from 1 ml of the $\text{CrO}_3\text{-H}_2\text{SO}_4$ solution (Selby and Creaser, 2003). The purified Re and Os fractions were loaded onto Ni and Pt filaments, respectively (Selby and Creaser, 2003) with the addition of $\sim 0.5 \mu\text{l}$ BaNO_3 and BaOH activator solutions, respectively. Isotope compositions were measured using negative thermal ion mass spectrometry (NTIMS; Creaser et al., 1991; Volkening et al., 1991) via faraday cups for Re and electron multiplier (SEM) in peak hopping mode for Os. All samples were analysed as one batch. For this batch the total procedural blank for Re and Os during this study is $13.3 \pm 1.8 \text{ pg}$ and $0.32 \pm 0.17 \text{ pg}$, respectively, with $^{187}\text{Os}/^{188}\text{Os}$ value of 0.19 ± 0.05 . Uncertainties for $^{187}\text{Re}/^{188}\text{Os}$ and $^{187}\text{Os}/^{188}\text{Os}$ are determined through full propagation of uncertainties in Re and Os mass spectrometer measurements, blank abundances and isotopic compositions, spike calibrations and reproducibility of standard Re and Os isotopic values. In-house standard solutions (DROsS and Re Std) are 0.16094 ± 0.00030 and 0.59795 ± 0.0032 (2sd), which are consistent within uncertainty to those published by Nowell et al. (2008).

6.3 Results

All $^{187}\text{Os}/^{188}\text{Os}$ and Os concentrations, as well as $^{187}\text{Re}/^{188}\text{Os}$ and Re for the organic-rich sediments, are presented in Table 6.1 with corresponding lithophile element concentrations and isotopic ratios from the literature. All lavas apart from the most mafic sample, (Grenada picrite; $\text{MgO} = 17$ wt. %), have more radiogenic $^{187}\text{Os}/^{188}\text{Os}$ than the depleted mantle range (DMM; $^{187}\text{Os}/^{188}\text{Os} = 0.1238 \pm 0.0042$; Rudnick and Walker, 2009) and variable $^{187}\text{Os}/^{188}\text{Os}$ ratios and Os concentrations ranging between 0.127-0.202 and 0.005-0.362 ppb respectively (Fig. 6.3). The $^{187}\text{Os}/^{188}\text{Os}$ ratio of the altered basalt is 0.466 and this sample has very low Os abundance (0.0095 ppb). The organic-poor claystone from DSDP site 543 is enriched in Os (11.15 ppb) and possess moderately radiogenic $^{187}\text{Os}/^{188}\text{Os}$ (0.185). The organic-rich sedimentary units from DSDP 144 have moderate to highly radiogenic $^{187}\text{Os}/^{188}\text{Os}$ (0.32-3.52), and variable Os concentrations from 0.09 to 34.48 ppb (Fig. 6.3). The Os isotope ratios of the sediments get progressively more radiogenic from Late Albian to Turonian and less radiogenic from Turonian to Santonian. The same variations through time can also be observed in the calculated initial $^{187}\text{Os}/^{188}\text{Os}$ ratio (using sediment ages from Hayes et al. (1972) and Carpentier et al. (2008); Table 6.1). Therefore, the isotopic variations observed in the organic-rich sediment are not due to variations in Re content, but instead, are inherited from sea water compositional variations during sediment deposition.

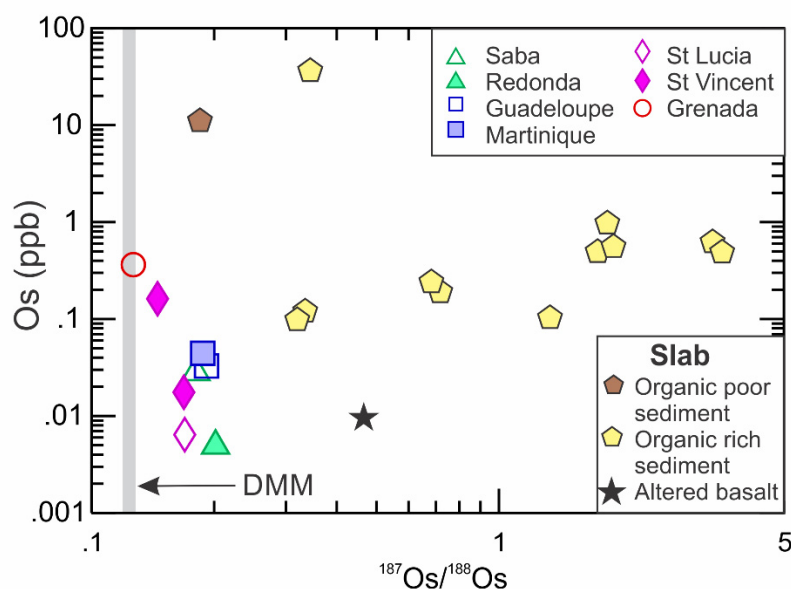


Fig. 6.3. Os (ppb) vs. $^{187}\text{Os}/^{188}\text{Os}$ of the lavas and subducting slab. DMM = Depleted MORB mantle from Rudnick and Walker (2009). Note logarithmic scales. Data presented in Table 6.1.

6.4 Discussion

6.4.1 Crustal assimilation control on $^{187}\text{Os}/^{188}\text{Os}$

If transfer of slab-derived Os into the mantle wedge was to be reflected in the isotopic variations observed in the lavas, a north-south trend to more radiogenic $^{187}\text{Os}/^{188}\text{Os}$ in the lavas should be observed. This is because the dominantly organic-poor sediment sequences subducted in the north have markedly less radiogenic $^{187}\text{Os}/^{188}\text{Os}$ than the sequences subducted in the south which comprise organic-rich sediments. However, no such geographic variation is observed. Indeed the least radiogenic compositions are observed in lavas from the south of the arc, in Grenada and St Vincent. These observations argue against the direct control of lava isotopic variations by slab-derived Os. Instead, the samples form inverse correlations between $^{187}\text{Os}/^{188}\text{Os}$ and both Os (0.005-0.36) (Fig. 6.4a) and MgO (Fig. 6.4b) with compositions of the southern lavas plotting on a steeper trend than the northern islands (from Martinique northward). These negative correlations between an index of differentiation and $^{187}\text{Os}/^{188}\text{Os}$ cannot easily be explained by a source process since the latter would need to be able to both enrich the source in $^{187}\text{Os}/^{188}\text{Os}$ and additionally control the future extent of magmatic differentiation. Therefore, the $^{187}\text{Os}/^{188}\text{Os}$ variations in the Lesser Antilles arc lavas need to be accounted for by a process(es) which postdates mantle melting. Since both trends formed by lavas from the southern and northern islands back project toward the composition of the Grenada picrite (Fig. 6.4), they can be explained by evolution from a common parental magma. The differences in subsequent magmatic evolution may reflect either different phases fractionated during crust assimilation with different partitioning for MgO and Os, different rates of assimilation or slightly different $^{187}\text{Os}/^{188}\text{Os}$ ratios of the putative assimilants.

Control of the osmium isotopic composition by crust assimilation rather than by slab contributions is emphasized when the $^{187}\text{Os}/^{188}\text{Os}$ ratios of both lavas and sediments are plotted against Sr isotope ratios (Fig. 6.5a). Once again, a negative correlation is observed for the lavas with a decrease in $^{87}\text{Sr}/^{86}\text{Sr}$ with increasing $^{187}\text{Os}/^{188}\text{Os}$. This negative correlation precludes involvement of any sediment-derived Os in the lavas sources since the sediments display both radiogenic Sr and Os and a mixing line between the mantle and the sediments would therefore have a positive slope which is the opposite of that observed (Fig. 6.5a). Although the altered basalt from the slab has

a lower Sr isotopic composition than the sediment, mixing of fluids derived from this component with the mantle wedge would also result in a positive trend.

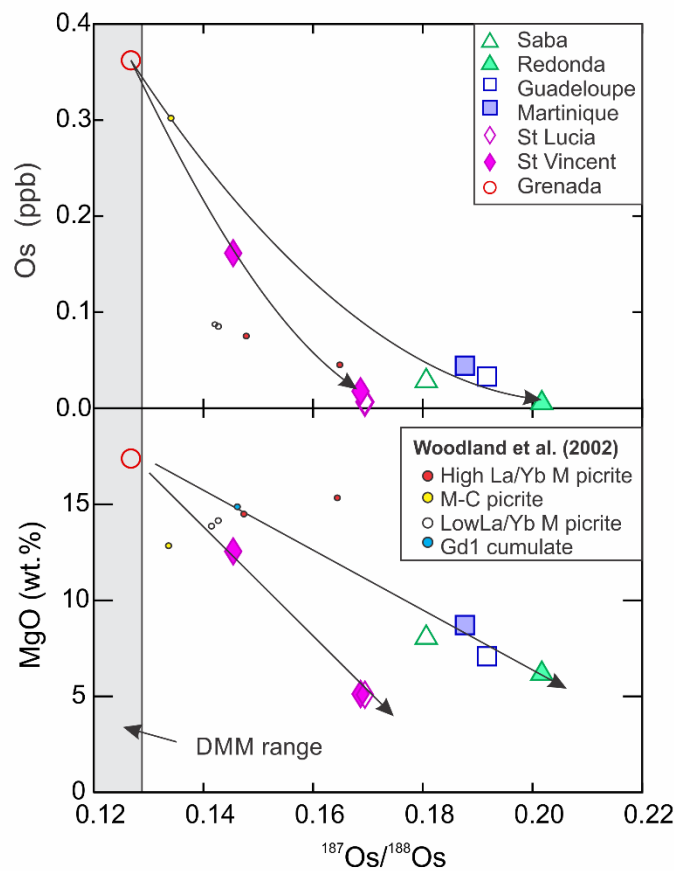


Fig. 6.4. Lavas Os (ppb) and MgO (wt. %) against $^{187}\text{Os}/^{188}\text{Os}$. Same legend as in Fig. 6.3. The same negative correlation is also observed between $^{187}\text{Os}/^{188}\text{Os}$ and Mg#. Woodland et al. (2002) data on different Grenada lavas are shown for comparison.

A source process capable of increasing slab-derived Os while decreasing slab derived Sr in the mantle is inconsistent with the decrease in Os concentrations observed with increasing $^{187}\text{Os}/^{188}\text{Os}$ (Fig. 6.4a). So too, stabilisation of an Os-bearing phase in the mantle wedge due to fluid fluxing from the slab (Borg et al., 2000) is inconsistent with the covariant decrease in both MgO and Os (Fig. 6.4a, b).

An increase in slab derived Os mobility in response to increasing the oxidation state of the mantle through time (Suzuki et al., 2011) is inconsistent with the decrease in $^{87}\text{Sr}/^{86}\text{Sr}$ observed with the increasing $^{187}\text{Os}/^{188}\text{Os}$ (Fig. 6.5a). Indeed slab derived Sr mobility is very unlikely to be sensitive to variation in oxygen fugacity given that, unlike Os, Sr displays only one valence state (bivalent) under normal geological

conditions. Instead, the contents of slab-derived Sr in the mantle are likely to be controlled by the extent of slab-derived fluid fluxing through the wedge, the latter fluid being also responsible for the increase in mantle oxygen fugacity through time (Brandon and Draper, 1996). Therefore, an increase rather than a decrease in slab derived Sr with increasing mantle oxygen fugacity would be expected. For example, such positive correlation between Sr concentration and oxygen fugacity was observed in melt inclusions from primitive lavas in the Cascades (Rowe et al., 2009). Finally, because the increase in $^{187}\text{Os}/^{188}\text{Os}$ ratios correlates inversely with MgO, any postulated increase in oxygen fugacity of the mantle would need to have a tight control on the future degree of differentiation of the magma, which seems very unlikely. Therefore we have confidence that the trends defined by the lavas are due to process occurring after melting in the source, i.e. crustal assimilation.

6.4.2 Source $^{187}\text{Os}/^{188}\text{Os}$

Since crustal assimilation affected $^{187}\text{Os}/^{188}\text{Os}$ during differentiation in the Lesser Antilles, the only sample suitable for constraining source characteristics is the sample with the highest MgO and highest Os concentrations, which is the picrite from Grenada (LAG4). This picrite $^{187}\text{Os}/^{188}\text{Os}$ (0.1267) plots within the mantle range (0.1238 ± 0.0042) (Fig. 4a, b) which indicates that assimilation had no, or very limited, effect on its composition. The apparent absence of radiogenic Os from either the subducting altered basalt or sediments in the Grenada picrite indicates either that (1) Os from the subducting slab is not transported into the magma source regions or (2) that it was retained in a residual mantle phase before the primitive Grenada melts were generated.

Conversely, the Grenada picrite has very radiogenic $^{87}\text{Sr}/^{88}\text{Sr}$ (0.70508; Fig 5a) which indicates that, as expected, Sr was mobilised from the slab into the wedge. As mentioned earlier, the more radiogenic Sr isotopic ratio of the Grenada picrite analysed, compared to other islands of the arc, is a general feature of Grenada mafic lavas, which has often been interpreted to reflect a greater contribution of sediment to the mantle source (Thirlwall et al., 1996). However, we show that Sr isotopes correlate inversely with Os which appear to be controlled by assimilation. Therefore, the decrease in $^{87}\text{Sr}/^{86}\text{Sr}$ observed in the Lesser Antilles lavas needs to be accounted for by the same process.

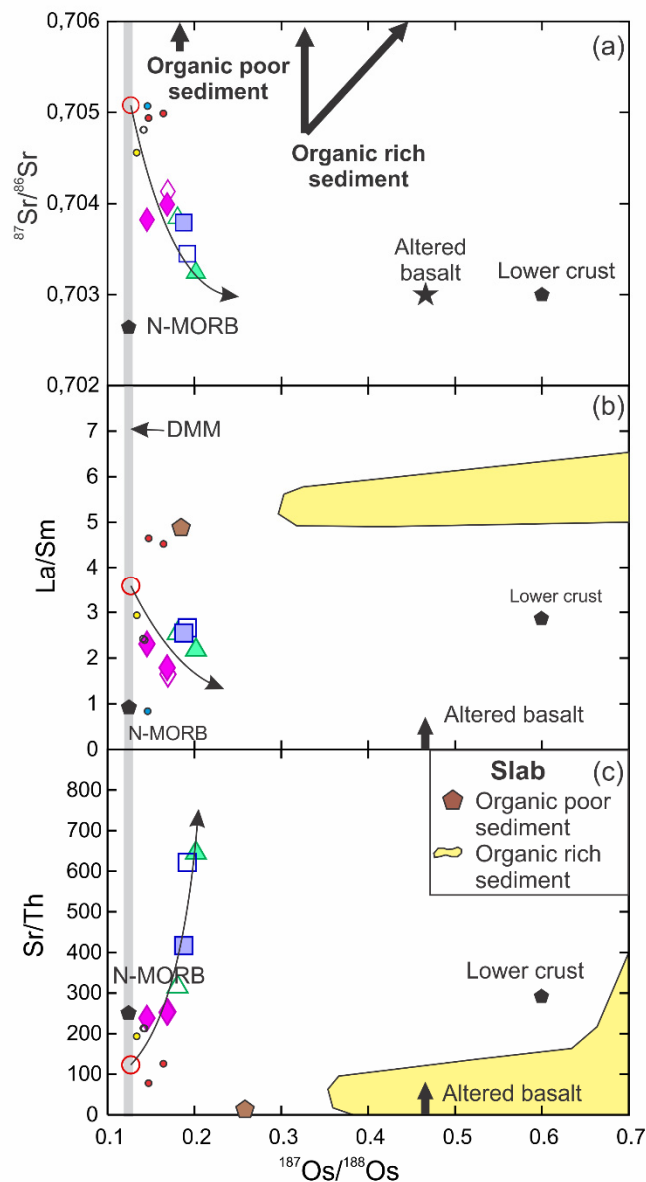


Fig. 6.5. Lavas (a) $^{87}\text{Sr}/^{86}\text{Sr}$, (b) La/Sm and (c) Sr/Th against $^{187}\text{Os}/^{188}\text{Os}$. Data for lavas, sediment and altered basalt presented in Table 6.1. DMM = depleted mantle from Rudnick and Walker (2009); Lower continental lower crust composition from Saal et al. (1999), N-MORB trace element composition is from Sun and McDonough (1989).

Hence $^{87}\text{Sr}/^{88}\text{Sr}$ in the Grenada picrite may not be more radiogenic than primary magmas of the other islands along the arc but instead provide the only true representative indication of source $^{87}\text{Sr}/^{86}\text{Sr}$ prior to crustal assimilation. In this case, estimations of slab contributions to the magma source based on Sr isotopes in mafic lavas have historically been misestimated for most islands.

6.4.3 Characteristics and nature of the assimilant

6.4.3.1 Trace element and isotopic characteristics

As described in section 4.1, the lavas show an inverse correlation between $^{87}\text{Sr}/^{86}\text{Sr}$ and $^{187}\text{Os}/^{188}\text{Os}$ (Fig. 6.5a). However, unlike MgO and Os vs. $^{187}\text{Os}/^{188}\text{Os}$, where two trends are observed, no north-south separation of the data exists. Given that isotopic ratios are not affected by crystal fractionation, we suggest that the same assimilant is present in both the north and the south of the arc and that the separated northern and southern arc trends observed on plots of MgO and Os vs. $^{187}\text{Os}/^{188}\text{Os}$ can be accounted for by different fractionated assemblages during assimilation (i.e. different bulk partition coefficients). For example, fractionation of olivine during assimilation will produce a steeper decrease in MgO and Os compared with clinopyroxene fractionation.

Given that $^{87}\text{Sr}/^{86}\text{Sr}$ decreases down to ~ 0.703 , the assimilant must have $^{87}\text{Sr}/^{86}\text{Sr}$ close to the DMM (Rudnick and Walker, 2009), which precludes any sedimentary origin. This is in agreement with the mantle-like clinopyroxene and olivine $\delta^{18}\text{O}$ data available for some of the high $^{187}\text{Os}/^{188}\text{Os}$ lavas, which are similar to those of Grenada picrites (Saba: $\delta^{18}\text{O}_{\text{ol}} = 5.13$ and $\delta^{18}\text{O}_{\text{cpx}} = 5.74$ for LAS1; Guadeloupe: $\delta^{18}\text{O}_{\text{ol}} = 5.00$ - 5.12 and $\delta^{18}\text{O}_{\text{cpx}} = 5.51$ for GUAD510; Grenada: $\delta^{18}\text{O}_{\text{ol}} = 5.18$ for LAG4; Van Soest et al., 2002). No clear correlation between Pb isotopes and $^{187}\text{Os}/^{188}\text{Os}$ can be observed and no correlation between $^{143}\text{Nd}/^{144}\text{Nd}$ and $^{187}\text{Os}/^{188}\text{Os}$ exist (not shown). This could either indicate that the isotopic composition of the assimilant is similar to that of the primitive magma, or that the concentrations in Pb and Nd in the assimilant are not high enough to buffer existing source variations between islands.

When La/Sm or La/Yb are plotted against $^{187}\text{Os}/^{188}\text{Os}$ (Fig. 6.5b), the same negative correlation observed on plots of MgO and Os vs. $^{187}\text{Os}/^{188}\text{Os}$ exists. Such correlations indicate that the REE were affected during assimilation. As with MgO and Os, we suggest that the similar separation of the samples into two trends is due to different phases being fractionated during assimilation. The decrease in L/M-HREE in itself (observed in both trends) could therefore reflect the interplay of the progressive incorporation of a low La/Sm assimilant and of fractional crystallisation of minerals that fractionate L/M-HREE (such as clinopyroxene or amphibole).

Finally, Sr/Th is also affected by crustal assimilation since it correlates negatively with $^{187}\text{Os}/^{188}\text{Os}$ (Fig. 6.5c). The correlation is clearly due to increasing Sr since Th does not decrease with $^{187}\text{Os}/^{188}\text{Os}$. As for $^{87}\text{Sr}/^{88}\text{Sr}$ vs. $^{187}\text{Os}/^{188}\text{Os}$, no distinction between the north-south sections of the arc can be observed, consistent with a common assimilant composition along the arc. The assimilant must also have very high Sr content with a minimum Sr/Th of 624 (the highest ratio found in the lavas).

In summary, one of the assimilants present in the basement of Lesser Antilles islands (the other being continent-derived sediment, not discussed here) displays a mantle-like $^{87}\text{Sr}/^{88}\text{Sr}$ ratio, a $^{187}\text{Os}/^{188}\text{Os}$ higher than 0.2, a high Sr/Th (> 620), and a low La/Sm (< 1.6) and La/Yb (< 1.7) coupled with modestly high Os (> 30 ppt) content. Lower Os concentrations would require unreasonably large degrees of assimilation. Significantly, thermobarometric estimations performed on St Vincent picrite (STV301) indicate that it was last stored at depths corresponding to the arc middle-lower crust (Heat et al., 1998; Pichavant et al., 2007). This would imply that assimilation would need to have occurred at depths equivalent to or greater than these.

6.4.3.2 Nature of the assimilant

Recent (\sim late Cretaceous to Paleogene) altered Mid-Ocean Ridge Basalts (MORB) or Fore-arc Basalts (FAB) could have a DMM-like $^{87}\text{Sr}/^{86}\text{Sr}$ with $^{187}\text{Os}/^{188}\text{Os}$ higher than 0.2 and low L/M-HREE (typically < 1), but their Sr concentration is typically far too low (typically ≤ 90 ppm) to be able to modify the primitive magma concentrations. Bulk mafic MORB or FAB cumulates would also be too depleted in Sr to represent an appropriate assimilant. Instead, we suggest that the assimilant could be a MORB or FAB plagioclase-rich cumulates present in the lower crust. Given that the Lesser Antilles arc is thought to be built after a slab rollback that displaced the activity eastward of the Aves ridge (extinct arc), on stretched arc and forearc rocks, FAB cumulates are more likely to be present at the base of the Lesser Antilles arc than MORB cumulates. Such rocks would likely occur under every island and meet the geochemical requirements of the assimilant described above. They could comprise mafic layers, but the more felsic sections would be preferentially assimilated by primitive magmas. While the mafic layers of cumulates tend to concentrate the iridium platinum group element (IPGE) because the latter are removed from the melt early during differentiation and concentrate in cumulus phases such as olivine or chromite,

plagioclase rich layers tend to concentrate more Re (and palladium platinum group elements: PPGE) since the latter remain longer in the melt and is more likely to be present as interstitial sulfides. Radiogenic Os, produced by Re decay, is therefore more likely to be present in such layers. Since the Lesser Antilles arc started accreting during the Oligocene (Germa et al., 2011), the early-arc FAB lavas and cumulates would have a moderately radiogenic $^{187}\text{Os}/^{188}\text{Os}$, consistent with the signature of the assimilant. The mantle-like Sr isotopic composition of the cumulate would also be consistent with their production early in the arc existence, prior to significant fluids fluxing through the mantle.

Finally, none of the lavas analysed have a europium positive anomaly, the latter being expected in the case of assimilation of large amounts of plagioclase. However, all but one lava (STV301) contains plagioclase phenocrysts which indicate that plagioclase fractionation may have erased any such positive anomaly. The absence of any Eu anomaly in the plagioclase-free high-MgO basalt from St Vincent could be explained by the apparent low amount of assimilation involved in that lava (one of the most limited increase in $^{187}\text{Os}/^{188}\text{Os}$; Fig. 6.5a) or if the assimilated plagioclase cumulates did not have a significant positive Eu anomaly. A low Eu anomaly in plagioclase can only occur in highly oxidised magmas. Since the plagioclase cumulates are likely to have crystallised at the initiation of the subduction zone, their oxygen fugacity is likely to be similar to that of FAB erupted at the onset of the Mariana subduction, which have been shown to present high oxygen fugacity (QFM +0.4; Brounce et al., 2013), and are likely to crystallise plagioclase with small Eu anomalies.

6.4.3.3 Assimilation and fractional crystallisation (AFC) modelling

The AFC equation (DePaolo, 1981) can be used to model the $^{187}\text{Os}/^{188}\text{Os}$, $^{87}\text{Sr}/^{88}\text{Sr}$, La/Sm and Sr/Th relationships using reasonable parameters (Fig. 6a, b, c). We used the Grenada picrite (LAG4) for the initial magma composition, since it plots within the mantle range in terms of $^{187}\text{Os}/^{188}\text{Os}$ and its Os concentration (360ppt Os) is consistent with that expected with a melt in equilibrium with sulfide-bearing mantle. The range of Os, Sr, Th, La and Sm bulk partition coefficients (D) (Table 6.2) were estimated by dividing the concentration of these elements in the Grenada picrite by their concentration in the most differentiated samples. Sr, Th, La and Sm bulk D's obtained are consistent with fractionation of the observed phenocryst assemblages

(olivine \pm pyroxene \pm plagioclase). The Os bulk partition coefficients used ($D = 9$ -10) are in agreement with that expected for $\sim 0.5\%$ of chromian-spinel fractionation (Chesley et al., 2002; Richter et al., 2002). The $^{187}\text{Os}/^{188}\text{Os}$ ratio of the assimilant can be easily produced by radiogenic ingrowth of a DMM composition with an initial ratio of $^{187}\text{Os}/^{188}\text{Os}$ (0.127). This could occur within the 25 My since magmatism was initiated in the Lesser Antilles (Germa et al., 2011), even if the initial $^{187}\text{Re}/^{188}\text{Os}$ is lower than MORB (~ 600).

Table 6.2. AFC model parameters.

Endmember compositions^a		
	Initial Magma	Assimilant
Sr (ppm)	296	790
Os (ppb)	0.36	0.04
La (ppm)	9.32	4.00
Sm (ppm)	2.60	1.84
Th (ppm)	2.41	0.50
$^{87}\text{Sr}/^{86}\text{Sr}$	0.7051	0.7023
$^{187}\text{Os}/^{188}\text{Os}$	0.1268	0.2450
Bulk partition coefficients		
	Model 1	Model 2
DSr	1.4	1.8
Dos	13	10
DTh	2.8	2.3
DLa	2	2.6
DSm	1.3	1.3
$r = \text{Ma/Mc}$	0.56	0.70

^aused in both model 1 and 2

All data could be modeled using the same starting (LAG-4) and assimilant composition (Table 6.2) and with a fraction of melt remaining (F) > 0.8 . In $^{87}\text{Sr}/^{86}\text{Sr}$ vs. $^{187}\text{Os}/^{188}\text{Os}$ space, the lavas fall on two trends produced by different rates of assimilation and small variations in D_{Sr} ($r = 0.56$ vs. 0.70 ; $D_{\text{Sr}} = 1.6$ -1.8). On trace element ratio vs. isotope diagrams (Fig. 6.6b, c), the effect of variations in the fractionating assemblage during assimilation on different islands (= variation in D) is reflected by small displacement of the samples on these trends compared to isotope-isotope space (Fig. 6.6a). The northern and southern trends observed in La/Sm vs. $^{187}\text{Os}/^{188}\text{Os}$ can be easily produced by increasing $D_{\text{La/Sm}}$. We suggest that such north-south variations in $D_{\text{La/Sm}}$ could be related to the depth at which AFC occurs. In this case, the assemblage fractionated during assimilation in the north of the arc depleted La less than the assemblage fractionated in the south for a constant D_{Sm} . For example, it would be the case if, during assimilation, the fractionated assemblage is dominated

by olivine ($D_{La/Sm} \sim 1$) in the south of the arc and by clinopyroxene ($D_{La/Sm} < 1$) in the north of the arc.

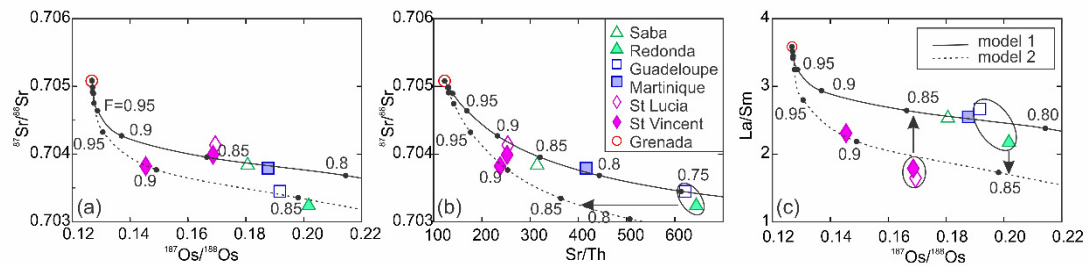


Fig. 6.6. Assimilation during Fractional Crystallisation (AFC) models of the $^{87}\text{Sr}/^{86}\text{Sr}$ (a, b), $^{187}\text{Os}/^{188}\text{Os}$ (a, c), Sr/Th (b) and La/Sm (c) of the Lesser Antilles primitive lavas using DePaolo (1981) equation. Model 1 and 2 parameters are shown in Table 6.2. Dots represent the fraction of melt remaining (F).

6.4.4 Implications

6.4.4.1 The Lesser Antilles

Although assimilation of sediment (high $\delta^{18}\text{O}$, $^{87}\text{Sr}/^{86}\text{Sr}$, $^{208-207-206}\text{Pb}/^{204}\text{Pb}$ and low $^{176}\text{Hf}/^{177}\text{Hf}$ and $^{143}\text{Nd}/^{144}\text{Nd}$ ratios) has been shown to modify some lava compositions in the central-southern part of the arc (Thirlwall and Graham, 1984; Davidson, 1987; Davidson and Harmon, 1989; Smith et al., 1996; Thirlwall et al., 1996; Van Soest et al., 2002; Bezard et al., 2014), assimilation of another component in the deep crust of the Lesser Antilles arc (Fig. 6.7) was not anticipated and differences between the Grenada picrite compositions and the rest of the arc lavas have traditionally been attributed to differences in source composition. This work suggests that the Grenada picrites might provide the only true estimates of the source composition in terms of $^{87}\text{Sr}/^{86}\text{Sr}$, $^{187}\text{Os}/^{188}\text{Os}$, Sr and REE. Thus, the use of such proxies in less primitive lavas to constrain the relative contributions of fluids versus sediment in the arc source may need reappraisal. Variations in the source from north to south might exist, although all the arc data seem to back-project toward a primitive magma with the Grenada picrite composition (Fig. 6.4). Since the Grenada picrite is the only silica undersaturated lava, this suggests that primitive magma along the arc in general could be of a similar alkaline nature before AFC, as suggested by Macdonald et al. (2000). The absence of cumulate assimilation by Grenada picrites could be either due to a lack of a significant amount of cumulate at the base of the island crust, or to the presence of crustal structures allowing the magma to reach the surface with minimal stalling at the base of the crust. The latter hypothesis could be supported by the presence of a transform

fault in Grenada, which has been suggested to control the emplacement of the most recent products (Arculus, 1976).

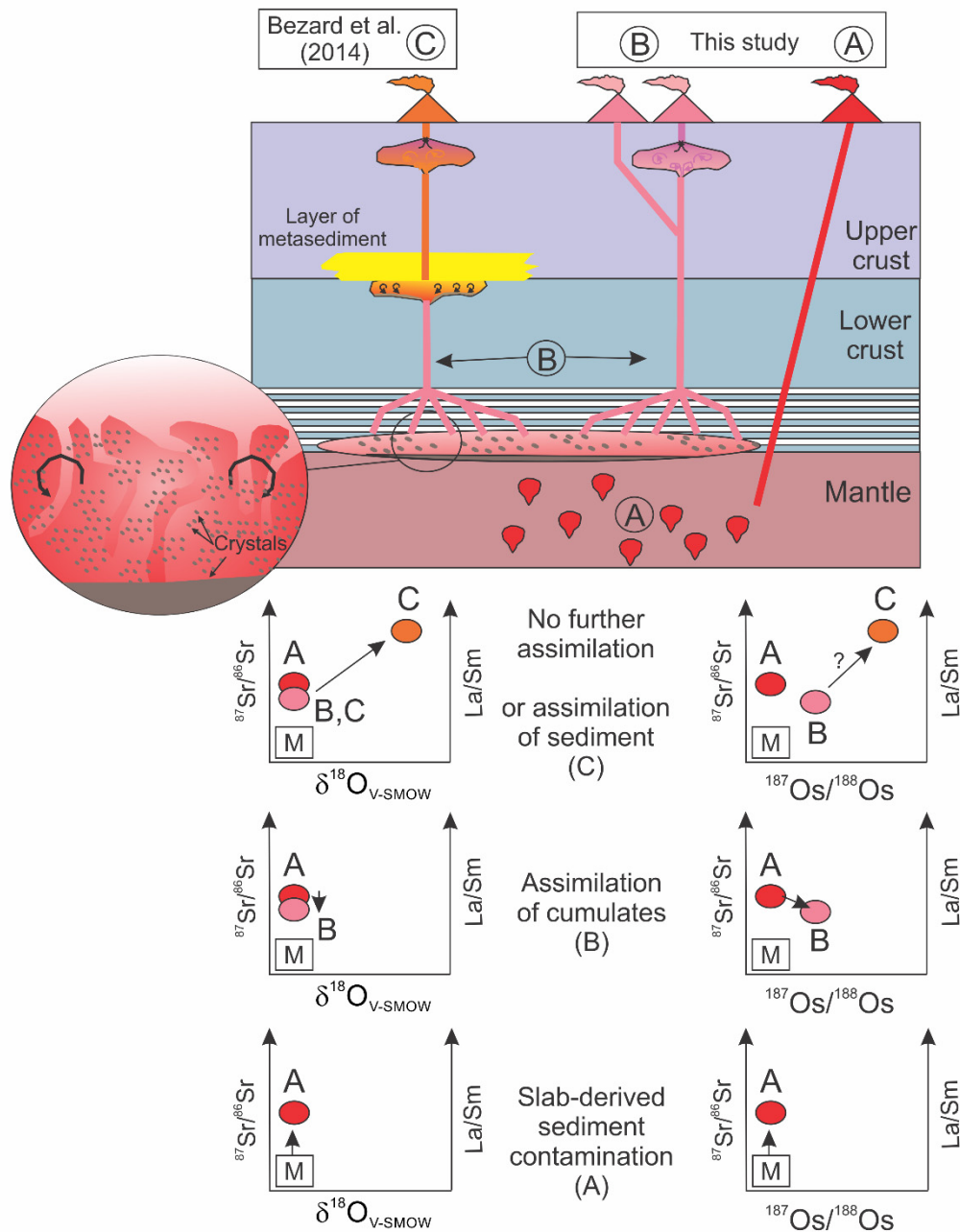


Fig. 6.7. Schematic model for the Lesser Antilles plumbing system to explain the main factors influencing the compositional variations of the arc lavas. The figure illustrates both the locus (cartoon) and the impact (diagrams) of cumulate assimilation on the lava's $^{187}\text{Os}/^{188}\text{Os}$, $^{87}\text{Sr}/^{86}\text{Sr}$, La/Sm and $\delta^{18}\text{O}$ compositions (evolution of Sr/Th ratio is not shown). The impact of subsequent assimilation of sediment (Bezard et al., 2014), which is not discussed in this contribution, is also shown for a full illustration of the arc processes. The arc primary magmas would come from a source strongly influence by the subducted sediment. Grenada picrite (A) would have avoided any storage in the arc crust and retained the primitive magma composition. All the less primitive lavas (B) would have spent variable amounts of time in contact with a plagioclase-rich cumulate in the lower parts of the crust. The resulting magmas

would have either ascended directly to the surface (B) or assimilated some sediment during the ascent (C). M = mantle composition.

6.4.4.2 Other arcs

The correlation between Os (or 1/Os) and $^{187}\text{Os}/^{188}\text{Os}$ observed in the Lesser Antilles arc is not unique and has been noted in most continental and oceanic arc lavas (Fig. 6.8a; Alves et al., 1999; Borg et al., 2000; Chesley et al. 2002; Woodland et al., 2002; Woodhead et al., 2004; Turner et al., 2009; Righter et al., 2012). However, clear correlations between Os isotopes and both Os concentrations and indices of differentiation (MgO, SiO₂), have only been noted in continental arcs (Lassiter and Luhr, 2001; Chesley et al., 2002). The absence of clear MgO-SiO₂ correlations with $^{187}\text{Os}/^{188}\text{Os}$ in oceanic arc lavas (Fig. 6.8b) led previous studies to suggest source control of the inverse correlation between Os concentration and $^{187}\text{Os}/^{188}\text{Os}$ (Alves et al., 1999). Our Lesser Antilles study suggests that the correlations between $^{187}\text{Os}/^{188}\text{Os}$ and Os content and the radiogenic $^{187}\text{Os}/^{188}\text{Os}$ ratios observed in oceanic arcs could reflect crustal assimilation and that slab-derived Os may not be transferred into the magma source regions, as proposed by Righter et al. (2012). It also suggests, based on the radiogenic $^{187}\text{Os}/^{188}\text{Os}$ ratio in the St Vincent high-MgO lavas (MgO = 12.6 wt. %), that the process can affect very primitive magmas. Although the conditions of assimilation may be different in every arc, early assimilation during differentiation could explain the radiogenic $^{187}\text{Os}/^{188}\text{Os}$ observed in early crystallising phases such as Cr-spinel in Bonin Islands tholeiites (Suzuki et al, 2011).

Unlike the correlation between Os isotopes and Os concentrations, the covariation of Os isotopes with lithophile isotope or trace element ratios observed in the Lesser Antilles (e.g. Sr isotopes, Sr/Th and La/Sm) is not ubiquitous in other arcs (e.g. Fig. 6.8c, d), with only the Cascades lavas showing similarly clear correlations between $^{187}\text{Os}/^{188}\text{Os}$ and $^{87}\text{Sr}/^{86}\text{Sr}$ ratios and Sr concentrations (Borg et al., 2000; Fig. 6.8c, d). This lack of obvious co-variation could be explained by more limited compositional differences between the primary magma and the assimilant which would rend the impact of assimilation harder to observe. Indeed, in the Lesser Antilles, the $^{87}\text{Sr}/^{86}\text{Sr}$, Sr/Th and La/Sm ratios of the primitive magmas differs significantly from those of the assimilant, which results in obvious mixing lines. However, such differences might be unusual since favored by the more “sediment-like” isotopic and trace element

signatures of the Lesser Antilles primitive magmas compared to other arcs (e.g. picrites from the Vanuatu or Salomon islands have $^{87}\text{Sr}/^{86}\text{Sr} \sim 0.703\text{--}0.7045$ contrasting with the $^{87}\text{Sr}/^{86}\text{Sr}$ of ~ 0.7051 of the most primitive picrite in Grenada; Peate et al., 1997; Schuth et al., 2004). In addition, the rocks assimilated in other arcs might have lower Sr concentrations, rendering the impact of the process on Sr/Th and $^{87}\text{Sr}/^{86}\text{Sr}$ hard to fingerprint. Alternatively, along-arc primitive magma compositional variations may exist, interfering with the variations produced by assimilation.

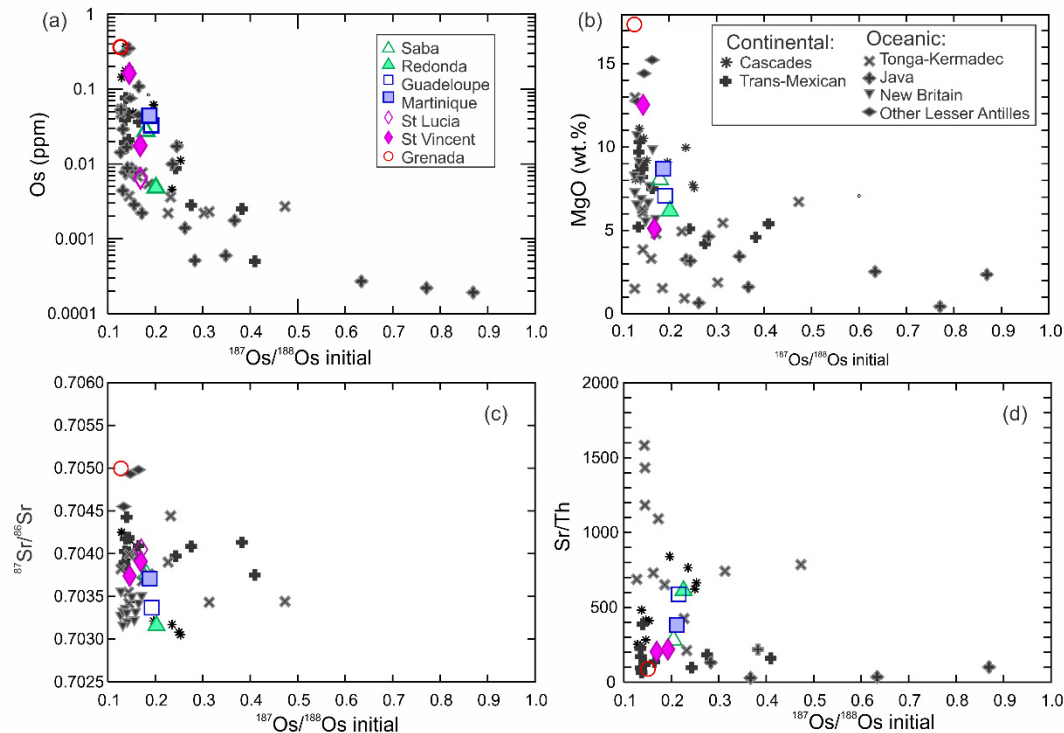


Fig. 6.8. Comparison of the Lesser Antilles arc compositions with those of other arcs (continental and oceanic). The negative correlation observed between Os isotopes and Os concentrations (a) is ubiquitous in arcs. On the other hand, negative correlations between Os isotopes and MgO (b) or Sr isotopes (c) as well as a positive correlation between Sr/Th (d) and Os isotopes are not observed in every arcs. Lava compositions are from Borg et al., (2000) for the Cascades, Chesley et al. (2002) for the Trans-Mexican arc, Turner et al. (2009) for the Tonga-Kermadec, Alves et al. (1999) for Java, Woodhead and Brauns (2004) for New Britain and Woodland et al. (2002) for the additional Lesser Antilles arc data.

6.5 Conclusions

Our observations suggest that no slab derived Os is present in the primitive magmas of the Lesser Antilles arc. The increase in Os isotopic ratios observed in the lavas is due to crustal assimilation in the deep crust of the arc. The assimilant is similar all

along the arc and displays lower $^{87}\text{Sr}/^{86}\text{Sr}$ (MORB-like), La/Sm and higher $^{187}\text{Os}/^{188}\text{Os}$, Sr and Sr/Th than the primitive magma. We suggest that the assimilant could be a plagioclase rich cumulate present at the base of the arc. Such cumulate could have been produced during the early-arc stage, prior to significant amount of fluids/sediments fluxing in the mantle.

Chapter 7

Conclusions and future work

7.1 Introduction

This thesis investigated the involvement of crustal assimilation in the Lesser Antilles arc magma signatures using (1) lavas from St Lucia and (2) some of the most mafic and well constrained lavas from other islands in the arc including Saba, Redonda, Guadeloupe, Martinique, St Vincent and Grenada.

At St Lucia (1), it was first demonstrated that assimilation of sediment in the arc crust significantly overprinted the source signatures of the magmas (Chapter 3). The detailed impact of assimilation on the magma compositions, the amount and the nature of the sediment assimilated were explored to subsequently constrain the composition of the mantle source (Chapter 4). The conditions during sediment assimilation and the involvement of this process in the production of large volumes of silicic magmas were investigated using mineral in-situ analyses (Chapter 5). Finally, the compositions of mafic lavas from along the arc (2) were explored to test how well they preserved their mantle source characteristics (Chapter 6), and revealed that igneous basement rocks were also assimilated by the arc magmas.

Below are presented the main conclusions obtained in Chapters 3-6. These are also illustrated in Fig. 7.1 which presents a summary of the context of assimilation of both sediment and igneous basement beneath St Lucia and other islands of the arc. It also shows some representative trace element and isotopic changes produced by these processes. Potential future research directions are subsequently discussed.

7.2 Conclusions

7.2.1 Impact of sediment assimilation on the Lesser Antilles arc lava compositions

The compositional range of the St Lucia lavas investigated in this thesis covers most of the Lesser Antilles arc Sr, Nd, Hf and Pb isotopic compositions, ranging from “typical oceanic arc” signatures to more “continental” compositions that overlap the local terrigenous sediments. The “continental” isotopic signatures are found in lavas and volcanoclastic rocks from the silicic Soufriere Volcanic Complex (SVC) while the “typical oceanic arc” compositions (Pre-SVC1), as well as some intermediate isotopic

compositions (Pre-SVC2) between Pre-SVC1 and SVC lavas, are found in the older and generally more mafic lava flows. The occurrence of crustal assimilation by St Lucia lavas is supported by (1) the $^{87}\text{Sr}/^{86}\text{Sr}$ composition of single plagioclase crystals from four of the SVC lavas which revealed isotopic heterogeneity both amongst and within hand samples and (2) the $\delta^{18}\text{O}$ composition of the Pre-SVC2 and SVC crystals which plot well beyond the mantle range. The control of crustal assimilation on the bulk lava isotopic compositions was demonstrated by the co-variation of the radiogenic isotope ratios of Pre-SVC2 and SVC lavas with both SiO_2 and mineral $\delta^{18}\text{O}$ data. Since no evidence for the presence of continental basement beneath the arc exists and since the assimilant is characterised by high Sr, Pb and $\delta^{18}\text{O}$ isotope ratios (with low Nd and Hf isotope ratios), the assimilant needs to be of sedimentary origin. Sediment assimilation also impacted on the trace element composition of the lavas as demonstrated by the co-variation of radiogenic isotopes with light/middle-heavy rare earth element (L/M-HREE) and Th/Th* ratios ($\text{Th}_\text{N} / ((\text{Ba}_\text{N} + \text{U}_\text{N})/2)$).

Assimilation during Fractional Crystallisation (AFC) models showed that a high rate ($r = 0.8$) of assimilation of a mix of biogenic and terrigenous sediments reproduces the spectrum of St Lucia lavas. Lavas that were the most affected by crustal assimilation are dacites and silica-rich andesites from the SVC, but the composition of lavas (from Pre-SVC2) as mafic as basaltic andesites were also significantly modified. This demonstrates the need for a careful mineral investigation to exclude the possibility of sediment assimilation, even in the most mafic lavas, before constraining the source characteristics.

The decrease in Hf and Nd isotope ratios accompanied by an increase in Th/Th*, L/M-HREE and Sr and Pb isotope ratios observed in St Lucia lavas also characterises the lavas from Martinique, which display the largest range of isotopic compositions in the arc. This suggests that sediment assimilation is responsible for all the extreme isotopic compositions observed along the Lesser Antilles arc.

7.2.2 Conditions of sediment assimilation and development of a silicic complex

St Lucia magmas that were the most affected by sediment assimilation were erupted at the SVC which is one of the largest silicic centres in the Lesser Antilles arc. The

SVC represents a locality of choice to understand the impact of the recycling of continental crust via sediment assimilation, on the production of new silicic arc crust. A detailed mineral study, including in-situ Sr isotopes in plagioclase and in-situ $\delta^{18}\text{O}$ in dated zircons, of both SVC and Pre-SVC lavas showed that the production of the erupted silicic lavas was tightly linked with crustal assimilation and occurred in two stages.

The first stage involved the differentiation of mafic magma by sediment assimilation and mineral fractionation in the middle-lower crust of the arc to produce magmas with intermediate compositions. These intermediate magmas were water rich (~ 7 wt. %), had high Sr isotope ratios, high La/Sm (~ 5) and high Ba and Sr concentrations compared to Pre-SVC1 lavas. They were also likely to be characterised by high Pb isotopes and Th/Th* ratios, and low Nd and Hf isotopes ratios, since these proxies are all correlated with Sr isotopes in the SVC lavas. The trace element and isotopic compositions of these magmas were nearly constant throughout the SVC lifespan which suggest that the process involved in their production was persistent over the last 600 kys.

In the second stage, the intermediate magmas ascended to a shallower and more differentiated chamber (~ 6 km depth). During ascent, any crystals or xenocrysts residual from the deeper chamber became fully resorbed, due to the decrease of pressure and the high water content of the magma, but hornblende microphenocrysts, and anorthite-rich plagioclase started crystallising. On reaching the shallow chamber, intermediate magmas mixed with resident rhyodacitic magmas produced by crystal fractionation of earlier magma batches. During mixing, both plagioclase from the recharging magma and crystals in equilibrium with the resident magma were partially resorbed. The recharge event triggered chamber wide convection, responsible for the wavy-oscillatory texture observed in most plagioclase phenocrysts mantle-rims. Mixing is thought to have triggered the eruptions of the silicic complex.

7.2.3 Impact of assimilation of the igneous arc roots on magma compositions

Analysis of $^{187}\text{Os}/^{188}\text{Os}$ in some of the most mafic lavas found along the arc, including the most mafic lava from St Lucia, showed that all but the most primitive lava (17 wt.

% MgO) were affected by assimilation of the igneous arc roots. Assimilation affected the Os and Sr isotopic compositions and the L/M-HREE and Sr/Th ratios of the lavas. The assimilant is inferred to have a Mid-Oceanic Ridge Basalt (MORB)-like $^{87}\text{Sr}/^{86}\text{Sr}$ ratio with high Sr content (>700 ppm), low L/M-HREE ($\text{La}/\text{Sm} < 1.6$; $\text{La}/\text{Yb} < 1.7$) and $^{187}\text{Os}/^{188}\text{Os} > 0.2$. Such compositional features are likely to correspond to Fore-arc Basalt (FAB) plagioclase-rich cumulates produced during the early stages of the subduction zone, during crystallisation from magma extracted before significant fluids were fluxed through the mantle. These results have important implications for the interpretation of the mafic lava compositions, since it shows that most of them are not fully representative of the source, at least in the Lesser Antilles arc.

7.2.4 The arc mantle source composition

Based on trace elements and Sr, Nd, Hf and Pb isotopes, St Lucia lavas that escaped sediment assimilation (mainly mafic) have a typical oceanic arc signature. They display similar Ba/Th, La/Sm and Nd isotopic compositions but have slightly more radiogenic Sr and Pb isotopes than lavas further north in the arc. Calculations indicate that addition of less than 2% of the local subducting sediments can explain these compositions; this estimate is similar to those previously obtained for the northern arc. Therefore, after removal of the effects of sediment assimilation, St Lucia lavas have only slightly more radiogenic Pb and Sr signatures compared to the northern islands, which could be attributed to differences in the isotopic composition of the subducting sediment rather than greater sediment input, as has been previously proposed. Comparison of St Lucia with the other southern Lesser Antilles islands suggests similar source compositions could exist beneath Martinique, St Vincent and maybe Bequia, while a more “continental” source might characterize Ile de Caille, Kick'em Jenny and Grenada.

However, $^{187}\text{Os}/^{188}\text{Os}$ investigation of the most mafic lavas (having escaped sediment assimilation) showed that care must be applied to use the lithophile trace element and isotope ratios mentioned above to interpret the source characteristics. Indeed, as explained in section 7.2.3, variations in Os and Sr isotopes and La/Sm and Sr/Th ratios amongst mafic lavas from along the Lesser Antilles arc appear to be mainly controlled by assimilation of plagioclase-rich cumulates, with only the most mafic lava, a picrite with 17 wt. % MgO from Grenada, possibly representing the arc source composition.

Based on the Grenada picrite composition, the mantle source is likely to have radiogenic $^{87}\text{Sr}/^{86}\text{Sr}$ (0.705), high La/Sm ratio (3.6), low Sr/Th ratio (123) but an $^{187}\text{Os}/^{188}\text{Os}$ ratio that overlaps the mantle range (0.127).

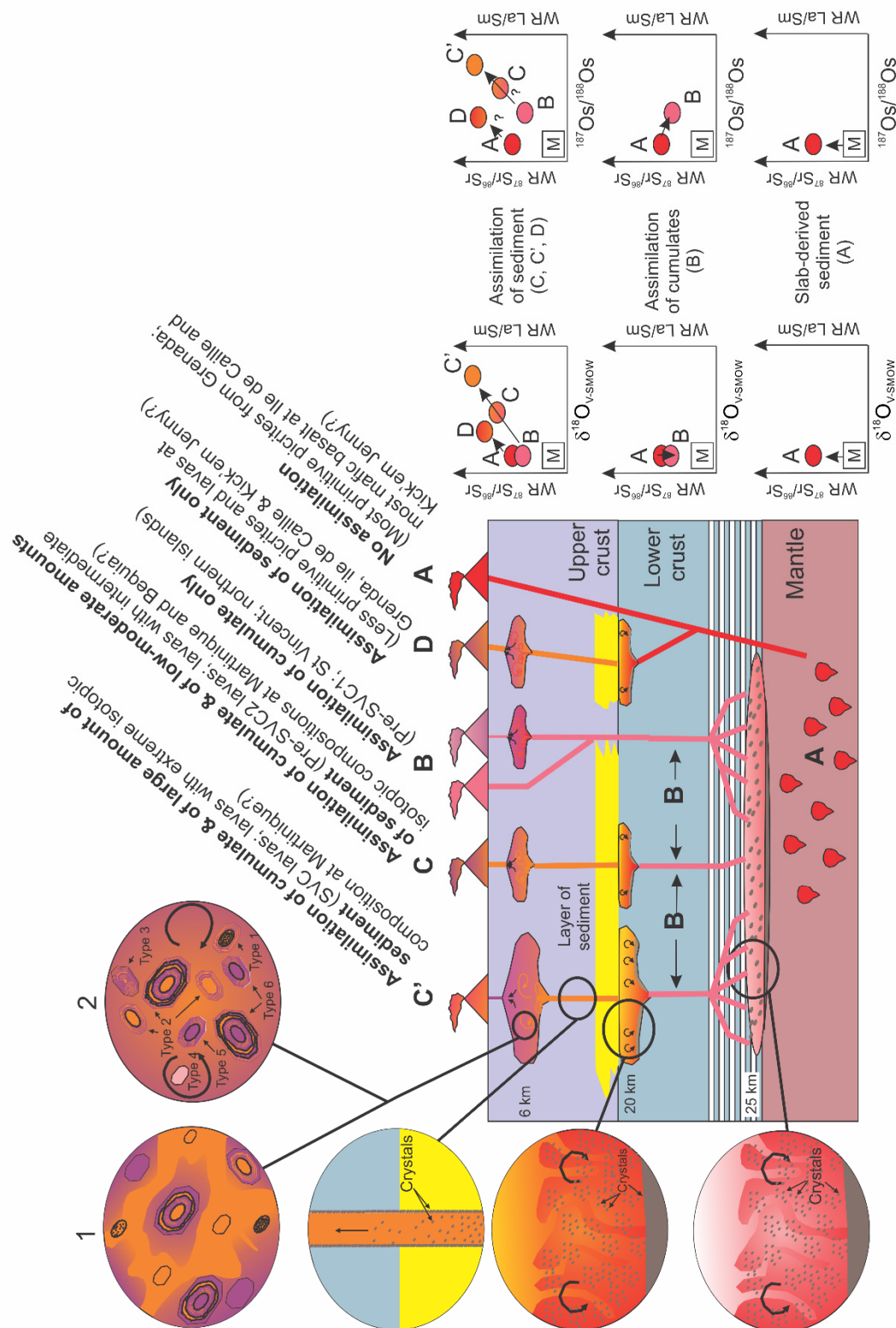


Fig. 7.1. Cartoon illustrating the locus of both cumulate and sediment assimilation in the Lesser Antilles arc and their impact on some representative isotope and trace elements ratios. The primary magma (A)

would have been influenced by fluids and sediments from the subducting slab and have high Sr and Pb isotopes with low Nd and Hf isotopes and high L/M-HREE and Sr/Th (not shown). It may only have erupted in Grenada. Other mafic lavas from the arc would have stalled at the base of the arc and assimilated some cumulates with FAB composition. Assimilation would have decreased $^{87}\text{Sr}/^{86}\text{Sr}$ and La/Sm ratios, and increased the Sr/Th ratio of the magmas (B). Magmas would have subsequently ascended to shallower storage levels or directly to the surface without further assimilation (B; e.g. Pre-SVC1). Some would have been stored in contact with a sediment-rich layer, when present in the middle to lower crust, which is the case of Pre-SVC2 and SVC lavas. The study of the SVC and Pre-SVC lavas suggested that magmas having had interacted with the sediment layer (C and C') would have experienced assimilation during fractional crystallisation (AFC) resulting in a significant decrease in Nd and Hf isotopes and increase in Sr, and Pb isotopes, but also in L/M-HREE and in Th, Sr and H₂O concentrations. The resulting magmas would then have ascended to a shallower reservoir. During ascent, crystals from the previous storage would be digested on their way up, and amphibole and anorthite-rich plagioclase would have started crystallising up to the mixing with the cooler and more differentiated magma of the shallow chamber. During mixing, both anorthite-rich crystals from the recharging melt and the anorthite-poor crystals from the differentiated chamber would have partially resorbed, followed by the growth of an oscillatory-zoned rim before eruption. The range of textures (Types 1-6) observed in the SVC and Pre-SVC lavas would all have been produced in the shallow chamber.

7.3 Future work

7.3.1 St Lucia

7.3.1.1 Plutonic enclaves

In-situ trace element and isotopic analyses in the crystals of the SVC lavas provided some important insights into the conditions of the shallow chamber beneath the complex. Complementary information could be obtained by performing a detailed trace element and isotopic study of the plutonic enclaves transported by the SVC lavas.

In addition, Pre-SVC1 lava flows could be examined for plutonic xenoliths. If plutonic xenoliths could be found, mineral isotope analysis might reveal important insights into the processes of arc igneous root assimilation.

7.3.1.2 $^{187}\text{Os}/^{188}\text{Os}$ in SVC lavas

Since the goal of the Os isotopic investigation was to understand the source composition, no SVC lavas were analysed. However, the $^{187}\text{Os}/^{188}\text{Os}$ composition of

the SVC lavas could provide important information on the nature of the assimilated sediment. Indeed, lithophile element isotopes (Sr, Nd, Hf and Pb) suggested that black shales (similar to DSDP site 144) were unlikely to be assimilated by the SVC magmas. This could be confirmed using Os isotopes since black-shales and organic-poor sediment analysed during this study were shown to have distinct Os isotopic compositions. Therefore, comparison of the SVC lava signatures with these sediments would be a good way to refine the nature of the assimilant in the arc basement.

7.3.2. The rest of the arc

7.3.2.1 Detection of sediment assimilation in other islands

Mineral oxygen isotopes were demonstrated to be a powerful tool to detect crustal assimilation on St Lucia. The use of mineral $\delta^{18}\text{O}$ in Martinique, where lavas with the highest Sr and Pb isotope ratios of the arc occur, would confirm or refute the involvement of sediment assimilation in the production of all the “continental” isotopic compositions of the arc.

7.3.2.2 Detection of igneous arc root assimilation

The modification of the Sr isotopes and trace element composition of the most mafic lavas along the arc by assimilation of a plagioclase-rich cumulate at the base of the arc crust could be confirmed by a detailed mineral $^{87}\text{Sr}/^{86}\text{Sr}$ analysis of the most primitive lavas and plutonic xenoliths of St Vincent. Indeed, more radiogenic $^{87}\text{Sr}/^{86}\text{Sr}$ ratios in olivine compared to clinopyroxene separates have already been observed in Saba and in St Vincent lavas and plutonic xenoliths (Van Soest et al., 2000; unpublished data from Simon Turner), and could result from crustal assimilation between the growth of these two phases. However, in both studies, the amount of data is very limited and a detailed mass balance calculation, using modal abundances in the samples, would need to be done to rule out any alteration effects on the mineral $^{87}\text{Sr}/^{86}\text{Sr}$ ratios. A detailed $^{87}\text{Sr}/^{86}\text{Sr}$ mineral study of several high-MgO lavas from St Vincent and of some plutonic xenoliths could therefore bring important insight into the mafic magma differentiation processes. If more than 2g of each single phases could be separated, the $^{187}\text{Os}/^{188}\text{Os}$ of olivine and pyroxene phenocryst could also be analysed and compared.

7.3.3 Other arcs

In the Lesser Antilles, $^{87}\text{Sr}/^{86}\text{Sr}$, La/Sm and Sr/Th ratios co-vary with Os isotopes, which suggest their modification by crustal assimilation. In most other arcs, the correlation between Os isotopes and lithophile trace elements or Sr isotope ratios is not obvious, with the exception of the Cascades. As suggested in Chapter 6, the absence of clear correlations in other arcs could be due to smaller compositional differences between the assimilant and the primary magma. This hypothesis could be tested by a detailed Os and Sr isotopic study of an island containing both picrites and basaltic lavas. Indeed, no picrites from arcs other than the Lesser Antilles have yet been analysed for Os isotopes. Os isotopic compositions of high-MgO picrites in other arcs would confirm or refute the mantle-like $^{187}\text{Os}/^{188}\text{Os}$ ratio of primary magmas, while the presence of Os isotopic variations amongst more differentiated mafic lavas from a same island, back-projecting toward the picrite composition, would confirm the occurrence of crustal assimilation. In the latter case, the correlation of Os isotopes with lithophile isotope and trace element ratios would reveal information about the nature of the assimilant.

References

- Agner-Torres, M., Blundy, J., Ulmer, P., Pettke, T., 2007. Laser Ablation ICPMS study of trace element partitioning between plagioclase and basaltic melts: an experimental approach. *Contributions to Mineralogy and Petrology* 153, 647-667.
- Aitken, T., Mann, P., Escalona, A., Christeson, G.L., 2011. Evolution of the Grenada and Tobago Basins and implications for arc migration. *Marine and Petroleum Geology* 28, 235-258.
- Allègre, C.J., Dupré, B., Nègre, P., Gaillardet, J., 1996. Sr–Nd–Pb isotope systematics in Amazon and Congo River systems: Constraints about erosion processes. *Chemical Geology* 131, 93-112.
- Alves, S., Schiano, P., Allegre, C.J., 1999. Rhenium-osmium isotopic investigation of Java subduction zone lavas. *Earth and Planetary Science Letters* 168, 65-77.
- Annen, C. and Sparks, R.S.J., 2002. Effects of repetitive emplacement of basaltic intrusions on thermal evolution and melt generation in the crust. *Earth and Planetary Science Letters* 203, 937-955.
- Annen, C., Blundy, J.D., Sparks, R.S.J., 2006. The Genesis of Intermediate and silicic magmas in deep crustal hot zones. *Journal of Petrology* 47, 505-539.
- Aquater, SpA, 1982. Exploration of St. Lucia's Geothermal Resources, Annex A-Geological Survey. The Government of St Lucia Ministry of Finance and Planning.
- Arculus, R.J., 1973. The alkali basalt, andesite association of Grenada, Lesser Antilles. PhD thesis, Durham, England, University of Durham.
- Arculus, R., 1976. Geology and geochemistry of the alkali basalt-andesite association of Grenada. Lesser Antilles island arc. *Geological Society of America Bulletin* 87, 612-624.
- Arculus, R.J., Wills, K.J.A., 1980. The petrology of plutonic blocks and inclusions from the Lesser Antilles island arc. *Journal of Petrology* 21, 743-799.
- Arth, J.G., 1976. Behaviour of trace elements during magmatic processes-a summary of theoretical models and their applications. *Journal of Research US Geological Survey* 4, 41-47.
- Bacon, C., R., 1986. Magmatic inclusions in silicic and intermediate volcanic rocks. *Journal of Geophysical Research-Solid Earth and Planets* 91, 6091-6112.
- Bacon, C.R., Adami, L.H., Lanphere, M.A., 1989. Direct evidence for the origin of low ^{18}O silicic magmas: Quenched samples of a magma chamber's

- partially-fused granitoid walls, Crater Lake, Oregon. *Earth and Planetary Science Letters*, 96, 199-208.
- Baker, 1984. Geochemical evolution of St Kitts and Montserrat, Lesser Antilles. *Journal of the Geological Society of London* 141, 401-411.
- Ballhaus, C., Berry, R.F., Green, D.H., 1991. High pressure experimental calibration of the olivine–orthopyroxene–spinel oxygen barometer: implications for the oxidation state of the upper mantle. *Contributions to Mineralogy and Petrology* 107, 27-40.
- Barclay, J., Rutherford, M.J., Carroll, M.R., Murphy, M.D., Devine, J.D., Gardner, J., Sparks, R.S.J., 1998. Experimental phase equilibria constraints on pre-eruptive storage conditions of the Soufriere Hills magma. *Geophysical Research Letters* 25, 3437-3440.
- Beard, J.S., Ragland, P.C., Crawford, M.L., 2005. Reactive bulk assimilation: A model for crust-mantle mixing in silicic magmas. *Geology* 3, 681-684.
- Beccaluva, L., Chinchilla Chaves, A.L., Coltorti, M., Giunta, G., Siena, F., Vaccaro, C., 1999. The St. Helena-Nicoya Ophiolitic Complex in Costa Rica and its geodynamic implications for the Caribbean Plate Evolution. *European Journal of Mineralogy* 11, 1091-1107.
- Bédard, J.H., 1999. Petrogenesis of Boninites from the Betts Cove Ophiolite, Newfoundland, Canada: Identification of Subducted Source Components. *Journal of Petrology*, 40, 1853-1889.
- Berlo, K., Blundy, J., Turner, S., 2007. Textural and chemical variation in plagioclase phenocrysts from the 1980 eruptions of Mount St. Helens, USA. *Contributions to Mineralogy and Petrology* 154, 291-308.
- Bezard, R., Davidson, J.P., Turner, S., Macpherson, C.G., Lindsay, J.M., Boyce, A.J., 2014. Assimilation of sediments embedded in the oceanic arc crust: myth or reality? *Earth and Planetary Science Letters* 395, 51-60.
- Biju-Duval, B., Quéléec, P.L., Mascle, A., Renard, V., Valéry, P., 1982. Multibeam bathymetric survey and high resolution seismic investigations on the Barbados ridge complex (Eastern Caribbean): a key to the knowledge and interpretation of an accretionary wedge. *Tectonophysics* 86, 275-304.
- Biju-Duval, B., et al., 1984. Initial Reports of the Deep Sea Drilling Project 78A. U.S. Government Printing Office, Washington.
- Biju-Duval, B., et al., 1985. The terrigenous and pelagic series of Barbados Island: Paleocene to middle Miocene slope deposits accreted to the Lesser Antilles margin. In: Mascle, A. (Ed.), *Géodynamique des Caraïbes*. Technip, Paris.

- Bindeman, I., 2008. Oxygen Isotopes in Mantle and Crustal Magmas as Revealed by Single Crystal Analysis. *Reviews in Mineralogy and Geochemistry* 69, 445-478.
- Bindeman, I.N., Valley, J.W., 2002. Oxygen isotope study of the Long Valley magma system, California: isotope thermometry and convection in large silicic magma bodies. *Contributions to Mineralogy and Petrology* 144, 185-205.
- Bindeman, I.N., Ponomareva, V.V., Bailey, J.C., Valley, J.W., 2004. Volcanic arc of Kamchatka: a province with high- $\delta^{18}\text{O}$ magma sources and large-scale $^{18}\text{O}/^{16}\text{O}$ depletion of the upper crust. *Geochimica et Cosmochimica Acta* 68, 841-865.
- Blundy, J. D., Shimizu, N., 1991. Trace element evidence for plagioclase recycling in calc-alkaline magmas. *Earth and Planetary Science Letters* 102, 178-197.
- Blundy, J.D., Wood, B.J., 1991. Crystal-chemical controls on the partitioning of Sr and Ba between plagioclase feldspar silicate melts and hydrothermal solutions. *Geochimica et Cosmochimica Acta* 55, 193-209.
- Bolz, V., 2001. The oxygen isotope geochemistry of zircon as a petrographic tracer in high temperature contact metamorphic and granitic rocks. MS thesis, University of Edinburgh, 208 p.
- Borg, L.E., Brandon, A.D., Clyne, M.A., Walker, R.J., 2000. Re-Os isotopic systematics of primitive lavas from the Lassen region of the Cascade Arc, California. *Earth and Planetary Science Letters* 177, 301-317.
- Bottinga, Y., Kudo, A., Weill, D., 1996. Some observation on oscillatory zoning and crystallization of magmatic plagioclase. *American Mineralogist* 51, 792-806.
- Bouysse, P., 1984. The Lesser Antilles island arc: structure and geodynamic evolution. In: Biju-Duval, B., Moore, J.C. et al. _Eds., Initial Rep. Deep Sea Drill. Proj. 78A, Government Printing Office, Washington, DC, 83-103.
- Bouysse, P., Westercamp, D., 1990. Subduction of Atlantic aseismic ridges and Late Cenozoic evolution of the Lesser Antilles island-arc. *Tectonophysics* 175, 349-390.
- Bowles, F.A., Fleischer, P., 1985. Orinoco and Amazon River sediment input to the eastern Caribbean Basin. *Marine Geology* 68, 53-72.
- Brandon, A.D., Draper, D.S., 1996. Constraints on the origin of the oxidation state of the mantle overlying subduction zones: an example from Simcoe, Washington, USA. *Geochimica Cosmochimica Acta* 60, 1739-1749.

- Brandon, A.D., Creaser, R.A., Shirey, S.B., Carlson, R.W., 1996. Os recycling in subduction zones. *Science* 272, 861-864.
- Briden, J.C., Rex, D.C., Faller, A.M., Tomblin, J.F., 1979. K-Ar geochronology and paleomagnetism of volcanic rocks in the Lesser Antilles island arc. *Philosophical Transactions of the Royal Society of London A291*, 485-528.
- Brounce, M.N., Kelley, K., Cottrell, E., 2013. Temporal evolution of fO_2 in the Mariana mantle wedge. *American Geophysical Union abstract*.
- Brown, M., 2007. Crustal melting and melt extraction, ascent and emplacement in orogens: mechanisms and consequences. *Journal of the Geological Society* 164, 709-730.
- Burke, K., 1988. Tectonic evolution of the Caribbean. *Annual Review of Earth and Planetary Sciences* 16, 201-230.
- Burton, K.W., Ling, H.F., O'Nions, R.K., 1997. Closure of the Central American Isthmus and its effect on the deep-water formation in the North Atlantic. *Nature* 386, 382-385.
- Carpentier, M., Chauvel, C., Mattielli, N., 2008. Pb-Nd isotopic constraints on sedimentary input into the Lesser Antilles arc system. *Earth Planetary Science Letters* 272, 199-211.
- Carpentier, M., Chauvel, C., Maury, R.C., Mattielli, N., 2009. The 'Zircon effect' as recorded by the chemical and Hf isotopic composition of Lesser Antilles forearc sediments. *Earth and Planetary Science Letters* 287, 86-99.
- Cashman, K.V., 1990. Textural Constraints on the kinetics of crystallization of igneous rocks. In: Nichols J., Russel, J.K. (eds) *Modern methods of igneous petrology, understanding magmatic processes*. Mineralogical Society of America, Washington, D.C. Review in *Mineralogy* 24, 259-314.
- Cashman, K., 1992. Groundmass crystallisation of Mt St. Helens dacite, 1980-1986: a tool for interpreting shallow magmatic processes. *Contributions to Mineralogy and Petrology* 109, 431-449.
- Charlier, B.L.A., Ginibre, C., Morgan, D., Nowell, G.M., Pearson, D.G., Davidson, J.P., Ottley, C.J., 2006. Methods for the microsampling and high-precision analysis of strontium and rubidium isotopes at single crystal scale for petrological and geochronological applications. *Chemical Geology* 232, 114-133.

- Chase, R.L., Bunce, E.T., 1969. Underthrusting of the eastern margin of the Antilles by the floor of the western North Atlantic ocean, and origin of the Barbados Ridge. *Journal of Geophysical Research* 74, 1413-1420.
- Chazot, G., Lowry, D., Menzies, M., Matthey, D., 1997. Oxygen isotopic composition of hydrous and anhydrous mantle peridotites. *Geochimica et Cosmochimica Acta* 61, 161-169.
- Cherniak, D.J., 1999. Ba diffusion in Feldspars. In: AGU Fall Meeting 1999. EOS transactions American Geophysical Union 80 Supplement 46, F1078.
- Cherniak, D.J., 2003. REE diffusion in feldspar. *Chemical Geology* 193, 25-41.
- Cherniak, D.J., Watson, B., 1994. A study of diffusion in plagioclase using Rutherford backscattering spectrometry. *Geochimica et Cosmochimica Acta* 58, 5179-5190.
- Chesley, J., Ruiz, J., Richter, K., Ferrari, L., Gomez-Tuena, A., 2002. Source contamination versus assimilation: an exemple from the Trans-Mexican Volcanic Arc. *Earth and Planetary Science Letters* 195, 211-221.
- Chiba, H., Chacko, T., Clayton, R.N., Goldsmith, J.R., 1989. Oxygen isotope fractionations involving diopside, forsterite, magnetite, and calcite: Application to geothermometry. *Geochimica et Cosmochimica Acta* 53, 2985-2995.
- Cohen, A.S., Waters, F.G., 1996. Separation of osmium from geological materials by solvent extraction for analysis by thermal ionisation mass spectrometry. *Analytica Chimica Acta* 332, 269-275.
- Coulon, C., Clocchiatti, R., Maury, R.C., Westercamp, D., 1984. Petrology of basaltic xenoliths in andesitic to dacitic host lavas from Martinique (Lesser Antilles): evidence for magma mixing. *Bulletin of Volcanology* 47, 705-734.
- Creaser, R.A., Selby, D., 2009. ^{187}Re - ^{187}Os geochronology of Precambrian organic-rich sedimentary rocks. *Geological Society of London Special Publication* 326, 85-107.
- Creaser, R.A., Papanastassiou, D.A., Wasserburg, G.J., 1991. Negative thermal ion mass spectrometry of osmium, rhenium and iridium. *Geochimica Cosmochimica Acta* 55, 397-401.
- Davidson, J.P., 1983. Lesser Antilles isotopic evidence of the role of subducted sediments in island arc magma genesis. *Nature* 306, 253-256.
- Davidson, J.P., 1984. Petrogenesis of Lesser Antilles island arc magmas: Isotopic and geochemical constraints. PhD thesis, Uni. Leeds, U.K. 308 pp.

- Davidson, J.P., 1985. Mechanisms of contamination in Lesser Antilles island arc magmas from radiogenic and oxygen isotope relationships. *Earth and Planetary Science Letters* 72, 163-174.
- Davidson, J. P., 1986. Isotopic and trace element constraints on the petrogenesis of subduction-related lavas from Martinique, Lesser Antilles. *Journal of Geophysical Research* 91, 5943-5962.
- Davidson, J.P., 1987. Crustal contamination versus subduction zone enrichment: example from the Lesser Antilles and implications for mantle source compositions of island arc volcanic rocks. *Geochimica et Cosmochimica Acta* 51, 2185-2198.
- Davidson, J.P., Harmon, R.S., 1989. Oxygen isotope constraints on the petrogenesis of volcanic arc magmas from Martinique, Lesser Antilles. *Earth and Planetary Science Letters* 95, 255-270.
- Davidson, J.P., Tepley, F.J., 1997. Recharge in Volcanic Systems: Evidence from isotope Profiles of Phenocrysts. *Science* 275, 826-829.
- Davidson, J.P., Arculus, R.J., 2006. The significance of Phanerozoic arc magmatism in generating continental crust. In: Brown, M. and Rusmer, T. (eds) *Evolution and Differentiation of the Continental Crust*. Cambridge: Cambridge University Press, pp. 135-172.
- Davidson, J.P., Wilson, M., 2011. Differentiation and Source Processes at Mt Pelée and the Quill; Active Volcanoes in the Lesser Antilles Arc. *Journal of Petrology* 52, 1493-1531.
- Davidson, J.P., Morgan, D.J., Charlier, B.L.A., Harlou, R., Hora, J. M., 2007. Microsampling and isotopic analysis of igneous rocks: implications for the study of magmatic systems. *Annual Review of Earth and Planetary Sciences* 35, 273-311.
- Davidson, J., Turner, S., Handley, H., Macpherson, C., Dosseto, A., 2007. Amphibole “sponge” in arc crust? *Geology* 35, 787-790.
- Davidson, J., Turner, S., Plank, T., 2013. Dy/Dy*: Variations Arising from Mantle Sources and Petrogenetic Processes. *Journal of Petrology* 54, 525-537.
- De Kerneizon, M.L., Bellon, H., Carron, J.P., Maury, R.C., 1983. The island of St-Lucia-petrochemistry and geochronology of the main magmatic series. *Bulletin de la Societe Géologique de France* 25, 845-853.
- DePaolo, D.J., 1981. Trace element and isotopic effects of combined wallrock assimilation and fractional crystallization. *Earth and Planetary Science Letters* 53, 189-202.

- Devine, J.D., 1995. Petrogenesis of the basalt-andesite-dacite association of Grenada, Lesser Antilles island arc, revisited. *Journal of Volcanology and Geothermal Research* 69, 1-33.
- Devine, J.E., Murphy, M.D., Rutherford, M.J., Barclay, J., Sparks, R.S.J., Carroll, M.R., Young, S.R., Gardner, J.E., 1998. Petrologic evidence for pre-eruptive pressure-temperature conditions, and recent reheating of andesitic magma erupting at the Soufriere Hills Volcano, Montserrat, W.I. *Geophysical Research Letters* 25, 3669-3672.
- Donnelly, R.W., Roger, J.J.W., Pushkar, P., Armstrong, R.S., 1971. Chemical evolution of the igneous rocks of the eastern West Indies: an investigation of thorium, uranium and lead and strontium isotopic ratios. *Geological Society of America Memoirs* 130, 81-224.
- Donovan, S.K., 2005. The Geology of Barbados: a field guide. *Caribbean Journal of Earth Sciences* 38, 21-33.
- Dostal, J., Dupuy, C., Carron, J.P., Le Guen de Kerneizon, M., Maury, R.C., 1983. Partition coefficients of trace elements: application to volcanic rocks of St Vincent, West Indies. *Geochimica et Cosmochimica Acta* 47, 525-533.
- Druitt, T.H., Bacon, C.R., 1989. Petrology of the zoned calcalkaline magma chamber of Mount Mazama, Crater Lake, Oregon. *Contributions to Mineralogy and Petrology* 101, 245-259.
- Dufrane, S.A., Turner, S., Dosseto, A., Van Soest, M., 2009. Reappraisal of fluid and sediment contributions to Lesser Antilles magma. *Chemical Geology* 265, 272-278.
- Eiler, M.J., Crawford, A., Elliott, K.A.F., Valley, J.W. and Stolper, E.M., 2000. Oxygen Isotope Geochemistry of Oceanic-Arc Lavas. *Journal of petrology* 41, 229-256.
- Elliott, T., Plank, T., Zindler, A., White, W., Bourdon, B., 1997. *Journal of Geophysical Research* 102, 14991-15019.
- Fujimaki, H., Tatsumoto, M., Aoki, K., 1984. Partition coefficients of Hf, Zr and REE between phenocrysts and groundmasses. *Proceedings of the fourteenth lunar and planetary science conference, Part 2. Journal of Geophysical Research* 89, B662-B672.
- Galer, S.J.G., 1997. Optimal triple spiking for high precision lead isotope ratio determination. *Terra Nova* 9, 441.
- Germa, A., Quidelleur, X., Labanieh, S., Chauvel, C., Lahitte, P., 2011. The volcanic evolution of Martinique Island: Insights from K-Ar dating into the Lesser Antilles arc migration since the Oligocene. *Journal of Volcanology and Geothermal Research* 208, 122-135.

- Geschwind, C.H., Rutherford, M.J., 1992. Cummingtonite and the evolution of the Mount St. Helens (Washington) magma system: An experimental study. *Geology* 20, 1011-1014.
- Gill, J.B., 1981. *Orogenic Andesites and Plate Tectonics*. Springer, New York.
- Ginibre, C., Worner, G., Kronz, A., 2002. Minor- and trace-element zoning in plagioclase: implications for magma chamber processes at Parinacota volcano, northern Chile. *Contributions to Mineralogy and Petrology* 143, 300-315.
- Giunta, G., Beccaluva, L., Siena, F., 2006. Caribbean Plate margin evolution: constraints and current problems. *Geologica Acta* 4, 265-277.
- Goldstein, S.L., Jacobsen, S.B., 1988. Nd and Sr isotopic systematics of river water suspended material: implications for crustal evolution. *Earth and Planetary Science Letters* 87, 249-265.
- Goldstein, S.L., O'Nions, R.K., Hamilton, P.J., 1984. A Sm–Nd isotopic study of atmospheric dusts and particulates from major river systems. *Earth and Planetary Science Letters* 70, 221–236.
- Goldstein, S.L., Arndt, N.T., Stallard, R.F., 1997. The history of a continent from U-Pb ages of zircons from Orinoco River sand and Sm–Nd isotopes in Orinoco basin river sediments. *Chemical Geology* 139, 271-286.
- Green, T.H., Pearson, N.J., 1985. Experimental determination of REE partition coefficients between amphibole and basaltic to andesitic liquids at high pressure. *Geochimica Cosmochimica Acta* 49, 1465-1468.
- Green, T.H., Sie, S.H., Ryan, C.G., Cousens, D.R., 1989. Proton microprobe-determined partitioning of Nb, Ta, Zr, Sr and Y between garnet, clinopyroxene and basaltic magma at high pressure and temperature. *Chemical Geology* 74, 201-216.
- Grove, T.H., Baker, M.B., Kinzler, R.J., 1984. Coupled CaAl–Na–Si diffusion in plagioclase feldspar: Experiments and applications to cooling rate speedometry. *Geochimica et Cosmochimica Acta*, 48, 211-2121.
- Grove, T.L., Elkins-Tanton, L.T., Parman, S.W., Chatterjee, N., Muntener, O., Gaetani, G.A., 2003. Fractional crystallisation and mantle melting controls on calc-alkaline differentiation trends. *Contributions to Mineralogy and Petrology* 145, 515-533.
- Gurenko, A.A., Trumbull, R.B., Thomas, R., Lindsay, J.M., 2005. A melt inclusion record of volatiles, trace elements and Li–B isotope variations in a single magma system from the Plat Pays Volcanic Complex, Dominica, Lesser Antilles. *Journal of Petrology* 12, 24495-2526.

- Hammer, J.E., Rutherford, M.J., 2002. An experimental study of the kinetics of decompression-induced crystallisation in silicic melt. *Journal of Geophysical Research* 107 B1 ECV 8, 1-24.
- Hawkesworth, C.J., Powell, M., 1980. Magma genesis in the Lesser Antilles island arc. *Earth and Planetary Science Letters* 51, 297-308.
- Hawkesworth, C.J., O’Nions, R.K., Arculus, R.J., 1979. Nd and Sr isotope geochemistry of island arc volcanics, Grenada, Lesser Antilles. *Earth and Planetary Science Letters* 45, 237-248.
- Hayes, D.E., et al., 1972. Initial Reports of the Deep Sea Drilling Project 14. U.S. Government Printing Office, Washington.
- Heath, E., Macdonald, R., Belkin, H.E., Hawkesworth, C.J., Sigurdsson, H., 1998. Magmagenesis at the Soufriere St. Vincent Volcano, Lesser Antilles arc. *Journal of Petrology* 39, 1721-1764.
- Hemleben, C., Troester, J., 1984. Campanian–Maestrichtian deep-water foraminifers from Hole 543A, Deep Sea Drilling Project. In: Biju-Duval, B., Moore, J.C. (Eds.), Initial Reports of the Deep Sea Drilling Project 78A. U.S. Government Printing Office, Washington, pp. 509-524.
- Hermann, J., Rubatto, D., 2009. Accessory phase control on the trace element signature of sediment melts in subduction zones. *Chemical Geology* 265, 512-526.
- Horsfield, W.T., 1975. Quaternary Vertical Movements in the Greater Antilles. *Geological Society Bulletin of America* 86, 933-938.
- Huang, F., Lundstrom, C.C., Sigurdsson, H., Zhang, Z., 2011. U-series disequilibria in Kick’em Jenny submarine volcano lavas: A new view of time-scales of magmatism in convergent margins. *Geochimica et Cosmochimica Acta* 75, 195-212.
- Irvine, T.N., Baragar, W.R.A., 1971. A guide to the chemical classification of the common volcanic rocks. *Canadian Journal of Earth Sciences* 8, 523-548.
- Jackson, M. D., Cheadle, M. J., Atherton, M. P., 2003. Quantitative modeling of granitic melt generation and segregation in the continental crust. *Journal of Geophysical Research* 108, article number 2332.
- James, D.E., 1981. The combined used of oxygen and radiogenic isotopes as indicators of crustal contamination. *Annual Review of Earth and Planetary Sciences* 9, 311-344.
- Johnson, M.C., Plank, T., 1999. Dehydration and melting experiments constrain the fate of subducted sediments. *Geochemistry, Geophysics, Geosystems*, doi: 10.1029/1999GC000014.

- Kasper, D.C., Larue, D.K., 1986. Paleogeographic and tectonic implications of quartzose sandstones of Barbados. *Tectonics* 5, 837-854.
- Kent, A.J.R., Darr, C., Koleszar, A.M., Salisbury, M.J., Cooper, K.M., 2010. Preferential eruption of andesitic magmas through recharge filtering. *Nature Geoscience* 3, 631-636.
- Kerr, A. C., White, R.V., Thompson, P.M.E., Tarney, J., Saunders, A.D., 2003. No oceanic plateau-no Caribbean plate? The seminal role of an oceanic plateau in Caribbean plate evolution. In Bartolini, C., Buffler, R.T., Blickwede, J. eds., *The Circum-Gulf of Mexico and the Caribbean: Hydrocarbon habitats, basin formation, and plate tectonics*. AAPG Memoir 79, 126-168.
- Kessel, R., Schmidt M.W., Ulmer, P., Pettke, T., 2005. Trace element signature of subduction-zone fluids, melts and supercritical liquids at 120-180 km depth. *Nature* 437, 724-727.
- Labanieh, S., Chauvel, C., Germa, A., Quidelleur X., Lewin E., 2010. Isotopic hyperbolas constrain sources and processes under the Lesser Antilles arc. *Earth and Planetary Science Letters* 298, 35-46.
- Labanieh, S., Chauvel, C., Germa, A., Quidelleur, X., 2012. Martinique: a clear case for sediment melting and slab dehydration as a function of distance to the trench. *Journal of Petrology* 53, 2441-2464.
- Larue, D.K., Smith, A.L., Schellekens, J.H., 1991. Oceanic island arc stratigraphy in the Caribbean region: don't take it for granite. *Sedimentary Geology* 74, 289-308.
- Leat, P.T., Larter, R.D., 2003. Intra-oceanic subduction systems: introduction. *Geological Society of London* 219, 1-17.
- Le-Guen de Kerneizon, M., Carron, J.P., Bellon, H., Maury, R.C., 1981. Enclaves métamorphiques et plutoniques, provenant du substratum des Petites Antilles, dans les formations volcaniques de l'île de Sainte Lucie. *CR Academie de Science de Paris* 292, 899-902.
- Le-Guen de Kerneizon, M., Bellon, H., Carron, J.P., Maury, R.C., 1983. L'île de Sainte- Lucie (Petites Antilles); distinction des principales series magmatiques a partir des donnees petrochimiques et geochronologiques (Saint Lucia (Lesser Antilles): Distinction of principal magmatic series from petrochemical and geochronologic data). *Bulletin de la Societe Geologique de France* 25, 845-853.
- Lindsay, J.M., 2005. Saint Lucia. In: Lindsay, J.M., Robertson, R., Shepherd, J., Ali, S. (Eds.), *Volcanic Hazard Atlas of the Lesser Antilles*. Trinidad and Tobago. The Seismic Research Unit, University of the West Indies, pp. 218-238.

- Lindsay, J., David, J., Shepherd, J., Ephraim, J., 2002. Volcanic Hazard Assessment for Saint Lucia, Lesser Antilles. Unpublished report presented to the Government of Saint Lucia, August 2002.
- Lindsay, J.M., Trumbull, R.B., Siebel, W., 2005. Geochemistry and petrogenesis of late Pleistocene to Recent volcanism in Southern Dominica, Lesser Antilles. *Journal of Volcanology and Geothermal Research* 148, 253-294.
- Lindsay, J.M., Trumbull, R.B., Schmitt, A.K., Stockli, D.F., Shane, P., Howe, T., 2013. Volcanic stratigraphy and geochemistry of the Soufrière Volcanic Center, Saint Lucia with implications for volcanic hazards. *Journal of Volcanology and Geothermal Research* 258, 126-142.
- Lindsley, D.H., 1983. Pyroxene thermometry. *American Mineralogist* 68, 477-493.
- Lofgren, G.E., 1980. Experimental studies on the dynamic crystallization of silicate melts. In R.B. Hargraves, Ed., *Physics of magmatic processes*, p.487-551. Princeton University Press, Princeton, New Jersey.
- Macdonald, K.C., Holcombe, T.L., 1978. Investigations of magnetic anomalies and sea floor spreading in the Cayman Trough. *Earth and Planetary Science Letters* 40, 407-414.
- Macdonald, R., Hawkesworth, C.J., Heath, E., 2000. The Lesser Antilles volcanic chain: a study in arc magmatism. *Earth-Science Reviews* 49, 1-76.
- Macpherson, C.G., Matthey, D.P., 1998. Oxygen isotope variations in Lau Basin basalts. *Chemical Geology* 144, 177-194.
- Macpherson, C.G., Gamble, J.A., Matthey, D.P., 1998. Oxygen isotope geochemistry of lavas from an oceanic to continental arc transition, kermadec-Hikurangi margin, SW pacific. *Earth and Planetary Science Letters* 160, 609-620.
- Macpherson, C.G., Hall, R., Thirlwall, M.F., 2003. Geochemical evolution of magmatism in an arc-arc collision: the Halmahera and Sangihe arcs, eastern Indonesia. In: Larter, R.D., Leat, P.T. (eds). *Intra-oceanic Subduction Systems: Tectonic and Magmatic Processes*. Geological Society of London 219, 207-220.
- Mahoney, J.B., Weiss, D., Keiffer, B., Friedman, R., Pretorius, W., Scoates, J., Goolaerts, A., Maerschalk, C., 2003. Ongoing isotopic characterization of USGS standards: MC-ICPMS and TIMS data from the Pacific Centre for isotopic and geochemical research, University of British Columbia, Paper 117-118, Geological Society of America 2003, Seattle Annual Meeting.

- Marsh, B.D., 1989. Magma chambers. *Annual Review of Earth and Planetary Sciences* 17, 439-474.
- Martel, C., Pichavant, M., Bourdier, J.-L., Traineau, H., Holtz, F., Scaillet, B., 1998. Magma storage conditions and control of eruption regime in silicic volcanoes: experimental evidence from Mt. Pelee. *Earth and Planetary Science Letters* 156, 89-99.
- Mattey, D., Macpherson, C., 1993. High-precision oxygen isotope microanalysis of ferromagnesian minerals by laser-fluorination. *Chemical Geology* 105, 305-318.
- Mattey, D.P., Lowry, D., Macpherson, C., 1994. Oxygen isotope composition of mantle peridotite. *Earth and Planetary Science Letters* 128, 231-241.
- McCann, W.R., Sykes, L.R., 1984. Subduction of aseismic ridges beneath the Caribbean plate: Implications for the tectonics and seismic potential of the Northeastern Caribbean. *Journal of Geophysical Research* 89, 4493-4519.
- McInnes, B.I.A., McBride, J.S., Evans, N.J., Lambert, D.D., Andrew, A.S., 1999. Osmium Isotope Constraints on Ore Metal Recycling in Subduction zones. *Science* 286, 512.
- McKay, G.A., Weill, D.F., 1977. KREEP petrogenesis revisited, *Proceeding Eight Lunar Science Conference* pp 2339-2355.
- McKenzie, D., 1985. The extraction of magma from the crust and mantle. *Earth and Planetary Science Letters* 74, 81-91.
- McKenzie, D., O’Nions, R.K., 1991. Partial Melt Distributions from Inversion of Rare Earth Element Concentrations. *Journal of Petrology* 32, 1021-1091.
- McLennan, S.M., 2001. Relationships between the trace element composition of sedimentary rocks and upper continental crust. *Geochemistry Geophysics Geosystems* 22000GC000109.
- Moore, J.C., Biju-Duval, B., Bergen, J.A., Blackington, G., Claypool, G.E., Cowan, D.S., Duennebier, F., Guerra, R.T., Hemleben, C.H.J., Hussong, D., Marlow, M.S., Natland, J.H., Pudsey, C.J., Renz, G.W., Tardy, M., Willis, M.E., Wilson, D., Wright, A.A., 1982. Offscraping and underthrusting of sediment at the deformation front of the Barbados Ridge: Deep Sea Drilling Project Leg 78A. *Geological Society of America Bulletin* 93, 1065-1077.
- Muntener, O., Kelemen, P.B., Grove, T.L., 2001. The role of H₂O during crystallization of primitive arc magmas under uppermost mantle conditions and genesis of igneous pyroxenites: an experimental study. *Contributions to Mineralogy and Petrology* 141, 643-658.

- Murphy, M.D., Sparks, R.S.J., Barclay, J., Carroll, M.R., Lejeune, A.-M., Brewer, T.S., Macdonald, R., Black, S., Young, S., 1998. The role of magma mixing in triggering the current eruption at the Soufriere Hills Volcano, Montserrat, West Indies. *Geophysical Research Letters* 25, 3433-3436.
- Nakamura, M., Shimakita, S., 1998. Dissolution origin and syn-entrapment compositional changes of melt inclusions in plagioclase. *Earth and Planetary Sciences Letter* 161, 119-133.
- Nash, W.P., Crecraft, H.R., 1985. Partition coefficients for trace elements in silicic magmas. *Geochimica et Cosmochimica Acta* 49, 2309-2322.
- Nelson, S.T., Montana, A., 1992. Sieve-textured plagioclases in volcanic rocks produced by rapid decompression. *American Mineralogist* 77, 1242-1249.
- Nimis, P., Taylor, W.R., 2000. Single clinopyroxene thermobarometry for garnet peridotites. Part I. Calibration and testing of a Cr-in-Cpx barometer and an enstatite-in Cpx thermometer. *Contributions to Mineralogy and Petrology* 139, 541-554.
- Nowell, G., Parrish, R.R., 2001. Simultaneous acquisition of isotope compositions and parent/daughter ratios by non-isotope dilution solution-mode plasma ionisation multi-collector mass spectrometry (PIMMS). In: *Plasma Source Mass Spectrometry: The New Millennium*. Royal Geological Society of London 267, 305 pp.
- Nowell, G.M., Kempton, P.D., Noble, S.R., Fitton, J.G., Saunders, A.D., Mahoney, J.J., Taylor, R.N., 1998. High precision Hf isotope measurements of MORB and OIB by thermal ionisation mass spectrometry: insights into the depleted mantle. *Chemical Geology* 149, 211-233.
- Nowell, G.M., Luguet, A., Pearson, D.G., Horstwood, M.S.A., 2008. Precise and accurate $^{186}\text{Os}/^{188}\text{Os}$ and $^{187}\text{Os}/^{188}\text{Os}$ measurements by multi-collector plasma ionisation mass spectrometry (MC-ICP-MS) part I: Solution analyses. *Chemical Geology* 248, 363-393.
- O'Nions, R.K., Frank, M., Von Blanckenburg, F., Ling, H.F., 1998. Secular variation of Nd and Pb isotopes in ferromanganese crusts from the Atlantic, Indian and Pacific oceans. *Earth and Planetary Science Letters* 155, 15-28.
- Ottley, C.J., Pearson, D.G., Irvine, G.J., 2003. A routine method for the dissolution of geological samples for the analysis of REE and trace elements via ICP-MS. *Plasma Source Mass Spectrometry*. Special Publication of the Royal Society of Chemistry, pp 221-230.

- Parkinson, J.J., Hawkesworth, C.J., Cohen, A.S., 1998a. Ancient mantle in a modern arc: osmium isotopes in Izu-Bonin-Mariana forearc peridotites. *Science* 281, 2011-2013.
- Parra, M., Faugères, J.C., Grousset, F., Pujol, C., 1997. Sr-Nd isotopes as tracers of finegrained detrital sediments: the south-Barbados accretionary prism during the last 150 kyr. *Marine Geology* 136, 225-243.
- Paster, T.P., Schauwecker, D.S., Haskin, L.A., 1974. The behaviour of some trace elements during solidification of the Skaergaard layered series. *Geochimica et Cosmochimica Acta* 38, 1549-1577.
- Pearce, J.A., Peate, D.W., 1995. Tectonic implications of the composition of volcanic arc magmas. *Annual Review of Earth and Planetary Sciences* 23, 251-285.
- Peate, D.W., Pearce, J.A., Hawkesworth, C.J., Colley, H., Edwards, C.M.H., Hirose, K., 1997. *Journal of petrology* 38, 1331-1358.
- Peck, W.H., Valley, J.W., Graham, C.M., 2003. Slow oxygen diffusion rates in igneous zircons from metamorphic rocks. *American Mineralogist* 88, 1003-1014.
- Pichavant, M., Mysen, B.O., Macdonald, R., 2002a. Source and H₂O content of high-MgO magmas in island arc settings: An experimental study of a primitive calc-alkaline basalt from St. Vincent, Lesser Antilles arc. *Geochimica et Cosmochimica Acta* 66, 2193-2209.
- Pichavant, M., Martel, C., Bourdier, J. L., Scaillet, B., 2002b. Physical conditions, structure, and dynamics of a zoned magma chamber: Mount Pelee (Martinique, Lesser Antilles Arc). *Journal of Geophysical Research* 107, doi: 10.1029/2001JB000315.
- Pin, C., Francisco, J., Zalduegui, S., 1997. Sequential separation of light rare-earth elements, thorium and uranium by miniaturized extraction chromatography: Application to isotopic analyses of silicate rocks. *Analytica Chimica Acta* 339, 79-89.
- Pindell, J.L., 1993. Regional synopsis of Gulf of Mexico and Caribbean evolution. In Pindell, J.L., and Perkins, R.F., eds., *Trans. 13th Annu. GCSSEPM Res. Conference*, Houston, TX, 251-274.
- Pindell, J.L., Kennan, L., Stanek, K.P., Maresch, W.V., Draper, G., 2006. Foundations of Gulf of Mexico and Caribbean evolution: Eight controversies resolved. *Geologica Acta* 4, 89-128.
- Plank, T., Langmuir, C.H., 1998. The chemical composition of subducting sediment and its consequences for the crust and mantle. *Chemical Geology* 145, 325-394.

- Plank, T., Kelley, K.A., Zimmer, M.M., Haury, E.H., Wallace, P.J., 2013. Why do mafic arc magmas contain ~4 wt% water on average? *Earth and Planetary Science Letters* 364, 168-179.
- Prouteau, G., Scaillet, B., 2003. Experimental constraints on the origin of the 1991 Pinatubo dacite. *Journal of Petrology* 44, 2203-2241.
- Pudsey, C.J., Reading, H.G., 1982. Sedimentology and structure of the Scotland group, Barbados. Geological Society of London, Special Publication 10, 291-308.
- Pushkar, P., Steuber, A.M., Tomblin, J.F., Julian, G.M., 1973. Strontium isotopic ratios in volcanic rocks from St Vincent and St Lucia, Lesser Antilles. *Journal of Geophysical Research* 78, 1279-1287.
- Ridolfi, F., Renzulli, A., Puerini, M., 2010. Stability and chemical equilibrium of amphibole in calc-alkaline magmas: an overview, new thermobarometric formulations and application to subduction-related volcanoes. *Contributions to Mineralogy and Petrology* 160, 45-66.
- Righter, K., Chesley, J.T., Ruiz, J., 2002. Genesis of primitive, arc type basalt: Constraints from Re, Os, and Cl on the depth of melting and role of fluids. *Geology* 30, 619-622.
- Roobol, M.J., Wright, J.V., Smith, A.L., 1983. Calderas or gravity slide structures in the Lesser Antilles island arc? *Journal of Volcanology and Geothermal Research* 19, 121-134.
- Royse, K., Kempton, P., Darbyshire, D.P.F. 1998. Procedure for the analysis for Rubidium-Strontium and Samarium-Neodymium isotopes at the NERC Isotope Geosciences Laboratory. NERC Isotope Geoscience Laboratory Report Series 121.
- Rudnick, R.L., Fountain, D.M., 1995. Nature and composition of the continental crust: a lower crustal perspective. *Review in Geophysics* 33, 267-309.
- Rudnick, R., Walker, R.J., 2009. Interpreting ages from Re-Os isotopes in peridotites. *Lithos* 102S, 1083-1095.
- Saal, A.E., Rudnick, R.L., Ravizza, G.E., Hart, S.R., 1998. Re-Os isotope evidence for the composition, formation and age of the lower continental crust. *Letters to Nature* 393, 58-61.
- Salters, V.J.M., Longhi, J., 1999. Trace element partitioning during the initial stages of melting beneath mid-ocean ridges. *Earth and Planetary Science Letters* 166, 15-30.
- Samper, A., Quidelleur, X., Boudon, G., Le Friant, A., Komorowski, J.C., 2008. Radiometric dating of three large volume flank collapses in the Lesser

- Antilles Arc. *Journal of Volcanology and Geothermal Research* 176, 485-492.
- Schmitt, A.K., Stockli, D.F., Lindsay, J.M., Robertson, R., Lovera, O.M., Kislitsyn, R., 2010. Episodic growth and homogenization of plutonic roots in arc volcanoes from combined U-Th and (U-Th)/He zircon dating. *Earth and Planetary Science Letters* 295, 91-103.
- Schuth, S., Rohrbach, A., Munker, C., Ballaus, C., Garbe-Schonberg, D., Qopoto, C., 2004. Geochemical constraints on the petrogenesis of arc picrites and basalts, New Georgia Group, Solomon Islands. *Contributions to Mineralogy and Petrology* 148, 288-304.
- Selby, D., Creaser, R.A., 2003. Re-Os geochronology of organic rich sediments: an evaluation of organic matter analysis methods. *Chemical Geology* 200, 225-240.
- Senda, R., Tanaka, T., Suzuki, K., 2007. Os, Nd and Sr isotopic and chemical compositions of ultramafic xenoliths from Kurose, SW Japan: Implications for contribution of slab-derived material to wedge mantle. *Lithos* 95, 229-242.
- Sharp, Z.D., 1990. A laser-based microanalytical method for the in situ determination of oxygen isotope ratios in silicates and oxides. *Geochimica et Cosmochimica Acta* 54, 1353-1357.
- Sherman, S. B., 1992. Geochemistry and petrogenesis of Saba, Lesser Antilles. MSc thesis, University of South Florida, Tampa, pp 114.
- Singer, B.S., Dungan, M.A., Layne, G., 1995. Textures and Sr, Ba, Mg, Fe, K and Ti compositional profiles in volcanic plagioclase: Clues to the dynamics of calc-alkaline magma chambers. *American Mineralogist* 80, 776-798.
- Smith, A.L., Roobol, M.J., 1990. Mt. Pelee, Martinique: a study of an active island-arc volcano. *Geological Society of America Memoirs* 175, 105.
- Smith, T.E., Thirlwall, M.F., Macpherson, C., 1996. Trace element and Isotope Geochemistry of the Volcanic Rocks of Bequia, Grenadine Islands, Lesser Antilles Arc: a Study of Subduction Enrichment and Intra-crustal Contamination. *Journal of Petrology* 37, 117-143.
- Speed, R.C., Walker, J.A., 1991. Oceanic-crust of the Grenada Basin in the southern Lesser Antilles arc platform. *Journal of Geophysical Research-Solid Earth Planets* 96, 3835-3851.
- Stormer, J.C., Nicholls, J., 1978. XLFRAC; a program for the interactive testing of magmatic differentiation models. *Computer Geosciences* 4, 143-159.

- Sun, S.S., McDonough, W., 1989. Chemical and isotopic systematics of ocean arc basalts: implications for mantle composition and processes. In: Saunders, A. D., Norry, M. J. (ed) *Magmatism in the Ocean Basins*. Geological Society of London Special Publication 42, pp 313-345.
- Suzuki, K., Senda, R., Shimizu, K., 2011. Osmium behaviour in a subduction system elucidated from chromian spinel in Bonin Island beach sands. *Geology* 39, 999-1002.
- Tatsumi, Y., Eggins, S., 1995. *Subduction Zone Magmatism*. Oxford: Blackwell Scientific.
- Thirlwall, M.F., 1991. Long-term reproducibility of multicollector Sr and Nd isotope ratio analysis. *Chemical Geology* 94, 85-104.
- Thirlwall, M.F., Graham, A.M., 1984. Evolution of high-Ca, high-Sr C-series basalts from Grenada, Lesser Antilles: the effects of intra-crustal contamination. *Journal of the Geological Society of London* 141, 427-445.
- Thirlwall, M.F., Graham, A.M., Arculus, R.J., Harmon, R.S., Macpherson, C.G., 1996. Resolution of the effects of crustal contamination, sediment subduction, and fluid transport in island arc magmas: Pb-Sr-Nd-O isotope geochemistry of Grenada, Lesser Antilles. *Geochimica et Cosmochimica Acta* 60, 4785-4810.
- Tollan, P.M.E., Bindeman, I., Blundy, J.D., 2012. Cumulate xenoliths from St. Vincent, Lesser Antilles Island Arc: a window into upper crustal differentiation of mantle-derived basalts. *Contributions to Mineralogy and Petrology* 163, 189-208.
- Tomblin, J.F., 1964. The volcanic history and petrology of the Soufrière region, St. Lucia. PhD Thesis, University of Oxford.
- Toothill, J., Williams, C.A., Macdonald, R., Turner, S.P., Rogers, N.W., Hawkesworth, C.J., Jerram, D.A., Ottley, C.J., Tindle, A.G., 2007. A complex petrogenesis for an arc magmatic suite, St Kitts, Lesser Antilles. *Journal of Petrology* 48, 3-42.
- Torrini Jr, R., Speed, R.C., 1989. Tectonic wedging in the forearc basin: Accretionary prism transition, Lesser Antilles forearc. *Journal of Geophysical Research* 94, 10549-10584.
- Turgeon, S., Creaser, R.A., 2008. Cretaceous oceanic anoxic event 2 triggered by a massive magmatic episode. *Nature* 454, 323-326.
- Turner, S., Hawkesworth, C., Van Calsteren, P., Heath, E., Macdonald, R., Black, S., 1996. U-series isotopes and destructive plate margin magma genesis in the Lesser Antilles. *Earth and Planetary Science Letters* 142, 191-207.

- Turner, S., Handler, M., Bindeman, I., Suzuki, K., 2009. New insights into the origin of O-Hf-Os isotope signatures in arc lavas from Tonga-Kermadec. *Chemical Geology* 266, 187-193.
- Valley, J.W., 2003. Oxygen isotopes in zircon. *Reviews in mineralogy and geochemistry* 53, 343-385.
- Valley, J.W., Kitchen, N., Kohn, M.J., Niendorf, C.R., Spicuzza, 1995. UWG-2, a garnet standard for oxygen isotope ratios: Strategies for high precision and accuracy with laser heating. *Geochimica et Cosmochimica Acta* 59, 5223-5231.
- Van Soest, M.C., 2000. Sediment Subduction and Crustal Contamination in the Lesser Antilles Island Arc. PhD thesis, University of Vrije, Amsterdam, pp 287.
- Van Soest, M.C., Hilton, D.R., Macpherson, C.G., Matthey, D.P., 2002. Resolving sediment subduction and crustal contamination in the Lesser Antilles arc: a combined He-O-Sr Isotope approach. *Journal Petrology* 43, 143-170.
- Vidal, P., Le Guen de Kerneizon, M., Maury, R.C., Dupre, B., White, W.M., 1991. Large role of sediments in the genesis of some Lesser Antilles andesites and dacites (Soufriere, St Lucia): isotopic constraints. *Bulletin de la Societe Geologique de France* 162, 993-1002.
- Volkening, J., Walczyk, T., Heumann, K.G., 1991. Osmium isotope ratio determinations by negative thermal ionization mass spectrometry. *Internal Journal of Mass Spectrometry and Ion Processes* 105, 147-159.
- Von Huene, R., Scholl, D.W., 1991. Observations at convergent margins concerning sediment subduction, subduction erosion, and growth of the continental crust. *Reviews of Geophysics*, 29, 279-316.
- Wadge, G., Shepherd, J.B., 1984. Segmentation of the Lesser Antilles subduction zone. *Earth and Planetary Science Letters* 71, 297-304.
- Watson, E.B., Cherniak D.J., 1997. Oxygen diffusion in zircon. *Earth and Planetary Science Letters* 148, 527-544.
- Weis, D., Kieffer, B., Hanano, D., Silva, I.N., Barling, J., Pretorius, W., Maerschalk, C., Mattielli, 2007. Hf isotope composition of U.S. Geological Survey reference materials. *Geochemistry, Geophysics, Geosystems* 8, Q06006.
- Westbrook, G.K., Smith, M.J., 1983. Long décollements and mud volcanoes: evidence from the Barbados Ridge Complex for the role of high pore-fluid pressure in the development of an accretionary complex. *Geology* 11, 279-283.

- Westbrook, G.K., Smith, M.J., Peacock, J.H., Poulter, M.J., 1982. Extensive underthrusting of undeformed sediment beneath the accretionary complex of the Lesser Antilles subduction zone. *Nature* 300, 625-628.
- Westercamp, D., Tomblin, J.F., 1979. Le volcanisme recent et les eruptions historiques dans la partie centrale de l'arc insulaire des Petites Antilles. *Bulletin du Bureau de Recherche Geologiques et Minieres* 3-4, 293-319.
- White, W.M., Patchett, P.J., 1984. Hf-Nd-Sr isotopes and incompatible element abundances in island arcs: implications for magma origins and crust-mantle evolution. *Earth and Planetary Science Letters* 67, 167-185.
- White, W.M., Dupré, B., Vidal, P., 1985. Isotope and trace element geochemistry of sediments from the Barbados Ridge-Demerara Plain region, Atlantic Ocean. *Geochimica et Cosmochimica Acta* 49, 1875-1886.
- White, W.M., Dupré, B., 1986. Sediment Subduction and Magma Genesis in the Lesser Antilles: Isotopic and Trace Element Constraints. *Journal of Geophysical Research* 91, 5927-5941.
- Widom, E., Kepezhinskas, P., Defant, M., 2003. The nature of metasomatism in the sub-arc mantle wedge: evidence from Re-Os isotopes in Kamchatka peridotite xenoliths. *Chemical Geology* 196, 283-306.
- Wohletz, K., Heiken, G., Ander, M., Goff, F., Vuataz, F.D., Wadge, G., 1986. The Qualibou Caldera, St. Lucia, West Indies. *Journal of Volcanology and Geothermal Research* 27, 77-115.
- Woodhead, J., Brauns, M., 2004. Current limitations to the understanding of Re-Os behaviour in subduction systems, with an exemple from New Britain. *Earth and Planetary Science Letters* 221, 309-323.
- Woodhead, J.D., Eggins, S.M., Johnson, R.W., 1998. Magma genesis in the New Britain island arc: further insights into melting and mass transfer processes. *Journal of Petrology* 39, 1641-1668.
- Woodland, S.J., Pearson, D.G., Thirlwall, M.F., 2002. A Platinum Group Element and Re-Os Isotope Investigation of Siderophile Element Recycling in Subduction Zones: Comparison of Grenada, Lesser Antilles Arc, and the Izu-Bonin Arc. *Journal of Petrology* 43, 171-198.
- Workman, R.K., Hart, S.R., 2005. Major and trace element composition of the depleted MORB mantle (DMM). *Earth and Planetary Science Letters* 231, 53-72.
- Wright, J.V., Roobol, M.J., Smith, A.L., Sparks, R.S.J., Brazier, S.A., Rose Jr., W.I., Sigurdsson, H., 1984. Late Quaternary explosive silicic volcanism on St. Lucia, West Indies. *Geological Magazine* 121, 1-15.

- Xiong, Y., Wood, S.A., 1999. Experimental determination of the solubility of ReOs and the dominant oxidation state of rhenium in hydrothermal systems. *Chemical Geology* 158, 245-256.
- Xiong, Y., Wood, S.A., 2000. Experimental quantification of hydrothermal solubility of platinum group elements with special reference to porphyry copper environments. *Mineralogy and Petrology* 68, 1-28.
- Yogodzinsky, G.M., Kelemen, P.B., 1998. Slab melting in the Aleutians: implications of an ion probe study of clinopyroxene in primitive adakite and basalt. *Earth and Planetary Science Letters* 158, 53-65.
- Ysaccis, R., 1997. Tertiary evolution of the northeastern Venezuela offshore. Ph.D. thesis, Rice University, Houston. 285 pp.
- Zack, T., Brumm, R., 1998. Ilmenite/liquid partition coefficients of 26 trace elements determined through ilmenite/clinopyroxene partitioning in garnet pyroxenites. Seventh International Kimberlite Conference, Cape Town, pp. 986-988.
- Zheng, Y.F., Fu, B., 1998. Estimation of oxygen diffusivity from anion porosity in minerals. *Geochemical Journal* 32, 71-89.

Appendix A

Name, type and location of the
samples analysed

Content

Table A.1. List of St Lucia samples and their location. 263

Table A.2. List of the samples analysed for Os isotopes. 264

All whole rock, mineral and in-situ analysis of St Lucia lavas presented in this thesis were carried on the samples listed in Table A1. The list of samples from other islands of the arc and from the subducting slab analysed for their Os isotopic composition are presented in Table A.2.

Table A.1. List of St Lucia samples and their location

Sample name	Composition Group	Eruption age group	Latitude	Longitude	Location	Rock type	Lithology
SL-83-03	SVC	2?	13°50'23.30"N	61°01'18.30"W	St philip dacite dome	Lava	Dacite
SL-83-08	SVC	3	13°49'13.80"N	61°02'21.70"W	Belfond dacite dome	Lava	Dacite
SL-83-12	SVC	?	13°49'21.80"N	61°03'4.50"W	Plaisance piton dome	Lava	Dacite
S-L83-15	SVC	1?	13°50'53.67"N	61°03'38.87"W	Coubaril dark andesite dome	Lava	Andesite
SL-83-16	SVC	3	13°50'16.75"N	61°02'3907"W	Terre Blanche dacite dome	Lava	Dacite
SL-83-17	SVC	1?	13°48'47.20"N	61°03'8.30"W	Fond doux piton dome	Lava	Andesite
SL-83-19	SVC	2	13°48'1.63"N	61°04'4.97"W	Gros piton dome	Lava	Dacite
SL-83-24	SVC	2	13°49'55.94"N	61°04'5.89"W	Petit piton dome	Lava	Dacite
SL-JL-02	SVC	1	13°51'51.41"N	61°02'17.50"W	Morne Tabac	Lava	Andesite
SL-JL-22	SVC	3	13°50'39.5"N	61°02'07.1"W	Terre Blanche dacite dome	Lava	Low-silica dacite
SL-JL-23	SVC	1	13°49'45.7"N	61°01'51.3"W	Morne Bonin dome	Lava	Low-silica dacite
SL-JL-24	SVC	3	13°50'15.1"N	61°01'09.9"W	Near Migny	Pumice	Dacite
SL-JL-33	SVC	2	13°47'17.3"	61°03'47.95"W	Near La Pointe	Pumice	Dacite
SL-JL-51	SVC	3	13°49'13.80"N	61°02'21.70"W	Belfond bloc & ash flow	Lava	Dacite
SL-JL-57	SVC	1	13°48'6.10"N	61°02'12.80"W	Near Dugard	Pumice	Dacite
SL-JL-61	SVC	3	13°50'15.1"N	61°01'09.9"W	Near Migny (same as JL-24)	Pumice	Dacite
SL-JL-79	SVC	2	13°46'45.3"	61°03'12.3"W	Anse John Beach	Pumice	Dacite
SL-JL-83	SVC	2	13°49'04.0"N	61°04'03.3"W	Gros Piton dome	Lava	Dacite
SL-JL-84	SVC	2	13°50'20.9"N	61°03'52.6"W	Petit Piton dome	Lava	Low-silica dacite
SL-83-26	Pre-SVC2		13°45'7.74"N	60°59'23.56"W	East of Laborie	Lava	Basaltic andesite
SL-83-38	Pre-SVC2		13°45'39.00"N	60°56'1.89"W	NE of Vieux Fort	Lava	Basaltic andesite
SL-83-39	Pre-SVC2		13°44'32.72"N	60°56'43.9"W	NE of Vieux Fort	Lava	Low-silica andesite
SL-83-23	Pre-SVC1		13°50'46.45"N	61°03'46.81"W	Basalt flow, Soufriere Bay	Lava	Basaltic andesite
SL-83-25	Pre-SVC1		13°50'4.30"N	61°03'29.7"W	Basalt flow, Anse des Pitons	Lava	Basaltic andesite
SL-83-30	Pre-SVC1		13°50'24.70"N	61°01'3.40"W	Basalt flow	Lava	Basaltic andesite
SL-83-32	Pre-SVC1		14°1'1.57"N	60°59'55.83"W	NW of Castries	Lava	Low-silica andesite
SL-83-40	Pre-SVC1		13°43'6.39"N	60°57'2.92"W	S of Vieux Fort	Lava	Basaltic andesite
SL-83-41	Pre-SVC1		14°4'21.02"N	60°57'45.54"W	SW of Gros Islets	Lava	High-silica andesite
SL-83-42	Pre-SVC1		14°5'31.23"N	60°57'9.15"W	NW of Gros Islets	Lava	Basalt
SL-83-44	Pre-SVC1		14°6'3.84"N	60°55'7.18"W	basalt flow	Lava	Basalt
SL-83-45	Pre-SVC1		14°1'25.89"N	60°58'26.56"W	NE of Castries	Lava	Rhyolite

SVC = Soufriere Volcanic Complex; Age groups correspond to eruption periods of the SVC determined by Schmitt et al. (2010) and Lindsay et al. (2013) using (U-Th)/He zircon dating.

Table A.2. List of samples analysed for their Os isotopic composition. It comprises Lesser Antilles lavas from along the arc and an altered basalt and sediments from the subducting slab.

Sample name	Location	Age (ka)	Rock type	Lithology
<u>Lavas</u>				
LAS1	Saba	<10	lava	Basalt
R8204	Redonda	1000	lava	Basalt
GUAD510	Guadeloupe	500	lava	Basalt
M8328	Martinique	<1000	lava	Basaltic andesite
SL-83-44	St Lucia	11400	lava	Basalt
STV301	St Vincent	180	lava	Basalt
STV324	St Vincent	<3.6	lava	Basalt
LAG4	Grenada	<10	lava	Picrite
543A-15-3 piece 2A	DSDP site 543	—	Altered lava	Basalt
<u>Sediment</u>				
78A-543-17-3-120-124	Site DSDP 546	16000	sediment	organic-poor
14-144Z-4-2 interval 60-64	Site DSDP 144	93000	sediment	organic-rich
14-144Z-4-2 interval 143-146	Site DSDP 144	93000	sediment	organic-rich
14-144Z-4-3 interval 31-33	Site DSDP 144	93000	sediment	organic-rich
14-144Z-4-3 interval 100-103	Site DSDP 144	93000	sediment	organic-rich
14-144Z-5-1 interval 5-6	Site DSDP 144	98000	sediment	organic-rich
14-144Z-5-1 interval 143-143	Site DSDP 144	98000	sediment	organic-rich
14-144Z-7-1 interval 136-137	Site DSDP 144	106000	sediment	organic-rich
14-144Z-7-1 interval 123-124	Site DSDP 144	106000	sediment	organic-rich
14-144Z-8-3 interval 136-137	Site DSDP 144	113000	sediment	organic-rich
14-144A-5-1 interval 123-124	Site DSDP 144	85000	sediment	organic-rich
14-144A-6-1 interval 70-110	Site DSDP 144	89000	sediment	organic-rich

Appendix B

Supplementary data file
of Chapter 3

Content

Table B.1. Details of the analyses of international standard solutions NBS981 obtained during Sr isotope analyses of St Lucia lavas on the MC-ICPMS at the Durham Geochemistry Centre (DGC) and at the Geochemical Analysis Unit (GAU) of Macquarie University.	267
Table B.2. Details of the analyses of standard solutions obtained during Nd isotope analyses of St Lucia lavas. In house J & M and J & M doped solutions were analysed at DGC during analyses on the MC-ICPMS and international standard NBS987 was analysed at the GAU.	268
Table B.3. Details of the analyses of the international standard solution NBS981 obtained on the MC-ICPMS at DGC during Pb isotope analyses of St Lucia lavas.	269
Table B.4. Details of the analyses of blanks and international standard solutions NBS981 obtained during Sr isotope analyses of single plagioclase crystals at DGC.	270
Table B.5. Details of the analyses of international and in-house standards obtained during single mineral $\delta^{18}\text{O}$ analyses by laser-fluorination at East Kilbride (NERC facilities).	270

Table B.1. Details of the analyses of international standard solutions NBS981 obtained during Sr isotope analyses of St Lucia lavas on the MC-ICPMS at Durham Geochemistry Centre (DGC) and at the Geochemical Analysis Unit (GAU) of Macquarie University.

MC-ICPMS at DGC NBS987		TIMS at the GAU NBS987	
⁸⁷ Sr/ ⁸⁶ Sr	2 SE	⁸⁷ Sr/ ⁸⁶ Sr	2 SE
0.710272	0.000009	0.710211	0.000006
0.710264	0.000009	0.710210	0.000006
0.710267	0.000009	0.710231	0.000006
0.710269	0.000008	0.710229	0.000006
0.710279	0.000009		
0.710284	0.000009	Average:	0.710220
0.710261	0.000008	2 sd:	0.000023
0.710260	0.000010		
0.710270	0.000010		
0.710263	0.000010		
0.710273	0.000009		
0.710273	0.000009		
0.710285	0.000012		
Average:	0.710271		
2 sd:	0.000016		

Table B.2. Details of the analyses of standard solutions obtained during Nd isotope analyses of St Lucia lavas. In house J & M and J & M doped solutions were analysed at DGC during analyses on the MC-ICPMS and international standard NBS987 was analysed at the GAU.

MC-ICPMS at DGC			TIMS at the GAU		
J & M			JMC 321		
$^{143}\text{Nd}/^{144}\text{Nd}$	2 SE		$^{143}\text{Nd}/^{144}\text{Nd}$	2 SE	
0.511100	0.000009		0.511120	0.000007	
0.511101	0.000008		0.511122	0.000020	
0.511104	0.000009		0.511127	0.000023	
0.511102	0.000010				
0.511108	0.000008				
0.511103	0.000007	Average: 2 sd	0.511123		
0.511103	0.000007		0.000007		
0.511104	0.000007				
Average	0.511103				
2 sd	0.000005				
MC-ICPMS at DGC					
J & M doped					
$^{143}\text{Nd}/^{144}\text{Nd}$	2 SE				
0.511101	0.000010				
0.511099	0.000008				
0.511107	0.000009				
0.511112	0.000007				
0.511114	0.000007				
0.511107	0.000006				
0.511116	0.000008				
Average	0.511108				
2 sd	0.000013				

Table B.3. Details of the analyses of the international standard solution NBS981 obtained on the MC-ICPMS at DGC during Pb isotope analyses of St Lucia lavas.

MC-ICPMS at DGC					
NBS981					
$^{206}\text{Pb}/^{204}\text{Pb}$	2 SE	$^{207}\text{Pb}/^{204}\text{Pb}$	2 SE	$^{208}\text{Pb}/^{204}\text{Pb}$	2 SE
16.94051	0.00059	15.49776	0.00079	36.71598	0.00318
16.93939	0.00083	15.49624	0.00097	36.71084	0.00335
16.93986	0.00064	15.49691	0.00087	36.71362	0.00325
16.93967	0.00079	15.49657	0.00078	36.71541	0.00367
16.93951	0.00088	15.49643	0.00075	36.71252	0.00254
16.93980	0.00085	15.49637	0.00093	36.71312	0.00379
16.94045	0.00066	15.49681	0.00075	36.71419	0.00372
16.94177	0.00075	15.49675	0.00080	36.71339	0.00340
16.94276	0.00065	15.49712	0.00067	36.71544	0.00328
16.94221	0.00080	15.49664	0.00080	36.71323	0.00238
16.94421	0.00075	15.49782	0.00079	36.71742	0.00315
16.93984	0.00065	15.49705	0.00068	36.71424	0.00270
16.93981	0.00082	15.49705	0.00096	36.71569	0.00323
16.94078	0.00079	15.49781	0.00081	36.71648	0.00259
16.94171	0.00067	15.49796	0.00073	36.71861	0.00320
16.94092	0.00055	15.49762	0.00070	36.71631	0.00258
16.94069	0.00055	15.49789	0.00068	36.71705	0.00200
16.94120	0.00061	15.49807	0.00064	36.71764	0.00188
16.94092	0.00063	15.49807	0.00065	36.71795	0.00186
16.94098	0.00054	15.49787	0.00064	36.71643	0.00248
16.93994	0.00058	15.49702	0.00065	36.71454	0.00246
16.93990	0.00057	15.49708	0.00067	36.71412	0.00234
16.93988	0.00052	15.49652	0.00065	36.71311	0.00291
16.93942	0.00070	15.49634	0.00076	36.71367	0.00361
Average	16.94067	15.49716		36.71504	
2 sd	0.00237	0.00124		0.00393	

Table B.4. Details of the analyses of blanks and international standard solutions NBS981 obtained during Sr isotope analyses of single plagioclase crystals at DGC.

DGC micro-Sr NBS987 (12 ng Sr)		DGC micro-Sr Blank	
$^{87}\text{Sr}/^{86}\text{Sr}$	2 SE	Sr (pg)	%age of smallest sample (~66 ng)
0.710239	0.000007	18	0.03
0.710248	0.000007	32	0.05
0.710243	0.000007		
Average	0.710243	Average	25
2 sd	0.000009		

Table B.5. Details of the analyses of international and in-house standards obtained during single mineral $\delta^{18}\text{O}$ analyses by laser-fluorination at East Kilbride (NERC facilities).

Period 1 March 2012 $\delta^{18}\text{O}$ VSMOW			Period 2 (November 2012) $\delta^{18}\text{O}$ VSMOW		
SES (Quartz)	GP147 (Garnet)	UWG2 (Garnet)	SES (Quartz)	GP147 (Garnet)	UWG2 (Garnet)
10.9	7.0	5.8	10.4	7.0	5.9
10.9	7.3	5.7	10.0	7.3	5.8
10.3	7.4	5.6	10.2		
10.5		5.8	10.2		
10.1		5.3	10.1		
10.3		5.6	10.2		
9.9		5.7			
10.4		5.4	10.2	7.2	5.9
10.3		5.8	0.3	0.4	0.2
		5.6			
		5.8			
Average	10.4	7.2	5.7		
2 sd	0.6	0.4	0.3		

Appendix C

Supplementary data file
of chapter 4

Content

Table C.1. Details of the analyses of the international standard solution JMC 475 obtained during $^{176}\text{Hf}/^{177}\text{Hf}$ analyses of St Lucia lavas by MC-ICPMS at DGC and by TIMS at the GAU.	273
Table C.2. Details of the composition of international rock standards BHVO-1, BHVO-2, BIR-1, NBS 688, BCR-2, AGV-1 and W2 obtained during trace element analyses of St Lucia lavas at both DGC and the GAU.	274
Table C.3. Assimilation during Fractional Crystallization (AFC) models with assimilant “minimum” isotopic composition allowing to model the most extreme SVC lava compositions with ~15% fraction of melt remaining (F) in agreement with the least squares models.	277
Table C.4. Assimilation during Fractional Crystallization (AFC) models with assimilant “minimum” isotopic composition allowing to model the most extreme SVC lava compositions with ~ 55% fraction of melt remaining (F).	281
Table C.5. Bulk sediment composition at DSDP sites 543 and 144 and Barbados and partition coefficients used to calculate sediment melt compositions.	285
Table C.6. Composition of the most mafic lavas presented in Fig. 11.	286

Table C.1. Details of the analyses of the international standard solution JMC 475 obtained during $^{176}\text{Hf}/^{177}\text{Hf}$ analyses of St Lucia lavas by MC-ICPMS at DGC and by TIMS at the GAU.

MC-ICPMS at DGC JMC 475			TIMS at the GAU JMC 475	
$^{176}\text{Hf}/^{177}\text{Hf}$	2 SE		$^{176}\text{Hf}/^{177}\text{Hf}$	2 SE
0.282142	0.000009		0.282170	0.000007
0.282140	0.000007		0.282156	0.000005
0.282146	0.000008		0.282141	0.000007
0.282142	0.000007		0.282180	0.000007
0.282145	0.000006			
0.282150	0.000007	Average 2 sd	0.282162	
0.282148	0.000006		0.000034	
0.282141	0.000006			
0.282145	0.000005			
0.282142	0.000006			
Average	0.282144			
2 sd	0.000006			

Table C.2. Details of the composition of international rock standards BHVO-1, BHVO-2, BIR-1, NBS 688, BCR-2, AGV-1 and W2 obtained during trace element analyses of St Lucia lavas at both DGC and the GAU. Concentrations are reported in ppm unless stated otherwise.

BHVO-2			
GAU powder digestion (n=3):			
	Accepted value:	This study	1sd
Ti (wt. %)	2.72	2.84	0.03
V	317	320	5
Ga	22.00	21.11	0.24
Rb	9.11	9.64	0.04
Sr	396	387	3
Y	26.00	28.36	0.19
Zr	172	179	2
Nb	18.10	18.73	0.32
Ba	131	130	0
La	15.20	15.35	0.15
Ce	37.50	37.02	0.32
Pr	5.35	5.44	0.04
Nd	24.50	24.10	0.27
Sm	6.07	6.11	0.07
Eu	2.07	2.00	0.03
Tb	0.92	0.96	0.02
Gd	6.24	6.27	0.11
Dy	5.31	5.19	0.09
Ho	0.98	0.99	0.02
Er	2.54	2.50	0.06
Yb	2.00	1.94	0.05
Lu	0.27	0.27	0.01
Hf	4.36	4.26	0.13
Ta	1.14	1.11	0.03
Pb	1.60	1.55	0.06
Th	1.22	1.22	0.04
U	0.40	0.40	0.02

BHVO-1						
	Macquarie fused disk laser ablation (n = 2)			Durham powder digestion (n = 4)		Durham fused disk digestion (n = 1)
	Accepted value	This study	1sd	This study	1sd	This study
Ti (wt. %)	2.72	2.89	0.02	2.78	0.07	2.72
V	317	314	1	309	18	305
Ga	22.00	20.21	0.53	20.74	0.64	20.96
Rb	9.11	9.07	0.04	9.32	0.42	9.62
Sr	396	402	1	402	13	400
Y	26.00	27.30	0.27	27.40	0.52	27.09
Zr	172	192	0	174	7	177
Nb	18.10	19.70	0.69	19.05	0.56	19.51
Ba	131	129	1	141	9	136
La	15.20	15.36	0.13	15.07	0.42	–
Ce	37.50	36.12	0.27	36.37	0.77	38.78
Pr	5.35	5.40	0.04	5.62	0.19	5.61
Nd	24.50	26.24	0.59	26.20	1.08	25.10
Sm	6.07	6.66	0.34	6.27	0.22	6.20
Eu	2.07	2.03	0.12	2.09	0.06	2.08
Tb	0.92	0.96	0.02	0.98	0.03	0.96
Gd	6.24	6.32	0.29	6.56	0.32	6.31
Dy	5.31	5.66	0.08	5.36	0.16	5.15
Ho	0.98	1.02	0.02	1.00	0.02	0.96
Er	2.54	2.82	0.21	2.42	0.05	2.45
Yb	2.00	2.05	0.01	2.03	0.04	1.95
Lu	0.27	0.26	0.00	0.31	0.01	0.30
Hf	4.36	5.00	0.12	4.39	0.07	4.37
Ta	1.14	1.22	0.03	1.24	0.03	1.25
Pb	2.40	2.37	0.16	2.26	0.14	2.29
Th	1.22	1.28	0.09	1.24	0.05	1.15
U	0.40	0.42	0.02	0.42	0.01	0.42

Table C.2. (continued).

	BIR-1			NBS 688		
	Macquarie powder digestion (n=3)			Durham powder digestion (n = 3)		
	Accepted value	This study	1 sd	Accepted value	This study	1 sd
Ti (wt.%)	0.93	0.99	0.01		1.15	0.03
V	319	326	3	242	245	2
Ga	15.30	15.04	0.20	17.00	15.54	0.10
Rb	0.20	0.21	0.00	1.91	1.97	0.09
Sr	109	105	1	169	169	4
Y	15.60	17.12	0.24	17.00	20.75	0.21
Zr	14.00	15.28	0.16	61.0	53.8	1.1
Nb	0.55	0.55	0.01	5.00	4.26	0.05
Ba	7.14	6.54	0.14	200	186	7
La	0.62	0.67	0.02	5.30	5.08	—
Ce	1.92	1.99	0.04	13.00	11.44	0.20
Pr	0.37	0.40	0.01	2.40	1.84	0.05
Nd	2.38	2.36	0.05	9.60	9.02	0.36
Sm	1.12	1.11	0.01	2.50	2.48	0.08
Eu	0.53	0.50	0.01	1.01	1.01	0.04
Tb	0.36	0.35	0.01	0.52	0.54	0.01
Gd	1.87	1.89	0.03	3.20	3.10	0.10
Dy	2.51	2.50	0.04	3.40	3.45	0.10
Ho	0.56	0.57	0.01		0.75	0.02
Er	1.66	1.70	0.03	2.10	2.07	0.05
Yb	1.65	1.60	0.03	2.05	2.12	0.05
Lu	0.25	0.24	0.01	0.35	0.34	0.00
Hf	0.58	0.56	0.01	1.55	1.49	0.02
Ta	0.04	0.04	0.00	0.31	0.30	0.01
Pb	3.10	2.92	0.06	3.30	3.65	1.05
Th	0.03	0.04	0.00	0.33	0.33	0.01
U	0.01	0.01	0.00	0.31	0.27	0.04

	BCR-2				
	Macquarie powder digestion (n = 2)			Macquarie fusion (n = 2)	
	Accepted value	This study	1 sd	This study	1 sd
Ti (wt.%)	2.25	2.31	0.06	2.39	0.09
V	416	401	7	421	18
Ga	23.00	21.62	0.66	21.60	1.46
Rb	48.00	47.00	0.82	45.93	2.49
Sr	346	328	1	344	9
Y	37.00	37.98	0.03	36.41	3.65
Zr	188	192	0	205	21
Nb	12.00	12.56	0.12	13.33	1.17
Ba	683	660	2	672	10
La	25.00	24.92	0.22	25.81	0.50
Ce	53.00	51.82	0.13	51.73	1.26
Pr	6.80	6.85	0.03	6.73	0.21
Nd	28.00	28.27	0.07	29.95	1.47
Sm	6.70	6.60	0.01	6.86	0.42
Eu	2.00	2.05	0.01	2.00	0.04
Tb	1.07	1.08	0.01	0.98	0.05
Gd	6.80	6.82	0.03	6.68	0.64
Dy	6.41	6.28	0.00	6.52	0.45
Ho	1.33	1.31	0.01	1.34	0.11
Er	3.66	3.65	0.01	3.77	0.44
Yb	3.50	3.29	0.01	3.38	0.17
Lu	0.51	0.49	0.00	0.52	0.06
Hf	4.80	4.78	0.02	5.24	0.57
Ta	0.74	0.75	0.00	0.80	0.10
Pb	11.00	10.31	0.01	9.92	0.82
Th	5.70	6.07	0.05	6.34	0.38
U	1.69	1.67	0.01	1.69	0.10

Table C.2. (continued).

AGV-1					
	Durham powder digestion (n = 9)			Durham fusion (n = 5)	
	Accepted value	This study	1 sd	This study	1 sd
Ti (wt. %)	1.05	1.01	0.03	0.82	0.05
V	119	119	3	95.53	5.07
Ga	20.20	20.03	0.27	18.19	0.48
Rb	66.6	67.2	1.2	67.89	1.89
Sr	660	661	8	651.94	12.69
Y	19.00	19.86	0.23	18.95	0.54
Zr	231	225	6	220.08	1.78
Nb	14.60	14.42	0.22	13.69	0.12
Ba	1200	1232	25	1215.80	11.95
La	38.20	37.72	0.82	—	0.65
Ce	67.6	66.8	1.2	63.98	0.83
Pr	8.30	8.76	0.13	7.04	0.11
Nd	31.70	33.42	0.55	31.86	0.26
Sm	5.72	5.87	0.06	5.54	0.06
Eu	1.58	1.65	0.05	1.55	0.03
Tb	0.69	0.68	0.02	0.66	0.02
Gd	4.70	5.23	0.38	4.87	0.14
Dy	3.55	3.56	0.04	3.32	0.07
Ho	0.68	0.68	0.01	0.64	0.01
Er	1.82	1.75	0.01	1.62	0.02
Yb	1.63	1.66	0.02	1.57	0.02
Lu	0.244	0.27	0.00	0.25	0.00
Hf	5.1	5.01	0.08	4.81	0.06
Ta	0.87	0.90	0.01	0.85	0.01
Pb	37.4	35.70	0.25	36.01	0.42
Th	6.4	6.23	0.19	6.23	0.09
U	1.93	1.88	0.02	1.85	0.03

W2					
	Durham powder digestion (n = 4)			Durham fusion (n = 2)	
	Accepted value	This study	1 sd	This study	1 sd
Ti (wt. %)	1.06	1.02	0.05	0.93	0.20
V	268	257	13	243	50
Ga	18.00	16.85	0.47	16.35	1.75
Rb	21.00	19.25	0.55	19.52	1.17
Sr	196	192	4	191	11
Y	22.00	21.92	0.48	21.19	1.18
Zr	92.0	86.7	3.4	91.7	7.2
Nb	7.50	7.40	0.19	7.34	0.55
Ba	172	177	7	160	14
La	10.80	10.13	0.30	—	2.52
Ce	23.40	21.57	0.59	21.62	2.52
Pr	3.00	3.06	0.10	2.91	0.28
Nd	13.00	13.47	0.55	12.50	1.29
Sm	3.30	3.29	0.11	3.15	0.30
Eu	1.08	1.09	0.03	1.04	0.10
Tb	0.62	0.63	0.01	0.60	0.03
Gd	3.66	3.83	0.13	3.57	0.30
Dy	3.79	3.80	0.05	3.57	0.28
Ho	0.79	0.79	0.01	0.73	0.07
Er	2.22	2.11	0.04	2.07	0.16
Yb	2.05	2.05	0.02	1.99	0.14
Lu	0.31	0.33	0.00	0.31	0.02
Hf	2.45	2.38	0.08	2.31	0.28
Ta	0.47	0.49	0.01	0.47	0.04
Pb	7.70	7.55	0.14	7.40	0.72
Th	2.17	2.18	0.12	1.88	0.24
U	0.51	0.50	0.01	0.47	0.05

Table C.3. Assimilation during Fractional Crystallization (AFC) models with assimilant “minimum” isotopic composition allowing to model the most extreme SVC lava compositions with ~15% fraction of melt remaining (F) in agreement with the least squares models. Model 1 and 2 use both the trace element concentrations and the isotopic composition of SL-83-44 and only differ by their fractionating assemblage. Model 3 and 4 use trace element concentration of SL-83-44 (most mafic lava) but the isotopic composition of SL-83-25. r = rate of assimilation; Kd = partition coefficient; D = bulk partition coefficient.

Kd:	Plag	Cpx	Opx	Ilm	Am	D
La	0.0348	0.1047	0.002	0.098	0.5442	0.06661
Nd	0.0179	0.2866	0.03	0.14	1.3395	0.11919
Sm	0.0132	0.4774	0.05	0.15	1.8035	0.17331
Yb	0.0155	0.601	0.34	0.17	1.642	0.21200
Hf	0.0092	0.1208	0.01	0.38	1.5335	0.10411
Sr	1.67	0.07	0.04	0.01	0.48	0.99316
Ba	0.29	0.001	0.011	0.00034	0.16	0.17020
Th	0.25	0.012	0.0012	0.00055	0.004	0.14817
U	0.25	0.012	0.0012	0.00055	0.004	0.14817
Pb	0.36	0.0102	0.0013	0.01	0.1	0.21371

AFC model 1: using SL-83-44 as a starting composition and fractionating assemblage of least squares model 2 (with am)

Fractionated assemblage:				
Least square model 2 (normalized to 100%)				
Plag	Cpx	Opx	Ilm	Am
0.58	0.26	0.01	0.13	0.01

r	0.8
---	-----

	Initial magma	Assimilant
	SL-83-44	
¹⁴³ Nd/ ¹⁴⁴ Nd	0.51296	0.51205
⁸⁷ Sr/ ⁸⁸ Sr	0.70413	0.70910
²⁰⁶ Pb/ ²⁰⁴ Pb	19.3401	19.81
²⁰⁷ Pb/ ²⁰⁴ Pb	15.747	15.848
²⁰⁸ Pb/ ²⁰⁴ Pb	39.110	39.540
¹⁷⁶ Hf/ ¹⁷⁷ Hf	0.28312	0.28227
Sr	177.70	382.88
Ba	79.60	562.15
La	3.34	25.16
Nd	6.75	22.68
Sm	2.03	4.48
Yb	1.92	1.90
Hf	1.41	2.47
Pb	2.31	12.97
Th	0.70	7.81
U	0.28	2.17

F	1	0.99	0.98	0.95	0.9	0.8	0.7	0.55	0.2	0.1
La	3.34	4.38	5.43	8.71	14.57	28.09	44.76	78.90	300.29	565.45
Nd	6.75	7.69	8.65	11.60	16.81	28.58	42.61	69.95	218.65	361.90
Sm	2.03	2.21	2.40	2.96	3.96	6.14	8.67	13.34	34.66	51.02
Yb	1.92	2.00	2.07	2.31	2.71	3.58	4.57	6.32	13.42	18.03
Hf	1.41	1.51	1.62	1.95	2.55	3.89	5.51	8.71	27.01	45.79
Sr	177.70	185.85	193.75	216.07	248.90	300.13	335.51	366.71	385.83	386.16
Ba	79.60	102.34	125.34	195.99	319.64	592.49	907.66	1493.02	4191.00	6288.96
Th	0.70	1.02	1.34	2.33	4.06	7.92	12.45	21.02	63.46	99.67
U	0.28	0.37	0.46	0.74	1.22	2.29	3.55	5.93	17.73	27.80
Pb	2.31	2.83	3.35	4.95	7.74	13.76	20.53	32.61	81.13	112.49
⁸⁷ Sr/ ⁸⁸ Sr	0.70413	0.70454	0.70489	0.70577	0.70676	0.70789	0.70846	0.70888	0.70910	0.70910
¹⁴³ Nd/ ¹⁴⁴ Nd	0.51296	0.51285	0.51276	0.51259	0.51243	0.51228	0.51221	0.51216	0.51210	0.51209
¹⁷⁶ Hf/ ¹⁷⁷ Hf	0.28312	0.28306	0.28301	0.28289	0.28276	0.28261	0.28253	0.28245	0.28237	0.28235
²⁰⁶ Pb/ ²⁰⁴ Pb	19.3407	19.4273	19.4874	19.5924	19.6711	19.7326	19.7586	19.7781	19.7981	19.8018
²⁰⁷ Pb/ ²⁰⁴ Pb	15.7472	15.7658	15.7787	15.8013	15.8182	15.8314	15.8370	15.8412	15.8454	15.8462
²⁰⁸ Pb/ ²⁰⁴ Pb	39.1099	39.1893	39.2444	39.3406	39.4127	39.4690	39.4929	39.5108	39.5291	39.5325
La/Sm	1.65	1.98	2.27	2.94	3.68	4.57	5.16	5.92	8.66	11.08
Ba/Th	113.28	100.43	93.59	84.28	78.74	74.79	72.93	71.01	66.04	63.10
Th/Th*	0.71	0.79	0.84	0.93	0.98	1.03	1.05	1.07	1.11	1.13
La/Yb	1.74	2.19	2.62	3.77	5.38	7.84	9.80	12.48	22.38	31.36

Table C.3. (continued).

Kd:	Plag	Cpx	Opx	Ilm	D
La	0.0348	0.1047	0.002	0.098	0.03616
Nd	0.0179	0.2866	0.03	0.14	0.05870
Sm	0.0132	0.4774	0.05	0.15	0.08700
Yb	0.0155	0.601	0.34	0.17	0.18302
Hf	0.0092	0.1208	0.01	0.38	0.02912
Sr	1.67	0.07	0.04	0.01	0.99676
Ba	0.29	0.001	0.011	0.00034	0.17267
Th	0.25	0.012	0.0012	0.00055	0.14812
U	0.25	0.012	0.0012	0.00055	0.14812
Pb	0.36	0.0102	0.0013	0.01	0.21235

	Initial magma	Assimilant
	SL-83-44	
¹⁴³ Nd/ ¹⁴⁴ Nd	0.51296	0.51205
⁸⁷ Sr/ ⁸⁸ Sr	0.70413	0.70910
²⁰⁶ Pb/ ²⁰⁴ Pb	19.341	19.810
²⁰⁷ Pb/ ²⁰⁴ Pb	15.747	15.848
²⁰⁸ Pb/ ²⁰⁴ Pb	39.110	39.540
¹⁷⁶ Hf/ ¹⁷⁷ Hf	0.28312	0.28227
Sr	177.70	382.88
Ba	79.60	562.15
La	3.34	25.16
Nd	6.75	22.68
Sm	2.03	4.48
Yb	1.92	1.90
Hf	1.41	2.47
Pb	2.31	12.97
Th	0.70	7.81
U	0.28	2.17

AFC model 2: using SL-83-44 as a starting composition and fractionating assemblage of least squares model 1 (no am)

Fractionated assemblage:			
Least square model 1			
Plag	Cpx	Opx	Ilm
0.58	0.13	0.27	0.01

r	0.8
---	-----

F	1	0.99	0.98	0.95	0.9	0.8	0.7	0.55	0.2	0.1
La	3.34	4.38	5.44	8.75	14.71	28.65	46.16	83.08	348.79	709.32
Nd	6.75	7.72	8.70	11.74	17.20	29.83	45.49	77.80	293.00	559.27
Sm	2.03	2.22	2.42	3.02	4.10	6.56	9.56	15.58	52.02	92.15
Yb	1.92	2.00	2.08	2.32	2.75	3.67	4.74	6.69	15.32	21.68
Hf	1.41	1.52	1.63	1.99	2.63	4.13	6.03	10.05	39.74	81.19
Sr	177.70	185.81	193.69	215.91	248.56	299.45	334.51	365.33	384.10	384.41
Ba	79.60	102.32	125.31	195.90	319.38	591.56	905.47	1487.12	4147.05	6193.93
Th	0.70	1.02	1.34	2.33	4.06	7.92	12.45	21.03	63.48	99.70
U	0.28	0.37	0.46	0.74	1.22	2.29	3.55	5.93	17.74	27.81
Pb	2.31	2.83	3.35	4.96	7.74	13.77	20.56	32.68	81.58	113.37
⁸⁷ Sr/ ⁸⁸ Sr	0.70413	0.70454	0.70489	0.70577	0.70677	0.70789	0.70846	0.70888	0.70910	0.70910
¹⁴³ Nd/ ¹⁴⁴ Nd	0.51296	0.51285	0.51276	0.51259	0.51243	0.51228	0.51221	0.51216	0.51210	0.51209
¹⁷⁶ Hf/ ¹⁷⁷ Hf	0.28312	0.28306	0.28301	0.28289	0.28276	0.28261	0.28252	0.28245	0.28237	0.28236
²⁰⁶ Pb/ ²⁰⁴ Pb	19.341	19.427	19.487	19.592	19.671	19.733	19.759	19.778	19.798	19.802
²⁰⁷ Pb/ ²⁰⁴ Pb	15.747	15.766	15.779	15.801	15.818	15.831	15.837	15.841	15.845	15.846
²⁰⁸ Pb/ ²⁰⁴ Pb	39.110	39.189	39.244	39.341	39.413	39.469	39.493	39.511	39.529	39.532
La/Sm	1.65	1.97	2.25	2.90	3.59	4.37	4.83	5.33	6.71	7.70
Ba/Th	113.28	100.42	93.57	84.24	78.68	74.67	72.75	70.73	65.33	62.12
Th/Th*	0.71	0.79	0.84	0.93	0.98	1.03	1.05	1.07	1.11	1.14
La/Yb	1.74	2.19	2.62	3.77	5.36	7.80	9.75	12.42	22.76	32.72

Table C.3. (continued).

Kd:	Plag	Cpx	Opx	Ilm	Am	D
La	0.0348	0.1047	0.002	0.098	0.5442	0.06661
Nd	0.0179	0.2866	0.03	0.14	1.3395	0.11919
Sm	0.0132	0.4774	0.05	0.15	1.8035	0.17331
Yb	0.0155	0.601	0.34	0.17	1.642	0.21110
Hf	0.0092	0.1208	0.01	0.38	1.5335	0.10411
Sr	1.67	0.07	0.04	0.01	0.48	0.99315
Ba	0.29	0.001	0.011	0.00034	0.16	0.17020
Th	0.25	0.012	0.0012	0.00055	0.004	0.14817
U	0.25	0.012	0.0012	0.00055	0.004	0.14817
Pb	0.36	0.0102	0.0013	0.01	0.1	0.21371

	Initial magma	Assimilant
	SL-83-25	
¹⁴³ Nd/ ¹⁴⁴ Nd	0.51295	0.51205
⁸⁷ Sr/ ⁸⁸ Sr	0.70439	0.70910
²⁰⁶ Pb/ ²⁰⁴ Pb	19.291	19.810
²⁰⁷ Pb/ ²⁰⁴ Pb	15.748	15.848
²⁰⁸ Pb/ ²⁰⁴ Pb	38.930	39.540
¹⁷⁶ Hf/ ¹⁷⁷ Hf	0.28303	0.28227
Sr	177.70	382.88
Ba	79.60	562.15
La	3.34	25.16
Nd	6.75	22.68
Sm	2.03	4.48
Yb	1.92	1.90
Hf	1.41	2.47
Pb	2.31	12.97
Th	0.70	7.81
U	0.28	2.17

AFC model 3: using SL-83-25 as a starting composition and fractionating assemblage of least squares model 2 (with am)

Fractionated assemblage:				
Least square model 2 (normalized to 100%)				
Plag	Cpx	Opx	Ilm	Am
0.58	0.26	0.01	0.13	0.01

r	0.8
---	-----

F	1	0.99	0.98	0.95	0.9	0.8	0.7	0.55	0.2	0.1
La	3.34	4.38	5.43	8.71	14.57	28.09	44.76	78.90	300.29	565.45
Nd	6.75	7.69	8.65	11.60	16.81	28.58	42.61	69.95	218.65	361.90
Sm	2.03	2.21	2.40	2.96	3.96	6.14	8.67	13.34	34.66	51.02
Yb	1.92	2.00	2.07	2.31	2.71	3.58	4.57	6.32	13.42	18.03
Hf	1.41	1.51	1.62	1.95	2.55	3.89	5.51	8.71	27.01	45.79
Sr	177.70	185.85	193.75	216.07	248.90	300.13	335.51	366.71	385.83	386.16
Ba	79.60	102.34	125.34	195.99	319.64	592.49	907.66	1493.02	4191.00	6288.96
Th	0.70	1.02	1.34	2.33	4.06	7.92	12.45	21.02	63.46	99.67
U	0.28	0.37	0.46	0.74	1.22	2.29	3.55	5.93	17.73	27.80
Pb	2.31	2.83	3.35	4.95	7.74	13.76	20.53	32.61	81.13	112.49
⁸⁷ Sr/ ⁸⁸ Sr	0.70439	0.70478	0.70512	0.70594	0.70689	0.70795	0.70849	0.70889	0.70910	0.70910
¹⁴³ Nd/ ¹⁴⁴ Nd	0.51295	0.51284	0.51276	0.51258	0.51242	0.51228	0.51221	0.51216	0.51210	0.51209
¹⁷⁶ Hf/ ¹⁷⁷ Hf	0.28303	0.28298	0.28293	0.28283	0.28271	0.28257	0.28250	0.28243	0.28236	0.28234
²⁰⁶ Pb/ ²⁰⁴ Pb	19.291	19.387	19.453	19.569	19.656	19.724	19.753	19.775	19.797	19.801
²⁰⁷ Pb/ ²⁰⁴ Pb	15.748	15.766	15.779	15.802	15.818	15.831	15.837	15.841	15.845	15.846
²⁰⁸ Pb/ ²⁰⁴ Pb	38.930	39.043	39.121	39.257	39.360	39.439	39.473	39.499	39.524	39.529
La/Sm	1.65	1.98	2.27	2.94	3.68	4.57	5.16	5.92	8.66	11.08
Ba/Th	113.28	100.43	93.59	84.28	78.74	74.79	72.93	71.01	66.04	63.10
Th/Th*	0.71	0.79	0.84	0.93	0.98	1.03	1.05	1.07	1.11	1.13
La/Yb	1.74	2.19	2.62	3.77	5.38	7.84	9.80	12.48	22.38	31.36

Table C.3. (continued).

Kd:	Plag	Cpx	Opx	Ilm	D
La	0.0348	0.1047	0.002	0.098	0.03616
Nd	0.0179	0.2866	0.03	0.14	0.05870
Sm	0.0132	0.4774	0.05	0.15	0.08700
Yb	0.0155	0.601	0.34	0.17	0.18302
Hf	0.0092	0.1208	0.01	0.38	0.02912
Sr	1.67	0.07	0.04	0.01	0.99676
Ba	0.29	0.001	0.011	0.00034	0.17267
Th	0.25	0.012	0.0012	0.00055	0.14812
U	0.25	0.012	0.0012	0.00055	0.14812
Pb	0.36	0.0102	0.0013	0.01	0.21235

	Initial magma	Assimilant
	SL-83-25	
¹⁴³ Nd/ ¹⁴⁴ Nd	0.51295	0.51205
⁸⁷ Sr/ ⁸⁸ Sr	0.70439	0.70910
²⁰⁶ Pb/ ²⁰⁴ Pb	19.291	19.81
²⁰⁷ Pb/ ²⁰⁴ Pb	15.748	15.848
²⁰⁸ Pb/ ²⁰⁴ Pb	38.93	39.54
¹⁷⁶ Hf/ ¹⁷⁷ Hf	0.28303	0.28227
Sr	177.70	382.88
Ba	79.60	562.15
La	3.34	25.16
Nd	6.75	22.68
Sm	2.03	4.48
Yb	1.92	1.90
Hf	1.41	2.47
Pb	2.31	12.97
Th	0.70	7.81
U	0.28	2.17

AFC model 4: using SL-83-25 as a starting composition (isotopes) and fractionating assemblage of least squares model 1 (no am)

Fractionated assemblage:					
Least square model 1					
Plag	Cpx	Opx	Ilm	r	0.8
0.58	0.13	0.27	0.01		

F	1	0.99	0.98	0.95	0.9	0.8	0.7	0.55	0.2	0.1
La	3.34	4.38	5.44	8.75	14.71	28.65	46.16	83.08	348.79	709.32
Nd	6.75	7.72	8.70	11.74	17.20	29.83	45.49	77.80	293.00	559.27
Sm	2.03	2.22	2.42	3.02	4.10	6.56	9.56	15.58	52.02	92.15
Yb	1.92	2.00	2.08	2.32	2.75	3.67	4.74	6.69	15.32	21.68
Hf	1.41	1.52	1.63	1.99	2.63	4.13	6.03	10.05	39.74	81.19
Sr	177.70	185.81	193.69	215.91	248.56	299.45	334.51	365.33	384.10	384.41
Ba	79.60	102.32	125.31	195.89	319.33	591.37	905.03	1485.94	4138.25	6174.97
Th	0.70	1.02	1.34	2.33	4.06	7.92	12.45	21.02	63.45	99.65
U	6.75	7.74	8.74	11.88	17.58	31.12	48.53	86.51	396.68	884.08
Pb	2.31	2.83	3.35	4.96	7.74	13.77	20.56	32.68	81.58	113.37
⁸⁷ Sr/ ⁸⁸ Sr	0.70439	0.70478	0.70512	0.70594	0.70689	0.70795	0.70850	0.70889	0.70910	0.70910
¹⁴³ Nd/ ¹⁴⁴ Nd	0.51295	0.51284	0.51276	0.51259	0.51243	0.51229	0.51223	0.51218	0.51213	0.51212
¹⁷⁶ Hf/ ¹⁷⁷ Hf	0.28303	0.28298	0.28293	0.28282	0.28270	0.28257	0.28250	0.28243	0.28236	0.28235
²⁰⁶ Pb/ ²⁰⁴ Pb	19.291	19.387	19.453	19.569	19.656	19.724	19.753	19.775	19.797	19.801
²⁰⁷ Pb/ ²⁰⁴ Pb	15.748	15.766	15.779	15.802	15.818	15.831	15.837	15.841	15.845	15.846
²⁰⁸ Pb/ ²⁰⁴ Pb	38.930	39.043	39.121	39.257	39.359	39.439	39.473	39.499	39.524	39.529
La/Sm	1.65	1.97	2.25	2.90	3.59	4.37	4.83	5.33	6.71	7.70
Ba/Th	113.28	100.42	93.56	84.24	78.67	74.65	72.72	70.68	65.22	61.97
Th/Th*	0.06	0.07	0.08	0.10	0.12	0.13	0.13	0.13	0.09	0.06
La/Yb	1.74	2.19	2.62	3.77	5.36	7.80	9.75	12.42	22.76	32.72

Table C.4. Assimilation during Fractional Crystallization (AFC) models with assimilant “minimum” isotopic composition allowing to model the most extreme SVC lava compositions with ~55% fraction of melt remaining (F). Model 1 and 2 use both the trace element concentrations and the isotopic composition of SL-83-44 and only differ by their fractionating assemblage. Model 3 and 4 use trace element concentration of SL-83-44 (most mafic lava) but the isotopic composition of SL-83-25. r = rate of assimilation; Kd = partition coefficient; D = bulk partition coefficient.

Kd:	Plag	Cpx	Opx	Ilm	Am	D
La	0.0348	0.1047	0.002	0.098	0.5442	0.06661
Nd	0.0179	0.2866	0.03	0.14	1.3395	0.11919
Sm	0.0132	0.4774	0.05	0.15	1.8035	0.17331
Yb	0.0155	0.601	0.34	0.17	1.642	0.21200
Hf	0.0092	0.1208	0.01	0.38	1.5335	0.10411
Sr	1.67	0.07	0.04	0.01	0.48	0.99315
Ba	0.29	0.001	0.011	0.00034	0.16	0.17020
Th	0.25	0.012	0.0012	0.00055	0.004	0.14817
U	0.25	0.012	0.0012	0.00055	0.004	0.14817
Pb	0.36	0.0102	0.0013	0.01	0.1	0.21371

AFC model 1: using SL-83-44 as a starting composition and fractionating assemblage of least squares model 2 (with am)

Fractionated assemblage:				
Least square model 2				
Plag	Cpx	Opx	Ilm	Am
0.58	0.26	0.01	0.13	0.01

r	0.8
---	-----

F	1	0.99	0.98	0.95	0.9	0.8	0.7	0.55	0.2	0.1
La	3.34	4.38	5.43	8.71	14.57	28.09	44.76	78.90	300.29	565.45
Nd	6.75	7.69	8.65	11.60	16.81	28.58	42.61	69.95	218.65	361.90
Sm	2.03	2.21	2.40	2.96	3.96	6.14	8.67	13.34	34.66	51.02
Yb	1.92	2.00	2.07	2.31	2.71	3.58	4.57	6.32	13.42	18.03
Hf	1.41	1.51	1.62	1.95	2.55	3.89	5.51	8.71	27.01	45.79
Sr	177.70	185.85	193.75	216.07	248.90	300.13	335.51	366.71	385.83	386.16
Ba	79.60	102.34	125.34	195.99	319.64	592.49	907.66	1493.02	4191.00	6288.96
Th	0.70	1.02	1.34	2.33	4.06	7.92	12.45	21.02	63.46	99.67
U	0.28	0.37	0.46	0.74	1.22	2.29	3.55	5.93	17.73	27.80
Pb	2.31	2.83	3.35	4.95	7.74	13.76	20.53	32.61	81.13	112.49
⁸⁷ Sr/ ⁸⁸ Sr	0.70413	0.70455	0.70493	0.70583	0.70687	0.70804	0.70863	0.70907	0.70930	0.70930
¹⁴³ Nd/ ¹⁴⁴ Nd	0.51296	0.51284	0.51274	0.51255	0.51238	0.51221	0.51214	0.51208	0.51201	0.51200
¹⁷⁶ Hf/ ¹⁷⁷ Hf	0.28312	0.28306	0.28300	0.28288	0.28273	0.28257	0.28248	0.28240	0.28230	0.28228
²⁰⁶ Pb/ ²⁰⁴ Pb	19.341	19.431	19.494	19.603	19.685	19.749	19.776	19.797	19.818	19.821
²⁰⁷ Pb/ ²⁰⁴ Pb	15.747	15.766	15.779	15.802	15.820	15.833	15.839	15.843	15.847	15.848
²⁰⁸ Pb/ ²⁰⁴ Pb	39.110	39.189	39.244	39.341	39.413	39.469	39.493	39.511	39.529	39.532
La/Sm	1.65	1.98	2.27	2.94	3.68	4.57	5.16	5.92	8.66	11.08
Ba/Th	113.28	100.43	93.59	84.28	78.74	74.79	72.93	71.01	66.04	63.10
Th/Th*	0.71	0.79	0.84	0.93	0.98	1.03	1.05	1.07	1.11	1.13
La/Yb	1.74	2.19	2.62	3.77	5.38	7.84	9.80	12.48	22.38	31.36

	Initial magma SL-83-44	Assimilant
¹⁴³ Nd/ ¹⁴⁴ Nd	0.51296	0.51196
⁸⁷ Sr/ ⁸⁸ Sr	0.70413	0.70930
²⁰⁶ Pb/ ²⁰⁴ Pb	19.341	19.830
²⁰⁷ Pb/ ²⁰⁴ Pb	15.747	15.850
²⁰⁸ Pb/ ²⁰⁴ Pb	39.110	39.540
¹⁷⁶ Hf/ ¹⁷⁷ Hf	0.28312	0.28220
Sr	177.70	382.88
Ba	79.60	562.15
La	3.34	25.16
Nd	6.75	22.68
Sm	2.03	4.48
Yb	1.92	1.90
Hf	1.41	2.47
Pb	2.31	12.97
Th	0.70	7.81
U	0.28	2.17

Table C.4. (continued).

Kd	Plag	Cpx	Opx	Ilm	D
La	0.0348	0.1047	0.002	0.098	0.03616
Nd	0.0179	0.2866	0.03	0.14	0.05870
Sm	0.0132	0.4774	0.05	0.15	0.08700
Yb	0.0155	0.601	0.34	0.17	0.18302
Hf	0.0092	0.1208	0.01	0.38	0.02912
Sr	1.67	0.07	0.04	0.01	0.99676
Ba	0.29	0.001	0.011	0.00034	0.17267
Th	0.25	0.012	0.0012	0.00055	0.14812
U	0.25	0.012	0.0012	0.00055	0.14812
Pb	0.36	0.0102	0.0013	0.01	0.21235

	Initial magma	Assimilant
	SL-83-44	
¹⁴³ Nd/ ¹⁴⁴ Nd	0.51296	0.51196
⁸⁷ Sr/ ⁸⁸ Sr	0.70413	0.70930
²⁰⁶ Pb/ ²⁰⁴ Pb	19.341	19.830
²⁰⁷ Pb/ ²⁰⁴ Pb	15.747	15.850
²⁰⁸ Pb/ ²⁰⁴ Pb	39.110	39.540
¹⁷⁶ Hf/ ¹⁷⁷ Hf	0.28312	0.28220
Sr	177.70	382.88
Ba	79.60	562.15
La	3.34	25.16
Nd	6.75	22.68
Sm	2.03	4.48
Yb	1.92	1.90
Hf	1.41	2.47
Pb	2.31	12.97
Th	0.70	7.81
U	0.28	2.17

AFC model 2: using SL-83-44 as a starting composition and fractionating assemblage of least squares model 1 (no am)

Fractionated assemblage:			
Least square model 1			
Plag	Cpx	Opx	Ilm
0.58	0.13	0.27	0.01

r	0.8
---	-----

F	1	0.99	0.98	0.95	0.9	0.8	0.7	0.55	0.2	0.1
La	3.34	4.38	5.44	8.75	14.71	28.65	46.16	83.08	348.79	709.32
Nd	6.75	7.72	8.70	11.74	17.20	29.83	45.49	77.80	293.00	559.27
Sm	2.03	2.22	2.42	3.02	4.10	6.56	9.56	15.58	52.02	92.15
Yb	1.92	2.00	2.08	2.32	2.75	3.67	4.74	6.69	15.32	21.68
Hf	1.41	1.52	1.63	1.99	2.63	4.13	6.03	10.05	39.74	81.19
Sr	177.70	185.81	193.69	215.91	248.56	299.45	334.51	365.33	384.10	384.41
Ba	79.60	102.32	125.31	195.90	319.38	591.56	905.47	1487.12	4147.05	6193.93
Th	0.70	1.02	1.34	2.33	4.06	7.92	12.45	21.03	63.48	99.70
U	0.28	0.37	0.46	0.74	1.22	2.29	3.55	5.93	17.74	27.81
Pb	2.31	2.83	3.35	4.96	7.74	13.77	20.56	32.68	81.58	113.37
⁸⁷ Sr/ ⁸⁸ Sr	0.70413	0.70455	0.70493	0.70583	0.70687	0.70804	0.70864	0.70907	0.70930	0.70930
¹⁴³ Nd/ ¹⁴⁴ Nd	0.51296	0.51284	0.51274	0.51255	0.51238	0.51221	0.51214	0.51208	0.51201	0.51200
¹⁷⁶ Hf/ ¹⁷⁷ Hf	0.28312	0.28306	0.28300	0.28288	0.28274	0.28258	0.28249	0.28241	0.28233	0.28231
²⁰⁶ Pb/ ²⁰⁴ Pb	19.341	19.431	19.494	19.603	19.685	19.749	19.776	19.797	19.817	19.821
²⁰⁷ Pb/ ²⁰⁴ Pb	15.747	15.766	15.779	15.802	15.820	15.833	15.839	15.843	15.847	15.848
²⁰⁸ Pb/ ²⁰⁴ Pb	39.110	39.189	39.244	39.341	39.413	39.469	39.493	39.511	39.529	39.532
La/Sm	1.65	1.97	2.25	2.90	3.59	4.37	4.83	5.33	6.71	7.70
Ba/Th	113.28	100.42	93.57	84.24	78.68	74.67	72.75	70.73	65.33	62.12
Th/Th*	0.71	0.79	0.84	0.93	0.98	1.03	1.05	1.07	1.11	1.14
La/Yb	1.74	2.19	2.62	3.77	5.36	7.80	9.75	12.42	22.76	32.72

Table C.4. (continued).

	Plag	Cpx	Opx	Ilm	Am	D
La	0.0348	0.1047	0.002	0.098	0.5442	0.06661
Nd	0.0179	0.2866	0.03	0.14	1.3395	0.11919
Sm	0.0132	0.4774	0.05	0.15	1.8035	0.17331
Yb	0.0155	0.601	0.34	0.17	1.642	0.21200
Hf	0.0092	0.1208	0.01	0.38	1.5335	0.10411
Sr	1.67	0.07	0.04	0.01	0.48	0.99315
Ba	0.29	0.001	0.011	0.00034	0.16	0.17020
Th	0.25	0.012	0.0012	0.00055	0.004	0.14817
U	0.25	0.012	0.0012	0.00055	0.004	0.14817
Pb	0.36	0.0102	0.0013	0.01	0.1	0.21371

	Initial magma	Assimilant
	SL-83-44	
¹⁴³ Nd/ ¹⁴⁴ Nd	0.51295	0.51196
⁸⁷ Sr/ ⁸⁶ Sr	0.70439	0.70930
²⁰⁶ Pb/ ²⁰⁴ Pb	19.291	19.830
²⁰⁷ Pb/ ²⁰⁴ Pb	15.748	15.850
²⁰⁸ Pb/ ²⁰⁴ Pb	38.930	39.540
¹⁷⁶ Hf/ ¹⁷⁷ Hf	0.28303	0.28220
Sr	177.70	382.88
Ba	79.60	562.15
La	3.34	25.16
Nd	6.75	22.68
Sm	2.03	4.48
Yb	1.92	1.90
Hf	1.41	2.47
Pb	2.31	12.97
Th	0.70	7.81
U	0.28	2.17

AFC model 3: using SL-83-25 as a starting composition and fractionating assemblage of least squares model 2 (with am)

Fractionated assemblage:				
Least square model 2				
Plag	Cpx	Opx	Ilm	Am
0.58	0.26	0.01	0.13	0.01

r	0.8
---	-----

F	1	0.99	0.98	0.95	0.9	0.8	0.7	0.55	0.2	0.1
La	3.34	4.38	5.43	8.71	14.57	28.09	44.76	78.90	300.29	565.45
Nd	6.75	7.69	8.65	11.60	16.81	28.58	42.61	69.95	218.65	361.90
Sm	2.03	2.21	2.40	2.96	3.96	6.14	8.67	13.34	34.66	51.02
Yb	1.92	2.00	2.07	2.31	2.71	3.58	4.57	6.32	13.42	18.03
Hf	1.41	1.51	1.62	1.95	2.55	3.89	5.51	8.71	27.01	45.79
Sr	177.70	185.85	193.75	216.07	248.90	300.13	335.51	366.71	385.83	386.16
Ba	79.60	102.34	125.34	195.99	319.64	592.49	907.66	1493.02	4191.00	6288.96
Th	0.70	1.02	1.34	2.33	4.06	7.92	12.45	21.02	63.46	99.67
U	0.28	0.37	0.46	0.74	1.22	2.29	3.55	5.93	17.73	27.80
Pb	2.31	2.83	3.35	4.95	7.74	13.76	20.53	32.61	81.13	112.49
⁸⁷ Sr/ ⁸⁶ Sr	0.70439	0.70479	0.70515	0.70601	0.70699	0.70810	0.70867	0.70908	0.70930	0.70930
¹⁴³ Nd/ ¹⁴⁴ Nd	0.51295	0.51283	0.51274	0.51255	0.51237	0.51221	0.51214	0.51208	0.51201	0.51200
¹⁷⁶ Hf/ ¹⁷⁷ Hf	0.28303	0.28297	0.28292	0.28281	0.28268	0.28253	0.28245	0.28238	0.28229	0.28228
²⁰⁶ Pb/ ²⁰⁴ Pb	19.291	19.390	19.460	19.580	19.671	19.741	19.771	19.793	19.816	19.821
²⁰⁷ Pb/ ²⁰⁴ Pb	15.748	15.767	15.780	15.803	15.820	15.833	15.839	15.843	15.847	15.848
²⁰⁸ Pb/ ²⁰⁴ Pb	38.930	39.043	39.121	39.257	39.360	39.439	39.473	39.499	39.524	39.529
La/Sm	1.65	1.98	2.27	2.94	3.68	4.57	5.16	5.92	8.66	11.08
Ba/Th	113.28	100.43	93.59	84.28	78.74	74.79	72.93	71.01	66.04	63.10
Th/Th*	0.71	0.79	0.84	0.93	0.98	1.03	1.05	1.07	1.11	1.13
La/Yb	1.74	2.19	2.62	3.77	5.38	7.84	9.80	12.48	22.38	31.36

Table C.4. (continued).

	Plag	Cpx	Opx	Ilm	D
La	0.0348	0.1047	0.002	0.098	0.0361 6
Nd	0.0179	0.2866	0.03	0.14	0.0587 0
Sm	0.0132	0.4774	0.05	0.15	0.0870 0
Yb	0.0155	0.601	0.34	0.17	0.1830 2
Hf	0.0092	0.1208	0.01	0.38	0.0291 2
Sr	1.67	0.07	0.04	0.01	0.9967 6
Ba	0.29	0.001	0.011	0.00034	0.1726 7
Th	0.25	0.012	0.001	0.00055	0.1481 2
U	0.25	0.012	0.001	0.00055	0.1481 2
Pb	0.36	0.0102	0.001	0.01	0.2123 5

	Initial magma	Assimilant
	SL-83-44	
¹⁴³ Nd/ ¹⁴⁴ Nd	0.51295	0.51196
⁸⁷ Sr/ ⁸⁸ Sr	0.70439	0.70930
²⁰⁶ Pb/ ²⁰⁴ Pb	19.291	19.83
²⁰⁷ Pb/ ²⁰⁴ Pb	15.748	15.85
²⁰⁸ Pb/ ²⁰⁴ Pb	38.930	39.54
¹⁷⁶ Hf/ ¹⁷⁷ Hf	0.28303	0.28220
Sr	177.70	382.88
Ba	79.60	562.15
La	3.34	25.16
Nd	6.75	22.68
Sm	2.03	4.48
Yb	1.92	1.90
Hf	1.41	2.47
Pb	2.31	12.97
Th	0.70	7.81
U	0.28	2.17

AFC model 4: using SL-83-25 as a starting composition (isotopes) and fractionating assemblage of least squares model 1 (no am)

Fractionated assemblage:			
Least square model 2			
Plag	Cpx	Opx	Ilm
0.58	0.13	0.27	0.01

r	0.8
---	-----

F	1	0.99	0.98	0.95	0.9	0.8	0.7	0.55	0.2	0.1
La	3.34	4.38	5.44	8.75	14.71	28.65	46.16	83.08	348.79	709.32
Nd	6.75	7.72	8.70	11.74	17.20	29.83	45.49	77.80	293.00	559.27
Sm	2.03	2.22	2.42	3.02	4.10	6.56	9.56	15.58	52.02	92.15
Yb	1.92	2.00	2.08	2.32	2.75	3.67	4.74	6.69	15.32	21.68
Hf	1.41	1.52	1.63	1.99	2.63	4.13	6.03	10.05	39.74	81.19
Sr	177.70	185.81	193.69	215.91	248.56	299.45	334.51	365.33	384.10	384.41
Ba	79.60	102.32	125.31	195.89	319.33	591.37	905.03	1485.94	4138.25	6174.97
Th	0.70	1.02	1.34	2.33	4.06	7.92	12.45	21.02	63.45	99.65
U	6.75	7.74	8.74	11.88	17.58	31.12	48.53	86.51	396.68	884.08
Pb	2.31	2.83	3.35	4.96	7.74	13.77	20.56	32.68	81.58	113.37
⁸⁷ Sr/ ⁸⁸ Sr	0.70439	0.70479	0.70515	0.70601	0.70699	0.70810	0.70867	0.70908	0.70930	0.70930
¹⁴³ Nd/ ¹⁴⁴ Nd	0.51295	0.51283	0.51274	0.51255	0.51238	0.51223	0.51216	0.51210	0.51204	0.51204
¹⁷⁶ Hf/ ¹⁷⁷ Hf	0.28303	0.28297	0.28292	0.28281	0.28268	0.28254	0.28246	0.28239	0.28232	0.28230
²⁰⁶ Pb/ ²⁰⁴ Pb	19.291	19.390	19.460	19.580	19.670	19.741	19.771	19.793	19.816	19.820
²⁰⁷ Pb/ ²⁰⁴ Pb	15.748	15.767	15.780	15.803	15.820	15.833	15.839	15.843	15.847	15.848
²⁰⁸ Pb/ ²⁰⁴ Pb	38.930	39.043	39.121	39.257	39.359	39.439	39.473	39.499	39.524	39.529
La/Sm	1.65	1.97	2.25	2.90	3.59	4.37	4.83	5.33	6.71	7.70
Ba/Th	113.28	100.42	93.56	84.24	78.67	74.65	72.72	70.68	65.22	61.97
Th/Th*	0.06	0.07	0.08	0.10	0.12	0.13	0.13	0.13	0.09	0.06
La/Yb	1.74	2.19	2.62	3.77	5.36	7.80	9.75	12.42	22.76	32.72

Table C.5. Bulk sediment composition at DSDP sites 543 and 144 and Barbados and partition coefficients used to calculate sediment melt compositions.

Bulk sediment composition							
	Sr	Nd	Hf	Pb	Sr/Nd	Pb/Hf	Nd/Hf
Site 543 Bulk	110	30.6	2.79	18.7	3.59	6.70	10.97
Site 144 Bulk	656	14.8	2.15	7.24	44.32	3.37	6.88
Barbados Bulk	103	23.3	4.78	13.1	4.42	2.74	4.87
Bulk partion coefficients							
	Sr	Nd	Hf	Pb	Sr/Nd	Pb/Hf	Nd/Hf
	0.67	4.41	1.78	0.78	0.15	0.44	2.48
Sediment melt composition							
	Sr	Nd	Hf	Pb	Sr/Nd	Pb/Hf	Nd/Hf
Site 543 Bulk melt	73.70	134.95	4.97	14.59	0.55	2.94	27.17
Site 144 Bulk melt	439.52	65.27	3.83	5.65	6.73	1.48	17.05
Barbados Bulk melt	69.01	102.75	8.51	10.22	0.67	1.20	12.08

Sediment compositions are from Carpentier et al. (2008; 2009). Bulk partition coefficients for Sr, Nd and Pb are from Johnson and Plank (1999) and obtained at 2 Gpa and 800°C. Hf bulk partition coefficient is from Hermann and Rubatto (2009) and obtained at 2.5 Gpa and 800°C

Table C.6. Composition of the most mafic lavas presented in Fig. 11. Major element composition are anhydrous and normalised to 100%.

Sample ID	Island	Reference:	SiO ₂	TiO ₂	Al ₂ O ₃	Fe ₂ O ₃	MnO	MgO	CaO	Na ₂ O	K ₂ O	P ₂ O ₅	Total
LAS1	Saba	DuFrane et al. (2009)	51.67	0.79	17.19	8.29	0.16	8.05	10.35	2.71	0.67	0.10	100.00
8248	Statia	Davidson (1984)	53.39	0.85	18.87	8.67	0.19	4.39	9.45	3.52	0.57	0.10	100.00
Kit59	St Kitts	Toothhill et al. (2007)	48.67	0.92	19.43	9.30	0.16	6.88	11.82	2.45	0.30	0.08	100.00
95Isn5	Nevis	Van Soest (2000)	64.12	0.44	17.19	5.32	0.14	2.09	5.81	3.53	1.21	0.14	100.00
8202	Redonda	Davidson (1984)	48.74	0.77	19.43	10.14	0.19	6.25	11.18	2.67	0.52	0.10	100.00
LSM07	Montserrat	DuFrane et al. (2009)	51.42	0.92	18.72	9.06	0.15	5.31	10.86	2.61	0.84	0.12	100.00
GUAD510	Guadeloupe	Van Soest (2000)	46.74	0.85	18.32	10.23	0.15	7.08	14.97	1.34	0.26	0.06	100.00
168	Dominica	Davidson (1984)	50.96	0.89	20.66	9.77	0.19	4.18	10.02	2.71	0.49	0.14	100.00
IAR	Martinique	Labanieh et al. (2010;2012)	47.84	0.75	15.55	9.68	0.16	12.44	11.18	2.04	0.29	0.07	100.00
SL8344	St Lucia	This study	51.77	0.78	18.87	9.35	0.18	5.14	11.02	2.47	0.34	0.09	100.00
STV 315	St Vincent	Heath et al. (1998)	51.68	0.83	17.04	9.03	0.16	7.83	10.65	2.35	0.33	0.09	100.00
BQ5	Bequia	Smith et al. (1996)	50.09	0.74	16.70	10.11	0.24	8.00	11.11	2.59	0.32	0.10	100.00
RW 33	Ile de Caille	Turner et al. (1996)	48.25	0.88	15.42	9.44	0.16	11.72	11.17	2.31	0.54	0.11	100.00
KEJ017	Kick'em Jenny	Huang et al. (2011)	47.50	1.00	16.56	9.27	0.15	11.83	11.11	2.07	0.51	0.26	100.26
LAG4	Grenada	Van Soest (2000)	45.99	0.78	13.05	10.15	0.17	17.38	10.16	1.75	0.44	0.12	100.00

Sample ID	Cr	Ni	Cu	Zn	V	Sc	Rb	Sr	Y	Zr	Ba	Pb	Th	Nb	La
LAS1	271	63	49	27	248	n.a.	10.60	321	18.60	58	226	1.80	1.02	1.80	5.80
8248	9	7	38	52	228	25.50	9.00	288	21.00	60	110	2.13	0.48	1.60	3.50
Kit59	109	39	65	70	303	41.60	5.05	235	18.60	44	62	1.10	0.39	1.50	2.93
95Isn5	2	5	18	41	51	n.a.	20.29	238	12.50	82	257	7.00	2.16	2.02	5.47
8202	29	10	51	74	n.a.	n.a.	4.00	484	12.00	43	56	1.57	0.87	n.a.	3.89
LSM07	71	16	92	70	323	n.a.	9.90	488	15.40	70	148	6.00	2.82	3.13	10.40
GUAD510	120	40	89	68	405	n.a.	2.90	261	11.70	21	45	1.20	0.42	0.76	3.70
168	10	10	97	74	252	32.30	10.70	270	19.40	45	113	2.67	0.96	1.60	4.60
IAR	875	255	n.a.	n.a.	315	54.00	3.75	181	20.10	33	59	1.41	0.26	0.56	2.50
SL8344	n.a.	n.a.	n.a.	n.a.	236	33.31	7.71	178	17.63	49	80	2.31	0.70	1.11	3.34
STV 315	303	75	n.a.	n.a.	277	39.00	8.00	167	18.00	51	81	n.a.	0.49	2.90	3.20
BQ5	148	67	70	73	270	41.00	6.40	200	21.00	48	94	0.90	0.80	n.a.	3.83
RW 33	413	674	68	66	249	n.a.	13.68	261	17.41	67	106	2.45	2.05	3.96	5.91
KEJ017	n.a.	n.a.	n.a.	n.a.	n.a.	55.10	14.20	266	18.50	49	95	n.a.	1.15	n.a.	4.11
LAG4	1120	255	76	77	234	n.a.	12.67	296	16.10	50	110	0.50	2.41	4.55	9.32

Table C.6. (continued).

Sample ID	Ce	Nd	Sm	Eu	Gd	Dy	Er	Yb	Lu	U	Tb	Ta	Hf	Cs
LAS1	12.31	8.05	2.29	0.84	2.70	2.98		1.83	0.29	0.48	0.48	0.10	1.70	0.29
8248	9.60	7.30	2.20	0.81	2.70	3.22	2.01	2.09	0.33	n.a.	n.a.	n.a.	n.a.	n.a.
Kit59	7.45	6.22	2.03	0.78	2.67	2.99	1.87	1.84	0.30	0.17	0.47	0.09	1.25	n.a.
95lsn5	13.56	6.80	1.69	0.62	1.94	1.96	1.36	1.54	0.23	0.76	0.32	0.16	2.45	0.41
8202	9.41	6.39	1.71	0.67	2.05	2.45	1.45	1.40	0.21	n.a.	n.a.	n.a.	n.a.	n.a.
LSM07	23.12	11.38	2.39	0.91	2.84	2.63	n.a.	1.61	0.24	0.76	0.47	0.18	2.22	0.23
GUAD510	8.84	6.07	1.40	0.57	1.62	2.06	n.a.	1.12	0.17	0.13	0.31	0.03	0.75	0.11
168	13.00	8.50	n.a.	n.a.	n.a.	n.a.	n.a.	n.a.	n.a.	n.a.	n.a.	n.a.	n.a.	n.a.
IAR	5.74	5.77	1.94	0.72	2.75	3.22	2.08	1.94	0.28	0.09	0.44	0.04	1.04	0.15
SL8344	8.08	6.75	2.03	0.74	2.57	2.98	1.80	1.92	0.31	0.28	0.46	0.11	1.41	0.40
STV 315	8.20	8.30	2.24	0.83	n.a.	n.a.	n.a.	2.37	0.39	0.26	0.58	0.10	1.75	n.a.
BQ5	8.48	6.72	2.02	0.74	2.66	3.24	2.04	1.99	0.30	0.36	n.a.	n.a.	n.a.	n.a.
RW 33	13.60	8.49	2.29	0.81	2.79	2.99	1.78	1.72	0.27	0.76	0.47	0.25	1.82	0.43
KEJ017	9.50	7.00	2.25	0.85	2.90	3.55	2.02	1.83	0.29	0.58	n.a.	0.19	1.58	n.a.
LAG4	18.11	10.17	2.60	0.86	2.79	2.76	1.67	1.52	0.23	0.86	0.46	0.24	n.a.	0.75

Sample ID	⁸⁷ Sr/ ⁸⁶ Sr	¹⁴³ Nd/ ¹⁴⁴ Nd	²⁰⁶ Pb/ ²⁰⁴ Pb	²⁰⁷ Pb/ ²⁰⁴ Pb	²⁰⁸ Pb/ ²⁰⁴ Pb
LAS1	0.70371	0.51296	18.73	15.64	38.37
8248	0.70361	0.51303	n.a.	n.a.	n.a.
Kit59	0.70359	0.51300	18.96	15.63	38.65
95lsn5	0.70355	n.a.	n.a.	n.a.	n.a.
8202	0.70322	0.51303	18.93	15.62	38.57
LSM07	0.70384	0.51295	18.92	15.63	38.62
GUAD510	0.70378	0.51286	19.05	15.68	38.75
168	0.70461	0.51280	18.97	15.69	38.81
IAR	0.70382	0.51295	19.05	15.66	38.80
SL8344	0.70413	0.51296	19.34	15.75	39.11
STV 315	0.70391	0.51298	19.16	15.70	38.77
BQ5	0.70434	0.51298	19.51	15.74	39.01
RW 33	0.70516	0.51287	19.45	15.73	38.98
KEJ017	0.70564	n.a.	n.a.	n.a.	n.a.
LAG4	0.70508	0.51284	19.38	15.73	38.99

Appendix D

Supplementary data file
of Chapter 5

Content

Table D.1. Details of the analyses of the international standard solutions NBS987 (8ng Sr) and micro-drilled NIST 611 and BCR2 glass standards during in situ Sr isotope analyses by microdrilling + TIMS at the GAU.	292
Table D.2. Details of the Sr blank processed during the analyses of in-situ Sr isotopes by microdrilling + TIMS at the GAU.	292
Table D.3. Details of the composition of the zircon standard 91500 obtained during the in-situ $\delta^{18}\text{O}$ zircon analyses performed at UCLA.	293
Table D.4. Details of the BCR2-G compositions obtained during mineral analyses using LA-ICPMS at the GAU.	294
Table D.5. Representative plagioclase major element composition obtained by electron microprobe.	295
Table D.6. Representative clinopyroxene major element composition obtained by electron microprobe.	297
Table D.7. Representative orthopyroxene major element composition obtained by electron microprobe.	298
Table D.8. Representative amphibole major element composition obtained by electron microprobe	298
Table D.9. Representative biotite major element analyses obtained by electron microprobe.	299
Table D.10. Matrix composition of St Lucia lavas obtained by EDS Zeiss EVO at the GAU.	299
Table D.11. In-situ plagioclase major and trace element concentrations obtained for Pre-SVC1 basalt and rhyolite by LA-ICPMS at the GAU and the calculated Ba, Sr, La and Sm concentrations in the melt in equilibrium with the crystals.	300
Table D.12. In-situ plagioclase major and trace element concentrations obtained for Pre-SVC2 basaltic andesite and SVC1 andesite and dacite by LA-ICPMS at the GAU and the calculated Ba, Sr, La and Sm concentrations in the melt in equilibrium with the crystals.	304
Table D.13. In-situ plagioclase major and trace element concentrations obtained for orthopyroxene- and cummingtonite- bearing SVC 2, 3 dacites by LA-ICPMS at the GAU and the calculated Ba, Sr, La and Sm concentrations in the melt in equilibrium with the crystals.	308
Table D.14. In-situ pyroxene and amphibole major and trace element concentrations obtained for Pre-SVC and SVC lavas by LA-ICPMS at the GAU.	312

Table D.15. In-situ groundmass major and trace element concentrations obtained for Pre-SVC and SVC lavas by LA-ICPMS at the GAU. 313

Table D.16. In-situ zircon $\delta^{18}\text{O}$ compositions in St Lucia lavas obtained using the CAMECA ims 1270 at UCLA and the corresponding U-Th age from Schmitt et al. (2010). 315

Table D.1. Details of the analyses of the international standard solutions NBS987 (8ng Sr) and micro-drilled NIST 611 and BCR2 glass standards during in situ Sr isotope analyses by microdrilling + TIMS at the GAU.

GAU micro-Sr NBS987 (8ng Sr)		GAU micro-Sr NIST 611 Glass (~20 ng Sr)		GAU micro-Sr BCR2-Glass (~ 20 ng Sr)	
$^{87}\text{Sr}/^{86}\text{Sr}$	2 SE	$^{87}\text{Sr}/^{86}\text{Sr}$	2 SE	$^{87}\text{Sr}/^{86}\text{Sr}$	2 SE
0.710246	0.000023	0.709649	0.000011	0.705016	0.00001 1
0.710218	0.000013	0.709630	0.000010	0.705031	0.00001 3
0.710234	0.000011	0.709673	0.000013	0.705013	0.00001 3
0.710251	0.000012	0.709662	0.000012	0.705045	0.00001 7
0.710239	0.000013				
0.710243	0.000007	Average 0.709653		Average 0.705026	
0.710239	0.000017	2 sd 0.000037		2 sd 0.000030	
0.710227	0.000011				
Average	0.710237				
2 sd	0.000021				

Table D.2. Details of the Sr blank processed during the analyses of in-situ Sr isotopes by microdrilling + TIMS at the GAU.

GAU micro-Sr	
Sr (pg)	%tage of smallest sample (~10 ng)
22.0	0.22
33.0	0.33
7.0	0.07
Average:	20.7

Table D.3. Details of the composition of the zircon standard 91500 obtained during the in-situ $\delta^{18}\text{O}$ zircon analyses performed at UCLA

UCLA		
Zircon standard 91500		
	$\delta^{18}\text{O}$ VSMOW	1 SE
	9.96	0.16
	9.85	0.16
	10.06	0.16
	9.68	0.16
	9.88	0.16
	9.71	0.21
	9.86	0.21
	9.49	0.21
	9.83	0.21
	9.51	0.21
Average:	9.78	
2 sd:	0.37	

Table D.4. Details of the BCR2-G compositions obtained during mineral analyses using LA-ICPMS at the GAU. All concentrations are expressed in ppm.

BCR2-G							
Element	55 µm spot size		30 µm * 120 µm line (raster mode)		85 µm spot (for matrix analysis run)	GeoReM preferred value	
	Average (n = 8)	2 sd	Average (n=5)	2sd	Average (n=1)		2 sd
Na23	23340.43	1138.38	21800.74	1079.35	22444.41	23962	1038
Mg25	20125.97	1950.91	19560.89	1482.04	19452.43	22700	1086
Al27	73155.07	3285.82	75477.06	3753.87	74329.30	70920	4234
Si29	274993.28	14363.08	251159.67	14020.48	273952.31	254287	3740
P31	1279.95	58.31	1201.58	98.96	1268.03	1615	88
K39	16228.25	379.07	16105.22	351.30	15224.97	14445.00	664
Ca42	50290.11	851.55	50637.86	312.02	51029.66	50458.00	1572
Ca43	51029.64	0.01	50943.22	149.70	51525.50	50458.00	1572
Sc45	33.01	2.54	33.76	3.29	31.66	33.00	4
Ti47	14599.44	611.91	14219.44	377.73	15093.99	14100.00	2000
V51	429.96	28.95	401.72	18.67	419.69	425.00	36
Cr53	14.82	0.51	13.87	1.29	14.56	17.00	4
Mn55	1603.36	70.20	1460.38	44.47	1516.85	1550.00	140
Fe57	87385.08	11732.18	83042.27	1131.08	84887.99	97475.00	4664
Co59	37.23	2.30	34.92	1.40	34.00	38.00	4
Ni60	11.73	0.24	10.58	0.18	11.16	13.00	4
Ni62	12.20	0.86	12.22	0.61	12.97	13.00	4
Cu63	17.78	2.15	15.71	1.35	17.29	21.00	10
Cu65	18.04	2.53	15.45	0.80	18.41	21.00	10
Zn66	154.22	26.59	143.85	11.29	144.69	125.00	10
Ga69	42.81	38.15	31.67	3.51	35.52	23.00	2
Ga71	23.04	0.89	21.37	0.91	21.22	23.00	2
Rb85	50.13	2.84	47.62	1.14	45.65	47.00	1
Sr86	342.92	4.43	333.81	10.37	344.35	342.00	8
Sr88	345.69	4.49	342.38	3.42	344.16	342.00	8
Y89	33.34	1.79	34.95	5.63	31.11	35.00	6
Zr90	188.78	7.77	195.19	28.92	178.64	184.00	30
Nb93	13.43	1.38	13.53	0.08	12.70	12.50	2
Cs133	1.14	0.04	1.09	0.01	1.05	1.16	0.14
Ba137	690.22	36.50	658.89	35.28	689.28	683	14
La139	24.67	0.45	24.76	1.69	23.19	24.70	0.6
Ce140	52.36	1.48	50.29	1.41	48.98	53.30	1
Pr141	6.87	0.16	6.83	0.19	6.50	6.70	0.8
Nd146	29.31	1.11	29.37	2.17	29.94	28.90	0.6
Sm147	6.54	0.45	6.46	0.44	6.64	6.59	0.14
Eu153	1.97	0.08	1.95	0.08	1.82	1.97	0.04
Gd157	6.44	0.31	6.50	0.79	6.37	6.71	0.14
Tb159	0.97	0.02	0.99	0.12	0.89	1.02	0.16
Dy161	6.34	0.34	6.11	0.70	6.20	6.44	0.12
Ho165	1.25	0.05	1.30	0.13	1.17	1.27	0.16
Er167	3.51	0.19	3.59	0.81	3.45	3.70	0.08
Tm169	0.49	0.03	0.50	0.06	0.45	0.51	0.08
Yb173	3.41	0.18	3.45	0.07	3.37	3.39	0.06
Lu175	0.49	0.04	0.50	0.09	0.45	0.50	0.01
Hf178	4.86	0.21	4.94	0.55	4.84	4.84	0.56
Ta181	0.79	0.02	0.81	0.05	0.73	0.78	0.12
Pb208	11.03	0.46	10.43	1.58	10.15	11.00	2
Th232	6.03	0.19	6.06	0.66	5.63	5.90	0.6
U238	1.84	0.19	1.70	0.24	1.67	1.69	0.24

Table D.5. Representative plagioclase major element composition obtained by electron microprobe. P = phenocryst; MP = microphenocryst; incl = inclusion; Osci = oscillatory; An = anorthite; Ab = albite; Or = orthoclase.

Group	Pre-SVC1 basalt				Pre-SVC1 basaltic andesite			
Sample	SL8344				SL8325			
Name	C3-PI2-d0	C3-PI2-d621	C3-PI2-d777	C3-PI2-d932	C2-PI1-d0	C2-PI1-d53	C2-PI1-d66	C2-PI1-d185
Type	P				P			
Position	Core	mantle	Incl. rich mantle	rim	Core	An rich mantle	An-poor mantle	rim
<i>wt.% oxide</i>								
SiO ₂	44.28	44.50	46.20	48.51	46.65	47.60	47.57	55.60
Al ₂ O ₃	35.60	35.53	34.30	31.38	32.43	32.19	32.12	26.89
MgO	0.09	0.09	0.11	0.81	0.06	0.09	0.09	0.13
CaO	18.91	18.79	17.67	15.27	17.18	16.83	16.62	10.41
FeO	0.50	0.46	0.45	1.28	0.77	0.73	0.71	1.09
Na ₂ O	0.84	0.89	1.61	2.40	1.92	2.16	2.12	5.72
K ₂ O	b.d.l.	b.d.l.	b.d.l.	0.07	0.04	0.06	0.04	0.24
P ₂ O ₅	0.43	0.30	0.31	0.27	n.a	n.a	n.a	n.a
Total	100.7	100.6	100.7	100.0	99.08	99.72	99.29	100.18
An	92.51	92.1	85.75	77.58	83.02	80.85	81.02	49.46
Ab	7.42	7.87	14.11	22.03	16.76	18.81	18.75	49.19
Or	0.07	0.04	0.14	0.40	0.21	0.34	0.24	1.35

Group	Pre-SVC1 rhyolite				Pre-SVC2				
Sample	SL-83-45				SL8326				
Name	C3-PI2-d0	C3-PI2-d530	C1-PI2-d0	C1-PI2-d473	C6-PI3-d56	C6-PI3-d278	C2-PI1-d25	C2-PI1-d688	C2-PI1-d714
Type	P with normal zoning		P with inverse zoning		P Type 1		P Type 2		
Position	core	rim	core	rim	core	Mantle osci.	Core	Mantle Osci. An-rich	Mantle Osci. An-poor
<i>wt.% oxide</i>									
SiO ₂	58.16	58.75	59.67	58.03	42.12	46.61	43.37	47.84	49.76
Al ₂ O ₃	26.61	26.15	26.05	26.90	36.40	33.30	36.17	32.53	31.26
MgO	b.d.l	b.d.l	b.d.l.	b.d.l	b.d.l.	0.07	b.d.l.	0.11	0.11
CaO	8.06	7.54	7.13	8.08	18.53	15.37	18.46	14.67	13.22
FeO	0.33	0.27	0.26	0.34	0.72	0.91	0.71	0.79	0.67
Na ₂ O	6.76	7.05	7.14	6.74	1.14	2.94	1.30	3.38	4.20
K ₂ O	0.17	0.18	0.20	0.20	b.d.l.	0.10	b.d.l.	0.10	0.17
P ₂ O ₅	0.21	0.13	b.d.l	b.d.l	0.44	0.32	0.40	b.d.l	0.35
Total	100.30	100.09	100.43	100.29	99.42	99.67	100.50	99.47	99.80
An	39.34	36.75	35.14	39.39	89.81	73.86	88.57	70.14	62.86
Ab	59.69	62.19	63.69	59.44	10.00	25.55	11.25	29.27	36.19
Or	0.97	1.05	1.16	1.17	0.19	0.59	0.18	0.60	0.95

Group	Pre-SVC2				SVC1		
Sample	SL8326				SLJL02		
Name	C1-PI2-d103	C1-PI2-d668	C1-PI2-d796	C6-PI1-d0	C4-PI1-d0	C4-PI1-d283	C4-PI1-d397
Type	P Type 3		Type 4		P Type 1		
Position	Core	Mantle Osci An-rich			core	Mantle Osci Low An	Mantle Osci High An
<i>wt.% oxide</i>							
SiO ₂	45.39	45.66	49.55	41.94	48.84	53.03	51.07
Al ₂ O ₃	35.84	34.62	31.53	37.40	33.27	30.15	31.85
MgO	0.05	0.04	0.09	0.05	b.d.l	b.d.l	b.d.l
CaO	17.55	16.82	13.58	19.69	15.21	11.61	13.36
FeO	0.74	0.71	0.85	0.55	0.11	0.13	0.11
Na ₂ O	1.74	2.16	3.80	0.60	2.90	4.78	3.96
K ₂ O	0.05	0.06	0.15	b.d.l	0.11	0.23	0.16
P ₂ O ₅	0.44	0.32	0.05	0.39	0.25	0.28	0.24
Total	101.85	100.46	99.66	100.65	100.69	100.18	100.74
An	84.57	80.84	65.82	94.81	73.86	56.56	64.53
Ab	15.17	18.80	33.34	5.21	25.49	42.12	34.58
Or	0.26	0.36	0.84	0.00	0.65	1.32	0.90

Table D.5. (continued).

Group Sample	SVC1			SVC1			SVC1			
	SLJL02			SLJL02			SLJL23			
Name	C4-PI3- d0	C4-PI3- d821	C4-PI3- d719	C2-PI2- d0	C2-PI2- d546	C2-PI2- d598	C2- PI1- d106	C2-PI1- d27	C2-PI1- d400	C2-PI1- d373
Type	P Type 2			P Type 3			P Type 5			
Position	Mantle Osci			Mantle Osci			Mantle Incl. rich			
	Core	An-rich	Mantle Osci An- poor	Core	An-rich	An-poor	Core	An-rich	An-rich	Rim Osci An-poor
<i>wt. % oxide</i>										
SiO ₂	46.17	49.16	54.99	47.53	49.40	53.57	55.41	48.55	49.24	52.97
Al ₂ O ₃	35.24	33.44	29.52	33.82	33.28	30.26	28.90	32.58	32.74	29.86
MgO	b.d.l	b.d.l	b.d.l	b.d.l	b.d.l	b.d.l	b.d.l	b.d.l	b.d.l	b.d.l
CaO	17.53	15.13	10.53	15.78	15.01	11.57	10.60	15.40	15.15	12.22
FeO	0.15	0.16	0.18	0.14	0.09	0.11	0.09	0.16	0.15	0.13
Na ₂ O	1.75	2.98	5.45	2.62	3.06	4.87	5.44	2.78	2.96	4.65
K ₂ O	0.04	0.15	0.29	0.09	0.14	0.23	0.32	0.11	0.11	0.22
P ₂ O ₅	0.24	0.01	b.d.l	0.18	0.15	0.15	0.04	0.26	0.39	0.14
Total	101.18	101.07	100.99	100.16	101.11	100.78	100.8	99.86	100.69	100.15
An	84.47	73.13	50.80	76.46	72.44	55.99	50.89	74.89	73.38	58.48
Ab	15.27	26.03	47.55	23.00	26.77	42.67	47.29	24.49	25.96	40.28
Or	0.26	0.85	1.65	0.54	0.78	1.34	1.82	0.63	0.65	1.23

Group Sample	SVC1			SVC1		Opx-bearing SVC 2,3			
	SLJL02			SLJL02		SLJL83			
Name	C3-PI2- d0	C3-PI2- d299	C3-PI2- d209	C1-PI1- d0	C1-PI1- d38	C5-PI1- d153	C5-PI1- d867	C5-PI1- d994	C5-PI1- d1020
Type	P Type 6			Microlite		P Type 5			
Position	Mantle- rim					Mantle			
	Sodic core	Osci An-rich	Mantle-rim Osci An- poor	Core	Rim	Sodic Core	Incl. rich An-rich	Rim Osci An-rich	Rim Osci An-poor
<i>wt. % oxide</i>									
SiO ₂	53.72	50.77	53.71	51.59	54.28	53.03	46.98	49.88	53.37
Al ₂ O ₃	29.25	31.54	28.75	32.11	29.72	30.14	35.16	32.76	30.41
MgO	b.d.l	b.d.l	b.d.l	b.d.l	b.d.l	b.d.l	b.d.l	b.d.l	b.d.l
CaO	10.80	13.32	10.57	13.31	10.95	11.07	16.26	13.92	11.11
FeO	0.12	0.11	0.13	0.19	0.27	0.12	0.11	0.14	0.13
Na ₂ O	5.31	3.89	5.40	3.85	5.30	5.05	2.38	3.59	4.87
K ₂ O	0.25	0.17	0.27	0.20	0.30	0.25	0.12	0.15	0.28
P ₂ O ₅	0.19	0.09	0.09	b.d.l	0.40	b.d.l	0.12	0.28	0.10
Total	99.65	99.90	98.96	101.17	101.24	99.61	101.13	100.72	100.29
An	52.17	64.78	51.16	64.89	52.41	53.99	78.51	67.60	54.85
Ab	46.40	34.22	47.26	33.94	45.86	44.55	20.79	31.51	43.51
Or	1.43	1.00	1.58	1.17	1.73	1.45	0.71	0.89	1.64

Group Sample	Opx-bearing SVC 2,3			Opx-bearing SVC 2,3		Cgt-bearing SVC2,3			
	SL8303			SLJL83		SLJL51			
Name	C1-PI6- d655	C1-PI6- d218	C1-PI6- d246	C1-PI3- d60	C1-PI3- d0	C3-PI1- d0	C3-PI1- d713	C3-PI1- d535	C3-PI1- d815
Type	P Type 6			Microlite		P Type 2			
Position	Mantle-rim					Mantle			
	An-poor core	Osci An- rich	Mantle-rim Osci An- poor	Core	Rim	Core	Osci An-rich	Mantle Osci An-poor	Mantle incl. rich An-rich
<i>wt. % oxide</i>									
SiO ₂	54.55	50.91	56.62	43.60	45.33	47.08	50.50	52.40	48.04
Al ₂ O ₃	28.00	30.18	26.81	36.43	35.67	34.83	32.13	29.47	34.06
MgO	b.d.l	b.d.l	b.d.l	0.04	b.d.l	b.d.l	b.d.l	b.d.l	b.d.l
CaO	10.83	13.51	9.55	18.59	17.47	15.82	13.19	10.69	14.81
FeO	0.17	0.12	0.11	0.36	0.43	0.10	0.11	0.08	0.12
Na ₂ O	5.28	3.79	6.11	1.12	1.61	2.53	3.92	4.89	3.16
K ₂ O	0.23	0.14	0.34	b.d.l	b.d.l	0.09	0.17	0.27	0.13
P ₂ O ₅	n.a	n.a	n.a	0.22	0.50	0.11	0.40	0.42	0.29
Total	99.10	98.66	99.55	100.42	101.06	100.56	100.41	98.21	100.62
An	52.45	65.77	45.48	90.07	85.57	77.19	64.36	53.84	71.64
Ab	46.22	33.43	52.60	9.78	14.28	22.30	34.63	44.56	27.63
Or	1.33	0.79	1.92	0.14	0.16	0.51	1.01	1.61	0.73

Table D.5. (continued).

Group Sample	Cgt-bearing SVC2,3 SL8308		Cgt-bearing SVC2,3						
	C1-PI7- d27	C1-PI7- d242	SLJL51		SL-JL-51		SL-JL-51		
Name			C4-PI2- d109	C4-PI2- d136	C4-PI2- d109	C1-PI4- d0	C1-PI4- d58	C1-PI3- d0	C1-PI3- d102
Type	P Type 5		P Type 6			An-poor core microlite		An-rich-core microlite	
Position	An-poor Core	Mantle Incl. rich high An	An-poor core	Mantle-rim Osci High An	Mantle- rim Osci Low An	Core	Rim	Core	Rim
wt.% oxide									
SiO ₂	56.25	49.56	55.37	49.44	55.37	53.37	52.86	44.33	49.96
Al ₂ O ₃	27.35	31.90	28.76	32.28	28.76	29.36	30.15	36.56	31.49
MgO	b.d.l	b.d.l	b.d.l	b.d.l	b.d.l	b.d.l	b.d.l	b.d.l	b.d.l
CaO	10.03	15.29	9.30	13.48	9.30	10.46	11.08	17.90	12.75
FeO	0.10	0.10	0.07	0.08	0.07	0.08	0.17	0.10	0.11
Na ₂ O	5.70	2.87	5.81	3.62	5.81	5.49	5.23	1.57	4.40
K ₂ O	0.32	0.12	0.34	0.15	0.34	0.28	0.27	0.04	0.19
P ₂ O ₅	n.a	n.a	0.20	0.08	0.20	b.d.l	b.d.l	0.31	0.19
Total	99.77	99.85	99.81	99.11	99.81	98.92	99.58	100.82	99.09
An	48.40	74.13	46.01	66.68	46.01	50.46	53.11	86.13	60.90
Ab	49.74	25.18	52.01	32.43	52.01	47.95	45.37	13.64	38.05
Or	1.86	0.69	1.98	0.88	1.98	1.59	1.52	0.23	1.06

Table D.6. Representative clinopyroxene major element composition obtained by electron microprobe. P = phenocryst; MP = microphenocryst; incl = inclusion; Mg# = 100*Mg/(Mg+Fe (ii)) with Fe (ii) and Fe (iii) calculated based on the minimum amount of Fe (iii) permissible in the structural formula. En = enstatite; Fs = ferrosilite; Wo = wollastonite.

Group Sample	Pre-SVC1 basalt SL-83-44				Pre-SVC1 rhyolite SL-83-45	Pre-SVC2 basaltic andesite SL-83-26	
	C2-Py1- d132	C2-Py1- d239	C2-Py1- d451	C2-Py1- d560	C3-Py1	C1-opx2a	C1Opx2B
Type	P				P	P	
Position	Core	Mantle Incl. rich	Mantle no incl.	rim	core	Core	Rim
wt. % oxide							
SiO ₂	51.13	50.67	51.51	51.98	49.00	48.60	48.78
TiO ₂	0.34	0.36	0.28	0.28	0.31	0.42	0.56
Al ₂ O ₃	2.30	3.22	2.42	2.25	1.00	2.46	2.15
FeO*	6.85	6.75	7.01	6.78	23.04	8.35	12.49
MnO	0.20	0.18	0.20	0.19	0.98	0.22	0.34
MgO	17.01	16.39	17.20	17.54	6.11	15.58	15.65
CaO	21.06	21.38	20.57	20.48	19.01	21.68	18.31
Na ₂ O	0.19	0.20	0.20	0.18	0.25	0.20	0.21
K ₂ O	b.d.l.	b.d.l.	b.d.l.	b.d.l.	b.d.l.	b.d.l.	b.d.l.
Cr ₂ O ₃	0.16	0.18	0.14	0.12	b.d.l.	b.d.l.	b.d.l.
NiO	b.d.l.	b.d.l.	0.03	0.04	b.d.l.	b.d.l.	b.d.l.
Total	99.49	99.72	99.83	100.24	99.91	98.16	98.78
En	0.47	0.46	0.48	0.48	0.18	0.43	0.43
Fs	0.11	0.11	0.11	0.11	0.39	0.13	0.19
Wo	0.42	0.43	0.41	0.41	0.41	0.43	0.37
Mg#	0.83	0.90	0.89	0.89	0.33	0.77	0.69

Group Sample	SVC1 SL-JL-02	Opx-bearing SVC2,3 SL-JL-83		
	C4-Py1	C3-Py1- d25	C3-Py1- d136	C3-Py1- d123
Type	MP	MP		
Position	core	Core	Mantle Osci En-rich	Mantle Osci En-rich
wt. % oxide				
SiO ₂	47.74	50.14	48.09	47.65
TiO ₂	1.34	0.29	0.54	0.66
Al ₂ O ₃	7.98	3.62	6.19	6.42
FeO*	5.32	3.66	4.47	5.45
MnO	0.11	0.09	0.08	0.16
MgO	13.96	17.11	15.62	15.03
CaO	22.54	23.63	23.57	23.02
Na ₂ O	0.22	0.18	0.21	0.19
K ₂ O	b.d.l.	b.d.l.	b.d.l.	b.d.l.
Cr ₂ O ₃	0.14	0.84	0.80	0.22
NiO	b.d.l.	b.d.l.	0.03	0.03
Total	99.79	100.00	99.77	99.15
En	0.42	0.47	0.44	0.43
Fs	0.09	0.06	0.07	0.09
Wo	0.49	0.47	0.48	0.48
Mg#	0.88	0.91	0.93	0.55

Table D.7. Representative orthopyroxene major element composition obtained by electron microprobe. P = phenocryst; MP = microphenocryst; incl = inclusion; Mg# = $100 \cdot \text{Mg} / (\text{Mg} + \text{Fe (ii)})$ with Fe (ii) and Fe (iii) calculated based on the minimum amount of Fe (iii) permissible in the structural formula. En = enstatite; Fs = ferrosilite; Wo = wollastonite.

Group	Pre-SVC2 basaltic andesite	SVC1 dacite			Opx-SVC2,3	
Sample	SL-83-26	SL-JL-23			SL-83-03	
Name	C3-Py1B	C4-Py2- d0	C4-Py2- d343	C4-Py2- d581	C3-Py1	C3- PY2
Grain	P	P			P	
	Core	Core En- poor	Mantle. En- rich	Rim En- poor.	Core	Rim
<i>Wt. % oxide</i>						
SiO ₂	49.85	50.04	50.88	50.27	51.30	51.03
TiO ₂	0.40	0.10	0.19	0.14	0.11	0.10
Al ₂ O ₃	1.34	0.46	0.89	0.48	0.65	0.68
FeO*	21.32	29.29	25.64	30.88	33.74	32.97
MnO	0.49	0.76	0.66	0.81	0.92	1.00
MgO	23.02	17.81	20.19	16.41	12.95	13.23
CaO	2.25	0.93	1.04	1.00	0.81	1.46
Na ₂ O	0.01	0.01	b.d.l.	0.01	b.d.l.	0.02
K ₂ O	b.d.l.	b.d.l.	0.01	b.d.l.	b.d.l.	0.01
Cr ₂ O ₃	b.d.l.	b.d.l.	b.d.l.	b.d.l.	0.01	b.d.l.
NiO	0.05	0.01	0.01	b.d.l.	b.d.l.	0.02
Total	98.72	99.44	99.53	100.02	100.49	100.80
En	0.62	0.50	0.57	0.47	0.39	0.40
Fs	0.32	0.46	0.40	0.50	0.57	0.55
Wo	0.04	0.02	0.02	0.02	0.02	0.03
Mg#	0.66	0.51	0.57	0.48	0.41	0.42

Table D.8. Representative amphibole major element composition obtained by electron microprobe. P = phenocryst; MP = microphenocryst; Mg# = $100 \cdot \text{Mg} / (\text{Mg} + \text{Fe (ii)})$ with Fe (ii) and Fe (iii) calculated based on the minimum amount of Fe (iii) permissible in the structural formula. Mg## = $100 \cdot \text{Mg} / (\text{Mg} + \text{Fetot})$; Mg-Hst = Magnesio-hastingsite; Tsch = tschermakite; Mg-Hbl = magnesio-hornblende; T, P, oxygen fugacity and water in the melt were calculated using the model of Ridolfi et al. (2009).

Group	Opx-bearing SVC2,3 dacite		Opx-bearing SVC2,3 dacite		Opx-bearing SVC2,3 dacite	Cgt-bearing SVC2,3 dacite		
Sample	SL-JL-83		SL-83-03		SL-JL-22	SL-83-08		
Name	C1-Am1	C2-Am1	C3-Am1	C3-Am2	C5-Am2	C1-Am1	C1-Am2	C4-Am1
Grain	High Mg## MP	High Mg## MP	MP	MP	MP	MP	MP	P
Position	Core	Core	Core	Rim	Core	Cgt	Cgt	Cgt
<i>Wt. % oxide</i>								
SiO ₂	40.86	41.39	45.05	45.48	47.16	53.47	54.03	52.75
TiO ₂	1.79	1.66	1.38	1.48	1.54	0.39	0.31	0.42
Al ₂ O ₃	14.95	14.08	9.79	9.56	7.41	2.75	2.30	3.00
FeO	8.35	9.69	21.70	23.34	14.92	26.62	26.61	26.50
MnO	0.10	0.14	0.43	0.43	0.32	0.78	0.74	0.78
MgO	15.99	15.80	9.17	9.23	14.74	13.83	14.50	13.67
CaO	12.36	11.99	10.16	10.02	10.76	1.68	1.53	1.78
Na ₂ O	2.01	2.06	2.08	2.19	1.22	0.43	0.34	0.40
K ₂ O	0.44	0.34	0.36	0.23	0.30	0.02	0.01	0.02
Cr ₂ O ₃	0.01	0.08	0.01	0.02	0.04	0.00	0.03	0.00
NiO	0.03	0.03	b.d.l.	b.d.l.	b.d.l.	0.01	b.d.l.	0.01
Total	96.88	97.25	100.13	101.99	98.42	99.99	100.40	99.33
Si/Al	2.3	2.5	3.90	4.04	5.40	16.47	19.90	14.91
Ti	0.19	0.18	0.15	0.16	0.17	0.04	0.03	0.05
Al ^{Tot}	2.54	2.40	1.72	1.65	1.27	0.47	0.39	0.52
Fe(iii)/Fetot	0.63	0.555	0	0.00	0.17	0.00	0.00	0.00
Mg#	0.90	0.87	0.43	0.41	0.68	0.48	0.49	0.48
Mg##	0.77	0.74	0.43	0.41	0.64	0.48	0.49	0.48
Name	Mg-Hst	Tsch	Mg-Hbl	Tsch	Mg-Hbl	Cgt	Cgt	Cgt
T (°C)	1044	1016	821	814	841	-	-	-
1 SE	22	22	22	22	22	-	-	-
P (MPa)	724	580	212	192	114	-	-	-
1 SE	80	64	53	48	13	-	-	-
ΔNNO	1.42	1.51	0.01	0.09	1.94	-	-	-
logfO ₂	-8.02	-8.38	-13.37	-13.45	-11.09	-	-	-
1 SE	0.4	0.4	0.4	0.4	0.4	-	-	-
H ₂ O _{melt} (wt.%)	7.98	7.58	7.45	7.14	5.37	-	-	-
1 SE	1.20	1.14	0.40	1.07	0.40	-	-	-

Table D.9. Representative biotite major element analyses obtained by electron microprobe. P = phenocryst; MP = microphenocryst; Res = resorbed; Mg# = $100 \cdot \text{Mg} / (\text{Mg} + \text{Fe (ii)})$. OH was calculated following Tindle and Webb (1990).

Group Sample	Opx-bearing SVC 2,3 dacite SL-83-24		Cgt-bearing SVC 2,3 dacite SL-83-08	
	C1-Bi1	C4-Bi1	C2-Bi2	C1-Bi1
Grain	Res. P	Res. P	MP	MP
Position	Core	Core	Core	Core
<i>Wt. % oxide</i>				
SiO ₂	35.06	35.71	37.44	37.50
TiO ₂	4.58	4.36	4.35	4.44
Al ₂ O ₃	14.73	14.84	15.71	15.92
FeO	21.61	21.55	20.41	20.32
MnO	0.16	0.16	0.13	0.15
MgO	11.40	11.54	10.02	10.27
CaO	0.00	0.03	0.00	0.04
Na ₂ O	0.52	0.53	0.37	0.42
K ₂ O	8.80	8.85	8.14	8.13
Cr ₂ O ₃	0.01	0.00	0.02	0.03
NiO	0.02	0.00	0.02	0.00
Total	96.88	97.58	96.60	97.22
Mg#	0.42	0.42	0.42	0.42

Table D.10. Matrix composition of St Lucia lavas obtained by EDS Zeiss EVO at the GAU.

Group	Pre-SVC1 basalt	Pre-SVC1 basaltic andesite	Pre-SVC1 rhyolite	Pre-SVC2 basaltic andesite	SVC1	SVC1	Opx-bearing SVC2,3	Opx-bearing SVC2,4	Opx-bearing SVC2,5	Opx-bearing SVC2,5	Cgt-bearing SVC2,3	Cgt-bearing SVC2,3
WR Sample	SL8344	SL8325	SL8345	SL8326	SLJL02	SLJL23	SLJL83	SL 8324	SLJL22	SL8303	SLJL51	SLJL33
SiO ₂	55.18	60.72	74.31	59.38	75.90	77.92	73.49	73.56	72.71	70.96	73.45	76.50
TiO ₂	0.78	1.38	0.20	1.18	0.22	0.28	0.17	0.30	0.37	0.52	0.38	0.11
Al ₂ O ₃	18.46	16.26	13.39	16.45	14.36	14.30	13.70	15.17	13.64	15.08	14.24	13.65
FeOt	7.61	7.49	3.05	8.55	1.32	1.25	2.48	1.94	3.00	3.67	2.22	0.94
MnO	0.22	0.16	0.09	0.21	b.d.l.	0.00	0.03	0.03	0.11	0.03	0.07	0.07
MgO	4.72	2.36	0.18	2.45	0.20	0.25	1.05	0.75	1.40	1.11	0.58	0.16
CaO	9.54	6.52	2.14	7.11	2.19	2.45	2.92	2.38	3.30	3.27	2.48	1.57
Na ₂ O	3.01	3.91	4.69	3.34	2.64	2.96	3.05	2.72	2.86	2.91	2.98	3.45
K ₂ O	0.53	1.30	1.92	1.29	3.08	3.00	2.97	3.15	2.72	2.51	3.59	3.69
Cr ₂ O ₃	b.d.l.	b.d.l.	0.02	0.04	0.02	b.d.l.	0.01	b.d.l.	b.d.l.	b.d.l.	0.01	-0.02
NiO	0.02	-0.02	0.02	0.05	0.08	0.01	0.10	0.03	-0.03	-0.04	0.00	-0.05
Total	100.00	100.00	100.00	100.00	100.00	102.34	100.00	100.00	100.00	100.00	100.00	100.00
Matrix classification	basaltic andesite	andesite	rhyolite	basaltic andesite	rhyolite	ryolite	rhyolite	rhyolite	rhyolite	rhyolite	Dacite	rhyolite
WR SiO ₂	52.26	56.43	72.22	53.96	62.82	63.94	66.49	65.97	63.56	64.36	66.39	67.12

Table D.11. In-situ plagioclase major and trace element concentrations obtained for Pre-SVC1 basalt and rhyolite by LA-ICPMS at the GAU and the calculated Ba, Sr, La and Sm concentrations in the melt in equilibrium with the crystals. Ba and Sr melt concentrations were calculated using both Blundy and Wood (1991) (B & W, 1991) and Bindeman et al. (1998) (B (1998)) equations. Melt La and Sm concentrations were calculated using Kds from Table 5.3. # = number; An = the anorthite content obtained by electron microprobe for each spot analysis.

Name	Zone type	Zone texture/comment	Type	#	Na	Mg	Al	Si	P	K	Ca	Sc	Ti	V	Cr	Mn	Fe
<i>Pre-SVC1 basalt:</i>																	
44C2PLP1	Core	Inclusion-rich	-	45	10317	760	186461	223167	22	185	130125	1.01	96	2.67	<0,41	42	3890
44C2PLP2	Outer rim	Homogeneous & inclusion-free	-	46	16678	1077	154657	208578	23	430	102945	1.06	158	2.58	<0,33	40	3897
44C2-2R1	Outer rim	Homogeneous & inclusion-free	-	51	12650	1043	151268	193912	16	369	102917	2.83	154	3.37	<0,84	45	3387
8344C3P1	Core	Homogeneous & inclusion-free	-	47	7946	964	189057	228642	18	163	134449	1.00	82	2.44	<0,42	41	4334
8344C3P2	Mantle	Inclusion-rich	-	48	9999	755	182219	227834	21	178	128739	1.03	96	2.24	<0,39	37	3867
44C3-2P1	Mantle	Inclusion-poor	-	58	7207	608	185012	221946	36	188	133649	3.18	73	1.88	<0,30	38	2733
8344C3P4	Mantle	Inclusion-rich	-	49	7839	558	180391	222067	25	124	127656	0.99	73	2.15	0.51	38	3649
8344C3P5	Outer rim	Inclusion-rich	-	50	13041	917	158269	215053	19	293	108473	0.98	122	2.59	<0,37	39	3940
44C3-2P2	Outer rim	Inclusion-poor	-	59	11642	780	158180	195632	18	238	109349	2.82	107	2.09	0.47	35	2643
44C2-3P1	Core	Homogeneous & inclusion-free	-	52	7200	546	178396	199062	15	117	133792	3.35	69	2.17	<0,29	35	2110
44C2-3P2	Mantle	inclusion-rich	-	53	11288	892	182952	230940	20	235	131076	3.47	110	2.72	<0,35	43	2823
44C2-3P3	Outer rim	Normal zoning & inclusion-free	-	54	19525	1093	153875	219220	12	576	105776	3.28	190	3.36	<0,26	46	3247
44C3-1P1	Core	Homogeneous & inclusion-free	-	55	7700	602	187500	220811	19	124	134006	3.26	72	1.98	<0,34	38	2527
44C3-1P2	Mantle	inclusion-rich	-	56	9019	665	180775	210168	15	146	132220	3.13	84	2.26	<0,29	36	2640
44C3-1R3	Outer rim	Normal zoning & inclusion-free	-	57	12064	813	156915	190761	<7,46	218	105775	3.03	129	2.23	<0,80	32	2770
<i>Pre-SVC1 rhyolite:</i>																	
45C1-2P1	Core	Homogeneous & inclusion-free	-	61	61065	51.2	143166.88	311537	15.8	2009.24	50386	3.22	72	0.01	<0,28	33	1937
45C1-2P2	Outer rim	Homogeneous & inclusion-free	-	62	56622	131	145182.89	312610	13.4	1775.06	56890	3.67	76	<0,0078	<0,23	40	2149
45C3-2P1	Core	Homogeneous & inclusion-free	-	63	64970	84	149605.06	340355	14.8	1977.41	57105	3.67	90	0.01	0.42	40	2323
45C3-2P2	Outer rim	Homogeneous & inclusion-free	-	64	57437	73	143595.44	313453	12.8	1709.52	54960	3.15	73	<0,0137	<0,39	38	1962

Table D.11. (continued).

Name	Zone type	Zone texture/comment	Type	#	Co	Ni	Cu	Zn	Ga	Rb	Sr	Y	Zr	Nb	Cs	Ba	La
<i>Pre-SVC1 basalt:</i>																	
44C2PLP1	Core	Inclusion-rich	-	45	0.674	<0,078	43.9	2.66	19.8	<0,041	284	0.12	0.027	<0,0077	<0,0188	10.90	0.23
44C2PLP2	Outer rim	Homogeneous & inclusion-free	-	46	0.842	0.214	9.2	3.79	15.2	0.075	264	0.12	0.105	<0,0065	<0,0151	14.91	0.19
44C2-2R1	Outer rim	Homogeneous & inclusion-free	-	51	0.740	0.33	12.2	4.37	14.8	0.340	247	0.19	0.293	0.064	0.016	12.49	0.30
8344C3P1	Core	Homogeneous & inclusion-free	-	47	0.852	0.676	19.1	2.16	22.2	0.107	303	0.10	0.146	0.004	<0,0197	9.03	0.16
8344C3P2	Mantle	Inclusion-rich	-	48	0.585	0.196	25.8	3.51	18.3	<0,040	280	0.11	<0,0163	<0,0032	<0,0192	9.78	0.16
44C3-2P1	Mantle	Inclusion-poor	-	58	0.451	0.162	23.9	2.78	18.1	0.083	268	0.09	<0,0076	<0,0033	<0,0055	8.28	0.15
8344C3P4	Mantle	Inclusion-rich	-	49	0.466	<0,067	18.2	2.07	18.8	0.045	264	0.09	0.016	<0,0093	<0,0173	7.35	0.13
8344C3P5	Outer rim	Inclusion-rich	-	50	0.867	0.279	12.5	3.27	19.1	<0,041	247	0.12	0.092	<0,0060	<0,0153	11.32	0.21
44C3-2P2	Outer rim	Inclusion-poor	-	59	0.615	0.072	7.9	2.77	16.3	0.047	243	0.09	<0,0107	<0,0024	<0,0041	10.54	0.15
44C2-3P1	Core	Homogeneous & inclusion-free	-	52	0.460	0.074	12.6	1.81	16.6	0.033	270	0.12	<0,0078	<0,0031	0.262	8.27	0.14
44C2-3P2	Mantle	inclusion-rich	-	53	0.785	0.316	12.2	3.06	20.4	0.060	277	0.11	0.141	<0,0059	<0,0054	10.63	0.18
44C2-3P3	Outer rim	Normal zoning & inclusion-free	-	54	0.839	0.131	9.6	6.26	17.6	0.184	266	0.14	0.049	<0,0032	<0,0046	17.55	0.24
44C3-1P1	Core	Homogeneous & inclusion-free	-	55	0.445	0.164	27.1	1.88	18.1	0.019	272	0.09	0.005	<0,0037	<0,0054	8.05	0.13
44C3-1P2	Mantle	inclusion-rich	-	56	0.538	0.128	16.8	2.80	17.7	0.025	268	0.11	0.016	<0,0037	<0,0041	9.24	0.16
44C3-1R3	Outer rim	Normal zoning & inclusion-free	-	57	0.593	<0,103	13.7	3.97	13.9	0.056	247	0.10	<0,022	<0,0053	<0,0195	10.79	0.15
<i>Pre-SVC1 rhyolite:</i>																	
45C1-2P1	Core	Homogeneous & inclusion-free	-	61	0.050	<0,031	3.23	16.56	29.3	0.280	422	0.22	0.010	<0,00158	<0,0067	151	1.40
45C1-2P2	Outer rim	Homogeneous & inclusion-free	-	62	0.040	0.040	3.04	18.89	28.3	0.290	430	0.19	0.210	<0,0026	0.013	106	1.29
45C3-2P1	Core	Homogeneous & inclusion-free	-	63	0.130	0.030	3.02	15.05	33.0	0.230	457	0.21	0.040	<0,0035	<0,0083	123	1.32
45C3-2P2	Outer rim	Homogeneous & inclusion-free	-	64	0.080	<0,036	3.03	14.89	30.7	0.160	432	0.19	0.020	<0,0063	<0,0075	111	1.41

Table D.11. (continued).

Name	Zone type	Zone texture/comment	Type	#	Ce	Pr	Nd	Sm	Eu	Gd	Tb	Dy	Ho	Er	Tm	Yb	Lu
<i>Pre-SVC1 basalt:</i>																	
44C2PLP1	Core	Inclusion-rich	-	45	0.43	0.041	0.19	0.049	0.22	<0,031	0.007	<0,046	0.009	0.030	0.006	<0,038	<0,00294
44C2PLP2	Outer rim	Homogeneous & inclusion-free	-	46	0.43	0.065	0.12	0.061	0.16	<0,040	0.005	<0,037	<0,0035	<0,015	<0,00233	<0,021	<0,0043
44C2-2R1	Outer rim	Homogeneous & inclusion-free	-	51	0.44	0.042	0.14	<0,042	0.18	0.105	<0,0072	0.035	0.011	<0,052	<0,0124	<0,066	<0,0134
8344C3P1	Core	Homogeneous & inclusion-free	-	47	0.35	0.060	0.25	<0,039	0.22	0.063	0.0049	<0,022	<0,0095	<0,034	0.001	0.022	<0,0068
8344C3P2	Mantle	Inclusion-rich	-	48	0.31	0.049	0.26	0.033	0.17	0.048	<0,0055	<0,032	<0,0062	0.021	<0,0052	<0,040	0.0073
44C3-2P1	Mantle	Inclusion-poor	-	58	0.28	0.042	0.20	0.035	0.14	0.020	<0,0045	<0,0162	0.003	<0,0159	<0,00274	<0,0126	<0,0021
8344C3P4	Mantle	Inclusion-rich	-	49	0.27	0.037	0.15	<0,037	0.16	<0,039	0.0070	0.038	0.006	<0,031	<0,0070	<0,033	0.0037
8344C3P5	Outer rim	Inclusion-rich	-	50	0.37	0.046	0.17	0.089	0.19	0.033	<0,0065	<0,045	0.006	0.018	<0,0054	<0,030	<0,0045
44C3-2P2	Outer rim	Inclusion-poor	-	59	0.31	0.045	0.23	0.029	0.17	0.039	0.0066	0.035	0.003	<0,0101	<0,0030	<0,0178	<0,0023
44C2-3P1	Core	Homogeneous & inclusion-free	-	52	0.31	0.034	0.22	0.043	0.16	0.060	0.005	0.060	0.009	0.014	0.008	<0,00	<0,0030
44C2-3P2	Mantle	inclusion-rich	-	53	0.35	0.053	0.21	0.064	0.17	0.033	0.003	0.035	0.006	0.015	<0,0040	<0,0157	<0,00260
44C2-3P3	Outer rim	Normal zoning & inclusion-free	-	54	0.45	0.062	0.30	0.062	0.24	0.085	0.002	0.030	0.004	<0,0120	<0,0020	<0,0073	<0,00271
44C3-1P1	Core	Homogeneous & inclusion-free	-	55	0.29	0.037	0.15	<0,027	0.14	0.030	0.006	<0,0218	<0,0036	0.014	<0,0021	<0,0259	<0,0043
44C3-1P2	Mantle	inclusion-rich	-	56	0.34	0.039	0.28	<0,022	0.17	0.037	<0,0025	0.039	<0,0032	0.016	<0,0027	<0,0150	<0,0032
44C3-1R3	Outer rim	Normal zoning & inclusion-free	-	57	0.30	0.047	0.13	0.060	0.10	<0,090	<0,0079	<0,033	<0,0063	<0,042	<0,0110	<0,057	<0,0064
<i>Pre-SVC1 rhyolite:</i>																	
45C1-2P1	Core	Homogeneous & inclusion-free	-	61	2.47	0.250	1.19	0.180	3.14	0.089	0.016	0.040	0.006	0.040	<0,0033	<0,0174	<0,0022
45C1-2P2	Outer rim	Homogeneous & inclusion-free	-	62	2.49	0.290	1.12	0.180	3.00	0.100	0.010	0.077	<0,0041	0.013	0.004	<0,011	<0,00180
45C3-2P1	Core	Homogeneous & inclusion-free	-	63	2.37	0.230	1.09	0.240	3.11	0.105	0.010	0.046	0.015	0.020	<0,0039	<0,020	<0,0016
45C3-2P2	Outer rim	Homogeneous & inclusion-free	-	64	2.45	0.250	1.14	0.110	3.17	0.138	0.010	0.061	0.010	0.011	0.005	<0,022	<0,0062

Table D.11. (continued).

Name	Zone type	Zone texture/comment	Type	#	Hf	Ta	Pb	Th	U	An	B & W (1991) Melt Sr	B & W (1991) Melt Ba	B (1998) Melt Sr	B (1998) Melt Ba	Melt La	Melt Sm	Melt La/Sm
<i>Pre-SVC1 basalt:</i>																	
44C2PLP1	Core	Inclusion-rich	-	45	<0,029	<0,0079	0.17	<0,0113	<0,0070	88	206	99	239	171	6.49	3.71	1.75
44C2PLP2	Outer rim	Homogeneous & inclusion-free	-	46	<0,0117	<0,00251	0.20	<0,0034	<0,0083	70	139	71	155	105	6.06	6.74	0.90
44C2-2R1	Outer rim	Homogeneous & inclusion-free	-	51	<0,028	<0,0095	0.24	0.0126	0.014	80	122	71	133	92	5.55	4.62	1.20
8344C3P1	Core	Homogeneous & inclusion-free	-	47	<0,0175	<0,0031	0.23	<0,0071	<0,0080	92	244	94	286	174	4.71		
8344C3P2	Mantle	Inclusion-rich	-	48	<0,0131	<0,0068	0.18	<0,0100	<0,0118	88	155	79	176	125	4.22	4.55	0.93
44C3-2P1	Mantle	Inclusion-poor	-	58	<0,0117	<0,0026	0.22	<0,0056	<0,0053	92	203	88	235	152	4.63	2.50	1.85
8344C3P4	Mantle	Inclusion-rich	-	49	<0,0232	<0,0057	0.13	0.0060	<0,0082	86	182	62	209	103	3.71		
8344C3P5	Outer rim	Inclusion-rich	-	50	<0,0086	<0,0074	0.18	<0,0093	<0,0081	78	216	87	253	161	4.39	2.65	1.65
44C3-2P2	Outer rim	Inclusion-poor	-	59	<0,0094	0.00169	0.16	0.0026	<0,0027	78	147	85	166	131	8.56		
44C2-3P1	Core	Homogeneous & inclusion-free	-	52	0.019	<0,0027	0.15	<0,0043	<0,00161	91	214	84	250	155	4.17	3.26	1.28
44C2-3P2	Mantle	inclusion-rich	-	53	<0,0120	<0,00214	0.21	<0,0048	<0,0018	89	207	100	241	177	5.05	4.85	1.04
44C2-3P3	Outer rim	Normal zoning & inclusion-free	-	54	<0,0043	<0,00298	0.22	<0,00173	<0,0036	72	129	89	142	121	6.90	4.70	1.47
44C3-1P1	Core	Homogeneous & inclusion-free	-	55	<0,0163	<0,0040	0.13	<0,0061	0.0043	91	215	82	252	151	3.79		
44C3-1P2	Mantle	inclusion-rich	-	56	0.0094	<0,0032	0.14	<0,0068	<0,0030	90	205	90	238	161	4.45		
44C3-1R3	Outer rim	Normal zoning & inclusion-free	-	57	<0,0216	<0,0078	0.14	<0,0120	<0,0078	82	136	151	143	171	14.2	2.35	6.04
<i>Pre-SVC1 rhyolite:</i>																	
45C1-2P1	Core	Homogeneous & inclusion-free	-	61	0.0078	<0,0028	1.08	<0,00315	<0,00263	35	59	213	56	151	40	13.64	2.94
45C1-2P2	Outer rim	Homogeneous & inclusion-free	-	62	<0,0090	<0,0023	1.07	0.0086	0.0064	39	69	180	67	139	37	13.71	2.69
45C3-2P1	Core	Homogeneous & inclusion-free	-	63	<0,0114	<0,0036	0.95	<0,0057	<0,0064	39	73	208	71	160	38	18	2.10
45C3-2P2	Outer rim	Homogeneous & inclusion-free	-	64	0.016	<0,00255	1.08	0.0107	<0,0058	38	66	178	64	133	40	8.03	5.03

Table D.12. In-situ plagioclase major and trace element concentrations obtained for Pre-SVC2 basaltic andesite and SVC1 andesite and dacite by LA-ICPMS at the GAU and the calculated Ba, Sr, La and Sm concentrations in the melt in equilibrium with the crystals. Ba and Sr melt concentrations were calculated using both Blundy and Wood (1991) (B & W, 1991) and Bindeman et al. (1998) (B (1998)) equations. Melt La and Sm concentrations were calculated using Kds from Table 5.3. # = number; An = the anorthite content obtained by electron microprobe for each spot analysis.

Name	Zone type	Zone texture/comment	Type	#	Na	Mg	Al	Si	P	K	Ca	Sc	Ti	V	Cr	Mn	Fe
<i>Pre-SVC2 basaltic andesite:</i>																	
8326P1_2	Core	Homogeneous & inclusion-free	Type 1 alt.	3	19590	612	188595	256471	24.9	713	120194	2.36	216	4.18	<2,09	54	4342
8626P1_3	Mantle	Oscillatory-inclusion free	Type 1 alt.	1	27741	787	167700	258962	13.4	1300	97818	2.74	351	5.40	<1,19	52	4546
8626P1_4	Rim	Oscillatory-inclusion free	Type 1 alt.	2	19045	568	148729	211908	26.0	807	91947	2.18	224	4.05	<1,03	47	3805
8326C1P2	Mantle-rim	Oscillatory-inclusion free	Type 3	5	19577	745	173665	243289	31.1	753	116849	1.92	185	4.26	<0,27	58	4992
8326C1P3	Mantle-rim	Oscillatory-inclusion free	Type 3	4	19150	641	166991	223123	29.1	729	112147	1.88	189	3.91	0.25	52	4551
8326C2P1	Core	Homogeneous & inclusion-free	Type 2	6	9428	324	180554	222460	17.8	251	129385	1.79	111	3.46	<0,29	57	3918
8326C2P2	Mantle-rim	Flame texture & inclusion-rich	Type 2	7	18956	599	161834	225902	28.9	732	107442	1.75	222	5.10	<0,26	52	4682
8326C2P3	Mantle-rim	Homogeneous & inclusion-free	Type 2	8	21393	623	177146	253981	28.9	796	117720	1.96	218	4.95	<0,29	56	5112
8326C2P4	Mantle-rim	Oscillatory & inclusion-free	Type 2	9	27781	708	170068	267795	28.9	1170	107020	1.82	274	4.84	<0,26	53	5204
8326C2P6	Mantle-rim	Inclusion-rich	Type 2	10	29198	742	157413	257610	26.8	1283	95951	1.84	291	4.71	<0,27	49	5200
26C6-1P1	Core	Homogeneous & Inclusion-bearing	Type 4	11	3940	523	186531	207824	14.5	49.4	139246	1.39	51	1.33	<0,34	25	2781
26C6-3P1	Core	Flame texture & inclusion-rich	Type 1	12	14064	531	177212	224583	25.8	491	123663	1.88	168	4.84	<0,33	55	4586
<i>SVC1:</i>																	
02C4-1P2	Mantle-rim	Homogeneous & inclusion-free	Type 1	13	39553	72	154926	267012	8.3	2288	80256	1.44	41	0.31	<0,30	28	825
02C4-3P1	Core	Homogeneous & inclusion-free	Type 2	14	9790	52	181267	212330	26.1	270	125801	0.96	38	0.16	<0,30	40	830
02C4-3P2	Mantle-rim	Oscillatory & inclusion-free	Type 2	15	35833	174	141361	244275	23.3	2334	73010	1.16	41	0.30	0.27	25	853
02C5P1	Core	Slightly norm. zoned & inclusion-free	Type 2	16	16852	80	175775	239244	21.9	573	117580	1.03	71	0.63	<0,33	34	877
JL23C2P2	Core	Homogeneous & inclusion-free	Type 5	18	37307	88	161685	262494	33.9	2815	84400	1.13	36	0.16	<0,35	27	914
JL23C2R1	Mantle	Flame texture & inclusion-rich	Type 5	17	16464	82	178548	192946	28.3	694	109651	0.99	31	0.28	<0,98	33	859
23C2-1P1	Core	Oscillatory & inclusion-free	Type 5	67	42590	132	169950	311139	26.3	3084	84335	2.97	61	0.27	0.50	29	1000
23C2-1R2	Mantle-rim	Oscillatory & inclusion-free	Type 5	68	29913	103	202495	279634	47.3	1421	110779	3.12	50	0.41	<1,19	37	1105
JL23C2P3	Mantle-rim	Oscillatory & inclusion-free	Type 5	19	36724	93	162912	267914	53.1	2217	86006	1.18	48	0.28	<0,37	27	906
JL23C2R4	Mantle-rim	Oscillatory & inclusion-free	Type 5	20	21270	74	173749	212065	27.6	981	106907	0.97	47	0.36	<0,99	38	814
JL23C2P5	Mantle-rim			21	37010	97	160909	275617	46.0	2170	85279	1.26	46.66	0.29	<0,33	32	947
JL23C4P1	Core	Homogeneous & inclusion-free	Type 2	22	8063	89	195473	222899	44.6	219	136331	1.02	37	0.11	<0,42	50	968
JL23C4R2	Mantle-rim	Oscillatory & inclusion-free	Type 2	23	34178	109	162733	263580	20.5	2313	83076	1.31	56	0.43	<0,25	27	946
23C4-1R2	Mantle-rim	Oscillatory & inclusion-free	Type 2	69	40509	109	176634	309707	26.5	2742	83620	2.95	50	0.25	<0,91	31	1047

Table D.12. (continued).

Name	Zone type	Zone texture/comment	Type	#	Co	Ni	Cu	Zn	Ga	Rb	Sr	Y	Zr	Nb	Cs	Ba	La
<i>Pre-SVC2 basaltic andesite:</i>																	
8326P1_2	Core	Homogeneous & inclusion-free	Type 1 alt.	3	0.66	<0,190	2.12	8.39	25.4	0.18	374	0.25	0.04	<0,0268	<0,0188	49	0.61
8626P1_3	Mantle	Oscillatory-inclusion free	Type 1 alt.	1	1.17	<0,147	10.2	11.3	23.9	0.73	366	0.27	0.31	<0,0202	<0,0246	67	0.89
8626P1_4	Rim	Oscillatory-inclusion free	Type 1 alt.	2	0.80	<0,111	6.56	8.10	20.1	0.39	314	0.21	0.17	0.011	<0,0113	51	0.64
8326C1P2	Mantle-rim	Oscillatory-inclusion free	Type 3	5	0.84	0.08	4.33	5.68	24.8	0.48	366	0.20	0.43	<0,0070	0.013	45	0.66
8326C1P3	Mantle-rim	Oscillatory-inclusion free	Type 3	4	0.80	0.09	4.19	6.25	21.6	0.36	365	0.22	0.35	<0,0044	<0,0116	46	0.69
8326C2P1	Core	Homogeneous & inclusion-free	Type 2	6	0.43	0.10	1.05	2.94	22.4	0.08	343	0.29	0.02	<0,0044	<0,0098	26	0.51
8326C2P2	Mantle-rim	Flame texture & inclusion-rich	Type 2	7	0.78	<0,038	3.37	5.40	22.7	0.40	342	0.32	0.50	0.013	<0,0101	52	0.85
8326C2P3	Mantle-rim	Homogeneous & inclusion-free	Type 2	8	0.86	0.05	5.74	7.21	24.5	0.26	376	0.25	0.14	<0,0047	0.014	51	0.78
8326C2P4	Mantle-rim	Oscillatory & inclusion-free	Type 2	9	1.03	0.07	8.03	8.10	24.4	0.37	384	0.19	0.10	0.010	0.010	66	0.78
8326C2P6	Mantle-rim	Inclusion-rich	Type 2	10	1.19	0.08	7.61	8.35	23.9	0.47	370	0.20	0.15	0.007	<0,0085	68	0.75
26C6-1P1	Core	Homogeneous & Inclusion-bearing	Type 4	11	0.47	<0,058	0.24	1.33	14.7	<0,023	285	0.03	<0,0078	<0,0057	<0,0112	12.4	0.21
26C6-3P1	Core	Flame texture & inclusion-rich	Type 1	12	0.72	0.06	8.23	5.24	20.7	0.24	366	0.33	0.36	0.022	<0,0127	38	0.56
<i>SVC1:</i>																	
02C4-1P2	Mantle-rim	Homogeneous & inclusion-free	Type 1	13	0.09	0.07	2.67	6.44	35.5	0.70	645	0.30	0.16	0.007	<0,0119	163	5.68
02C4-3P1	Core	Homogeneous & inclusion-free	Type 2	14	0.03	0.17	0.39	2.67	20.9	<0,036	611	0.35	0.020	<0,0059	<0,0145	62	2.66
02C4-3P2	Mantle-rim	Oscillatory & inclusion-free	Type 2	15	0.12	0.10	1.64	7.80	29.4	0.60	577	0.35	0.31	0.010	<0,0132	150	5.22
02C5P1	Core	Slightly norm. zoned & inclusion-free	Type 2	16	0.07	0.09	2.36	5.68	22.3	0.05	734	0.21	0.033	<0,0046	<0,0137	75	1.98
JL23C2P2	Core	Homogeneous & inclusion-free	Type 5	18	0.06	<0,078	2.60	8.07	29.9	1.24	688	0.45	0.34	0.034	0.046	191	9.03
JL23C2R1	Mantle	Flame texture & inclusion-rich	Type 5	17	0.07	0.18	1.99	6.75	23.5	0.40	631	0.48	0.14	<0,0178	<0,048	102	9.88
23C2-1P1	Core	Oscillatory & inclusion-free	Type 5	67	0.09	0.08	5.37	12.4	34.9	1.03	724	0.47	0.05	0.043	0.011	226	8.87
23C2-1R2	Mantle-rim	Oscillatory & inclusion-free	Type 5	68	0.11	<0,148	5.07	15.5	38.7	0.46	757	0.79	0.10	<0,0131	<0,025	163	8.08
JL23C2P3	Mantle-rim	Oscillatory & inclusion-free	Type 5	19	0.12	<0,062	2.25	10.3	34.7	0.52	704	0.59	0.038	0.004	<0,0156	195	8.86
JL23C2R4	Mantle-rim	Oscillatory & inclusion-free	Type 5	20	0.05	<0,18	3.22	9.6	25.3	0.25	684	0.48	0.08	0.020	<0,058	122	6.57
JL23C2P5	Mantle-rim			21	0.08	<0,076	1.91	11.4	34.8	0.47	717	0.50	0.042	0.007	<0,0123	190	8.20
JL23C4P1	Core	Homogeneous & inclusion-free	Type 2	22	0.06	<0,083	0.97	2.90	26.4	0.13	634	0.11	0.20	0.016	<0,0176	31	1.75
JL23C4R2	Mantle-rim	Oscillatory & inclusion-free	Type 2	23	0.07	<0,065	1.95	12.5	31.8	1.25	680	0.34	0.11	0.024	0.042	192	8.18
23C4-1R2	Mantle-rim	Oscillatory & inclusion-free	Type 2	69	<0,030	0.13	2.85	19.2	36.3	0.55	777	0.63	0.09	<0,0129	<0,018	226	9.68

Table D.12. (continued).

Name	Zone type	Zone texture/comment	Type	#	Ce	Pr	Nd	Sm	Eu	Gd	Tb	Dy	Ho	Er	Tm	Yb	Lu
<i>Pre-SVC2 basaltic andesite:</i>																	
8326P1_2	Core	Homogeneous & inclusion-free	Type 1 alt.	3	1.21	0.13	0.54	<0,081	0.45	0.09	<0,0223	<0,064	0.016	<0,051	<0,0157	<0,093	<0,0118
8626P1_3	Mantle	Oscillatory-inclusion free	Type 1 alt.	1	1.37	0.13	0.56	0.06	0.39	<0,084	0.010	0.06	0.017	0.049	<0,0097	<0,040	0.003
8626P1_4	Rim	Oscillatory-inclusion free	Type 1 alt.	2	1.15	0.16	0.42	0.09	0.36	0.11	<0,0077	0.05	<0,0084	0.019	<0,0077	<0,045	<0,0129
8326C1P2	Mantle-rim	Oscillatory-inclusion free	Type 3	5	1.19	0.14	0.52	0.09	0.36	0.09	<0,0035	0.06	0.010	<0,0139	<0,0055	<0,024	0.004
8326C1P3	Mantle-rim	Oscillatory-inclusion free	Type 3	4	1.12	0.14	0.49	0.12	0.32	0.11	0.011	0.05	0.008	<0,0152	<0,0021	<0,019	<0,0031
8326C2P1	Core	Homogeneous & inclusion-free	Type 2	6	0.95	0.13	0.45	0.06	0.29	0.09	0.012	0.04	0.009	0.032	0.005	<0,018	<0,0035
8326C2P2	Mantle-rim	Flame texture & inclusion-rich	Type 2	7	1.47	0.17	0.42	0.14	0.44	0.06	0.019	0.07	0.018	0.026	<0,0038	0.043	<0,0027
8326C2P3	Mantle-rim	Homogeneous & inclusion-free	Type 2	8	1.35	0.15	0.44	0.11	0.43	0.04	0.012	0.02	0.015	0.046	0.006	0.012	<0,0045
8326C2P4	Mantle-rim	Oscillatory & inclusion-free	Type 2	9	1.32	0.15	0.64	0.09	0.53	0.17	<0,0036	0.03	0.005	<0,0101	<0,0035	0.025	<0,0041
8326C2P6	Mantle-rim	Inclusion-rich	Type 2	10	1.33	0.14	0.58	0.07	0.40	0.12	0.016	0.05	0.005	0.030	<0,0033	<0,019	0.003
26C6-1P1	Core	Homogeneous & Inclusion-bearing	Type 4	11	0.31	0.05	0.15	<0,025	0.14	<0,024	0.002	<0,0144	<0,0047	<0,0081	<0,0031	<0,020	<0,0043
26C6-3P1	Core	Flame texture & inclusion-rich	Type 1	12	1.13	0.12	0.58	0.09	0.29	0.05	0.015	0.13	0.014	0.037	<0,0055	<0,016	<0,00277
<i>SVC1:</i>																	
02C4-1P2	Mantle-rim	Homogeneous & inclusion-free	Type 1	13	8.27	0.80	2.20	0.27	1.41	0.22	0.019	0.05	0.010	<0,016	<0,0051	<0,019	<0,00270
02C4-3P1	Core	Homogeneous & inclusion-free	Type 2	14	4.66	0.55	1.68	0.17	1.07	0.17	0.008	0.07	0.006	0.027	<0,0051	<0,034	<0,0044
02C4-3P2	Mantle-rim	Oscillatory & inclusion-free	Type 2	15	8.00	0.74	2.31	0.33	1.29	0.16	0.010	0.10	0.020	0.060	<0,0034	0.06	0.010
02C5P1	Core	Slightly norm. zoned & inclusion-free	Type 2	16	3.50	0.36	1.18	0.11	0.87	0.07	0.017	0.04	0.005	0.043	0.006	<0,030	<0,0032
JL23C2P2	Core	Homogeneous & inclusion-free	Type 5	18	13.9	1.23	4.00	0.35	1.67	0.24	0.017	0.12	<0,0042	0.056	<0,0046	0.05	<0,0065
JL23C2R1	Mantle	Flame texture & inclusion-rich	Type 5	17	14.7	1.52	4.22	0.43	1.62	0.24	<0,0188	0.16	0.026	<0,079	<0,0178	0.07	<0,0167
23C2-1P1	Core	Oscillatory & inclusion-free	Type 5	67	13.2	1.19	3.57	0.38	1.75	0.19	0.013	0.09	0.010	0.027	0.008	0.04	<0,0044
23C2-1R2	Mantle-rim	Oscillatory & inclusion-free	Type 5	68	14.3	1.65	4.27	0.48	1.55	0.11	0.048	0.16	0.025	<0,080	0.012	<0,117	<0,0092
JL23C2P3	Mantle-rim	Oscillatory & inclusion-free	Type 5	19	13.4	1.29	4.23	0.50	1.66	0.26	0.038	0.11	0.017	0.053	0.008	0.05	<0,0056
JL23C2R4	Mantle-rim	Oscillatory & inclusion-free	Type 5	20	11.3	1.00	3.41	0.50	1.66	0.28	<0,0118	0.13	0.040	0.13	<0,029	<0,109	<0,0135
JL23C2P5	Mantle-rim			21	12.9	1.20	3.83	0.47	1.69	0.24	0.023	0.14	0.022	0.036	<0,0064	<0,038	<0,0034
JL23C4P1	Core	Homogeneous & inclusion-free	Type 2	22	2.74	0.28	1.01	0.12	0.97	<0,042	<0,0054	0.06	<0,0068	0.021	<0,0057	<0,036	0.004
JL23C4R2	Mantle-rim	Oscillatory & inclusion-free	Type 2	23	12.4	1.15	3.84	0.42	1.62	0.20	0.018	0.10	0.011	0.049	<0,0052	0.03	0.004
23C4-1R2	Mantle-rim	Oscillatory & inclusion-free	Type 2	69	14.8	1.29	4.31	0.65	2.43	0.33	<0,0116	0.15	0.018	<0,050	<0,0129	0.08	<0,0131

Table D.12. (continued).

Name	Zone type	Zone texture/comment	Type	#	Hf	Ta	Pb	Th	U	An	B & W (1991) Melt Sr	B & W (1991) Melt Ba	B (1998) Melt Sr	B (1998) Melt Ba	Melt La	Melt Sm	Melt La/Sm
<i>Pre-SVC2 basaltic andesite:</i>																	
8326P1_2	Core	Homogeneous & inclusion-free	Type 1 alt.	3	<0,091	<0,0181	0.97	<0,0246	<0,0192	77.74	211	309	236	458	17		
8626P1_3	Mantle	Oscillatory-inclusion free	Type 1 alt.	1	<0,025	0.001	1.00	0.014	<0,0102	66.64	156	285	168	354	25	4.17	6.1
8626P1_4	Rim	Oscillatory-inclusion free	Type 1 alt.	2	<0,035	<0,01	0.75	<0,0120	0.009	70.14	147	244	160	320	18	6.44	2.9
8326C1P2	Mantle-rim	Oscillatory-inclusion free	Type 3	5	<0,0096	<0,0028	0.85	0.006	0.004	79.28	215	298	242	452	19	6.67	2.8
8326C1P3	Mantle-rim	Oscillatory-inclusion free	Type 3	4	0.011	0.005	0.71	0.008	0.005	75.07	193	261	214	370	20.0	9.17	2.2
8326C2P1	Core	Homogeneous & inclusion-free	Type 2	6	<0,0104	<0,0047	0.69	<0,0059	<0,0044	87.85	250	236	290	411	15	4.70	3.1
8326C2P2	Mantle-rim	Flame texture & inclusion-rich	Type 2	7	<0,0129	<0,0051	0.80	0.014	0.010	75.17	181	299	201	426	24	10.30	2.4
8326C2P3	Mantle-rim	Homogeneous & inclusion-free	Type 2	8	0.007	<0,00242	0.93	<0,0057	<0,0042	77.89	213	324	239	481	22	7.95	2.8
8326C2P4	Mantle-rim	Oscillatory & inclusion-free	Type 2	9	<0,0113	<0,0044	1.01	<0,0032	<0,0046	67.74	169	290	182	366	22	6.97	3.2
8326C2P6	Mantle-rim	Inclusion-rich	Type 2	10	0.015	<0,0022	1.02	0.008	<0,0043	67.84	163	298	176	378	21	5.00	4.3
26C6-1P1	Core	Homogeneous & Inclusion-bearing	Type 4	11	<0,0158	<0,0027	0.15	<0,0026	0.001	94.33	245	143	290	275	5.89		
26C6-3P1	Core	Flame texture & inclusion-rich	Type 1	12	<0,0114	<0,0052	0.65	<0,0080	<0,0048	83.76	241	299.00	275	487	16	7.05	2.3
<i>SVC1:</i>																	
02C4-1P2	Mantle-rim	Homogeneous & inclusion-free	Type 1	13	<0,0111	<0,00273	7.50	0.039	<0,0056	56.00	171	570	178	603	163	20.61	7.9
02C4-3P1	Core	Homogeneous & inclusion-free	Type 2	14	<0,0195	0.001	5.07	0.006	<0,0053	85.38	390	764	459	1406	76.4	13.03	5.9
02C4-3P2	Mantle-rim	Oscillatory & inclusion-free	Type 2	15	<0,0160	0.001	6.00	<0,0055	0.010	53.55	142	475	147	480	150	24.92	6.0
02C5P1	Core	Slightly norm. zoned & inclusion-free	Type 2	16	<0,0131	<0,0046	5.14	<0,0075	<0,0038	81.03	411	771	476	1307	57	8.26	6.9
JL23C2P2	Core	Homogeneous & inclusion-free	Type 5	18	<0,0231	<0,0078	7.60	0.083	0.013	54.72	176	633	182	655	259	26.44	9.8
JL23C2R1	Mantle	Flame texture & inclusion-rich	Type 5	17	<0,080	<0,0216	5.73	0.028	<0,0223	74.89	294	803	332	1213	284	32.50	8.7
23C2-1P1	Core	Oscillatory & inclusion-free	Type 5	67	0.026	<0,0040	8.14	0.020	0.018	54.72	185	749	191	774	255	28.48	8.9
23C2-1R2	Mantle-rim	Oscillatory & inclusion-free	Type 5	68	<0,058	<0,0148	7.89	0.047	<0,0119	65.19	264	846	286	1065	232	36.36	6.4
JL23C2P3	Mantle-rim	Oscillatory & inclusion-free	Type 5	19	<0,0169	<0,0036	7.45	0.012	0.007	58.41	201	760	211	842	255	37.50	6.8
JL23C2R4	Mantle-rim	Oscillatory & inclusion-free	Type 5	20	0.040	<0,017	6.78	0.030	0.030	73.38	305	902	342	1324	189	37.88	5.0
JL23C2P5	Mantle-rim			21	<0,0115	<0,0049	8.04	0.018	<0,0082	58.25	203	735	214	812	236	35.61	6.6
JL23C4P1	Core	Homogeneous & inclusion-free	Type 2	22	0.03	<0,0062	1.90	0.012	0.008	91.90	492	507	595	1054	50	8.86	5.7
JL23C4R2	Mantle-rim	Oscillatory & inclusion-free	Type 2	23	0.01	<0,0040	6.83	0.016	0.010	55.55	178	662	185	694	235	31.82	7.4
23C4-1R2	Mantle-rim	Oscillatory & inclusion-free	Type 2	69	0.01	<0,0071	7.88	<0,0134	0.035	62.45	250	1045	267	12489	278	49.24	5.7

Table D.13. In-situ plagioclase major and trace element concentrations obtained for orthopyroxene- and cummingtonite- bearing SVC 2, 3 dacites by LA-ICPMS at the GAU and the calculated Ba, Sr, La and Sm concentrations in the melt in equilibrium with the crystals. Ba and Sr melt concentrations were calculated using both Blundy and Wood (1991) (B & W, 1991) and Bindeman et al. (1998) (B (1998)) equations. Melt La and Sm concentrations were calculated using Kds from Table 5.3. # = number; An = the anorthite content obtained by electron microprobe for each spot analysis.

Name	Zone type	Zone texture/comment	Type	#	Na	Mg	Al	Si	P	K	Ca	Sc	Ti	V	Cr	Mn	Fe
<i>Opx-bearing SVC2,3 :</i>																	
83C1P1P2	Core	Flame texture & inclusion-rich	Type 5	35	38516	52	151189	256790	27	2352	75773	0.92	21	0.04	<0,33	38	716
83C1-1P1	Mantle-rim	Homogeneous & inclusion-free	Type 5	75	22501	59	193002	264239	48	873	119355	2.35	25	0.18	0.74	59	863
83C1P1P3	Mantle-rim	Oscillatory & inclusion-free	Type 5	36	46350	63	163246	297535	38	2961	77599	1.06	30	0.06	<0,36	34	756
83C1-1P2	Mantle-rim	Oscillatory & inclusion-free	Type 5	76	43210	68	165365	299022	27	2524	80761	2.31	30	0.13	0.48	37	793
JL83C5P1	Core	Homogeneous & inclusion-free	Type 5	37	45715	50	161361	294454	25	2912	76548	1.17	22	0.02	<0,43	33	737
83C5-1P2	Mantle-rim	oscillatory & inclusion-free	Type 5	77	24583	45	145475	230663	29	1179	80761	1.78	45	0.07	<0,32	43	757
83C1-2P1	Core	Unzoned & inclusion-free	Type 5	72	38927	51	163108	288299	23	2164	82476	2.45	29	0.08	<0,32	39	764
83C1-2R2	Mantle-rim	Flame texture & inclusion-rich	Type 5	73	18183	51	187137	247952	31	653	118855	2.72	33	0.10	<0,99	52	817
83C1-2R3	Mantle-rim	Oscillatory & inclusion-free	Type 6	74	42417	51	171493	303587	19	3007	85192	2.68	28	0.25	<0,83	31	808
<i>Cgt-bearing SVC2,3:</i>																	
1AC3P1	Mantle-rim	Oscillatory & inclusion-free	Type 2	24	38556	49	162939	282514	40	2235	86429	1.13	23	0.05	<0,29	42	679
1AC3-1P1	Mantle-rim	Oscillatory & inclusion-free	Type 2	70	47668	61	206163	380797	40	2538	110779	3.33	32	0.12	<0,42	65	882
1AC3P2	Mantle-rim	Oscillatory & inclusion-free	Type 2	25	33761	42	158318	252704	29	1789	87243	1.06	20	0.07	<0,32	47	626
1AC3P3	Mantle-rim	Homogeneous & inclusion-free	Type 2	26	40945	48	157127	276699	28	2419	79078	1.18	22	0.04	<0,33	38	627
1AC3P4	Mantle-rim	Flame texture & inclusion-rich	Type 2	27	38742	49	181466	289398	34	2181	97520	1.25	28	0.08	<0,38	53	761
1AC3P5	Mantle-rim	Oscillatory & inclusion-free	Type 2	28	41692	48	153230	275955	32	2498	75551	1.14	21	0.04	<0,31	34	635
1AC4P1	Core	Homogeneous & inclusion-free	Type 6	29	42449	42	139658	262033	18	2732	64883	1.00	19	<0,0171	<0,33	35	565
1AC4P2	Core	Unzoned & inclusion-free	Type 6	30	39308	43	149873	266080	28	2267	77630	1.09	24	0.03	<0,32	44	625
1AC4P3	Mantle-rim	Oscillatory & inclusion-free	Type 6	31	35924	42	136399	236425	46	2178	67806	0.91	27	0.07	0.45	38	564
1AC4-2R1	Mantle-rim	Oscillatory & inclusion-free	Type 6	71	49729	55	195378	345821	14.4	3049	90481	3.47	39	0.07	<0,96	47	761
1AC5P1	Core	Slightly oscillatory & inclusion-free	Type 2	32	16166	81	183645	236456	38	581	120669	0.97	62	0.23	<0,37	56	974
1AC5P2	Mantle-rim	Slightly-oscillatory & inclusion-free	Type 2	33	27550	50	148549	230679	42	1469	86358	0.90	50	0.07	<0,30	40	696
8308C1P1	Core	Homogeneous & inclusion-free	Type 5	38	42751	48	151628	287397	13.6	2738	71847	1.06	22	0.06	<0,37	31	599
8308C2P1	Core	Homogeneous & inclusion-free	Type 5	41	45128	52	150159	292168	24	2997	68325	1.06	18.4	<0,0183	<0,37	32	623
8308C2P3	mantle	Flame texture & inclusion-rich	Type 5	39	52453	62	182556	338766	17.1	3428	84528	1.40	25	<0,024	<0,50	41	724
8308C2P2	mantle	Homogeneous & inclusion-free	Type 5	40	36020	47	137303	259141	28	2168	68285	0.94	21	0.08	<0,30	35	596
8308C3P1	Core	Slightly oscillatory & inclusion-free	Type 2	42	13362	293	189416	231740	37	420	125939	0.88	29	0.16	<0,36	93	1361
8308C3P2	Mantle-rim	Slightly oscillatory & inclusion-free	Type 2	43	41811	65	154207	278313	31	2561	76064	1.00	28	0.10	<0,33	37	679
8308C3P3	Mantle-rim	Slightly oscillatory & inclusion-free	Type 2	44	38211	58	164796	290247	36	2161	85448	1.06	101	0.14	<0,34	44	850

Table D.13. (continued).

Name	Zone type	Zone texture/comment	Type	#	Co	Ni	Cu	Zn	Ga	Rb	Sr	Y	Zr	Nb	Cs	Ba	La
<i>Opx-bearing SVC2,3 :</i>																	
83C1P1P2	Core	Flame texture & inclusion-rich	Type 5	35	0.06	<0,065	0.26	7.22	27	0.43	657	0.22	0.03	<0,0047	<0,0167	138	7.46
83C1-1P1	Mantle-rim	Homogeneous & inclusion-free	Type 5	75	0.09	0.08	3.08	5.83	31	0.16	701	0.34	0.05	0.005	<0,0086	93	8.09
83C1P1P3	Mantle-rim	Oscillatory & inclusion-free	Type 5	36	0.08	<0,087	0.33	8.38	33	0.52	724	0.31	0.03	<0,0070	<0,0189	168	7.86
83C1-1P2	Mantle-rim	Oscillatory & inclusion-free	Type 5	76	0.07	0.04	0.77	8.62	35	0.38	727	0.30	0.04	0.008	<0,0062	175	9.51
JL83C5P1	Core	Homogeneous & inclusion-free	Type 5	37	0.06	<0,082	0.24	8.30	29	0.45	740	0.22	<0,0115	<0,0077	<0,0170	131	8.44
83C5-1P2	Mantle-rim	oscillatory & inclusion-free	Type 5	77	0.07	0.04	1.08	6.14	25	0.27	590	0.16	0.02	0.013	<0,0061	91	3.86
83C1-2P1	Core	Unzoned & inclusion-free	Type 5	72	0.09	<0,033	0.20	8.22	33	0.32	660	0.33	<0,0079	<0,0028	<0,0067	154	8.77
83C1-2R2	Mantle-rim	Flame texture & inclusion-rich	Type 5	73	<0,026	<0,107	0.87	5.59	25	<0,046	664	0.57	0.11	<0,0072	<0,0161	88	7.63
83C1-2R3	Mantle-rim	Oscillatory & inclusion-free	Type 6	74	<0,028	<0,13	0.63	9.76	31	0.48	716	0.25	0.13	0.015	<0,0177	188	9.28
<i>Cgt-bearing SVC2,3:</i>																	
1AC3P1	Mantle-rim	Oscillatory & inclusion-free	Type 2	24	0.07	<0,064	0.91	8.58	34	0.51	690	0.39	0.14	0.017	<0,0109	123	9.51
1AC3-1P1	Mantle-rim	Oscillatory & inclusion-free	Type 2	70	0.10	<0,055	3.97	11.02	47	0.44	841	0.35	0.01	<0,0060	0.009	139	12.2
1AC3P2	Mantle-rim	Oscillatory & inclusion-free	Type 2	25	0.05	<0,060	0.58	6.48	31	0.27	658	0.35	<0,0095	0.003	<0,0095	97	9.94
1AC3P3	Mantle-rim	Homogeneous & inclusion-free	Type 2	26	0.05	<0,074	0.44	8.19	32	0.34	668	0.30	0.01	<0,0028	<0,0121	117	8.96
1AC3P4	Mantle-rim	Flame texture & inclusion-rich	Type 2	27	0.06	<0,075	0.90	7.52	35	0.87	739	0.47	0.40	0.016	0.024	121	11.2
1AC3P5	Mantle-rim	Oscillatory & inclusion-free	Type 2	28	0.07	<0,068	0.55	7.55	31	0.43	675	0.34	<0,0154	<0,0071	<0,0132	132	7.73
1AC4P1	Core	Homogeneous & inclusion-free	Type 6	29	0.06	<0,077	0.48	6.48	25	0.55	630	0.28	0.03	<0,0061	<0,0108	130	6.56
1AC4P2	Core	Unzoned & inclusion-free	Type 6	30	0.19	0.06	0.44	6.79	30	0.35	656	0.31	<0,0074	<0,0027	<0,0125	123	7.79
1AC4P3	Mantle-rim	Oscillatory & inclusion-free	Type 6	31	0.05	<0,058	0.52	6.75	25	0.32	639	0.46	0.01	<0,0060	<0,0121	122	9.37
1AC4-2R1	Mantle-rim	Oscillatory & inclusion-free	Type 6	71	<0,033	<0,086	3.57	10.33	40	0.47	823	0.51	0.02	<0,0234	<0,023	189	14.0
1AC5P1	Core	Slightly oscillatory & inclusion-free	Type 2	32	0.08	<0,070	0.97	6.02	25	0.20	664	0.16	0.03	<0,0031	<0,0135	40	1.67
1AC5P2	Mantle-rim	Slightly-oscillatory & inclusion-free	Type 2	33	0.08	<0,078	0.99	6.37	28	0.34	611	0.41	0.02	0.029	<0,0134	93	5.67
8308C1P1	Core	Homogeneous & inclusion-free	Type 5	38	0.07	<0,064	1.49	7.10	29	0.43	660	0.17	<0,0144	<0,0040	<0,0126	125	7.85
8308C2P1	Core	Homogeneous & inclusion-free	Type 5	41	0.08	0.10	1.95	11.45	26	0.53	655	0.18	<0,0153	<0,0043	<0,0156	144	5.55
8308C2P3	mantle	Flame texture & inclusion-rich	Type 5	39	0.07	<0,096	1.67	9.01	33	0.61	803	0.33	0.06	0.015	<0,0176	177	8.49
8308C2P2	mantle	Homogeneous & inclusion-free	Type 5	40	0.10	0.07	1.52	7.85	30	0.33	606	0.28	0.02	<0,0056	<0,0127	124	8.07
8308C3P1	Core	Slightly oscillatory & inclusion-free	Type 2	42	0.12	0.09	0.69	5.78	28	0.08	681	0.29	<0,0138	<0,0045	<0,0149	47	3.70
8308C3P2	Mantle-rim	Slightly oscillatory & inclusion-free	Type 2	43	0.06	<0,080	1.10	7.65	32	0.40	677	0.29	<0,0146	<0,0081	<0,0161	143	9.17
8308C3P3	Mantle-rim	Slightly oscillatory & inclusion-free	Type 2	44	0.28	<0,092	6.07	8.85	32	0.35	701	0.43	0.04	0.22	<0,0158	141	10.1

Table D.13. (continued).

Name	Zone type	Zone texture/comment	Type	#	Ce	Pr	Nd	Sm	Eu	Gd	Tb	Dy	Ho	Er	Tm	Yb	Lu
<i>Opx-bearing SVC2,3 :</i>																	
83C1P1P2	Core	Flame texture & inclusion-rich	Type 5	35	10.8	0.97	3.05	0.24	1.41	0.05	0.014	<0,025	0.010	0.018	<0,0022	<0,036	<0,0057
83C1-1P1	Mantle-rim	Homogeneous & inclusion-free	Type 5	75	12.9	1.21	3.78	0.44	1.63	0.16	0.010	0.09	0.006	0.052	0.005	<0,025	<0,0053
83C1P1P3	Mantle-rim	Oscillatory & inclusion-free	Type 5	36	11.2	1.00	2.96	0.27	1.57	0.14	0.012	0.06	0.012	<0,028	<0,0079	0.03	<0,0071
83C1-1P2	Mantle-rim	Oscillatory & inclusion-free	Type 5	76	13.9	1.15	3.71	0.34	1.66	0.15	0.013	0.12	0.008	0.030	0.004	0.03	<0,0051
JL83C5P1	Core	Homogeneous & inclusion-free	Type 5	37	11.8	1.11	3.19	0.35	1.72	0.11	0.011	<0,035	0.006	0.031	<0,0048	0.009	<0,0042
83C5-1P2	Mantle-rim	oscillatory & inclusion-free	Type 5	77	6.3	0.61	2.17	0.19	1.21	0.02	0.018	<0,0202	<0,00286	<0,013	<0,00308	0.08	<0,0041
83C1-2P1	Core	Unzoned & inclusion-free	Type 5	72	13.6	1.17	3.58	0.37	1.64	0.22	0.016	0.09	0.012	0.014	<0,0034	<0,033	<0,0037
83C1-2R2	Mantle-rim	Flame texture & inclusion-rich	Type 5	73	10.8	1.03	4.03	0.31	1.51	0.30	0.046	0.12	0.03	<0,068	<0,0152	<0,122	<0,0164
83C1-2R3	Mantle-rim	Oscillatory & inclusion-free	Type 6	74	14.4	1.28	3.63	0.46	1.38	0.24	0.032	<0,0259	<0,015	<0,036	<0,0080	0.17	<0,013
<i>Cgt-bearing SVC2,3:</i>																	
1AC3P1	Mantle-rim	Oscillatory & inclusion-free	Type 2	24	13.8	1.20	3.77	0.34	1.56	0.18	0.016	1.20	0.009	0.033	0.005	0.04	<0,0051
1AC3-1P1	Mantle-rim	Oscillatory & inclusion-free	Type 2	70	19.2	1.64	5.08	0.44	1.95	0.29	0.016	0.10	0.007	0.13	<0,0040	<0,033	0.009
1AC3P2	Mantle-rim	Oscillatory & inclusion-free	Type 2	25	14.8	1.35	3.70	0.40	1.54	0.21	0.014	0.08	0.009	0.034	<0,0048	<0,021	<0,0051
1AC3P3	Mantle-rim	Homogeneous & inclusion-free	Type 2	26	13.0	1.09	3.31	0.32	1.61	0.16	0.012	0.07	0.007	0.025	<0,0038	<0,031	<0,0053
1AC3P4	Mantle-rim	Flame texture & inclusion-rich	Type 2	27	16.8	1.64	4.28	0.57	1.57	0.23	0.03	0.10	0.017	0.063	<0,0060	<0,027	0.006
1AC3P5	Mantle-rim	Oscillatory & inclusion-free	Type 2	28	11.4	1.02	3.03	0.31	1.60	0.12	0.015	0.10	0.013	0.028	<0,0030	0.01	<0,0039
1AC4P1	Core	Homogeneous & inclusion-free	Type 6	29	10.0	0.85	2.68	0.18	1.40	0.13	<0,0046	0.08	0.008	<0,0097	<0,0049	0.04	<0,00
1AC4P2	Core	Unzoned & inclusion-free	Type 6	30	12.1	1.03	3.37	0.30	1.46	0.22	0.010	0.11	0.008	<0,019	<0,0037	<0,030	0.006
1AC4P3	Mantle-rim	Oscillatory & inclusion-free	Type 6	31	13.4	1.08	4.29	0.32	1.39	0.19	0.022	0.14	0.012	<0,014	0.006	<0,0189	<0,0051
1AC4-2R1	Mantle-rim	Oscillatory & inclusion-free	Type 6	71	22.5	1.91	5.59	0.52	2.30	0.18	0.031	0.26	<0,012	<0,040	<0,0115	<0,055	<0,0056
1AC5P1	Core	Slightly oscillatory & inclusion-free	Type 2	32	2.6	0.29	0.87	0.12	0.89	0.10	0.012	0.05	0.005	0.022	<0,0055	<0,031	<0,0052
1AC5P2	Mantle-rim	Slightly-oscillatory & inclusion-free	Type 2	33	9.5	0.91	3.00	0.37	1.30	0.21	0.025	0.03	0.021	<0,0091	0.007	0.04	0.004
8308C1P1	Core	Homogeneous & inclusion-free	Type 5	38	11.4	1.01	2.86	0.17	1.50	0.13	0.012	0.06	0.006	<0,020	<0,0056	<0,020	<0,0054
8308C2P1	Core	Homogeneous & inclusion-free	Type 5	41	8.3	0.69	2.12	0.20	1.49	0.10	<0,0061	0.04	<0,0045	<0,0188	<0,0060	<0,026	<0,0052
8308C2P3	mantle	Flame texture & inclusion-rich	Type 5	39	12.5	1.10	3.31	0.26	1.93	0.20	0.016	<0,039	0.013	0.006	<0,0054	0.06	0.006
8308C2P2	mantle	Homogeneous & inclusion-free	Type 5	40	12.0	1.07	3.28	0.28	1.47	0.14	0.009	0.07	<0,0063	<0,020	<0,0051	<0,042	0.004
8308C3P1	Core	Slightly oscillatory & inclusion-free	Type 2	42	6.1	0.67	2.01	0.18	1.26	0.23	0.008	0.06	<0,0048	<0,020	0.002	<0,049	<0,0062
8308C3P2	Mantle-rim	Slightly oscillatory & inclusion-free	Type 2	43	13.3	1.14	3.40	0.38	1.51	0.18	0.010	0.06	0.021	0.041	<0,00	0.022	<0,0049
8308C3P3	Mantle-rim	Slightly oscillatory & inclusion-free	Type 2	44	15.6	1.43	4.36	0.55	1.75	0.24	0.022	0.13	0.014	0.028	0.012	0.05	0.010

Table D.13. (continued).

Name	Zone type	Zone texture/comment	Type	#	Hf	Ta	Pb	Th	U	An	B & W (1991) Melt Sr	B & W (1991) Melt Ba	B (1998) Melt Sr	B (1998) Melt Ba	Melt La	Melt Sm	Melt La/Sm
<i>Opx-bearing SVC2,3 :</i>																	
83C1P1P2	Core	Flame texture & inclusion-rich	Type 5	35	<0,0111	<0,0058	9.2	<0,01	<0,0062	53.59	162	438	167	443	214	18.4	11.6
83C1-1P1	Mantle-rim	Homogeneous & inclusion-free	Type 5	75	0.02	<0,0042	8.4	<0,0071	<0,0023	72.62	306	667	341	966	232	33.3	7.0
83C1P1P3	Mantle-rim	Oscillatory & inclusion-free	Type 5	36	<0,0090	<0,0047	10.8	0.015	<0,0078	50.45	163	464	166	443	226	20.7	10.9
83C1-1P2	Mantle-rim	Oscillatory & inclusion-free	Type 5	76	<0,0084	<0,0042	9.5	0.008	0.012	53.70	180	558	186	565	273	25.5	10.7
JL83C5P1	Core	Homogeneous & inclusion-free	Type 5	37	<0,0141	<0,0060	11.3	<0,0107	<0,0050	54.08	185	422	191	430	243	26.2	9.2
83C5-1P2	Mantle-rim	oscillatory & inclusion-free	Type 5	77	<0,0131	<0,0034	7.1	0.007	0.007	61.22	183	401	195	468	111	14.0	7.9
83C1-2P1	Core	Unzoned & inclusion-free	Type 5	72	<0,0162	<0,0028	9.8	0.016	<0,0040	56.43	177	548	185	585	252	28.3	8.9
83C1-2R2	Mantle-rim	Flame texture & inclusion-rich	Type 5	73	<0,047	<0,018	7.4	<0,017	<0,014	77.77	337	783	385	1249	219	23.5	9.3
83C1-2R3	Mantle-rim	Oscillatory & inclusion-free	Type 6	74	0.02	<0,00	10.2	<0,0193	<0,0164	58.14	202	721	213	795	267	34.9	7.7
<i>Cgt-bearing SVC2,3:</i>																	
1AC3P1	Mantle-rim	Oscillatory & inclusion-free	Type 2	24	<0,0098	0.003	11.9	0.017	0.030	60.88	212	532	225	617	273	26.1	10.5
1AC3-1P1	Mantle-rim	Oscillatory & inclusion-free	Type 2	70	<0,0243	<0,0044	15.2	<0,0077	<0,0073	56.77	228	503	239	541	350	33.6	10.4
1AC3P2	Mantle-rim	Oscillatory & inclusion-free	Type 2	25	<0,0140	<0,0021	10.5	<0,0107	<0,0061	60.88	202	421	215	488	286	30.1	9.5
1AC3P3	Mantle-rim	Homogeneous & inclusion-free	Type 2	26	<0,0111	<0,0067	11.5	<0,0045	<0,0056	55.16	173	397	179	414	257	24.2	10.6
1AC3P4	Mantle-rim	Flame texture & inclusion-rich	Type 2	27	<0,026	<0,0046	11.3	0.07	0.030	63.74	247	589	266	721	323	43.1	7.5
1AC3P5	Mantle-rim	Oscillatory & inclusion-free	Type 2	28	<0,0076	<0,0051	10.6	<0,0043	<0,0038	52.65	162	402	166	400	222	23.2	9.6
1AC4P1	Core	Homogeneous & inclusion-free	Type 6	29	<0,0174	<0,0040	10.1	0.008	<0,0062	45.57	122	292	122	254	189	13.3	14.1
1AC4P2	Core	Unzoned & inclusion-free	Type 6	30	<0,0154	<0,00	10.3	<0,0063	<0,0083	51.32	151	353	155	342	224	22.4	10.0
1AC4P3	Mantle-rim	Oscillatory & inclusion-free	Type 6	31	0.01	<0,0040	8.7	0.020	<0,0067	48.97	137	315	139	293	269	23.9	11.3
1AC4-2R1	Mantle-rim	Oscillatory & inclusion-free	Type 6	71	<0,038	<0,0114	13.3	<0,0151	<0,0083	51.33	190	542	194	525	403	39.4	10.2
1AC5P1	Core	Slightly oscillatory & inclusion-free	Type 2	32	<0,0231	<0,01	2.5	<0,0100	<0,0070	83.03	395	446	461	786	47.8	8.7	5.5
1AC5P2	Mantle-rim	Slightly-oscillatory & inclusion-free	Type 2	33	<0,0126	<0,0044	7.0	0.020	<0,0045	58.57	175	365	184	405	162	28.0	5.8
8308C1P1	Core	Homogeneous & inclusion-free	Type 5	38	<0,0183	<0,0043	10.5	<0,0081	<0,0087	49.62	144	333	147	312	225	12.7	17.8
8308C2P1	Core	Homogeneous & inclusion-free	Type 5	41	<0,0173	<0,0078	10.4	<0,0093	<0,0043	47.56	135	353	136	318	159	15.5	10.3
8308C2P3	mantle	Flame texture & inclusion-rich	Type 5	39	<0,0193	0.006	11.7	<0,0120	<0,0130	60.07	240	738	255	844	244	19.6	12.4
8308C2P2	mantle	Homogeneous & inclusion-free	Type 5	40	<0,0198	<0,0049	9.6	<0,0080	<0,0070	47.56	125	304	126	274	232	20.8	11.1
8308C3P1	Core	Slightly oscillatory & inclusion-free	Type 2	42	<0,0207	<0,0068	6.8	<0,0075	<0,0073	85.35	434	574	511.42	1055.49	106.32	13.9	7.6
8308C3P2	Mantle-rim	Slightly oscillatory & inclusion-free	Type 2	43	<0,02	<0,00	10.0	0.012	<0,0077	51.45	156	413	160.08	400.92	263.51	28.8	9.2
8308C3P3	Mantle-rim	Slightly oscillatory & inclusion-free	Type 2	44	<0,020	0.011	11.1	<0,0082	<0,0055	51.45	162	405	165.81	393.91	290.80	41.8	7.0

Table D.14. In-situ pyroxene and amphibole major and trace element concentrations obtained for Pre-SVC and SVC lavas by LA-ICPMS at the GAU.

Name	Zone type	Mineral type	Na	Mg	Al	Si	P	K	Ca	Sc	Ti	V	Cr	Mn	Fe	Co	Ni
Pre-SVC1 basalt:																	
8344C2P1	core	Clinopyroxene	1680	101925	17753	278862	28	39	161696	167	2625	505	825	1824	59662	48	67
8344C2P2	rim	Clinopyroxene	1461	104458	13261	273377	22	<1,02	163163	132	1936	377	717	1796	54660	46	83
SVC1:																	
23C4PY1	Core	Orthopyroxene	63.5	107353	2332	265202	354	1.16	8005	46	613	117	37	6601	230047	53	15.4
23C4PY2	Mantle	Orthopyroxene	81.7	121224	5272	295459	63	4.45	9692	57	1151	188	46	6085	226139	65	26
23C4PY3	Rim	Orthopyroxene	69.5	99512	3802	268152	248	3.73	8034	57	814	146	26	6723	237853	44	9.2
Orthopyroxene bearing SVC2,3																	
JL83C3P1	Core	Clinopyroxene	1545	101322	27275	266594	24	<0,93	193509	151	2949	356	5231	821	31498	28	134
JL83C3R2	Rim	Clinopyroxene	1544	91069	32575	233244	20	<2,73	171991	155	4164	460	2678	850	34120	26	103
83C1B1P1	Core	Hornblend	16370	85087	80313	196176	60	4133	87236	71	10123	599	33	909	68527	53	65
Cummingtonite bearing SVC2,3																	
1AC1P1	Core	Cummingtonite	3180	96676	16711	339855	54	195	15547	82	2570	132	73	9633	255646	49	15.4
8308C4P1	Rim	Cummingtonite	2917	76433	14646	263292	76	138	12516	90	2386	169	44	6110	195398	39	13.6

Name	Zone type	Mineral type	Cu	Zn	Ga	Rb	Sr	Y	Zr	Nb	Cs	Ba	La	Ce	Pr	Nd	Sm
Pre-SVC1 basalt:																	
8344C2P1	core	Clinopyroxene	31	41	5.83	0.15	12.2	13.4	9.9	0.027	0.024	0.11	0.25	1.27	0.30	2.41	1.16
8344C2P2	rim	Clinopyroxene	7.5	36	4.03	0.04	10.5	10.4	5.7	0.007	<0,0126	0.05	0.19	0.91	0.24	1.72	0.86
SVC1:																	
23C4PY1	Core	Orthopyroxene	2.87	716	2.93	<0,032	1.11	11.2	1.05	<0,0058	0.014	0.18	3.12	6.26	1.09	5.23	1.47
23C4PY2	Mantle	Orthopyroxene	2.35	601	4.50	0.03	0.16	6.71	3.49	0.003	<0,0124	0.09	0.09	0.35	0.07	0.50	0.24
23C4PY3	Rim	Orthopyroxene	2.86	729	3.87	0.04	1.33	12.0	2.64	0.019	0.010	0.16	0.96	2.68	0.41	2.05	0.59
Orthopyroxene bearing SVC2,3																	
JL83C3P1	Core	Clinopyroxene	1.17	16.4	5.70	<0,030	19.66	9.65	8.68	0.008	<0,0152	0.08	0.23	1.04	0.27	2.05	1.01
JL83C3R2	Rim	Clinopyroxene	2.45	17.7	7.05	<0,091	19.00	13.65	18	0.029	<0,050	<0,069	0.48	2.37	0.52	3.59	1.73
83C1B1P1	Core	Hornblend	2.13	50.1	15.02	2.74	167	29.0	45	1.57	<0,0140	79.98	2.57	9.79	1.94	11.43	3.79
Cummingtonite bearing SVC2,3																	
1AC1P1	Core	Cummingtonite	0.29	830	8.74	0.04	3.84	55.7	11.2	3.23	<0,0136	1.13	0.68	3.54	0.99	6.90	3.64
8308C4P1	Rim	Cummingtonite	0.80	620	7.51	0.04	3.89	61.1	11.1	3.15	<0,0103	0.51	0.56	3.12	0.86	6.48	3.98

Table D.14. (continued).

Name	Zone type	Mineral type	Eu	Gd	Tb	Dy	Ho	Er	Tm	Yb	Lu	Hf	Ta	Pb	Th	U
Pre-SVC1 basalt:																
8344C2P1	core	Clinopyroxene	0.58	1.84	0.32	2.44	0.56	1.41	0.17	1.26	0.22	0.58	<0,00	0.16	<0,0064	<0,0062
8344C2P2	rim	Clinopyroxene	0.34	1.47	0.26	1.93	0.44	1.15	0.17	1.15	0.16	0.30	<0,0050	<0,0173	<0,0086	<0,0075
SVC1:																
23C4PY1	Core	Orthopyroxene	0.04	1.24	0.21	1.73	0.48	1.35	0.20	2.42	0.37	0.04	<0,0087	0.010	0.15	0.06
23C4PY2	Mantle	Orthopyroxene	0.01	0.44	0.11	0.89	0.27	0.88	0.18	1.85	0.26	0.16	<0,0042	<0,0150	0.012	<0,0057
23C4PY3	Rim	Orthopyroxene	0.03	1.04	0.19	1.70	0.45	1.73	0.30	2.27	0.44	0.14	<0,0058	0.05	0.08	0.04
Orthopyroxene bearing SVC2,3																
JL83C3P1	Core	Clinopyroxene	0.38	1.58	0.27	1.96	0.38	1.08	0.14	0.96	0.12	0.61	<0,0039	0.035	<0,0075	<0,0084
JL83C3R2	Rim	Clinopyroxene	0.58	2.30	0.44	2.57	0.63	1.25	0.16	1.10	0.18	1.04	0.024	0.090	<0,031	<0,0156
83C1B1P1	Core	Hornblende	1.24	5.01	0.77	5.57	1.14	3.27	0.42	2.71	0.39	2.25	0.10	0.55	0.22	0.02
Cummingtonite bearing SVC2,3																
1AC1P1	Core	Cummingtonite	0.14	5.45	1.11	8.55	2.02	6.07	1.03	7.46	1.20	0.64	0.12	0.21	0.020	0.01
8308C4P1	Rim	Cummingtonite	0.17	5.54	1.15	9.70	2.30	7.01	1.16	9.04	1.30	0.72	0.12	0.10	<0,0057	0.01

Table D.15. In-situ groundmass major and trace element concentrations obtained for Pre-SVC and SVC lavas by LA-ICPMS at the GAU.

Sample ID	Lava type	Na	Mg	Al	Si	P	K	Ca	Ca	Sc	Ti	V	Cr	Mn	Fe	Co	Ni	Cu	Zn
Pre-SVC1																			
44C3M	basalt	24248	12704	110219	262634	516	6613	68182	68451	19.1	4561	104.20	3.56	858	37888	13.9	6.14	169	61
25C2M	basaltic andesite	20628	18993	65654	238779	664	7781	46599	46623	38.9	7834	288.05	4.64	1218	61758	21.6	7.52	267	106
25C2M2	basaltic andesite	21888	21917	67911	258208	818	9246	46599	46498	40.5	10832	400.97	4.94	1468	80205	28.4	8.83	341	183
45C3M	rhyolite	33833	4675	32898	219195	71.5	8422	15295	15551	7.61	623	0.29	0.40	549	10364	0.26	0.41	14.9	44
Pre-SVC2:																			
26C2M	basaltic andesite	14213	7019	74831	182841	223	4446	47242	47113	14.2	3451	142.19	0.83	686	29682	11.4	1.69	81	51
26C2M2	basaltic andesite	19784	17287	65699	243937	399	7947	47242	47129	35.4	7352	326.13	2.32	1417	62723	25.2	3.82	121	106
SVC1:																			
23C4M	dacite	12324	669	48540	169775	62.6	9845	17510	17655	3.32	2413	12.14	2.63	77.7	6538	0.88	0.61	4.1	24
23C4M2	dacite	28420	1602	87157	498200	474	34696	17510	18661	12.1	16009	70.	16.08	310	25309	3.14	1.86	12.5	78
Orthopyroxene bearing SVC2,3:																			
83C1M	dacite	34959	10487	32833	240609	117	13990	20869	20956	4.90	747	14.9	6.75	314	10551	2.77	4.29	5.6	30

Table D.15. (continued).

Sample ID	Lava type	Ga	Rb	Sr	Y	Zr	Nb	Cs	Ba	La	Ce	Pr	Nd	Sm	Eu	Gd	Tb	Dy	Ho
Pre-SVC1																			
44C3M	basalt	17.5	18.7	210	22.1	78	1.87	0.89	128.2	5.69	14.5	2.09	10.8	3.11	1.00	3.36	0.52	3.98	0.79
25C2M	basaltic andesite	14.4	13.3	159	28.1	117	3.58	0.31	188.2	5.81	15.3	2.37	12.6	3.85	1.14	4.49	0.71	5.14	1.04
25C2M2	basaltic andesite	16.7	18.9	164	32.6	140	4.31	0.35	235.4	7.04	18.9	2.90	15.2	4.50	1.23	5.19	0.80	5.92	1.17
45C3M	rhyolite	8.0	24.1	46	20.4	112	2.19	0.78	163.8	5.12	12.4	1.79	9.08	2.55	0.53	2.89	0.46	3.54	0.72
Pre-SVC2:																			
26C2M	basaltic andesite	12.2	54	151	11.8	56	1.76	1.29	155.9	5.46	12.0	1.52	6.83	1.71	0.50	1.89	0.29	2.17	0.43
26C2M2	basaltic andesite	14.5	100	135	24.4	107	3.30	2.24	271.7	9.75	21.4	2.72	12.6	3.31	0.86	3.79	0.58	4.52	0.88
SVC1:																			
23C4M	dacite	10.1	48	149	5.7	40	7.08	1.92	343.2	8.27	14.7	1.60	6.07	1.13	0.43	1.00	0.14	1.00	0.20
23C4M2	dacite	20.2	174	174	24.3	102	27.7	6.78	1108.1	34.9	74.9	8.49	33.6	6.39	0.72	5.34	0.70	4.58	0.84
Orthopyroxene bearing SVC2,3:																			
83C1M	dacite	7.2	66	75	5.5	32	1.80	2.22	366.9	11.1	21.6	2.38	9.17	1.57	0.27	1.21	0.15	0.98	0.18

Sample ID	Lava type	Er	Tm	Yb	Lu	Hf	Ta	Pb	Th	U	La/Sm
Pre-SVC1											
44C3M	basalt	2.43	0.34	2.55	0.35	2.10	0.11	3.62	1.17	0.49	1.8
25C2M	basaltic andesite	3.16	0.42	3.17	0.43	3.27	0.21	4.40	1.44	0.77	1.5
25C2M2	basaltic andesite	3.53	0.48	3.56	0.49	3.81	0.26	5.91	1.72	0.88	1.6
45C3M	rhyolite	2.31	0.32	2.44	0.35	3.12	0.14	3.55	1.45	0.88	2.0
Pre-SVC2:											
26C2M	basaltic andesite	1.30	0.18	1.37	0.19	1.57	0.09	3.64	1.98	0.80	3.2
26C2M2	basaltic andesite	2.75	0.36	2.85	0.38	2.93	0.17	6.31	3.47	1.42	2.9
SVC1:											
23C4M	dacite	0.59	0.09	0.67	0.09	1.23	0.30	7.56	3.29	1.62	7.3
23C4M2	dacite	2.39	0.31	2.33	0.32	3.48	1.47	24.76	13.8	4.53	5.5
Orthopyroxene bearing SVC2,3:											
83C1M	dacite	0.52	0.07	0.55	0.08	0.92	0.20	8.87	44.0	1.11	7.1

Table D.16. In-situ zircon $\delta^{18}\text{O}$ compositions in St Lucia lavas obtained using the CAMECA ims 1270 at UCLA and the corresponding U-Th age from Schmitt et al. (2010).

WR sample name	Analysis name	Eruption period	$\delta^{18}\text{O}$ VSMOW	1 SE	Name of U-Th data	Polishing:	m	1SE	Th age (ka)	1SE	U ppm	Nature
SVC1:												
SL-JL-57	SLJL57@1.ais	SVC1	8.26	0.21	2009_06_22Jun\ SLJL57-2@1.ais	unpolished	1.03	0.09	-	-	586	Near dugard_pumice dark andesite
SL-JL-57	SLJL57@2.ais	SVC1	8.57	0.21	2009_06_22Jun\ SLJL57-2@2.ais	unpolished	0.92	0.03	272	45	764	Near dugard_pumice dark andesite
SL-JL-57	SLJL57@3.ais	SVC1	8.02	0.21	2009_06_22Jun\ SLJL57-2@3.ais	unpolished	0.88	0.04	232	40	683	Near dugard_pumice dark andesite
SL-JL-57	SLJL57@4.ais	SVC1	8.28	0.21	2009_06_22Jun\ SLJL57-2@4.ais	unpolished	0.94	0.05	299	81	564	Near dugard_pumice dark andesite
SL-JL-57	SLJL57@5.ais	SVC1	9.22	0.21	2009_06_22Jun\ SLJL57-2@5.ais	unpolished	1.00	0.05	605	1301	390	Near dugard_pumice dark andesite
SL-JL-57	SLJL57@5_2.ais	SVC1	8.80	0.21	2009_06_22Jun\ SLJL57-2@5.ais	unpolished	1.00	0.05	605	1301	390	Near dugard_pumice dark andesite
SL-JL-57	SLJL57@6.ais	SVC1	8.26	0.21	2009_06_22Jun\ SLJL57-2@6.ais	unpolished	0.99	0.07	557	1306	682	Near dugard_pumice dark andesite
SL-JL-57	SLJL57@7.ais	SVC1	7.79	0.21	2009_06_22Jun\ SLJL57-2@7.ais	unpolished	0.94	0.05	300	86	652	Near dugard_pumice dark andesite
SL-JL-57	SLJL57@8.ais	SVC1	8.07	0.21	2009_06_22Jun\ SLJL57-2@8.ais	unpolished	0.85	0.05	210	35	338	Near dugard_pumice dark andesite
SL-JL-57	SLJL57@9.ais	SVC1	8.76	0.21	2009_06_22Jun\ SLJL57-2@9.ais	unpolished	1.03	0.04	-	-	425	Near dugard_pumice dark andesite
SL-JL-57	SLJL57@10.ais	SVC1	7.60	0.21	2009_06_22Jun\ SLJL57-2@10.ais	unpolished	0.92	0.04	276	55	387	Near dugard_pumice dark andesite
SL-JL-57	SLJL57@11.ais	SVC1	8.22	0.21	2009_06_22Jun\ SLJL57-2@11.ais	unpolished	0.88	0.03	233	29	944	Near dugard_pumice dark andesite
SL-JL-75	SLJL75@1_2.ais	SVC1	8.63	0.20	2009_06_22Jun\ SLJL75@1.ais	unpolished	1.07	0.16	-	-	448	Choiseul pyroclastic formation_crystal poor pumice
SL-JL-75	SLJL75@2.ais	SVC1	8.74	0.20	2009_06_22Jun\ SLJL75@2.ais	unpolished	0.94	0.05	302	83	436	Choiseul pyroclastic formation_crystal poor pumice
Orthopyroxee bearing SVC2,2												
SL-JL-83	SLJL83@1_2.ais	SVC2	7.89	0.20	2009_07_01July\ SLJL83-2@1.ais	unpolished	0.835	0.077	197	51	1227	Gros piton_lava dacite
SL-JL-83	SLJL83@2.ais	SVC2	8.13	0.20	2009_07_01July\ SLJL83-2@2.ais	unpolished	0.754	0.047	153	21	710	Gros piton_lava dacite
SL-JL-83	SLJL83@3.ais	SVC2	8.04	0.20	2009_07_01July\ SLJL83-2@3.ais	unpolished	0.551	0.043	87	10	609	Gros piton_lava dacite
SL-JL-83	SLJL83@4.ais	SVC2	7.42	0.20	2009_07_01July\ SLJL83-2@4.ais	unpolished	0.671	0.037	121	12	960	Gros piton_lava dacite
SL-JL-83	SLJL83@5.ais	SVC2	8.07	0.20	2009_07_01July\ SLJL83-2@5.ais	unpolished	0.604	0.039	101	11	769	Gros piton_lava dacite
SL-JL-83	SLJL83@6.ais	SVC2	8.43	0.20	2009_07_01July\ SLJL83-2@6.ais	unpolished	0.901	0.132	252	145	1030	Gros piton_lava dacite
SL-JL-83	SLJL83@7.ais	SVC2	7.41	0.20	2009_07_01July\ SLJL83-2@7.ais	unpolished	0.568	0.036	92	9	850	Gros piton_lava dacite
SL-JL-83	SLJL83@8.ais	SVC2	8.35	0.20	2009_07_01July\ SLJL83-2@8.ais	unpolished	0.629	0.030	108	9	733	Gros piton_lava dacite
SL-JL-83	SLJL83@9.ais	SVC2	8.14	0.20	2009_07_01July\ SLJL83-2@9.ais	unpolished	0.556	0.030	89	7	918	Gros piton_lava dacite
SL-JL-83	SLJL83@10.ais	SVC2	7.82	0.20	2009_07_01July\ SLJL83-2@10.ais	unpolished	0.696	0.047	130	17	773	Gros piton_lava dacite
SL-JL-83	SLJL83@11.ais	SVC2	8.17	0.20	2009_07_01July\ SLJL83-2@11.ais	unpolished	0.929	0.049	288	75	544	Gros piton_lava dacite
SL-JL-83	SLJL83@12.ais	SVC2	8.34	0.20	2009_07_01July\ SLJL83-2@12.ais	unpolished	0.612	0.031	104	9	756	Gros piton_lava dacite
SL-JL-83	SLJL83@13.ais	SVC2	7.77	0.20	2009_07_01July\ SLJL83-2@13.ais	unpolished	0.864	0.063	218	51	438	Gros piton_lava dacite
SL-JL-83	SLJL83@14.ais	SVC2	7.93	0.20	2009_07_01July\ SLJL83-2@14.ais	unpolished	0.508	0.032	77	7	601	Gros piton_lava dacite
SL-JL-83	SLJL83@15.ais	SVC2	7.98	0.20	2009_07_01July\ SLJL83-2@15.ais	unpolished	0.665	0.040	120	13	589	Gros piton_lava dacite
SL-JL-79	SLJL79@21.ais	SVC2	7.84	0.17	2009_06_22Jun\ SLJL79-2@1.ais	unpolished	0.78	0.05	167	24	703	Anse John beach_pumice
SL-JL-79	SLJL79@22.ais	SVC2	8.25	0.17	2009_06_22Jun\ SLJL79-2@2.ais	unpolished	0.73	0.04	142	15	591	Anse John beach_pumice
SL-JL-79	SLJL79@22_2.ais	SVC2	8.86	0.17	2009_06_22Jun\ SLJL79-2@2.ais	unpolished	0.73	0.04	142	15	591	Anse John beach_pumice
SL-JL-79	SLJL79@25.ais	SVC2	7.66	0.17	2009_06_22Jun\ SLJL79-2@5.ais	unpolished	0.71	0.03	136	12	862	Anse John beach_pumice
SL-JL-79	SLJL79@26.ais	SVC2	8.42	0.17	2009_06_22Jun\ SLJL79-2@6.ais	unpolished	0.68	0.04	123	13	733	Anse John beach_pumice
SL-JL-79	SLJL79@27.ais	SVC2	8.66	0.17	2009_06_22Jun\ SLJL79-2@7.ais	unpolished	0.74	0.03	148	12	740	Anse John beach_pumice
SL-JL-79	SLJL79@29.ais	SVC2	7.70	0.17	2009_06_22Jun\ SLJL79-2@9.ais	unpolished	1.01	0.10	-	-	1134	Anse John beach_pumice
SL-JL-79	SLJL79@30.ais	SVC2	8.55	0.17	2009_06_22Jun\ SLJL79-2@10.ais	unpolished	0.66	0.03	118	9	753	Anse John beach_pumice
SL-JL-79	SLJL79@31.ais	SVC2	8.03	0.17	2009_06_22Jun\ SLJL79-2@11.ais	unpolished	0.95	0.12	317	243	1665	Anse John beach_pumice
SL-JL-79	SLJL79@32.ais	SVC2	8.12	0.17	2009_06_22Jun\ SLJL79-2@12.ais	unpolished	0.78	0.07	165	32	325	Anse John beach_pumice
SL-JL-79	SLJL79@33.ais	SVC2	7.79	0.17	2009_06_22Jun\ SLJL79-2@13.ais	unpolished	0.81	0.05	182	26	637	Anse John beach_pumice
SL-JL-79	SLJL79@34.ais	SVC2	8.43	0.17		unpolished	-	-	-	-		Anse John beach_pumice
SL-JL-79	SLJL79@35.ais	SVC2	8.04	0.17	2009_06_22Jun\ SLJL79-2@15.ais	unpolished	0.69	0.03	129	11	646	Anse John beach_pumice
SL-JL-79	SLJL79@36.ais	SVC2	8.02	0.17	2009_06_22Jun\ SLJL79-2@16.ais	unpolished	0.93	0.03	285	52	523	Anse John beach_pumice

Table D.16. (continued).

WR sample name	Analysis name	Eruption period	$\delta^{18}\text{O}$ V-SMOW	1 SE	Name of U-Th data	Polishing:	m	1SE	Th age (ka)	1SE	U ppm	Nature
<i>Orthopyroxee bearing SVC2,2</i>												
SL-JL-24	SLJL24@10.ais	SVC3	7.01	0.41	2007_12_08Dec\ SLJL24@10.ais	polished	0.62	0.03	106	8	744	Belfond pyroclastic formation_pumice
SL-JL-24	SLJL24@11.ais	SVC3	7.53	0.41	2007_12_08Dec\ SLJL24@11.ais	polished	0.72	0.04	138	14	583	Belfond pyroclastic formation_pumice
SL-JL-24	SLJL24@12.ais	SVC3	7.45	0.41	2007_12_08Dec\ SLJL24@12.ais	polished	0.80	0.03	174	18	559	Belfond pyroclastic formation_pumice
SL-JL-24	SLJL24@13.ais	SVC3	7.58	0.41	2007_12_08Dec\ SLJL24@13.ais	polished	0.53	0.03	82	7	572	Belfond pyroclastic formation_pumice
SL-JL-24	SLJL24@14.ais	SVC3	7.89	0.41	2007_12_08Dec\ SLJL24@14.ais	polished	0.62	0.03	107	9	970	Belfond pyroclastic formation_pumice
SL-JL-24	SLJL24@15.ais	SVC3	7.74	0.41	2007_12_08Dec\ SLJL24@15.ais	polished	0.47	0.02	70	4	866	Belfond pyroclastic formation_pumice
SL-JL-24	SLJL24@16.ais	SVC3	8.24	0.41	2007_12_08Dec\ SLJL24@16.ais	polished	0.33	0.02	45	3	1446	Belfond pyroclastic formation_pumice
SL-JL-24	SLJL24@17.ais	SVC3	7.71	0.41	2007_12_08Dec\ SLJL24@17.ais	polished	0.51	0.02	78	5	893	Belfond pyroclastic formation_pumice
SL-JL-24	SLJL24@18.ais	SVC3	8.15	0.41	2007_12_08Dec\ SLJL24@18.ais	polished	0.67	0.04	123	12	371	Belfond pyroclastic formation_pumice
SL-JL-24	SLJL24@19.ais	SVC3	8.79	0.41	2007_12_08Dec\ SLJL24@19.ais	polished	0.79	0.04	171	19	436	Belfond pyroclastic formation_pumice
SL-JL-24	SLJL24@20_2.ais	SVC3	7.83	0.41	2007_12_08Dec\ SLJL24@20.ais	polished	0.50	0.03	76	6	712	Belfond pyroclastic formation_pumice
SL-JL-24	SLJL24@21.ais	SVC3	8.73	0.41	2007_12_08Dec\ SLJL24@21.ais	polished	0.55	0.02	88	6	986	Belfond pyroclastic formation_pumice
SL-JL-24	SLJL24@22.ais	SVC3	7.38	0.41	2007_12_08Dec\ SLJL24@22.ais	polished	0.62	0.04	107	10	726	Belfond pyroclastic formation_pumice
SL-JL-24	SLJL24@23.ais	SVC3	8.35	0.41	2007_12_08Dec\ SLJL24@23.ais	polished	0.63	0.03	109	8	908	Belfond pyroclastic formation_pumice
SL-JL-24	SLJL24@24.ais	SVC3	7.47	0.41	2007_12_08Dec\ SLJL24@24.ais	polished	0.28	0.02	35	2	1525	Belfond pyroclastic formation_pumice
SL-JL-24	SLJL24@25.ais	SVC3	8.54	0.41	2007_12_08Dec\ SLJL24@25.ais	polished	0.76	0.03	155	15	1126	Belfond pyroclastic formation_pumice
SL-JL-22	SLJL22@1.ais	SVC3	7.72	0.20	2009_06_22Jun\ SLJL22-2@1.ais	unpolished	0.43	0.03	61	5	1038	Terre blanche dome_ lava grey dacite
SL-JL-22	SLJL22@2.ais	SVC3	8.11	0.20	2009_06_22Jun\ SLJL22-2@2.ais	unpolished	0.39	0.03	54	5	808	Terre blanche dome_ lava grey dacite
SL-JL-22	SLJL22@3.ais	SVC3	8.16	0.20	2009_06_22Jun\ SLJL22-2@3.ais	unpolished	0.22	0.02	28	3	761	Terre blanche dome_ lava grey dacite
SL-JL-22	SLJL22@4.ais	SVC3	8.09	0.20	2009_06_22Jun\ SLJL22-2@4.ais	unpolished	0.23	0.02	29	2	1454	Terre blanche dome_ lava grey dacite
SL-JL-22	SLJL22@5.ais	SVC3	8.15	0.20	2009_06_22Jun\ SLJL22-2@5.ais	unpolished	0.61	0.05	102	13	912	Terre blanche dome_ lava grey dacite
SL-JL-22	SLJL22@6.ais	SVC3	8.18	0.20	2009_06_22Jun\ SLJL22-2@6.ais	unpolished	0.40	0.04	56	6	899	Terre blanche dome_ lava grey dacite
SL-JL-22	SLJL22@7.ais	SVC3	8.88	0.20	2009_06_22Jun\ SLJL22-2@7.ais	unpolished	0.33	0.03	44	6	690	Terre blanche dome_ lava grey dacite
SL-JL-22	SLJL22@7_2.ais	SVC3	7.93	0.20	2009_06_22Jun\ SLJL22-2@7.ais	unpolished	0.33	0.03	44	6	690	Terre blanche dome_ lava grey dacite
SL-JL-22	SLJL22@8.ais	SVC3	8.25	0.20	2009_06_22Jun\ SLJL22-2@8.ais	unpolished	0.27	0.02	35	4	855	Terre blanche dome_ lava grey dacite
SL-JL-22	SLJL22@9.ais	SVC3	8.06	0.20	2009_06_22Jun\ SLJL22-2@9.ais	unpolished	0.26	0.02	32	4	829	Terre blanche dome_ lava grey dacite
SL-JL-22	SLJL22@10.ais	SVC3	7.28	0.20	2009_06_22Jun\ SLJL22-2@10.ais	unpolished	0.39	0.03	54	5	1558	Terre blanche dome_ lava grey dacite
SL-JL-22	SLJL22_UTh@1.ais	SVC3	8.28	0.24	2008_06_03June\ SLJL22_MMCC@1.ais	polished	0.47	0.03	69	7	765	Terre blanche dome_ lava grey dacite
SL-JL-22	SLJL22_UTh@2.ais	SVC3	8.47	0.24	2008_06_03June\ SLJL22_MMCC@2.ais	polished	0.57	0.03	92	9	615	Terre blanche dome_ lava grey dacite
SL-JL-22	SLJL22_UTh@3.ais	SVC3	9.36	0.24	—	polished	—	—	—	—	—	Terre blanche dome_ lava grey dacite
SL-JL-22	SLJL22_UTh@4.ais	SVC3	9.04	0.24	2008_06_03June\ SLJL22_MMCC@4.ais	polished	0.53	0.04	83	9	460	Terre blanche dome_ lava grey dacite
SL-JL-22	SLJL22_UTh@5.ais	SVC3	8.26	0.24	2008_06_03June\ SLJL22_MMCC@5.ais	polished	0.66	0.03	117	11	696	Terre blanche dome_ lava grey dacite
SL-JL-22	SLJL22_UTh@6.ais	SVC3	8.27	0.24	2008_06_03June\ SLJL22_MMCC@6.ais	polished	0.66	0.03	119	10	972	Terre blanche dome_ lava grey dacite
SL-JL-22	SLJL22_UTh@9.ais	SVC3	8.00	0.24	2008_06_03June\ SLJL22_MMCC@9.ais	polished	0.72	0.03	138	13	927	Terre blanche dome_ lava grey dacite
SL-JL-22	SLJL22_UTh@10.ais	SVC3	8.99	0.24	2008_06_03June\ SLJL22_MMCC@10.ais	polished	0.73	0.04	142	17	648	Terre blanche dome_ lava grey dacite
SL-JL-22	SLJL22_UTh@10_2.ais	SVC3	7.74	0.24	2008_06_03June\ SLJL22_MMCC@10.ais	polished	0.73	0.04	142	17	648	Terre blanche dome_ lava grey dacite
SL-JL-22	SLJL22_UTh@11.ais	SVC3	7.23	0.24	2008_06_03June\ SLJL22_MMCC@11.ais	polished	0.88	0.08	235	138	327	Terre blanche dome_ lava grey dacite
SL-JL-22	SLJL22_UTh@13.ais	SVC3	8.68	0.24	2008_06_03June\ SLJL22_MMCC@13.ais	polished	0.72	0.09	139	40	1149	Terre blanche dome_ lava grey dacite
SL-JL-22	SLJL22_UTh@14.ais	SVC3	8.21	0.24	2008_06_03June\ SLJL22_MMCC@14.ais	polished	0.52	0.03	81	7	783	Terre blanche dome_ lava grey dacite
SL-JL-22	SLJL22_UTh@16.ais	SVC3	8.41	0.24	—	polished	—	—	—	—	—	Terre blanche dome_ lava grey dacite
SL-JL-22	SLJL22_UTh@18.ais	SVC3	13.07	0.24	—	polished	—	—	—	—	—	Terre blanche dome_ lava grey dacite
SL-JL-22	SLJL22_UTh@19.ais	SVC3	7.82	0.24	2008_06_03June\ SLJL22_MMCC@19.ais	polished	0.46	0.03	67	6	732	Terre blanche dome_ lava grey dacite
SL-JL-22	SLJL22_UTh@20.ais	SVC3	7.52	0.24	2008_06_03June\ SLJL22_MMCC@20.ais	polished	0.51	0.03	77	7	666	Terre blanche dome_ lava grey dacite
SL-JL-22	SLJL22_UTh@21.ais	SVC3	7.37	0.24	2008_06_03June\ SLJL22_MMCC@21.ais	polished	0.72	0.04	138	18	568	Terre blanche dome_ lava grey dacite

Table D.16. (continued).

WR sample name	Analysis name	Eruption period	$\delta^{18}\text{O}_{\text{V-SMOW}}$	1 SE	Name of U-Th data	Polishing:	m	1SE	Th age (ka)	1SE	U ppm	Nature
<i>Cummingtonite bearing SVC2,2</i>												
SL-JL-25	SLJL25@11.ais	SVC3	5.56	0.41	2007_12_08Dec\ SLJL25@11.ais	polished	0.43	0.02	61	4	1252	Belfond dome_dacite lava clast
SL-JL-25	SLJL25@12.ais	SVC3	8.53	0.41	2007_12_08Dec\ SLJL25@12.ais	polished	0.84	0.02	202	17	2434	Belfond dome_dacite lava clast
SL-JL-25	SLJL25@13.ais	SVC3	8.15	0.41	2007_12_08Dec\ SLJL25@13.ais	polished	0.90	0.05	256	53	391	Belfond dome_dacite lava clast
SL-JL-25	SLJL25@14.ais	SVC3	8.57	0.41	2007_12_08Dec\ SLJL25@14.ais	polished	0.22	0.02	27	3	1099	Belfond dome_dacite lava clast
SL-JL-25	SLJL25@15.ais	SVC3	8.70	0.41	2007_12_08Dec\ SLJL25@15.ais	polished	0.50	0.02	75	5	1055	Belfond dome_dacite lava clast
SL-JL-25	SLJL25@16.ais	SVC3	7.75	0.41	2007_12_08Dec\ SLJL25@16.ais	polished	0.27	0.02	34	3	1072	Belfond dome_dacite lava clast
SL-JL-25	SLJL25@17.ais	SVC3	8.45	0.41	2007_12_08Dec\ SLJL25@17.ais	polished	0.32	0.02	43	3	1053	Belfond dome_dacite lava clast
SL-JL-25	SLJL25@18.ais	SVC3	7.89	0.41	2007_12_08Dec\ SLJL25@18.ais	polished	0.53	0.03	82	6	653	Belfond dome_dacite lava clast
SL-JL-25	SLJL25@1.ais	SVC3	7.41	0.20	2009_06_22Jun\ SLJL25-2@1.ais	unpolished	0.26	0.03	33	4	910	Belfond dome_dacite lava clast
SL-JL-25	SLJL25@2.ais	SVC3	8.29	0.20	2009_06_22Jun\ SLJL25-2@2.ais	unpolished	0.24	0.02	29	3	1484	Belfond dome_dacite lava clast
SL-JL-25	SLJL25@3.ais	SVC3	8.17	0.20	2009_06_22Jun\ SLJL25-2@3.ais	unpolished	0.28	0.02	36	4	689	Belfond dome_dacite lava clast
SL-JL-25	SLJL25@4.ais	SVC3	7.71	0.20	2009_06_22Jun\ SLJL25-2@4.ais	unpolished	0.49	0.03	74	7	696	Belfond dome_dacite lava clast
SL-JL-25	SLJL25@5.ais	SVC3	7.68	0.20	2009_06_22Jun\ SLJL25-2@5.ais	unpolished	0.48	0.02	71	5	790	Belfond dome_dacite lava clast
SL-JL-25	SLJL25@6.ais	SVC3	8.00	0.20	2009_06_22Jun\ SLJL25-2@6.ais	unpolished	0.32	0.02	42	3	1085	Belfond dome_dacite lava clast
SL-JL-25	SLJL25@7.ais	SVC3	8.53	0.20	2009_06_22Jun\ SLJL25-2@7.ais	unpolished	0.22	0.02	27	3	1166	Belfond dome_dacite lava clast
SL-JL-25	SLJL25@8.ais	SVC3	7.73	0.20	2009_06_22Jun\ SLJL25-2@8.ais	unpolished	0.27	0.02	35	3	1205	Belfond dome_dacite lava clast
SL-JL-25	SLJL25@9.ais	SVC3	8.08	0.20	2009_06_22Jun\ SLJL25-2@9.ais	unpolished	0.23	0.02	29	3	894	Belfond dome_dacite lava clast
SL-JL-25	SLJL25@10.ais	SVC3	8.27	0.20	2009_06_22Jun\ SLJL25-2@10.ais	unpolished	0.19	0.02	22	2	1006	Belfond dome_dacite lava clast
SL-JL-25	SLJL25@11.ais	SVC3	8.34	0.20	2009_06_22Jun\ SLJL25-2@11.ais	unpolished	0.36	0.02	48	4	1055	Belfond dome_dacite lava clast
SL-JL-25	SLJL25@12.ais	SVC3	7.94	0.20	2009_06_22Jun\ SLJL25-2@12.ais	unpolished	0.50	0.03	76	7	802	Belfond dome_dacite lava clast
SL-JL-25	SLJL25@13.ais	SVC3	8.27	0.20	2009_06_22Jun\ SLJL25-2@13.ais	unpolished	0.24	0.02	31	3	720	Belfond dome_dacite lava clast
SL-JL-25	SLJL25@14.ais	SVC3	9.07	0.20	2009_06_22Jun\ SLJL25-2@14.ais	unpolished	0.29	0.02	37	3	715	Belfond dome_dacite lava clast
SL-JL-25	SLJL25@14_2.ais	SVC3	8.33	0.20	2009_06_22Jun\ SLJL25-2@14.ais	unpolished	0.29	0.02	37	3	715	Belfond dome_dacite lava clast
SL-JL-25	SLJL25@15.ais	SVC3	7.33	0.20	2009_06_22Jun\ SLJL25-2@15.ais	unpolished	0.57	0.03	93	8	554	Belfond dome_dacite lava clast

Table D.16. (continued).

WR sample name	Analysis name	Eruption period	$\delta^{18}\text{O}_{\text{V-SMOW}}$	1 SE	Name of U-Th data	Polishing:	m	1SE	Th age (ka)	1SE	U ppm	Nature	
Plutonic xenoliths found in Cumingtonite bearing dome:													
SL-JL-52	SLJL52@1.ais	—	8.55	0.36	2009_03_26Mar\	SLJL52@1.ais	unpolished	0.28	0.02	36	3	730	Belfond dome_ biotite rich xeno 10 cm
SL-JL-52	SLJL52@2.ais	—	7.40	0.36	2009_03_26Mar\	SLJL52@2.ais	unpolished	0.38	0.02	52	4	504	Belfond dome_ biotite rich xeno 10 cm
SL-JL-52	SLJL52@3.ais	—	7.78	0.36	2009_03_26Mar\	SLJL52@3.ais	unpolished	0.60	0.04	99	10	440	Belfond dome_ biotite rich xeno 10 cm
SL-JL-52	SLJL52@4.ais	—	8.35	0.36	2009_03_26Mar\	SLJL52@4.ais	unpolished	0.28	0.02	35	3	635	Belfond dome_ biotite rich xeno 10 cm
SL-JL-52	SLJL52@5.ais	—	8.07	0.36	2009_03_26Mar\	SLJL52@5.ais	unpolished	0.33	0.02	44	4	493	Belfond dome_ biotite rich xeno 10 cm
SL-JL-52	SLJL52@6.ais	—	7.96	0.36	2009_03_26Mar\	SLJL52@6.ais	unpolished	0.51	0.04	79	10	702	Belfond dome_ biotite rich xeno 10 cm
SL-JL-52	SLJL52@7.ais	—	7.59	0.36	2009_03_26Mar\	SLJL52@7.ais	unpolished	0.33	0.02	44	4	587	Belfond dome_ biotite rich xeno 10 cm
SL-JL-52	SLJL52@7_2.ais	—	7.49	0.36	2009_03_26Mar\	SLJL52@7.ais	unpolished	0.33	0.02	44	4	587	Belfond dome_ biotite rich xeno 10 cm
SL-JL-52	SLJL52@8.ais	—	7.49	0.36	2009_03_26Mar\	SLJL52@8.ais	unpolished	0.33	0.02	44	3	481	Belfond dome_ biotite rich xeno 10 cm
SL-JL-52	SLJL52@9.ais	—	7.72	0.36	2009_03_26Mar\	SLJL52@9.ais	unpolished	0.43	0.03	62	5	557	Belfond dome_ biotite rich xeno 10 cm
SL-JL-52	SLJL52@10.ais	—	8.33	0.36	2009_03_26Mar\	SLJL52@10.ais	unpolished	0.32	0.02	42	3	616	Belfond dome_ biotite rich xeno 10 cm
SL-JL-52	SLJL52@11.ais	—	8.66	0.36	2009_03_26Mar\	SLJL52@11.ais	unpolished	0.36	0.04	49	6	532	Belfond dome_ biotite rich xeno 10 cm
SL-JL-52	SLJL52@12 mean (n=2)	—	9.28	0.36	2009_03_26Mar\	SLJL52@12.ais	unpolished	0.35	0.02	47	3	725	Belfond dome_ biotite rich xeno 10 cm
SL-JL-52	SLJL52@13.ais	—	8.21	0.36	2009_03_26Mar\	SLJL52@13.ais	unpolished	0.37	0.03	50	4	489	Belfond dome_ biotite rich xeno 10 cm
SL-JL-52	SLJL52@14.ais	—	8.50	0.36	2009_03_26Mar\	SLJL52@14.ais	unpolished	0.81	0.07	179	38	547	Belfond dome_ biotite rich xeno 10 cm
SL-JL-52	SLJL52@14_2.ais	—	7.75	0.36	2009_03_26Mar\	SLJL52@14.ais	unpolished	0.81	0.07	179	38	547	Belfond dome_ biotite rich xeno 10 cm
SL-JL-52	SLJL52@15.ais	—	8.56	0.36	2009_03_26Mar\	SLJL52@15.ais	unpolished	0.32	0.02	42	3	613	Belfond dome_ biotite rich xeno 10 cm

Appendix E

Supplementary data file
of Chapter 6

Content

Table E.1. Details of the composition of the in-house solution standard JMC-2 and of the international rock standard WPR-1 obtained during the Os isotopic analyses of the Lesser Antilles lavas by N-TIMS.	321
--	-----

Table E.1. Details of the composition of the in-house solution standard JMC-2 and of the international rock standard WPR-1 obtained during the Os isotopic analyses of the Lesser Antilles lavas by N-TIMS. The Os concentration of the processed blank used to correct the $^{187}\text{Os}/^{188}\text{Os}$ ratio of the samples and WPR-1 is also presented.

GAU TIMMS JMC-2			GAU TIMMS WPR-1			GAU TIMMS Blank Os (pg)
$^{187}\text{Os}/^{188}\text{Os}$	2 SE		$^{187}\text{Os}/^{188}\text{Os}$	2 SE	Os (ppb)	
0.18335	0.00003		0.145402	0.000083	17.27	6.30
0.18301	0.00003		0.144109	0.000081	17.62	
0.18309	0.00004		0.145838	0.000074	16.91	
0.18300	0.00004		0.144922	0.000116	16.97	
Average:	0.18311	Average:	0.1451		17.19	
2 sd:	0.00032	2 sd:	0.0015		0.65	

Appendix F

Detailed analytical techniques

Content

F.1 Introduction	326
F.2 Whole rock trace elements	326
F.2.1 Sample preparation	326
F.2.2 Beaker cleaning	326
F.2.3 Dissolution procedure	327
F.2.4 Fusion procedure	329
F.2.5 Measurement	330
F.3 Whole rock Sr-Nd-Hf-Pb isotopes	331
F.3.1 Sample Preparation	331
F.3.2 Beaker cleaning	331
F.3.4 Dissolution procedure	332
F.3.5 Column chemistry procedure	333
F.3.6 Measurement	339
F.3.6.1 Sr isotopes	339
F.3.6.2 Nd isotopes	340
F.3.6.3 Pb isotopes	341
F.3.6.4 Hf isotopes	341
F.4 Os isotopes	342
F.4.1 Sample preparation	342
F.4.2 Beaker and Carius tube cleaning	342
F.4.3 Dissolution procedure	343
F.4.4 Os extraction and purification	344
F.4.5 Measurement	345
F.5 Single mineral $\delta^{18}\text{O}$	346
F.5.1 Sample preparation	346
F.5.2 Laser-Fluorination	346
F.5.3 Measurement	347
F.6 Single plagioclase $^{87}\text{Sr}/^{86}\text{Sr}$ and trace elements	347
F.6.1 Sample preparation	347
F.6.2 Beaker cleaning	347
F.6.3 Sample digestion	348
F.6.4 Column chemistry procedure	349
F.6.5 $^{87}\text{Sr}/^{86}\text{Sr}$ analysis	350

F.6.6 Mineral trace element analysis	350
F.7 Imaging and in-situ major elements	351
F.8 In-situ trace elements	352
F.9 In-situ $\delta^{18}\text{O}$ in zircons	352
F.10 In-situ $^{87}\text{Sr}/^{86}\text{Sr}$ in plagioclase	353
F.10.1 Beaker cleaning	353
F.10.2. Resin cleaning	354
F.10.3 Making the high purity TaF_5 activator	354
F.10.4 Microdrilling	355
F.10.5. Digestion	356
F.10.6 Column work	356
F.10.7 Analysis	357

F.1 Introduction

In the following sections, the detailed methodology for sample preparation, chemistry and measurement of all the data obtained in the thesis is presented. More succinct descriptions can be found in the method section of each chapter.

F.2 Whole rock trace elements

F.2.1 Sample preparation

Rock chips and rock powders had already been prepared and stored by Jon Davidson for part of the lava samples (All SL-83- samples). Samples that were not already processed (all SL-JL), were cleared of weathering surfaces using a hammer. The samples were then reduced to a smaller fraction using a hammer. The rock chips were subsequently crushed using a fly-press at Durham University. Finally, the crushed samples were transferred into agate ball mill for 30 min to be powdered. All these steps were performed at Durham Geochemistry centre (DGC), Durham University.

Samples were dissolved and analysed at both DGC and the Geochemical Unit (GAU) of Macquarie University. At both DGC and the GAU, samples were analysed twice: once on crushed powder and once on fused glass to obtain Zr, Hf, U and Ti in zircon bearing rocks.

F.2.2 Beaker cleaning

At DGC:

1. Place the open beaker upside down in the dishwasher
2. Remove from the dishwasher
2. Add 2 ml of 16N Analar HNO₃ and place on the hot plate at 130-150°C for 24h
3. Turn the hot plate off, allow the beaker to cool and discard acid
4. Fill the beaker with MQ H₂O, close and shake
5. Repeat step 4
6. Close the beaker. It is now ready for sample loading.

At the GAU:

1. Remove old labels with ethanol and rinse beaker and cap with MQ H₂O

2. Add 2 ml of 16N TD HNO₃ to each beaker and reflux overnight at 120-150°C
3. Remove from the hot plate, leave it cool and discard acid
4. Rinse 3 times with MQ H₂O
5. Add 2 ml of 12N TD HCl to each beaker and reflux overnight at 120°C
6. Rinse 3 times with MQ H₂O
7. Add 2-3 ml of 4N Suprapur® HF to each beaker and reflux overnight at 120°C
8. Rinse 3 times with MQ H₂O
9. Add MQ H₂O to the beaker, let sit until needed

F.2.3 Dissolution procedure

At DGC:

1. Weight 0.1g of sample using weighing paper and transfer into clean Teflon beaker
2. Add 1 ml of Aristar® 15N HNO₃ to each beaker and wait 5 min
3. Add 4 ml of Aristar® 12N HF to each beaker and close cap tightly
4. Place the beaker on the hot plate at 130°C-150°C for 48 h
5. Remove the beaker from the hot plate and let it cool
6. Remove the cap and place the beaker on hot plate at 130-150°C. Dry to paste (a few µl should remain)
7. Remove from the hot plate, put the cap on, let the sample cool
8. Add 1 ml of Aristar® 15N HNO₃ to each beaker
9. Place the sample on hot plate without the cap. Dry to paste
10. Repeat steps 8 and 9
11. Remove the beaker from the hot plate and let the sample cool
12. Add 2.5 ml of Aristar® 15N HNO₃ to each beaker and add 10-15 ml of MQ water
13. Place the beaker on the hot plate with the caps on for 30 min at 110-130°C
14. Add 1 ml of internal standard (2 ppm Bi, Re and Rh solution)
15. Transfer the solution from Teflon beaker to a pre-cleaned 50 ml polypropylene volumetric flask. Rinse the beaker with MQ and transfer the washings to polypropylene flask, repeat 2-3 times. Make the flask up to 50 ml with MQ H₂O.

16. Transfer the content of the volumetric flasks into a 60 ml bottle pre-cleaned with 5-10% HNO₃ and rinsed with MQ H₂O.
17. Sample is ready for analysis

At the GAU:

1. Weight 0.1g of sample powder in each beaker
2. Add a few drops of 2% single Teflon distilled (TD) HNO₃
3. Add 2 ml of 29N Suprapur® HF + 2 ml of 16N TD HNO₃
4. Close the beaker and put on hot plate at 130-140°C for 48h
5. Take the beaker off the hot plate, let it cool for 1/2h
6. Open the cap, and put both the cap and beaker on the hot plate to dry overnight at 100-150°C
7. Repeat steps 3-6 once
8. Add 1 ml of 29N TD HF + 1 ml of 12N Suprapur® HCL0₄ to dissolve fluorides
9. Place the beaker on hot plate overnight at 130°C with cap on
10. Open the beaker and dry the samples at around 200°C for a day
11. Let the sample cool down and add 2-3 ml of 6N TD HCL
12. Put the beaker, with cap on, on hot plate overnight at 130-150°C
13. Dry the sample down at 150-170°C
14. Let the sample cool down and add 6N TD HNO₃
15. Leave on hot plate overnight at 130-150°C
16. Dry it down to a paste
17. Add 4-5 ml of 2% TD HNO₃ + 0.5% Suprapur® HF
18. Label a 100 ml pre-cleaned polypropylene bottle and a small pre-cleaned polypropylene 5 ml beaker for analysis
19. Weight each bottle and tare it
20. Transfer all the sample in the bottle
21. Wash cap and Teflon beaker 3 times with 2% TD HNO₃ + traces of Suprapur® HF
22. Fill the bottle until 100g ± 1% with 2% TD HNO₃ + traces of Suprapur® HF
23. Shake the bottle
24. Add 20µl of spike (Li⁶, Ar, Rh, In, Tm, Bi) in a 5 ml beaker (± 1%), write weight

25. Fill the ~5 ml beaker with 5 ml of sample in 2% TD HNO₃ + traces of Suprapur® HF and write weight.
26. The solution is ready for analysis

F.2.4 Fusion procedure

At DGC:

1. Label 5 ml pre-cleaned plastic beaker
2. Weight 2.25g of Li₂B₄O₇ flux
3. Weight 0.45g of sample powder and shake powder extensively to homogenise
4. Turn the furnace on 3h before placing the samples in (set at 1050°C)
5. Transfer the powders in platinum crucibles pre-cleaned in 50% MQ H₂O + 50% 11N AnalaR® HCl at 150°C on hot plate.
6. Place the crucible in the oven for 35 min with platinum lids on
7. Poor the melt into cylindrical stainless steel mold and “stamp it” within less than 2 seconds
8. Let the glass cool
9. Place the glass in a small labelled sample bag
10. Crush the glass disk in an agate bowl and transfer the powder in a sample bag.
11. The powder is ready to be digested as described in section G.2.2.1

At the GAU:

1. Add 1.5g (± 1%) of Li₂B₄O₇ flux in a platinum crucible
2. Add 0.5 g (± 1%) of sample powder
3. Mix it with spatula
2. Put in furnace and leave it for 1/2 h with temperature set at 1100°C
3. Turn the “agitation” mode on and wait for 20 min
4. Add Ammonium iodide in crucible (1 pill) in the melt and wait for 5 min
6. Poor melt in the press preheated for ½ h at 250°C
7. Let the disks cool and place it in a plastic sample bag.

F.2.5 Measurement

At DGC:

At DGC, trace element concentrations in both the rock powders and the crushed glass disks were analysed in solution by inductively coupled plasma mass spectrometry (ICP-MS) using the Thermo Scientific X-Series 2 instrument using the technique described by Ottley et al. (2003). Calibration was done using total procedural blanks and 3 processed international rock standards (see Table C.2.). Instrumental drift was corrected using the internal standard.

At the GAU:

At GAU, rock powders were analysed in solution using Agilent 7500 Series instrument. Instrument drift was corrected using the internal standard and elemental concentrations were calibrated using international rock standards (see Table C.2.).

Fused disks were analysed using a NewWave UP-213 laser ablation system linked to an Agilent 7700 Series ICP-MS system. Ablation of the samples was performed in a helium-filled chamber using a frequency of 5 Hz and an ablation spot size of 50 μm wide * 240 μm long. CaO from XRF analyses was used as an internal standard.

At Both DGC and the GAU:

Repeatability of the data was checked by analysing 3 replicates of the same sample in each batch. Standard deviation between the 3 replicates of each batch was less than 3% for all elements presented. Three blanks and three international rock standards (Durham: W2, BHVO-1, AGV-1; Macquarie: BCR-2; BIR-1; BHVO-2) were processed in each batch of sample. The inter-lab reproducibility of the data was verified by analysing BHVO-1 or BHVO-2 (which are identical for the elements presented, except for Pb) in every batch of samples. BHVO-1, W2, AGV-1 and BCR-2 and BIR-1 compositions are presented in Table C2. Differences between our measured BHVO-1 concentrations in every batch and the Georem preferred values (<http://georem.mpch-mainz.gwdg.de>) are less than 5% for all trace elements presented in this thesis.

F.3 Whole rock Sr-Nd-Hf-Pb isotopes

F.3.1 Sample Preparation

Rock powders for dissolution were prepared using the same method as described in section F.2.1.

F.3.2 Beaker cleaning

At DGC:

1. Fill both the cap and the beaker with MQ H₂O and discard
2. Check if any residues can be seen in the beaker. If any: wipe it using micropure wipe
3. Fill $\frac{3}{4}$ beakers with 6N AnalaR® HCl, put the cap on, shake and discard
4. Fill the cap with 6N AnalaR® HCl and discard
5. Add 2 ml of 29N TD HF in each beaker, close the cap and place on hot plate at 100°C for 24h
6. Remove the beaker from the hot plate, let it cool and discard HF
7. Rinse with MQ H₂O
8. Place open beaker and cap in large glass beaker (4 L) of 1N TD HNO₃ on hot plate at 70°C for 24h
9. Remove from the hot plate, let it cool and discard acid
10. Place the open beaker and the cap in a large glass beaker (4 L) of MQ H₂O and place on hot plate at 70°C for 24h
11. Discard MQ H₂O
12. Rinse both the beaker and the cap with MQ H₂O
13. Add 2 ml of 29N TD HF in each beaker and place them on hot plate at 100°C for 24h
14. Remove from hot plate, leave it cool and discard acid
15. Rinse with MQ H₂O
16. Close and store beaker.

At the GAU:

Same method as in section F.2.2.

F.3.4 Dissolution procedure

At DGC:

1. Weight 0.1 g of sample and place it into a clean Teflon beaker
2. Add 1 ml of 16N TD HNO₃ and 3 ml of 29N TD HF.
3. Place the beaker on the hot plate for 24h at 100°C with cap on.
4. Dry down to paste (2-6 h)
5. Add 1 ml of 16N TD HNO₃ and put on hot plate for 24h at 100°C with cap on.
6. Remove the beaker from the hot plate, take the cap off and dry down the sample for ~1h at 150°C
7. Add 1 ml of 16N TD HNO₃ and put samples back on the hot plate with lid off to dry them down for ~1h at 150°C.
8. Add 0.5 ml of 3N TD HNO₃ place the sample on hot plate with cap on for 1 h at 100°C
9. Pre-clean 1.5 ml centrifuge tube with MQ H₂O (5 min) followed by 3N TD HCl (for 15 min).
10. Transfer the sample solution in the centrifuge tube and centrifuge at 13000 rpm for 15 min: ready for column chemistry work.
11. Add 0.5 ml of 6N TD HCl to the empty Teflon beaker, to clean it before re-use. Place it on hot plate at 100°C for ~ 1h
12. Throw 6N TD HCl and rinse with MQ H₂O

At the GAU:

1. Weight 0.1g of each sample
2. Add a few drops of 2% TD HNO₃
3. Add 2 ml of 29N Suprapur® HF + 2 ml of 16N TD HNO₃
4. Close the beaker and put on hot plate at 130-140°C for 48h
5. Take the beaker off the hot plate, let it cool for ½ h
6. Open the cap, and put both the cap and the beaker on the hot plate to dry overnight at 100°C
7. Repeat steps 3-6 once
8. Add 1 ml of 29N Suprapur® HF + 1 ml of suprapur® HClO₄ to dissolve fluorides
9. Place the beaker on the hot plate overnight at 130°C with cap on

10. Open the beaker and dry the sample at around 200°C for a day
11. Let the sample cool down and add 2-3 ml of 6N TD HCL
12. Put the beaker, with cap on, on hot plate overnight at 130-150°C
13. Dry the sample down at 150-170°C
14. Let the sample cool down
15. Add 1.4 ml of 2.5N TD HCl + 0.1N Suprapur® HF to dried down sample
16. Ready for column chemistry

F.3.5 Column chemistry procedure

At DGC:

Column 1: separation of sample into Sr + Pb + Hf-Nd cuts

1. Prepare columns by cutting the end of 1 ml blue pipette tips and adding a frit at the bottom
2. Rinse column with 1 column volume (CV) of MQ H₂O.
3. Rinse column with 1 CV 6N TD HCL
4. Rinse column with 1 CV MQ H₂O
5. Add 2 drops (~ 6 µl) of Sr-Spec Resin (Eichrom)
6. Rinse resin with 1 CV of 6N TD HCl
7. Rinse resin with 2 CV of MQ H₂O
8. Pre-condition the resin with 200 µl of 3N HNO₃
9. Label and place clean Teflon beaker under the columns to collect Nd-Hf cut
10. Load the sample by pipetting the sample solution from the centrifuge tube (~300 µl), making sure no residue is added on to the resin.
11. Elute 2 times 250 µl of 3N TD HNO₃ and close beaker. **The Nd-Hf cut is now collected.**
12. Place Teflon beaker used for dissolution (cleaned with 6N TD HCl) under the column to collect Sr cuts.
13. Elute 2 times 200 µl of MQ water and close the beaker. **The Sr cut is now collected.**
14. Place the waste under the column
15. Elute 2 times 100 µl of 2.5N TD HCl to waste

16. Place 7 ml Teflon beaker under the columns for Pb collection
17. Elute 2 times 50 μ l of 8N TD HCl. **The Pb cut is now collected**
18. Wrap and discard column in glad wrap to avoid any resin particles in the room.
19. Dry Sr and Pb cuts on the hotplate at 80°C and dry Nd-Hf fraction on hotplate at 100°C
20. Add 500 μ l of 3% TD HNO₃ to the Pb sample with cap on at 40°C on hot plate for 30 min
21. Add 1 ml of 3% TD HNO₃ to dry sample and place on hot plate at ~70°C with cap on for ~ 30 min
22. Transfer both the Pb and the Sr sample solutions in 1.5 ml centrifuge tubes pre-cleaned with 6N TD HCl and rinsed with MQ H₂O
23. Centrifuge both Pb and Sr cuts at 13000 rpm for 15 min
24. Transfer sample solutions in new pre-cleaned 1.5 ml centrifuge tubes.
25. Pb and Sr are ready for analysis

Column 2: separation of Hf and Nd cuts

1. Add 1 ml of 1N TD HCl on the dry Hf-Nd cut and place on hot plate at 100°C for ~30 min with cap on.
2. Transfer the sample solution in pre-cleaned 1.5 ml centrifuge tube. Centrifuge for 15 min at 13000 rpm for 15 min.
3. Add 1 ml of 6N TD HCl in the dirty Teflon beaker and place it on the hot plate for ~ 30 min.
4. Rinse resin with 5 ml of 29N TD HF
5. Rinse resin with 10 ml of MQ H₂O
6. Pre-condition resin with 10 ml of 1N TD HF + 1N TD HCL
7. Recover Teflon beaker from hot plate, rinse with MQ H₂O.
8. Place beakers under the columns
9. Load sample solution (1ml) in the columns
10. Elute 3 ml of 1N TD HF-1N TD HCl and close beaker. **The Hf cut is now collected**
11. Place waste under the column
12. Elute 14 ml of 2.5N TD HCl
13. Elute 10 ml of 2N TD HNO₃

14. Recover Teflon beaker from hotplate, discard 6N TD HCl and rinse with MQ H₂O
15. Place the Teflon beaker under column
16. Elute 12 ml of 6N TD HCl. Close beaker. **The Nd cut is now collected**
17. Dry down the Nd cut at 130°C
18. Add 400 µl of 3% HNO₃ in sample and place on hot plate at 60°C for ~ 2h.
19. Pre-clean 1.5 ml centrifuge tubes with 1 ml 6N TD HCl for 1h and rinse with MQ H₂O
20. Transfer the sample solution in the centrifuge tube: Nd cut ready for analysis.
21. Clean the resin with 5 ml of 29N TD HF,
22. Clean the resin with 10 ml of MQ H₂O
23. Clean the resin with 10 ml of 6N TD HCl
24. Store columns in 6N TD HCl

Column 3: Separation of Ti from Hf

1. Dry down the sample cut collected at column 2 at 100°C
2. Add 1 ml of 0.52N TD H₂SO₄ - 5% H₂O₂ on sample
3. Rinse resin with 5 ml of 29N TD HF
4. Rinse resin with 5 ml of MQ H₂O
5. Rinse resin with 4 ml of 12N H₂SO₄
6. Rinse resin with 5 ml of MQ H₂O
7. Pre-condition resin with 5 ml of 0.52N TD H₂SO₄ – 5% H₂O₂
8. Place the waste under the column
9. Load the sample (1 ml)
10. Elute 5 ml of 0.52N TD H₂SO₄ – 5% H₂O₂
11. Repeat step 6.
12. Place clean Teflon beaker under column
13. Elute 4 ml of 1N TD HF-2N TD HCl. **The final Hf cut is now collected**
14. Dry down the cut at 100-110°C overnight
15. Remove the beaker from hot plate and add 20µl of H₂O₂ on samples (cover with parafilm during injection to protect from projections).
16. Dry down the cut at 200°C for ~3 days.
17. Add 5µl of HF on warm sample,

18. Add 500 μ l of 3% TD HNO₃ on sample and place on hot plate for 1/2h
19. Transfer sample in 1.5 ml centrifuge tube pre-cleaned with 6N TD HCl for 1h and rinsed with MQ H₂O
20. Centrifuge sample at 13000 rpm for 15 min.
21. Clean the resin following steps 3-6 and store columns in 6N TD HCl.

At the GAU:

Column 1: separation of Hf cut from Sr cut and Nd cut

Biorad AG 50W-X8 (100-200 mesh size) anionic resin and Teflon columns were used.

1. Pre-clean the resin 5-6 times with MQ H₂O before adding it to the Teflon column
2. Add resin to the columns and place waste under the columns
3. Rinse resin with 25 ml of 4 N suprapur® HF
4. Rinse resin with 25 ml of MQ H₂O and back-flush the resin to remove bubbles
5. Rinse resin with 25 ml of 6N TD HCl
6. Pre-condition resin with 25 mls of 2.5N HCl / 0.1N supra HF
2. Place a 15 ml clean Teflon beaker (with flat bottom) under the column
3. Load the 1.4 ml of sample solution
4. Elute 4 times 1 ml of 2.5N TD HCl-0.1N suprapur® HF
5. Close beaker. **The Hf cut is now collected**
6. Place the waste under column
7. Elute 21.5 ml of 2.5N TD HCl
8. Place 15 ml Teflon beaker for Sr collection
9. Elute 8 ml of 2.5N TD HCl
10. Close beaker. **Sr cut is now collected.**
11. Place the waste under column
12. Elute 7 ml of 6N TD HCl
13. Place a 15 ml Teflon beaker under the column for Nd cut collection
14. Elute 7 ml of 6N TD HCl
15. Close beaker. **Nd cut in now collected**
16. Dry down the Sr cut, add 1 drop of 16N TD HNO₃ then dry it down: the sample is ready to load.

Column 2: Purification of Hf cut

Biorad AG1-X8 (100-200 mesh size) anionic resin and Teflon columns were used.

1. Dry the Hf cut from column 1 at 150°C for 1-2h
2. Add 200 ml of H₂O₂ + 4 ml of 6N TD HCl, put cap on at >150°C for 1-2h
3. Dry sample at 120°C
4. Add 1-1.4 ml of 0.5N TD HCl-0.5N TD HF
5. Transfer the sample solution into pre-cleaned 1.5 ml centrifuge tubes and centrifuge at 5000 rpm for 5 min
6. Rinse the Teflon beakers with MQ and clean by adding 1 ml of 6N TD HCl and placing the beakers on the hot plate at 120°C
7. Load 1.8-2 ml (~2.7 ml wet) of AG1-X8 Anionic exchange resin (100-200 mesh) into 0.8*4 cm Bio-Rad Poly-Prep columns
8. Place the waste under column
9. Rinse the column and resin with 1 full reservoir (FR) of 4N suprapur® HF
10. Rinse the column and resin with 1 FR of 6N TD HCl
11. Pre-condition resin with 1 FR of 0.5N TD HCl-0.5N suprapur® HF
12. Pre-condition resin with 4 ml of 0.5N HCl-0.5N supra HF
13. Load sample (1-1.4 ml)
14. Elute 3 times 1 ml 0.5N TD HCl-0.5N suprapur® HF
15. Elute 16 ml of 0.5N TD HCl-0.5N HF
16. Recover used beaker from the hot plate, discard 6N TD HCl and rinse with MQ H₂O
17. Place the beaker under the column
18. Elute 10 ml of 6N HCl
19. Close the beaker. The second Hf cut (comprising HFSE) is now collected
20. Discard column

Column 3: Purify Hf cut second stage

Biorad AG50W-X8 (100-200 mesh size) anionic resin and Teflon columns were used.

1. Dry down the Hf cut from column 2
2. Add 3 drops of 12N suprapur® HClO₄ on the dry sample,
3. Evaporate to a small drop at 120°C and evaporate totally at 170-200°C
4. Add 3 drops of 12N suprapur® HClO₄ and evaporate totally at 170-200°C
5. Repeat step 4.

6. Add 1.4 ml of 2.5N TD HCl
7. Transfer sample solution into pre-cleaned 1.5 ml micro tubes, centrifuge for 5 min at 5000 rpm.
8. Rinse the Teflon beaker with MQ H₂O, and clean by adding 1 ml of 6N TD HCl and place at 120°C on hot plate for 1h.
9. Place the waste under the column
10. Add 60 µl H₂O₂ in centrifuge tube before loading (Brown-coloured Ti indicator)
11. Clean resin with 25 ml of 4N TD HF
12. Clean resin with 25 ml MQ H₂O and backflush the resin
13. Clean the resin with 25 ml of 6N TD HCl
14. Pre-condition resin with 25 ml of 2.5N HCl
15. Pre-condition resin with 5 ml of 2.5N TD HCl
16. Load sample solutions (~1.4 ml)
17. Elute 3 times 1 ml of 2.5N TD HCl
18. Elute 1.5 ml of 2.5N TD HCl
19. Recover Teflon beaker from hot plate, throw the 6N TD HCl and rinse with MQ H₂O
20. Place Teflon beaker under column
- 21. Elute 12 ml of 2.5N TD HCl-0.1N TD HF. The Final Hf is now collected**
22. Dry the Hf cuts at 120°C
23. Add 1 drop of 16N TD HNO₃ and dry down at 120-150°C to remove any organic material from resin.
24. Dilute the sample in 2 ml of 2% TD HNO₃ and place on hot plate at 100°C for 60 min. Place in ultrasonic bath if any particles can be observed. The sample is ready for analysis.

Column 4: Nd cut purification

Eichrom Ln Spec resin and Glass biorad columns were used for Nd purification.

1. Dry down the Nd cuts from column 1.
2. Add a drop of 16N TD HNO₃ and dry down at 120-150°C
3. Add 0.7 ml of 0.05N HNO₃ on the samples
4. Load 5 ml of resin in the columns
5. Rinse the resin with 5 ml of 0.25N TD HCl

6. Rinse the resin with 4 times 3 ml of 0.25N TD HCl
7. Place the waste under the column
8. Load the sample by increment: 3 times 0.2 ml and 1 time 0.1 ml.
9. Elute 3 times 0.75 ml of 0.25N TD HCl (remove Ba, La and Ce).
10. Place clean Teflon beaker under the column
11. Elute 4 ml of 0.25N TD HCl to collect Nd.
12. Dry down the sample at 150°C. The sample is ready for analysis on TIMS.

F.3.6 Measurement

F.3.6.1 Sr isotopes

At DGC:

Sr isotope ratios were analysed by plasma ionisation multicollector mass spectrometry (PIMMS) using a Thermo Scientific Neptune instrument. During the $^{87}\text{Sr}/^{86}\text{Sr}$ analytical sessions, instrument performance was monitored by analysis of NBS987 and within-run instrument mass fractionation was corrected using an exponential law and the normalising value of $^{88}\text{Sr}/^{86}\text{Sr} = 8.375209$ (equivalent to $^{86}\text{Sr}/^{88}\text{Sr} = 0.1194$). The average $^{87}\text{Sr}/^{86}\text{Sr}$ for NBS987 was 0.710272 ± 0.000020 (2sd; $n = 14$). The details of all NBS987 values are presented in Table B1. $^{87}\text{Sr}/^{86}\text{Sr}$ ratios are reported relative to NBS987 standard value of 0.71024 (Thirlwall, 1991). The $^{87}\text{Sr}/^{86}\text{Sr}$ ratio of the two international rock standards BHVO-1 and BIR-1 were 0.703463 and 0.703115 and respectively.

At the GAU:

At the GAU, $^{87}\text{Sr}/^{86}\text{Sr}$ ratios were measured by TIMS using a Thermo-Fisher Triton instrument. Samples were loaded on Re filaments using 1N TD HNO_3 and TaCl_5 activator. During the analytical session, instrument performance was monitored by analyses of Sr standards NBS987 and mass bias was corrected as in DGC. The average $^{87}\text{Sr}/^{86}\text{Sr}$ for NBS987 was 0.710220 ± 0.000022 (2sd, $n = 4$). The details of all NBS987 data are presented in Table B1. During the course of this study, analyses of processed international BHVO-2 standard yielded average $^{87}\text{Sr}/^{86}\text{Sr}$ of 0.703469 ± 0.000012 (2sd; $n = 4$).

F.3.6.2 Nd isotopes

At DGC:

$^{143}\text{Nd}/^{144}\text{Nd}$ compositions were analysed by PIMMS using a Thermo Scientific Neptune instrument. During the analytical sessions, the instrument performance was monitored by analysis of an in house J&M Nd standards and within-run instrument mass fractionation was corrected using an exponential law and the normalising value of $^{146}\text{Nd}/^{145}\text{Nd} = 2.079143$ (equivalent $^{146}\text{Nd}/^{144}\text{Nd} = 0.7219$). Since Nd was analysed as part of a total REE cut, the data required an algebraic correction for Sm interference on Nd based on the approach of Nowell and Parrish (2001). The accuracy of this correction was monitored by analysis of Sm-doped J&M, with a Sm/Nd ratio of ~ 0.25 . The average $^{143}\text{Nd}/^{144}\text{Nd}$ for both pure and Sm-doped J&M was 0.511105 ± 0.00002 (2sd; $n = 15$). The details of all pure and SM-doped J & M data are presented in Table B2. The $^{143}\text{Nd}/^{144}\text{Nd}$ ratio of the two international rock standards BHVO-1 and BIR-1 were 0.512989 and 0.513073 respectively. The accuracy of the Sm correction on the $^{143}\text{Nd}/^{144}\text{Nd}$ ratio is illustrated by the analysis of BHVO-1, which after Sm correction is identical to the ratio of 0.512986 ± 0.000009 (2sd; $n = 19$) that Weis et al. (2005) obtained by thermal ionisation mass spectrometry (TIMS).

At the GAU:

$^{143}\text{Nd}/^{144}\text{Nd}$ ratios were measured by TIMS using a Thermo-Fisher Triton instrument. Samples were loaded on Re filaments with a mix of HCl and orthophosphoric acid (activator solution). During the analytical session, instrument performance was monitored by analyses Nd standard JMC321 and mass bias was corrected as in DGC. The average $^{143}\text{Nd}/^{144}\text{Nd}$ for JMC321 was 0.511123 ± 0.000006 (2sd; $n = 3$; see table B2 for the detail of all JMC321 compositions). $^{143}\text{Nd}/^{144}\text{Nd}$ were not reported relative to a literature value. During the course of this study, analyses of processed international BHVO-2 standard yielded average $^{143}\text{Nd}/^{144}\text{Nd}$ ratios of 0.512976 ± 0.000012 (2sd; $n = 4$).

F.3.6.3 Pb isotopes

At DGC:

$^{206}\text{Pb}/^{204}\text{Pb}$, $^{207}\text{Pb}/^{204}\text{Pb}$ and $^{208}\text{Pb}/^{204}\text{Pb}$ compositions were analysed by PIMMS using a Thermo Scientific Neptune instrument. Pb cuts, diluted in 0.5 ml of 3% HNO_3 , were analysed for their Pb concentrations before isotopic measurements, in order to calculate the appropriate amount of Tl spike to add to obtain a Pb/Tl ratio of ~ 12 . This minimizes the tail from ^{205}Tl onto ^{204}Pb and from ^{206}Pb onto ^{204}Tl . During isotopic measurements, the samples were introduced into the Neptune using an ESI PFA50 nebulizer and a Cinnabar cyclonic spray-chamber. The normal H skimmer cone was used. Sensitivity for Pb on the Neptune using such setup was around 100 V total Pb ppm^{-1} at an uptake rate of $90 \mu\text{m min}^{-1}$. Pb mass bias was corrected externally using the $^{205}\text{Tl}/^{203}\text{Tl}$ ratio of the spike and an exponential law. The $^{205}\text{Tl}/^{203}\text{Tl}$ used for correction was determined for each analytical session ($^{205}\text{Tl}/^{203}\text{Tl} = 2.3885$ for session 1 and 2.3882 for session 2) by minimizing the difference in offset between the session average Pb ratios and the Galer (1997) triple spike Pb isotope values. The Tl isotope ratio was calculated to yield the best fit to all the Pb isotope ratios of Galer (1997) simultaneously. During the analytical sessions, the NBS981 standard solution was analysed regularly ($n = 16$). The average ratios were: $^{206}\text{Pb}/^{204}\text{Pb} = 16.941 \pm 0.0024$ (2sd), $^{207}\text{Pb}/^{204}\text{Pb} = 15.497 \pm 0.0012$ (2sd), $^{208}\text{Pb}/^{204}\text{Pb} = 36.715 \pm 0.0039$ (2sd). The detail of all NBS981 solution data are presented in Table B3. A total procedural BHVO-1 was analysed. The $^{206}\text{Pb}/^{204}\text{Pb}$, $^{207}\text{Pb}/^{204}\text{Pb}$, $^{208}\text{Pb}/^{204}\text{Pb}$ ratios obtained were 18.687, 15.568 and 38.342, respectively which is in good agreement with the GEOREM accepted value ($^{206}\text{Pb}/^{204}\text{Pb} = 18.692 \pm 0.008$ (2sd); $^{207}\text{Pb}/^{204}\text{Pb} = 15.572 \pm 0.006$ (2 sd); $^{208}\text{Pb}/^{204}\text{Pb} = 38.355 \pm 0.022$ (2sd)).

F.3.6.4 Hf isotopes

DGC:

Twenty samples were analysed by PIMMS using the Thermo Scientific Neptune instrument. The measurements were made using the static-collection mode and mass bias was corrected using a $^{179}\text{Hf}/^{177}\text{Hf}$ ratio of 0.7325 and an exponential law. At Durham, 10 JMC475 solutions were analysed during the analytical session. The average $^{176}\text{Hf}/^{177}\text{Hf}$ was 0.282144 ± 0.000006 (2sd). The details of all JMC475 solution

compositions are presented in Table C1. $^{176}\text{Hf}/^{177}\text{Hf}$ ratios are reported relative to the JMC475 standard value of 0.282160 (Nowell et al., 1998). The $^{176}\text{Hf}/^{177}\text{Hf}$ ratios of the two international rock standards BIR-1 and BHVO-1 analysed were 0.283239 and 0.283105, respectively.

GAU:

The samples were analysed by PIMMS using a Nu plasma instrument at Macquarie. The measurements were made using the static-collection mode and mass bias was corrected using a $^{179}\text{Hf}/^{177}\text{Hf}$ ratio of 0.7325 and an exponential law. Four JMC475 solutions were analysed during the analytical session. The average was 0.282162 ± 0.000017 (2sd) which is in very good agreement with the accepted value (See Table C1 for the details of all JMC475 analyses). $^{176}\text{Hf}/^{177}\text{Hf}$ ratios were not reported to a literature value. The $^{176}\text{Hf}/^{177}\text{Hf}$ of a total procedural BHVO-1 was 0.2831074, which is in excellent agreement with Weiss et al. (2007) (0.283106 ± 12 ; 2sd) and with the BHVO-1 composition obtained in DGC which demonstrates the excellent inter-lab reproducibility.

F.4 Os isotopes

Os isotopic digestion, extraction and analysis were performed at the GAU. All reagents used were doubled distilled or ultra-pure grades. In addition, HNO_3 was sparged after distillation. All pipette tips used were leached in 1N 2TD HNO_3 and rinsed three times with MQ H_2O .

F.4.1 Sample preparation

Samples were very finely crushed following the protocol described in F.2.1

F.4.2 Beaker and Carius tube cleaning

Carius tube cleaning:

1. Fill a large glass beaker and the Carius tubes (CTs) with MQ H_2O .
2. Place on hot plate at 100°C for 3-4 h
3. Rinse the CTs with MQ H_2O
4. Fill the large glass beaker with MQ H_2O

5. Fill the CTs with 33% 2TD HNO₃ and leave on hot plate overnight at 100°C
6. Rinse the CTs with MQ H₂O
7. Dry Carius tubes horizontally in clean oven at 100°C
8. Check for white residues
9. Seal tubes with parafilm
10. Ready to load powders

Beaker cleaning:

1. Rinse with MQ H₂O
2. Wipe inside with kim wipes if any visible residue remain in the beaker
3. Put open beakers into large glass beaker with MQ H₂O overnight on hot plate at 110°C
4. Rinse with MQ H₂O (one by one)
5. Put open beakers into large glass beaker filled with 33% Analar® aquaregia.
6. Discard aquaregia and rinse with MQ H₂O (one by one)
7. Add 12N 2TD HCl in each beaker and leach overnight at 110°C
8. Empty and rinse with MQ H₂O
9. Add 16N 2TD HNO₃ in each beaker and leach overnight at 110°C
10. Empty and rinse with MQ H₂O
11. Add 16N 2TD HNO₃ in each beaker and leach overnight at 110°C
12. Empty and rinse with MQ H₂O
13. Add 16N 2TD HNO₃ in each beaker and leach overnight at 110°C
14. Empty and rinse with MQ H₂O
15. Place in the clean beaker Tupperware box.

F.4.3 Dissolution procedure

Calculation of mass of sample and spike:

The minimum mass of powder needed and the amount of Os spike to add in the CTs was estimated based on the predicted Os content of each sample. The estimates of Os content of the lavas were done based on the MgO and NiO concentrations of the lavas. For most lavas, ~ 5g of powder was processed. Rock powdered were introduced in the CTs using weighting paper (cone shape). CTs were sealed with parafilm. Os spike was weighted directly in 5 ml Teflon beakers.

Tube sealing:

1. Fill the liquid nitrogen tank
2. Fill a bucket with liquid nitrogen under the hood
3. Place CTs 1 by 1 in the liquid nitrogen and let them freeze for 15 min.
4. Inject 1 ml of 12N 2TD HCl in each CT
5. Add 4 ml of 12N 2TD HCl in each spike beaker.
6. Transfer the 12N 2TD HCl + spike incrementally: 4 times 1 ml
7. Inject 2 times 5 ml of 16N 2TD HNO₃ in each CT
8. Refill the liquid nitrogen
9. Turn Torch on (oxygen and acetylene torch), make sure the flame is blue.
10. Place the neck of the CTs in the flame at ~ 5 cm from the torch and keep turning the tube until the tube is fully sealed
11. Roll the CTs in aluminium foil and place them in metal capsules in oven.
12. Leave the CTs in the oven at 120°C for 1h and 3 days at 220°C

F.4.4 Os extraction and purification

Os was separated by solvent extraction following Cohen and Waters (1996)

Os extraction:

1. Turn the oven off the night before opening the tubes
2. Prepare: liquid nitrogen + CCl₄ + Teflon beaker + Teflon tape + 5 ml pipette
3. Open the metal capsules one by one carefully
4. Plate the CTs in liquid nitrogen
5. Cut most of each CT neck with glass cutter and finish by smashing the glass with a hammer
6. Close each CT with parafilm and place it in a beaker with cold water (to unfreeze)
7. Label a 30 ml Teflon beaker and place Teflon tape around its neck
8. Pour the sample solution in the Teflon beaker, avoiding residues
9. Add 5 ml of CCl₄. Close tight.
10. Place the beaker under the hood overnight: 3 layers will appear (top = aqua regia; middle = solid residue; bottom = CCl₄+Os)
11. Pipette the aqua regia (dark yellow layer) and the residue into waste
12. Add 10 ml of 15N suprapur® HBr in the CCl₄ + Os (light orange layer)

13. Leave under the hood overnight: 2 layers will appear (top: orange HBr + Os; bottom = brown CCl₄)
14. Pipette the HBr layer (containing Os) in clean 15 ml beaker avoiding any residue and CCl₄
15. Discard CCl₄ + residue in the CCl₄ waste
16. Place the HBr + Os layer on hot plate at 100°C and with heating lamps overnight

Microdistillation

1. Add 15 µl 15N suprapur® HBr in the tip of a conical beaker
2. Add 2 drops of CrO₃ + H₂SO₄ solution on the lid
3. Pipette 5µl of 15N suprapur® H₂SO₄ and add on dry sample.
4. Pick the sample and inject it in the Cr₂O₃+H₂SO₄ mix drop
5. Close the conical beaker carefully and wrap it in foil
6. Place sample on hot plate at 80°C for 1h to 1h15 min
7. Open beaker and wash lid with MQ H₂O
8. Dry both the lid and the beaker containing Os + HBr for ~2h at 80°C
9. Close the lid. The sample is ready to load

F.4.5 Measurement

Given the young age of the samples, no age correction on the $^{187}\text{Os}/^{188}\text{Os}$ ratio was necessary and Re was not analysed. Os was analysed by N-TIMS on a Thermo-Finnigan Triton mass spectrometer at Macquarie University in dynamic mode. All data were blank corrected using the total procedural blank (TPB) processed with the samples analysed. TPB was 6.30 pg Os with an $^{187}\text{Os}/^{188}\text{Os}$ ratio of 0.1821 ($n = 1$). This corresponds to corrections of 0-12% except for the two lavas with the lowest abundances where these corrections amounted to 21 and 25%. During the analytical session, instrument performance was monitored by the analysis of Os in-house solution standard JMC-2. $^{187}\text{Os}/^{188}\text{Os}$ for 5 ng loads in dynamic collection mode was 0.18311 ± 0.00016 (2sd; $n = 4$; see Table E1 for the details of all JMC-2 analysed) which is in good agreement with the long term running means of 5ng JMC-2 in dynamic mode of 0.18294 ± 0.00070 (2sd; $n = 17$ since 2006). The average $^{187}\text{Os}/^{188}\text{Os}$ ratio of the WPR-1 international rock standard was 0.1451 ± 0.0013 (2sd; $n = 4$) with

concentrations of $17.19 \text{ ppb} \pm 0.71$ (2sd; $n = 4$) which is in good agreement with the accepted values (Cohen and Waters, 1996; $^{187}\text{Os}/^{188}\text{Os} = 0.14543 \pm 0.00018$ (2 sd) and $\text{Os} = 16.06 \text{ ppb} \pm 0.8$ (2 sd)).

F.5. Single mineral $\delta^{18}\text{O}$

F.5.1 Sample preparation

Lavas and pumices from the SVC and Pre-SVC groups were lightly crushed using a fly-press at DGC. Rock fragments were sieved to keep only fractions $> 500 \text{ }\mu\text{m}$. Fragments were then sprayed with acetone to clear the crystals with rock fine particules (dust size). Plagioclase, quartz, pyroxene and amphibole were hand-picked with stainless twizzles under the binocular microscope and placed in a 1.5 ml precleaned polypropylene vial. In mafic lavas, additional crystals were separated by fragmentation of hand samples using the Selfrag instrument at the GAU (high voltage pulses of electricity), sprayed with ethanol and hand-picked under the microscope. Grains selected were between 0.9 and 3.7 mg and free of inclusion and glass adhering to the grains.

F.5.2 Laser-Fluorination

O was extracted using a laser-fluorination line at the Scottish Universities Environmental Research Centre (SUERC), following the method of Sharp (1990). All fluorinations resulted in 100% release of O_2 from mineral lattice. The detailed procedure is described below:

1. Load grains and standards in a circular stainless bloc with 12 holes (for 12 samples).
2. Place the holder in the chamber and vacuum air for at least 1h
2. Pre-fluorinate the sample: injection of ClF_3 (reagent) in the chamber before analysis to react any particles, other than the sample, with the reagent before analysis. Pre-fluorination time is different for each mineral. Quartz, pyroxene and amphibole pre-fluorination was $\sim 16\text{h}$ while plagioclase was only pre-fluorinated for $\sim 1/2\text{h}$ (since it is more reactive).
3. Release the ClF_3 of the pre-fluorination and refill the chamber with “clean” ClF_3 .
3. Laser the sample. The silicate sample will react with ClF_3 to liberate O_2
4. Convert O_2 in CO_2 using carbon rode

5. Collect gas in glass bottles

F.5.3 Measurement

The recovered samples were analyzed on a VG Optima mass spectrometer. Oxygen isotope ($\delta^{18}\text{O}$) values are reported as per mil (‰) deviations relative to Vienna Standard Mean Ocean Water (V-SMOW). Samples were analysed during two periods. During the first period (March 2012) 31 unknowns were analysed along with the international and in-house standards UWG2 and SES and GP147. The average $\delta^{18}\text{O}$ values obtained for UWG2 (garnet, $+5.7\text{‰} \pm 0.2$ (2sd), $n = 11$), SES (quartz, $+10.4\text{‰} \pm 0.6$ (2sd), $n = 10$) and GP147 (garnet, $+7.2\text{‰} \pm 0.4$ (2sd), $n = 3$) are in very good agreement with their accepted values of $+5.8\text{‰}$ (Valley et al., 1995), $+10.2\text{‰}$ and $+7.2\text{‰}$ (Mattey and Macpherson, 1996) respectively. The internal SES standard has been run many hundreds of time over the past 20 years in SUERC, and is well calibrated against UWG2, NBS 28 and NBS 30, as well as GP147. Twelve unknowns were analysed during the second period of study (November 2012) when the average $\delta^{18}\text{O}$ values for UWG2, SES and GP147 were $+5.9\text{‰} \pm 0.2$ (2 sd, $n = 2$), $+10.2\text{‰} \pm 0.3$ (2 sd, $n = 6$), $+7.15\text{‰} \pm 0.4$ (2 sd, $n = 2$) respectively. The details of all standard analyses are presented in Table B.5.

F.6 Single plagioclase $^{87}\text{Sr}/^{86}\text{Sr}$ and trace elements

Single mineral $^{87}\text{Sr}/^{86}\text{Sr}$ analyses were performed at DGC. During the chemistry, only Romil UPA grade acids were used.

F.6.1 Sample preparation

Plagioclase (20 grains) from the SVC lavas were hand-picked following the method described in section F.5.1 at DGC. All pipette tips were leached in 1N UPA HNO_3 and rinsed with MQ H_2O before use.

F.6.2 Beaker cleaning

1. Remove the label with ethanol on the Teflon beaker
2. Rinse out with MQ H_2O

3. Wipe inside with Micro-pure tissue if there is any visible residue in the beaker
4. Leach with 500 μ l of 6N UPA HCl overnight on hot plate (80°C)
5. Empty and rinse with MQ H₂O
5. Put closed Teflon beaker into large Teflon beaker with MQ H₂O overnight on hot-plate at 80°C
6. Empty and rinse with MQ H₂O
7. Put each open Teflon beaker in a large Teflon beaker with dilute HNO₃ (1N UPA HNO₃) overnight on hot plate at 80°C
8. Put each open beaker in a large Teflon beaker with MQ H₂O overnight on hot plate at 80°C
9. Rinse out with MQ H₂O and repeat step 8.
10. Rinse out with MQ H₂O
11. Leach with 6M UPA HCl overnight on the hot plate at 80°C
12. Empty and rinse with MQ H₂O
13. Leach with MQ H₂O overnight on the hot plate at 80°C
14. Empty and rinse with MQ H₂O
15. Leach with 6N UPA HCl overnight on the hot plate at 80°C
16. Empty and rinse with MQ H₂O
17. Leach with MQ overnight on the hot plate at 80°C
18. Empty and rinse with MQ H₂O
19. Put cap on and place in clean micro-Sr beaker box.

F.6.3 Sample digestion

1. Weigh the grain and place it in 5 ml Teflon beaker
2. Add 100 μ l of 16N UPA HNO₃ and 300 μ l of 29N UPA HF and place on the hot plate for 48 h at 100°C with cap on.
3. Take the cap off and dry down to paste (~3h) on the hot plate at 80°C
4. Add 100 μ l of 16N UPA HNO₃ and place on hot plate at 100°C with cap on for 15 min, then open the cap and dry
5. Add 100 μ l of 16N UPA HNO₃ and dry down directly at 100°C
6. Add 500 μ l of 3N UPA HNO₃ and put on hot plate for 1h at 100°C with cap on
7. Prepare another set of beakers for TE aliquots

8. Add rapidly 50µl of the sample solution (~10%) in the new Teflon beaker. Record the weight of the TE aliquot, and the new weight of the aliquot for isotopes chemistry
9. We now have two aliquots: (1) for column chemistry and (2) for trace element analysis

F.6.4 Column chemistry procedure

Columns were made of 1 ml blue pipette tips cut obliquely at the tip, with a white frit.

1. Place the waste under the column
2. Rinse the column with a full volume (1 CV) of MQ H₂O
3. Repeat step 1
4. Add 2 drops of resin
5. Rinse resin with 1CV or 6N UPA HCl
6. Rinse resin with 2 CV of MQ H₂O
7. Pre-condition resin with 2 times 100 µl of 3N HNO₃
8. Load sample solution
9. Collect to beaker and reload
10. Add 500 µl of 6N UPA HCl to the empty beaker and place on hot plate at 80°C with cap on
11. Elute 50 µl of 3N UPA HNO₃
12. Elute 100 µl of 3N UPA HNO₃
13. Elute 300 µl of 3N UPA HNO₃
14. Recover the beaker from hot plate and discard 6N UPA HCl
15. Place the Teflon beaker under the column
16. Elute 200 µl 2.5N MQ H₂O
17. Repeat step 16. **Sr is now collected.**
18. Wrap column in plastic glad wrap and discard
19. Dry the sample down at 80°C (~2h). The sample is now ready to be loaded.

F.6.5 $^{87}\text{Sr}/^{86}\text{Sr}$ analysis

Samples were loaded on Re filaments using a high Purity TaF5 activator. Purification of the TaF5 activator was done following the method described in Charlier et al. (2006). $^{87}\text{Sr}/^{86}\text{Sr}$ was measured by TIMS using the Thermo Fisher Triton using the static collection mode at DGC. Sr samples were run unspiked since the young age (< 20 Ma) and low Rb/Sr (0.44-0.02) of St Lucia lavas precluded the need of isotopic dilution to age correct the measured ratios. Rb was monitored and burned off the filament during slow heating prior to analysis. During the TIMS analyses, the average $^{87}\text{Sr}/^{86}\text{Sr}$ ratio for NBS987 obtained on 12ng of Sr was 0.710243 ± 0.000009 (2sd, n = 3). Within-run instrument mass fractionation was corrected using an exponential law and the normalising value of $^{88}\text{Sr}/^{86}\text{Sr} = 8.375209$ (equivalent to $^{86}\text{Sr}/^{88}\text{Sr} = 0.1194$). This is in excellent agreement with the value reported by Thirlwall (1991) of 0.710248 ± 0.000023 (2sd, n = 427). Two total procedural blanks contained 18 and 32 pg of Sr which represent 0.03 and 0.05% of the lowest sample Sr concentration analysed and are therefore negligible. The details of NBS987 solution analyses and of the blanks are presented in Table B.4.

F.6.6 Mineral trace element analysis

The trace element concentration of the plagioclase crystals was determined from the aliquot separated as described in section F.6.2.

Before analysis:

1. Dry down the aliquot
2. Calculate the minimum amount of 3.5% UPA HNO_3 to add to the sample before analysis: in our case 2.5 ml. The added volume of acid was calculated based on the following parameters: (1) the trace element concentrations in the sample solution must be higher than the detection limit (1) the volume of sample solution needs to be high enough to leave enough time to analyse all the elements requested, taking into account the uptake of ~1 ml/min. Trace element concentration of plagioclase was estimated using whole rock concentrations and partition coefficients from the literature.
3. Prepare international standards solutions (BHVO-1, W2 and AGV1) with similar concentrations to the samples.

Trace element concentrations were analysed using the Thermo scientific ICPMS Xseries 2 and calibrated using the international rock standards BHVO-1, AGV-1 and W2 and the same three standards diluted 10 times. Given the low level of concentrations, no international standard was introduced in the samples to avoid any contamination. Instrumental drift was reduced by running a short run, and monitored by analysing multiple times AGV-1 during the run, and all the standards at the beginning and the end of the run. However, even with these precautions, a drifting affected the data during the run. The compositions obtained were not presented in any of the chapters, and are shown in Table H.2. The composition of BHVO-1, AGV-1 and W2 (and the same standards diluted by 10) for the elements analysed are presented in Table H.1.

F.7 Imaging and in-situ major elements

Over 200 back-scattered electron images of thick sections of representative samples were collected using a Zeiss EVO MA15 scanning electron microscope at the GAU, with an accelerating voltage of 15 kV. Brightness and contrast were varied to accentuate the textures. A few images of the thick sections were also obtained by cathodo-luminescence with a fixed voltage of 15 kV and variable current. Imaging of zircon mounts was performed at University of California in Los Angeles (UCLA) using a LEO 1430 VP Scanning Electron Microscope (SEM) and similar analytical conditions.

Mineral major element analyses were done using a CAMECA SX100 electron microprobe either at the GAU or at the Australian National University (ANU) with an accelerating voltage of 15kV, a 20 nA beam current and a beam diameter of 1-2µm. Calibration at Macquarie was based on the following standards: orthoclase (K), wollastonite (Ca, Si), albite (Na), Hematite (Fe), Kyanite (Al), chromium (Cr), rutile (Ti), Olivine (Mg). At ANU, the following standards were used: albite (Na), K412 glass (Mg, Al, Fe), chromite (Cr), rhodonite (Mn), Sanidine (K), rutile (Ti), P on #375 glass.

Major element compositions of the lava groundmasses were determined using an energy dispersive spectrometer (X-max Oxford Instruments) attached to the Zeiss EVO scanning electron microscope at operating conditions of 20 kV and 8-10 nA, at

the GAU. The instrument (spectrum) was calibrated using a thin pure copper grid attached to each section analysed.

F.8 In-situ trace elements

In-situ trace element concentrations were determined on thick sections (100 μm) using a New Wave UP-213 laser ablation system linked to an Agilent 7700 Series ICP-MS system at the GAU. Ablation of the thick sections was performed in a helium chamber using a frequency of 5 Hz and an ablation size of 55 μm for single spots or a line of 120 μm long and 30 μm large when rastering was needed. Concentrations and detection limits were obtained using GLITTER software (<http://www.glitter-gemoc.com/>). The instrument was calibrated using the NIST610 glass standard and CaO (wt. %) obtained from the electron microprobe was used as an internal standard for each analysis. The BCR-2 standard was analysed at least at the beginning and the end of each analytical session. Results for BCR-2 are presented in Table E4. Differences between our measured BCR-2 concentrations in every batch and the Georem preferred values are less than 5% for all elements presented. Given the presence of melt inclusions in most crystals and in order to ensure data quality incompatible trace elements in the mineral analysed were carefully checked and all abnormal data (e.g. unreasonable enrichment in elements incompatible in plagioclase) were discarded. Furthermore, every LA-ICPMS analysis included major elements allowing comparison with the major element obtained by electron microprobe, and the calculation of the structural formula for every spot.

F.9 In-situ $\delta^{18}\text{O}$ in zircons

Oxygen isotope ratios in the SVC zircons were analysed using the CAMECA ims 1270 high-resolution ion microprobe at UCLA using multi-collection analysis as described in Trail et al. (2007). Zircons were mounted in indium metal and previously analysed using the same instrument for U-Th (Schmitt et al., 2010). Zircon mounts were polished, to remove any $^{16}\text{O}^-$ from the U-Th analysis, using 1200 silicon carbide paper mats, 1 μm polycrystalline diamond suspension water base spray and de-ionised water. Mounts were cleaned in ultrasonic bath with methanol for 3s and were gold coated. Oxygen isotope ($\delta^{18}\text{O}$) values are reported in the standard per mil (‰) notation relative

to the Vienna Standard Mean Ocean Water (V-SMOW). Standard AS3 ($\delta^{18}\text{O}_{\text{VSMOW}} = 5.34\text{‰}$; Trail et al., 2007) was analysed several times ($n = 80$) at the beginning, during and at the end of each analytical sessions to determine instrumental mass fractionation. The accuracy of the measurements was confirmed by replicate analysis of the in house zircon standard 91500 ($\delta^{18}\text{O} = 9.78 \pm 0.37$ (2 sd; $n = 10$; see Table D.3 for the details of all 91500 data).

F.10 In-situ $^{87}\text{Sr}/^{86}\text{Sr}$ in plagioclase

In-situ analysis of $^{87}\text{Sr}/^{86}\text{Sr}$ in plagioclase were performed at the GAU following the method of Charlier (2006). They were performed by microdrilling thick sections (100 μm) following imaging (SEM) major (electron microprobe) and trace element (LA-ICPMS) analyses on the crystals.

F.10.1 Beaker cleaning

1. Remove labels with ethanol
2. Rinse out with MQ H_2O
3. Wipe inside with kim-wipes any visible residue in beaker
4. Wash cap and beaker with 6N TD HCl
5. Rinse out cap and beaker with MQ H_2O
6. Put open beaker in large Teflon beaker with dilute SeastarTM HNO_3 overnight on hot plate at 80°C
7. Put open beakers in large Teflon beaker with MQ H_2O overnight on hot plate at 80°C
8. Empty and rinse out with MQ H_2O
9. Leach with 500 μl of 16N SeastarTM HF overnight at 80°C
10. Empty and rinse out with MQ H_2O
11. Leach with 500 μl of 16N SeastarTM HNO_3 overnight at 80°C
12. Empty and rinse out with MQ H_2O
13. Leach with 500 μl of 6N SeastarTM HCl overnight at 80°C
14. Empty and rinse with MQ H_2O
15. Repeat steps 13 and 14
16. Leach with 1ml of MQ H_2O overnight at 80°C

16. Empty and rinse with MQ
17. Leach with 6N SeastarTM HCl overnight at 80°C
18. Empty and rinse with MQ H₂O
19. Leach with MQ H₂O overnight at 80°C
20. Empty and rinse with MQ H₂O
21. Place in clean beaker Tupperware

F.10.2 Resin cleaning

Sr-spec resin (Eichrom) was purified before use:

1. Add 2 ml of resin powder in a BioradTM glass column with a 225 ml reservoir attached.
2. Elute 225 ml of MQ H₂O twice
3. Elute 40 ml of 6N SeastarTM HCl
4. Elute 225 ml of MQ H₂O twice
5. Elute 225 ml of 0.1 M Suprapur[®] H₂SO₄ twice
6. Elute 225 ml of 0.05N seastar[®] HNO₃ twice
7. Repeat 4 times steps 1-6.

F.10.3 Making the high purity TaF₅ activator

Activator was prepared following the method of Charlier et al. (2006):

1. Weight 250 mg of Ta₂O₅ powder
2. Dissolve in 10 ml of 29N SeastarTM HF at 80°C for 7 days
3. Dry down
4. Add 1 ml of 29N SeastarTM HF
5. Transfer in pre-cleaned centrifuge tube with 1N SeastarTM HCl and MQ H₂O
6. Leach Teflon beaker with 2 ml of 6N SeastarTM HCl at 100°C for 1h
7. Add 6 ml of MQ H₂O in centrifuge tube
8. Add drops of ordinary grade ammonia solution drop by drop
9. White crystals of Ta(OH)₅ will precipitate from the solution
10. Add ammonia solution until no more precipitation occurs
11. Centrifuge at 5000 rpm for 10 min and discard supernatant
12. Add 6 ml of MQ H₂O and repeat step 10

13. Repeat step 11
14. Recover the Teflon beaker from the hot plate, discard acid and rinse with MQ H₂O
15. Add MQ H₂O in the centrifuge tube and transfer the content back in the Teflon beaker
16. Dry down
17. Repeat steps 4-16
18. Add 370 µl 29N SeastarTM HF + 270 µl conc. Suprapur[®] H₃PO₄ + 2125 µl 3N SeastarTM HNO₃ + 16.55 ml MQ H₂O.
19. Equilibrate on hot plate at 80°C for 1h.

F.10.4 Microdrilling

Microdrilling was performed following the guide written by Victoria Martin at Durham. It was performed on 100 µm thick sections at Macquarie University using a Merchantek[®] micromill.

1. Leach pipette tips with end cut at 45°C in 1N SeastarTM HCl for 3 days on the hot plate at 60°C
2. Pre-clean 2 large polypropylene centrifuge tube with MQ H₂O
3. Rinse tubes and pipette tips with MQ H₂O
4. Place the thick section in one of the centrifuge tube filled with MQ H₂O in an ultrasonic bath for 1-2 min
5. Place the drill bits in the second centrifuge tube filled with Ethanol
6. Remove the thin section with plastic tweezers pre-cleaned in MQ H₂O
7. Let the section dry and stick it on the drill stage using double sided tape and a scalpel
8. Place a Parafilm[®] ring (~2.5 mm diameter hole) around the zone to be microdrilled. Parafilm[®] rings were previously leached in MQ H₂O and heated under a red lamp to make it become “sticky” before placing it on the section. Make sure there is no bubbles between the ring and the section
9. Rinse the drill bit with MQ H₂O and load it on the drill
10. Calibrate the surface in the software (z axis)
11. Calibrate the x-y axis by drilling a glass spot on the edge of the thin section
12. Spray the drill bit with ethanol

13. Select the zone to be microdrilled and calibrate the drill with the following parameters: 1 Passing; 50 μm spacing; 55 μm depth; 85% drill speed; Dwell time 5 seconds; 750 $\mu\text{m/s}$ drill plunge speed; Enable drilling during scan.
14. Go in Drill mode and place a drop on MQ H_2O on the drill bit (in the Parafilm[®] ring)
15. Start drilling
16. Label a clean Teflon beaker
17. When drilling is finished, pipette in and out in the slurry to keep the particles in suspension in the drop.
18. Pipette the sample in the beaker. Add a new drop of MQ H_2O on the sample and transfer it to the beaker. Repeat until no sample particles are left on the section.
19. Clean the drill bit and the thick section using steps 1-5 before micro-drilling a new zone

F.10.5 Digestion

Digestion method is similar to Charlier et al. (2006).

1. Dry down the slurry at 80°C
 2. Add 300 μl of 29N Seastar[™] HF and 100 μl 16N seastar[™] HNO_3 for 48h at 100°C
 3. Dry to paste at 110°C (~ 1h)
 4. Add 100 μl 16N Seastar[™] HNO_3 . Put the cap on for 15 min at 80°C and then take the cap off and dry (~ 30 min) at 100°C
 5. Add 100 μl 16N seastar[™] HNO_3 and dry directly at 110°C
 5. Add 180 μl of 3N seastar HNO_3 , close cap, put on the hot plate for 1h at 80°C:
- The sample is ready for column work.

F.10.6 Column work

Column work was performed as described in section F.6.4 for the bulk plagioclase analysis at Durham.

F.10.7 Analysis

Samples were loaded using 16N Seastar™ HNO₃ and high purity TaF₅ activator on Re filaments. They were analysed at the GAU using a Finnigan Triton TIMS instrument in static collection mode. Correction for within-run mass fractionation was done using an exponential law and the normalising value of $^{86}\text{Sr}/^{88}\text{Sr} = 0.1194$. Sr samples were run unspiked since the young age (< 20 Ma) and low Rb/Sr (0.44-0.02) of St Lucia lavas precluded the need of isotopic dilution to age correct the measured ratios. Rb was monitored and burnt off the filament during slow heating prior to analysis. During the analytical session instrument performance was monitored by analyses of Sr standard NBS987. The average $^{87}\text{Sr}/^{86}\text{Sr}$ ratio for NBS987 obtained on 8 ng Sr was 0.710237 ± 0.000021 (2sd; n = 8). This is in very good agreement with the value reported by Thirlwall (1991) of 0.710248 ± 0.000023 (2sd, n = 427). During the course of this study, analyses of microdrilled international glass standards NIST611 and BCR-2G (~ 20 ng Sr loads) were carried out and the average $^{87}\text{Sr}/^{86}\text{Sr}$ was 0.70965 ± 0.000037 (2sd; n = 4) and 0.705026 ± 0.000030 (2sd; n = 4) respectively. BCR-2G values are identical to values determined for big loads of Sr (>100 ng Sr) by Mahoney et al. (2003) of 0.705024 ± 0.000010 (2sd). Three total procedure blanks contained 22, 33 and 7 pg of Sr which represent 0.22, 0.33 and 0.07 % of the smallest Sr sample analysed (10 ng) and are therefore negligible. The details of all the standards and blanks analysed are presented in Table E1.

Appendix G

All mineral major element data

Content

Table G.1. Plagioclase major element compositions obtained by electron microprobe	361
Table G.2. Clinopyroxene major element compositions obtained by electron microprobe	394
Table G.3. Orthopyroxene major element compositions obtained by electron microprobe	396
Table G.4. Amphibole major element compositions obtained by electron microprobe	401
Table G.5. Biotite major element compositions obtained by electron microprobe	404
Table G.6. Ilmenite major element compositions obtained by electron microprobe	405

Table G.1. Plagioclase major element compositions obtained by electron microprobe.

Group:	Pre-SVC1 B		Pre-SVC1 B			Pre-SVC1 B				
Sample:	SL-83-44		SL-83-44			SL-83-44				
Name:	C1-PI3	C1-PI2A	Profile P1			Profile P3				
Grain:	G	G	G			P with incl. poor C				
Position:	C	C	C	C	R	C	C	C	C	M
Dist.:	0	29	57	0	27	54	81	134	161	
SiO ₂	49.03	48.97	44.23	44.58	56.21	44.60	43.99	44.05	44.11	48.56
Al ₂ O ₃	31.28	31.07	34.89	34.79	24.85	35.18	35.24	35.31	34.96	31.49
MgO	0.20	0.18	0.12	0.11	0.45	0.08	0.08	0.07	0.06	0.27
CaO	14.51	14.82	18.33	18.26	10.19	18.74	18.72	18.81	18.61	15.18
FeO	0.89	0.75	0.55	0.51	1.75	0.48	0.45	0.51	0.50	0.82
Na ₂ O	3.33	3.24	1.17	1.20	4.47	1.02	1.01	0.96	1.03	2.79
K ₂ O	0.08	0.07	b.d.l.	b.d.l.	0.58	b.d.l.	b.d.l.	b.d.l.	b.d.l.	0.09
P ₂ O ₅	0.10	b.d.l.	0.25	0.24	0.16	0.39	0.30	0.27	0.21	0.37
Total	99.50	99.20	99.58	99.73	98.93	100.54	99.85	100.01	99.53	99.61
Si	9.04	9.06	8.22	8.27	10.29	8.21	8.16	8.16	8.21	8.94
Al	6.80	6.78	7.65	7.61	5.36	7.63	7.70	7.71	7.67	6.84
Mg	0.05	0.05	0.03	0.03	0.12	0.02	0.02	0.02	0.02	0.07
Ca	2.87	2.94	3.65	3.63	2.00	3.70	3.72	3.73	3.71	2.99
Fe (ii)	0.14	0.12	0.09	0.08	0.27	0.07	0.07	0.08	0.08	0.13
Na	1.19	1.16	0.42	0.43	1.59	0.36	0.36	0.34	0.37	1.00
K	0.02	0.02	0.01	0.00	0.14	0.00	0.00	0.00	0.00	0.02
P	0.02	0.00	0.04	0.04	0.02	0.06	0.05	0.04	0.03	0.06
Total	20.13	20.13	20.11	20.09	19.82	20.06	20.10	20.09	20.09	20.06
An	70.37	71.40	89.55	89.24	53.72	90.98	91.07	91.46	90.83	74.65
Ab	29.19	28.21	10.32	10.64	42.63	8.92	8.86	8.44	9.08	24.83
Or	0.44	0.40	0.13	0.12	3.66	0.10	0.07	0.09	0.09	0.52

Group:	Pre-SVC1 B									
Sample:	SL-83-44									
Name:	Profile P3									
Grain:	P with incl. poor core									
Position:	M	M	M	M	M	M	M	M	M	R
Dist.:	215	241	268	295	322	349	376	402	429	483
SiO ₂	45.80	44.44	44.47	44.48	44.33	45.04	44.99	44.40	43.94	46.24
Al ₂ O ₃	33.37	34.46	34.86	34.66	34.63	34.75	33.88	34.72	35.01	33.42
MgO	0.19	0.10	0.06	0.05	0.11	0.09	0.10	0.08	0.10	0.15
CaO	17.04	18.29	18.36	18.38	18.22	18.21	17.65	18.63	18.41	17.13
FeO	0.66	0.52	0.58	0.46	0.53	0.52	0.60	0.55	0.58	0.61
Na ₂ O	1.93	1.36	1.20	1.17	1.24	1.29	1.61	1.06	1.12	1.88
K ₂ O	0.04	b.d.l.	b.d.l.	b.d.l.	b.d.l.	b.d.l.	b.d.l.	b.d.l.	b.d.l.	0.05
P ₂ O ₅	0.29	0.46	0.15	0.21	0.39	0.08	0.36	0.19	0.06	0.14
Total	99.38	99.68	99.73	99.49	99.46	100.02	99.25	99.62	99.23	99.66
Si	8.51	8.25	8.26	8.27	8.25	8.33	8.38	8.25	8.21	8.56
Al	7.31	7.54	7.63	7.60	7.59	7.57	7.44	7.61	7.70	7.29
Mg	0.05	0.03	0.02	0.01	0.03	0.02	0.03	0.02	0.03	0.04
Ca	3.39	3.64	3.65	3.66	3.63	3.61	3.52	3.71	3.68	3.40
Fe (ii)	0.10	0.08	0.09	0.07	0.08	0.08	0.09	0.09	0.09	0.10
Na	0.69	0.49	0.43	0.42	0.45	0.46	0.58	0.38	0.41	0.67
K	0.01	0.01	0.00	0.01	0.00	0.01	0.01	0.00	0.00	0.01
P	0.05	0.07	0.02	0.03	0.06	0.01	0.06	0.03	0.01	0.02
Total	20.12	20.11	20.11	20.09	20.09	20.10	20.11	20.09	20.13	20.10
An	82.85	88.01	89.29	89.50	88.95	88.54	85.68	90.60	89.96	83.19
Ab	16.94	11.84	10.59	10.34	10.94	11.32	14.16	9.36	9.92	16.52
Or	0.21	0.14	0.12	0.15	0.11	0.14	0.16	0.04	0.11	0.29

Group:	Pre-SVC1 B		Pre-SVC1 B							
Sample:	SL-83-44		SL-83-44							
Name:	Profile P3		Profile P4							
Grain:	P with incl. poor C		P with incl. rich C							
Position:	R	R	C	C	C	C	C	C	C	C
Dist.:	510	536	0	28	55	83	111	138	166	194
SiO ₂	47.99	51.73	45.97	45.15	44.80	44.78	44.02	46.73	45.13	44.69
Al ₂ O ₃	32.35	28.73	33.95	33.98	34.24	34.66	35.05	33.14	34.17	34.81
MgO	0.19	0.22	0.11	0.10	0.14	0.09	0.07	0.12	0.07	0.11
CaO	15.80	12.46	17.57	17.81	17.96	18.29	18.66	16.80	17.93	18.11
FeO	0.77	1.34	0.56	0.56	0.55	0.49	0.53	0.57	0.56	0.58
Na ₂ O	2.71	4.36	1.71	1.46	1.49	1.21	1.03	2.11	1.44	1.31
K ₂ O	0.05	0.16	0.03	b.d.l.	b.d.l.	b.d.l.	b.d.l.	0.04	0.03	b.d.l.
P ₂ O ₅	0.26	0.22	0.42	b.d.l.	0.37	0.14	0.18	0.25	0.31	0.11
Total	100.16	99.31	100.32	98.99	99.61	99.69	99.60	99.80	99.65	99.76
Si	8.81	9.52	8.45	8.43	8.32	8.31	8.19	8.63	8.37	8.29
Al	7.00	6.23	7.36	7.48	7.49	7.58	7.69	7.21	7.47	7.61
Mg	0.05	0.06	0.03	0.03	0.04	0.03	0.02	0.03	0.02	0.03
Ca	3.11	2.45	3.46	3.56	3.57	3.64	3.72	3.32	3.56	3.60
Fe (ii)	0.12	0.21	0.09	0.09	0.09	0.08	0.08	0.09	0.09	0.09
Na	0.96	1.55	0.61	0.53	0.54	0.44	0.37	0.75	0.52	0.47
K	0.01	0.04	0.01	0.00	0.00	0.00	0.01	0.01	0.01	0.01
P	0.04	0.03	0.07	b.d.l.	0.06	0.02	0.03	0.04	0.05	0.02
Total	20.11	20.10	20.08	20.11	20.11	20.09	20.11	20.09	20.08	20.12
An	76.08	60.67	84.88	86.99	86.88	89.20	90.79	81.30	87.17	88.33
Ab	23.61	38.40	14.94	12.89	13.03	10.71	9.09	18.46	12.68	11.54
Or	0.31	0.93	0.18	0.12	0.08	0.09	0.13	0.24	0.15	0.13

Group: B = basalt; BA = basaltic andesite; A = andesite; D = dacite; R = rhyolite; Opx/Cgt-SVC 2, 3 = orthopyroxene/cummingtonite-bearing SVC 2; 3 lavas; **Grain:** P = phenocryst; MC = microphenocryst; G = groundmass; C = core; INC = inclusion (mineral included within is stated in parentheses); **Position:** C = core; M = mantle; R = rim, osci. = oscillatory; **Other:** UNZ = unzoned; Dist. = distance from the core (µm); An = anorthite; Ab = albite; Or = orthoclase.

Table G.1. (continued).

Group: Sample: Name: Grain:	Pre-SVC1 B SL-83-44 Profile P4 P with incl. rich C		Pre-SVC1 B SL-83-44 Profile P5 P with incl. free C								
Dist.:	R 249	C 0	C 27	C 54	C 81	C 108	C 135	C 162	C 188	C 215	C 242
SiO ₂	49.61	44.72	44.89	44.94	44.88	44.56	44.66	44.73	44.42	44.34	44.87
Al ₂ O ₃	30.69	35.44	34.99	35.22	35.37	35.13	35.32	35.55	35.51	35.04	35.57
MgO	0.11	0.07	0.06	0.09	0.09	0.07	0.11	0.07	0.07	0.08	0.09
CaO	14.39	18.91	18.91	18.43	18.51	18.78	18.69	18.64	18.88	18.69	18.75
FeO	0.82	0.50	0.49	0.49	0.47	0.50	0.45	0.49	0.44	0.45	0.50
Na ₂ O	3.37	0.89	0.94	1.12	1.06	0.96	1.01	0.99	0.97	1.06	1.08
K ₂ O	0.10	b.d.l.	b.d.l.	b.d.l.	b.d.l.	b.d.l.	b.d.l.	b.d.l.	b.d.l.	b.d.l.	b.d.l.
P ₂ O ₅	0.32	0.55	0.28	0.33	0.44	0.16	0.27	0.32	0.50	0.65	0.54
Total	99.48	101.07	100.56	100.68	100.85	100.18	100.56	100.80	100.81	100.36	101.42
Si	9.13	8.18	8.26	8.25	8.22	8.24	8.22	8.21	8.15	8.17	8.18
Al	6.66	7.64	7.59	7.62	7.64	7.65	7.66	7.69	7.68	7.61	7.64
Mg	0.03	0.02	0.02	0.02	0.02	0.02	0.03	0.02	0.02	0.02	0.02
Ca	2.84	3.71	3.73	3.63	3.63	3.72	3.68	3.66	3.71	3.69	3.66
Fe (ii)	0.13	0.08	0.08	0.08	0.07	0.08	0.07	0.07	0.07	0.07	0.08
Na	1.20	0.32	0.34	0.40	0.38	0.34	0.36	0.35	0.34	0.38	0.38
K	0.02	0.00	0.01	0.00	0.00	0.01	0.00	0.00	0.00	0.00	0.00
P	0.05	0.09	0.04	0.05	0.07	0.02	0.04	0.05	0.08	0.10	0.08
Total	20.07	20.03	20.05	20.06	20.04	20.07	20.07	20.05	20.06	20.06	20.06
An	69.82	92.07	91.59	90.00	90.53	91.45	90.98	91.14	91.43	90.63	90.47
Ab	29.60	7.87	8.27	9.89	9.37	8.42	8.91	8.75	8.47	9.30	9.44
Or	0.59	0.05	0.14	0.11	0.10	0.13	0.10	0.11	0.10	0.07	0.09

Group: Sample: Name: Grain:	Pre-SVC1 B SL-83-44 Profile P5 P with incl. free C										Pre-SVC1 B SL-83-44 Profile P6 P with incl. free C
Dist.:	C 269	M 296	M 323	M 350	M 377	M 404	M 431	M 458	M 485	M 512	C 0
SiO ₂	44.64	45.69	45.38	46.11	45.17	45.34	45.63	45.29	44.66	47.26	44.28
Al ₂ O ₃	35.27	34.36	34.83	34.31	34.90	34.70	34.60	34.90	34.97	33.49	35.60
MgO	0.12	0.10	0.09	0.13	0.06	0.09	0.08	0.11	0.07	0.15	0.09
CaO	18.60	18.17	18.26	17.71	18.65	18.43	18.29	18.61	18.54	16.92	18.91
FeO	0.47	0.51	0.59	0.48	0.55	0.48	0.51	0.51	0.47	0.50	0.50
Na ₂ O	1.05	1.35	1.28	1.58	1.10	1.18	1.24	1.10	1.20	2.04	0.84
K ₂ O	b.d.l.	b.d.l.	b.d.l.	b.d.l.	b.d.l.	b.d.l.	b.d.l.	b.d.l.	b.d.l.	b.d.l.	b.d.l.
P ₂ O ₅	0.23	0.42	0.43	0.41	0.20	0.11	b.d.l.	0.08	0.26	0.23	0.43
Total	100.43	100.64	100.88	100.78	100.62	100.38	100.35	100.63	100.22	100.66	100.70
Si	8.22	8.38	8.31	8.44	8.31	8.35	8.40	8.33	8.25	8.64	8.14
Al	7.66	7.43	7.52	7.40	7.56	7.53	7.51	7.56	7.61	7.22	7.71
Mg	0.03	0.03	0.02	0.03	0.02	0.03	0.02	0.03	0.02	0.04	0.03
Ca	3.67	3.57	3.58	3.47	3.67	3.64	3.61	3.66	3.67	3.32	3.72
Fe (ii)	0.07	0.08	0.09	0.07	0.09	0.07	0.08	0.08	0.07	0.08	0.08
Na	0.38	0.48	0.45	0.56	0.39	0.42	0.44	0.39	0.43	0.72	0.30
K	0.00	0.01	0.00	0.01	0.00	0.00	0.00	0.00	0.00	0.01	0.00
P	0.04	0.07	0.07	0.06	0.03	0.02	0.00	0.01	0.04	0.04	0.07
Total	20.08	20.04	20.06	20.05	20.07	20.07	20.06	20.07	20.10	20.06	20.05
An	90.64	88.05	88.64	85.97	90.24	89.51	89.00	90.24	89.44	81.91	92.51
Ab	9.27	11.80	11.25	13.88	9.64	10.41	10.91	9.65	10.45	17.89	7.42
Or	0.08	0.15	0.11	0.15	0.12	0.09	0.10	0.11	0.11	0.19	0.07

Group: Sample: Name: Grain:	Pre-SVC1 B SL-83-44 Profile P6 P with incl. free C										
Dist.:	C 26	C 52	C 78	C 104	C 129	C 155	C 181	C 207	M 233	M 259	M 285
SiO ₂	44.56	44.54	45.24	44.72	44.88	44.84	44.86	44.17	44.75	44.90	45.01
Al ₂ O ₃	35.44	35.54	34.87	35.16	35.27	35.44	35.23	35.40	35.31	34.95	34.90
MgO	0.08	0.04	0.15	0.10	0.08	0.05	0.07	0.10	0.08	0.48	0.44
CaO	18.75	18.91	18.55	18.78	18.71	18.78	18.75	18.90	18.83	18.56	18.51
FeO	0.49	0.45	0.60	0.47	0.52	0.52	0.51	0.49	0.48	0.69	0.61
Na ₂ O	0.89	0.89	1.00	0.98	0.94	0.98	0.96	0.86	0.89	0.89	0.95
K ₂ O	b.d.l.	b.d.l.	0.05	b.d.l.	b.d.l.	b.d.l.	b.d.l.	b.d.l.	b.d.l.	b.d.l.	b.d.l.
P ₂ O ₅	0.15	0.03	0.49	0.40	0.26	0.33	0.13	0.04	0.31	0.33	0.23
Total	100.42	100.46	100.95	100.63	100.70	100.96	100.57	100.00	100.67	100.83	100.72
Si	8.21	8.21	8.28	8.22	8.24	8.22	8.25	8.18	8.22	8.24	8.27
Al	7.70	7.72	7.52	7.62	7.63	7.65	7.64	7.73	7.65	7.56	7.56
Mg	0.02	0.01	0.04	0.03	0.02	0.01	0.02	0.03	0.02	0.13	0.12
Ca	3.70	3.73	3.64	3.70	3.68	3.69	3.70	3.75	3.71	3.65	3.64
Fe (ii)	0.07	0.07	0.09	0.07	0.08	0.08	0.08	0.08	0.07	0.11	0.09
Na	0.32	0.32	0.35	0.35	0.33	0.35	0.34	0.31	0.32	0.32	0.34
K	0.01	0.00	0.01	0.00	0.00	0.00	0.00	0.00	0.00	0.01	0.01
P	0.02	0.00	0.08	0.06	0.04	0.05	0.02	0.01	0.05	0.05	0.04
Total	20.06	20.08	20.02	20.05	20.04	20.05	20.06	20.09	20.04	20.06	20.07
An	91.97	92.08	90.88	91.24	91.60	91.35	91.42	92.30	92.07	91.88	91.31
Ab	7.90	7.85	8.84	8.66	8.33	8.59	8.47	7.62	7.88	7.97	8.49
Or	0.13	0.08	0.28	0.10	0.07	0.06	0.11	0.08	0.05	0.15	0.19

Group: B = basalt; BA = basaltic andesite; A = andesite; D = dacite; R = rhyolite; Opx/Cgt-SVC 2, 3 = orthopyroxene/cummingtonite-bearing SVC 2; 3 lavas; **Grain:** P = phenocryst; MC = microphenocryst; G = groundmass; C = core; INC = inclusion (mineral included within is stated in parentheses); **Position:** C = core; M = mantle; R = rim, osci. = oscillatory; **Other:** UNZ = unzoned; Dist. = distance from the core (μm); An = anorthite; Ab = albite; Or = orthoclase.

Table G.1. (continued).

Group:	Pre-SVC1 B										
Sample:	SL-83-44										
Name:	Profile P6										
Grain:	P with incl. free C										
Position:	M	M	M	M	M	M	M	M	M	M	M
Dist.:	311	337	362	388	414	440	466	492	518	544	570
SiO ₂	44.68	44.51	44.54	44.60	44.87	46.16	45.69	45.56	45.67	45.09	44.90
Al ₂ O ₃	35.39	35.27	35.32	35.47	35.22	34.73	34.64	34.52	34.85	35.19	35.19
MgO	0.08	0.08	0.05	0.06	0.08	0.12	0.11	0.11	0.12	0.09	0.05
CaO	18.87	18.74	19.01	18.89	18.69	17.93	18.09	17.87	18.08	18.39	18.85
FeO	0.43	0.51	0.53	0.48	0.48	0.51	0.54	0.52	0.50	0.49	0.45
Na ₂ O	0.94	0.96	0.92	0.90	0.95	1.37	1.36	1.44	1.29	1.18	0.95
K ₂ O	b.d.l.	b.d.l.	b.d.l.	b.d.l.	b.d.l.	b.d.l.	b.d.l.	b.d.l.	b.d.l.	b.d.l.	b.d.l.
P ₂ O ₅	0.44	0.24	0.48	0.11	0.17	0.08	0.35	0.48	0.24	0.42	0.43
Total	100.86	100.35	100.86	100.54	100.48	100.96	100.82	100.54	100.78	100.87	100.84
Si	8.19	8.21	8.18	8.21	8.26	8.44	8.37	8.36	8.37	8.26	8.23
Al	7.65	7.67	7.64	7.70	7.64	7.48	7.48	7.47	7.52	7.60	7.61
Mg	0.02	0.02	0.01	0.02	0.02	0.03	0.03	0.03	0.03	0.02	0.01
Ca	3.71	3.70	3.74	3.73	3.69	3.51	3.55	3.51	3.55	3.61	3.70
Fe (ii)	0.07	0.08	0.08	0.07	0.07	0.08	0.08	0.08	0.08	0.08	0.07
Na	0.33	0.34	0.33	0.32	0.34	0.48	0.48	0.51	0.46	0.42	0.34
K	0.00	0.00	0.00	0.00	0.00	0.01	0.01	0.00	0.00	0.00	0.00
P	0.07	0.04	0.07	0.02	0.03	0.01	0.05	0.07	0.04	0.06	0.07
Total	20.05	20.07	20.05	20.07	20.05	20.05	20.05	20.05	20.05	20.05	20.03
An	91.69	91.39	91.92	92.02	91.51	87.70	87.90	87.17	88.49	89.52	91.54
Ab	8.27	8.50	8.02	7.90	8.40	12.11	11.95	12.72	11.39	10.40	8.37
Or	0.05	0.11	0.05	0.08	0.08	0.19	0.16	0.11	0.12	0.09	0.09

Group:	Pre-SVC1 B										
Sample:	SL-83-44										
Name:	Profile P6										
Grain:	P with incl. free C										
Position:	M	M	M	M	M	M	M	M	M	M	M
Dist.:	595	621	647	673	699	725	751	777	803	828	854
SiO ₂	44.55	44.50	44.82	44.74	44.57	45.63	45.97	46.20	46.65	46.08	45.25
Al ₂ O ₃	35.34	35.53	35.06	35.42	35.50	34.36	34.26	34.30	34.08	34.36	34.66
MgO	0.07	0.09	0.07	0.07	0.03	0.11	0.12	0.11	0.07	0.10	0.07
CaO	18.82	18.79	18.71	18.97	18.95	17.97	17.58	17.67	17.60	17.82	18.55
FeO	0.44	0.46	0.49	0.45	0.50	0.55	0.55	0.45	0.49	0.55	0.48
Na ₂ O	0.92	0.89	0.93	0.91	0.91	1.40	1.60	1.61	1.65	1.48	1.10
K ₂ O	b.d.l.	b.d.l.	b.d.l.	b.d.l.	b.d.l.	b.d.l.	b.d.l.	b.d.l.	b.d.l.	b.d.l.	0.05
P ₂ O ₅	0.20	0.30	0.29	0.33	0.41	0.36	0.45	0.31	0.49	0.16	0.26
Total	100.37	100.60	100.39	100.90	100.89	100.40	100.61	100.70	101.09	100.58	100.42
Si	8.21	8.18	8.26	8.21	8.18	8.39	8.43	8.46	8.50	8.45	8.33
Al	7.68	7.70	7.61	7.65	7.68	7.45	7.40	7.40	7.32	7.43	7.52
Mg	0.02	0.03	0.02	0.02	0.01	0.03	0.03	0.03	0.02	0.03	0.02
Ca	3.72	3.70	3.69	3.73	3.73	3.54	3.45	3.47	3.44	3.50	3.66
Fe (ii)	0.07	0.07	0.08	0.07	0.08	0.09	0.08	0.07	0.08	0.08	0.07
Na	0.33	0.32	0.33	0.32	0.32	0.50	0.57	0.57	0.58	0.53	0.39
K	0.00	0.00	0.00	0.00	0.00	0.01	0.01	0.01	0.01	0.00	0.01
P	0.03	0.05	0.04	0.05	0.06	0.06	0.07	0.05	0.08	0.03	0.04
Total	20.06	20.05	20.04	20.05	20.05	20.05	20.05	20.05	20.02	20.06	20.05
An	91.82	92.10	91.67	91.93	91.95	87.53	85.68	85.75	85.37	86.82	90.05
Ab	8.12	7.87	8.22	7.99	7.96	12.32	14.12	14.11	14.46	13.08	9.68
Or	0.06	0.04	0.11	0.08	0.09	0.15	0.20	0.14	0.17	0.09	0.27

Group:	Pre-SVC1 B			SL-83-25 BA							
Sample:	SL-83-44			Pre-SVC1							
Name:	Profile P6			Profile C1-P11							
Grain:	P with incl. free C			P							
Position:	M	M	R	C	C	C	C	M	M	M	M
Dist.:	880	906	932	0	25	51	76	101	152	177	203
SiO ₂	45.74	44.81	48.51	48.73	47.53	47.76	46.85	46.96	47.38	47.50	47.82
Al ₂ O ₃	34.31	34.93	31.38	31.41	32.30	32.11	32.56	32.64	32.30	32.27	31.72
MgO	0.10	0.05	0.81	0.10	0.10	0.11	0.08	0.10	0.09	0.10	0.13
CaO	17.90	18.53	15.27	15.75	16.89	16.68	17.17	17.21	16.69	16.77	16.20
FeO	0.62	0.54	1.28	0.68	0.71	0.75	0.68	0.71	0.73	0.77	0.74
Na ₂ O	1.44	1.10	2.40	2.61	2.15	2.19	1.87	1.91	2.09	2.07	2.37
K ₂ O	0.03	b.d.l.	0.07	0.05	0.06	0.06	0.05	b.d.l.	0.04	0.04	0.04
P ₂ O ₅	0.16	0.77	0.27	n.a.	n.a.	n.a.	n.a.	n.a.	n.a.	n.a.	n.a.
Total	100.32	100.78	100.03	99.41	99.77	99.72	99.29	99.59	99.35	99.53	99.08
Si	8.42	8.22	8.91	9.00	8.78	8.82	8.70	8.70	8.79	8.79	8.88
Al	7.45	7.55	6.80	6.84	7.03	6.99	7.13	7.13	7.06	7.04	6.94
Mg	0.03	0.01	0.22	0.03	0.03	0.03	0.02	0.03	0.03	0.03	0.04
Ca	3.53	3.64	3.01	3.12	3.34	3.30	3.42	3.42	3.32	3.33	3.22
Fe (ii)	0.10	0.08	0.20	0.11	0.11	0.12	0.11	0.11	0.11	0.12	0.12
Na	0.51	0.39	0.85	0.93	0.77	0.78	0.68	0.68	0.75	0.74	0.85
K	0.01	0.00	0.02	0.01	0.01	0.01	0.01	0.01	0.01	0.01	0.01
P	0.02	0.12	0.04	n.a.	n.a.	n.a.	n.a.	n.a.	n.a.	n.a.	n.a.
Total	20.07	20.02	20.05	20.05	20.09	20.07	20.07	20.08	20.06	20.06	20.07
An	87.13	90.21	77.58	76.71	81.02	80.56	83.25	83.17	81.37	81.58	78.86
Ab	12.71	9.68	22.03	22.98	18.62	19.10	16.45	16.66	18.40	18.20	20.89
Or	0.16	0.11	0.40	0.31	0.36	0.34	0.30	0.17	0.23	0.22	0.25

Group: B = basalt; BA = basaltic andesite; A = andesite; D = dacite; R = rhyolite; Opx/Cgt-SVC 2, 3 = orthopyroxene/cummingtonite-bearing SVC 2; 3 lavas; **Grain:** P = phenocryst; MC = microphenocryst; G = groundmass; C = core; INC = inclusion (mineral included within is stated in parentheses); **Position:** C = core; M = mantle; R = rim, osci. = oscillatory; **Other:** UNZ = unzoned; Dist. = distance from the core (μm); An = anorthite; Ab = albite; Or = orthoclase.

Table G.1. (continued).

Group: Sample: Name: Grain:	SL-83-25 BA Pre-SVC1 Profile C1-P11 P					SL-83-25 BA Pre-SVC1 Profile C2-P11 P					
Position: Dist.:	M 228	M 254	M 279	M 304	R 330	C 0	C 13	C 26	C 40	C 53	C 66
SiO ₂	48.74	49.96	49.59	51.58	52.17	46.65	47.44	47.63	47.17	47.60	47.57
Al ₂ O ₃	31.22	30.30	30.67	29.33	28.95	32.43	32.39	32.20	32.37	32.19	32.12
MgO	0.12	0.12	0.14	0.10	0.13	0.06	0.11	0.09	0.07	0.09	0.09
CaO	15.65	14.65	15.09	13.57	13.03	17.18	16.90	16.87	16.84	16.83	16.62
FeO	0.80	0.80	0.81	0.87	0.93	0.77	0.68	0.76	0.73	0.73	0.71
Na ₂ O	2.78	3.31	3.06	3.96	4.26	1.92	2.11	2.19	2.06	2.16	2.12
K ₂ O	0.08	0.09	0.07	0.13	0.16	0.04	0.05	0.04	0.06	0.06	0.04
P ₂ O ₅	n.a.	n.a.	n.a.	n.a.	n.a.	n.a.	n.a.	n.a.	n.a.	n.a.	n.a.
Total	99.45	99.28	99.50	99.59	99.73	99.08	99.70	99.84	99.37	99.72	99.29
Si	9.01	9.22	9.14	9.46	9.55	8.69	8.77	8.80	8.75	8.80	8.82
Al	6.80	6.59	6.66	6.34	6.24	7.12	7.06	7.01	7.08	7.01	7.02
Mg	0.03	0.03	0.04	0.03	0.04	0.02	0.03	0.03	0.02	0.02	0.02
Ca	3.10	2.90	2.98	2.67	2.56	3.43	3.35	3.34	3.35	3.33	3.30
Fe (ii)	0.12	0.12	0.12	0.13	0.14	0.12	0.11	0.12	0.11	0.11	0.11
Na	1.00	1.18	1.09	1.41	1.51	0.69	0.76	0.78	0.74	0.78	0.76
K	0.02	0.02	0.02	0.03	0.04	0.01	0.01	0.01	0.01	0.01	0.01
P	n.a.	n.a.	n.a.	n.a.	n.a.	n.a.	n.a.	n.a.	n.a.	n.a.	n.a.
Total	20.09	20.08	20.07	20.08	20.09	20.09	20.08	20.09	20.08	20.08	20.05
An	75.31	70.65	72.87	64.94	62.24	83.02	81.35	80.77	81.64	80.85	81.02
Ab	24.22	28.85	26.71	34.31	36.83	16.76	18.38	18.99	18.04	18.81	18.75
Or	0.46	0.50	0.42	0.75	0.93	0.21	0.27	0.24	0.32	0.34	0.24

Group: Sample: Name: Grain:	SL-83-25 BA Pre-SVC1 Profile C2-P11 P										SL-83-25 BA Pre-SVC1 Profile C3-P11 P	
Position: Dist.:	M 79	M 92	M 106	M 119	M 132	M 145	M 158	M 172	R 185	M 0	M 26	
SiO ₂	50.32	49.66	49.45	51.98	50.59	52.71	53.10	52.19	55.60	51.07	46.82	
Al ₂ O ₃	29.93	30.80	31.13	29.30	30.39	28.79	28.56	28.88	26.89	29.61	32.50	
MgO	0.21	0.10	0.09	0.12	0.13	0.10	0.12	0.12	0.13	0.16	0.08	
CaO	14.46	15.06	15.35	13.40	14.53	12.87	12.51	12.92	10.41	13.90	17.10	
FeO	0.88	0.77	0.84	0.76	0.81	0.86	0.87	0.90	1.09	0.75	0.74	
Na ₂ O	3.36	3.11	2.96	4.15	3.41	4.36	4.62	4.28	5.72	3.83	1.88	
K ₂ O	0.09	0.07	0.06	0.11	0.09	0.13	0.13	0.14	0.24	0.11	0.04	
P ₂ O ₅	n.a.	n.a.	n.a.	n.a.	n.a.	n.a.	n.a.	n.a.	n.a.	n.a.	n.a.	
Total	99.29	99.60	99.90	99.87	100.00	99.91	100.01	99.51	100.18	99.49	99.20	
Si	9.28	9.14	9.09	9.50	9.26	9.62	9.67	9.57	10.06	9.39	8.71	
Al	6.51	6.68	6.74	6.31	6.56	6.19	6.13	6.24	5.73	6.41	7.12	
Mg	0.06	0.03	0.02	0.03	0.03	0.03	0.03	0.03	0.04	0.04	0.02	
Ca	2.86	2.97	3.02	2.62	2.85	2.52	2.44	2.54	2.02	2.74	3.41	
Fe (ii)	0.14	0.12	0.13	0.12	0.12	0.13	0.13	0.14	0.17	0.12	0.12	
Na	1.20	1.11	1.05	1.47	1.21	1.54	1.63	1.52	2.01	1.36	0.68	
K	0.02	0.02	0.01	0.03	0.02	0.03	0.03	0.03	0.05	0.03	0.01	
P	n.a.	n.a.	n.a.	n.a.	n.a.	n.a.	n.a.	n.a.	n.a.	n.a.	n.a.	
Total	20.07	20.07	20.07	20.08	20.07	20.06	20.08	20.08	20.09	20.10	20.07	
An	70.05	72.51	73.91	63.71	69.84	61.56	59.49	62.03	49.46	66.31	83.20	
Ab	29.44	27.07	25.76	35.68	29.63	37.71	39.78	37.17	49.19	33.06	16.55	
Or	0.51	0.42	0.33	0.61	0.53	0.72	0.73	0.80	1.35	0.64	0.25	

Group: Sample: Name: Grain:	SL-83-25 BA Pre-SVC1 Profile C3-P11 P										Pre- SVC1 R SL-83-45 C2-P11 G
Position: Dist.:	M 53	M 79	M 105	M 131	M 158	M 184	M 210	M 237	M 263	M 289	C
SiO ₂	46.91	48.26	46.87	48.04	48.93	47.12	48.98	49.30	50.12	52.27	57.47
Al ₂ O ₃	32.21	31.60	32.48	31.88	31.21	32.30	31.07	30.76	30.34	28.93	27.01
MgO	0.09	0.09	0.08	0.11	0.12	0.06	0.12	0.09	0.09	0.06	b.d.l.
CaO	16.88	16.04	16.84	16.37	15.71	17.00	15.62	15.28	14.77	12.92	8.19
FeO	0.77	0.76	0.75	0.66	0.75	0.76	0.79	0.84	0.85	0.85	0.50
Na ₂ O	2.08	2.55	1.97	2.33	2.82	2.02	2.82	3.00	3.27	4.32	6.83
K ₂ O	0.05	0.05	0.05	0.05	0.05	0.05	0.07	0.09	0.09	0.16	0.17
P ₂ O ₅	n.a.	n.a.	n.a.	n.a.	n.a.	n.a.	n.a.	n.a.	n.a.	n.a.	b.d.l.
Total	99.07	99.36	99.06	99.49	99.64	99.35	99.51	99.38	99.60	99.58	100.20
Si	8.74	8.93	8.72	8.88	9.02	8.75	9.04	9.11	9.23	9.57	10.29
Al	7.07	6.89	7.13	6.95	6.78	7.07	6.76	6.70	6.58	6.24	5.70
Mg	0.03	0.03	0.02	0.03	0.03	0.02	0.03	0.02	0.02	0.02	b.d.l.
Ca	3.37	3.18	3.36	3.24	3.10	3.38	3.09	3.03	2.91	2.54	1.57
Fe (ii)	0.12	0.12	0.12	0.10	0.12	0.12	0.12	0.13	0.13	0.13	0.07
Na	0.75	0.92	0.71	0.84	1.01	0.73	1.01	1.07	1.17	1.53	2.37
K	0.01	0.01	0.01	0.01	0.01	0.01	0.02	0.02	0.02	0.04	0.04
P	n.a.	n.a.	n.a.	n.a.	n.a.	n.a.	n.a.	n.a.	n.a.	n.a.	0.00
Total	20.10	20.08	20.07	20.06	20.09	20.08	20.08	20.08	20.07	20.08	20.05
An	81.50	77.39	82.32	79.28	75.30	82.08	75.10	73.43	71.00	61.74	39.48
Ab	18.21	22.30	17.42	20.46	24.43	17.64	24.50	26.05	28.47	37.37	59.57
Or	0.28	0.31	0.27	0.27	0.27	0.28	0.40	0.52	0.53	0.89	0.96

Group: B = basalt; BA = basaltic andesite; A = andesite; D = dacite; R = rhyolite; Opx/Cgt-SVC 2, 3 = orthopyroxene/cummingtonite-bearing SVC 2; 3 lavas; **Grain:** P = phenocryst; MC = microphenocryst; G = groundmass; C = core; INC = inclusion (mineral included within is stated in parentheses); **Position:** C = core; M = mantle; R = rim, osci. = oscillatory; **Other:** UNZ = unzoned; Dist. = distance from the core (µm); An = anorthite; Ab = albite; Or = orthoclase.

Table G.1. (continued).

Group: Sample: Name: Grain:	Pre-SVC1 R SL-83-45 C2-PI1 C6-PI3 G G		Pre-SVC1 R SL-83-45 Profile P1 P with normal zoning							
Position:	C	C	C	C	C	C	C	C	C	R
Dist.:			0	28	55	83	111	139	166	194
SiO ₂	59.98	60.39	57.67	57.83	57.64	57.24	57.88	57.35	57.97	57.29
Al ₂ O ₃	25.39	25.14	27.27	27.35	27.23	27.27	26.53	27.39	27.38	27.45
MgO	b.d.l.	b.d.l.	b.d.l.	b.d.l.	b.d.l.	b.d.l.	0.11	b.d.l.	b.d.l.	b.d.l.
CaO	6.50	6.11	8.42	8.40	8.56	8.69	8.51	8.65	8.56	8.71
FeO	0.47	0.51	0.37	0.38	0.33	0.39	0.47	0.36	0.38	0.31
Na ₂ O	7.57	7.45	6.55	6.58	6.51	6.47	6.70	6.58	6.39	6.39
K ₂ O	0.28	0.62	0.17	0.16	0.16	0.14	0.17	0.16	0.15	0.15
P ₂ O ₅	b.d.l.	b.d.l.	0.09	0.27	0.22	0.04	0.08	0.15	0.19	0.10
Total	100.10	100.20	100.56	100.95	100.70	100.29	100.49	100.66	101.06	100.44
Si	10.69	10.75	10.28	10.26	10.26	10.24	10.34	10.22	10.27	10.23
Al	5.33	5.27	5.73	5.72	5.71	5.75	5.59	5.75	5.72	5.78
Mg	b.d.l.	b.d.l.	b.d.l.	b.d.l.	b.d.l.	b.d.l.	0.03	b.d.l.	b.d.l.	b.d.l.
Ca	1.24	1.17	1.61	1.60	1.63	1.67	1.63	1.65	1.63	1.67
Fe (ii)	0.07	0.08	0.05	0.06	0.05	0.06	0.07	0.05	0.06	0.05
Na	2.62	2.57	2.26	2.26	2.25	2.25	2.32	2.28	2.20	2.21
K	0.06	0.14	0.04	0.04	0.04	0.03	0.04	0.04	0.03	0.03
P	b.d.l.	b.d.l.	0.01	0.04	0.03	0.01	0.01	0.02	0.03	0.02
Total	20.00	19.98	19.99	19.97	19.97	20.01	20.03	20.02	19.94	19.98
An	31.66	30.05	41.13	40.98	41.68	42.24	40.84	41.67	42.15	42.59
Ab	66.71	66.31	57.89	58.10	57.40	56.94	58.17	57.40	56.94	56.53
Or	1.63	3.64	0.98	0.92	0.92	0.82	0.99	0.93	0.91	0.88

Group: Sample: Name: Grain:	Pre-SVC1 R SL-83-45 Profile P1 P with normal zoning				Pre-SVC1 R SL-83-45 Profile P2 P with normal zoning						Pre-SVC1 R SL-83-45 Profile P3 P with inverse zoning
Position:	R	R	R	R	C	C	C	C	R	R	C
Dist.:	250	277	305	333	0	31	62	94	125	156	0
SiO ₂	58.15	59.32	58.86	61.89	58.20	57.57	57.64	57.74	59.16	57.73	59.67
Al ₂ O ₃	25.54	26.55	26.56	22.35	26.63	26.99	27.42	27.51	26.22	26.94	26.05
MgO	0.11	b.d.l.	b.d.l.	b.d.l.	b.d.l.	b.d.l.	b.d.l.	b.d.l.	b.d.l.	b.d.l.	b.d.l.
CaO	7.42	7.42	7.57	5.54	7.78	8.47	8.59	8.63	7.35	8.11	7.13
FeO	1.14	0.36	0.34	1.71	0.40	0.39	0.40	0.37	0.37	0.35	0.26
Na ₂ O	6.47	7.12	6.93	6.47	6.73	6.48	6.34	6.29	7.07	6.37	7.14
K ₂ O	0.28	0.18	0.20	0.66	0.21	0.17	0.15	0.17	0.18	0.26	0.20
P ₂ O ₅	0.23	0.19	0.29	b.d.l.	0.20	0.09	b.d.l.	0.07	0.42	0.23	b.d.l.
Total	99.40	101.13	100.75	98.84	100.2	100.2	100.5	100.8	100.8	100.0	100.43
Si	10.48	10.47	10.43	11.16	10.39	10.30	10.28	10.26	10.47	10.33	10.59
Al	5.43	5.52	5.55	4.75	5.60	5.69	5.76	5.76	5.47	5.68	5.45
Mg	0.03	b.d.l.	b.d.l.	b.d.l.	b.d.l.	b.d.l.	b.d.l.	b.d.l.	b.d.l.	b.d.l.	b.d.l.
Ca	1.43	1.40	1.44	1.07	1.49	1.62	1.64	1.64	1.39	1.55	1.36
Fe (ii)	0.17	0.05	0.05	0.26	0.06	0.06	0.06	0.05	0.05	0.05	0.04
Na	2.26	2.44	2.38	2.26	2.33	2.25	2.19	2.17	2.43	2.21	2.46
K	0.06	0.04	0.04	0.15	0.05	0.04	0.04	0.04	0.04	0.06	0.04
P	0.04	0.03	0.04	b.d.l.	0.03	0.01	b.d.l.	0.01	0.06	0.04	b.d.l.
Total	19.91	19.96	19.94	19.69	19.95	19.98	19.96	19.94	19.93	19.92	19.93
An	38.13	36.18	37.21	30.72	38.50	41.52	42.40	42.72	36.09	40.66	35.14
Ab	60.18	62.77	61.63	64.94	60.24	57.50	56.69	56.30	62.84	57.80	63.69
Or	1.69	1.06	1.16	4.34	1.25	0.98	0.91	0.98	1.07	1.54	1.16

Group: Sample: Name: Grain:	Pre-SVC1 R SL-83-45 Profile P3 P with inverse zoning									
Position:	C	C	C	C	C	C	C	C	R	R
Dist.:	26	53	79	105	131	158	184	210	263	289
SiO ₂	59.06	59.18	59.04	59.34	59.26	59.59	59.38	59.74	59.27	59.35
Al ₂ O ₃	26.30	26.01	25.98	26.02	26.09	25.81	25.91	26.20	26.13	26.32
MgO	b.d.l.	b.d.l.	b.d.l.	b.d.l.	b.d.l.	b.d.l.	b.d.l.	b.d.l.	b.d.l.	b.d.l.
CaO	7.14	7.11	7.01	7.00	7.14	7.02	6.96	6.95	7.38	7.33
FeO	0.31	0.29	0.30	0.25	0.25	0.27	0.29	0.27	0.29	0.23
Na ₂ O	7.15	7.14	7.26	7.09	7.19	7.10	7.30	7.33	7.05	7.17
K ₂ O	0.20	0.23	0.20	0.22	0.19	0.22	0.22	0.21	0.18	0.20
P ₂ O ₅	0.11	0.22	0.14	0.28	0.15	0.13	0.10	0.42	b.d.l.	0.04
Total	100.31	100.15	99.92	100.18	100.28	100.16	100.15	101.09	100.18	100.65
Si	10.51	10.54	10.54	10.55	10.54	10.60	10.58	10.53	10.56	10.52
Al	5.51	5.46	5.47	5.45	5.47	5.41	5.44	5.44	5.49	5.50
Mg	b.d.l.	b.d.l.	b.d.l.	b.d.l.	b.d.l.	b.d.l.	b.d.l.	b.d.l.	b.d.l.	b.d.l.
Ca	1.36	1.36	1.34	1.33	1.36	1.34	1.33	1.31	1.41	1.39
Fe (ii)	0.05	0.04	0.04	0.04	0.04	0.04	0.04	0.04	0.04	0.03
Na	2.47	2.46	2.51	2.44	2.48	2.45	2.52	2.50	2.43	2.46
K	0.04	0.05	0.05	0.05	0.04	0.05	0.05	0.05	0.04	0.04
P	0.02	0.03	0.02	0.04	0.02	0.02	0.02	0.06	b.d.l.	0.01
Total	19.97	19.94	19.97	19.91	19.95	19.91	19.97	19.93	19.96	19.97
An	35.14	35.03	34.38	34.86	35.02	34.89	34.08	33.96	36.27	35.70
Ab	63.71	63.64	64.45	63.86	63.87	63.80	64.67	64.82	62.65	63.16
Or	1.15	1.33	1.18	1.28	1.11	1.31	1.26	1.22	1.08	1.15

Group: B = basalt; BA = basaltic andesite; A = andesite; D = dacite; R = rhyolite; Opx/Cgt-SVC 2, 3 = orthopyroxene/cummingtonite-bearing SVC 2; 3 lavas; **Grain:** P = phenocryst; MC = microphenocryst; G = groundmass; C = core; INC = inclusion (mineral included within is stated in parentheses); **Position:** C = core; M = mantle; R = rim, osci. = oscillatory; **Other:** UNZ = unzoned; Dist. = distance from the core (µm); An = anorthite; Ab = albite; Or = orthoclase.

Table G.1. (continued).

Group: Sample: Name: Grain:	Pre-SVC1 R SL-83-45 Profile P3 P with inverse zoning						Pre-SVC1 R SL-83-45 Profile P4 P with inverse zoning				
Position: Dist.:	R 341	R 368	R 394	R 420	R 447	R 473	C 0	C 16	C 32	R 48	R 64
SiO ₂	59.08	58.73	58.26	58.04	57.78	58.03	59.77	59.39	60.12	59.00	59.03
Al ₂ O ₃	26.30	26.69	26.65	26.77	27.16	26.90	25.69	25.56	25.73	26.31	26.52
MgO	b.d.l.	b.d.l.	b.d.l.	b.d.l.	b.d.l.	b.d.l.	b.d.l.	b.d.l.	b.d.l.	b.d.l.	b.d.l.
CaO	7.44	7.69	7.95	7.95	8.13	8.08	6.78	6.81	6.79	7.40	7.55
FeO	0.30	0.27	0.34	0.31	0.36	0.34	0.31	0.24	0.35	0.32	0.29
Na ₂ O	6.97	6.84	6.83	6.67	6.65	6.74	7.10	7.25	7.38	7.09	7.07
K ₂ O	0.19	0.18	0.17	0.17	0.18	0.20	0.32	0.21	0.21	0.19	0.19
P ₂ O ₅	0.21	0.21	0.17	0.33	0.09	0.00	0.21	0.28	0.10	0.17	0.25
Total	100.54	100.64	100.40	100.25	100.38	100.29	100.23	99.75	100.67	100.48	100.90
Si	10.49	10.42	10.38	10.35	10.31	10.36	10.62	10.60	10.64	10.48	10.45
Al	5.50	5.58	5.60	5.63	5.71	5.66	5.38	5.38	5.37	5.51	5.53
Mg	b.d.l.	b.d.l.	b.d.l.	b.d.l.	b.d.l.	b.d.l.	b.d.l.	b.d.l.	b.d.l.	b.d.l.	b.d.l.
Ca	1.42	1.46	1.52	1.52	1.55	1.55	1.29	1.30	1.29	1.41	1.43
Fe (ii)	0.05	0.04	0.05	0.05	0.05	0.05	0.05	0.04	0.05	0.05	0.04
Na	2.40	2.35	2.36	2.31	2.30	2.33	2.45	2.51	2.53	2.44	2.43
K	0.04	0.04	0.04	0.04	0.04	0.05	0.07	0.05	0.05	0.04	0.04
P	0.03	0.03	0.03	0.05	0.01	0.00	0.03	0.04	0.01	0.03	0.04
Total	19.93	19.94	19.98	19.93	19.98	20.00	19.90	19.92	19.94	19.96	19.96
An	36.69	37.92	38.76	39.31	39.93	39.39	33.90	33.73	33.26	36.20	36.71
Ab	62.18	61.05	60.24	59.67	59.04	59.43	64.20	65.01	65.51	62.69	62.17
Or	1.12	1.03	1.00	1.02	1.03	1.17	1.90	1.26	1.23	1.11	1.12

Group: Sample: Name: Grain:	Pre-SVC1 R SL-83-45 Profile P4 P with inverse zoning					Pre-SVC1 R SL-83-45 Profile P5 P with normal zoning					
Position: Dist.:	R 80	R 96	R 112	R 128	R 144	C 0	C 27	C 53	C 80	C 106	C 133
SiO ₂	58.56	59.14	59.44	59.36	58.58	58.16	58.03	57.80	58.20	58.29	58.15
Al ₂ O ₃	26.29	26.35	26.47	26.25	26.28	26.61	26.78	26.38	26.43	26.25	26.28
MgO	b.d.l.	b.d.l.	b.d.l.	b.d.l.	b.d.l.	b.d.l.	b.d.l.	b.d.l.	b.d.l.	b.d.l.	b.d.l.
CaO	7.49	7.18	7.13	7.34	7.27	8.06	8.04	7.85	7.77	7.75	7.67
FeO	0.28	0.28	0.32	0.32	0.31	0.33	0.33	0.28	0.31	0.34	0.37
Na ₂ O	7.11	7.18	7.15	7.02	7.15	6.76	6.78	6.81	6.92	7.01	6.92
K ₂ O	0.19	0.20	0.20	0.22	0.33	0.17	0.17	0.17	0.18	0.18	0.19
P ₂ O ₅	0.19	0.20	0.16	0.11	0.17	0.21	0.16	0.32	0.07	0.12	b.d.l.
Total	100.12	100.54	100.89	100.63	100.06	100.30	100.30	99.62	99.90	99.99	99.56
Si	10.45	10.50	10.51	10.53	10.46	10.37	10.36	10.37	10.42	10.43	10.45
Al	5.53	5.51	5.51	5.49	5.53	5.59	5.63	5.58	5.58	5.54	5.57
Mg	b.d.l.	b.d.l.	b.d.l.	b.d.l.	b.d.l.	b.d.l.	b.d.l.	b.d.l.	b.d.l.	b.d.l.	b.d.l.
Ca	1.43	1.37	1.35	1.39	1.39	1.54	1.54	1.51	1.49	1.49	1.48
Fe (ii)	0.04	0.04	0.05	0.05	0.05	0.05	0.05	0.04	0.05	0.05	0.06
Na	2.46	2.47	2.45	2.41	2.48	2.34	2.35	2.37	2.40	2.43	2.41
K	0.04	0.04	0.05	0.05	0.07	0.04	0.04	0.04	0.04	0.04	0.04
P	0.03	0.03	0.02	0.02	0.03	0.03	0.02	0.05	0.01	0.02	b.d.l.
Total	19.99	19.96	19.95	19.94	20.01	19.97	19.98	19.97	19.99	20.01	20.00
An	36.39	35.19	35.10	36.14	35.29	39.34	39.22	38.54	37.90	37.51	37.57
Ab	62.50	63.67	63.71	62.57	62.82	59.69	59.82	60.45	61.07	61.43	61.35
Or	1.12	1.14	1.18	1.29	1.90	0.97	0.96	1.01	1.03	1.06	1.09

Group: Sample: Name: Grain:	Pre-SVC1 R SL-83-45 Profile P5 P with normal zoning										
Position: Dist.:	R 186	R 212	R 239	R 265	R 318	R 345	R 371	R 398	R 424	R 451	R 477
SiO ₂	58.32	58.33	58.14	58.29	58.55	58.66	57.71	57.83	58.65	57.66	58.09
Al ₂ O ₃	26.63	26.51	26.31	26.29	26.38	26.30	26.23	26.44	26.56	26.46	26.82
MgO	b.d.l.	b.d.l.	b.d.l.	b.d.l.	b.d.l.	b.d.l.	b.d.l.	b.d.l.	b.d.l.	b.d.l.	b.d.l.
CaO	7.73	7.64	7.71	7.68	7.69	7.76	7.88	7.91	7.57	7.73	7.84
FeO	0.31	0.32	0.30	0.30	0.32	0.32	0.35	0.32	0.30	0.52	0.28
Na ₂ O	7.05	6.95	6.91	6.94	7.07	6.84	6.80	6.84	6.97	6.72	6.83
K ₂ O	0.18	0.18	0.18	0.17	0.18	0.18	0.18	0.17	0.18	0.18	0.18
P ₂ O ₅	0.15	0.27	0.39	0.12	0.12	0.14	0.37	0.35	0.05	0.20	0.13
Total	100.37	100.19	99.98	99.83	100.32	100.22	99.51	99.85	100.30	99.50	100.17
Si	10.40	10.41	10.39	10.44	10.44	10.46	10.37	10.36	10.45	10.37	10.37
Al	5.59	5.57	5.54	5.55	5.54	5.53	5.56	5.58	5.58	5.61	5.64
Mg	b.d.l.	b.d.l.	b.d.l.	b.d.l.	b.d.l.	b.d.l.	b.d.l.	b.d.l.	b.d.l.	b.d.l.	b.d.l.
Ca	1.48	1.46	1.48	1.47	1.47	1.48	1.52	1.52	1.44	1.49	1.50
Fe (ii)	0.05	0.05	0.05	0.05	0.05	0.05	0.05	0.05	0.04	0.08	0.04
Na	2.44	2.40	2.39	2.41	2.44	2.37	2.37	2.37	2.41	2.34	2.36
K	0.04	0.04	0.04	0.04	0.04	0.04	0.04	0.04	0.04	0.04	0.04
P	0.02	0.04	0.06	0.02	0.02	0.02	0.06	0.05	0.01	0.03	0.02
Total	20.01	19.97	19.96	19.98	20.00	19.95	19.97	19.98	19.97	19.97	19.98
An	37.34	37.38	37.77	37.57	37.16	38.13	38.63	38.63	37.12	38.46	38.40
Ab	61.62	61.59	61.18	61.45	61.82	60.82	60.33	60.38	61.82	60.46	60.53
Or	1.03	1.03	1.05	0.98	1.01	1.05	1.04	0.99	1.06	1.08	1.07

Group: B = basalt; BA = basaltic andesite; A = andesite; D = dacite; R = rhyolite; Opx/Cgt-SVC 2, 3 = orthopyroxene/cummingtonite-bearing SVC 2; 3 lavas; **Grain:** P = phenocryst; MC = microphenocryst; G = groundmass; C = core; INC = inclusion (mineral included within is stated in parentheses); **Position:** C = core; M = mantle; R = rim, osci. = oscillatory; **Other:** UNZ = unzoned; Dist. = distance from the core (µm); An = anorthite; Ab = albite; Or = orthoclase.

Table G.1. (continued).

Group: Sample: Name: Grain:	Pre-SVC1 R SL-83-45 Profile P5 P with normal zoning					Pre-SVC2 BA SL-83-26 Profile P1 P Type 1 Alternative texture					
Position: Dist.:	R 504	R 530	R 557	R 583	R 610	C 0	C 27	C 54	C 81	C 108	An-rich M 134
SiO ₂	58.50	58.75	58.49	58.24	58.81	46.24	46.20	46.39	46.68	46.31	46.51
Al ₂ O ₃	26.25	26.15	26.53	26.70	26.63	34.19	34.08	34.18	34.23	34.03	33.37
MgO	b.d.l.	b.d.l.	b.d.l.	b.d.l.	b.d.l.	0.08	0.08	0.06	0.06	0.08	0.08
CaO	7.60	7.54	7.74	7.81	7.67	16.26	16.25	16.20	16.16	16.19	15.44
FeO	0.33	0.27	0.31	0.34	0.38	0.73	0.69	0.76	0.74	0.64	0.71
Na ₂ O	7.03	7.05	6.93	6.92	6.88	2.54	2.53	2.52	2.53	2.46	2.93
K ₂ O	0.19	0.18	0.18	0.18	0.32	0.07	0.07	0.09	0.07	0.07	0.09
P ₂ O ₅	0.17	0.13	0.26	0.28	b.d.l.	0.20	0.29	0.04	0.10	0.25	0.40
Total	100.06	100.09	100.49	100.49	100.68	100.36	100.22	100.28	100.58	100.07	99.57
Si	10.45	10.49	10.41	10.37	10.45	8.50	8.50	8.54	8.55	8.53	8.60
Al	5.53	5.50	5.56	5.60	5.58	7.41	7.39	7.41	7.39	7.38	7.27
Mg	b.d.l.	b.d.l.	b.d.l.	b.d.l.	b.d.l.	0.02	0.02	0.02	0.02	0.02	0.02
Ca	1.45	1.44	1.47	1.49	1.46	3.20	3.20	3.19	3.17	3.19	3.06
Fe (ii)	0.05	0.04	0.05	0.05	0.06	0.11	0.11	0.12	0.11	0.10	0.11
Na	2.44	2.44	2.39	2.39	2.37	0.90	0.90	0.90	0.90	0.88	1.05
K	0.04	0.04	0.04	0.04	0.07	0.02	0.02	0.02	0.02	0.02	0.02
P	0.03	0.02	0.04	0.04	b.d.l.	0.03	0.05	0.01	0.02	0.04	0.06
Total	19.98	19.97	19.97	19.98	19.99	20.20	20.19	20.21	20.18	20.16	20.20
An	36.98	36.75	37.77	38.02	37.43	77.66	77.69	77.60	77.60	78.16	74.06
Ab	61.92	62.19	61.19	60.96	60.72	21.92	21.89	21.89	22.00	21.44	25.41
Or	1.09	1.05	1.04	1.02	1.85	0.42	0.42	0.51	0.41	0.39	0.53

Group: Sample: Name: Grain:	Pre-SVC2 BA SL-83-26 Profile P1 P Type 1 Alternative texture							Pre-SVC2 BA SL-83-26 Profile P2 P Type 3			
Position: Dist.:	An-rich M 161	An-rich M 242	An-poor M 269	An-poor M 296	An-poor M 323	An-poor M 349	An-poor M 376	R 403	C 0	C 51	C 77
SiO ₂	46.03	45.65	48.58	50.23	49.13	49.37	47.56	50.46	46.00	47.58	45.78
Al ₂ O ₃	34.37	34.65	32.96	31.43	32.00	31.71	33.08	31.00	34.08	33.61	35.24
MgO	0.06	0.04	0.09	0.22	0.10	0.10	0.09	0.07	0.08	0.13	0.11
CaO	16.60	16.84	14.75	13.64	14.09	13.74	15.22	12.89	16.18	15.52	16.74
FeO	0.85	0.74	0.85	1.16	0.75	0.75	0.84	0.95	0.76	0.81	0.85
Na ₂ O	2.26	2.10	3.23	3.78	3.63	3.79	2.87	4.30	2.46	2.90	2.13
K ₂ O	0.07	0.06	0.10	0.17	0.11	0.14	0.11	0.21	0.08	0.11	0.07
P ₂ O ₅	0.35	0.42	0.39	0.28	0.23	0.40	0.37	0.21	0.28	0.18	0.16
Total	100.63	100.54	100.99	101.01	100.09	100.05	100.14	100.16	99.97	100.90	101.14
Si	8.44	8.38	8.83	9.11	8.99	9.03	8.73	9.21	8.49	8.68	8.36
Al	7.43	7.50	7.06	6.72	6.90	6.83	7.15	6.67	7.41	7.23	7.59
Mg	0.02	0.01	0.02	0.06	0.03	0.03	0.02	0.02	0.02	0.04	0.03
Ca	3.26	3.31	2.87	2.65	2.76	2.69	2.99	2.52	3.20	3.03	3.28
Fe (ii)	0.13	0.11	0.13	0.18	0.11	0.11	0.13	0.15	0.12	0.12	0.13
Na	0.80	0.75	1.14	1.33	1.29	1.34	1.02	1.52	0.88	1.03	0.75
K	0.02	0.01	0.02	0.04	0.03	0.03	0.03	0.05	0.02	0.02	0.02
P	0.05	0.07	0.06	0.04	0.04	0.06	0.06	0.03	0.04	0.03	0.02
Total	20.17	20.15	20.13	20.14	20.16	20.14	20.13	20.18	20.19	20.19	20.19
An	79.89	81.33	71.21	65.99	67.75	66.19	74.10	61.61	78.06	74.26	80.96
Ab	19.71	18.35	28.22	33.06	31.61	33.02	25.26	37.20	21.50	25.14	18.65
Or	0.40	0.32	0.58	0.95	0.64	0.79	0.63	1.18	0.44	0.60	0.39

Group: Sample: Name: Grain:	Pre-SVC2 BA SL-83-26 Profile P2 P Type 3										
Position: Dist.:	C 103	C 154	C 180	C 205	C 231	C 257	C 283	M 308	M 334	M 360	M 385
SiO ₂	45.39	45.05	45.28	45.54	46.43	46.55	46.26	46.99	45.97	47.57	45.51
Al ₂ O ₃	35.84	35.69	34.87	34.90	34.36	33.87	34.08	33.89	34.41	32.76	34.87
MgO	0.05	0.05	0.04	0.08	0.04	0.11	0.07	0.09	0.07	0.09	0.08
CaO	17.55	17.50	17.01	17.03	16.36	15.99	16.31	15.29	16.52	15.04	16.91
FeO	0.74	0.78	0.71	0.76	0.78	0.79	0.79	0.77	0.79	0.78	0.73
Na ₂ O	1.74	1.68	2.01	2.04	2.35	2.60	2.41	2.98	2.24	3.00	2.12
K ₂ O	0.05	0.04	0.05	0.06	0.07	0.08	0.09	0.11	0.07	0.10	0.06
P ₂ O ₅	0.44	0.38	0.21	0.41	0.22	0.45	0.52	0.15	0.26	0.08	0.25
Total	101.85	101.24	100.20	100.86	100.64	100.46	100.58	100.31	100.39	99.48	100.60
Si	8.24	8.23	8.35	8.34	8.51	8.54	8.48	8.62	8.45	8.79	8.36
Al	7.66	7.68	7.58	7.53	7.42	7.32	7.36	7.33	7.45	7.13	7.55
Mg	0.01	0.01	0.01	0.02	0.01	0.03	0.02	0.02	0.02	0.02	0.02
Ca	3.41	3.42	3.36	3.34	3.21	3.14	3.20	3.01	3.25	2.98	3.33
Fe (ii)	0.11	0.12	0.11	0.12	0.12	0.12	0.12	0.12	0.12	0.12	0.11
Na	0.61	0.59	0.72	0.72	0.84	0.93	0.86	1.06	0.80	1.08	0.75
K	0.01	0.01	0.01	0.02	0.02	0.02	0.02	0.03	0.02	0.02	0.01
P	0.07	0.06	0.03	0.06	0.03	0.07	0.08	0.02	0.04	0.01	0.04
Total	20.14	20.14	20.18	20.16	20.15	20.17	20.15	20.22	20.16	20.17	20.19
An	84.57	84.99	82.13	81.87	79.03	76.90	78.54	73.44	79.96	73.01	81.25
Ab	15.17	14.77	17.56	17.76	20.58	22.66	20.97	25.94	19.65	26.40	18.41
Or	0.26	0.25	0.31	0.37	0.39	0.44	0.50	0.62	0.39	0.58	0.34

Group: B = basalt; BA = basaltic andesite; A = andesite; D = dacite; R = rhyolite; Opx/Cgt-SVC 2, 3 = orthopyroxene/cummingtonite-bearing SVC 2; 3 lavas; **Grain:** P = phenocryst; MC = microphenocryst; G = groundmass; C = core; INC = inclusion (mineral included within is stated in parentheses); **Position:** C = core; M = mantle; R = rim, osci. = oscillatory; **Other:** UNZ = unzoned; Dist. = distance from the core (µm); An = anorthite; Ab = albite; Or = orthoclase.

Table G.1. (continued).

Group: Sample: Name: Grain:	Pre-SVC2 BA SL-83-26 Profile P2 P Type 3										
Position: Dist.:	M 411	M 437	M 462	M 488	M 514	M 539	M 565	M 616	M 642	M 668	M 693
SiO ₂	45.74	46.40	46.75	48.71	46.54	49.96	49.82	47.45	46.96	45.66	48.82
Al ₂ O ₃	34.39	34.36	32.95	32.08	34.15	31.45	31.94	33.81	33.61	34.62	32.66
MgO	0.04	0.06	0.11	0.14	0.06	0.10	0.08	0.07	0.11	0.04	0.09
CaO	16.34	16.06	15.27	13.92	16.10	13.57	13.76	15.65	15.56	16.82	14.27
FeO	0.73	0.69	0.93	0.71	0.80	0.84	0.78	0.79	0.82	0.71	0.75
Na ₂ O	2.36	2.51	2.77	3.78	2.54	3.92	3.82	2.83	2.79	2.16	3.46
K ₂ O	0.07	0.07	0.09	0.13	0.08	0.16	0.14	0.09	0.08	0.06	0.11
P ₂ O ₅	0.34	0.22	0.31	0.36	0.24	0.05	0.14	0.49	0.47	0.32	0.15
Total	100.04	100.40	99.25	99.83	100.56	100.10	100.51	101.17	100.45	100.46	100.33
Si	8.43	8.51	8.67	8.94	8.53	9.14	9.07	8.63	8.60	8.39	8.92
Al	7.47	7.43	7.20	6.94	7.38	6.78	6.85	7.24	7.26	7.50	7.03
Mg	0.01	0.02	0.03	0.04	0.02	0.03	0.02	0.02	0.03	0.01	0.03
Ca	3.23	3.16	3.03	2.74	3.16	2.66	2.68	3.05	3.05	3.31	2.79
Fe (ii)	0.11	0.11	0.14	0.11	0.12	0.13	0.12	0.12	0.13	0.11	0.11
Na	0.85	0.89	0.99	1.34	0.90	1.39	1.35	1.00	0.99	0.77	1.22
K	0.02	0.02	0.02	0.03	0.02	0.04	0.03	0.02	0.02	0.01	0.03
P	0.05	0.03	0.05	0.06	0.04	0.01	0.02	0.07	0.07	0.05	0.02
Total	20.18	20.17	20.16	20.19	20.18	20.17	20.16	20.15	20.16	20.17	20.15
An	78.95	77.65	74.90	66.59	77.42	65.05	66.00	75.00	75.14	80.84	69.09
Ab	20.66	21.92	24.56	32.69	22.09	34.05	33.17	24.51	24.43	18.80	30.28
Or	0.39	0.43	0.54	0.71	0.48	0.91	0.83	0.49	0.43	0.36	0.64
Group: Sample: Name: Grain:	Pre-SVC2 BA SL-83-26 Profile P2 P Type 3						Pre-SVC2 BA SL-83-26 Profile P3 MP in incl. in cpx				
Position: Dist.:	M 719	M 745	M 770	M 796	M 822	R 847	C 0	C 28	M 56	M 84	R 112
SiO ₂	50.21	47.94	45.34	49.55	49.07	46.91	43.94	44.46	43.09	43.13	43.33
Al ₂ O ₃	31.41	32.46	34.85	31.53	31.52	33.51	34.36	35.22	36.03	36.56	36.85
MgO	0.09	0.07	0.06	0.09	0.10	0.07	0.21	0.08	0.07	0.03	0.07
CaO	13.16	14.71	17.16	13.58	13.82	15.40	17.24	17.67	18.58	18.51	18.49
FeO	0.71	0.83	0.76	0.85	0.83	0.86	1.88	1.30	0.66	0.67	0.75
Na ₂ O	4.10	3.27	1.97	3.80	3.80	2.86	1.42	1.49	1.26	1.20	1.22
K ₂ O	0.15	0.11	0.04	0.15	0.13	0.10	0.09	0.09	b.d.l.	b.d.l.	b.d.l.
P ₂ O ₅	0.07	0.23	0.33	0.05	b.d.l.	0.24	0.25	0.08	0.35	0.32	0.27
Total	99.96	99.67	100.59	99.66	99.30	99.97	99.44	100.42	100.13	100.44	101.02
Si	9.18	8.84	8.33	9.10	9.06	8.64	8.22	8.22	7.99	7.97	7.96
Al	6.77	7.05	7.55	6.83	6.86	7.27	7.58	7.68	7.88	7.96	7.98
Mg	0.03	0.02	0.02	0.03	0.03	0.02	0.06	0.02	0.02	0.01	0.02
Ca	2.58	2.90	3.38	2.67	2.73	3.04	3.46	3.50	3.69	3.66	3.64
Fe (ii)	0.11	0.13	0.12	0.13	0.13	0.13	0.29	0.20	0.10	0.10	0.11
Na	1.45	1.17	0.70	1.35	1.36	1.02	0.52	0.53	0.45	0.43	0.43
K	0.04	0.02	0.01	0.03	0.03	0.02	0.02	0.02	0.01	0.01	0.01
P	0.01	0.04	0.05	0.01	b.d.l.	0.04	0.04	0.01	0.06	0.05	0.04
Total	20.16	20.17	20.17	20.16	20.21	20.19	20.19	20.19	20.21	20.19	20.20
An	63.41	70.89	82.57	65.82	66.29	74.44	86.53	86.34	88.92	89.34	89.18
Ab	35.71	28.50	17.17	33.34	32.94	25.00	12.92	13.14	10.92	10.48	10.65
Or	0.88	0.61	0.25	0.84	0.77	0.56	0.55	0.53	0.16	0.18	0.17
Group: Sample: Name: Grain:	Pre-SVC2 BA SL-83-26 Profile 4 MP						Pre-SVC2 BA SL-83-26 Profile P5 P Type 2				
Position: Dist.:	C 0	C 29	M 88	M 117	M 146	R 175	C 0	C 25	C 51	C 76	C 102
SiO ₂	49.68	49.20	46.88	47.73	46.85	49.29	42.89	43.37	43.89	44.38	43.77
Al ₂ O ₃	31.60	32.01	31.80	31.82	33.44	32.09	35.77	36.17	36.04	35.32	36.30
MgO	0.09	0.10	0.16	0.23	0.05	0.09	0.03	b.d.l.	0.05	0.04	0.04
CaO	13.58	13.65	15.07	14.43	15.63	14.11	18.38	18.46	17.92	17.67	18.46
FeO	0.84	0.79	1.24	2.25	0.79	0.87	0.65	0.71	0.71	0.81	0.74
Na ₂ O	3.90	3.70	2.87	2.88	2.73	3.60	1.26	1.30	1.46	1.61	1.28
K ₂ O	0.16	0.15	0.11	0.11	0.09	0.15	0.03	0.03	0.04	0.05	0.03
P ₂ O ₅	0.32	0.18	0.02	0.31	0.19	0.26	0.26	0.40	0.41	0.25	0.09
Total	100.23	99.83	98.20	99.78	99.79	100.49	99.27	100.50	100.50	100.17	100.75
Si	9.07	9.02	8.80	8.83	8.64	8.99	8.02	8.01	8.09	8.21	8.06
Al	6.80	6.92	7.04	6.94	7.27	6.90	7.88	7.87	7.83	7.70	7.88
Mg	0.02	0.03	0.04	0.06	0.01	0.02	0.01	b.d.l.	0.01	0.01	0.01
Ca	2.66	2.68	3.03	2.86	3.09	2.76	3.68	3.65	3.54	3.50	3.64
Fe (ii)	0.13	0.12	0.20	0.35	0.12	0.13	0.10	0.11	0.11	0.12	0.11
Na	1.38	1.31	1.04	1.03	0.98	1.27	0.46	0.46	0.52	0.58	0.46
K	0.04	0.03	0.03	0.03	0.02	0.03	0.01	0.01	0.01	0.01	0.01
P	0.05	0.03	0.00	0.05	0.03	0.04	0.04	0.06	0.06	0.04	0.01
Total	20.16	20.15	20.20	20.15	20.17	20.15	20.21	20.19	20.17	20.18	20.20
An	65.19	66.55	73.91	72.99	75.61	67.85	88.78	88.57	86.92	85.59	88.67
Ab	33.89	32.61	25.45	26.35	23.89	31.32	11.02	11.25	12.84	14.14	11.16
Or	0.93	0.84	0.64	0.67	0.50	0.83	0.20	0.18	0.24	0.28	0.17

Group: B = basalt; BA = basaltic andesite; A = andesite; D = dacite; R = rhyolite; Opx/Cgt-SVC 2, 3 = orthopyroxene/cummingtonite-bearing SVC 2; 3 lavas; **Grain:** P = phenocryst; MC = microphenocryst; G = groundmass; C = core; INC = inclusion (mineral included within is stated in parentheses); **Position:** C = core; M = mantle; R = rim, osci. = oscillatory; **Other:** UNZ = unzoned; Dist. = distance from the core (µm); An = anorthite; Ab = albite; Or = orthoclase.

Table G.1. (continued).

Group: Sample: Name: Grain:	Pre-SVC2 BA SL-83-26 Profile P5 P Type 2										
Position: Dist.:	C 128	C 153	M 178	M 204	M 229	M 255	M 280	M 382	M 408	M 459	M 484
SiO ₂	43.66	43.11	46.60	47.59	49.15	47.83	46.44	45.99	45.20	45.67	46.42
Al ₂ O ₃	36.53	37.01	33.93	32.80	32.08	32.85	34.19	34.11	34.79	34.67	33.72
MgO	0.05	0.05	0.07	0.06	0.12	0.11	0.07	0.07	0.07	0.07	0.08
CaO	18.35	18.80	15.76	15.00	13.89	14.96	16.35	16.50	16.77	17.02	16.09
FeO	0.59	0.69	0.77	0.73	0.78	0.76	0.83	0.83	0.76	0.71	0.73
Na ₂ O	1.29	1.04	2.68	3.12	3.71	3.17	2.36	2.36	2.14	1.97	2.45
K ₂ O	0.03	b.d.l.	0.09	0.10	0.13	0.10	0.07	0.07	0.06	0.05	0.07
P ₂ O ₅	0.16	0.24	0.33	0.27	0.24	0.21	0.39	0.34	0.26	0.02	0.44
Total	100.70	100.97	100.27	99.72	100.14	99.99	100.77	100.33	100.09	100.23	100.02
Si	8.04	7.93	8.56	8.77	8.99	8.79	8.50	8.46	8.35	8.42	8.55
Al	7.93	8.02	7.34	7.12	6.92	7.11	7.37	7.40	7.57	7.53	7.32
Mg	0.01	0.01	0.02	0.02	0.03	0.03	0.02	0.02	0.02	0.02	0.02
Ca	3.62	3.70	3.10	2.96	2.72	2.95	3.21	3.25	3.32	3.36	3.17
Fe (ii)	0.09	0.11	0.12	0.11	0.12	0.12	0.13	0.13	0.12	0.11	0.11
Na	0.46	0.37	0.95	1.11	1.31	1.13	0.84	0.84	0.77	0.70	0.88
K	0.01	0.01	0.02	0.02	0.03	0.02	0.02	0.02	0.01	0.01	0.02
P	0.03	0.04	0.05	0.04	0.04	0.03	0.06	0.05	0.04	0.00	0.07
Total	20.19	20.19	20.17	20.17	20.17	20.18	20.15	20.18	20.19	20.16	20.14
An	88.56	90.76	76.11	72.24	66.92	71.88	78.97	79.12	80.99	82.48	78.04
Ab	11.29	9.10	23.38	27.19	32.32	27.55	20.64	20.49	18.68	17.23	21.53
Or	0.15	0.14	0.51	0.58	0.76	0.56	0.39	0.40	0.33	0.29	0.43

Group: Sample: Name: Grain:	Pre-SVC2 BA SL-83-26 Profile P5 P Type 2										
Position: Dist.:	M 510	M 535	M 561	M 586	M 612	M 637	M 663	M 688	M 714	M 739	M 765
SiO ₂	46.82	46.67	46.26	49.00	48.01	50.16	48.06	47.84	49.76	47.28	46.68
Al ₂ O ₃	33.60	34.18	34.48	32.30	32.84	30.78	33.02	32.53	31.26	33.38	33.83
MgO	0.07	0.07	0.06	0.07	0.03	0.10	0.07	0.11	0.11	0.09	0.06
CaO	15.45	16.04	16.35	14.09	14.98	13.09	14.67	14.67	13.22	15.45	15.61
FeO	0.77	0.71	0.76	0.71	0.69	0.88	0.82	0.79	0.67	0.76	0.79
Na ₂ O	3.00	2.59	2.39	3.52	3.16	4.12	3.39	3.38	4.20	2.85	2.75
K ₂ O	0.10	0.08	0.06	0.13	0.10	0.20	0.11	0.10	0.17	0.10	0.09
P ₂ O ₅	0.15	0.12	0.30	0.21	0.27	0.02	0.07	0.00	0.35	0.26	0.26
Total	100.01	100.50	100.72	100.11	100.13	99.43	100.23	99.47	99.80	100.19	100.08
Si	8.63	8.56	8.47	8.96	8.80	9.23	8.81	8.84	9.12	8.68	8.59
Al	7.30	7.39	7.44	6.96	7.10	6.67	7.13	7.09	6.75	7.22	7.34
Mg	0.02	0.02	0.02	0.02	0.01	0.03	0.02	0.03	0.03	0.02	0.02
Ca	3.05	3.15	3.21	2.76	2.94	2.58	2.88	2.90	2.59	3.04	3.08
Fe (ii)	0.12	0.11	0.12	0.11	0.11	0.14	0.13	0.12	0.10	0.12	0.12
Na	1.07	0.92	0.85	1.25	1.12	1.47	1.20	1.21	1.49	1.02	0.98
K	0.02	0.02	0.01	0.03	0.02	0.05	0.02	0.02	0.04	0.02	0.02
P	0.02	0.02	0.05	0.03	0.04	0.00	0.01	0.00	0.05	0.04	0.04
Total	20.23	20.19	20.17	20.14	20.15	20.18	20.22	20.23	20.19	20.16	20.18
An	73.56	77.01	78.78	68.33	72.00	62.97	70.11	70.14	62.86	74.54	75.41
Ab	25.85	22.55	20.86	30.90	27.45	35.86	29.29	29.27	36.19	24.92	24.08
Or	0.59	0.44	0.36	0.77	0.55	1.17	0.60	0.60	0.95	0.55	0.51

Group: Sample: Name: Grain:	Pre-SVC2 BA SL-83-26 Profile P5 P Type 2					Pre-SVC2 BA SL-83-26 Profile P6 P Type 4					
Position: Dist.:	M 816	M 841	M 867	M 892	M 918	R 943			UNZ 275		
SiO ₂	48.56	49.91	48.21	48.66	47.99	47.56	41.94	42.49	42.40	42.11	42.28
Al ₂ O ₃	32.59	31.58	32.46	32.51	32.45	33.19	37.40	37.14	37.50	37.56	37.51
MgO	0.05	0.10	0.06	0.09	0.08	0.07	0.05	0.01	0.07	0.09	0.04
CaO	14.35	13.35	14.62	14.31	14.81	14.98	19.69	19.41	19.48	19.42	19.41
FeO	0.74	0.79	0.71	0.76	0.79	0.87	0.55	0.49	0.38	0.38	0.44
Na ₂ O	3.56	3.99	3.29	3.46	3.28	3.22	0.60	0.69	0.61	0.62	0.70
K ₂ O	0.12	0.15	0.12	0.12	0.11	0.10	b.d.l.	b.d.l.	b.d.l.	b.d.l.	b.d.l.
P ₂ O ₅	0.13	0.35	b.d.l.	0.41	b.d.l.	0.25	0.39	0.47	b.d.l.	0.23	0.47
Total	100.13	100.29	99.46	100.34	98.79	100.31	100.65	100.74	100.45	100.40	100.90
Si	8.90	9.10	8.90	8.89	8.94	8.72	7.75	7.83	7.84	7.79	7.78
Al	7.04	6.78	7.06	7.00	7.13	7.17	8.15	8.07	8.18	8.19	8.14
Mg	0.01	0.03	0.02	0.03	0.02	0.02	0.01	0.00	0.02	0.03	0.01
Ca	2.82	2.61	2.89	2.80	2.96	2.94	3.90	3.83	3.86	3.85	3.83
Fe (ii)	0.11	0.12	0.11	0.12	0.12	0.13	0.08	0.08	0.06	0.06	0.07
Na	1.26	1.41	1.18	1.23	1.18	1.14	0.21	0.25	0.22	0.22	0.25
K	0.03	0.03	0.03	0.03	0.03	0.02	b.d.l.	0.00	0.00	0.00	0.00
P	0.02	0.05	b.d.l.	0.06	b.d.l.	0.04	0.06	0.07	b.d.l.	0.04	0.07
Total	20.19	20.14	20.18	20.14	20.27	20.21	20.18	20.14	20.18	20.17	20.16
An	68.56	64.34	70.60	69.05	70.98	71.61	94.81	93.88	94.55	94.52	93.78
Ab	30.78	34.82	28.73	30.26	28.41	27.80	5.21	6.02	5.37	5.45	6.14
Or	0.66	0.83	0.67	0.69	0.61	0.58	b.d.l.	0.10	0.08	0.03	0.08

Group: B = basalt; BA = basaltic andesite; A = andesite; D = dacite; R = rhyolite; Opx/Cgt-SVC 2, 3 = orthopyroxene/cummingtonite-bearing SVC 2; 3 lavas; **Grain:** P = phenocryst; MC = microphenocryst; G = groundmass; C = core; INC = inclusion (mineral included within is stated in parentheses); **Position:** C = core; M = mantle; R = rim, osci. = oscillatory; **Other:** UNZ = unzoned; Dist. = distance from the core (µm); An = anorthite; Ab = albite; Or = orthoclase.

Table G.1. (continued).

Group: Sample: Name: Grain:	Pre-SVC2 BA SL-83-26 Profile P6 P Type 4					Pre-SVC2 BA SL-83-26 Profile P7 MP				
Position:	UNZ					C	C	C	C	C
Dist.:	689	826	964	1102	1240	0	27	53	80	107
SiO ₂	43.28	42.00	41.85	41.41	41.92	42.46	42.10	41.99	42.36	42.52
Al ₂ O ₃	36.82	37.67	37.93	37.67	37.24	37.02	37.24	37.12	36.88	36.98
MgO	0.14	b.d.l.	0.04	0.05	0.10	0.03	0.05	0.05	0.05	0.02
CaO	19.04	19.56	19.47	19.69	19.68	19.17	19.08	19.09	19.29	19.16
FeO	0.45	0.46	0.41	0.41	0.62	0.56	0.57	0.58	0.54	0.53
Na ₂ O	1.04	0.57	0.57	0.47	0.53	0.80	0.79	0.78	0.75	0.81
K ₂ O	0.04	b.d.l.	b.d.l.	b.d.l.	b.d.l.	b.d.l.	b.d.l.	b.d.l.	b.d.l.	b.d.l.
P ₂ O ₅	0.27	0.24	0.44	0.26	0.31	0.43	0.45	0.26	0.19	0.18
Total	101.10	100.56	100.71	99.98	100.48	100.52	100.29	99.90	100.07	99.86
Si	7.95	7.77	7.72	7.71	7.77	7.85	7.80	7.82	7.87	7.88
Al	7.97	8.21	8.25	8.26	8.13	8.06	8.13	8.14	8.08	8.08
Mg	0.04	b.d.l.	0.01	0.02	0.03	0.01	0.01	0.01	0.01	0.00
Ca	3.75	3.87	3.85	3.93	3.91	3.79	3.79	3.81	3.84	3.81
Fe (ii)	0.07	0.07	0.06	0.06	0.10	0.09	0.09	0.09	0.08	0.08
Na	0.37	0.21	0.20	0.17	0.19	0.29	0.29	0.28	0.27	0.29
K	0.01	0.00	0.00	0.00	0.00	0.00	0.00	0.00	0.01	0.00
P	0.04	0.04	0.07	0.04	0.05	0.07	0.07	0.04	0.03	0.03
Total	20.19	20.18	20.16	20.19	20.18	20.16	20.17	20.19	20.19	20.18
An	90.80	94.91	94.91	95.81	95.32	92.89	92.95	93.08	93.32	92.79
Ab	9.00	5.04	5.02	4.15	4.63	7.04	7.00	6.85	6.55	7.14
Or	0.20	0.05	0.07	0.04	0.05	0.08	0.05	0.08	0.13	0.08

Group: Sample: Name: Grain:	Pre-SVC2 BA SL-83-26 Profile P7 MP		Pre-SVC2 BA SL-83-26 Profile P8 P Type 1							
Position:	R	R	C	C	C	C	C	C	C	R
Dist.:	187	214	0	28	56	83	111	139	195	250
SiO ₂	47.90	47.11	43.16	45.28	42.12	43.93	44.55	45.29	44.15	44.63
Al ₂ O ₃	32.91	33.14	35.84	34.03	36.40	35.71	34.99	34.63	34.79	34.62
MgO	0.08	0.06	0.07	0.07	b.d.l.	b.d.l.	0.05	0.07	0.05	0.06
CaO	14.92	15.30	18.19	16.30	18.53	17.89	16.96	16.72	17.29	16.80
FeO	0.76	0.84	0.70	0.85	0.72	0.75	0.85	0.67	0.80	0.71
Na ₂ O	3.22	3.08	1.40	2.38	1.14	1.53	1.98	2.25	1.82	2.10
K ₂ O	0.10	0.10	0.04	0.08	0.03	0.04	0.06	0.06	0.04	0.06
P ₂ O ₅	0.18	0.22	0.24	0.34	0.44	0.44	0.19	0.29	0.17	0.35
Total	100.09	99.89	99.66	99.33	99.42	100.33	99.69	100.02	99.18	99.39
Si	8.79	8.69	8.04	8.42	7.88	8.11	8.27	8.36	8.25	8.33
Al	7.12	7.20	7.87	7.46	8.02	7.77	7.66	7.54	7.66	7.57
Mg	0.02	0.02	0.02	0.02	b.d.l.	b.d.l.	0.01	0.02	0.01	0.02
Ca	2.93	3.02	3.63	3.25	3.71	3.54	3.37	3.31	3.46	3.34
Fe (ii)	0.12	0.13	0.11	0.13	0.11	0.12	0.13	0.10	0.13	0.11
Na	1.14	1.10	0.50	0.86	0.41	0.55	0.71	0.81	0.66	0.75
K	0.02	0.02	0.01	0.02	0.01	0.01	0.01	0.01	0.01	0.01
P	0.03	0.03	0.04	0.05	0.07	0.07	0.03	0.05	0.03	0.06
Total	20.19	20.22	20.22	20.20	20.22	20.17	20.21	20.20	20.21	20.19
An	71.53	72.87	87.61	78.78	89.81	86.43	82.26	80.15	83.75	81.27
Ab	27.90	26.55	12.17	20.78	10.00	13.34	17.41	19.53	15.99	18.37
Or	0.57	0.58	0.23	0.44	0.19	0.23	0.33	0.32	0.25	0.36

Group: Sample: Name: Grain:	Pre-SVC2 BA SL-83-26 Profile P8 P Type 1		Pre-SVC2 BA SL-86-26 C1 PI5A C1 PI5B C1 PI5C C2-PI3A C2-PI3B C1-Cpx1 MP Type 1 INC (px)					SVC1 A SL-JL-02 C2-PI3 C5-PI2 G G		SVC1 A SL-JL-02 Profile P1 G
Position:	R	R	C	M	R	C	R	R	C	C
Dist.:	278	306								0
SiO ₂	46.61	48.96	46.77	46.13	49.08	43.60	48.12	46.64	54.63	49.26
Al ₂ O ₃	33.30	31.46	33.86	34.34	31.95	36.19	32.43	33.68	29.37	33.43
MgO	0.07	0.07	0.06	0.07	0.09	b.d.l.	0.09	0.07	b.d.l.	b.d.l.
CaO	15.37	13.49	15.97	16.81	13.80	18.32	14.55	15.99	10.86	15.19
FeO	0.91	1.06	0.74	0.85	0.88	0.71	0.88	0.78	0.15	0.15
Na ₂ O	2.94	3.85	2.57	1.97	3.71	1.34	3.29	2.68	5.07	2.88
K ₂ O	0.10	0.17	0.08	0.06	0.14	0.04	0.13	0.08	0.28	0.13
P ₂ O ₅	0.32	0.41	0.36	0.34	0.18	0.20	0.38	b.d.l.	0.21	b.d.l.
Total	99.67	99.54	100.50	100.60	99.90	100.50	99.90	100.00	100.60	101.00
Si	8.62	9.01	8.57	8.46	9.00	8.05	8.84	8.61	9.79	8.92
Al	7.26	6.83	7.31	7.42	6.91	7.88	7.02	7.33	6.21	7.13
Mg	0.02	0.02	0.02	0.02	0.02	b.d.l.	0.02	0.02	b.d.l.	b.d.l.
Ca	3.04	2.66	3.14	3.30	2.71	3.63	2.86	3.16	2.09	2.95
Fe (ii)	0.14	0.16	0.11	0.13	0.13	0.11	0.13	0.12	0.02	0.02
Na	1.05	1.38	0.91	0.70	1.32	0.48	1.17	0.96	1.76	1.01
K	0.02	0.04	0.02	0.01	0.03	0.01	0.03	0.02	0.06	0.03
P	0.05	0.06	0.06	0.05	0.03	0.03	0.06	0.00	0.03	b.d.l.
Total	20.21	20.18	20.15	20.11	20.17	20.20	20.15	20.21	19.97	20.05
An	73.86	65.27	77.09	82.22	66.74	88.13	70.47	76.38	53.35	73.91
Ab	25.55	33.73	22.46	17.43	32.48	11.67	28.81	23.16	45.02	25.34
Or	0.59	0.99	0.45	0.35	0.78	0.20	0.72	0.45	1.63	0.76

Group: B = basalt; BA = basaltic andesite; A = andesite; D = dacite; R = rhyolite; Opx/Cgt-SVC 2, 3 = orthopyroxene/cummingtonite-bearing SVC 2; 3 lavas; **Grain:** P = phenocryst; MC = microphenocryst; G = groundmass; C = core; INC = inclusion (mineral included within is stated in parentheses); **Position:** C = core; M = mantle; R = rim, osci. = oscillatory; **Other:** UNZ = unzoned; Dist. = distance from the core (μm); An = anorthite; Ab = albite; Or = orthoclase.

Table G.1. (continued).

Group: Sample: Name: Grain:	SVC1 A SL-JL-02 Profile P1 G		SVC1 A SL-JL-02 Profile P2 P Type 5								
Position: Dist.:	C 19	R 38	C 0	C 26	C 52	C 78	C 104	C 131	C 183	M 287	M 313
SiO ₂	50.82	54.28	53.24	53.85	52.89	51.81	52.72	52.46	52.81	50.92	51.69
Al ₂ O ₃	31.73	29.72	30.02	29.97	30.77	32.17	30.69	30.47	29.86	31.17	31.49
MgO	b.d.l.	b.d.l.	b.d.l.	b.d.l.	b.d.l.	b.d.l.	b.d.l.	b.d.l.	b.d.l.	b.d.l.	b.d.l.
CaO	13.33	10.95	11.58	11.46	12.31	12.32	11.89	12.32	11.31	12.67	12.97
FeO	0.15	0.27	0.10	0.16	0.12	0.11	0.08	0.10	0.15	0.15	0.12
Na ₂ O	3.78	5.30	4.86	4.94	4.45	4.14	4.61	4.36	4.81	4.05	4.12
K ₂ O	0.22	0.30	0.25	0.26	0.24	0.24	0.27	0.23	0.30	0.20	0.22
P ₂ O ₅	0.31	0.40	0.25	0.38	0.29	0.22	b.d.l.	0.27	0.25	0.30	0.26
Total	100.31	101.24	100.30	101.04	101.08	101.00	100.28	100.19	99.51	99.44	100.87
Si	9.21	9.69	9.60	9.63	9.48	9.29	9.52	9.48	9.60	9.29	9.31
Al	6.78	6.25	6.38	6.32	6.50	6.80	6.53	6.49	6.40	6.70	6.68
Mg	b.d.l.	b.d.l.	b.d.l.	b.d.l.	b.d.l.	b.d.l.	b.d.l.	b.d.l.	b.d.l.	b.d.l.	b.d.l.
Ca	2.59	2.09	2.24	2.20	2.36	2.37	2.30	2.39	2.20	2.48	2.50
Fe (ii)	0.02	0.04	0.02	0.02	0.02	0.02	0.01	0.02	0.02	0.02	0.02
Na	1.33	1.83	1.70	1.71	1.55	1.44	1.62	1.53	1.69	1.43	1.44
K	0.05	0.07	0.06	0.06	0.05	0.05	0.06	0.05	0.07	0.05	0.05
P	0.05	0.06	0.04	0.06	0.04	0.03	b.d.l.	0.04	0.04	0.05	0.04
Total	20.02	20.04	20.03	20.01	20.00	20.00	20.05	20.00	20.03	20.02	20.04
An	65.22	52.41	56.00	55.35	59.64	61.32	57.86	60.12	55.50	62.61	62.68
Ab	33.50	45.86	42.58	43.18	39.00	37.28	40.59	38.53	42.72	36.19	36.03
Or	1.28	1.73	1.42	1.47	1.36	1.40	1.55	1.35	1.78	1.20	1.29

Group: Sample: Name: Grain:	SVC1 A SL-JL-02 Profile P2 P Type 5										
Position: Dist.:	M 339	M 392	M 444	M 470	M 496	M 522	M 548	M 574	M 600	M 653	M 679
SiO ₂	52.30	50.08	45.96	51.46	51.75	53.12	53.05	51.74	50.52	50.69	52.01
Al ₂ O ₃	30.85	32.61	33.64	31.45	31.32	30.43	30.06	31.47	32.19	32.02	31.31
MgO	b.d.l.	b.d.l.	b.d.l.	b.d.l.	b.d.l.	b.d.l.	b.d.l.	b.d.l.	b.d.l.	b.d.l.	b.d.l.
CaO	12.39	14.18	16.16	13.27	12.79	11.99	11.96	12.95	13.88	13.85	12.96
FeO	0.12	0.15	0.11	0.12	0.13	0.12	0.10	0.13	0.15	0.14	0.13
Na ₂ O	4.34	3.41	2.07	4.14	4.18	4.69	4.52	4.15	3.55	3.67	4.19
K ₂ O	0.27	0.18	0.08	0.18	0.16	0.20	0.20	0.17	0.14	0.15	0.18
P ₂ O ₅	0.52	0.16	0.22	0.24	b.d.l.	0.10	0.11	0.19	0.26	0.20	0.23
Total	100.88	100.77	98.23	100.88	100.26	100.64	100.04	100.84	100.69	100.72	101.01
Si	9.40	9.06	8.59	9.28	9.37	9.56	9.59	9.32	9.13	9.16	9.35
Al	6.53	6.95	7.41	6.68	6.68	6.45	6.41	6.68	6.86	6.82	6.63
Mg	b.d.l.	b.d.l.	b.d.l.	b.d.l.	b.d.l.	b.d.l.	b.d.l.	b.d.l.	b.d.l.	b.d.l.	b.d.l.
Ca	2.39	2.75	3.23	2.56	2.48	2.31	2.32	2.50	2.69	2.68	2.50
Fe (ii)	0.02	0.02	0.02	0.02	0.02	0.02	0.02	0.02	0.02	0.02	0.02
Na	1.51	1.20	0.75	1.45	1.47	1.64	1.58	1.45	1.25	1.29	1.46
K	0.06	0.04	0.02	0.04	0.04	0.05	0.05	0.04	0.03	0.03	0.04
P	0.08	0.02	0.04	0.04	b.d.l.	0.02	0.02	0.03	0.04	0.03	0.03
Total	20.00	20.05	20.04	20.07	20.05	20.04	19.99	20.04	20.02	20.04	20.03
An	60.26	68.94	80.85	63.28	62.24	57.89	58.69	62.67	67.78	67.04	62.43
Ab	38.18	30.05	18.70	35.71	36.81	40.97	40.11	36.37	31.40	32.12	36.53
Or	1.56	1.01	0.45	1.01	0.95	1.14	1.20	0.96	0.82	0.85	1.04

Group: Sample: Name: Grain:	SVC1 A SL-JL-02 Profile P2 P Type 5		SVC1 A SL-JL-02 Profile P3 P Type 3								
Position: Dist.:	M 705	R 809	C 0	M 26	M 52	M 78	M 130	M 156	M 182	M 208	M 234
SiO ₂	51.42	49.07	47.53	48.20	49.09	50.88	48.57	50.43	51.37	50.41	48.04
Al ₂ O ₃	31.49	33.13	33.82	33.08	32.13	31.60	33.13	32.24	31.12	31.64	32.94
MgO	b.d.l.	b.d.l.	b.d.l.	b.d.l.	b.d.l.	b.d.l.	b.d.l.	b.d.l.	b.d.l.	b.d.l.	b.d.l.
CaO	13.10	14.76	15.78	14.88	14.17	13.45	15.02	12.95	12.96	13.50	15.15
FeO	0.16	0.26	0.14	0.21	0.16	0.16	0.17	0.18	0.14	0.15	0.16
Na ₂ O	3.96	3.08	2.62	3.27	3.50	3.86	3.20	3.75	4.14	3.84	2.94
K ₂ O	0.21	0.13	0.09	0.12	0.18	0.20	0.13	0.22	0.19	0.18	0.10
P ₂ O ₅	0.51	0.17	0.18	0.32	0.39	0.28	0.30	0.25	0.10	0.31	b.d.l.
Total	100.88	100.60	100.16	100.05	99.58	100.43	100.55	100.04	99.99	100.04	99.34
Si	9.26	8.91	8.70	8.82	9.00	9.22	8.84	9.16	9.34	9.17	8.85
Al	6.68	7.09	7.30	7.13	6.94	6.75	7.11	6.90	6.67	6.79	7.15
Mg	b.d.l.	b.d.l.	b.d.l.	b.d.l.	b.d.l.	b.d.l.	b.d.l.	b.d.l.	b.d.l.	b.d.l.	b.d.l.
Ca	2.53	2.87	3.09	2.92	2.78	2.61	2.93	2.52	2.52	2.63	2.99
Fe (ii)	0.02	0.04	0.02	0.03	0.02	0.02	0.03	0.03	0.02	0.02	0.03
Na	1.38	1.08	0.93	1.16	1.24	1.35	1.13	1.32	1.46	1.35	1.05
K	0.05	0.03	0.02	0.03	0.04	0.05	0.03	0.05	0.04	0.04	0.02
P	0.08	0.03	0.03	0.05	0.06	0.04	0.05	0.04	0.02	0.05	0.00
Total	20.00	20.06	20.09	20.13	20.08	20.04	20.12	20.02	20.06	20.06	20.10
An	63.83	72.04	76.46	71.03	68.44	65.08	71.63	64.74	62.63	65.35	73.60
Ab	34.94	27.20	23.00	28.27	30.54	33.76	27.65	33.95	36.26	33.63	25.84
Or	1.22	0.77	0.54	0.70	1.02	1.17	0.71	1.31	1.11	1.01	0.55

Group: B = basalt; BA = basaltic andesite; A = andesite; D = dacite; R = rhyolite; Opx/Cgt-SVC 2, 3 = orthopyroxene/cummingtonite-bearing SVC 2; 3 lavas; **Grain:** P = phenocryst; MC = microphenocryst; G = groundmass; C = core; INC = inclusion (mineral included within is stated in parentheses); **Position:** C = core; M = mantle; R = rim, osci. = oscillatory; **Other:** UNZ = unzoned; Dist. = distance from the core (µm); An = anorthite; Ab = albite; Or = orthoclase.

Table G.1. (continued).

Group: Sample: Name: Grain:	SVC1 A SL-JL-02 Profile P3 P Type 3										
Position: Dist.:	M 260	M 286	M 312	M 338	M 364	M 390	M 416	M 442	M 494	M 520	M 546
SiO ₂	48.52	53.60	51.26	48.75	48.86	51.75	48.66	50.34	50.14	48.53	49.40
Al ₂ O ₃	32.82	29.75	31.38	32.84	33.19	30.81	33.16	31.54	31.92	32.69	33.28
MgO	b.d.l.	b.d.l.	b.d.l.	b.d.l.	b.d.l.	b.d.l.	b.d.l.	b.d.l.	b.d.l.	b.d.l.	b.d.l.
CaO	15.06	11.36	12.80	14.98	15.02	13.87	15.40	13.56	13.91	14.69	15.01
FeO	0.12	0.11	0.14	0.13	0.11	0.22	0.15	0.08	0.17	0.16	0.09
Na ₂ O	3.12	5.01	4.18	3.06	2.97	2.81	2.81	3.84	3.70	2.92	3.06
K ₂ O	0.12	0.25	0.19	0.12	0.13	0.31	0.10	0.17	0.19	0.13	0.14
P ₂ O ₅	0.38	0.12	0.34	0.10	0.21	0.14	0.40	0.13	b.d.l.	0.35	0.15
Total	100.15	100.16	100.27	100.00	100.48	99.92	100.69	99.70	100.02	99.47	101.11
Si	8.86	9.68	9.28	8.92	8.89	9.40	8.84	9.20	9.15	8.91	8.92
Al	7.06	6.33	6.70	7.08	7.11	6.59	7.10	6.79	6.86	7.07	7.08
Mg	b.d.l.	b.d.l.	b.d.l.	b.d.l.	b.d.l.	b.d.l.	b.d.l.	b.d.l.	b.d.l.	b.d.l.	b.d.l.
Ca	2.95	2.20	2.48	2.94	2.93	2.70	3.00	2.65	2.72	2.89	2.90
Fe (ii)	0.02	0.02	0.02	0.02	0.02	0.03	0.02	0.01	0.03	0.02	0.01
Na	1.11	1.75	1.47	1.08	1.05	0.99	0.99	1.36	1.31	1.04	1.07
K	0.03	0.06	0.04	0.03	0.03	0.07	0.02	0.04	0.04	0.03	0.03
P	0.06	0.02	0.05	0.02	0.03	0.02	0.06	0.02	b.d.l.	0.05	0.02
Total	20.08	20.04	20.04	20.08	20.05	19.80	20.03	20.08	20.10	20.01	20.05
An	72.22	54.78	62.16	72.52	73.08	71.83	74.78	65.47	66.77	72.97	72.44
Ab	27.09	43.77	36.73	26.77	26.14	26.29	24.67	33.55	32.18	26.26	26.77
Or	0.69	1.45	1.11	0.71	0.78	1.88	0.55	0.97	1.06	0.77	0.78

Group: Sample: Name: Grain:	SVC1 A SL-JL-02 Profile P3 P Type 3										SVC1 A SL-JL-02 Profile P4 P Type 6
Position: Dist.:	M 598	M 650	M 702	M 728	M 754	M 780	M 806	M 832	M 858	R 910	C 0
SiO ₂	53.57	51.43	52.67	53.34	53.22	52.63	50.20	51.92	52.28	51.05	53.72
Al ₂ O ₃	30.26	30.50	30.58	29.77	29.95	30.68	32.37	31.05	30.74	31.67	29.25
MgO	b.d.l.	b.d.l.	b.d.l.	b.d.l.	b.d.l.	b.d.l.	b.d.l.	b.d.l.	b.d.l.	b.d.l.	b.d.l.
CaO	11.57	12.40	12.19	11.23	11.25	12.33	14.28	12.64	12.21	13.15	10.80
FeO	0.11	0.12	0.12	0.14	0.12	0.10	0.11	0.14	0.14	0.14	0.12
Na ₂ O	4.87	4.19	4.51	5.04	4.98	4.46	3.55	4.29	4.57	4.10	5.31
K ₂ O	0.23	0.20	0.18	0.23	0.23	0.20	0.12	0.17	0.18	0.22	0.25
P ₂ O ₅	0.15	0.41	b.d.l.	b.d.l.	0.19	b.d.l.	100.6	0.17	0.15	0.30	0.19
Total	100.78	99.25	100.20	99.82	99.93	100.42	5	100.40	100.23	100.62	99.65
Si	9.61	9.39	9.53	9.67	9.63	9.50	9.10	9.38	9.46	9.23	9.74
Al	6.40	6.56	6.52	6.36	6.38	6.53	6.91	6.61	6.55	6.75	6.25
Mg	b.d.l.	b.d.l.	b.d.l.	b.d.l.	b.d.l.	b.d.l.	b.d.l.	b.d.l.	b.d.l.	b.d.l.	b.d.l.
Ca	2.22	2.43	2.36	2.18	2.18	2.38	2.77	2.45	2.37	2.55	2.10
Fe (ii)	0.02	0.02	0.02	0.02	0.02	0.02	0.02	0.02	0.02	0.02	0.02
Na	1.70	1.48	1.58	1.77	1.75	1.56	1.25	1.50	1.60	1.44	1.87
K	0.05	0.05	0.04	0.05	0.05	0.05	0.03	0.04	0.04	0.05	0.06
P	0.02	0.06	b.d.l.	0.00	0.03	b.d.l.	0.01	0.03	0.02	0.05	0.03
Total	20.03	19.99	20.04	20.06	20.04	20.04	20.08	20.04	20.05	20.07	20.06
An	55.99	61.35	59.26	54.49	54.76	59.74	68.47	61.33	59.00	63.16	52.17
Ab	42.67	37.49	39.67	44.20	43.92	39.12	30.85	37.66	39.94	35.60	46.40
Or	1.34	1.16	1.06	1.30	1.32	1.14	0.68	1.00	1.06	1.23	1.43

Group: Sample: Name: Grain:	SVC1 A SL-JL-02 Profile P3 P Type 3										SVC1 A SL-JL-02 Profile P5 P Type 1
Position: Dist.:	M 60	M 90	M 120	M 179	M 209	M 299	M 359	R 388	C 0	C 57	C 113
SiO ₂	52.10	50.35	52.58	53.08	53.71	50.77	51.36	51.23	48.84	49.03	50.15
Al ₂ O ₃	30.20	31.58	30.46	30.20	28.75	31.54	29.74	31.72	33.27	32.74	32.29
MgO	b.d.l.	b.d.l.	b.d.l.	b.d.l.	b.d.l.	b.d.l.	b.d.l.	b.d.l.	b.d.l.	b.d.l.	b.d.l.
CaO	11.93	13.29	12.10	11.75	10.57	13.32	11.84	13.27	15.21	14.36	14.03
FeO	0.15	0.12	0.12	0.11	0.13	0.11	0.16	0.16	0.11	0.15	0.10
Na ₂ O	4.73	3.98	4.74	4.84	5.40	3.89	4.50	4.11	2.90	3.36	3.60
K ₂ O	0.22	0.15	0.19	0.23	0.27	0.17	0.23	0.21	0.11	0.14	0.18
P ₂ O ₅	0.19	0.14	b.d.l.	0.18	0.09	0.09	0.14	0.41	0.25	0.33	0.38
Total	99.51	99.63	100.21	100.39	98.96	99.90	97.98	101.10	100.69	100.10	100.70
Si	9.49	9.20	9.51	9.57	9.80	9.24	9.50	9.22	8.87	8.94	9.07
Al	6.48	6.80	6.50	6.42	6.18	6.77	6.49	6.73	7.12	7.04	6.89
Mg	b.d.l.	b.d.l.	b.d.l.	b.d.l.	b.d.l.	b.d.l.	b.d.l.	b.d.l.	b.d.l.	b.d.l.	b.d.l.
Ca	2.33	2.60	2.35	2.27	2.07	2.60	2.35	2.56	2.96	2.81	2.72
Fe (ii)	0.02	0.02	0.02	0.02	0.02	0.02	0.02	0.02	0.02	0.02	0.02
Na	1.67	1.41	1.66	1.69	1.91	1.37	1.61	1.43	1.02	1.19	1.26
K	0.05	0.04	0.04	0.05	0.06	0.04	0.05	0.05	0.03	0.03	0.04
P	0.03	0.02	0.00	0.03	0.01	0.01	0.02	0.06	0.04	0.05	0.06
Total	20.08	20.09	20.09	20.05	20.07	20.06	20.05	20.07	20.04	20.07	20.05
An	57.50	64.31	57.91	56.55	51.16	64.78	58.46	63.31	73.86	69.72	67.58
Ab	41.26	34.82	41.01	42.15	47.26	34.22	40.20	35.49	25.49	29.48	31.36
Or	1.24	0.87	1.08	1.30	1.58	1.00	1.34	1.20	0.65	0.80	1.06

Group: B = basalt; BA = basaltic andesite; A = andesite; D = dacite; R = rhyolite; Opx/Cgt-SVC 2, 3 = orthopyroxene/cummingtonite-bearing SVC 2; 3 lavas; **Grain:** P = phenocryst; MC = microphenocryst; G = groundmass; C = core; INC = inclusion (mineral included within is stated in parentheses); **Position:** C = core; M = mantle; R = rim, osci. = oscillatory; **Other:** UNZ = unzoned; Dist. = distance from the core (μm); An = anorthite; Ab = albite; Or = orthoclase.

Table G.1. (continued).

Group: Sample: Name: Grain:	SVC1 A SL-JL-02 Profile P5 P Type 1									SVC1 A SL-JL-02 Profile P6 P Type 2	
Position:	C	M	M	M	M	M	M	M	M	C	C
Dist.:	227	283	340	397	453	510	567	623	680	0	26
SiO ₂	50.06	53.03	53.75	51.07	51.75	52.61	53.07	51.47	50.85	46.17	46.18
Al ₂ O ₃	32.34	30.15	30.11	31.85	31.14	30.51	30.18	31.42	31.77	35.24	35.66
MgO	b.d.l.	b.d.l.	b.d.l.	b.d.l.	b.d.l.	b.d.l.	b.d.l.	b.d.l.	b.d.l.	b.d.l.	b.d.l.
CaO	14.14	11.61	11.43	13.36	12.59	11.87	11.60	13.19	13.44	17.53	17.43
FeO	0.11	0.13	0.11	0.11	0.11	0.11	0.13	0.14	0.12	0.15	0.13
Na ₂ O	3.42	4.78	4.92	3.96	4.33	4.73	4.76	4.04	3.93	1.75	1.73
K ₂ O	0.14	0.23	0.24	0.16	0.19	0.22	0.21	0.16	0.14	0.04	0.04
P ₂ O ₅	0.18	0.28	b.d.l.	0.24	0.12	0.25	0.41	0.12	0.32	0.24	0.03
Total	100.34	100.18	100.53	100.74	100.25	100.34	100.36	100.53	100.59	101.18	101.19
Si	9.09	9.58	9.67	9.22	9.37	9.50	9.56	9.31	9.20	8.40	8.40
Al	6.92	6.41	6.38	6.78	6.64	6.49	6.41	6.70	6.77	7.56	7.64
Mg	b.d.l.	b.d.l.	b.d.l.	b.d.l.	b.d.l.	b.d.l.	b.d.l.	b.d.l.	b.d.l.	b.d.l.	b.d.l.
Ca	2.75	2.24	2.20	2.58	2.44	2.30	2.24	2.55	2.60	3.42	3.40
Fe (ii)	0.02	0.02	0.02	0.02	0.02	0.02	0.02	0.02	0.02	0.02	0.02
Na	1.20	1.67	1.71	1.38	1.52	1.66	1.66	1.42	1.38	0.62	0.61
K	0.03	0.05	0.06	0.04	0.04	0.05	0.05	0.04	0.03	0.01	0.01
P	0.03	0.04	b.d.l.	0.04	0.02	0.04	0.06	0.02	0.05	0.04	0.01
Total	20.03	20.02	20.03	20.05	20.06	20.05	20.00	20.04	20.05	20.07	20.08
An	69.01	56.56	55.45	64.53	60.96	57.37	56.69	63.74	64.87	84.47	84.60
Ab	30.20	42.12	43.16	34.58	37.95	41.38	42.08	35.32	34.30	15.27	15.17
Or	0.79	1.32	1.40	0.90	1.09	1.25	1.24	0.94	0.82	0.26	0.23

Group: Sample: Name: Grain:	SVC1 A SL-JL-02 Profile P6 P Type 2										
Position:	C	C	C	C	C	M	M	M	M	M	M
Dist.:	51	77	128	154	180	231	257	282	308	334	359
SiO ₂	45.83	45.24	44.67	45.70	46.02	51.96	52.98	56.98	54.46	53.81	53.95
Al ₂ O ₃	35.51	35.87	36.01	35.66	35.45	30.68	30.64	27.41	29.31	30.22	29.84
MgO	b.d.l.	b.d.l.	b.d.l.	b.d.l.	b.d.l.	b.d.l.	b.d.l.	b.d.l.	b.d.l.	b.d.l.	b.d.l.
CaO	17.54	17.46	18.15	17.57	17.50	12.29	11.90	9.65	10.75	11.51	10.84
FeO	0.13	0.10	0.18	0.13	0.17	0.12	0.16	0.24	0.11	0.14	0.11
Na ₂ O	1.67	1.74	1.33	1.63	1.61	4.48	4.72	5.16	5.23	4.98	5.22
K ₂ O	0.04	0.04	0.03	0.05	0.06	0.21	0.22	0.53	0.31	0.24	0.25
P ₂ O ₅	0.30	0.34	0.39	0.23	0.18	0.27	0.16	0.16	0.20	0.23	0.21
Total	101.04	100.77	100.73	100.96	101.01	100.00	100.79	100.15	100.39	101.09	100.48
Si	8.35	8.27	8.18	8.33	8.39	9.42	9.52	10.21	9.79	9.62	9.69
Al	7.63	7.73	7.77	7.67	7.61	6.56	6.49	5.79	6.21	6.37	6.32
Mg	b.d.l.	b.d.l.	b.d.l.	b.d.l.	b.d.l.	b.d.l.	b.d.l.	b.d.l.	b.d.l.	b.d.l.	b.d.l.
Ca	3.42	3.42	3.56	3.43	3.42	2.39	2.29	1.85	2.07	2.21	2.09
Fe (ii)	0.02	0.01	0.03	0.02	0.03	0.02	0.02	0.04	0.02	0.02	0.02
Na	0.59	0.62	0.47	0.57	0.57	1.57	1.64	1.79	1.82	1.73	1.82
K	0.01	0.01	0.01	0.01	0.01	0.05	0.05	0.12	0.07	0.05	0.06
P	0.05	0.05	0.06	0.04	0.03	0.04	0.03	0.02	0.03	0.03	0.03
Total	20.07	20.10	20.08	20.07	20.05	20.05	20.04	19.82	20.01	20.03	20.04
An	85.07	84.54	88.13	85.41	85.45	59.56	57.50	49.18	52.23	55.31	52.66
Ab	14.68	15.21	11.69	14.30	14.22	39.26	41.23	47.60	45.97	43.32	45.90
Or	0.25	0.25	0.18	0.29	0.33	1.19	1.28	3.22	1.80	1.38	1.44

Group: Sample: Name: Grain:	SVC1 A SL-JL-02 Profile P6 P Type 2										
Position:	M	M	M	M	M	M	M	M	M	M	M
Dist.:	385	411	436	462	488	513	539	565	590	616	642
SiO ₂	54.29	53.81	51.77	51.38	52.80	52.39	53.39	51.39	51.96	53.35	52.85
Al ₂ O ₃	29.58	30.14	31.09	31.49	30.55	30.63	30.47	31.64	30.89	30.27	30.71
MgO	b.d.l.	b.d.l.	b.d.l.	b.d.l.	b.d.l.	b.d.l.	b.d.l.	b.d.l.	b.d.l.	b.d.l.	b.d.l.
CaO	10.81	11.27	12.80	13.32	12.02	12.16	11.73	13.05	12.25	11.87	12.06
FeO	0.10	0.08	0.13	0.13	0.13	0.13	0.08	0.16	0.16	0.13	0.15
Na ₂ O	5.35	5.18	4.18	4.06	4.69	4.53	4.84	4.13	4.60	4.73	4.58
K ₂ O	0.25	0.23	0.17	0.16	0.20	0.20	0.21	0.18	0.19	0.20	0.21
P ₂ O ₅	0.18	0.33	b.d.l.	0.40	b.d.l.	0.05	0.28	0.25	b.d.l.	b.d.l.	0.03
Total	100.58	101.03	100.22	100.97	100.39	100.08	100.99	100.84	100.16	100.43	100.63
Si	9.75	9.63	9.38	9.25	9.53	9.49	9.56	9.26	9.42	9.62	9.52
Al	6.26	6.35	6.64	6.68	6.50	6.54	6.43	6.72	6.60	6.43	6.52
Mg	b.d.l.	b.d.l.	b.d.l.	b.d.l.	b.d.l.	b.d.l.	b.d.l.	b.d.l.	b.d.l.	b.d.l.	b.d.l.
Ca	2.08	2.16	2.49	2.57	2.32	2.36	2.25	2.52	2.38	2.29	2.33
Fe (ii)	0.01	0.01	0.02	0.02	0.02	0.02	0.01	0.02	0.02	0.02	0.02
Na	1.86	1.80	1.47	1.42	1.64	1.59	1.68	1.44	1.62	1.65	1.60
K	0.06	0.05	0.04	0.04	0.05	0.05	0.05	0.04	0.04	0.05	0.05
P	0.03	0.05	0.00	0.06	0.00	0.01	0.04	0.04	0.01	-0.02	0.00
Total	20.04	20.05	20.05	20.04	20.06	20.05	20.02	20.06	20.09	20.04	20.04
An	51.98	53.86	62.22	63.85	57.92	59.05	56.54	62.94	58.91	57.41	58.56
Ab	46.60	44.82	36.79	35.22	40.90	39.81	42.24	36.04	40.01	41.42	40.24
Or	1.42	1.32	0.98	0.93	1.18	1.15	1.22	1.02	1.09	1.17	1.20

Group: B = basalt; BA = basaltic andesite; A = andesite; D = dacite; R = rhyolite; Opx/Cgt-SVC 2, 3 = orthopyroxene/cummingtonite-bearing SVC 2; 3 lavas; **Grain:** P = phenocryst; MC = microphenocryst; G = groundmass; C = core; INC = inclusion (mineral included within is stated in parentheses); **Position:** C = core; M = mantle; R = rim, osci. = oscillatory; **Other:** UNZ = unzoned; Dist. = distance from the core (µm); An = anorthite; Ab = albite; Or = orthoclase.

Table G.1. (continued).

Group: Sample: Name: Grain:	SVC1 A SL-JL-02 Profile P6 P Type 2										
Position: Dist.:	M 667	M 693	M 719	M 744	M 770	M 796	M 821	M 847	M 873	M 924	M 950
SiO ₂	50.78	50.65	54.99	54.80	50.76	52.40	49.16	50.33	51.87	51.05	52.71
Al ₂ O ₃	32.06	32.31	29.52	29.68	32.18	31.47	33.44	32.42	31.30	32.10	30.87
MgO	b.d.l.	b.d.l.	b.d.l.	b.d.l.	b.d.l.	b.d.l.	b.d.l.	b.d.l.	b.d.l.	b.d.l.	b.d.l.
CaO	13.55	13.79	10.53	10.80	13.51	13.04	15.13	14.07	12.72	13.74	12.22
FeO	0.11	0.15	0.18	0.13	0.16	0.16	0.16	0.11	0.12	0.16	0.10
Na ₂ O	3.96	3.75	5.45	5.33	3.79	4.18	2.98	3.66	4.35	3.77	4.57
K ₂ O	0.15	0.15	0.29	0.28	0.16	0.25	0.15	0.14	0.18	0.16	0.20
P ₂ O ₅	0.11	0.15	b.d.l.	0.13	b.d.l.	0.25	b.d.l.	0.23	0.22	0.19	0.11
Total	100.72	100.99	100.99	101.18	100.57	101.80	101.07	100.99	100.79	101.18	100.80
Si	9.18	9.14	9.83	9.77	9.19	9.35	8.90	9.08	9.34	9.18	9.48
Al	6.83	6.87	6.22	6.24	6.86	6.62	7.13	6.90	6.64	6.81	6.54
Mg	b.d.l.	b.d.l.	b.d.l.	b.d.l.	b.d.l.	b.d.l.	b.d.l.	b.d.l.	b.d.l.	b.d.l.	b.d.l.
Ca	2.62	2.66	2.02	2.06	2.62	2.49	2.93	2.72	2.46	2.65	2.35
Fe (ii)	0.02	0.02	0.03	0.02	0.02	0.02	0.02	0.02	0.02	0.02	0.02
Na	1.39	1.31	1.89	1.84	1.33	1.45	1.04	1.28	1.52	1.32	1.59
K	0.03	0.03	0.07	0.06	0.04	0.06	0.03	0.03	0.04	0.04	0.05
P	0.02	0.02	b.d.l.	0.02	0.00	0.04	0.00	0.03	0.03	0.03	0.02
Total	20.09	20.07	20.04	20.03	20.06	20.03	20.07	20.07	20.06	20.05	20.04
An	64.86	66.42	50.80	51.98	65.70	62.38	73.13	67.46	61.18	66.20	58.97
Ab	34.28	32.73	47.55	46.29	33.39	36.20	26.03	31.77	37.82	32.90	39.88
Or	0.86	0.85	1.65	1.63	0.91	1.42	0.85	0.78	1.00	0.91	1.16

Group: Sample: Name: Grain:	SVC1 A SL-JL-02 Profile P6 P Type 2								SVC1 A SL-JL-02 Profile P7 MP Type 2		
Position: Dist.:	M 975	M 1001	M 1027	M 1078	M 1104	M 1129	M 1155	rim 1181	C 0	C 27	C 55
SiO ₂	51.81	50.44	49.00	54.15	49.41	48.96	47.37	49.80	46.31	45.16	46.86
Al ₂ O ₃	31.52	32.94	33.34	30.34	32.90	33.39	34.93	32.91	34.60	35.56	34.61
MgO	b.d.l.	b.d.l.	b.d.l.	b.d.l.	b.d.l.	b.d.l.	b.d.l.	b.d.l.	b.d.l.	b.d.l.	b.d.l.
CaO	13.05	14.38	15.07	11.24	14.65	15.18	16.60	14.59	16.61	17.60	16.30
FeO	0.13	0.17	0.12	0.18	0.16	0.13	0.16	0.12	0.10	0.12	0.15
Na ₂ O	4.05	3.33	3.08	5.06	3.25	2.88	2.26	3.25	2.30	1.70	2.47
K ₂ O	0.17	0.13	0.12	0.28	0.14	0.13	0.08	0.16	0.07	0.04	0.08
P ₂ O ₅	0.12	0.40	0.33	b.d.l.	0.08	0.14	0.35	0.09	0.18	0.35	b.d.l.
Total	100.86	101.73	101.07	101.26	100.61	100.81	101.78	100.86	100.19	100.50	100.46
Si	9.33	9.03	8.86	9.67	8.97	8.88	8.54	9.01	8.50	8.28	8.57
Al	6.69	6.95	7.11	6.38	7.04	7.13	7.43	7.02	7.48	7.68	7.46
Mg	b.d.l.	b.d.l.	b.d.l.	b.d.l.	b.d.l.	b.d.l.	b.d.l.	b.d.l.	b.d.l.	b.d.l.	b.d.l.
Ca	2.52	2.76	2.92	2.15	2.85	2.95	3.21	2.83	3.27	3.46	3.20
Fe (ii)	0.02	0.03	0.02	0.03	0.02	0.02	0.02	0.02	0.02	0.02	0.02
Na	1.41	1.16	1.08	1.75	1.14	1.01	0.79	1.14	0.82	0.60	0.88
K	0.04	0.03	0.03	0.06	0.03	0.03	0.02	0.04	0.02	0.01	0.02
P	0.02	0.06	0.05	0.00	0.01	0.02	0.05	0.01	0.03	0.05	b.d.l.
Total	20.03	20.00	20.06	20.04	20.08	20.05	20.07	20.05	20.13	20.10	20.15
An	63.38	69.95	72.50	54.25	70.81	73.86	79.81	70.64	79.65	84.93	78.10
Ab	35.63	29.30	26.81	44.14	28.39	25.39	19.70	28.47	19.96	14.83	21.45
Or	0.99	0.74	0.69	1.61	0.80	0.74	0.48	0.90	0.39	0.23	0.45

Group: Sample: Name: Grain:	SVC1 A SL-JL-02 Profile P7 MP Type 2						SVC1 A SL-83-17 Profile C1-P11 P Type 1				
Position: Dist.:	C 82	M 109	M 137	M 164	M 191	R 219	C 0	C 25	C 75	C 100	C 125
SiO ₂	46.28	49.35	50.53	52.59	50.78	52.65	47.45	47.72	48.18	48.17	48.18
Al ₂ O ₃	34.85	32.67	32.17	30.48	31.91	30.73	33.67	33.33	33.50	33.23	33.38
MgO	b.d.l.	b.d.l.	b.d.l.	b.d.l.	b.d.l.	b.d.l.	b.d.l.	b.d.l.	b.d.l.	b.d.l.	b.d.l.
CaO	16.90	14.31	13.75	11.88	13.24	11.65	17.10	16.82	16.68	16.60	16.69
FeO	0.12	0.13	0.17	0.11	0.15	0.14	0.14	0.18	0.15	0.11	0.17
Na ₂ O	2.09	3.44	3.67	4.85	4.01	4.87	1.92	2.12	2.23	2.23	2.11
K ₂ O	0.06	0.13	0.18	0.21	0.18	0.28	0.06	0.06	0.07	0.07	0.07
P ₂ O ₅	0.37	0.37	0.20	0.16	0.09	0.41	n.a.	n.a.	n.a.	n.a.	n.a.
Total	100.67	100.40	100.68	100.31	100.37	100.74	100.35	100.24	100.82	100.45	100.67
Si	8.45	8.97	9.14	9.50	9.21	9.47	8.69	8.74	8.77	8.80	8.78
Al	7.50	7.00	6.86	6.49	6.82	6.51	7.26	7.20	7.19	7.15	7.17
Mg	b.d.l.	b.d.l.	b.d.l.	b.d.l.	b.d.l.	b.d.l.	b.d.l.	b.d.l.	b.d.l.	b.d.l.	b.d.l.
Ca	3.31	2.79	2.66	2.30	2.57	2.24	3.35	3.30	3.25	3.25	3.26
Fe (ii)	0.02	0.02	0.03	0.02	0.02	0.02	0.02	0.03	0.02	0.02	0.03
Na	0.74	1.21	1.29	1.70	1.41	1.70	0.68	0.75	0.79	0.79	0.75
K	0.02	0.03	0.04	0.05	0.04	0.07	0.01	0.01	0.02	0.02	0.02
P	0.06	0.06	0.03	0.02	0.01	0.06	n.a.	n.a.	n.a.	n.a.	n.a.
Total	20.09	20.07	20.05	20.09	20.09	20.07	20.03	20.04	20.04	20.03	20.01
An	81.41	69.15	66.75	56.82	63.96	56.01	82.81	81.18	80.19	80.13	81.03
Ab	18.22	30.11	32.21	41.98	35.03	42.37	16.86	18.49	19.40	19.46	18.54
Or	0.37	0.74	1.04	1.20	1.01	1.62	0.33	0.33	0.42	0.41	0.43

Group: B = basalt; BA = basaltic andesite; A = andesite; D = dacite; R = rhyolite; Opx/Cgt-SVC 2, 3 = orthopyroxene/cummingtonite-bearing SVC 2; 3 lavas; **Grain:** P = phenocryst; MC = microphenocryst; G = groundmass; C = core; INC = inclusion (mineral included within is stated in parentheses); **Position:** C = core; M = mantle; R = rim, osci. = oscillatory; **Other:** UNZ = unzoned; Dist. = distance from the core (µm); An = anorthite; Ab = albite; Or = orthoclase.

Table G.1. (continued).

Group:	SVC1 A										
Sample:	SL-83-17										
Name:	Profile C1-Pl1										
Grain:	P Type 1										
Position:	C	C	C	C	C	C	C	C	C	C	C
Dist.:	176	201	276	301	351	376	401	426	502	527	552
SiO ₂	47.78	47.45	47.26	48.90	48.89	49.05	49.51	48.88	48.19	48.44	49.20
Al ₂ O ₃	33.41	33.62	33.83	32.58	32.78	32.73	32.47	32.44	33.26	32.99	32.48
MgO	b.d.l.	b.d.l.	b.d.l.	b.d.l.	b.d.l.	b.d.l.	0.04	b.d.l.	b.d.l.	b.d.l.	b.d.l.
CaO	16.73	17.00	17.08	15.99	15.99	15.87	15.65	15.74	16.52	16.17	15.68
FeO	0.20	0.15	0.19	0.18	0.12	0.13	0.11	0.15	0.13	0.17	0.18
Na ₂ O	2.14	1.97	1.91	2.71	2.53	2.65	2.85	2.68	2.29	2.46	2.73
K ₂ O	0.08	0.06	0.05	0.11	0.11	0.11	0.11	0.11	0.08	0.05	0.08
P ₂ O ₅	n.a.	n.a.	n.a.	n.a.	n.a.	n.a.	n.a.	n.a.	n.a.	n.a.	n.a.
Total	100.38	100.27	100.32	100.52	100.46	100.57	100.79	100.05	100.55	100.29	100.36
Si	8.74	8.69	8.66	8.92	8.91	8.93	8.99	8.95	8.79	8.85	8.97
Al	7.20	7.26	7.30	7.00	7.04	7.02	6.95	7.00	7.15	7.11	6.98
Mg	b.d.l.	b.d.l.	b.d.l.	b.d.l.	b.d.l.	b.d.l.	0.01	b.d.l.	b.d.l.	b.d.l.	b.d.l.
Ca	3.28	3.34	3.35	3.12	3.12	3.09	3.04	3.09	3.23	3.17	3.06
Fe (ii)	0.03	0.02	0.03	0.03	0.02	0.02	0.02	0.02	0.02	0.03	0.03
Na	0.76	0.70	0.68	0.96	0.89	0.93	1.00	0.95	0.81	0.87	0.97
K	0.02	0.01	0.01	0.03	0.02	0.03	0.02	0.03	0.02	0.01	0.02
P	n.a.	n.a.	n.a.	n.a.	n.a.	n.a.	n.a.	n.a.	n.a.	n.a.	n.a.
Total	20.04	20.03	20.04	20.07	20.02	20.04	20.05	20.04	20.04	20.04	20.03
An	80.83	82.35	82.94	76.05	77.28	76.33	74.75	75.97	79.58	78.20	75.67
Ab	18.69	17.31	16.77	23.34	22.11	23.04	24.65	23.39	19.96	21.54	23.86
Or	0.48	0.34	0.30	0.62	0.61	0.63	0.60	0.64	0.46	0.26	0.47

Group:	SVC1 A										
Sample:	SL-83-17										
Name:	Profile C1-Pl1										
Grain:	P Type 1										
Position:	C	C	C	C	C	C	An-rich M	An-rich M	An-rich M	An-rich M	An-rich M
Dist.:	577	627	652	677	702	727	752	803	828	853	878
SiO ₂	51.82	49.17	48.32	48.49	48.27	48.06	48.15	53.44	47.44	47.81	53.08
Al ₂ O ₃	30.96	32.42	33.07	33.05	33.36	33.28	32.84	29.88	33.66	33.41	30.54
MgO	b.d.l.	b.d.l.	b.d.l.	b.d.l.	b.d.l.	b.d.l.	b.d.l.	b.d.l.	b.d.l.	b.d.l.	0.03
CaO	14.91	15.52	16.47	16.18	16.62	16.50	16.43	12.37	16.92	16.75	12.54
FeO	0.15	0.16	0.13	0.15	0.17	0.17	0.17	0.17	0.17	0.15	0.17
Na ₂ O	2.69	2.75	2.29	2.42	2.32	2.26	2.33	4.56	1.98	2.14	4.23
K ₂ O	0.35	0.13	0.09	0.08	0.09	0.07	0.10	0.25	0.06	0.06	0.20
P ₂ O ₅	n.a.	n.a.	n.a.	n.a.	n.a.	n.a.	n.a.	n.a.	n.a.	n.a.	n.a.
Total	100.94	100.20	100.38	100.40	100.87	100.36	100.05	100.69	100.28	100.39	100.80
Si	9.35	8.98	8.83	8.85	8.79	8.79	8.83	9.62	8.69	8.74	9.54
Al	6.58	6.98	7.12	7.11	7.16	7.17	7.10	6.34	7.27	7.20	6.47
Mg	b.d.l.	b.d.l.	b.d.l.	b.d.l.	b.d.l.	b.d.l.	b.d.l.	b.d.l.	b.d.l.	b.d.l.	0.01
Ca	2.88	3.04	3.22	3.16	3.24	3.23	3.23	2.39	3.32	3.28	2.42
Fe (ii)	0.02	0.02	0.02	0.02	0.03	0.03	0.03	0.03	0.03	0.02	0.03
Na	0.94	0.97	0.81	0.86	0.82	0.80	0.83	1.59	0.70	0.76	1.47
K	0.08	0.03	0.02	0.02	0.02	0.02	0.02	0.06	0.01	0.01	0.05
P	n.a.	n.a.	n.a.	n.a.	n.a.	n.a.	n.a.	n.a.	n.a.	n.a.	n.a.
Total	19.87	20.03	20.03	20.03	20.06	20.04	20.04	20.03	20.03	20.04	19.98
An	73.85	75.15	79.46	78.33	79.39	79.80	79.14	59.12	82.23	80.96	61.40
Ab	24.08	24.09	20.01	21.18	20.07	19.80	20.30	39.45	17.42	18.68	37.44
Or	2.07	0.76	0.54	0.49	0.54	0.39	0.56	1.43	0.35	0.36	1.16

Group:	SVC1 A		SVC1 A				SVC1 A			
Sample:	SL-83-17		SL-83-17				SL-83-17			
Name:	Profile C1-Pl1		Profile C3-Pl2				Profile C4-Pl1			
Grain:	P Type 1		P Indiff.				P Type 1			
Position:	An-rich									
Dist.:	M	R	C	C	M	M	R	C	C	C
	903	978	0	27	55	110	192	0	27	53
SiO ₂	48.37	56.56	50.55	50.07	50.43	52.55	53.67	47.32	48.44	48.16
Al ₂ O ₃	33.13	27.64	31.24	31.55	31.31	30.65	29.25	33.27	32.55	32.86
MgO	b.d.l.	b.d.l.	b.d.l.	b.d.l.	b.d.l.	b.d.l.	b.d.l.	b.d.l.	b.d.l.	b.d.l.
CaO	16.39	9.91	14.61	14.83	14.43	13.14	12.04	16.90	16.07	16.33
FeO	0.17	0.19	0.18	0.14	0.15	0.13	0.25	0.12	0.18	0.13
Na ₂ O	2.35	5.83	3.43	3.23	3.42	4.17	4.76	2.04	2.53	2.30
K ₂ O	0.11	0.46	0.13	0.14	0.13	0.18	0.24	0.05	0.10	0.07
P ₂ O ₅	n.a.	n.a.	n.a.	n.a.	n.a.	n.a.	n.a.	n.a.	n.a.	n.a.
Total	100.54	100.60	100.20	100.00	99.90	100.85	100.27	99.73	99.90	99.87
Si	8.83	10.13	9.21	9.15	9.21	9.47	9.70	8.72	8.89	8.84
Al	7.12	5.83	6.71	6.79	6.74	6.51	6.23	7.22	7.04	7.11
Mg	b.d.l.	b.d.l.	b.d.l.	b.d.l.	b.d.l.	b.d.l.	b.d.l.	b.d.l.	b.d.l.	b.d.l.
Ca	3.20	1.90	2.85	2.90	2.82	2.54	2.33	3.34	3.16	3.21
Fe (ii)	0.03	0.03	0.03	0.02	0.02	0.02	0.04	0.02	0.03	0.02
Na	0.83	2.03	1.21	1.15	1.21	1.46	1.67	0.73	0.90	0.82
K	0.03	0.10	0.03	0.03	0.03	0.04	0.05	0.01	0.02	0.02
P	n.a.	n.a.	n.a.	n.a.	n.a.	n.a.	n.a.	n.a.	n.a.	n.a.
Total	20.04	20.02	20.05	20.04	20.04	20.03	20.04	20.04	20.05	20.02
An	78.89	47.16	69.63	71.15	69.43	62.84	57.50	81.81	77.39	79.35
Ab	20.48	50.23	29.60	28.08	29.82	36.12	41.16	17.88	22.06	20.26
Or	0.63	2.60	0.76	0.77	0.75	1.03	1.34	0.30	0.55	0.39

Group: B = basalt; BA = basaltic andesite; A = andesite; D = dacite; R = rhyolite; Opx/Cgt-SVC 2, 3 = orthopyroxene/cummingtonite-bearing SVC 2; 3 lavas; **Grain:** P = phenocryst; MC = microphenocryst; G = groundmass; C = core; INC = inclusion (mineral included within is stated in parentheses); **Position:** C = core; M = mantle; R = rim, osci. = oscillatory; **Other:** UNZ = unzoned; Dist. = distance from the core (µm); An = anorthite; Ab = albite; Or = orthoclase.

Table G.1. (continued).

Group:	SVC1 A										
Sample:	SL-83-17										
Name:	Profile C4-Pl1										
Grain:	P Type 1										
Position:	C	C	C	C	M	M	M	M	M	M	M
Dist.:	107	134	160	187	214	240	267	294	321	347	374
SiO ₂	48.34	48.79	48.62	49.33	50.78	52.28	52.26	51.98	49.65	51.23	54.29
Al ₂ O ₃	32.74	32.22	32.40	31.98	31.01	29.94	30.63	30.30	31.70	30.75	28.68
MgO	b.d.l.	b.d.l.	b.d.l.	0.04	b.d.l.	b.d.l.	b.d.l.	0.06	b.d.l.	b.d.l.	b.d.l.
CaO	16.29	15.71	16.02	15.25	14.16	13.00	12.94	13.23	15.22	13.90	11.48
FeO	0.20	0.15	0.13	0.16	0.12	0.13	0.14	0.12	0.15	0.19	0.16
Na ₂ O	2.42	2.54	2.60	2.95	3.58	4.27	4.21	4.03	3.01	3.71	5.12
K ₂ O	0.09	0.12	0.08	0.10	0.17	0.19	0.18	0.16	0.11	0.16	0.22
P ₂ O ₅	n.a.	n.a.	n.a.	n.a.	n.a.	n.a.	n.a.	n.a.	n.a.	n.a.	n.a.
Total	100.12	99.55	99.87	99.84	99.84	99.83	100.42	99.90	99.86	99.98	99.99
Si	8.86	8.97	8.92	9.04	9.27	9.51	9.45	9.46	9.09	9.33	9.82
Al	7.07	6.98	7.01	6.90	6.67	6.42	6.53	6.49	6.84	6.60	6.11
Mg	b.d.l.	b.d.l.	b.d.l.	0.01	b.d.l.	b.d.l.	b.d.l.	b.d.l.	b.d.l.	b.d.l.	b.d.l.
Ca	3.20	3.09	3.15	2.99	2.77	2.53	2.51	2.58	2.99	2.71	2.22
Fe (ii)	0.03	0.02	0.02	0.02	0.02	0.02	0.02	0.02	0.02	0.03	0.02
Na	0.86	0.91	0.93	1.05	1.27	1.51	1.48	1.42	1.07	1.31	1.80
K	0.02	0.03	0.02	0.02	0.04	0.04	0.04	0.04	0.03	0.04	0.05
P	n.a.	n.a.	n.a.	n.a.	n.a.	n.a.	n.a.	n.a.	n.a.	n.a.	n.a.
Total	20.05	20.01	20.04	20.05	20.04	20.05	20.04	20.02	20.03	20.04	20.04
An	78.46	76.82	76.94	73.64	67.96	62.07	62.27	63.88	73.21	66.81	54.65
Ab	21.05	22.50	22.63	25.82	31.08	36.86	36.69	35.21	26.16	32.25	44.09
Or	0.49	0.68	0.43	0.55	0.97	1.07	1.04	0.91	0.63	0.94	1.26

Group:	SVC1 A										
Sample:	SL-83-17										
Name:	Profile C5 -Pl1										
Grain:	P Type 5										
Position:	C	An-rich	An-rich	An-rich	An-rich	An-rich	An-rich	An-rich	An-rich	An-rich	An-rich
Dist.:	0	M 25	M 100	M 125	M 175	M 225	M 250	M 275	M 350	M 400	M 425
SiO ₂	53.90	52.03	48.39	52.25	49.26	48.00	48.42	47.51	46.82	46.59	47.24
Al ₂ O ₃	28.44	29.60	31.69	29.52	31.50	32.17	32.12	33.25	33.14	34.73	32.78
MgO	b.d.l.	b.d.l.	b.d.l.	b.d.l.	b.d.l.	b.d.l.	b.d.l.	b.d.l.	b.d.l.	b.d.l.	b.d.l.
CaO	11.38	13.41	15.38	12.48	15.24	16.12	16.06	16.50	17.17	17.52	16.72
FeO	0.16	0.18	0.13	0.12	0.15	0.13	0.13	0.12	0.13	0.14	0.06
Na ₂ O	5.22	4.02	2.98	4.44	3.02	2.53	2.57	2.28	1.91	1.79	2.17
K ₂ O	0.29	0.21	0.15	0.26	0.14	0.08	0.09	0.08	0.05	0.06	0.08
P ₂ O ₅	n.a.	n.a.	n.a.	n.a.	n.a.	n.a.	n.a.	n.a.	n.a.	n.a.	n.a.
Total	99.45	99.48	98.81	99.11	99.35	99.07	99.43	99.77	99.22	100.84	99.06
Si	9.82	9.52	8.98	9.57	9.07	8.89	8.93	8.74	8.68	8.51	8.76
Al	6.10	6.38	6.93	6.37	6.84	7.02	6.98	7.21	7.24	7.47	7.16
Mg	b.d.l.	b.d.l.	b.d.l.	b.d.l.	b.d.l.	b.d.l.	b.d.l.	b.d.l.	b.d.l.	b.d.l.	b.d.l.
Ca	2.22	2.63	3.06	2.45	3.01	3.20	3.17	3.25	3.41	3.43	3.32
Fe (ii)	0.02	0.03	0.02	0.02	0.02	0.02	0.02	0.02	0.02	0.02	0.01
Na	1.84	1.43	1.07	1.58	1.08	0.91	0.92	0.81	0.69	0.63	0.78
K	0.07	0.05	0.04	0.06	0.03	0.02	0.02	0.02	0.01	0.01	0.02
P	n.a.	n.a.	n.a.	n.a.	n.a.	n.a.	n.a.	n.a.	n.a.	n.a.	n.a.
Total	20.08	20.03	20.11	20.06	20.06	20.06	20.05	20.07	20.05	20.08	20.06
An	53.75	64.03	73.39	59.91	73.02	77.52	77.12	79.59	82.99	84.12	80.63
Ab	44.61	34.76	25.75	38.62	26.19	22.00	22.35	19.93	16.74	15.56	18.89
Or	1.64	1.21	0.87	1.47	0.79	0.47	0.54	0.48	0.27	0.32	0.48

Group:	SVC1 A										
Sample:	SL-83-17										
Name:	Profile C5 -Pl1										
Grain:	P Type 5										
Position:	An-rich	An-rich	An-rich	An-rich	An-rich	An-rich	An-poor	An-poor	An-poor	An-poor	An-poor
Dist.:	M 450	M 475	M 500	M 525	M 575	M 600	M 625	M 650	M 675	M 700	M 725
SiO ₂	47.34	46.88	47.54	47.12	48.09	51.92	54.16	54.38	54.66	54.00	53.13
Al ₂ O ₃	32.64	32.68	32.69	32.99	32.43	30.17	28.00	28.16	29.34	27.82	28.87
MgO	b.d.l.	b.d.l.	b.d.l.	b.d.l.	b.d.l.	b.d.l.	b.d.l.	b.d.l.	b.d.l.	b.d.l.	b.d.l.
CaO	16.71	16.68	16.76	16.58	16.35	13.48	11.27	11.16	10.86	10.91	11.91
FeO	0.14	0.10	0.09	0.14	0.15	0.13	0.12	0.14	0.12	0.15	0.12
Na ₂ O	2.19	2.19	2.11	2.05	2.46	3.99	5.14	5.16	5.55	5.26	4.88
K ₂ O	0.09	0.10	0.08	0.09	0.10	0.19	0.30	0.29	0.30	0.31	0.26
P ₂ O ₅	n.a.	n.a.	n.a.	n.a.	n.a.	n.a.	n.a.	n.a.	n.a.	n.a.	n.a.
Total	99.10	98.66	99.30	98.99	99.59	99.92	99.03	99.33	100.84	98.46	99.22
Si	8.78	8.74	8.79	8.74	8.86	9.45	9.89	9.90	9.80	9.91	9.71
Al	7.13	7.18	7.12	7.21	7.04	6.47	6.03	6.04	6.20	6.02	6.22
Mg	b.d.l.	b.d.l.	b.d.l.	b.d.l.	b.d.l.	b.d.l.	b.d.l.	b.d.l.	b.d.l.	b.d.l.	b.d.l.
Ca	3.32	3.33	3.32	3.30	3.23	2.63	2.21	2.18	2.09	2.15	2.33
Fe (ii)	0.02	0.02	0.01	0.02	0.02	0.02	0.02	0.02	0.02	0.02	0.02
Na	0.79	0.79	0.76	0.74	0.88	1.41	1.82	1.82	1.93	1.87	1.73
K	0.02	0.02	0.02	0.02	0.02	0.05	0.07	0.07	0.07	0.07	0.06
P	n.a.	n.a.	n.a.	n.a.	n.a.	n.a.	n.a.	n.a.	n.a.	n.a.	n.a.
Total	20.06	20.08	20.03	20.03	20.07	20.04	20.04	20.03	20.10	20.05	20.08
An	80.39	80.35	81.04	81.28	78.15	64.41	53.85	53.54	51.10	52.44	56.55
Ab	19.11	19.09	18.49	18.21	21.31	34.48	44.45	44.82	47.25	45.78	41.96
Or	0.51	0.56	0.46	0.51	0.55	1.11	1.71	1.64	1.66	1.78	1.48

Group: B = basalt; BA = basaltic andesite; A = andesite; D = dacite; R = rhyolite; Opx/Cgt-SVC 2, 3 = orthopyroxene/cummingtonite-bearing SVC 2; 3 lavas; **Grain:** P = phenocryst; MC = microphenocryst; G = groundmass; C = core; INC = inclusion (mineral included within is stated in parentheses); **Position:** C = core; M = mantle; R = rim, osci. = oscillatory; **Other:** UNZ = unzoned; Dist. = distance from the core (µm); An = anorthite; Ab = albite; Or = orthoclase.

Table G.1. (continued).

Group: Sample: Name: Grain:	SVC1 A SL-83-17 Profile C5 -P1 P Type 5									SVC1 D SL-JL-23 Profile P1 P Type 5	
Position: Dist.:	An-poor M 750	An-poor M 800	An-poor M 825	An-poor M 850	An-poor M 875	An-poor M 900	An-poor M 925	An-poor M 950	R 975	An-rich M 0	An-rich M 27
SiO ₂	53.45	54.01	51.48	54.16	54.47	54.12	51.15	54.63	52.79	50.14	48.55
Al ₂ O ₃	29.42	28.63	29.88	28.40	27.91	28.24	30.35	27.95	29.75	32.28	32.58
MgO	b.d.l.	b.d.l.	b.d.l.	b.d.l.	b.d.l.	b.d.l.	b.d.l.	b.d.l.	b.d.l.	b.d.l.	b.d.l.
CaO	12.35	11.48	13.08	11.38	10.87	11.08	13.77	10.83	12.45	14.62	15.40
FeO	0.12	0.13	0.13	0.12	0.14	0.13	0.12	0.18	0.27	0.15	0.16
Na ₂ O	4.65	5.08	4.22	5.15	5.31	5.30	3.79	5.42	4.52	3.48	2.78
K ₂ O	0.24	0.27	0.20	0.28	0.32	0.29	0.16	0.33	0.20	0.15	0.11
P ₂ O ₅	n.a.	n.a.	n.a.	n.a.	n.a.	n.a.	n.a.	n.a.	n.a.	0.32	0.26
Total	100.25	99.61	99.04	99.52	99.06	99.19	99.40	99.35	100.01	101.17	99.86
Si	9.67	9.81	9.46	9.85	9.93	9.87	9.37	9.94	9.58	9.05	8.90
Al	6.27	6.13	6.47	6.08	6.00	6.07	6.55	5.99	6.36	6.87	7.03
Mg	b.d.l.	b.d.l.	b.d.l.	b.d.l.	b.d.l.	b.d.l.	b.d.l.	b.d.l.	b.d.l.	b.d.l.	b.d.l.
Ca	2.39	2.23	2.57	2.22	2.12	2.16	2.70	2.11	2.42	2.83	3.02
Fe (ii)	0.02	0.02	0.02	0.02	0.02	0.02	0.02	0.03	0.04	0.02	0.02
Na	1.63	1.79	1.50	1.82	1.88	1.87	1.35	1.91	1.59	1.22	0.99
K	0.06	0.06	0.05	0.07	0.07	0.07	0.04	0.08	0.05	0.03	0.03
P	n.a.	n.a.	n.a.	n.a.	n.a.	n.a.	n.a.	n.a.	n.a.	0.05	0.04
Total	20.04	20.05	20.08	20.05	20.04	20.07	20.04	20.06	20.05	20.07	20.03
An	58.65	54.67	62.40	54.09	52.13	52.71	66.09	51.49	59.64	69.35	74.89
Ab	39.98	43.77	36.46	44.30	46.05	45.63	32.96	46.66	39.20	29.83	24.49
Or	1.37	1.56	1.14	1.61	1.82	1.66	0.94	1.85	1.15	0.82	0.63

Group: Sample: Name: Grain:	SVC1 D SL-JL-23 Profile P1 P Type 5										
Position: Dist.:	C 53	C 80	C 107	C 133	C 186	C 293	Osci. M 320	Osci. M 346	Osci. M 373	Osci. M 400	Osci. M 426
SiO ₂	54.05	52.45	55.41	52.99	53.93	53.63	49.18	53.09	52.97	49.24	53.77
Al ₂ O ₃	29.24	30.42	28.90	29.84	29.49	29.54	32.66	29.81	29.86	32.74	29.93
MgO	b.d.l.	b.d.l.	b.d.l.	b.d.l.	b.d.l.	b.d.l.	b.d.l.	b.d.l.	b.d.l.	b.d.l.	b.d.l.
CaO	11.22	12.68	10.60	12.02	11.58	11.76	15.15	12.06	12.22	15.15	12.03
FeO	0.16	0.13	0.09	0.09	0.14	0.14	0.14	0.12	0.13	0.15	0.10
Na ₂ O	5.12	4.42	5.44	4.70	4.86	4.82	3.17	4.61	4.65	2.96	4.75
K ₂ O	0.28	0.21	0.32	0.27	0.37	0.31	0.13	0.23	0.22	0.11	0.22
P ₂ O ₅	0.19	0.26	0.04	0.11	0.17	0.09	0.39	0.27	0.14	0.39	0.24
Total	100.28	100.60	100.82	100.02	100.54	100.30	100.81	100.19	100.15	100.69	101.03
Si	9.74	9.46	9.91	9.60	9.70	9.68	8.92	9.59	9.59	8.93	9.63
Al	6.21	6.47	6.09	6.37	6.25	6.28	6.98	6.35	6.37	7.00	6.32
Mg	b.d.l.	b.d.l.	b.d.l.	b.d.l.	b.d.l.	b.d.l.	b.d.l.	b.d.l.	b.d.l.	b.d.l.	b.d.l.
Ca	2.17	2.45	2.03	2.33	2.23	2.27	2.94	2.33	2.37	2.94	2.31
Fe (ii)	0.02	0.02	0.01	0.01	0.02	0.02	0.02	0.02	0.02	0.02	0.02
Na	1.79	1.54	1.89	1.65	1.70	1.69	1.11	1.62	1.63	1.04	1.65
K	0.06	0.05	0.07	0.06	0.08	0.07	0.03	0.05	0.05	0.03	0.05
P	0.03	0.04	0.01	0.02	0.03	0.01	0.06	0.04	0.02	0.06	0.04
Total	20.03	20.04	20.01	20.04	20.02	20.03	20.07	20.00	20.04	20.01	20.00
An	53.90	60.59	50.89	57.63	55.63	56.40	72.04	58.34	58.49	73.38	57.58
Ab	44.49	38.20	47.29	40.80	42.27	41.84	27.24	40.36	40.28	25.96	41.15
Or	1.61	1.21	1.82	1.57	2.09	1.76	0.72	1.30	1.23	0.65	1.28

Group: Sample: Name: Grain:	SVC1 D SL-JL-23 Profile P1 P Type 5			SVC1 D SL-JL-23 Profile P2 P Type 1							
Position: Dist.:	Osci. M 453	Osci. M 479	Osci. R 506	C 0	C 27	C 80	C 214	C 241	C 268	C 295	M 321
SiO ₂	52.43	53.40	51.68	47.28	47.79	46.62	48.25	47.89	48.69	48.62	52.25
Al ₂ O ₃	30.15	29.24	30.90	34.07	33.89	35.19	33.43	33.45	33.04	33.56	30.53
MgO	b.d.l.	b.d.l.	b.d.l.	b.d.l.	b.d.l.	b.d.l.	b.d.l.	b.d.l.	b.d.l.	b.d.l.	b.d.l.
CaO	12.70	11.79	13.29	16.86	16.31	15.72	16.16	16.16	15.77	15.76	12.77
FeO	0.12	0.12	0.14	0.13	0.12	0.18	0.17	0.15	0.15	0.12	0.17
Na ₂ O	4.38	4.89	4.16	2.17	2.38	2.29	2.61	2.60	2.72	2.82	4.33
K ₂ O	0.20	0.26	0.22	0.09	0.09	0.08	0.09	0.09	0.10	0.10	0.19
P ₂ O ₅	0.18	b.d.l.	0.25	b.d.l.	0.26	0.13	0.38	0.20	0.25	0.29	0.40
Total	100.17	99.81	100.64	100.53	100.81	100.25	101.05	100.55	100.74	101.25	100.63
Si	9.50	9.69	9.34	8.65	8.69	8.52	8.75	8.74	8.85	8.79	9.42
Al	6.44	6.25	6.58	7.34	7.26	7.58	7.15	7.19	7.08	7.15	6.49
Mg	b.d.l.	b.d.l.	b.d.l.	b.d.l.	b.d.l.	b.d.l.	b.d.l.	b.d.l.	b.d.l.	b.d.l.	b.d.l.
Ca	2.47	2.29	2.57	3.30	3.18	3.08	3.14	3.16	3.07	3.05	2.47
Fe (iii)	0.02	0.02	0.02	0.02	0.02	0.03	0.03	0.02	0.02	0.02	0.02
Na	1.54	1.72	1.46	0.77	0.84	0.81	0.92	0.92	0.96	0.99	1.51
K	0.05	0.06	0.05	0.02	0.02	0.02	0.02	0.02	0.02	0.02	0.04
P	0.03	0.01	0.04	b.d.l.	0.04	0.02	0.06	0.03	0.04	0.04	0.06
Total	20.03	20.05	20.06	20.09	20.05	20.07	20.06	20.09	20.04	20.07	20.02
An	60.90	56.29	63.07	80.67	78.67	78.74	76.97	77.02	75.79	75.10	61.30
Ab	37.98	42.26	35.69	18.82	20.82	20.79	22.53	22.45	23.62	24.33	37.62
Or	1.12	1.45	1.23	0.50	0.51	0.47	0.51	0.52	0.59	0.57	1.08

Group: B = basalt; BA = basaltic andesite; A = andesite; D = dacite; R = rhyolite; Opx/Cgt-SVC 2, 3 = orthopyroxene/cummingtonite-bearing SVC 2; 3 lavas; **Grain:** P = phenocryst; MC = microphenocryst; G = groundmass; C = core; INC = inclusion (mineral included within is stated in parentheses); **Position:** C = core; M = mantle; R = rim, osci. = oscillatory; **Other:** UNZ = unzoned; Dist. = distance from the core (µm); An = anorthite; Ab = albite; Or = orthoclase.

Table G.1. (continued).

Group: Sample: Name: Grain:	SVC1 D SL-JL-23 Profile P2 P Type 1					SVC1 D SL-JL-23 Profile P3 MP Type 2				SVC1 D SL-JL-23 Profile P4 P Type 2	
Position: Dist.:	M 348	M 375	M 402	M 428	M 455	C 0	M 30	M 60	R 90	C 0	C 28
SiO ₂	51.69	53.04	54.25	53.63	50.79	45.67	48.25	52.45	52.12	43.74	43.77
Al ₂ O ₃	31.01	30.17	29.58	29.33	31.24	35.17	33.06	29.79	29.87	36.07	36.04
MgO	b.d.l.	b.d.l.	b.d.l.	b.d.l.	b.d.l.	b.d.l.	b.d.l.	b.d.l.	b.d.l.	b.d.l.	b.d.l.
CaO	13.11	12.46	11.55	11.73	13.49	18.09	15.70	12.43	12.01	19.43	19.46
FeO	0.16	0.12	0.14	0.12	0.19	0.10	0.17	0.15	0.23	0.17	0.11
Na ₂ O	3.99	4.56	5.08	4.99	4.00	1.43	2.80	4.56	4.48	0.69	0.70
K ₂ O	0.16	0.19	0.24	0.25	0.20	0.03	0.10	0.23	0.35	0.01	0.01
P ₂ O ₅	0.35	0.16	b.d.l.	0.21	0.07	0.32	0.19	0.15	0.21	0.36	0.32
Total	100.50	100.72	100.67	100.26	99.97	100.84	100.25	99.76	99.27	100.43	100.40
Si	9.34	9.55	9.75	9.68	9.26	8.35	8.82	9.54	9.52	8.06	8.07
Al	6.60	6.40	6.27	6.24	6.71	7.58	7.12	6.39	6.43	7.84	7.83
Mg	b.d.l.	b.d.l.	b.d.l.	b.d.l.	b.d.l.	b.d.l.	b.d.l.	b.d.l.	b.d.l.	b.d.l.	b.d.l.
Ca	2.54	2.40	2.22	2.27	2.63	3.54	3.08	2.42	2.35	3.84	3.84
Fe (ii)	0.02	0.02	0.02	0.02	0.03	0.02	0.03	0.02	0.04	0.03	0.02
Na	1.40	1.59	1.77	1.75	1.41	0.51	0.99	1.61	1.59	0.25	0.25
K	0.04	0.04	0.06	0.06	0.05	0.01	0.02	0.05	0.08	0.00	0.00
P	0.05	0.02	b.d.l.	0.03	0.01	0.05	0.03	0.02	0.03	0.06	0.05
Total	20.00	20.03	20.06	20.05	20.10	20.05	20.08	20.06	20.04	20.06	20.06
An	63.85	59.51	54.94	55.70	64.33	87.30	75.19	59.32	58.50	93.86	93.83
Ab	35.20	39.43	43.71	42.88	34.54	12.53	24.23	39.40	39.44	6.06	6.10
Or	0.95	1.06	1.36	1.42	1.14	0.17	0.58	1.28	2.06	0.08	0.07
Group: Sample: Name: Grain:	SVC1 D SL-JL-23 Profile P4 P Type 2										
Position: Dist.:	C 57	C 85	C 113	C 142	C 170	C 198	C 227	C 255	C 312	C 340	M 368
SiO ₂	43.84	44.03	43.75	43.76	44.48	44.45	44.25	44.67	44.64	45.07	49.13
Al ₂ O ₃	35.91	36.06	36.16	35.94	35.57	35.60	35.40	35.72	35.30	35.44	32.66
MgO	b.d.l.	b.d.l.	b.d.l.	b.d.l.	b.d.l.	b.d.l.	b.d.l.	b.d.l.	b.d.l.	b.d.l.	b.d.l.
CaO	19.31	19.30	19.54	19.35	18.69	18.97	18.87	18.84	18.50	18.64	15.35
FeO	0.10	0.14	0.11	0.13	0.16	0.09	0.15	0.12	0.18	0.13	0.11
Na ₂ O	0.79	0.74	0.68	0.80	1.08	1.03	1.01	1.03	1.18	1.28	2.98
K ₂ O	0.02	0.01	0.02	0.02	0.02	0.03	0.02	0.02	0.03	0.02	0.11
P ₂ O ₅	0.25	0.28	0.45	0.48	0.18	0.11	0.22	0.15	0.20	0.31	0.18
Total	100.22	100.57	100.73	100.47	100.23	100.29	99.93	100.54	100.04	100.92	100.57
Si	8.10	8.10	8.04	8.06	8.20	8.20	8.19	8.21	8.25	8.25	8.94
Al	7.82	7.82	7.83	7.80	7.73	7.74	7.72	7.74	7.68	7.65	7.00
Mg	b.d.l.	b.d.l.	b.d.l.	b.d.l.	b.d.l.	b.d.l.	b.d.l.	b.d.l.	b.d.l.	b.d.l.	b.d.l.
Ca	3.82	3.80	3.85	3.82	3.69	3.75	3.74	3.71	3.66	3.66	2.99
Fe (ii)	0.02	0.02	0.02	0.02	0.02	0.01	0.02	0.02	0.03	0.02	0.02
Na	0.28	0.26	0.24	0.28	0.38	0.37	0.36	0.37	0.42	0.45	1.05
K	0.00	0.00	0.00	0.00	0.01	0.01	0.01	0.01	0.01	0.00	0.02
P	0.04	0.04	0.07	0.07	0.03	0.02	0.04	0.02	0.03	0.05	0.03
Total	20.08	20.05	20.06	20.07	20.08	20.09	20.08	20.07	20.08	20.08	20.06
An	92.99	93.45	94.01	92.96	90.45	90.93	91.07	90.92	89.47	88.85	73.54
Ab	6.90	6.50	5.88	6.93	9.42	8.91	8.79	8.95	10.33	11.03	25.85
Or	0.10	0.05	0.11	0.10	0.14	0.16	0.14	0.12	0.20	0.12	0.61
Group: Sample: Name: Grain:	SVC1 D SL-JL-23 Profile P4 P Type 2									SVC1 D SL-JL-23 Profile P5 P Type 6	
Position: Dist.:	M 397	M 425	M 453	M 482	M 510	M 538	M 567	M 595	R 623	C 0	C 25
SiO ₂	50.55	54.17	53.33	49.35	49.62	48.08	48.45	51.81	55.80	52.83	54.02
Al ₂ O ₃	31.53	29.34	29.94	32.19	32.20	33.11	33.19	31.10	28.10	29.42	29.01
MgO	b.d.l.	b.d.l.	b.d.l.	b.d.l.	b.d.l.	b.d.l.	b.d.l.	b.d.l.	b.d.l.	b.d.l.	b.d.l.
CaO	13.97	11.46	11.85	14.88	14.73	15.91	15.89	13.14	9.91	11.68	11.06
FeO	0.12	0.18	0.13	0.20	0.17	0.18	0.19	0.16	0.21	0.16	0.15
Na ₂ O	3.77	5.08	4.86	3.21	3.25	2.61	2.66	4.23	5.89	4.98	5.36
K ₂ O	0.14	0.26	0.29	0.15	0.16	0.10	0.13	0.20	0.44	0.22	0.26
P ₂ O ₅	0.15	0.20	0.14	0.32	0.30	0.07	0.24	0.18	0.24	0.23	0.08
Total	100.25	100.70	100.55	100.29	100.39	100.10	100.71	100.82	100.60	99.55	99.92
Si	9.19	9.73	9.61	8.99	9.02	8.81	8.82	9.35	10.00	9.62	9.78
Al	6.76	6.21	6.36	6.91	6.90	7.15	7.12	6.61	5.93	6.31	6.19
Mg	b.d.l.	b.d.l.	b.d.l.	b.d.l.	b.d.l.	b.d.l.	b.d.l.	b.d.l.	b.d.l.	b.d.l.	b.d.l.
Ca	2.72	2.21	2.29	2.91	2.87	3.12	3.10	2.54	1.90	2.28	2.15
Fe (ii)	0.02	0.03	0.02	0.03	0.03	0.03	0.03	0.02	0.03	0.02	0.02
Na	1.33	1.77	1.70	1.13	1.14	0.93	0.94	1.48	2.05	1.76	1.88
K	0.03	0.06	0.07	0.03	0.04	0.02	0.03	0.05	0.10	0.05	0.06
P	0.02	0.03	0.02	0.05	0.05	0.01	0.04	0.03	0.04	0.04	0.01
Total	20.08	20.04	20.06	20.06	20.05	20.08	20.06	20.07	20.05	20.08	20.08
An	66.64	54.65	56.46	71.33	70.84	76.69	76.16	62.45	47.01	55.73	52.50
Ab	32.56	43.85	41.88	27.82	28.24	22.73	23.08	36.43	50.53	43.03	46.03
Or	0.81	1.50	1.66	0.85	0.91	0.58	0.76	1.12	2.46	1.24	1.47

Group: B = basalt; BA = basaltic andesite; A = andesite; D = dacite; R = rhyolite; Opx/Cgt-SVC 2, 3 = orthopyroxene/cummingtonite-bearing SVC 2; 3 lavas; **Grain:** P = phenocryst; MC = microphenocryst; G = groundmass; C = core; INC = inclusion (mineral included within is stated in parentheses); **Position:** C = core; M = mantle; R = rim, osci. = oscillatory; **Other:** UNZ = unzoned; Dist. = distance from the core (µm); An = anorthite; Ab = albite; Or = orthoclase.

Table G.1. (continued).

Group:	SVC1 D										
Sample:	SL-JL-23										
Name:	Profile P5										
Grain:	P Type 6										
Position:	C	C	C	C	M	M	M	M	M	M	M
Dist.:	51	76	101	126	152	177	253	278	303	328	354
SiO ₂	51.71	50.91	51.75	51.59	50.44	51.04	51.49	51.42	49.67	51.36	49.43
Al ₂ O ₃	30.44	30.29	30.11	30.68	31.21	30.93	30.77	29.57	31.39	30.61	31.79
MgO	b.d.l.	b.d.l.	b.d.l.	b.d.l.	b.d.l.	b.d.l.	b.d.l.	b.d.l.	b.d.l.	b.d.l.	b.d.l.
CaO	12.91	12.98	12.84	12.95	13.86	13.42	13.08	12.37	14.26	13.07	14.53
FeO	0.12	0.16	0.10	0.13	0.18	0.11	0.13	0.86	0.12	0.11	0.12
Na ₂ O	4.41	4.39	4.38	4.38	3.76	4.05	4.12	3.74	3.52	4.19	3.40
K ₂ O	0.19	0.21	0.22	0.23	0.19	0.23	0.26	0.28	0.18	0.25	0.17
P ₂ O ₅	0.34	0.35	0.33	0.25	0.38	0.17	0.05	0.07	0.26	0.20	0.08
Total	100.17	99.28	99.72	100.26	100.01	99.93	99.91	98.30	99.44	99.78	99.52
Si	9.38	9.33	9.43	9.36	9.19	9.30	9.37	9.51	9.12	9.36	9.08
Al	6.51	6.55	6.46	6.56	6.70	6.64	6.60	6.44	6.79	6.58	6.88
Mg	b.d.l.	b.d.l.	b.d.l.	b.d.l.	b.d.l.	b.d.l.	b.d.l.	b.d.l.	b.d.l.	b.d.l.	b.d.l.
Ca	2.51	2.55	2.51	2.52	2.71	2.62	2.55	2.45	2.80	2.55	2.86
Fe (ii)	0.02	0.02	0.02	0.02	0.03	0.02	0.02	0.13	0.02	0.02	0.02
Na	1.55	1.56	1.55	1.54	1.33	1.43	1.45	1.34	1.25	1.48	1.21
K	0.04	0.05	0.05	0.05	0.04	0.05	0.06	0.07	0.04	0.06	0.04
P	0.05	0.05	0.05	0.04	0.06	0.03	0.01	0.01	0.04	0.03	0.01
Total	20.08	20.11	20.06	20.10	20.06	20.08	20.07	19.96	20.07	20.07	20.09
An	61.14	61.33	61.04	61.21	66.33	63.86	62.76	63.50	68.43	62.41	69.55
Ab	37.78	37.51	37.73	37.48	32.60	34.85	35.76	34.79	30.53	36.19	29.48
Or	1.07	1.17	1.23	1.31	1.07	1.29	1.48	1.70	1.05	1.40	0.98

Group:	SVC1 D										
Sample:	SL-JL-23										
Name:	Profile P5										
Grain:	P Type 6										
Position:	M	M	M	M	M	M	M	M	M	M	M
Dist.:	379	404	429	455	480	505	530	556	581	606	632
SiO ₂	49.47	47.69	48.90	48.58	48.54	52.99	51.86	52.34	49.50	51.67	50.02
Al ₂ O ₃	31.42	32.75	32.35	32.74	32.50	29.51	29.62	30.17	31.79	30.17	31.61
MgO	b.d.l.	b.d.l.	b.d.l.	b.d.l.	b.d.l.	b.d.l.	b.d.l.	b.d.l.	b.d.l.	0.04	b.d.l.
CaO	14.18	15.64	14.72	15.32	15.29	11.76	12.18	12.22	14.44	12.69	13.97
FeO	0.11	0.10	0.19	0.11	0.12	0.15	0.11	0.14	0.12	0.14	0.13
Na ₂ O	3.48	2.76	3.30	3.01	3.00	4.95	4.67	4.74	3.50	4.43	3.74
K ₂ O	0.19	0.13	0.14	0.13	0.12	0.25	0.24	0.24	0.15	0.21	0.14
P ₂ O ₅	0.12	0.28	0.31	0.39	0.29	0.24	0.27	0.26	0.42	0.42	0.21
Total	98.95	99.32	99.92	100.31	99.82	99.86	98.97	100.10	99.92	99.75	99.81
Si	9.12	8.80	8.95	8.86	8.90	9.62	9.51	9.49	9.04	9.41	9.14
Al	6.83	7.12	6.98	7.04	7.02	6.31	6.40	6.45	6.85	6.47	6.81
Mg	b.d.l.	b.d.l.	b.d.l.	b.d.l.	b.d.l.	b.d.l.	b.d.l.	b.d.l.	b.d.l.	0.01	b.d.l.
Ca	2.80	3.09	2.89	2.99	3.00	2.29	2.39	2.37	2.83	2.47	2.73
Fe (ii)	0.02	0.01	0.03	0.02	0.02	0.02	0.02	0.02	0.02	0.02	0.02
Na	1.24	0.99	1.17	1.07	1.07	1.74	1.66	1.67	1.24	1.56	1.33
K	0.04	0.03	0.03	0.03	0.03	0.06	0.06	0.06	0.03	0.05	0.03
P	0.02	0.04	0.05	0.06	0.04	0.04	0.04	0.04	0.07	0.06	0.03
Total	20.08	20.08	20.09	20.07	20.07	20.07	20.08	20.09	20.07	20.06	20.09
An	68.51	75.22	70.60	73.20	73.30	55.93	58.23	57.95	68.93	60.58	66.82
Ab	30.42	24.05	28.59	26.04	26.03	42.63	40.43	40.67	30.22	38.24	32.41
Or	1.07	0.73	0.81	0.76	0.67	1.44	1.35	1.38	0.85	1.19	0.77

Group:	SVC1 D										
Sample:	SL-JL-23										
Name:	Profile P5										
Grain:	P Type 6										
Position:	M	M	M	M	M	M	M	M	M	M	R
Dist.:	657	682	707	733	758	808	834	859	884	909	935
SiO ₂	53.23	53.60	48.92	52.05	50.90	52.71	53.44	52.12	52.80	51.63	47.19
Al ₂ O ₃	28.80	28.61	32.30	29.89	30.00	29.62	29.17	29.99	29.84	30.32	33.20
MgO	b.d.l.	b.d.l.	b.d.l.	b.d.l.	b.d.l.	b.d.l.	b.d.l.	b.d.l.	b.d.l.	b.d.l.	b.d.l.
CaO	11.47	11.17	14.95	12.21	12.88	11.92	11.52	12.46	12.09	12.77	16.23
FeO	0.10	0.16	0.14	0.12	0.11	0.18	0.14	0.14	0.13	0.15	0.20
Na ₂ O	5.18	5.26	3.22	4.64	4.38	4.87	5.05	4.55	4.82	4.39	2.46
K ₂ O	0.24	0.24	0.10	0.20	0.17	0.23	0.22	0.18	0.20	0.18	0.07
P ₂ O ₅	0.29	0.18	0.46	0.10	0.29	0.14	b.d.l.	0.09	0.37	0.26	0.21
Total	99.34	99.28	100.11	99.21	98.73	99.68	99.56	99.53	100.30	99.73	99.52
Si	9.70	9.77	8.93	9.52	9.38	9.59	9.72	9.51	9.54	9.41	8.71
Al	6.19	6.15	6.95	6.44	6.52	6.35	6.25	6.45	6.36	6.51	7.22
Mg	b.d.l.	b.d.l.	b.d.l.	b.d.l.	b.d.l.	b.d.l.	b.d.l.	b.d.l.	b.d.l.	b.d.l.	b.d.l.
Ca	2.24	2.18	2.92	2.39	2.54	2.32	2.24	2.43	2.34	2.49	3.21
Fe (ii)	0.02	0.02	0.02	0.02	0.02	0.03	0.02	0.02	0.02	0.02	0.03
Na	1.83	1.86	1.14	1.65	1.56	1.72	1.78	1.61	1.69	1.55	0.88
K	0.05	0.06	0.02	0.05	0.04	0.05	0.05	0.04	0.05	0.04	0.02
P	0.04	0.03	0.07	0.01	0.04	0.02	0.00	0.01	0.06	0.04	0.03
Total	20.08	20.07	20.06	20.08	20.10	20.09	20.07	20.07	20.06	20.07	20.08
An	54.29	53.27	71.54	58.54	61.32	56.74	55.09	59.61	57.44	61.03	78.21
Ab	44.39	45.38	27.87	40.29	37.70	41.95	43.67	39.36	41.43	37.95	21.41
Or	1.33	1.35	0.59	1.17	0.98	1.30	1.24	1.03	1.13	1.02	0.38

Group: B = basalt; BA = basaltic andesite; A = andesite; D = dacite; R = rhyolite; Opx/Cgt-SVC 2, 3 = orthopyroxene/cummingtonite-bearing SVC 2; 3 lavas; **Grain:** P = phenocryst; MC = microphenocryst; G = groundmass; C = core; INC = inclusion (mineral included within is stated in parentheses); **Position:** C = core; M = mantle; R = rim, osci. = oscillatory; **Other:** UNZ = unzoned; Dist. = distance from the core (µm); An = anorthite; Ab = albite; Or = orthoclase.

Table G.1. (continued).

Group: Sample: Name: Grain:	SVC1 D SL-JL-23 Profile P5 P Type 6		Opx-SVC 2,3 D SL-JL-83 C4-Pl1 P	Opx-SVC 2, 3 D SL-JL-83 Profile P1 G			Opx-SVC 2, 3 D SL-JL-83 Profile P2 P Type 5				
Position:	R	R	C	C	C	R	C	C	C	C	C
Dist.:	960	985		0	30	60	0	26	51	77	103
SiO ₂	47.59	49.97	54.28	43.60	44.23	45.33	52.77	53.71	53.01	53.51	53.42
Al ₂ O ₃	33.14	31.82	29.41	36.43	36.80	35.67	30.13	30.48	30.39	30.00	30.17
MgO	b.d.l.	b.d.l.	b.d.l.	0.04	0.04	b.d.l.	b.d.l.	b.d.l.	b.d.l.	b.d.l.	b.d.l.
CaO	16.12	13.99	9.92	18.59	18.45	17.47	10.96	10.91	10.93	10.66	10.62
FeO	0.19	0.16	0.07	0.36	0.35	0.43	0.15	0.10	0.15	0.08	0.15
Na ₂ O	2.64	3.70	5.54	0.03	0.02	0.03	0.27	0.29	0.26	0.29	0.27
K ₂ O	0.07	0.18	0.24	1.12	1.05	1.61	4.93	5.04	4.86	4.98	5.12
P ₂ O ₅	0.23	0.30	0.05	0.22	0.15	0.50	0.16	b.d.l.	0.14	0.52	0.23
Total	99.96	100.11	99.50	100.42	101.09	101.06	99.35	100.38	99.73	100.01	99.96
Si	8.74	9.10	9.82	8.04	8.09	8.27	9.60	9.67	9.60	9.64	9.64
Al	7.17	6.83	6.27	7.92	7.93	7.67	6.46	6.46	6.48	6.37	6.42
Mg	b.d.l.	b.d.l.	b.d.l.	0.01	b.d.l.	b.d.l.	b.d.l.	b.d.l.	b.d.l.	b.d.l.	b.d.l.
Ca	3.17	2.73	1.92	3.67	3.61	3.41	2.14	2.10	2.12	2.06	2.05
Fe (ii)	0.03	0.02	0.01	0.06	0.05	0.07	0.02	0.02	0.02	0.01	0.02
Na	0.94	1.31	1.94	0.01	0.00	0.01	0.06	0.07	0.06	0.07	0.06
K	0.02	0.04	0.05	0.40	0.37	0.57	1.74	1.76	1.71	1.74	1.79
P	0.04	0.05	0.01	0.03	0.02	0.08	0.02	b.d.l.	0.02	0.08	0.04
Total	20.10	20.08	20.03	20.15	20.10	20.07	20.04	20.05	20.01	19.96	20.02
An	76.84	66.96	49.06	90.07	90.56	85.57	54.26	53.53	54.53	53.26	52.54
Ab	22.76	32.04	49.54	9.78	9.33	14.28	44.12	44.79	43.90	45.03	45.85
Or	0.40	1.00	1.40	0.14	0.11	0.16	1.61	1.69	1.57	1.71	1.61

Group: Sample: Name: Grain:	Opx-SVC 2, 3 D SL-JL-83 Profile P2 P Type 5										
Position:	C	An-rich M	C	C	An rich M	An rich M	An rich M	An rich M	An rich M	An rich M	An rich M
Dist.:	129	154	206	231	257	283	309	334	360	386	437
SiO ₂	53.36	50.27	53.79	53.38	49.83	46.30	50.30	46.60	46.13	49.67	47.61
Al ₂ O ₃	30.07	32.37	30.01	30.48	32.56	35.07	32.72	34.86	35.99	32.80	34.08
MgO	b.d.l.	b.d.l.	b.d.l.	b.d.l.	b.d.l.	b.d.l.	b.d.l.	b.d.l.	b.d.l.	b.d.l.	b.d.l.
CaO	10.78	12.89	10.87	11.12	13.66	16.41	13.48	16.46	17.12	13.88	15.44
FeO	0.09	0.12	0.20	0.09	0.12	0.10	0.11	0.16	0.17	0.13	0.13
Na ₂ O	0.27	0.18	0.31	0.24	0.16	0.07	0.19	0.08	0.06	0.16	0.11
K ₂ O	5.01	4.01	4.82	4.85	3.69	2.19	3.73	2.11	1.81	3.40	2.69
P ₂ O ₅	0.07	0.21	0.25	0.08	0.24	0.28	0.17	0.37	b.d.l.	0.23	0.16
Total	99.64	100.04	100.25	100.22	100.25	100.39	100.68	100.60	101.28	100.31	100.20
Si	9.67	9.14	9.68	9.62	9.05	8.47	9.09	8.50	8.38	9.02	8.70
Al	6.42	6.93	6.36	6.47	6.97	7.56	6.97	7.49	7.71	7.02	7.34
Mg	b.d.l.	b.d.l.	b.d.l.	b.d.l.	b.d.l.	b.d.l.	b.d.l.	b.d.l.	b.d.l.	b.d.l.	b.d.l.
Ca	2.09	2.51	2.09	2.15	2.66	3.21	2.61	3.22	3.33	2.70	3.02
Fe (ii)	0.01	0.02	0.03	0.01	0.02	0.02	0.02	0.02	0.03	0.02	0.02
Na	0.06	0.04	0.07	0.05	0.04	0.02	0.04	0.02	0.01	0.04	0.03
K	1.76	1.41	1.68	1.69	1.30	0.78	1.31	0.75	0.64	1.20	0.95
P	0.01	0.03	0.04	0.01	0.04	0.04	0.03	0.06	0.00	0.04	0.03
Total	20.02	20.08	19.96	20.00	20.08	20.09	20.06	20.05	20.09	20.03	20.08
An	53.44	63.28	54.46	55.09	66.55	80.18	65.91	80.77	83.64	68.62	75.54
Ab	44.97	35.65	43.68	43.51	32.53	19.40	32.98	18.75	16.03	30.45	23.82
Or	1.58	1.06	1.86	1.40	0.92	0.41	1.11	0.48	0.32	0.93	0.63

Group: Sample: Name: Grain:	Opx-SVC 2, 3 D SL-JL-83 Profile P2 P Type 5										
Position:	An rich M	An rich M	An rich M	An rich M	An rich M	An rich M	An rich M	An rich M	An rich M	An rich M	An rich M
Dist.:	463	489	566	592	617	643	694	720	746	772	797
SiO ₂	51.73	46.70	48.77	49.66	53.73	51.30	54.34	52.62	52.88	51.62	52.92
Al ₂ O ₃	31.19	34.79	33.81	33.18	30.07	31.75	29.83	31.04	30.66	31.67	30.44
MgO	b.d.l.	b.d.l.	b.d.l.	b.d.l.	b.d.l.	b.d.l.	b.d.l.	b.d.l.	b.d.l.	b.d.l.	b.d.l.
CaO	11.89	15.97	14.75	14.07	10.46	12.58	10.18	11.54	11.06	12.42	11.32
FeO	0.11	0.13	0.12	0.07	0.11	0.14	0.10	0.06	0.05	0.09	0.10
Na ₂ O	0.27	0.09	0.11	0.12	0.28	0.19	0.29	0.21	0.23	0.20	0.24
K ₂ O	4.37	2.49	3.11	3.51	5.18	4.25	5.34	4.71	4.98	4.23	4.87
P ₂ O ₅	0.24	0.40	0.11	0.39	0.05	0.13	0.13	b.d.l.	0.12	0.36	0.18
Total	99.76	100.57	100.80	100.98	99.88	100.28	100.20	100.19	99.98	100.57	100.05
Si	9.39	8.52	8.84	8.96	9.70	9.29	9.77	9.50	9.56	9.30	9.56
Al	6.67	7.48	7.22	7.05	6.40	6.77	6.32	6.61	6.53	6.73	6.48
Mg	b.d.l.	b.d.l.	b.d.l.	b.d.l.	b.d.l.	b.d.l.	b.d.l.	b.d.l.	b.d.l.	b.d.l.	b.d.l.
Ca	2.31	3.12	2.86	2.72	2.02	2.44	1.96	2.23	2.14	2.40	2.19
Fe (ii)	0.02	0.02	0.02	0.01	0.02	0.02	0.01	0.01	0.01	0.01	0.01
Na	0.06	0.02	0.03	0.03	0.06	0.04	0.07	0.05	0.05	0.05	0.05
K	1.54	0.88	1.09	1.23	1.81	1.49	1.86	1.65	1.75	1.48	1.70
P	0.04	0.06	0.02	0.06	0.01	0.02	0.02	b.d.l.	0.02	0.05	0.03
Total	20.02	20.10	20.08	20.05	20.02	20.06	20.01	20.05	20.05	20.01	20.04
An	59.09	77.55	71.92	68.40	51.89	61.38	50.45	56.80	54.33	61.13	55.47
Ab	39.34	21.92	27.44	30.88	46.47	37.54	47.86	41.96	44.30	37.67	43.14
Or	1.57	0.53	0.64	0.72	1.64	1.08	1.69	1.25	1.37	1.20	1.39

Group: B = basalt; BA = basaltic andesite; A = andesite; D = dacite; R = rhyolite; Opx/Cgt-SVC 2, 3 = orthopyroxene/cummingtonite-bearing SVC 2; 3 lavas; **Grain:** P = phenocryst; MC = microphenocryst; G = groundmass; C = core; INC = inclusion (mineral included within is stated in parentheses); **Position:** C = core; M = mantle; R = rim, osci. = oscillatory; **Other:** UNZ = unzoned; Dist. = distance from the core (μm); An = anorthite; Ab = albite; Or = orthoclase.

Table G.1. (continued).

Group:	Opx-SVC 2, 3 D										
Sample:	SL-JL-83										
Name:	Profile P2										
Grain:	P Type 5										
Position:	An rich	An rich	An rich	An rich	An rich	An rich	An rich	An rich	An rich	An rich	R
Dist.:	823	M 849	M 874	M 900	M 926	M 977	M 1003	M 1029	M 1080	M 1106	1132
SiO ₂	51.13	52.84	53.37	51.22	52.16	53.56	52.17	52.88	53.29	53.99	51.86
Al ₂ O ₃	31.55	30.60	29.73	31.60	30.87	30.15	30.88	30.50	29.86	30.54	31.25
MgO	b.d.l.	b.d.l.	b.d.l.	b.d.l.	b.d.l.	b.d.l.	b.d.l.	b.d.l.	b.d.l.	b.d.l.	b.d.l.
CaO	12.59	11.61	10.44	12.57	11.64	10.98	11.86	11.30	10.51	10.95	12.24
FeO	0.08	0.13	0.13	0.04	0.13	0.10	0.07	0.14	0.10	0.13	0.16
Na ₂ O	0.18	0.21	0.26	0.18	0.23	0.25	0.21	0.24	0.28	0.26	0.23
K ₂ O	4.15	4.72	5.15	4.17	4.67	4.95	4.64	4.89	5.22	4.98	4.32
P ₂ O ₅	0.22	b.d.l.	b.d.l.	0.33	0.29	0.22	0.03	0.03	0.33	0.07	0.26
Total	99.91	100.02	99.05	100.11	99.99	100.23	99.86	99.99	99.59	100.94	100.32
Si	9.29	9.56	9.72	9.28	9.44	9.64	9.47	9.57	9.65	9.65	9.37
Al	6.75	6.53	6.38	6.75	6.59	6.40	6.60	6.50	6.37	6.44	6.65
Mg	b.d.l.	b.d.l.	b.d.l.	b.d.l.	b.d.l.	b.d.l.	b.d.l.	b.d.l.	b.d.l.	b.d.l.	b.d.l.
Ca	2.45	2.25	2.04	2.44	2.26	2.12	2.30	2.19	2.04	2.10	2.37
Fe (ii)	0.01	0.02	0.02	0.01	0.02	0.02	0.01	0.02	0.01	0.02	0.02
Na	0.04	0.05	0.06	0.04	0.05	0.06	0.05	0.05	0.06	0.06	0.05
K	1.46	1.66	1.82	1.46	1.64	1.73	1.63	1.72	1.83	1.72	1.52
P	0.03	b.d.l.	b.d.l.	0.05	0.04	0.03	0.00	0.00	0.05	0.01	0.04
Total	20.04	20.05	20.03	20.02	20.05	20.00	20.07	20.06	20.03	20.00	20.03
An	62.00	56.90	52.03	61.84	57.15	54.27	57.83	55.28	51.82	54.02	60.17
Ab	36.97	41.85	46.42	37.11	41.51	44.27	40.93	43.33	46.56	44.43	38.47
Or	1.04	1.24	1.56	1.05	1.34	1.46	1.24	1.39	1.63	1.56	1.37

Group:	Opx-SVC 2, 3 D										
Sample:	SL-JL-83										
Name:	Profile P3										
Grain:	P Type 5										
Position:	C	An-rich	An-rich	An-rich	An-rich	An-rich	An-rich	An-rich	An-rich	An-rich	R
Dist.:	27	M 55	M 82	M 109	M 136	M 164	M 191	M 218	M 245	M 273	300
SiO ₂	52.32	48.77	49.04	48.06	47.95	45.92	53.66	47.51	51.95	45.94	52.04
Al ₂ O ₃	31.06	33.24	32.73	33.92	34.12	35.34	29.67	34.69	31.10	35.38	30.97
MgO	b.d.l.	b.d.l.	b.d.l.	b.d.l.	b.d.l.	b.d.l.	b.d.l.	b.d.l.	b.d.l.	b.d.l.	b.d.l.
CaO	11.54	14.16	14.17	15.23	15.35	16.63	10.58	15.67	11.65	16.68	11.92
FeO	0.14	0.12	0.15	0.13	0.16	0.18	0.15	0.14	0.06	0.11	0.12
Na ₂ O	0.25	0.15	0.17	0.13	0.12	0.10	0.30	0.11	0.27	0.08	0.28
K ₂ O	4.76	3.44	3.45	2.90	2.79	2.12	5.20	2.68	4.63	2.14	4.56
P ₂ O ₅	0.25	0.21	0.02	0.37	0.32	0.34	0.15	0.49	0.34	0.25	0.19
Total	100.33	100.13	99.72	100.72	100.83	100.65	99.71	101.27	99.94	100.55	100.10
Si	9.44	8.89	8.98	8.73	8.70	8.39	9.71	8.59	9.41	8.40	9.42
Al	6.61	7.14	7.06	7.26	7.30	7.61	6.33	7.39	6.64	7.62	6.61
Mg	b.d.l.	b.d.l.	b.d.l.	b.d.l.	b.d.l.	b.d.l.	b.d.l.	b.d.l.	b.d.l.	b.d.l.	b.d.l.
Ca	2.23	2.77	2.78	2.96	2.99	3.26	2.05	3.04	2.26	3.27	2.31
Fe (ii)	0.02	0.02	0.02	0.02	0.02	0.03	0.02	0.02	0.01	0.02	0.02
Na	0.06	0.04	0.04	0.03	0.03	0.02	0.07	0.03	0.06	0.02	0.06
K	1.67	1.22	1.22	1.02	0.98	0.75	1.82	0.94	1.63	0.76	1.60
P	0.04	0.03	0.00	0.06	0.05	0.05	0.02	0.08	0.05	0.04	0.03
Total	20.06	20.11	20.11	20.08	20.08	20.11	20.03	20.08	20.04	20.12	20.06
An	56.43	68.85	68.76	73.80	74.74	80.79	52.02	75.88	57.22	80.80	58.14
Ab	42.13	30.26	30.26	25.45	24.57	18.62	46.24	23.47	41.19	18.75	40.23
Or	1.44	0.90	0.97	0.76	0.68	0.59	1.74	0.65	1.59	0.45	1.63

Group:	Opx-SVC 2, 3 D										
Sample:	SL-JL-83										
Name:	Profile P4										
Grain:	P Type 5										
Position:	C	C	C	C	C	C	C	C	C	C	C
Dist.:	0	25	51	76	102	127	153	179	204	230	255
SiO ₂	53.15	51.43	53.18	52.63	52.86	52.84	53.03	53.07	52.91	53.11	53.62
Al ₂ O ₃	30.18	31.35	30.27	29.79	30.66	30.38	30.14	30.29	30.33	30.24	29.37
MgO	b.d.l.	b.d.l.	b.d.l.	b.d.l.	b.d.l.	b.d.l.	b.d.l.	b.d.l.	b.d.l.	b.d.l.	b.d.l.
CaO	11.04	12.39	11.05	10.98	11.48	11.20	11.07	11.12	11.13	10.99	10.24
FeO	0.08	0.07	0.10	0.07	0.10	0.10	0.12	0.07	0.15	0.10	0.08
Na ₂ O	0.24	0.20	0.26	0.30	0.24	0.25	0.25	0.25	0.25	0.26	0.32
K ₂ O	4.96	4.27	4.94	5.12	4.71	4.84	5.05	4.90	5.03	4.92	5.19
P ₂ O ₅	0.19	-0.08	0.08	0.22	0.27	0.36	b.d.l.	0.16	0.13	0.25	0.25
Total	99.82	99.61	99.89	99.07	100.31	99.96	99.61	99.85	99.85	99.85	99.09
Si	9.62	9.37	9.62	9.61	9.53	9.55	9.63	9.60	9.58	9.60	9.75
Al	6.43	6.73	6.45	6.41	6.51	6.47	6.45	6.46	6.47	6.44	6.29
Mg	b.d.l.	b.d.l.	b.d.l.	b.d.l.	b.d.l.	b.d.l.	b.d.l.	b.d.l.	b.d.l.	b.d.l.	b.d.l.
Ca	2.14	2.42	2.14	2.15	2.22	2.17	2.15	2.16	2.16	2.13	2.00
Fe (ii)	0.01	0.01	0.02	0.01	0.01	0.02	0.02	0.01	0.02	0.01	0.01
Na	0.06	0.05	0.06	0.07	0.05	0.06	0.06	0.06	0.06	0.06	0.07
K	1.74	1.51	1.73	1.81	1.64	1.70	1.78	1.72	1.76	1.72	1.83
P	0.03	b.d.l.	0.01	0.03	0.04	0.05	b.d.l.	0.02	0.02	0.04	0.04
Total	20.02	20.06	20.03	20.08	20.01	20.01	20.07	20.02	20.06	20.01	19.99
An	54.35	60.87	54.43	53.28	56.60	55.27	53.99	54.80	54.23	54.43	51.20
Ab	44.23	37.95	44.03	45.00	42.01	43.27	44.55	43.71	44.33	44.05	46.92
Or	1.42	1.17	1.54	1.72	1.39	1.46	1.45	1.49	1.44	1.52	1.88

Group: B = basalt; BA = basaltic andesite; A = andesite; D = dacite; R = rhyolite; Opx/Cgt-SVC 2, 3 = orthopyroxene/cummingtonite-bearing SVC 2; 3 lavas; **Grain:** P = phenocryst; MC = microphenocryst; G = groundmass; C = core; INC = inclusion (mineral included within is stated in parentheses); **Position:** C = core; M = mantle; R = rim, osci. = oscillatory; **Other:** UNZ = unzoned; Dist. = distance from the core (µm); An = anorthite; Ab = albite; Or = orthoclase.

Table G.1. (continued).

Group:	Opx-SVC 2, 3 D										
Sample:	SL-JL-83										
Name:	Profile P 4										
Grain:	P Type 5										
Position:	C	C	C	C	C	C	C	C	An-rich M	An-rich M	An-rich M
Dist.:	280	306	331	357	382	408	433	459	484	510	535
SiO ₂	52.48	53.40	52.62	52.99	53.11	53.10	53.64	53.48	51.21	50.36	50.25
Al ₂ O ₃	29.60	29.87	30.58	30.58	30.11	30.34	29.97	29.78	31.54	32.37	32.58
MgO	b.d.l.	b.d.l.	b.d.l.	b.d.l.	b.d.l.	b.d.l.	b.d.l.	b.d.l.	b.d.l.	b.d.l.	b.d.l.
CaO	10.77	10.56	11.60	11.34	10.94	10.78	10.84	10.72	12.42	13.18	13.25
FeO	0.08	0.09	0.12	0.08	0.13	0.12	0.17	0.17	0.12	0.14	0.12
Na ₂ O	0.28	0.27	0.22	0.24	0.26	0.27	0.27	0.31	0.23	0.17	0.20
K ₂ O	4.88	5.13	4.75	4.86	5.01	5.15	5.11	5.10	4.36	3.97	3.82
P ₂ O ₅	0.12	0.17	0.22	0.14	0.36	0.07	0.23	0.44	0.21	0.32	0.20
Total	98.24	99.49	100.14	100.20	99.93	99.83	100.26	99.95	100.07	100.49	100.43
Si	9.65	9.68	9.51	9.56	9.60	9.61	9.66	9.66	9.29	9.12	9.10
Al	6.41	6.38	6.51	6.50	6.41	6.47	6.36	6.34	6.74	6.91	6.96
Mg	b.d.l.	b.d.l.	b.d.l.	b.d.l.	b.d.l.	b.d.l.	b.d.l.	b.d.l.	b.d.l.	b.d.l.	b.d.l.
Ca	2.12	2.05	2.25	2.19	2.12	2.09	2.09	2.07	2.41	2.55	2.57
Fe (ii)	0.01	0.01	0.02	0.01	0.02	0.02	0.03	0.03	0.02	0.02	0.02
Na	0.06	0.06	0.05	0.06	0.06	0.06	0.06	0.07	0.05	0.04	0.05
K	1.74	1.80	1.67	1.70	1.75	1.81	1.78	1.78	1.53	1.39	1.34
P	0.02	0.03	0.03	0.02	0.06	0.01	0.03	0.07	0.03	0.05	0.03
Total	20.02	20.02	20.04	20.04	20.02	20.07	20.03	20.00	20.08	20.07	20.07
An	54.02	52.35	56.69	55.51	53.84	52.79	53.13	52.80	60.33	64.07	64.97
Ab	44.33	46.03	42.02	43.07	44.61	45.62	45.31	45.41	38.32	34.95	33.88
Or	1.65	1.62	1.29	1.42	1.55	1.59	1.56	1.80	1.35	0.98	1.15

Group:	Opx-SVC 2, 3 D										
Sample:	SL-JL-83										
Name:	Profile P 4										
Grain:	P Type 5										
Position:	An-rich M	An-rich M	An-rich M	An-rich M	An-rich M	An-rich M	An-rich M	An-rich M	An-rich M	An-rich M	An-rich M
Dist.:	587	612	637	663	688	714	739	765	790	816	841
SiO ₂	50.89	50.12	50.59	49.27	49.58	47.68	48.85	49.27	48.54	47.72	46.97
Al ₂ O ₃	32.09	32.35	32.64	33.19	32.91	34.08	33.65	30.05	33.82	34.43	34.93
MgO	b.d.l.	b.d.l.	b.d.l.	b.d.l.	b.d.l.	b.d.l.	b.d.l.	0.19	b.d.l.	b.d.l.	b.d.l.
CaO	12.78	13.45	13.45	14.30	13.99	15.39	14.96	12.34	14.89	15.70	16.09
FeO	0.16	0.10	0.13	0.12	0.17	0.15	0.18	0.39	0.17	0.14	0.15
Na ₂ O	0.27	0.22	0.21	0.18	0.18	0.10	0.22	0.69	0.14	0.12	0.13
K ₂ O	4.17	3.79	3.84	3.36	3.52	2.77	2.71	3.55	3.06	2.53	2.36
P ₂ O ₅	0.32	0.18	0.31	b.d.l.	0.29	0.10	0.34	0.11	0.15	0.18	0.01
Total	100.70	100.20	101.14	100.36	100.62	100.25	100.94	96.60	100.75	100.80	100.62
Si	9.19	9.11	9.10	8.96	8.98	8.71	8.84	9.30	8.81	8.67	8.57
Al	6.83	6.93	6.92	7.12	7.03	7.34	7.17	6.68	7.23	7.37	7.51
Mg	b.d.l.	b.d.l.	b.d.l.	b.d.l.	b.d.l.	b.d.l.	b.d.l.	0.05	b.d.l.	b.d.l.	b.d.l.
Ca	2.47	2.62	2.59	2.79	2.72	3.01	2.90	2.49	2.90	3.06	3.14
Fe (ii)	0.02	0.02	0.02	0.02	0.03	0.02	0.03	0.06	0.03	0.02	0.02
Na	0.06	0.05	0.05	0.04	0.04	0.02	0.05	0.17	0.03	0.03	0.03
K	1.46	1.34	1.34	1.18	1.24	0.98	0.95	1.30	1.08	0.89	0.84
P	0.05	0.03	0.05	b.d.l.	0.04	0.02	0.05	0.02	0.02	0.03	0.00
Total	20.09	20.08	20.06	20.10	20.07	20.10	20.00	20.07	20.09	20.06	20.11
An	61.91	65.40	65.13	69.47	68.05	74.96	74.29	63.02	72.34	76.88	78.41
Ab	36.54	33.34	33.68	29.52	30.94	24.44	24.40	32.77	26.85	22.41	20.83
Or	1.55	1.25	1.19	1.02	1.02	0.60	1.31	4.20	0.81	0.71	0.76

Group:	Opx-SVC 2, 3 D							Opx-SVC 2, 3 D			
Sample:	SL-JL-83							SL-83-03			
Name:	Profile P 4							C1-Pl6-1			
Grain:	P Type 5							P Type 6			
Position:	An-rich M	An-rich M	An-rich M	An-rich M	An-rich M	An-rich M	R	C	C	C	C
Dist.:	867	918	943	969	994	1020	1045	27	55	109	137
SiO ₂	46.98	47.85	49.59	51.88	49.88	53.37	53.14	55.56	55.71	55.94	55.63
Al ₂ O ₃	35.16	34.17	32.96	31.01	32.76	30.41	30.79	28.23	27.51	27.33	27.72
MgO	b.d.l.	b.d.l.	b.d.l.	b.d.l.	b.d.l.	b.d.l.	b.d.l.	b.d.l.	b.d.l.	b.d.l.	b.d.l.
CaO	16.26	15.48	14.03	11.92	13.92	11.11	11.46	10.76	10.13	9.99	10.34
FeO	0.11	0.17	0.11	0.09	0.14	0.13	0.15	0.18	0.12	0.12	0.09
Na ₂ O	0.12	0.10	0.14	0.24	0.15	0.28	0.28	5.43	5.68	5.89	5.63
K ₂ O	2.38	2.84	3.47	4.59	3.59	4.87	4.81	0.31	0.32	0.28	0.27
P ₂ O ₅	0.12	0.31	0.34	0.47	0.28	b.d.l.	0.21	n.a.	n.a.	n.a.	n.a.
Total	101.13	100.87	100.62	100.17	100.72	100.29	100.84	100.52	99.49	99.58	99.74
Si	8.53	8.69	8.98	9.38	9.02	9.61	9.53	9.98	10.09	10.12	10.05
Al	7.52	7.31	7.03	6.61	6.99	6.46	6.51	5.97	5.87	5.83	5.90
Mg	b.d.l.	b.d.l.	b.d.l.	b.d.l.	b.d.l.	b.d.l.	b.d.l.	b.d.l.	b.d.l.	b.d.l.	b.d.l.
Ca	3.16	3.01	2.72	2.31	2.70	2.14	2.20	2.07	1.96	1.94	2.00
Fe (ii)	0.02	0.03	0.02	0.01	0.02	0.02	0.02	0.03	0.02	0.02	0.01
Na	0.03	0.02	0.03	0.05	0.04	0.06	0.06	1.89	2.00	2.07	1.97
K	0.84	1.00	1.22	1.61	1.26	1.70	1.67	0.07	0.07	0.06	0.06
P	0.02	0.05	0.05	0.07	0.04	0.01	0.03	n.a.	n.a.	n.a.	n.a.
Total	20.11	20.10	20.05	20.04	20.07	20.02	20.03	20.01	20.01	20.03	20.01
An	78.51	74.63	68.53	58.12	67.60	54.85	55.90	51.37	48.71	47.62	49.59
Ab	20.79	24.78	30.68	40.51	31.51	43.51	42.46	46.87	49.46	50.80	48.89
Or	0.71	0.59	0.79	1.37	0.89	1.64	1.64	1.75	1.82	1.58	1.52

Group: B = basalt; BA = basaltic andesite; A = andesite; D = dacite; R = rhyolite; Opx/Cgt-SVC 2, 3 = orthopyroxene/cummingtonite-bearing SVC 2; 3 lavas; **Grain:** P = phenocryst; MC = microphenocryst; G = groundmass; C = core; INC = inclusion (mineral included within is stated in parentheses); **Position:** C = core; M = mantle; R = rim, osci. = oscillatory; **Other:** UNZ = unzoned; Dist. = distance from the core (μm); An = anorthite; Ab = albite; Or = orthoclase.

Table G.1. (continued).

Group:	Opx-SVC 2, 3 D										
Sample:	SL-83-03										
Name:	C1-Pl6-1										
Grain:	P Type 6										
Position:	C	C	C	C	C	C	C	C	C	C	C
Dist.:	164	191	219	246	273	300	328	355	382	410	437
SiO ₂	55.36	54.81	50.91	56.62	57.02	55.58	51.43	55.19	54.59	54.28	54.27
Al ₂ O ₃	27.46	27.83	30.18	26.81	26.71	27.18	30.30	27.64	28.63	28.16	28.45
MgO	b.d.l.	b.d.l.	b.d.l.	b.d.l.	b.d.l.	b.d.l.	b.d.l.	b.d.l.	b.d.l.	b.d.l.	b.d.l.
CaO	10.28	10.65	13.51	9.55	9.18	10.01	13.49	10.41	11.31	11.22	11.36
FeO	0.08	0.09	0.12	0.11	0.09	0.13	0.12	0.10	0.12	0.13	0.09
Na ₂ O	5.60	5.32	3.79	6.11	6.28	5.72	3.87	5.60	5.25	5.15	5.23
K ₂ O	0.25	0.24	0.14	0.34	0.35	0.29	0.14	0.26	0.21	0.22	0.24
P ₂ O ₅	n.a.	n.a.	n.a.	n.a.	n.a.	n.a.	n.a.	n.a.	n.a.	n.a.	n.a.
Total	99.06	98.94	98.66	99.55	99.69	98.93	99.37	99.21	100.13	99.16	99.64
Si	10.07	9.99	9.39	10.23	10.28	10.12	9.41	10.03	9.85	9.89	9.85
Al	5.88	5.98	6.56	5.71	5.67	5.83	6.54	5.92	6.09	6.05	6.09
Mg	b.d.l.	b.d.l.	b.d.l.	b.d.l.	b.d.l.	b.d.l.	b.d.l.	b.d.l.	b.d.l.	b.d.l.	b.d.l.
Ca	2.00	2.08	2.67	1.85	1.77	1.95	2.65	2.03	2.19	2.19	2.21
Fe (ii)	0.01	0.01	0.02	0.02	0.01	0.02	0.02	0.02	0.02	0.02	0.01
Na	1.97	1.88	1.36	2.14	2.19	2.02	1.37	1.97	1.84	1.82	1.84
K	0.06	0.05	0.03	0.08	0.08	0.07	0.03	0.06	0.05	0.05	0.06
P	n.a.	n.a.	n.a.	n.a.	n.a.	n.a.	n.a.	n.a.	n.a.	n.a.	n.a.
Total	20.00	19.99	20.03	20.02	20.02	20.01	20.02	20.03	20.04	20.02	20.05
An	49.65	51.83	65.77	45.48	43.78	48.33	65.29	49.93	53.68	53.95	53.82
Ab	48.92	46.81	33.43	52.60	54.21	50.02	33.90	48.57	45.12	44.81	44.83
Or	1.43	1.37	0.79	1.92	2.00	1.65	0.80	1.50	1.20	1.24	1.35

Group:	Opx-SVC 2, 3 D										
Sample:	SL-83-03										
Name:	C1-Pl6-1										
Grain:	P Type 6										
Position:	C	C	M	M	M	M	M	M	M	M	M
Dist.:	464	492	519	546	574	601	628	656	683	710	738
SiO ₂	54.17	53.74	53.57	54.53	51.33	54.28	54.11	54.55	54.37	52.57	53.94
Al ₂ O ₃	27.95	28.70	28.71	28.42	30.38	28.39	28.01	28.00	28.40	29.33	28.62
MgO	b.d.l.	b.d.l.	b.d.l.	b.d.l.	b.d.l.	b.d.l.	b.d.l.	b.d.l.	b.d.l.	0.04	b.d.l.
CaO	10.96	11.57	11.65	11.24	13.60	11.35	10.91	10.83	11.32	12.72	11.42
FeO	0.08	0.14	0.09	0.10	0.09	0.10	0.05	0.17	0.12	0.15	0.10
Na ₂ O	5.21	4.98	4.93	5.21	3.94	5.12	5.27	5.28	5.22	4.31	5.05
K ₂ O	0.23	0.21	0.22	0.22	0.12	0.23	0.24	0.23	0.23	0.21	0.21
P ₂ O ₅	n.a.	n.a.	n.a.	n.a.	n.a.	n.a.	n.a.	n.a.	n.a.	n.a.	n.a.
Total	98.64	99.35	99.18	99.75	99.51	99.49	98.65	99.10	99.68	99.33	99.39
Si	9.92	9.79	9.78	9.88	9.39	9.86	9.91	9.94	9.86	9.61	9.81
Al	6.03	6.16	6.17	6.07	6.55	6.08	6.04	6.01	6.07	6.32	6.14
Mg	b.d.l.	b.d.l.	b.d.l.	b.d.l.	b.d.l.	b.d.l.	b.d.l.	b.d.l.	b.d.l.	0.01	b.d.l.
Ca	2.15	2.26	2.28	2.18	2.66	2.21	2.14	2.11	2.20	2.49	2.23
Fe (ii)	0.01	0.02	0.01	0.02	0.01	0.02	0.01	0.03	0.02	0.02	0.01
Na	1.85	1.76	1.74	1.83	1.40	1.80	1.87	1.86	1.84	1.53	1.78
K	0.05	0.05	0.05	0.05	0.03	0.05	0.06	0.05	0.05	0.05	0.05
P	n.a.	n.a.	n.a.	n.a.	n.a.	n.a.	n.a.	n.a.	n.a.	n.a.	n.a.
Total	20.02	20.04	20.03	20.03	20.05	20.03	20.03	20.01	20.04	20.02	20.03
An	53.07	55.55	55.93	53.74	65.11	54.35	52.60	52.45	53.83	61.24	54.88
Ab	45.61	43.22	42.81	45.03	34.18	44.36	46.02	46.22	44.90	37.53	43.92
Or	1.31	1.23	1.26	1.23	0.71	1.29	1.38	1.33	1.28	1.22	1.20

Group:	Opx-SVC 2, 3 D				Opx-SVC 2, 3 D							
Sample:	SL-83-03				SL-83-03							
Name:	C1-Pl6-1				C3-Pl1-3							
Grain:	P Type 6				P Type 5							
Position:	M	R	An-rich M	An-rich M	An-rich M	An-rich M	An-rich M	C	C	C	C	C
Dist.:	765	792	0	96	121	169	217	241	410	434	482	482
SiO ₂	53.48	49.96	52.10	53.84	50.65	53.61	51.71	53.59	53.00	53.75	54.03	54.03
Al ₂ O ₃	28.90	31.07	29.52	27.99	30.55	28.70	29.79	28.03	28.91	27.87	27.65	27.65
MgO	b.d.l.	b.d.l.	b.d.l.	b.d.l.	b.d.l.	b.d.l.	b.d.l.	b.d.l.	b.d.l.	b.d.l.	b.d.l.	b.d.l.
CaO	11.89	14.69	12.71	11.15	13.84	11.62	13.09	11.14	12.04	10.94	10.81	10.81
FeO	0.09	0.13	0.11	0.10	0.09	0.09	0.13	0.13	0.12	0.10	0.10	0.10
Na ₂ O	4.81	3.26	4.18	5.03	3.72	4.96	4.18	5.03	4.75	5.23	5.32	5.32
K ₂ O	0.21	0.12	0.22	0.27	0.18	0.31	0.23	0.30	0.26	0.33	0.34	0.34
P ₂ O ₅	n.a.	n.a.	n.a.	n.a.	n.a.	n.a.	n.a.	n.a.	n.a.	n.a.	n.a.	n.a.
Total	99.39	99.24	98.86	98.40	99.05	99.32	99.15	98.26	99.09	98.25	98.30	98.30
Si	9.74	9.19	9.56	9.89	9.32	9.77	9.49	9.86	9.70	9.89	9.94	9.94
Al	6.20	6.74	6.39	6.06	6.62	6.17	6.44	6.08	6.23	6.04	5.99	5.99
Mg	b.d.l.	b.d.l.	b.d.l.	b.d.l.	b.d.l.	b.d.l.	b.d.l.	b.d.l.	b.d.l.	b.d.l.	b.d.l.	b.d.l.
Ca	2.32	2.89	2.50	2.19	2.73	2.27	2.57	2.20	2.36	2.16	2.13	2.13
Fe (ii)	0.01	0.02	0.02	0.02	0.01	0.01	0.02	0.02	0.02	0.02	0.02	0.02
Na	1.70	1.16	1.49	1.79	1.33	1.75	1.48	1.80	1.69	1.87	1.90	1.90
K	0.05	0.03	0.05	0.06	0.04	0.07	0.05	0.07	0.06	0.08	0.08	0.08
P	n.a.	n.a.	n.a.	n.a.	n.a.	n.a.	n.a.	n.a.	n.a.	n.a.	n.a.	n.a.
Total	20.03	20.03	20.01	20.01	20.05	20.05	20.06	20.03	20.06	20.06	20.06	20.06
An	57.05	70.87	61.90	54.19	66.62	55.43	62.58	54.05	57.44	52.61	51.85	51.85
Ab	41.75	28.42	36.81	44.22	32.37	42.81	36.11	44.19	41.06	45.50	46.20	46.20
Or	1.19	0.70	1.30	1.59	1.01	1.76	1.31	1.76	1.50	1.88	1.95	1.95

Group: B = basalt; BA = basaltic andesite; A = andesite; D = dacite; R = rhyolite; Opx/Cgt-SVC 2, 3 = orthopyroxene/cummingtonite-bearing SVC 2; 3 lavas; **Grain:** P = phenocryst; MC = microphenocryst; G = groundmass; C = core; INC = inclusion (mineral included within is stated in parentheses); **Position:** C = core; M = mantle; R = rim, osci. = oscillatory; **Other:** UNZ = unzoned; Dist. = distance from the core (µm); An = anorthite; Ab = albite; Or = orthoclase.

Table G.1. (continued).

Group: Sample: Name: Grain:	Opx-SVC 2, 3 D SL-83-03 C3-P11-3 P Type 5								Opx-SVC 2, 3 D SL-83-03 Profile C4-P11-7 P Type 5		
Position: Dist.:	C 506	C 530	An-rich M 579	An-rich M 603	An-rich M 627	An-rich M 820	An-rich M 844	An-poor R 892	C b.d.l.	C 25	C 199
SiO ₂	52.44	54.24	52.86	50.13	50.68	54.50	55.36	54.71	54.63	56.07	53.86
Al ₂ O ₃	28.73	27.91	29.25	30.83	29.73	27.37	27.01	27.30	27.52	27.25	28.07
MgO	b.d.l.	b.d.l.	b.d.l.	b.d.l.	b.d.l.	b.d.l.	b.d.l.	b.d.l.	b.d.l.	b.d.l.	b.d.l.
CaO	12.07	10.97	12.68	14.33	13.35	10.43	9.97	10.47	10.72	10.36	11.02
FeO	0.12	0.07	0.13	0.16	0.14	0.09	0.08	0.13	0.15	0.21	0.11
Na ₂ O	4.62	5.34	4.40	3.40	3.89	5.48	5.75	5.52	5.40	5.49	5.31
K ₂ O	0.26	0.35	0.24	0.14	0.20	0.28	0.30	0.32	0.35	0.44	0.30
P ₂ O ₅	n.a.	n.a.	n.a.	n.a.	n.a.	n.a.	n.a.	n.a.	n.a.	n.a.	n.a.
Total	98.30	98.92	99.68	99.06	98.03	98.20	98.52	98.46	98.77	99.81	98.71
Si	9.68	9.91	9.63	9.23	9.41	10.01	10.12	10.03	9.99	10.13	9.87
Al	6.25	6.01	6.28	6.69	6.51	5.93	5.82	5.90	5.93	5.80	6.06
Mg	b.d.l.	b.d.l.	b.d.l.	b.d.l.	b.d.l.	b.d.l.	b.d.l.	b.d.l.	b.d.l.	b.d.l.	b.d.l.
Ca	2.39	2.15	2.48	2.83	2.66	2.05	1.95	2.06	2.10	2.00	2.16
Fe (ii)	0.02	0.01	0.02	0.02	0.02	0.01	0.01	0.02	0.02	0.03	0.02
Na	1.65	1.89	1.55	1.21	1.40	1.95	2.04	1.96	1.91	1.92	1.89
K	0.06	0.08	0.06	0.03	0.05	0.07	0.07	0.07	0.08	0.10	0.07
P	n.a.	n.a.	n.a.	n.a.	n.a.	n.a.	n.a.	n.a.	n.a.	n.a.	n.a.
Total	20.05	20.07	20.03	20.04	20.06	20.03	20.02	20.04	20.04	19.99	20.08
An	58.21	52.14	60.61	69.39	64.72	50.43	48.10	50.24	51.29	49.77	52.50
Ab	40.31	45.90	38.03	29.81	34.14	47.96	50.17	47.96	46.74	47.74	45.78
Or	1.48	1.96	1.36	0.80	1.14	1.61	1.73	1.80	1.97	2.49	1.73

Group: Sample: Name: Grain:	Opx-SVC 2, 3 D SL-83-03 Profile C4-P11-7 P Type 5										
Position: Dist.:	C 224	An-rich M 249	An-rich M 273	An-rich M 298	An-rich M 323	An-rich M 348	An-rich M 373	An-rich M 447	An-rich M 646	An-rich M 696	An-rich M 820
SiO ₂	54.79	50.85	53.98	55.03	50.51	54.00	55.16	54.04	56.59	53.55	55.29
Al ₂ O ₃	27.92	30.29	28.29	27.45	30.51	27.95	27.01	28.03	26.90	27.90	28.21
MgO	b.d.l.	b.d.l.	b.d.l.	b.d.l.	b.d.l.	b.d.l.	b.d.l.	b.d.l.	b.d.l.	b.d.l.	b.d.l.
CaO	10.76	13.85	11.22	10.49	13.87	11.14	10.19	10.99	9.79	11.29	10.22
FeO	0.10	0.11	0.10	0.07	0.09	0.09	0.13	0.14	0.15	0.09	0.13
Na ₂ O	5.50	3.71	5.21	5.49	3.63	5.28	5.59	5.20	5.73	5.15	6.07
K ₂ O	0.31	0.17	0.30	0.32	0.19	0.32	0.38	0.34	0.49	0.33	0.36
P ₂ O ₅	n.a.	n.a.	n.a.	n.a.	n.a.	n.a.	n.a.	n.a.	n.a.	n.a.	n.a.
Total	99.42	98.99	99.12	98.87	98.80	98.80	98.49	98.79	99.69	98.35	100.28
Si	9.95	9.36	9.85	10.04	9.31	9.89	10.10	9.89	10.22	9.86	9.96
Al	5.98	6.57	6.09	5.90	6.63	6.03	5.83	6.05	5.72	6.05	5.99
Mg	b.d.l.	b.d.l.	b.d.l.	b.d.l.	b.d.l.	b.d.l.	b.d.l.	b.d.l.	b.d.l.	b.d.l.	b.d.l.
Ca	2.10	2.73	2.19	2.05	2.74	2.19	2.00	2.15	1.89	2.23	1.97
Fe (ii)	0.01	0.02	0.02	0.01	0.01	0.01	0.02	0.02	0.02	0.01	0.02
Na	1.94	1.32	1.84	1.94	1.30	1.87	1.98	1.84	2.01	1.84	2.12
K	0.07	0.04	0.07	0.07	0.04	0.08	0.09	0.08	0.11	0.08	0.08
P	n.a.	n.a.	n.a.	n.a.	n.a.	n.a.	n.a.	n.a.	n.a.	n.a.	n.a.
Total	20.06	20.04	20.06	20.02	20.04	20.07	20.02	20.05	19.98	20.07	20.14
An	51.05	66.71	53.42	50.40	67.14	52.85	49.09	52.84	47.18	53.73	47.25
Ab	47.18	32.34	44.86	47.77	31.78	45.32	48.72	45.23	50.01	44.38	50.79
Or	1.78	0.95	1.72	1.82	1.09	1.83	2.19	1.94	2.80	1.90	1.96

Group: Sample: Name: Grain:	Opx-SVC 2, 3 D SL-83-03 Profile C4-P11-11 P Indiff.										
Position: Dist.:	C b.d.l.	C 26	C 51	C 103	M 205	M 231	M 257	M 283	M 308	M 334	M 360
SiO ₂	52.79	53.04	52.13	53.21	56.00	56.09	56.48	55.90	55.66	55.64	55.38
Al ₂ O ₃	28.69	28.70	29.48	29.04	26.54	26.76	26.56	27.04	26.79	26.98	27.25
MgO	b.d.l.	0.04	b.d.l.	b.d.l.	b.d.l.	b.d.l.	b.d.l.	b.d.l.	b.d.l.	b.d.l.	b.d.l.
CaO	12.09	11.94	12.52	11.88	9.39	9.52	9.41	9.81	9.85	9.83	10.04
FeO	0.10	0.11	0.09	0.11	0.07	0.13	0.11	0.08	0.11	0.10	0.14
Na ₂ O	4.79	4.78	4.57	4.76	6.13	6.06	6.15	5.94	5.86	5.84	5.85
K ₂ O	0.23	0.21	0.19	0.20	0.35	0.33	0.35	0.32	0.33	0.32	0.37
P ₂ O ₅	n.a.	n.a.	n.a.	n.a.	n.a.	n.a.	n.a.	n.a.	n.a.	n.a.	n.a.
Total	98.71	98.82	99.04	99.22	98.48	98.95	99.10	99.13	98.62	98.74	99.08
Si	9.70	9.73	9.56	9.71	10.23	10.20	10.25	10.15	10.16	10.15	10.08
Al	6.21	6.20	6.37	6.25	5.71	5.74	5.68	5.79	5.76	5.80	5.85
Mg	b.d.l.	0.01	b.d.l.	b.d.l.	b.d.l.	b.d.l.	b.d.l.	b.d.l.	b.d.l.	b.d.l.	b.d.l.
Ca	2.38	2.35	2.46	2.32	1.84	1.85	1.83	1.91	1.93	1.92	1.96
Fe (ii)	0.02	0.02	0.01	0.02	0.01	0.02	0.02	0.01	0.02	0.02	0.02
Na	1.70	1.70	1.62	1.69	2.17	2.14	2.16	2.09	2.08	2.07	2.06
K	0.05	0.05	0.05	0.05	0.08	0.08	0.08	0.07	0.08	0.07	0.09
P	n.a.	n.a.	n.a.	n.a.	n.a.	n.a.	n.a.	n.a.	n.a.	n.a.	n.a.
Total	20.07	20.05	20.09	20.03	20.04	20.03	20.03	20.03	20.03	20.02	20.07
An	57.50	57.28	59.58	57.28	44.92	45.59	44.90	46.87	47.23	47.29	47.65
Ab	41.18	41.51	39.32	41.55	53.11	52.51	53.09	51.31	50.88	50.88	50.24
Or	1.32	1.21	1.10	1.17	1.97	1.90	2.01	1.82	1.89	1.83	2.11

Group: B = basalt; BA = basaltic andesite; A = andesite; D = dacite; R = rhyolite; Opx/Cgt-SVC 2, 3 = orthopyroxene/cummingtonite-bearing SVC 2; 3 lavas; **Grain:** P = phenocryst; MC = microphenocryst; G = groundmass; C = core; INC = inclusion (mineral included within is stated in parentheses); **Position:** C = core; M = mantle; R = rim, osci. = oscillatory; **Other:** UNZ = unzoned; Dist. = distance from the core (μm); An = anorthite; Ab = albite; Or = orthoclase.

Table G.1. (continued).

Group: Sample: Name: Grain:	Opx-SVC 2, 3 D SL-83-03 Profile C4-PI10-11 P Indiff.		Opx-SVC 2, 3 D SL-83-03 Profile C4-PI12-14 P Type 5		Cgt-SVC 2,3 D SL-11-01A C4-PI1A C4-PI1B MP			Cgt-SVC 2, 3 D SL-11-01A Profile P1 P Type 3			
Position:	M	M	C	C	M	C	R	C	C	C	C
Dist.:	385	411	80	106				0	26	51	77
SiO ₂	55.15	55.04	55.15	54.84	45.50	51.83	53.06	48.26	50.22	51.27	49.73
Al ₂ O ₃	27.20	27.61	27.42	27.29	36.29	31.18	30.39	32.84	31.41	30.28	31.40
MgO	b.d.l.	b.d.l.	b.d.l.	b.d.l.	b.d.l.	b.d.l.	b.d.l.	b.d.l.	b.d.l.	b.d.l.	b.d.l.
CaO	10.19	10.65	10.38	10.40	17.61	12.09	11.20	14.06	12.37	11.32	12.82
FeO	0.11	0.16	0.15	0.09	0.06	0.09	0.11	0.09	0.05	0.08	0.15
Na ₂ O	5.62	5.55	5.66	5.59	1.68	4.72	4.85	0.14	0.19	0.22	0.18
K ₂ O	0.39	0.34	0.32	0.35	0.05	0.22	0.27	3.68	4.56	5.16	4.29
P ₂ O ₅	n.a.	n.a.	n.a.	n.a.	0.41	0.14	0.32	0.31	0.32	b.d.l.	0.35
Total	98.67	99.35	99.10	98.55	101.60	100.20	100.20	99.35	99.14	98.25	98.91
Si	10.08	10.00	10.04	10.04	8.25	9.38	9.56	8.88	9.21	9.47	9.16
Al	5.86	5.91	5.88	5.89	7.75	6.65	6.46	7.12	6.79	6.59	6.81
Mg	b.d.l.	b.d.l.	b.d.l.	b.d.l.	b.d.l.	b.d.l.	b.d.l.	b.d.l.	b.d.l.	b.d.l.	b.d.l.
Ca	1.99	2.07	2.03	2.04	3.42	2.34	2.16	2.77	2.43	2.24	2.53
Fe (ii)	0.02	0.02	0.02	0.01	0.01	0.01	0.02	0.01	0.01	0.01	0.02
Na	1.99	1.96	2.00	1.98	0.59	1.66	1.70	0.03	0.04	0.05	0.04
K	0.09	0.08	0.07	0.08	0.01	0.05	0.06	1.31	1.62	1.85	1.53
P	n.a.	n.a.	n.a.	n.a.	0.06	0.02	0.05	0.05	0.05	b.d.l.	0.05
Total	20.03	20.05	20.05	20.05	20.09	20.11	20.01	20.17	20.15	20.20	20.14
An	48.94	50.47	49.42	49.70	85.00	57.89	55.17	67.31	59.34	54.10	61.66
Ab	48.85	47.60	48.76	48.32	14.69	40.87	43.25	31.91	39.58	44.64	37.31
Or	2.21	1.93	1.82	1.97	0.31	1.24	1.58	0.78	1.07	1.26	1.03

Group: Sample: Name: Grain:	Cgt-SVC 2, 3 D SL-11-01A Profile P1 P Type 3										
Position:	C	C	C	C	C	C	C	C	C	M	M
Dist.:	102	128	154	179	205	231	256	282	307	333	359
SiO ₂	48.83	50.50	51.46	50.41	50.42	51.33	50.75	51.20	50.86	52.54	54.00
Al ₂ O ₃	32.45	31.58	30.70	31.48	31.52	30.92	30.99	30.84	30.51	30.48	28.94
MgO	b.d.l.	b.d.l.	b.d.l.	b.d.l.	b.d.l.	b.d.l.	b.d.l.	b.d.l.	b.d.l.	b.d.l.	b.d.l.
CaO	13.54	12.28	11.79	12.64	12.06	11.73	12.01	11.80	11.52	10.78	9.53
FeO	0.08	0.11	0.10	0.07	0.06	0.07	0.04	0.04	0.09	0.09	0.11
Na ₂ O	0.16	0.20	0.22	0.19	0.21	0.23	0.20	0.22	0.23	0.25	0.32
K ₂ O	3.93	4.67	4.93	4.46	4.70	4.95	4.67	4.95	4.94	5.43	6.09
P ₂ O ₅	0.06	0.08	0.41	0.09	b.d.l.	0.11	0.21	0.21	0.27	b.d.l.	0.14
Total	99.04	99.44	99.56	99.28	98.94	99.37	98.91	99.23	98.39	99.59	99.16
Si	9.00	9.24	9.38	9.24	9.26	9.38	9.32	9.37	9.38	9.55	9.82
Al	7.05	6.81	6.59	6.80	6.83	6.66	6.70	6.65	6.63	6.53	6.20
Mg	b.d.l.	b.d.l.	b.d.l.	b.d.l.	b.d.l.	b.d.l.	b.d.l.	b.d.l.	b.d.l.	b.d.l.	b.d.l.
Ca	2.67	2.41	2.30	2.48	2.37	2.30	2.36	2.31	2.28	2.10	1.86
Fe (ii)	0.01	0.02	0.02	0.01	0.01	0.01	0.01	0.01	0.01	0.01	0.02
Na	0.04	0.05	0.05	0.04	0.05	0.05	0.05	0.05	0.05	0.06	0.07
K	1.40	1.66	1.74	1.59	1.67	1.75	1.66	1.75	1.77	1.91	2.15
P	0.01	0.01	0.06	0.01	0.00	0.02	0.03	0.03	0.04	0.00	0.02
Total	20.18	20.19	20.13	20.16	20.19	20.17	20.14	20.16	20.15	20.17	20.15
An	64.98	58.57	56.21	60.38	57.97	55.94	58.01	56.15	55.58	51.59	45.55
Ab	34.11	40.31	42.53	38.57	40.83	42.74	40.82	42.62	43.11	47.00	52.64
Or	0.91	1.11	1.26	1.06	1.19	1.32	1.17	1.23	1.30	1.42	1.80

Group: Sample: Name: Grain:	Cgt-SVC 2, 3 D SL-11-01A Profile P1 P Type 3										
Position:	M	M	M	M	M	M	M	M	M	M	M
Dist.:	384	410	436	461	487	512	538	564	589	615	641
SiO ₂	53.69	52.85	52.98	52.65	52.39	52.07	50.51	51.68	52.36	53.08	51.37
Al ₂ O ₃	29.11	29.91	30.03	29.92	30.03	30.41	31.50	30.58	29.49	29.75	31.36
MgO	b.d.l.	b.d.l.	b.d.l.	b.d.l.	b.d.l.	b.d.l.	b.d.l.	b.d.l.	b.d.l.	b.d.l.	b.d.l.
CaO	9.92	10.38	10.47	10.60	11.01	11.37	12.35	11.29	10.49	10.47	11.77
FeO	0.12	0.15	0.05	0.10	0.05	0.07	0.10	0.15	0.09	0.07	0.16
Na ₂ O	0.31	0.29	0.29	0.27	0.24	0.22	0.19	0.24	0.24	0.26	0.22
K ₂ O	5.86	5.64	5.63	5.49	5.37	5.08	4.55	5.14	5.44	5.44	4.88
P ₂ O ₅	b.d.l.	0.32	0.01	0.23	0.30	0.27	0.03	0.14	b.d.l.	0.05	0.07
Total	98.99	99.56	99.45	99.31	99.40	99.43	99.22	99.19	97.97	99.12	99.84
Si	9.79	9.60	9.64	9.59	9.54	9.48	9.26	9.45	9.67	9.67	9.34
Al	6.26	6.40	6.44	6.42	6.45	6.53	6.80	6.59	6.42	6.39	6.72
Mg	b.d.l.	b.d.l.	b.d.l.	b.d.l.	b.d.l.	b.d.l.	b.d.l.	b.d.l.	b.d.l.	b.d.l.	b.d.l.
Ca	1.94	2.02	2.04	2.07	2.15	2.22	2.42	2.21	2.07	2.04	2.29
Fe (ii)	0.02	0.02	0.01	0.01	0.01	0.01	0.01	0.02	0.01	0.01	0.02
Na	0.07	0.07	0.07	0.06	0.06	0.05	0.04	0.06	0.06	0.06	0.05
K	2.07	1.99	1.99	1.94	1.90	1.79	1.62	1.82	1.95	1.92	1.72
P	0.00	0.05	0.00	0.03	0.05	0.04	0.00	0.02	b.d.l.	0.01	0.01
Total	20.15	20.15	20.17	20.14	20.14	20.11	20.17	20.16	20.15	20.11	20.17
An	47.47	49.60	49.82	50.82	52.38	54.61	59.32	54.09	50.87	50.76	56.41
Ab	50.75	48.78	48.54	47.63	46.24	44.12	39.59	44.55	47.74	47.73	42.35
Or	1.78	1.62	1.64	1.55	1.37	1.27	1.08	1.36	1.39	1.51	1.24

Group: B = basalt; BA = basaltic andesite; A = andesite; D = dacite; R = rhyolite; Opx/Cgt-SVC 2, 3 = orthopyroxene/cummingtonite-bearing SVC 2; 3 lavas; **Grain:** P = phenocryst; MC = microphenocryst; G = groundmass; C = core; INC = inclusion (mineral included within is stated in parentheses); **Position:** C = core; M = mantle; R = rim, osci. = oscillatory; **Other:** UNZ = unzoned; Dist. = distance from the core (µm); An = anorthite; Ab = albite; Or = orthoclase.

Table G.1. (continued).

Group: Sample: Grain:	Cgt-SVC 2, 3 D SL-11-01A Profile P1 P Type 3									Cgt-SVC 2, 3 D SL-11-01A Profile P2 G	
Position: Dist.:	M 666	M 692	M 718	M 743	M 769	M 794	M 820	M 846	M 871	C 0	C 34
SiO ₂	50.94	51.79	52.44	52.06	53.40	52.86	52.45	51.84	51.59	44.33	44.27
Al ₂ O ₃	31.40	30.30	30.50	30.40	29.77	29.93	30.22	29.69	30.47	36.56	36.57
MgO	b.d.l.	b.d.l.	b.d.l.	b.d.l.	b.d.l.	b.d.l.	b.d.l.	b.d.l.	b.d.l.	b.d.l.	b.d.l.
CaO	12.23	11.48	11.22	11.20	10.58	10.62	10.86	11.11	11.38	17.90	17.96
FeO	0.11	0.12	0.11	0.06	0.06	0.11	0.11	0.12	0.13	0.10	0.12
Na ₂ O	0.21	0.23	0.24	0.25	0.27	0.28	0.26	0.25	0.25	0.04	0.03
K ₂ O	4.72	5.10	5.18	5.28	5.49	5.59	5.35	5.16	5.10	1.57	1.51
P ₂ O ₅	0.05	0.29	0.37	0.08	b.d.l.	0.19	0.10	0.35	0.10	0.31	0.39
Total	99.64	99.32	100.07	99.33	99.43	99.53	99.38	98.53	99.02	100.82	100.79
Si	9.30	9.46	9.49	9.50	9.71	9.61	9.56	9.53	9.45	8.12	8.11
Al	6.75	6.52	6.50	6.54	6.38	6.41	6.49	6.43	6.58	7.89	7.89
Mg	b.d.l.	b.d.l.	b.d.l.	b.d.l.	b.d.l.	b.d.l.	b.d.l.	b.d.l.	b.d.l.	b.d.l.	b.d.l.
Ca	2.39	2.25	2.17	2.19	2.06	2.07	2.12	2.19	2.23	3.51	3.52
Fe (ii)	0.02	0.02	0.02	0.01	0.01	0.02	0.02	0.02	0.02	0.01	0.02
Na	0.05	0.05	0.06	0.06	0.06	0.06	0.06	0.06	0.06	0.01	0.01
K	1.67	1.80	1.82	1.87	1.93	1.97	1.89	1.84	1.81	0.56	0.53
P	0.01	0.04	0.06	0.01	b.d.l.	0.03	0.01	0.06	0.02	0.05	0.06
Total	20.18	20.14	20.11	20.18	20.13	20.16	20.15	20.12	20.17	20.15	20.13
An	58.19	54.73	53.71	53.19	50.79	50.43	52.11	53.57	54.43	86.13	86.68
Ab	40.62	43.99	44.92	45.40	47.69	48.02	46.41	44.98	44.17	13.64	13.15
Or	1.19	1.28	1.37	1.41	1.52	1.56	1.48	1.45	1.40	0.23	0.17

Group: Sample: Grain:	Cgt-SVC 2, 3 D SL-11-01A Profile P2 G	Cgt-SVC 2, 3 D SL-11-01A Profile P3 G	Cgt-SVC 2, 3 D SL-11-01A Profile P4 P Type 6								
Position: Dist.:	R 102	C 0	R 58	C 0	C 26	C 52	C 78	C 104	M 130	M 156	M 182
SiO ₂	49.96	53.37	52.86	54.12	54.31	54.15	53.84	54.58	51.99	52.90	53.14
Al ₂ O ₃	31.49	29.36	30.15	29.29	29.00	29.12	29.13	28.90	30.76	30.21	29.88
MgO	b.d.l.	b.d.l.	b.d.l.	b.d.l.	b.d.l.	b.d.l.	b.d.l.	b.d.l.	b.d.l.	b.d.l.	b.d.l.
CaO	12.75	10.46	11.08	10.01	9.98	10.11	10.07	9.75	11.77	10.96	10.77
FeO	0.11	0.08	0.17	0.06	0.06	0.08	0.10	0.09	0.10	0.09	0.07
Na ₂ O	0.19	0.28	0.27	0.30	0.30	0.29	0.31	0.32	0.21	0.27	0.26
K ₂ O	4.40	5.49	5.23	5.51	5.55	5.46	5.53	5.58	4.64	5.15	5.00
P ₂ O ₅	0.19	b.d.l.	b.d.l.	0.16	0.26	b.d.l.	0.05	0.20	0.10	b.d.l.	0.39
Total	99.09	98.92	99.58	99.42	99.44	98.96	99.02	99.43	99.56	99.54	99.51
Si	9.18	9.75	9.61	9.81	9.83	9.87	9.81	9.88	9.46	9.61	9.63
Al	6.82	6.32	6.46	6.25	6.19	6.25	6.25	6.17	6.60	6.47	6.38
Mg	b.d.l.	b.d.l.	b.d.l.	b.d.l.	b.d.l.	b.d.l.	b.d.l.	b.d.l.	b.d.l.	b.d.l.	b.d.l.
Ca	2.51	2.05	2.16	1.94	1.94	1.97	1.97	1.89	2.29	2.13	2.09
Fe (ii)	0.02	0.01	0.03	0.01	0.01	0.01	0.02	0.01	0.01	0.01	0.01
Na	0.04	0.06	0.06	0.07	0.07	0.07	0.07	0.07	0.05	0.06	0.06
K	1.57	1.94	1.84	1.94	1.95	1.93	1.95	1.96	1.64	1.81	1.76
P	0.03	b.d.l.	b.d.l.	0.02	0.04	b.d.l.	0.01	0.03	0.01	b.d.l.	0.06
Total	20.17	20.11	20.14	20.03	20.02	20.06	20.07	20.01	20.06	20.10	19.99
An	60.90	50.46	53.11	49.20	48.95	49.70	49.27	48.19	57.64	53.24	53.51
Ab	38.05	47.95	45.37	49.06	49.30	48.59	48.91	49.93	41.12	45.23	44.93
Or	1.06	1.59	1.52	1.74	1.76	1.70	1.82	1.88	1.23	1.53	1.56

Group: Sample: Grain:	Cgt-SVC 2, 3 D SL-11-01A Profile P4 P Type 6										
Position: Dist.:	M 207	M 233	M 259	M 285	M 311	M 337	M 363	M 389	M 519	M 545	M 571
SiO ₂	52.30	51.92	52.61	53.17	54.29	52.42	53.44	52.66	52.87	50.46	53.09
Al ₂ O ₃	30.56	31.22	30.21	30.38	29.20	30.51	30.14	30.04	30.39	31.97	30.26
MgO	b.d.l.	b.d.l.	b.d.l.	b.d.l.	b.d.l.	b.d.l.	b.d.l.	b.d.l.	b.d.l.	b.d.l.	b.d.l.
CaO	11.36	12.04	11.08	11.09	10.16	11.43	10.76	10.97	10.96	12.95	11.10
FeO	0.07	0.12	0.10	0.06	0.06	0.10	0.08	0.09	0.10	0.11	0.09
Na ₂ O	0.23	0.21	0.25	0.25	0.29	0.24	0.27	0.25	0.27	0.18	0.25
K ₂ O	4.87	4.56	5.05	5.10	5.35	4.89	5.34	5.12	5.01	4.08	4.97
P ₂ O ₅	0.33	0.20	b.d.l.	0.27	b.d.l.	0.13	0.30	0.25	0.16	0.11	0.05
Total	99.74	100.27	99.14	100.28	99.28	99.73	100.38	99.39	99.77	99.88	99.81
Si	9.49	9.39	9.60	9.58	9.85	9.52	9.62	9.58	9.58	9.19	9.61
Al	6.53	6.65	6.50	6.45	6.24	6.53	6.39	6.44	6.49	6.86	6.46
Mg	b.d.l.	b.d.l.	b.d.l.	b.d.l.	b.d.l.	b.d.l.	b.d.l.	b.d.l.	b.d.l.	b.d.l.	b.d.l.
Ca	2.21	2.33	2.17	2.14	1.98	2.22	2.07	2.14	2.13	2.53	2.15
Fe (ii)	0.01	0.02	0.01	0.01	0.01	0.02	0.01	0.01	0.02	0.02	0.01
Na	0.05	0.05	0.06	0.06	0.07	0.06	0.06	0.06	0.06	0.04	0.06
K	1.71	1.60	1.79	1.78	1.88	1.72	1.86	1.81	1.76	1.44	1.74
P	0.05	0.03	b.d.l.	0.04	b.d.l.	0.02	0.05	0.04	0.02	0.02	0.01
Total	20.05	20.06	20.10	20.05	20.01	20.08	20.08	20.07	20.05	20.10	20.05
An	55.57	58.61	54.01	53.76	50.36	55.58	51.86	53.43	53.87	62.98	54.46
Ab	43.11	40.15	44.53	44.79	47.95	43.01	46.60	45.13	44.54	35.95	44.10
Or	1.32	1.24	1.46	1.44	1.69	1.41	1.54	1.44	1.58	1.07	1.45

Group: B = basalt; BA = basaltic andesite; A = andesite; D = dacite; R = rhyolite; Opx/Cgt-SVC 2, 3 = orthopyroxene/cummingtonite-bearing SVC 2; 3 lavas; **Grain:** P = phenocryst; MC = microphenocryst; G = groundmass; C = core; INC = inclusion (mineral included within is stated in parentheses); **Position:** C = core; M = mantle; R = rim, osci. = oscillatory; **Other:** UNZ = unzoned; Dist. = distance from the core (μm); An = anorthite; Ab = albite; Or = orthoclase.

Table G.1. (continued).

Group:	Cgt-SVC 2, 3 D											
Sample:	SL-11-01A											
Name:	Profile P4											
Grain:	P Type 6											
Position:	M	M	M	M	M	M	M	M	M	M	M	M
Dist.:	622	674	700	726	752	778	804	830	856	882	908	
SiO ₂	51.58	52.39	52.92	54.07	53.51	52.78	52.87	51.83	51.91	53.32	52.83	
Al ₂ O ₃	30.65	30.57	30.49	29.35	30.06	29.44	30.11	31.10	31.50	30.58	30.55	
MgO	b.d.l.	b.d.l.	b.d.l.	b.d.l.	b.d.l.	b.d.l.	b.d.l.	b.d.l.	b.d.l.	b.d.l.	b.d.l.	
CaO	11.45	11.54	10.88	10.13	10.68	10.29	10.98	12.04	12.21	10.96	11.30	
FeO	0.13	0.10	0.08	0.07	0.10	0.07	0.10	0.11	0.11	0.07	0.13	
Na ₂ O	0.25	0.23	0.26	0.28	0.26	0.27	0.26	0.22	0.21	0.26	0.24	
K ₂ O	4.61	4.72	5.09	5.46	5.13	5.30	5.15	4.53	4.47	4.96	4.86	
P ₂ O ₅	0.31	0.33	0.20	b.d.l.	0.14	b.d.l.	0.15	0.16	0.05	b.d.l.	0.08	
Total	98.98	99.85	99.93	99.33	99.88	98.17	99.62	99.98	100.45	100.19	99.99	
Si	9.43	9.49	9.57	9.81	9.67	9.71	9.60	9.40	9.37	9.61	9.56	
Al	6.61	6.53	6.50	6.28	6.40	6.38	6.44	6.65	6.70	6.50	6.51	
Mg	b.d.l.	b.d.l.	b.d.l.	b.d.l.	b.d.l.	b.d.l.	b.d.l.	b.d.l.	b.d.l.	b.d.l.	b.d.l.	
Ca	2.24	2.24	2.11	1.97	2.07	2.03	2.13	2.34	2.36	2.12	2.19	
Fe (ii)	0.02	0.02	0.01	0.01	0.02	0.01	0.02	0.02	0.02	0.01	0.02	
Na	0.06	0.05	0.06	0.07	0.06	0.06	0.06	0.05	0.05	0.06	0.06	
K	1.63	1.66	1.79	1.92	1.80	1.89	1.81	1.59	1.56	1.73	1.71	
P	0.05	0.05	0.03	b.d.l.	0.02	0.00	0.02	0.03	0.01	0.00	0.01	
Total	20.04	20.03	20.06	20.05	20.03	20.08	20.08	20.06	20.07	20.03	20.05	
An	57.00	56.69	53.34	49.79	52.72	50.91	53.27	58.72	59.44	54.15	55.42	
Ab	41.50	41.96	45.17	48.55	45.76	47.48	45.23	39.99	39.33	44.33	43.17	
Or	1.51	1.35	1.49	1.66	1.52	1.61	1.50	1.29	1.23	1.52	1.41	

Group:	Cgt-SVC 2, 3 D											
Sample:	SL-11-01A											
Name:	Profile P4											
Grain:	P Type 6											
Position:	M	M	M	M	M	M	M	M	M	M	M	M
Dist.:	934	986	1012	1037	1063	1089	1115	1141	1167	1193	1219	
SiO ₂	52.90	54.14	53.39	53.96	53.88	54.64	55.12	53.59	53.82	52.54	54.28	
Al ₂ O ₃	30.35	29.35	30.06	29.87	29.67	29.43	29.23	30.14	29.99	30.61	29.54	
MgO	b.d.l.	b.d.l.	b.d.l.	b.d.l.	b.d.l.	b.d.l.	b.d.l.	b.d.l.	b.d.l.	b.d.l.	b.d.l.	
CaO	11.33	10.21	10.68	10.29	10.45	10.01	9.62	10.82	10.68	11.40	10.15	
FeO	0.04	0.07	0.06	0.08	0.08	0.11	0.06	0.10	0.11	0.10	0.08	
Na ₂ O	0.26	0.29	0.27	0.28	0.29	0.31	0.32	0.26	0.26	0.25	0.29	
K ₂ O	4.93	5.49	5.19	5.35	5.33	5.58	5.77	5.23	5.10	4.78	5.46	
P ₂ O ₅	b.d.l.	0.34	0.35	0.43	0.21	0.03	0.08	0.15	0.07	0.03	0.14	
Total	99.77	99.86	100.03	100.27	99.92	100.07	100.19	100.32	100.02	99.72	99.93	
Si	9.59	9.77	9.63	9.70	9.73	9.84	9.90	9.65	9.71	9.53	9.79	
Al	6.49	6.24	6.39	6.33	6.31	6.24	6.18	6.40	6.37	6.55	6.28	
Mg	b.d.l.	b.d.l.	b.d.l.	b.d.l.	b.d.l.	b.d.l.	b.d.l.	b.d.l.	b.d.l.	b.d.l.	b.d.l.	
Ca	2.20	1.97	2.06	1.98	2.02	1.93	1.85	2.09	2.06	2.22	1.96	
Fe (ii)	0.01	0.01	0.01	0.01	0.01	0.02	0.01	0.01	0.02	0.02	0.01	
Na	0.06	0.07	0.06	0.06	0.07	0.07	0.07	0.06	0.06	0.06	0.07	
K	1.73	1.92	1.82	1.86	1.86	1.95	2.01	1.83	1.78	1.68	1.91	
P	b.d.l.	0.05	0.05	0.07	0.03	0.00	0.01	0.02	0.01	0.01	0.02	
Total	20.07	20.03	20.03	20.01	20.03	20.04	20.03	20.06	20.01	20.06	20.03	
An	55.10	49.84	52.37	50.67	51.15	48.92	47.08	52.52	52.81	56.01	49.81	
Ab	43.40	48.45	46.06	47.68	47.18	49.29	51.08	45.95	45.63	42.51	48.48	
Or	1.50	1.71	1.58	1.65	1.68	1.79	1.84	1.53	1.56	1.48	1.70	

Group:	Cgt-SVC 2, 3 D				Cgt-SVC 2, 3 D							
Sample:	SL-11-01A				SL-11-01A							
Name:	Profile P4				Profile P5							
Grain:	P Type 6				P Type 2							
Position:	M	R	C	C	C	C	M	M	M	M	M	M
Dist.:	1245	1271	0	25	51	76	102	127	153	178	204	
SiO ₂	53.63	53.72	47.08	47.34	46.77	48.32	50.26	52.31	51.20	50.42	52.79	
Al ₂ O ₃	30.05	29.75	34.83	34.62	33.06	33.52	32.51	30.65	31.94	31.78	30.72	
MgO	b.d.l.	b.d.l.	b.d.l.	b.d.l.	b.d.l.	b.d.l.	b.d.l.	b.d.l.	b.d.l.	b.d.l.	b.d.l.	
CaO	10.66	10.52	15.82	15.64	15.46	14.67	13.44	11.64	12.70	12.84	11.47	
FeO	0.10	0.10	0.10	0.09	0.12	0.08	0.10	0.08	0.07	0.11	0.10	
Na ₂ O	0.27	0.28	0.09	0.09	0.21	0.12	0.16	0.22	0.18	0.18	0.23	
K ₂ O	5.17	5.21	2.53	2.68	2.89	3.13	3.79	4.75	4.16	4.11	4.79	
P ₂ O ₅	0.08	0.09	0.11	0.32	0.24	0.13	0.24	0.22	0.25	0.28	b.d.l.	
Total	99.95	99.65	100.56	100.75	98.76	100.00	100.47	99.88	100.50	99.72	100.03	
Si	9.68	9.72	8.58	8.61	8.70	8.83	9.10	9.48	9.25	9.19	9.55	
Al	6.39	6.35	7.49	7.42	7.24	7.22	6.94	6.55	6.80	6.83	6.55	
Mg	b.d.l.	b.d.l.	b.d.l.	b.d.l.	b.d.l.	b.d.l.	b.d.l.	b.d.l.	b.d.l.	b.d.l.	b.d.l.	
Ca	2.06	2.04	3.09	3.05	3.08	2.87	2.61	2.26	2.46	2.51	2.22	
Fe (ii)	0.01	0.02	0.02	0.01	0.02	0.01	0.02	0.01	0.01	0.02	0.01	
Na	0.06	0.07	0.02	0.02	0.05	0.03	0.04	0.05	0.04	0.04	0.05	
K	1.81	1.83	0.89	0.95	1.04	1.11	1.33	1.67	1.46	1.45	1.68	
P	0.01	0.01	0.02	0.05	0.04	0.02	0.04	0.03	0.04	0.04	b.d.l.	
Total	20.04	20.03	20.10	20.09	20.17	20.09	20.06	20.05	20.05	20.08	20.07	
An	52.43	51.87	77.19	75.89	73.86	71.68	65.62	56.77	62.09	62.71	56.16	
Ab	45.99	46.47	22.30	23.58	24.97	27.64	33.45	41.96	36.84	36.27	42.48	
Or	1.58	1.66	0.51	0.53	1.17	0.69	0.92	1.27	1.07	1.02	1.36	

Group: B = basalt; BA = basaltic andesite; A = andesite; D = dacite; R = rhyolite; Opx/Cgt-SVC 2, 3 = orthopyroxene/cummingtonite-bearing SVC 2; 3 lavas; **Grain:** P = phenocryst; MC = microphenocryst; G = groundmass; C = core; INC = inclusion (mineral included within is stated in parentheses); **Position:** C = core; M = mantle; R = rim, osci. = oscillatory; **Other:** UNZ = unzoned; Dist. = distance from the core (µm); An = anorthite; Ab = albite; Or = orthoclase.

Table G.1. (continued).

Group: Sample: Name: Grain:	Cgt-SVC 2, 3 D SL-11-01A Profile P5 P Type 2										
Position: Dist.:	M 229	M 255	M 280	M 306	M 331	M 357	M 382	M 408	M 433	M 459	M 484
SiO ₂	51.39	50.20	51.16	51.64	51.68	50.60	51.64	52.10	50.46	51.32	52.39
Al ₂ O ₃	31.20	31.21	31.77	31.06	31.41	31.75	31.28	30.75	32.44	31.69	30.40
MgO	b.d.l.	b.d.l.	b.d.l.	b.d.l.	b.d.l.	b.d.l.	b.d.l.	b.d.l.	b.d.l.	b.d.l.	b.d.l.
CaO	12.25	12.52	12.66	12.01	11.94	12.84	12.33	11.73	13.30	12.51	11.35
FeO	0.10	0.08	0.09	0.05	0.06	0.10	0.06	0.09	0.09	0.12	0.04
Na ₂ O	0.20	0.20	0.19	0.22	0.22	0.22	0.21	0.22	0.18	0.20	0.26
K ₂ O	4.29	4.08	4.11	4.53	4.42	4.00	4.42	4.68	3.90	4.23	4.85
P ₂ O ₅	0.12	b.d.l.	b.d.l.	0.13	0.32	b.d.l.	0.13	0.32	0.17	0.04	0.15
Total	99.56	98.25	99.98	99.68	100.06	99.53	100.07	99.92	100.52	100.09	99.42
Si	9.36	9.28	9.29	9.39	9.35	9.24	9.36	9.44	9.13	9.31	9.53
Al	6.70	6.80	6.80	6.66	6.70	6.83	6.68	6.57	6.92	6.77	6.52
Mg	b.d.l.	b.d.l.	b.d.l.	b.d.l.	b.d.l.	b.d.l.	b.d.l.	b.d.l.	b.d.l.	b.d.l.	b.d.l.
Ca	2.39	2.48	2.46	2.34	2.32	2.51	2.39	2.28	2.58	2.43	2.21
Fe (ii)	0.02	0.01	0.01	0.01	0.01	0.01	0.01	0.01	0.01	0.02	0.01
Na	0.05	0.05	0.04	0.05	0.05	0.05	0.05	0.05	0.04	0.05	0.06
K	1.51	1.46	1.45	1.60	1.55	1.42	1.55	1.64	1.37	1.49	1.71
P	0.02	0.00	b.d.l.	0.02	0.05	b.d.l.	0.02	0.05	0.03	0.01	0.02
Total	20.05	20.07	20.06	20.07	20.03	20.08	20.07	20.05	20.07	20.06	20.06
An	60.48	62.16	62.26	58.65	59.12	63.16	59.94	57.34	64.66	61.31	55.53
Ab	38.32	36.67	36.62	40.08	39.61	35.57	38.88	41.37	34.32	37.50	42.97
Or	1.20	1.17	1.13	1.27	1.27	1.27	1.19	1.29	1.02	1.19	1.50

Group: Sample: Name: Grain:	Cgt-SVC 2, 3 D SL-11-01A Profile P5 P Type 2										
Position: Dist.:	M 510	M 535	M 560	M 586	M 611	M 637	M 662	M 688	M 713	M 739	M 790
SiO ₂	53.14	52.40	52.84	52.83	52.96	52.45	52.58	51.80	50.50	52.31	52.94
Al ₂ O ₃	30.15	29.47	30.47	30.62	30.75	31.12	30.26	30.92	32.13	30.56	30.50
MgO	b.d.l.	b.d.l.	b.d.l.	b.d.l.	b.d.l.	b.d.l.	b.d.l.	b.d.l.	b.d.l.	b.d.l.	b.d.l.
CaO	10.93	10.69	11.11	11.28	11.35	11.65	11.33	12.13	13.19	11.68	11.26
FeO	0.08	0.08	0.08	0.08	0.05	0.12	0.10	0.08	0.11	0.08	0.09
Na ₂ O	0.26	0.27	0.25	0.26	0.24	0.23	0.25	0.25	0.17	0.24	0.23
K ₂ O	4.94	4.89	4.94	4.84	4.91	4.74	4.83	4.60	3.92	4.79	4.88
P ₂ O ₅	b.d.l.	0.42	0.17	0.12	0.08	0.16	0.03	0.10	0.40	0.21	0.15
Total	99.42	98.21	99.86	100.06	100.32	100.46	99.40	99.90	100.41	99.87	100.06
Si	9.65	9.62	9.56	9.55	9.55	9.45	9.57	9.41	9.14	9.49	9.56
Al	6.46	6.38	6.50	6.52	6.53	6.61	6.49	6.62	6.85	6.53	6.49
Mg	b.d.l.	b.d.l.	b.d.l.	b.d.l.	b.d.l.	b.d.l.	b.d.l.	b.d.l.	b.d.l.	b.d.l.	b.d.l.
Ca	2.13	2.10	2.15	2.18	2.19	2.25	2.21	2.36	2.56	2.27	2.18
Fe (ii)	0.01	0.01	0.01	0.01	0.01	0.02	0.02	0.01	0.02	0.01	0.01
Na	0.06	0.06	0.06	0.06	0.06	0.05	0.06	0.06	0.04	0.05	0.05
K	1.74	1.74	1.73	1.69	1.72	1.66	1.70	1.62	1.38	1.68	1.71
P	b.d.l.	0.07	0.03	0.02	0.01	0.03	0.00	0.02	0.06	0.03	0.02
Total	20.04	19.99	20.05	20.04	20.06	20.06	20.06	20.10	20.05	20.07	20.04
An	54.15	53.84	54.59	55.44	55.28	56.80	55.63	58.45	64.36	56.63	55.28
Ab	44.31	44.56	43.94	43.03	43.33	41.85	42.88	40.13	34.63	42.00	43.37
Or	1.54	1.61	1.47	1.53	1.39	1.35	1.49	1.42	1.01	1.37	1.35

Group: Sample: Name: Grain:	Cgt-SVC 2, 3 D SL-11-01A Profile P5 P Type 2								Cgt-SVC 2, 3 D SL-11-01A Profile P6 P Type 6		
Position: Dist.:	M 815	M 866	M 917	M 943	M 968	M 994	M 1019	R 1045	C 0	C 27	C 54
SiO ₂	48.04	52.94	53.25	53.48	53.37	53.71	53.73	53.21	52.87	53.78	54.20
Al ₂ O ₃	34.06	30.80	29.66	30.23	30.11	29.98	30.69	30.05	30.37	29.80	28.95
MgO	b.d.l.	b.d.l.	b.d.l.	b.d.l.	b.d.l.	b.d.l.	b.d.l.	b.d.l.	b.d.l.	b.d.l.	b.d.l.
CaO	14.81	11.50	10.53	10.81	10.87	10.56	11.00	10.77	11.09	10.33	9.96
FeO	0.12	0.10	0.09	0.08	0.09	0.11	0.13	0.11	0.10	0.07	0.11
Na ₂ O	0.13	0.23	0.29	0.27	0.25	0.28	0.25	0.27	0.24	0.27	0.31
K ₂ O	3.16	4.87	5.23	5.10	5.04	5.35	5.22	5.08	4.94	5.46	5.52
P ₂ O ₅	0.29	0.20	0.15	0.18	0.37	0.22	0.24	0.25	0.30	0.31	0.06
Total	100.62	100.62	99.18	100.14	100.16	100.19	101.26	99.74	99.93	99.99	99.10
Si	8.73	9.52	9.69	9.64	9.62	9.68	9.59	9.63	9.56	9.70	9.85
Al	7.30	6.53	6.36	6.42	6.39	6.37	6.45	6.41	6.47	6.33	6.20
Mg	b.d.l.	b.d.l.	b.d.l.	b.d.l.	b.d.l.	b.d.l.	b.d.l.	b.d.l.	b.d.l.	b.d.l.	b.d.l.
Ca	2.89	2.21	2.05	2.09	2.10	2.04	2.10	2.09	2.15	2.00	1.94
Fe (ii)	0.02	0.01	0.01	0.01	0.01	0.02	0.02	0.02	0.02	0.01	0.02
Na	0.03	0.05	0.07	0.06	0.06	0.06	0.06	0.06	0.06	0.06	0.07
K	1.11	1.70	1.84	1.78	1.76	1.87	1.81	1.78	1.73	1.91	1.94
P	0.04	0.03	0.02	0.03	0.06	0.03	0.04	0.04	0.05	0.05	0.01
Total	20.12	20.05	20.05	20.03	20.01	20.06	20.06	20.03	20.03	20.05	20.04
An	71.64	55.85	51.80	53.08	53.58	51.33	53.04	53.07	54.59	50.33	49.04
Ab	27.63	42.83	46.53	45.37	44.94	47.03	45.55	45.33	43.98	48.11	49.15
Or	0.73	1.32	1.67	1.55	1.49	1.63	1.41	1.60	1.42	1.56	1.81

Group: B = basalt; BA = basaltic andesite; A = andesite; D = dacite; R = rhyolite; Opx/Cgt-SVC 2, 3 = orthopyroxene/cummingtonite-bearing SVC 2; 3 lavas; **Grain:** P = phenocryst; MC = microphenocryst; G = groundmass; C = core; INC = inclusion (mineral included within is stated in parentheses); **Position:** C = core; M = mantle; R = rim, osci. = oscillatory; **Other:** UNZ = unzoned; Dist. = distance from the core (μm); An = anorthite; Ab = albite; Or = orthoclase.

Table G.1. (continued).

Group:	Cgt-SVC 2, 3 D										
Sample:	SL-11-01A										
Name:	Profile P6										
Grain:	P Type 6										
Position:	C	C	M	M	M	M	M	M	M	M	M
Dist.:	82	109	136	190	218	245	272	299	327	354	381
SiO ₂	55.50	55.37	49.44	53.01	54.17	55.03	54.55	53.70	51.14	51.10	52.42
Al ₂ O ₃	28.48	28.76	32.28	30.50	30.03	28.94	29.43	29.71	31.62	32.08	30.60
MgO	b.d.l.	b.d.l.	b.d.l.	b.d.l.	b.d.l.	b.d.l.	b.d.l.	b.d.l.	b.d.l.	b.d.l.	b.d.l.
CaO	9.17	9.30	13.48	11.10	10.36	9.62	9.89	10.48	12.63	12.69	11.68
FeO	0.07	0.07	0.08	0.14	0.07	0.10	0.08	0.09	0.14	0.12	0.06
Na ₂ O	0.35	0.34	0.15	0.24	0.28	0.32	0.32	0.28	0.18	0.19	0.23
K ₂ O	5.93	5.81	3.62	4.95	5.42	5.74	5.62	5.31	4.11	4.08	4.46
P ₂ O ₅	0.13	0.20	0.08	0.10	0.15	0.06	0.07	0.17	0.23	0.19	0.34
Total	99.63	99.81	99.11	100.06	100.41	99.79	99.97	99.71	100.06	100.47	99.77
Si	10.01	9.96	9.08	9.58	9.72	9.92	9.83	9.72	9.28	9.23	9.50
Al	6.05	6.10	6.99	6.49	6.35	6.15	6.25	6.33	6.76	6.83	6.53
Mg	b.d.l.	b.d.l.	b.d.l.	b.d.l.	b.d.l.	b.d.l.	b.d.l.	b.d.l.	b.d.l.	b.d.l.	b.d.l.
Ca	1.77	1.79	2.65	2.15	1.99	1.86	1.91	2.03	2.46	2.46	2.27
Fe (ii)	0.01	0.01	0.01	0.02	0.01	0.01	0.01	0.01	0.02	0.02	0.01
Na	0.08	0.08	0.04	0.06	0.06	0.07	0.07	0.06	0.04	0.04	0.05
K	2.07	2.03	1.29	1.73	1.89	2.01	1.96	1.86	1.45	1.43	1.57
P	0.02	0.03	0.01	0.02	0.02	0.01	0.01	0.03	0.04	0.03	0.05
Total	20.02	19.99	20.07	20.05	20.04	20.03	20.05	20.04	20.04	20.04	19.97
An	45.12	46.01	66.68	54.56	50.55	47.19	48.38	51.33	62.24	62.51	58.33
Ab	52.83	52.01	32.43	44.01	47.85	50.93	49.77	47.03	36.68	36.39	40.32
Or	2.05	1.98	0.88	1.42	1.61	1.88	1.85	1.63	1.07	1.10	1.35

Group:	Cgt-SVC 2, 3 D				Cgt-SVC 2, 3 D						
Sample:	SL-11-01A				SL-11-01A						
Name:	Profile P6				Profile P7						
Grain:	P Type 6				MP Type 2						
Position:	M	R	C	C	C	C	C	C	C	C	R
Dist.:	408	435	0	27	53	80	107	160	186	213	240
SiO ₂	54.06	53.62	45.41	44.04	44.99	46.61	46.19	45.18	45.98	44.63	47.32
Al ₂ O ₃	29.59	29.90	35.98	36.77	35.97	34.86	35.18	35.78	35.35	36.27	33.96
MgO	b.d.l.	b.d.l.	b.d.l.	b.d.l.	b.d.l.	b.d.l.	b.d.l.	b.d.l.	b.d.l.	b.d.l.	b.d.l.
CaO	10.20	10.49	17.15	18.36	17.35	16.65	16.56	17.38	16.95	17.63	15.47
FeO	0.10	0.06	0.19	0.14	0.22	0.17	0.10	0.14	0.11	0.10	0.11
Na ₂ O	0.30	0.29	0.05	0.03	0.05	0.07	0.07	0.06	0.06	0.05	0.11
K ₂ O	5.40	5.17	1.90	1.28	1.80	2.30	2.26	1.79	2.01	1.60	2.73
P ₂ O ₅	0.23	0.21	0.28	0.26	0.34	0.22	0.35	0.41	b.d.l.	0.36	0.37
Total	99.88	99.77	100.96	100.90	100.72	100.85	100.71	100.71	100.47	100.62	100.06
Si	9.75	9.69	8.28	8.07	8.24	8.50	8.43	8.27	8.42	8.18	8.66
Al	6.29	6.37	7.73	7.94	7.76	7.49	7.57	7.71	7.63	7.83	7.33
Mg	b.d.l.	b.d.l.	b.d.l.	b.d.l.	b.d.l.	b.d.l.	b.d.l.	b.d.l.	b.d.l.	b.d.l.	b.d.l.
Ca	1.97	2.03	3.35	3.60	3.40	3.25	3.24	3.41	3.33	3.46	3.03
Fe (ii)	0.02	0.01	0.03	0.02	0.03	0.03	0.02	0.02	0.02	0.02	0.02
Na	0.07	0.07	0.01	0.01	0.01	0.02	0.02	0.01	0.01	0.01	0.03
K	1.89	1.81	0.67	0.45	0.64	0.81	0.80	0.64	0.71	0.57	0.97
P	0.03	0.03	0.04	0.04	0.05	0.03	0.05	0.06	b.d.l.	0.06	0.06
Total	20.02	20.02	20.12	20.13	20.13	20.12	20.11	20.11	20.12	20.11	20.09
An	50.17	51.94	83.07	88.68	83.92	79.64	79.90	83.99	82.04	85.68	75.33
Ab	48.07	46.34	16.62	11.16	15.79	19.95	19.72	15.68	17.60	14.04	24.04
Or	1.76	1.72	0.31	0.16	0.30	0.41	0.38	0.33	0.35	0.28	0.63

Group:	Cgt-SVC 2, 3 D				Cgt-SVC 2, 3 D						
Sample:	SL-11-01A				SL-83-08						
Name:	Profile P7				Profile C1-P11						
Grain:	MP Type 2				P Type 6						
Position:	R	C	C	C	C	C	C	C	C	C	C
Dist.:	266	0	25	51	76	102	127	152	178	203	229
SiO ₂	51.70	53.90	53.01	55.77	54.89	53.89	55.02	54.94	53.64	54.67	53.69
Al ₂ O ₃	31.14	28.85	29.59	27.60	28.32	28.95	28.23	28.39	29.10	28.36	29.14
MgO	b.d.l.	b.d.l.	b.d.l.	b.d.l.	b.d.l.	b.d.l.	b.d.l.	b.d.l.	b.d.l.	b.d.l.	b.d.l.
CaO	12.01	11.83	11.91	10.27	11.09	11.92	11.07	10.97	11.98	11.20	11.86
FeO	0.13	0.07	0.11	0.05	0.05	0.10	0.10	0.10	0.07	0.07	0.07
Na ₂ O	0.21	4.88	4.58	5.72	5.27	4.83	5.37	5.27	4.62	5.10	4.78
K ₂ O	4.55	0.23	0.20	0.29	0.25	0.24	0.27	0.27	0.22	0.24	0.21
P ₂ O ₅	0.26	n.a.	n.a.	n.a.	n.a.	n.a.	n.a.	n.a.	n.a.	n.a.	n.a.
Total	99.99	99.78	99.42	99.75	99.95	99.94	100.12	99.98	99.64	99.66	99.76
Si	9.37	9.78	9.65	10.07	9.92	9.76	9.93	9.92	9.74	9.90	9.74
Al	6.65	6.17	6.35	5.87	6.03	6.18	6.00	6.04	6.23	6.05	6.23
Mg	b.d.l.	b.d.l.	b.d.l.	b.d.l.	b.d.l.	b.d.l.	b.d.l.	b.d.l.	b.d.l.	b.d.l.	b.d.l.
Ca	2.33	2.30	2.32	1.99	2.15	2.31	2.14	2.12	2.33	2.17	2.31
Fe (ii)	0.02	0.01	0.02	0.01	0.01	0.02	0.01	0.01	0.01	0.01	0.01
Na	0.05	1.72	1.62	2.00	1.84	1.70	1.88	1.85	1.63	1.79	1.68
K	1.60	0.05	0.05	0.07	0.06	0.05	0.06	0.06	0.05	0.06	0.05
P	0.04	n.a.	n.a.	n.a.	n.a.	n.a.	n.a.	n.a.	n.a.	n.a.	n.a.
Total	20.07	20.03	20.01	20.02	20.02	20.02	20.04	20.01	19.99	19.99	20.01
An	58.57	56.50	58.28	48.99	53.01	56.91	52.44	52.67	58.14	54.08	57.12
Ab	40.18	42.21	40.54	49.39	45.54	41.75	46.02	45.81	40.57	44.53	41.66
Or	1.25	1.29	1.18	1.63	1.45	1.34	1.54	1.52	1.29	1.39	1.22

Group: B = basalt; BA = basaltic andesite; A = andesite; D = dacite; R = rhyolite; Opx/Cgt-SVC 2, 3 = orthopyroxene/cummingtonite-bearing SVC 2; 3 lavas; **Grain:** P = phenocryst; MC = microphenocryst; G = groundmass; C = core; INC = inclusion (mineral included within is stated in parentheses); **Position:** C = core; M = mantle; R = rim, osci. = oscillatory; **Other:** UNZ = unzoned; Dist. = distance from the core (µm); An = anorthite; Ab = albite; Or = orthoclase.

Table G.1. (continued).

Group:	Cgt-SVC 2, 3 D										
Sample:	SL-83-08										
Name:	Profile C1-P11										
Grain:	P Type 6										
Position:	C	C	C	C	C	C	M	M	M	M	M
Dist.:	254	279	305	330	356	381	406	432	457	508	533
SiO ₂	52.97	53.04	53.48	54.53	54.70	55.63	54.08	54.03	55.06	56.49	56.16
Al ₂ O ₃	28.84	29.70	29.33	29.27	28.44	27.82	28.88	28.78	28.19	27.21	27.48
MgO	b.d.l.	b.d.l.	b.d.l.	b.d.l.	b.d.l.	b.d.l.	b.d.l.	b.d.l.	b.d.l.	b.d.l.	b.d.l.
CaO	11.94	12.60	12.17	11.68	11.06	10.59	11.70	11.72	10.88	9.70	10.13
FeO	0.07	0.08	0.08	0.11	0.08	0.08	0.06	0.05	0.07	0.08	0.09
Na ₂ O	4.58	4.41	4.58	4.87	5.19	5.52	4.89	4.80	5.32	5.91	5.80
K ₂ O	0.22	0.20	0.20	0.22	0.26	0.30	0.24	0.22	0.25	0.35	0.29
P ₂ O ₅	n.a.	n.a.	n.a.	n.a.	n.a.	n.a.	n.a.	n.a.	n.a.	n.a.	n.a.
Total	98.63	100.07	99.84	100.70	99.73	99.94	99.90	99.60	99.80	99.78	100.02
Si	9.72	9.61	9.70	9.79	9.90	10.03	9.79	9.81	9.95	10.18	10.11
Al	6.24	6.34	6.27	6.19	6.07	5.91	6.16	6.15	6.01	5.78	5.83
Mg	b.d.l.	b.d.l.	b.d.l.	b.d.l.	b.d.l.	b.d.l.	b.d.l.	b.d.l.	b.d.l.	b.d.l.	b.d.l.
Ca	2.35	2.45	2.36	2.25	2.15	2.05	2.27	2.28	2.11	1.87	1.96
Fe (ii)	0.01	0.01	0.01	0.02	0.01	0.01	0.01	0.01	0.01	0.01	0.01
Na	1.63	1.55	1.61	1.69	1.82	1.93	1.72	1.69	1.86	2.06	2.02
K	0.05	0.05	0.05	0.05	0.06	0.07	0.06	0.05	0.06	0.08	0.07
P	n.a.	n.a.	n.a.	n.a.	n.a.	n.a.	n.a.	n.a.	n.a.	n.a.	n.a.
Total	20.00	20.01	20.00	19.99	20.01	20.01	20.01	19.99	20.00	20.00	20.01
An	58.29	60.52	58.82	56.29	53.26	50.57	56.15	56.68	52.28	46.61	48.33
Ab	40.44	38.32	40.05	42.44	45.23	47.73	42.48	42.07	46.27	51.39	50.03
Or	1.26	1.16	1.13	1.26	1.51	1.71	1.36	1.25	1.46	2.01	1.65

Group:	Cgt-SVC 2, 3 D										
Sample:	SL-83-08										
Name:	Profile C1-P11										
Grain:	P Type 6										
Position:	M	M	M	M	M	M	M	M	M	M	M
Dist.:	559	584	610	635	660	686	711	737	762	787	813
SiO ₂	56.25	55.76	55.81	56.52	57.03	56.76	53.04	54.83	54.08	54.96	55.35
Al ₂ O ₃	27.34	27.69	27.55	27.09	26.83	26.95	29.48	28.22	28.68	27.97	27.87
MgO	b.d.l.	b.d.l.	b.d.l.	b.d.l.	b.d.l.	b.d.l.	b.d.l.	b.d.l.	b.d.l.	b.d.l.	b.d.l.
CaO	9.86	10.32	10.25	9.80	9.53	9.44	12.50	11.04	11.76	10.66	10.65
FeO	0.12	0.07	0.09	0.08	0.04	0.07	0.07	0.09	0.08	0.07	0.05
Na ₂ O	5.84	5.60	5.63	5.65	5.84	5.85	4.36	5.10	4.70	4.95	5.24
K ₂ O	0.32	0.32	0.31	0.36	0.33	0.31	0.19	0.27	0.22	0.28	0.30
P ₂ O ₅	n.a.	n.a.	n.a.	n.a.	n.a.	n.a.	n.a.	n.a.	n.a.	n.a.	n.a.
Total	99.74	99.77	99.67	99.50	99.61	99.39	99.65	99.55	99.53	98.89	99.52
Si	10.15	10.07	10.09	10.21	10.27	10.25	9.64	9.94	9.82	10.00	10.02
Al	5.81	5.89	5.87	5.77	5.70	5.74	6.32	6.03	6.14	6.00	5.95
Mg	b.d.l.	b.d.l.	b.d.l.	b.d.l.	b.d.l.	b.d.l.	b.d.l.	b.d.l.	b.d.l.	b.d.l.	b.d.l.
Ca	1.90	2.00	1.98	1.90	1.84	1.83	2.43	2.14	2.29	2.08	2.07
Fe (ii)	0.02	0.01	0.01	0.01	0.01	0.01	0.01	0.01	0.01	0.01	0.01
Na	2.04	1.96	1.97	1.98	2.04	2.05	1.54	1.79	1.65	1.75	1.84
K	0.07	0.07	0.07	0.08	0.08	0.07	0.04	0.06	0.05	0.07	0.07
P	n.a.	n.a.	n.a.	n.a.	n.a.	n.a.	n.a.	n.a.	n.a.	n.a.	n.a.
Total	20.00	20.00	20.00	19.94	19.94	19.94	19.99	19.98	19.96	19.90	19.96
An	47.38	49.53	49.28	47.89	46.49	46.28	60.65	53.65	57.29	53.44	51.95
Ab	50.79	48.63	48.94	49.99	51.58	51.88	38.27	44.81	41.42	44.88	46.29
Or	1.83	1.84	1.78	2.12	1.94	1.83	1.08	1.54	1.29	1.68	1.76

Group:	Cgt-SVC 2, 3 D										
Sample:	SL-83-08										
Name:	Profile C1-P11										
Grain:	P Type 6										
Position:	M	M	M	M	M	M	M	M	M	M	M
Dist.:	838	864	889	915	965	991	1016	1042	1067	1092	1118
SiO ₂	55.75	54.32	53.98	54.62	55.09	55.35	55.34	55.57	55.26	56.16	55.75
Al ₂ O ₃	27.43	28.71	28.79	28.43	27.87	27.93	28.12	27.30	27.66	27.19	27.64
MgO	b.d.l.	b.d.l.	b.d.l.	b.d.l.	b.d.l.	b.d.l.	b.d.l.	b.d.l.	b.d.l.	b.d.l.	b.d.l.
CaO	10.20	11.48	11.71	11.12	10.76	10.72	10.77	10.50	10.53	9.96	10.40
FeO	0.06	0.10	0.08	0.07	0.10	0.10	0.09	0.10	0.10	0.10	0.12
Na ₂ O	5.49	4.83	4.66	5.03	5.19	5.16	5.22	5.31	5.40	5.74	5.59
K ₂ O	0.30	0.26	0.23	0.26	0.28	0.28	0.28	0.31	0.29	0.32	0.31
P ₂ O ₅	n.a.	n.a.	n.a.	n.a.	n.a.	n.a.	n.a.	n.a.	n.a.	n.a.	n.a.
Total	99.24	99.72	99.48	99.56	99.36	99.57	99.87	99.13	99.28	99.51	99.81
Si	10.11	9.84	9.81	9.90	10.00	10.01	9.99	10.10	10.03	10.16	10.07
Al	5.86	6.13	6.16	6.07	5.96	5.96	5.98	5.85	5.92	5.79	5.88
Mg	b.d.l.	b.d.l.	b.d.l.	b.d.l.	b.d.l.	b.d.l.	b.d.l.	b.d.l.	b.d.l.	b.d.l.	b.d.l.
Ca	1.98	2.23	2.28	2.16	2.09	2.08	2.08	2.04	2.05	1.93	2.01
Fe (ii)	0.01	0.02	0.01	0.01	0.02	0.02	0.01	0.02	0.02	0.01	0.02
Na	1.93	1.70	1.64	1.77	1.83	1.81	1.83	1.87	1.90	2.01	1.96
K	0.07	0.06	0.05	0.06	0.07	0.07	0.06	0.07	0.07	0.07	0.07
P	n.a.	n.a.	n.a.	n.a.	n.a.	n.a.	n.a.	n.a.	n.a.	n.a.	n.a.
Total	19.96	19.97	19.96	19.98	19.97	19.94	19.96	19.95	19.99	19.99	20.01
An	49.76	55.90	57.37	54.16	52.51	52.54	52.41	51.31	51.02	48.04	49.82
Ab	48.48	42.59	41.30	44.31	45.86	45.81	45.98	46.89	47.33	50.11	48.43
Or	1.76	1.51	1.33	1.53	1.64	1.66	1.60	1.80	1.65	1.85	1.75

Group: B = basalt; BA = basaltic andesite; A = andesite; D = dacite; R = rhyolite; Opx/Cgt-SVC 2, 3 = orthopyroxene/cummingtonite-bearing SVC 2; 3 lavas; **Grain:** P = phenocryst; MC = microphenocryst; G = groundmass; C = core; INC = inclusion (mineral included within is stated in parentheses); **Position:** C = core; M = mantle; R = rim, osci. = oscillatory; **Other:** UNZ = unzoned; Dist. = distance from the core (µm); An = anorthite; Ab = albite; Or = orthoclase.

Table G.1 (continued).

Group: Sample: Name: Grain:	Cgt-SVC 2,3 D SL-83-08 Profile C1-Pl1 P Type 6		Cgt-SVC 2, 3 D SL-83-08 Profile C1-Pl7-Pl8 P Type 5							Cgt-SVC 2, 3 D SL-83-08 C2-Pl1-5 P Type 5	
Position:	M	C	C	C	C	C	An-rich M	An-rich M	An-rich M	C	C
Dist.:	1143	0	27	54	135	162	189	242	269	0	24
SiO ₂	53.49	55.19	56.25	55.72	54.17	54.62	49.96	49.56	50.50	56.29	56.16
Al ₂ O ₃	29.09	27.99	27.35	27.54	28.60	28.40	31.15	31.90	30.95	27.10	27.16
MgO	b.d.l.	b.d.l.	b.d.l.	b.d.l.	b.d.l.	b.d.l.	b.d.l.	b.d.l.	b.d.l.	b.d.l.	b.d.l.
CaO	12.00	10.66	10.03	10.07	11.42	11.22	14.69	15.29	14.21	9.75	9.77
FeO	0.10	0.11	0.10	0.11	0.08	0.11	0.09	0.10	0.10	0.06	0.07
Na ₂ O	4.72	5.35	5.70	5.62	4.94	5.12	3.26	2.87	3.69	5.92	5.83
K ₂ O	0.24	0.28	0.32	0.30	0.20	0.23	0.12	0.12	0.17	0.32	0.31
P ₂ O ₅	n.a.	n.a.	n.a.	n.a.	n.a.	n.a.	n.a.	n.a.	n.a.	n.a.	n.a.
Total	99.68	99.58	99.77	99.37	99.49	99.74	99.32	99.85	99.64	99.53	99.33
Si	9.72	9.99	10.14	10.09	9.84	9.89	9.18	9.07	9.25	10.18	10.17
Al	6.23	5.97	5.81	5.88	6.12	6.06	6.75	6.88	6.68	5.77	5.80
Mg	b.d.l.	b.d.l.	b.d.l.	b.d.l.	b.d.l.	b.d.l.	b.d.l.	b.d.l.	b.d.l.	b.d.l.	b.d.l.
Ca	2.34	2.07	1.94	1.95	2.22	2.18	2.89	3.00	2.79	1.89	1.90
Fe (ii)	0.02	0.02	0.01	0.02	0.01	0.02	0.01	0.01	0.02	0.01	0.01
Na	1.66	1.88	1.99	1.97	1.74	1.80	1.16	1.02	1.31	2.08	2.05
K	0.06	0.06	0.07	0.07	0.05	0.05	0.03	0.03	0.04	0.07	0.07
P	n.a.	n.a.	n.a.	n.a.	n.a.	n.a.	n.a.	n.a.	n.a.	n.a.	n.a.
Total	20.03	19.99	19.98	19.99	19.99	20.00	20.04	20.01	20.09	20.01	19.99
An	57.60	51.55	48.40	48.93	55.44	54.03	70.83	74.13	67.36	46.77	47.20
Ab	41.01	46.85	49.74	49.36	43.40	44.63	28.48	25.18	31.68	51.39	51.00
Or	1.40	1.60	1.86	1.71	1.16	1.35	0.69	0.69	0.96	1.83	1.80

Group: Sample: Name: Grain:	Cgt-SVC 2, 3 D SL-83-08 C2-Pl1-5 P Type 5										
Position:	C	C	C	C	C	C	C	C	C	C	C
Dist.:	48	73	97	121	145	169	194	218	266	290	315
SiO ₂	56.06	56.28	56.41	56.41	55.76	55.50	54.62	55.34	55.49	54.93	56.27
Al ₂ O ₃	26.84	27.16	27.13	27.17	27.50	27.45	28.07	27.17	28.15	28.04	26.99
MgO	b.d.l.	b.d.l.	b.d.l.	b.d.l.	b.d.l.	b.d.l.	b.d.l.	b.d.l.	b.d.l.	b.d.l.	b.d.l.
CaO	9.81	9.75	9.82	9.78	10.22	10.12	10.96	10.10	10.93	10.72	9.79
FeO	0.07	0.06	0.11	0.09	0.06	0.10	0.12	0.10	0.10	0.10	0.11
Na ₂ O	5.76	5.93	5.99	5.82	5.62	5.64	5.29	5.57	5.33	5.34	5.88
K ₂ O	0.31	0.31	0.33	0.34	0.29	0.29	0.28	0.29	0.29	0.26	0.34
P ₂ O ₅	n.a.	n.a.	n.a.	n.a.	n.a.	n.a.	n.a.	n.a.	n.a.	n.a.	n.a.
Total	98.87	99.50	99.82	99.62	99.47	99.13	99.38	98.57	100.31	99.39	99.38
Si	10.20	10.17	10.17	10.18	10.09	10.08	9.93	10.11	9.98	9.97	10.19
Al	5.75	5.78	5.77	5.78	5.87	5.88	6.01	5.85	5.97	6.00	5.76
Mg	b.d.l.	b.d.l.	b.d.l.	b.d.l.	b.d.l.	b.d.l.	b.d.l.	b.d.l.	b.d.l.	b.d.l.	b.d.l.
Ca	1.91	1.89	1.90	1.89	1.98	1.97	2.13	1.98	2.11	2.08	1.90
Fe (ii)	0.01	0.01	0.02	0.01	0.01	0.01	0.02	0.01	0.01	0.02	0.02
Na	2.03	2.08	2.09	2.04	1.97	1.99	1.87	1.97	1.86	1.88	2.06
K	0.07	0.07	0.07	0.08	0.07	0.07	0.06	0.07	0.07	0.06	0.08
P	n.a.	n.a.	n.a.	n.a.	n.a.	n.a.	n.a.	n.a.	n.a.	n.a.	n.a.
Total	19.98	20.01	20.03	19.98	19.99	20.00	20.03	19.99	20.00	20.00	20.00
An	47.61	46.80	46.67	47.22	49.28	48.92	52.53	49.18	52.25	51.80	46.99
Ab	50.58	51.45	51.49	50.84	49.06	49.38	45.90	49.12	46.10	46.72	51.08
Or	1.81	1.75	1.84	1.94	1.66	1.70	1.58	1.70	1.65	1.48	1.92

Group: Sample: Name: Grain:	Cgt-SVC 2, 3 D SL-83-08 C2-Pl1-5 P Type 5										
Position:	C	C	An-rich M	An-rich M	An-rich M	An-rich M	An-rich M	An-rich M	An-poor M	An-poor M	An-poor M
Dist.:	339	363	387	411	436	460	484	508	532	557	581
SiO ₂	56.29	56.08	53.73	55.07	50.78	52.78	53.34	54.31	55.92	56.24	55.82
Al ₂ O ₃	27.05	27.34	28.82	27.76	30.86	29.29	29.09	28.45	27.24	27.21	27.32
MgO	b.d.l.	b.d.l.	b.d.l.	b.d.l.	b.d.l.	b.d.l.	b.d.l.	b.d.l.	b.d.l.	b.d.l.	b.d.l.
CaO	9.76	10.13	11.73	10.66	14.33	12.41	12.03	11.43	10.02	10.03	10.23
FeO	0.09	0.06	0.09	0.06	0.09	0.10	0.09	0.11	0.11	0.09	0.07
Na ₂ O	5.89	5.84	4.91	5.41	3.65	4.54	4.71	4.98	5.75	5.70	5.71
K ₂ O	0.32	0.32	0.21	0.26	0.14	0.21	0.22	0.23	0.29	0.31	0.30
P ₂ O ₅	n.a.	n.a.	n.a.	n.a.	n.a.	n.a.	n.a.	n.a.	n.a.	n.a.	n.a.
Total	99.44	99.83	99.56	99.28	99.88	99.33	99.52	99.53	99.35	99.62	99.48
Si	10.18	10.12	9.77	10.00	9.27	9.64	9.71	9.86	10.13	10.16	10.11
Al	5.77	5.81	6.18	5.94	6.64	6.30	6.24	6.09	5.82	5.79	5.83
Mg	b.d.l.	b.d.l.	b.d.l.	b.d.l.	b.d.l.	b.d.l.	b.d.l.	b.d.l.	b.d.l.	b.d.l.	b.d.l.
Ca	1.89	1.96	2.28	2.08	2.80	2.43	2.35	2.22	1.95	1.94	1.98
Fe (ii)	0.01	0.01	0.01	0.01	0.01	0.02	0.01	0.02	0.02	0.01	0.01
Na	2.07	2.04	1.73	1.91	1.29	1.61	1.66	1.75	2.02	2.00	2.00
K	0.07	0.07	0.05	0.06	0.03	0.05	0.05	0.05	0.07	0.07	0.07
P	n.a.	n.a.	n.a.	n.a.	n.a.	n.a.	n.a.	n.a.	n.a.	n.a.	n.a.
Total	20.00	20.03	20.03	20.01	20.07	20.04	20.03	20.00	20.00	19.98	20.01
An	46.93	48.06	56.24	51.34	67.92	59.46	57.77	55.14	48.23	48.40	48.92
Ab	51.23	50.15	42.59	47.17	31.29	39.34	40.96	43.52	50.11	49.79	49.40
Or	1.84	1.78	1.18	1.49	0.79	1.20	1.27	1.35	1.66	1.81	1.69

Group: B = basalt; BA = basaltic andesite; A = andesite; D = dacite; R = rhyolite; Opx/Cgt-SVC 2, 3 = orthopyroxene/cummingtonite-bearing SVC 2; 3 lavas; **Grain:** P = phenocryst; MC = microphenocryst; G = groundmass; C = core; INC = inclusion (mineral included within is stated in parentheses); **Position:** C = core; M = mantle; R = rim, osci. = oscillatory; **Other:** UNZ = unzoned; Dist. = distance from the core (µm); An = anorthite; Ab = albite; Or = orthoclase.

Table G.1. (continued).

Group: Sample: Name: Grain:	Cgt-SVC 2, 3 D SL-83-08 C2-P11-5 P Type 5										Cgt-SVC 2, 3 D SL-83-08 C3-P11-6 P Type 6
Position: Dist.:	An- poor M 605	An- poor M 629	An- poor M 653	An- poor M 678	An- poor M 702	An- poor M 726	An- poor M 750	An- poor M 774	An- poor M 799	An- poor M 823	C 0
SiO ₂	53.68	54.84	55.09	53.93	55.23	55.04	52.24	54.74	55.02	53.07	52.37
Al ₂ O ₃	28.89	27.98	27.81	28.60	27.60	27.94	29.45	28.01	27.77	28.87	29.32
MgO	b.d.l.	b.d.l.	b.d.l.	b.d.l.	b.d.l.	b.d.l.	b.d.l.	b.d.l.	b.d.l.	b.d.l.	b.d.l.
CaO	11.92	10.82	10.54	11.53	10.48	10.87	12.72	10.94	10.52	12.15	12.55
FeO	0.11	0.11	0.06	0.08	0.11	0.11	0.13	0.07	0.11	0.08	0.10
Na ₂ O	4.78	5.35	5.55	4.94	5.51	5.36	4.33	5.20	5.46	4.68	4.38
K ₂ O	0.21	0.26	0.32	0.25	0.31	0.24	0.19	0.25	0.25	0.23	0.20
P ₂ O ₅	n.a.	n.a.	n.a.	n.a.	n.a.	n.a.	n.a.	n.a.	n.a.	n.a.	n.a.
Total	99.63	99.38	99.41	99.37	99.24	99.59	99.10	99.25	99.14	99.09	98.94
Si	9.75	9.96	10.00	9.82	10.04	9.97	9.57	9.95	10.01	9.71	9.60
Al	6.19	5.99	5.95	6.14	5.91	5.97	6.36	6.00	5.95	6.22	6.34
Mg	b.d.l.	b.d.l.	b.d.l.	b.d.l.	b.d.l.	b.d.l.	b.d.l.	b.d.l.	b.d.l.	b.d.l.	b.d.l.
Ca	2.32	2.11	2.05	2.25	2.04	2.11	2.50	2.13	2.05	2.38	2.47
Fe (ii)	0.02	0.02	0.01	0.01	0.02	0.02	0.02	0.01	0.02	0.01	0.01
Na	1.68	1.88	1.95	1.74	1.94	1.88	1.54	1.83	1.93	1.66	1.56
K	0.05	0.06	0.07	0.06	0.07	0.06	0.04	0.06	0.06	0.05	0.05
P	n.a.	n.a.	n.a.	n.a.	n.a.	n.a.	n.a.	n.a.	n.a.	n.a.	n.a.
Total	20.02	20.02	20.04	20.02	20.01	20.01	20.04	19.99	20.01	20.04	20.03
An	57.26	52.00	50.31	55.53	50.33	52.15	61.21	52.97	50.80	58.16	60.58
Ab	41.54	46.49	47.89	43.05	47.92	46.49	37.69	45.57	47.74	40.53	38.27
Or	1.20	1.51	1.80	1.42	1.75	1.36	1.10	1.45	1.46	1.32	1.15

Group: Sample: Name: Grain:	Cgt-SVC 2, 3 D SL-83-08 C3-P11-6 P Type 6										C
Position: Dist.:	C 26	C 51	C 77	C 154	C 180	C 206	C 257	C 283	C 308	C 334	C 360
SiO ₂	53.00	54.17	54.40	54.62	53.04	54.14	53.25	54.26	54.43	54.40	54.96
Al ₂ O ₃	28.98	28.36	28.13	28.06	28.83	28.42	28.69	28.08	27.94	28.04	27.61
MgO	b.d.l.	b.d.l.	b.d.l.	b.d.l.	b.d.l.	b.d.l.	b.d.l.	b.d.l.	b.d.l.	b.d.l.	b.d.l.
CaO	12.14	11.42	11.13	11.05	12.03	11.36	11.77	11.22	11.00	11.01	10.69
FeO	0.09	0.05	0.09	0.10	0.10	0.10	0.12	0.09	0.06	0.09	0.08
Na ₂ O	4.65	5.02	5.13	5.22	4.71	5.04	4.77	5.08	5.23	5.19	5.37
K ₂ O	0.20	0.24	0.25	0.26	0.20	0.23	0.21	0.28	0.28	0.24	0.27
P ₂ O ₅	n.a.	n.a.	n.a.	n.a.	n.a.	n.a.	n.a.	n.a.	n.a.	n.a.	n.a.
Total	99.10	99.31	99.14	99.36	98.92	99.32	98.84	99.01	98.96	98.99	99.03
Si	9.69	9.86	9.91	9.93	9.71	9.85	9.75	9.90	9.93	9.92	10.01
Al	6.25	6.08	6.04	6.01	6.22	6.10	6.19	6.04	6.01	6.03	5.93
Mg	b.d.l.	b.d.l.	b.d.l.	b.d.l.	b.d.l.	b.d.l.	b.d.l.	b.d.l.	b.d.l.	b.d.l.	b.d.l.
Ca	2.38	2.23	2.17	2.15	2.36	2.22	2.31	2.19	2.15	2.15	2.09
Fe (ii)	0.01	0.01	0.01	0.02	0.02	0.01	0.02	0.01	0.01	0.01	0.01
Na	1.65	1.77	1.81	1.84	1.67	1.78	1.69	1.80	1.85	1.83	1.90
K	0.05	0.06	0.06	0.06	0.05	0.05	0.05	0.07	0.07	0.06	0.06
P	n.a.	n.a.	n.a.	n.a.	n.a.	n.a.	n.a.	n.a.	n.a.	n.a.	n.a.
Total	20.03	20.01	20.01	20.01	20.03	20.01	20.02	20.01	20.02	20.01	20.00
An	58.35	54.90	53.73	53.13	57.84	54.75	57.01	54.07	52.91	53.25	51.56
Ab	40.48	43.71	44.86	45.39	41.01	43.92	41.77	44.30	45.46	45.37	46.87
Or	1.17	1.38	1.41	1.48	1.15	1.33	1.22	1.63	1.63	1.39	1.57

Group: Sample: Name: Grain:	Cgt-SVC 2, 3 D SL-83-08 C3-P11-6 P Type 6										M
Position: Dist.:	C 411	C 437	C 462	C 514	C 539	M 591	M 617	M 642	M 668	M 694	M 719
SiO ₂	54.91	55.10	55.27	56.04	57.41	55.81	54.79	52.61	52.05	55.35	55.16
Al ₂ O ₃	27.76	27.37	27.67	27.03	26.14	27.18	27.97	29.05	29.59	27.41	27.53
MgO	b.d.l.	b.d.l.	b.d.l.	b.d.l.	b.d.l.	b.d.l.	b.d.l.	b.d.l.	b.d.l.	b.d.l.	b.d.l.
CaO	10.74	10.57	10.58	9.72	8.76	9.95	10.93	12.34	12.87	10.33	10.50
FeO	0.13	0.06	0.15	0.09	0.07	0.10	0.08	0.06	0.07	0.11	0.07
Na ₂ O	5.43	5.43	5.54	5.78	6.30	5.67	5.28	4.39	4.27	5.53	5.55
K ₂ O	0.28	0.30	0.28	0.31	0.41	0.31	0.28	0.19	0.19	0.30	0.28
P ₂ O ₅	n.a.	n.a.	n.a.	n.a.	n.a.	n.a.	n.a.	n.a.	n.a.	n.a.	n.a.
Total	99.25	98.86	99.51	98.97	99.09	99.03	99.35	98.74	99.07	99.04	99.11
Si	9.99	10.05	10.02	10.18	10.39	10.14	9.96	9.66	9.54	10.07	10.04
Al	5.95	5.88	5.91	5.79	5.57	5.82	5.99	6.28	6.39	5.88	5.90
Mg	b.d.l.	b.d.l.	b.d.l.	b.d.l.	b.d.l.	b.d.l.	b.d.l.	b.d.l.	b.d.l.	b.d.l.	b.d.l.
Ca	2.09	2.07	2.06	1.89	1.70	1.94	2.13	2.43	2.53	2.01	2.05
Fe (ii)	0.02	0.01	0.02	0.01	0.01	0.02	0.01	0.01	0.01	0.02	0.01
Na	1.91	1.92	1.95	2.03	2.21	2.00	1.86	1.56	1.52	1.95	1.96
K	0.07	0.07	0.06	0.07	0.09	0.07	0.07	0.05	0.04	0.07	0.07
P	n.a.	n.a.	n.a.	n.a.	n.a.	n.a.	n.a.	n.a.	n.a.	n.a.	n.a.
Total	20.03	20.00	20.03	19.98	19.98	19.98	20.01	20.00	20.04	20.00	20.02
An	51.39	50.96	50.54	47.32	42.45	48.32	52.47	60.15	61.79	49.90	50.30
Ab	47.00	47.32	47.90	50.86	55.21	49.86	45.91	38.74	37.15	48.37	48.09
Or	1.61	1.72	1.56	1.82	2.34	1.82	1.63	1.12	1.06	1.73	1.61

Group: B = basalt; BA = basaltic andesite; A = andesite; D = dacite; R = rhyolite; Opx/Cgt-SVC 2, 3 = orthopyroxene/cummingtonite-bearing SVC 2; 3 lavas; **Grain:** P = phenocryst; MC = microphenocryst; G = groundmass; C = core; INC = inclusion (mineral included within is stated in parentheses); **Position:** C = core; M = mantle; R = rim, osci. = oscillatory; **Other:** UNZ = unzoned; Dist. = distance from the core (μm); An = anorthite; Ab = albite; Or = orthoclase.

Table G.1. (continued).

Group:	Cgt-SVC 2, 3 D				Cgt-SVC 2, 3 D							
Sample:	SL-83-08				SL-83-08							
Name:	C3-PI1-6				C3-PI9-10							
Grain:	P Type 6				P Type 2							
Position:	M	M	M	M	C	C	C	M	M	M	M	M
Dist.:	745	771	822	848	0	26	52	78	104	130	156	182
SiO ₂	55.98	54.70	54.02	53.68	45.54	46.28	46.02	51.85	55.47	54.92	54.24	54.53
Al ₂ O ₃	27.02	27.80	28.21	28.52	33.52	33.03	33.25	29.56	27.55	27.67	28.16	27.90
MgO	b.d.l.	b.d.l.	b.d.l.	b.d.l.	b.d.l.	b.d.l.	b.d.l.	b.d.l.	b.d.l.	b.d.l.	b.d.l.	b.d.l.
CaO	9.96	10.73	11.41	11.65	17.99	17.34	17.60	12.80	10.37	10.70	11.21	10.76
FeO	0.13	0.06	0.12	0.11	0.12	0.09	0.09	0.10	0.13	0.11	0.08	0.11
Na ₂ O	5.73	5.27	5.14	4.76	1.43	1.79	1.71	4.24	5.69	5.43	5.18	5.48
K ₂ O	0.32	0.27	0.22	0.21	0.03	0.05	0.05	0.19	0.29	0.28	0.24	0.25
P ₂ O ₅	n.a.	n.a.	n.a.	n.a.	n.a.	n.a.	n.a.	n.a.	n.a.	n.a.	n.a.	n.a.
Total	99.16	98.85	99.16	98.99	98.66	98.58	98.74	98.76	99.50	99.16	99.11	99.06
Si	10.16	9.98	9.86	9.81	8.51	8.64	8.59	9.54	10.05	10.00	9.89	9.94
Al	5.78	5.98	6.06	6.14	7.39	7.27	7.31	6.41	5.88	5.93	6.05	5.99
Mg	b.d.l.	b.d.l.	b.d.l.	b.d.l.	b.d.l.	b.d.l.	b.d.l.	b.d.l.	b.d.l.	b.d.l.	b.d.l.	b.d.l.
Ca	1.94	2.10	2.23	2.28	3.60	3.47	3.52	2.52	2.01	2.09	2.19	2.10
Fe (ii)	0.02	0.01	0.02	0.02	0.02	0.01	0.01	0.02	0.02	0.02	0.01	0.02
Na	2.02	1.86	1.82	1.68	0.52	0.65	0.62	1.51	2.00	1.92	1.83	1.94
K	0.07	0.06	0.05	0.05	0.01	0.01	0.01	0.04	0.07	0.07	0.06	0.06
P	n.a.	n.a.	n.a.	n.a.	n.a.	n.a.	n.a.	n.a.	n.a.	n.a.	n.a.	n.a.
Total	19.99	19.99	20.05	19.99	20.06	20.05	20.07	20.04	20.04	20.03	20.03	20.06
An	48.11	52.13	54.42	56.80	87.25	84.00	84.79	61.84	49.35	51.27	53.71	51.31
Ab	50.08	46.33	44.33	41.96	12.59	15.72	14.90	37.07	49.01	47.11	44.93	47.29
Or	1.81	1.55	1.25	1.24	0.16	0.28	0.31	1.09	1.64	1.62	1.36	1.40

Group: B = basalt; BA = basaltic andesite; A = andesite; D = dacite; R = rhyolite; Opx/Cgt-SVC 2, 3 = orthopyroxene/cummingtonite-bearing SVC 2; 3 lavas; **Grain:** P = phenocryst; MC = microphenocryst; G = groundmass; C = core; INC = inclusion (mineral included within is stated in parentheses); **Position:** C = core; M = mantle; R = rim, osci. = oscillatory; **Other:** UNZ = unzoned; Dist. = distance from the core (µm); An = anorthite; Ab = albite; Or = orthoclase.

Table G.2. Clinopyroxene major element composition obtained by electron microprobe.

Group:	Pre-SVC1 B										
Sample:	SL-83-44										
Name:	Profile C2-Py1A-Py1B										
Grain:	P										
Position:	C	C	C	M	M	M	M	M	M	M	M
Dist:	0	27	53	80	106	133	159	186	212	239	265
SiO ₂	51.06	50.80	51.07	51.00	50.93	51.13	51.17	51.21	51.39	50.67	50.93
TiO ₂	0.36	0.35	0.33	0.30	0.33	0.34	0.34	0.34	0.37	0.36	0.34
Al ₂ O ₃	2.98	3.00	3.04	2.65	2.77	2.30	2.32	2.10	2.09	3.22	2.80
FeOtot	6.52	6.38	6.04	6.00	6.57	6.85	7.23	7.16	7.61	6.75	6.41
MnO	0.20	0.18	0.16	0.15	0.17	0.20	0.22	0.20	0.24	0.18	0.19
MgO	16.83	16.69	16.72	16.85	16.87	17.01	17.06	17.02	17.11	16.39	16.62
CaO	21.37	21.51	22.03	21.80	21.26	21.06	20.68	20.60	20.04	21.38	21.37
Na ₂ O	0.21	0.21	0.18	0.18	0.21	0.19	0.19	0.20	0.19	0.20	0.19
K ₂ O	b.d.l.	0.01	b.d.l.	b.d.l.	b.d.l.	b.d.l.	b.d.l.	b.d.l.	b.d.l.	b.d.l.	b.d.l.
Cr ₂ O ₃	0.16	0.17	0.18	0.11	0.15	0.16	0.11	0.10	0.11	0.18	0.19
NiO	b.d.l.	b.d.l.	b.d.l.	b.d.l.	b.d.l.	b.d.l.	b.d.l.	b.d.l.	b.d.l.	b.d.l.	b.d.l.
Total	100.05	99.86	99.80	99.23	99.62	99.49	99.57	99.23	99.39	99.72	99.07
Si	1.87	1.87	1.87	1.88	1.88	1.90	1.90	1.91	1.91	1.87	1.88
Ti	0.01	0.01	0.01	0.01	0.01	0.01	0.01	0.01	0.01	0.01	0.01
Al	0.13	0.13	0.13	0.12	0.12	0.10	0.10	0.09	0.09	0.14	0.12
Fe (iii)	0.11	0.12	0.11	0.10	0.11	0.02	0.05	0.03	0.05	0.11	0.10
Fe (ii)	0.09	0.08	0.07	0.09	0.10	0.19	0.17	0.19	0.18	0.10	0.10
Mn	0.00	0.00	0.00	0.00	0.00	0.00	0.00	0.00	0.00	0.00	b.d.l.
Mg	0.92	0.92	0.91	0.93	0.93	0.94	0.94	0.95	0.95	0.90	0.92
Ca	0.84	0.85	0.87	0.86	0.84	0.84	0.82	0.82	0.80	0.85	0.85
Na	0.01	0.01	0.01	0.01	0.01	0.01	0.01	0.01	0.01	0.01	0.01
Cr	0.00	0.01	0.01	0.00	0.00	0.00	0.00	0.00	0.00	0.01	0.01
Ni	0.01	0.01	0.00	0.00	0.01	0.01	0.01	0.01	0.01	0.01	0.01
Total	4.00	4.00	4.00	4.01	4.00	4.03	4.02	4.02	4.01	4.00	4.00
Mg#	91	92	93	91	91	83	84	83	84	90	90
En	47	47	47	47	47	47	47	47	48	46	47
Fs	10	10	9	9	10	11	11	11	12	11	10
Wo	43	43	44	44	43	42	41	41	40	43	43

Group:	Pre-SVC1 B										
Sample:	SL-83-44										
Name:	Profile C2-Py1A-Py1B										
Grain:	P										
Position:	M	M	M	M	M	M	M	M	M	M	R
Dist:	292	318	345	372	398	425	451	478	504	560	535
SiO ₂	50.53	51.02	50.86	51.04	51.57	51.42	51.51	49.37	51.58	51.98	52.72
TiO ₂	0.34	0.34	0.34	0.28	0.27	0.28	0.28	0.23	0.30	0.28	0.30
Al ₂ O ₃	3.14	2.71	2.92	2.22	2.34	2.24	2.42	3.63	2.26	2.25	2.20
FeOtot	6.07	6.81	6.00	6.82	6.55	6.98	7.01	8.61	6.85	6.78	6.70
MnO	0.16	0.21	0.14	0.21	0.21	0.20	0.20	0.20	0.18	0.19	0.22
MgO	16.53	16.78	16.58	17.36	17.15	17.28	17.20	17.01	17.22	17.54	17.85
CaO	22.04	21.12	21.85	20.78	20.86	20.57	20.57	16.21	20.45	20.48	20.49
Na ₂ O	0.19	0.20	0.16	0.16	0.17	0.18	0.20	0.15	0.18	0.18	0.17
K ₂ O	b.d.l.	b.d.l.	b.d.l.	b.d.l.	b.d.l.	b.d.l.	b.d.l.	0.07	b.d.l.	b.d.l.	b.d.l.
Cr ₂ O ₃	0.21	0.16	0.15	0.12	0.15	0.11	0.14	0.11	0.09	0.12	0.08
NiO	b.d.l.	0.04	b.d.l.	b.d.l.	b.d.l.	b.d.l.	0.03	b.d.l.	0.03	0.04	b.d.l.
Total	99.22	99.79	99.40	99.25	99.41	99.81	99.83	95.77	99.35	100.24	100.85
Si	1.86	1.88	1.88	1.90	1.90	1.90	1.89	1.89	1.90	1.90	1.91
Ti	0.01	0.01	0.01	0.01	0.01	0.01	0.01	0.01	0.01	0.01	0.01
Al	0.14	0.12	0.13	0.10	0.10	0.10	0.10	0.16	0.10	0.10	0.09
Fe (iii)	0.13	0.11	0.10	0.02	0.09	0.06	0.10	0.04	0.09	0.09	0.07
Fe (ii)	0.06	0.10	0.08	0.19	0.11	0.15	0.12	0.23	0.12	0.12	0.13
Mn	0.00	0.00	0.00	0.00	0.00	0.00	0.00	0.00	0.00	0.00	0.00
Mg	0.91	0.92	0.91	0.96	0.94	0.95	0.94	0.97	0.95	0.96	0.96
Ca	0.87	0.83	0.86	0.83	0.82	0.82	0.81	0.67	0.81	0.80	0.80
Na	0.01	0.01	0.01	0.01	0.01	0.01	0.01	0.01	0.01	0.01	0.01
Cr	0.01	0.00	0.00	0.00	0.00	0.00	0.00	0.00	0.00	0.00	0.00
Ni	0.00	0.01	0.00	0.01	0.01	0.01	0.01	0.01	0.01	0.01	0.01
Total	4.00	4.00	4.00	4.04	4.00	4.01	4.00	4.00	4.00	4.00	4.00
Mg#	94	90	92	83	89	86	89	81	88	89	88
En	46	47	46	48	48	48	48	51	48	49	49
Fs	10	11	9	11	10	11	11	14	11	11	10
Wo	44	42	44	41	42	41	41	35	41	41	41

Group: B = basalt; BA = basaltic andesite; A = andesite; D = dacite; R = rhyolite; Opx/Cgt-SVC 2, 3 = orthopyroxene/cummingtonite-bearing SVC 2, 3 lavas; **Grain:** P = phenocryst; MC = microphenocryst; G = groundmass; C = core; INC = inclusion (mineral included within is stated in parentheses); **Position:** C = core; M = mantle, R = rim, osci. = oscillatory; UNZ = unzoned; **Other:** Dist. = distance from the core (µm); En = enstatite; Fs = forsterite; Wo = wollastonite; Mg# = 100*Mg / (Mg + Fe (ii)); Fe (ii) and Fe (iii) were calculated based on the minimum amount of Fe (iii) permissible in the structural formula.

Table G.2. (continued).

Group: Sample:	Pre-SVC1 B SL-83-44	Pre-SVC1 R SL-83-45	Pre-SVC2 BA SL-83-26	SVC1 A SL-JL-02	Opx-SVC 2,3D SL-83-03	Opx-SVC 2, 3 D SL-JL-83
Name:	C2-Py2	C3-Py1 C4- Py1	C1-Opx2A	C4-Py1	C1-Py2	C3-Py1A-1B
Grain:	G	MP	P	MP	MP	MP
Position:	C	C	C	C	R	C
Dist:						C 0 12 25
SiO ₂	50.46	49.00	47.41	48.60	47.74	53.83
TiO ₂	0.68	0.31	0.50	0.42	1.34	0.33
Al ₂ O ₃	2.68	1.00	1.65	2.46	7.98	2.76
FeOtot	11.96	23.04	23.71	8.35	5.32	4.44
MnO	0.35	0.98	1.06	0.22	0.11	0.13
MgO	16.47	6.11	5.88	15.58	13.96	16.90
CaO	17.16	19.01	18.19	21.68	22.54	22.81
Na ₂ O	0.18	0.25	0.29	0.20	0.22	0.12
K ₂ O	b.d.l.	b.d.l.	b.d.l.	b.d.l.	b.d.l.	b.d.l.
Cr ₂ O ₃	0.04	b.d.l.	b.d.l.	b.d.l.	0.14	0.10
NiO	b.d.l.	b.d.l.	0.04	b.d.l.	b.d.l.	b.d.l.
Total	100.06	99.91	99.09	98.16	99.79	101.58
Si	1.88	1.95	1.92	1.87	1.76	1.94
Ti	0.02	0.01	0.02	0.01	0.04	0.01
Al	0.12	0.05	0.08	0.11	0.35	0.12
Fe (iii)	0.04	0.04	0.02	0.00	0.06	0.00
Fe (ii)	0.34	0.73	0.78	0.27	0.10	0.13
Mn	0.01	0.03	0.04	0.01	0.00	0.00
Mg	0.92	0.36	0.36	0.89	0.77	0.91
Ca	0.69	0.81	0.79	0.89	0.89	0.88
Na	0.01	0.02	0.02	0.02	0.02	0.01
Cr	0.00	b.d.l.	b.d.l.	b.d.l.	0.00	0.00
Ni	b.d.l.	b.d.l.	0.00	0.00	0.00	0.00
Total	4.02	4.00	4.02	4.07	4.00	4.00
Mg#	73	33	31	77	88	87
En	46	18	18	43	42	47
Fs	19	39	40	13	9	7
Wo	35	41	40	43	49	46
Group: Sample:	Opx-SVC 2, 3 D SL-JL-83	Opx-SVC 2, 3 D SL-JL-83				
Name:	C3-Py1A-1B	C3-Py1A-1B				
Grain:	MP	MP				
Position:	M	M	M	M	M	M
Dist:	37	49	62	74	87	99
SiO ₂	50.10	49.32	49.80	49.52	49.80	48.79
TiO ₂	0.30	0.34	0.36	0.37	0.37	0.42
Al ₂ O ₃	3.75	4.07	4.11	4.27	4.28	4.92
FeOtot	3.42	3.70	3.69	3.83	3.74	3.89
MnO	0.09	0.11	0.10	0.11	0.11	0.09
MgO	16.92	16.85	16.49	16.96	16.74	16.15
CaO	23.65	23.61	23.50	23.35	23.43	23.90
Na ₂ O	0.20	0.16	0.17	0.17	0.18	0.17
K ₂ O	b.d.l.	b.d.l.	b.d.l.	b.d.l.	b.d.l.	b.d.l.
Cr ₂ O ₃	0.85	0.79	0.73	0.76	0.72	0.84
NiO	b.d.l.	0.03	b.d.l.	b.d.l.	b.d.l.	b.d.l.
Total	99.67	99.18	99.43	99.92	99.42	99.80
Si	1.85	1.83	1.84	1.83	1.84	1.81
Ti	0.01	0.01	0.01	0.01	0.01	0.01
Al	0.16	0.18	0.18	0.19	0.19	0.21
Fe (iii)	0.05	0.07	0.06	0.06	0.06	0.07
Fe (ii)	0.05	0.05	0.06	0.06	0.06	0.05
Mn	0.00	0.00	0.00	0.00	0.00	0.00
Mg	0.93	0.93	0.91	0.93	0.92	0.89
Ca	0.93	0.94	0.93	0.92	0.93	0.95
Na	0.01	0.01	0.01	0.01	0.01	0.01
Cr	0.02	0.02	0.02	0.02	0.02	0.02
Ni	0.00	0.00	0.00	0.00	0.00	0.00
Total	4.03	4.03	4.02	4.03	4.03	4.03
Mg#	95	95	94	94	94	94
En	47	47	47	47	47	45
Fs	5	6	6	6	6	8
Wo	47	47	48	47	47	48

Group: B = basalt; BA = basaltic andesite; A = andesite; D = dacite; R = rhyolite; Opx/Cgt-SVC 2, 3 = orthopyroxene/cummingtonite-bearing SVC 2, 3 lavas; **Grain:** P = phenocryst; MC = microphenocryst; G = groundmass; C = core; INC = inclusion (mineral included within is stated in parentheses); **Position:** C = core; M = mantle, R = rim, osci. = oscillatory; UNZ = unzoned; **Other:** Dist. = distance from the core (µm); En = enstatite; Fs = forsterite; Wo = wollastonite; Mg# = 100*Mg / (Mg + Fe (ii)); Fe (ii) and Fe (iii) were calculated based on the minimum amount of Fe (iii) permissible in the structural formula.

Table G.3. Orthopyroxene major element composition obtained by electron microprobe.

Group: Sample: Name:	Pre-SVC2 BA SL-JL-26		SVC1 A SL-83-17 Profile C2-Py1								
Grain:	P	C1-Oi1 INC (cpx)	P								
Position: Dist.	C	C	C	C	C	C	C	C	C	C	C
	0	25	76	101	126	177	228	253	278		
SiO ₂	49.85	50.08	51.49	51.62	51.44	52.01	51.56	51.54	51.51	51.57	51.73
TiO ₂	0.40	0.31	0.13	0.10	0.13	0.17	0.25	0.14	0.11	0.12	0.12
Al ₂ O ₃	1.34	1.11	0.44	0.44	0.40	0.81	0.46	0.45	0.40	0.50	0.51
FeOtot	21.32	21.24	28.77	29.11	28.82	28.63	28.29	28.87	28.70	28.99	28.86
MnO	0.49	0.52	0.74	0.73	0.78	0.68	0.74	0.77	0.72	0.73	0.75
MgO	23.02	22.71	17.95	18.06	18.24	17.38	18.03	18.08	17.96	17.86	18.10
CaO	2.25	2.09	0.89	0.85	0.89	0.91	0.88	0.94	1.03	0.93	0.99
Na ₂ O	b.d.l.	b.d.l.	b.d.l.	b.d.l.	b.d.l.	b.d.l.	b.d.l.	b.d.l.	b.d.l.	b.d.l.	b.d.l.
K ₂ O	b.d.l.	b.d.l.	b.d.l.	b.d.l.	b.d.l.	b.d.l.	b.d.l.	b.d.l.	b.d.l.	b.d.l.	b.d.l.
Cr ₂ O ₃	b.d.l.	b.d.l.	b.d.l.	b.d.l.	b.d.l.	b.d.l.	b.d.l.	0.04	b.d.l.	0.04	b.d.l.
NiO	0.05	b.d.l.	n.a.	n.a.	n.a.	n.a.	n.a.	n.a.	n.a.	n.a.	n.a.
Total	98.72	98.13	100.44	100.96	100.70	100.67	100.24	100.86	100.44	100.78	101.09
Si	1.90	1.91	1.98	1.97	1.97	1.99	1.98	1.97	1.98	1.97	1.97
Ti	0.01	0.01	0.00	0.00	0.00	0.00	0.01	0.00	0.00	0.00	0.00
Al	0.06	0.05	0.02	0.02	0.02	0.04	0.02	0.02	0.02	0.02	0.02
Fe (iii)	0.00	0.00	0.00	0.00	0.00	0.00	0.00	0.00	0.00	0.00	0.00
Fe (ii)	0.68	0.68	0.92	0.93	0.92	0.91	0.91	0.92	0.92	0.93	0.92
Mn	0.02	0.02	0.02	0.02	0.03	0.02	0.02	0.02	0.02	0.02	0.02
Mg	1.31	1.29	1.03	1.03	1.04	0.99	1.03	1.03	1.03	1.02	1.03
Ca	0.09	0.09	0.04	0.03	0.04	0.04	0.04	0.04	0.04	0.04	0.04
Na	b.d.l.	b.d.l.	b.d.l.	b.d.l.	b.d.l.	b.d.l.	b.d.l.	b.d.l.	b.d.l.	b.d.l.	b.d.l.
Cr	b.d.l.	b.d.l.	b.d.l.	b.d.l.	b.d.l.	b.d.l.	b.d.l.	0.00	b.d.l.	0.00	b.d.l.
Ni	0.00	b.d.l.	n.a.	n.a.	n.a.	n.a.	n.a.	n.a.	n.a.	n.a.	n.a.
Total	4.06	4.05	4.01	4.01	4.02	3.99	4.00	4.02	4.01	4.01	4.01
Mg#	65.81	65.58	52.65	52.50	53.00	51.97	53.17	52.74	52.72	52.33	52.78
En	62.86	62.84	51.68	51.59	52.03	50.97	52.20	51.72	51.60	51.32	51.71
Fs	32.66	32.98	46.48	46.67	46.14	47.11	45.97	46.34	46.28	46.75	46.26
Wo	4.41	4.17	1.85	1.74	1.83	1.92	1.82	1.93	2.12	1.93	2.03

Group: Sample: Name:	SVC1 A SL-83-17 Profile C2-Py1									SVC1 A SL-83-17 Profile C3-Py1a-c	
Grain:	P									P	
Position: Dist.	C	M	M	M	M	M	M	R	R	C	C
	329	354	379	405	430	455	481	506	531	0	26
SiO ₂	51.60	51.94	51.69	51.88	51.70	51.43	51.08	51.27	51.32	51.86	51.79
TiO ₂	0.16	0.13	0.10	0.11	0.13	0.11	0.14	0.09	0.12	0.11	0.12
Al ₂ O ₃	0.41	0.45	0.51	0.40	0.44	0.71	0.83	0.37	0.35	0.62	0.65
FeOtot	29.01	26.98	28.83	28.60	29.12	28.90	29.19	29.93	30.04	28.55	28.66
MnO	0.79	0.75	0.78	0.70	0.72	0.78	0.73	0.75	0.76	0.72	0.70
MgO	17.96	19.19	18.01	18.19	17.86	18.05	17.29	16.87	17.00	18.09	18.23
CaO	0.98	0.95	0.87	0.90	0.96	0.72	1.04	1.02	0.94	0.83	0.82
Na ₂ O	b.d.l.	b.d.l.	b.d.l.	b.d.l.	b.d.l.	b.d.l.	b.d.l.	b.d.l.	b.d.l.	b.d.l.	b.d.l.
K ₂ O	b.d.l.	b.d.l.	b.d.l.	b.d.l.	b.d.l.	b.d.l.	b.d.l.	b.d.l.	b.d.l.	b.d.l.	b.d.l.
Cr ₂ O ₃	b.d.l.	b.d.l.	b.d.l.	b.d.l.	b.d.l.	b.d.l.	b.d.l.	b.d.l.	b.d.l.	b.d.l.	b.d.l.
NiO	n.a.	n.a.	n.a.	n.a.	n.a.	n.a.	n.a.	n.a.	n.a.	n.a.	n.a.
Total	100.94	100.42	100.79	100.80	100.96	100.69	100.34	100.35	100.58	100.79	101.01
Si	1.97	1.98	1.98	1.98	1.98	1.97	1.97	1.98	1.98	1.98	1.97
Ti	0.00	0.00	0.00	0.00	0.00	0.00	0.00	0.00	0.00	0.00	0.00
Al	0.02	0.02	0.02	0.02	0.02	0.03	0.04	0.02	0.02	0.03	0.03
Fe (iii)	0.00	0.00	0.00	0.00	0.00	0.00	0.00	0.00	0.00	0.00	0.00
Fe (ii)	0.93	0.86	0.92	0.91	0.93	0.92	0.94	0.97	0.97	0.91	0.91
Mn	0.03	0.02	0.03	0.02	0.02	0.03	0.02	0.02	0.02	0.02	0.02
Mg	1.02	1.09	1.03	1.03	1.02	1.03	0.99	0.97	0.98	1.03	1.03
Ca	0.04	0.04	0.04	0.04	0.04	0.03	0.04	0.04	0.04	0.03	0.03
Na	b.d.l.	b.d.l.	b.d.l.	b.d.l.	b.d.l.	b.d.l.	b.d.l.	b.d.l.	b.d.l.	b.d.l.	b.d.l.
Cr	b.d.l.	b.d.l.	b.d.l.	b.d.l.	b.d.l.	b.d.l.	b.d.l.	b.d.l.	b.d.l.	b.d.l.	b.d.l.
Ni	n.a.	n.a.	n.a.	n.a.	n.a.	n.a.	n.a.	n.a.	n.a.	n.a.	n.a.
Total	4.01	4.01	4.01	4.01	4.01	4.01	4.01	4.01	4.01	4.01	4.01
Mg#	52.46	55.89	52.67	53.13	52.21	52.67	51.35	50.12	50.21	53.03	53.13
En	51.40	54.81	51.73	52.15	51.18	51.89	50.24	49.05	49.23	52.11	52.23
Fs	46.58	43.25	46.48	46.01	46.84	46.62	47.60	48.82	48.82	46.16	46.08
Wo	2.02	1.94	1.80	1.85	1.98	1.48	2.17	2.14	1.95	1.73	1.69

Group: B = basalt; BA = basaltic andesite; A = andesite; D = dacite; R = rhyolite; Opx/Cgt-SVC 2, 3 = orthopyroxene/cummingtonite-bearing SVC 2, 3 lavas; **Grain:** P = phenocryst; MC = microphenocryst; G = groundmass; C = core; INC = inclusion (mineral included within is stated in parentheses); **Position:** C = core; M = mantle, R = rim, osci. = oscillatory; UNZ = unzoned; **Other:** Dist. = distance from the core (μm); En = enstatite; Fs = forsterite; Wo = wollastonite; Mg# = 100*Mg / (Mg + Fe (ii)); Fe (ii) and Fe (iii) were calculated based on the minimum amount of Fe (iii) permissible in the structural formula.

Table G.3. (continued).

Group:	SVC1 A										
Sample:	SL-83-17										
Name:	Profile C3-Py1a-c										
Grain:	P										
Position:	C	C	C	C	C	C	C	C	C	C	C
Dist.	51	77	102	127	153	178	204	229	255	281	306
SiO ₂	53.35	51.91	51.96	51.93	51.89	51.75	53.17	51.99	51.79	52.04	51.78
TiO ₂	0.08	0.12	0.11	0.12	0.16	0.09	0.09	0.14	0.13	0.10	0.10
Al ₂ O ₃	2.37	0.63	0.62	0.66	0.83	0.62	0.93	0.63	0.62	0.64	0.60
FeOtot	25.66	28.21	27.98	27.97	27.76	28.24	27.53	28.39	28.15	27.85	28.00
MnO	0.65	0.67	0.70	0.77	0.67	0.70	0.70	0.64	0.72	0.74	0.71
MgO	16.80	18.30	18.44	18.70	18.32	18.82	17.93	18.53	18.53	18.70	18.45
CaO	0.90	0.81	0.83	0.81	0.81	0.82	0.86	0.80	0.79	0.83	0.75
Na ₂ O	b.d.l.	b.d.l.	b.d.l.	b.d.l.	0.06	b.d.l.	b.d.l.	b.d.l.	b.d.l.	b.d.l.	b.d.l.
K ₂ O	0.40	b.d.l.	b.d.l.	b.d.l.	0.04	b.d.l.	b.d.l.	b.d.l.	b.d.l.	b.d.l.	b.d.l.
Cr ₂ O ₃	b.d.l.	b.d.l.	b.d.l.	b.d.l.	b.d.l.	b.d.l.	b.d.l.	b.d.l.	b.d.l.	b.d.l.	b.d.l.
NiO	n.a.	n.a.	n.a.	n.a.	n.a.	n.a.	n.a.	n.a.	n.a.	n.a.	n.a.
Total	100.58	100.67	100.65	100.99	100.54	101.08	101.24	101.12	100.75	100.93	100.40
Si	2.01	1.98	1.98	1.97	1.98	1.97	2.00	1.97	1.97	1.98	1.98
Ti	0.00	0.00	0.00	0.00	0.00	0.00	0.00	0.00	0.00	0.00	0.00
Al	0.11	0.03	0.03	0.03	0.04	0.03	0.04	0.03	0.03	0.03	0.03
Fe (iii)	0.00	0.00	0.00	0.00	0.00	0.00	0.00	0.00	0.00	0.00	0.00
Fe (ii)	0.81	0.90	0.89	0.89	0.88	0.90	0.87	0.90	0.90	0.88	0.89
Mn	0.02	0.02	0.02	0.02	0.02	0.02	0.02	0.02	0.02	0.02	0.02
Mg	0.94	1.04	1.05	1.06	1.04	1.07	1.01	1.05	1.05	1.06	1.05
Ca	0.04	0.03	0.03	0.03	0.03	0.03	0.03	0.03	0.03	0.03	0.03
Na	b.d.l.	b.d.l.	b.d.l.	b.d.l.	b.d.l.	b.d.l.	b.d.l.	b.d.l.	b.d.l.	b.d.l.	b.d.l.
Cr	b.d.l.	b.d.l.	b.d.l.	b.d.l.	b.d.l.	b.d.l.	b.d.l.	b.d.l.	b.d.l.	b.d.l.	b.d.l.
Ni	n.a.	n.a.	n.a.	n.a.	n.a.	n.a.	n.a.	n.a.	n.a.	n.a.	n.a.
Total	3.95	4.00	4.00	4.01	4.00	4.02	3.98	4.01	4.01	4.01	4.01
Mg#	53.85	53.61	54.02	54.36	54.04	54.28	53.72	53.77	53.98	54.47	54.00
En	52.76	52.71	53.09	53.45	53.12	53.37	52.74	52.89	53.11	53.53	53.16
Fs	45.21	45.60	45.20	44.88	45.18	44.95	45.44	45.47	45.27	44.76	45.28
Wo	2.03	1.69	1.71	1.67	1.70	1.68	1.81	1.64	1.62	1.71	1.56

Group:	SVC1 A										
Sample:	SL-83-17										
Name:	Profile C3-Py1a-c										
Grain:	P										
Position:	M	M	M	M	M	M	M	M	M	M	M
Dist.	332	357	382	408	459	536	561	586	612	663	688
SiO ₂	49.89	51.69	51.96	51.89	51.94	52.12	52.07	51.79	52.00	51.87	51.81
TiO ₂	0.11	0.11	0.10	0.13	0.15	0.11	0.10	0.06	0.11	0.08	0.11
Al ₂ O ₃	0.59	0.60	0.61	0.64	0.70	0.58	0.57	0.57	0.52	0.47	0.51
FeOtot	27.49	27.82	27.87	27.98	27.85	27.38	27.96	27.92	28.09	28.38	28.68
MnO	0.70	0.73	0.74	0.67	0.68	0.66	0.62	0.62	0.61	0.60	0.67
MgO	20.29	18.65	18.65	18.78	18.79	19.04	18.71	18.78	18.48	18.47	18.16
CaO	0.83	0.78	0.77	0.77	0.75	0.77	0.74	0.77	0.74	0.78	0.72
Na ₂ O	b.d.l.	b.d.l.	b.d.l.	b.d.l.	b.d.l.	b.d.l.	b.d.l.	b.d.l.	b.d.l.	b.d.l.	b.d.l.
K ₂ O	b.d.l.	b.d.l.	b.d.l.	b.d.l.	b.d.l.	b.d.l.	b.d.l.	b.d.l.	b.d.l.	b.d.l.	b.d.l.
Cr ₂ O ₃	b.d.l.	b.d.l.	b.d.l.	0.05	b.d.l.	b.d.l.	b.d.l.	b.d.l.	b.d.l.	b.d.l.	b.d.l.
NiO	n.a.	n.a.	n.a.	n.a.	n.a.	n.a.	n.a.	n.a.	n.a.	n.a.	n.a.
Total	99.94	100.39	100.75	100.93	100.87	100.69	100.81	100.53	100.57	100.69	100.71
Si	1.92	1.97	1.98	1.97	1.97	1.98	1.98	1.97	1.98	1.98	1.98
Ti	0.00	0.00	0.00	0.00	0.00	0.00	0.00	0.00	0.00	0.00	0.00
Al	0.03	0.03	0.03	0.03	0.03	0.03	0.03	0.03	0.02	0.02	0.02
Fe (iii)	0.00	0.00	0.00	0.00	0.00	0.00	0.00	0.00	0.00	0.00	0.00
Fe (ii)	0.89	0.89	0.89	0.89	0.88	0.87	0.89	0.89	0.90	0.91	0.92
Mn	0.02	0.02	0.02	0.02	0.02	0.02	0.02	0.02	0.02	0.02	0.02
Mg	1.16	1.06	1.06	1.06	1.06	1.08	1.06	1.07	1.05	1.05	1.03
Ca	0.03	0.03	0.03	0.03	0.03	0.03	0.03	0.03	0.03	0.03	0.03
Na	b.d.l.	b.d.l.	b.d.l.	b.d.l.	b.d.l.	b.d.l.	b.d.l.	b.d.l.	b.d.l.	b.d.l.	b.d.l.
Cr	b.d.l.	b.d.l.	b.d.l.	0.00	b.d.l.	b.d.l.	b.d.l.	b.d.l.	b.d.l.	b.d.l.	b.d.l.
Ni	n.a.	n.a.	n.a.	n.a.	n.a.	n.a.	n.a.	n.a.	n.a.	n.a.	n.a.
Total	4.06	4.01	4.01	4.01	4.01	4.01	4.01	4.01	4.00	4.01	4.01
Mg#	56.81	54.43	54.39	54.47	54.59	55.34	54.39	54.52	53.97	53.70	53.02
En	55.88	53.55	53.53	53.60	53.75	54.45	53.56	53.66	53.14	52.84	52.23
Fs	42.48	44.83	44.89	44.81	44.71	43.95	44.91	44.77	45.33	45.56	46.28
Wo	1.64	1.62	1.58	1.59	1.54	1.59	1.53	1.57	1.53	1.61	1.49

Group: B = basalt; BA = basaltic andesite; A = andesite; D = dacite; R = rhyolite; Opx/Cgt-SVC 2, 3 = orthopyroxene/cummingtonite-bearing SVC 2, 3 lavas; **Grain:** P = phenocryst; MC = microphenocryst; G = groundmass; C = core; INC = inclusion (mineral included within is stated in parentheses); **Position:** C = core; M = mantle, R = rim, osci. = oscillatory; UNZ = unzoned; **Other:** Dist. = distance from the core (µm); En = enstatite; Fs = forsterite; Wo = wollastonite; Mg# = 100*Mg / (Mg + Fe (ii)); Fe (ii) and Fe (iii) were calculated based on the minimum amount of Fe (iii) permissible in the structural formula.

Table G.3. (continued).

Group: Sample: Name: Grain:	SVC1 A SL-83-17 Profile C3-Py1a-c P									SVC1 A SL-83-17 Profile C3-Py1a-d P	
	M	M	M	M	M	M	M	M	R	C	C
	714	740	765	791	816	841	867	892	918	0	26
	Position: Dist.										
SiO ₂	51.65	49.82	51.69	51.44	51.35	51.38	51.41	51.29	50.27	51.64	51.68
TiO ₂	0.11	0.10	0.12	0.08	0.12	0.08	0.10	0.10	0.12	0.08	0.12
Al ₂ O ₃	0.46	0.51	0.39	0.42	0.44	0.41	0.37	0.36	0.39	0.62	0.61
FeOtot	28.78	27.94	29.24	29.50	29.70	30.22	30.22	30.11	29.45	28.29	28.35
MnO	0.73	0.76	0.73	0.71	0.79	0.76	0.78	0.83	0.69	0.69	0.74
MgO	17.96	16.87	17.46	17.60	17.26	17.05	16.79	16.86	16.73	18.11	18.15
CaO	0.96	2.56	1.02	1.13	0.89	0.80	0.96	1.01	2.28	0.81	0.83
Na ₂ O	b.d.l.	b.d.l.	b.d.l.	b.d.l.	b.d.l.	b.d.l.	b.d.l.	b.d.l.	b.d.l.	b.d.l.	b.d.l.
K ₂ O	b.d.l.	0.03	b.d.l.	b.d.l.	b.d.l.	b.d.l.	b.d.l.	b.d.l.	b.d.l.	b.d.l.	b.d.l.
Cr ₂ O ₃	b.d.l.	b.d.l.	b.d.l.	b.d.l.	b.d.l.	b.d.l.	b.d.l.	b.d.l.	b.d.l.	b.d.l.	b.d.l.
NiO	n.a.	n.a.	n.a.	n.a.	n.a.	n.a.	n.a.	n.a.	n.a.	n.a.	n.a.
Total	100.69	98.62	100.69	100.95	100.58	100.71	100.63	100.59	99.94	100.30	100.50
Si	1.98	1.96	1.98	1.97	1.98	1.98	1.98	1.98	1.96	1.98	1.97
Ti	0.00	0.00	0.00	0.00	0.00	0.00	0.00	0.00	0.00	0.00	0.00
Al	0.02	0.02	0.02	0.02	0.02	0.02	0.02	0.02	0.02	0.03	0.03
Fe (iii)	0.00	0.00	0.00	0.00	0.00	0.00	0.00	0.00	0.00	0.01	0.01
Fe (ii)	0.92	0.92	0.94	0.95	0.96	0.97	0.97	0.97	0.96	0.90	0.90
Mn	0.02	0.03	0.02	0.02	0.03	0.02	0.03	0.03	0.02	0.02	0.02
Mg	1.02	0.99	1.00	1.01	0.99	0.98	0.96	0.97	0.97	1.03	1.03
Ca	0.04	0.11	0.04	0.05	0.04	0.03	0.04	0.04	0.10	0.03	0.03
Na	b.d.l.	b.d.l.	b.d.l.	b.d.l.	b.d.l.	b.d.l.	b.d.l.	b.d.l.	b.d.l.	b.d.l.	b.d.l.
Cr	b.d.l.	b.d.l.	b.d.l.	b.d.l.	b.d.l.	b.d.l.	b.d.l.	b.d.l.	b.d.l.	b.d.l.	b.d.l.
Ni	n.a.	n.a.	n.a.	n.a.	n.a.	n.a.	n.a.	n.a.	n.a.	n.a.	n.a.
Total	4.01	4.03	4.01	4.02	4.01	4.01	4.01	4.01	4.03	4.00	4.00
Mg#	52.65	51.83	51.55	51.53	50.88	50.13	49.75	49.94	50.31	53.54	53.54
En	51.61	49.06	50.46	50.34	49.94	49.30	48.75	48.90	47.94	52.39	52.37
Fs	46.41	45.59	47.42	47.35	48.21	49.04	49.24	49.00	47.36	45.67	45.66
Wo	1.98	5.35	2.13	2.31	1.85	1.65	2.01	2.10	4.70	1.69	1.72

Group: Sample: Name: Grain:	SVC1 A SL-83-17 Profile C3-Py1a-d P									
	C	M	M	M	M	M	M	M	M	M
	53	79	106	132	159	185	211	238	264	291
	Position: Dist.									
SiO ₂	51.71	51.75	51.62	51.64	51.67	51.68	51.82	51.81	51.76	51.97
TiO ₂	0.12	0.09	0.09	0.11	0.10	0.12	0.09	0.09	0.09	0.09
Al ₂ O ₃	0.63	0.44	0.37	0.38	0.56	0.59	0.47	0.60	0.63	0.68
FeOtot	28.39	29.04	29.81	30.10	29.29	29.01	28.79	28.41	28.42	27.92
MnO	0.74	0.75	0.76	0.78	0.70	0.71	0.71	0.63	0.68	0.67
MgO	17.97	17.63	17.11	17.09	17.67	17.85	18.02	18.41	18.20	18.53
CaO	0.81	0.84	0.94	0.90	0.81	0.86	0.91	0.73	0.70	0.73
Na ₂ O	b.d.l.	b.d.l.	b.d.l.	b.d.l.	b.d.l.	b.d.l.	b.d.l.	b.d.l.	b.d.l.	b.d.l.
K ₂ O	b.d.l.	b.d.l.	b.d.l.	b.d.l.	b.d.l.	b.d.l.	b.d.l.	b.d.l.	b.d.l.	b.d.l.
Cr ₂ O ₃	b.d.l.	b.d.l.	b.d.l.	0.04	b.d.l.	b.d.l.	b.d.l.	b.d.l.	b.d.l.	b.d.l.
NiO	n.a.	n.a.	n.a.	n.a.	n.a.	n.a.	n.a.	n.a.	n.a.	n.a.
Total	100.38	100.57	100.74	101.05	100.83	100.84	100.84	100.70	100.51	100.63
Si	1.98	1.98	1.98	1.98	1.98	1.97	1.98	1.97	1.98	1.98
Ti	0.00	0.00	0.00	0.00	0.00	0.00	0.00	0.00	0.00	0.00
Al	0.03	0.02	0.02	0.02	0.03	0.03	0.02	0.03	0.03	0.03
Fe (iii)	0.01	0.01	0.01	0.01	0.01	0.01	0.01	0.01	0.01	0.01
Fe (ii)	0.90	0.92	0.95	0.95	0.93	0.92	0.91	0.90	0.90	0.88
Mn	0.02	0.02	0.02	0.03	0.02	0.02	0.02	0.02	0.02	0.02
Mg	1.02	1.01	0.98	0.98	1.01	1.02	1.02	1.05	1.04	1.05
Ca	0.03	0.03	0.04	0.04	0.03	0.04	0.04	0.03	0.03	0.03
Na	b.d.l.	b.d.l.	b.d.l.	b.d.l.	b.d.l.	b.d.l.	b.d.l.	b.d.l.	b.d.l.	b.d.l.
Cr	b.d.l.	b.d.l.	b.d.l.	0.00	b.d.l.	b.d.l.	b.d.l.	b.d.l.	b.d.l.	b.d.l.
Ni	n.a.	n.a.	n.a.	n.a.	n.a.	n.a.	n.a.	n.a.	n.a.	n.a.
Total	4.00	4.00	4.00	4.00	4.00	4.00	4.01	4.01	4.00	4.00
Mg#	53.25	52.22	50.81	50.55	52.05	52.55	52.97	53.84	53.55	54.44
En	52.11	51.06	49.57	49.36	50.93	51.37	51.73	52.78	52.52	53.36
Fs	45.96	46.95	48.22	48.53	47.14	46.59	46.14	45.46	45.77	44.87
Wo	1.69	1.75	1.98	1.87	1.69	1.80	1.88	1.51	1.46	1.53

Group: B = basalt; BA = basaltic andesite; A = andesite; D = dacite; R = rhyolite; Opx/Cgt-SVC 2, 3 = orthopyroxene/cummingtonite-bearing SVC 2, 3 lavas; **Grain:** P = phenocryst; MC = microphenocryst; G = groundmass; C = core; INC = inclusion (mineral included within is stated in parentheses); **Position:** C = core; M = mantle, R = rim, osci. = oscillatory; UNZ = unzoned; **Other:** Dist. = distance from the core (μm); En = enstatite; Fs = forsterite; Wo = wollastonite; Mg# = 100*Mg / (Mg + Fe (ii)); Fe (ii) and Fe (iii) were calculated based on the minimum amount of Fe (iii) permissible in the structural formula.

Table G.3. (continued).

Group: Sample:	SVC1 A SL-83-17		SVC1 A SL-JL-02				SVC1 D SL-JL-23				
Name: Grain:	Profile C3-Py1a-d P		C1- Py1A P	C1- Py1B P	C1- Ol1 P	C1- Ol2 MP	Profile C4-Py2 P				
Position: Dist.	M 344	R 370	C	R	C	C	C 0	C 26	C 53	M 79	M 106
SiO ₂	51.12	51.26	49.77	49.99	50.73	50.82	50.04	49.98	50.19	50.48	50.50
TiO ₂	0.19	0.10	0.13	0.12	0.12	0.07	0.10	0.11	0.12	0.10	0.10
Al ₂ O ₃	1.35	0.40	0.48	0.49	0.30	0.52	0.46	0.56	0.57	0.46	0.41
FeOtot	28.97	30.79	29.64	30.29	29.43	30.35	29.29	29.18	28.99	28.60	28.24
MnO	0.66	0.72	0.72	0.77	0.73	0.77	0.76	0.75	0.76	0.77	0.70
MgO	17.66	16.55	16.87	15.97	17.17	16.15	17.81	17.89	17.81	18.26	18.28
CaO	0.93	0.99	1.10	0.88	1.06	0.71	0.93	0.87	0.89	0.88	0.88
Na ₂ O	b.d.l.	b.d.l.	b.d.l.	b.d.l.	b.d.l.	b.d.l.	b.d.l.	b.d.l.	b.d.l.	b.d.l.	b.d.l.
K ₂ O	b.d.l.	b.d.l.	b.d.l.	b.d.l.	b.d.l.	b.d.l.	b.d.l.	b.d.l.	b.d.l.	b.d.l.	b.d.l.
Cr ₂ O ₃	b.d.l.	b.d.l.	b.d.l.	b.d.l.	b.d.l.	b.d.l.	b.d.l.	b.d.l.	b.d.l.	b.d.l.	0.04
NiO	n.a.	n.a.	b.d.l.	b.d.l.	b.d.l.	b.d.l.	b.d.l.	b.d.l.	b.d.l.	b.d.l.	b.d.l.
Total	100.89	100.85	98.86	98.69	99.61	99.42	99.44	99.40	99.37	99.57	99.20
Si	1.95	1.98	1.96	1.98	1.97	1.99	1.95	1.93	1.94	1.94	1.95
Ti	0.01	0.00	0.00	0.00	0.00	0.00	0.00	0.00	0.00	0.00	0.00
Al	0.06	0.02	0.02	0.02	0.01	0.02	0.02	0.03	0.03	0.02	0.02
Fe (iii)	0.01	0.01	0.00	0.00	0.00	0.00	0.00	0.09	0.08	0.08	0.08
Fe (ii)	0.92	0.98	0.98	1.00	0.96	0.99	0.96	0.85	0.85	0.84	0.83
Mn	0.02	0.02	0.02	0.03	0.02	0.03	0.03	0.02	0.02	0.03	0.02
Mg	1.00	0.95	0.99	0.94	1.00	0.94	1.04	1.03	1.03	1.05	1.05
Ca	0.04	0.04	0.05	0.04	0.04	0.03	0.04	0.04	0.04	0.04	0.04
Na	b.d.l.	b.d.l.	b.d.l.	b.d.l.	b.d.l.	b.d.l.	b.d.l.	b.d.l.	b.d.l.	b.d.l.	b.d.l.
Cr	b.d.l.	b.d.l.	b.d.l.	b.d.l.	b.d.l.	b.d.l.	b.d.l.	b.d.l.	b.d.l.	b.d.l.	0.00
Ni	n.a.	n.a.	b.d.l.	b.d.l.	b.d.l.	b.d.l.	b.d.l.	b.d.l.	b.d.l.	b.d.l.	b.d.l.
Total	4.01	4.01	4.03	4.01	4.01	4.00	4.03	4.00	4.00	4.00	4.00
Mg#	52.32	49.18	50.36	48.45	50.98	48.67	52.01	54.83	54.60	55.56	55.90
En	51.06	47.92	49.19	47.53	49.83	47.93	51.00	51.27	51.29	52.25	52.58
Fs	46.76	49.76	48.49	50.58	47.92	50.55	47.07	44.33	44.52	43.59	43.25
Wo	1.94	2.08	2.31	1.88	2.22	1.52	1.92	1.89	1.92	1.90	1.90
Group: Sample:	SVC1 D SL-JL-23										
Name: Grain:	Profile C4-Py2 P										
Position: Dist.	M 132	M 158	M 185	M 211	M 238	M 264	M 291	M 317	M 343	M 370	M 396
SiO ₂	50.70	50.22	50.65	50.51	50.58	49.89	50.45	50.63	50.88	50.99	51.06
TiO ₂	0.09	0.11	0.09	0.14	0.20	0.20	0.19	0.18	0.19	0.11	0.09
Al ₂ O ₃	0.67	0.57	0.51	0.67	0.79	0.99	0.96	0.89	0.89	0.73	0.69
FeOtot	27.72	28.68	28.59	28.23	28.35	27.94	27.21	26.95	25.64	27.02	26.02
MnO	0.73	0.75	0.75	0.70	0.71	0.72	0.69	0.66	0.66	0.65	0.79
MgO	18.61	18.57	18.40	18.35	18.44	18.35	18.82	19.24	20.19	19.51	20.57
CaO	0.88	0.84	0.91	0.96	1.08	1.17	1.27	1.11	1.04	0.82	0.85
Na ₂ O	b.d.l.	b.d.l.	b.d.l.	b.d.l.	b.d.l.	b.d.l.	b.d.l.	b.d.l.	b.d.l.	b.d.l.	b.d.l.
K ₂ O	b.d.l.	b.d.l.	b.d.l.	b.d.l.	b.d.l.	b.d.l.	b.d.l.	b.d.l.	b.d.l.	b.d.l.	b.d.l.
Cr ₂ O ₃	b.d.l.	b.d.l.	b.d.l.	b.d.l.	b.d.l.	b.d.l.	b.d.l.	b.d.l.	b.d.l.	b.d.l.	b.d.l.
NiO	b.d.l.	b.d.l.	0.04	b.d.l.	b.d.l.	0.03	b.d.l.	b.d.l.	b.d.l.	b.d.l.	b.d.l.
Total	99.40	99.77	99.97	99.56	100.18	99.28	99.63	99.70	99.53	99.91	100.38
Si	1.95	1.93	1.94	1.94	1.93	1.93	1.94	1.93	1.95	1.94	1.95
Ti	0.00	0.00	0.00	0.00	0.01	0.01	0.01	0.01	0.01	0.00	0.00
Al	0.03	0.03	0.02	0.03	0.04	0.04	0.04	0.04	0.04	0.03	0.03
Fe (iii)	0.08	0.08	0.08	0.08	0.08	0.08	0.00	0.09	0.00	0.09	0.00
Fe (ii)	0.81	0.84	0.83	0.83	0.82	0.82	0.88	0.77	0.82	0.77	0.83
Mn	0.02	0.02	0.02	0.02	0.02	0.02	0.02	0.02	0.02	0.02	0.03
Mg	1.06	1.06	1.05	1.05	1.05	1.06	1.08	1.09	1.15	1.11	1.17
Ca	0.04	0.03	0.04	0.04	0.04	0.05	0.05	0.05	0.04	0.03	0.03
Na	b.d.l.	b.d.l.	b.d.l.	b.d.l.	b.d.l.	b.d.l.	b.d.l.	b.d.l.	b.d.l.	b.d.l.	b.d.l.
Cr	b.d.l.	b.d.l.	b.d.l.	b.d.l.	b.d.l.	b.d.l.	b.d.l.	b.d.l.	b.d.l.	b.d.l.	b.d.l.
Ni	b.d.l.	b.d.l.	0.00	b.d.l.	b.d.l.	0.00	b.d.l.	b.d.l.	b.d.l.	b.d.l.	b.d.l.
Total	4.00	4.01	4.00	4.00	4.00	4.01	4.03	4.00	4.03	4.00	4.04
Mg#	56.79	55.91	55.76	56.00	56.03	56.25	55.21	58.56	58.40	58.84	58.49
En	53.48	52.65	52.40	52.60	52.50	52.60	53.76	54.71	57.14	55.32	57.49
Fs	42.39	43.30	43.36	43.09	42.96	42.63	43.61	40.45	40.71	40.43	40.80
Wo	1.89	1.78	1.94	2.06	2.31	2.51	2.60	2.38	2.12	1.75	1.71

Group: B = basalt; BA = basaltic andesite; A = andesite; D = dacite; R = rhyolite; Opx/Cgt-SVC 2, 3 = orthopyroxene/cummingtonite-bearing SVC 2, 3 lavas; **Grain:** P = phenocryst; MC = microphenocryst; G = groundmass; C = core; INC = inclusion (mineral included within is stated in parentheses); **Position:** C = core; M = mantle, R = rim, osci. = oscillatory; UNZ = unzoned; **Other:** Dist. = distance from the core (μm); En = enstatite; Fs = forsterite; Wo = wollastonite; Mg# = 100*Mg / (Mg + Fe (ii)); Fe (ii) and Fe (iii) were calculated based on the minimum amount of Fe (iii) permissible in the structural formula.

Table G.3. (continued).

Group: Sample: Name: Grain:	SVC1 D SL-JL-23 Pofile C4-Py2 P										SVC1 D SL-JL-23 Pofile C4-Py1 P
Position: Dist.	M 423	M 449	M 475	R 502	R 528	R 555	R 581	R 608	R 634	R 1930	C 0
SiO ₂	50.37	50.30	50.02	49.92	49.87	49.86	50.27	49.88	50.03	50.85	50.57
TiO ₂	0.10	0.10	0.11	0.10	0.11	0.10	0.14	0.12	0.13	0.13	0.16
Al ₂ O ₃	0.88	0.91	0.86	0.72	0.58	0.48	0.48	0.85	0.85	0.43	0.38
FeOtot	27.90	28.33	28.99	30.15	29.85	30.87	30.88	30.56	29.19	28.47	30.43
MnO	0.73	0.78	0.81	0.85	0.79	0.81	0.81	0.74	0.73	0.72	0.78
MgO	18.75	18.56	17.82	17.04	17.33	16.56	16.41	16.57	17.12	18.06	16.63
CaO	0.84	0.86	0.80	0.77	0.98	0.95	1.00	0.96	1.01	0.96	1.07
Na ₂ O	b.d.l.	b.d.l.	b.d.l.	b.d.l.	b.d.l.	b.d.l.	b.d.l.	b.d.l.	b.d.l.	b.d.l.	b.d.l.
K ₂ O	b.d.l.	b.d.l.	b.d.l.	b.d.l.	b.d.l.	b.d.l.	b.d.l.	b.d.l.	b.d.l.	b.d.l.	b.d.l.
Cr ₂ O ₃	b.d.l.	b.d.l.	b.d.l.	b.d.l.	b.d.l.	b.d.l.	b.d.l.	b.d.l.	b.d.l.	b.d.l.	b.d.l.
NiO	b.d.l.	b.d.l.	b.d.l.	b.d.l.	b.d.l.	b.d.l.	b.d.l.	b.d.l.	b.d.l.	b.d.l.	b.d.l.
Total	99.60	99.99	99.44	99.87	99.52	99.88	100.02	99.75	99.13	99.65	100.16
Si	1.95	1.94	1.95	1.95	1.95	1.96	1.96	1.95	1.96	1.97	1.97
Ti	0.00	0.00	0.00	0.00	0.00	0.00	0.00	0.00	0.00	0.00	0.00
Al	0.04	0.04	0.04	0.03	0.03	0.02	0.02	0.04	0.04	0.02	0.02
Fe (iii)	0.00	0.00	0.00	0.00	0.00	0.00	0.00	0.00	0.00	0.00	0.00
Fe (ii)	0.90	0.91	0.94	0.99	0.98	1.01	1.01	1.00	0.95	0.92	0.99
Mn	0.02	0.03	0.03	0.03	0.03	0.03	0.03	0.02	0.02	0.02	0.03
Mg	1.08	1.07	1.03	0.99	1.01	0.97	0.95	0.97	1.00	1.04	0.96
Ca	0.03	0.04	0.03	0.03	0.04	0.04	0.04	0.04	0.04	0.04	0.04
Na	b.d.l.	b.d.l.	b.d.l.	b.d.l.	b.d.l.	b.d.l.	b.d.l.	b.d.l.	b.d.l.	b.d.l.	b.d.l.
Cr	b.d.l.	b.d.l.	b.d.l.	b.d.l.	b.d.l.	b.d.l.	b.d.l.	b.d.l.	b.d.l.	b.d.l.	b.d.l.
Ni	b.d.l.	b.d.l.	b.d.l.	b.d.l.	b.d.l.	b.d.l.	b.d.l.	b.d.l.	b.d.l.	b.d.l.	b.d.l.
Total	4.03	4.03	4.03	4.03	4.03	4.03	4.02	4.03	4.02	4.02	4.02
Mg#	54.49	53.87	52.28	50.17	50.84	48.87	48.64	49.15	51.10	53.05	49.33
En	53.55	52.92	51.41	49.37	49.82	47.90	47.63	48.18	50.02	51.99	48.23
Fs	44.72	45.31	46.93	49.03	48.16	50.12	50.29	49.86	47.86	46.00	49.54
Wo	1.73	1.77	1.67	1.60	2.02	1.99	2.09	2.02	2.11	1.99	2.23

Group: Sample: Name: Grain:	SVC1 D SL-JL-23 Pofile C4-Py1 P								Opx-SVC 2, 3 D SL-83-03			
	C	M	M	M	M	M	M	R	C1- Py1 MP	C3- Py1 P	C3- Py2 P	C3- Py3 G
Position: Dist.	C 28	M 56	M 84	M 111	M 139	M 167	M 195	R 223	C	C	R	C
SiO ₂	50.44	46.16	49.13	50.39	50.94	50.25	50.36	51.02	50.98	51.30	51.03	50.59
TiO ₂	0.11	0.09	0.10	0.15	0.11	0.12	0.12	0.13	0.08	0.11	0.10	0.14
Al ₂ O ₃	0.33	0.36	0.30	0.45	0.38	0.74	0.56	0.48	0.59	0.65	0.68	0.68
FeOtot	30.42	27.75	29.45	29.37	30.20	29.85	30.51	28.82	33.20	33.74	32.97	31.34
MnO	0.78	0.71	0.72	0.79	0.76	0.78	0.81	0.73	0.95	0.92	1.00	1.03
MgO	16.67	15.18	16.21	17.52	17.25	17.25	16.49	17.85	12.64	12.95	13.23	13.24
CaO	1.03	5.63	2.33	0.96	0.99	0.98	1.04	1.07	0.77	0.81	1.46	0.80
Na ₂ O	b.d.l.	b.d.l.	b.d.l.	b.d.l.	b.d.l.	b.d.l.	b.d.l.	b.d.l.	b.d.l.	b.d.l.	b.d.l.	b.d.l.
K ₂ O	b.d.l.	b.d.l.	b.d.l.	b.d.l.	b.d.l.	b.d.l.	b.d.l.	b.d.l.	b.d.l.	b.d.l.	b.d.l.	b.d.l.
Cr ₂ O ₃	b.d.l.	b.d.l.	b.d.l.	b.d.l.	b.d.l.	b.d.l.	b.d.l.	b.d.l.	b.d.l.	b.d.l.	b.d.l.	b.d.l.
NiO	b.d.l.	b.d.l.	b.d.l.	b.d.l.	b.d.l.	b.d.l.	b.d.l.	b.d.l.	b.d.l.	b.d.l.	b.d.l.	b.d.l.
Total	99.82	99.94	99.70	99.74	101.01	99.99	99.98	100.12	99.26	100.49	100.80	97.84
Si	1.97	1.90	1.95	1.96	1.97	1.95	1.96	1.97	2.02	2.01	2.00	2.02
Ti	0.00	0.00	0.00	0.00	0.00	0.00	0.00	0.00	0.00	0.00	0.00	0.00
Al	0.02	0.02	0.01	0.02	0.02	0.03	0.03	0.02	0.03	0.03	0.03	0.03
Fe (iii)	0.00	0.00	0.00	0.00	0.00	0.00	0.00	0.00	0.00	0.00	0.00	0.00
Fe (ii)	0.99	0.96	0.98	0.96	0.97	0.97	1.00	0.93	1.10	1.11	1.08	1.05
Mn	0.03	0.02	0.02	0.03	0.02	0.03	0.03	0.02	0.03	0.03	0.03	0.03
Mg	0.97	0.93	0.96	1.02	0.99	1.00	0.96	1.03	0.75	0.76	0.77	0.79
Ca	0.04	0.25	0.10	0.04	0.04	0.04	0.04	0.04	0.03	0.03	0.06	0.03
Na	b.d.l.	b.d.l.	b.d.l.	b.d.l.	b.d.l.	b.d.l.	b.d.l.	b.d.l.	b.d.l.	b.d.l.	b.d.l.	b.d.l.
Cr	b.d.l.	b.d.l.	b.d.l.	b.d.l.	b.d.l.	b.d.l.	b.d.l.	b.d.l.	b.d.l.	b.d.l.	b.d.l.	b.d.l.
Ni	b.d.l.	b.d.l.	b.d.l.	b.d.l.	b.d.l.	b.d.l.	b.d.l.	b.d.l.	b.d.l.	b.d.l.	b.d.l.	b.d.l.
Total	4.02	4.09	4.04	4.02	4.02	4.03	4.02	4.02	3.96	3.97	3.98	3.96
Mg#	49.40	49.37	49.51	51.53	50.45	50.73	49.07	52.46	40.42	40.62	41.70	42.95
En	48.32	43.65	47.11	50.50	49.42	49.71	48.02	51.31	39.71	39.90	40.35	42.16
Fs	49.50	44.76	48.04	47.50	48.54	48.28	49.84	46.49	58.52	58.31	56.42	55.99
Wo	2.15	11.64	4.88	2.00	2.04	2.03	2.17	2.20	1.74	1.79	3.20	1.82

Group: B = basalt; BA = basaltic andesite; A = andesite; D = dacite; R = rhyolite; Opx/Cgt-SVC 2, 3 = orthopyroxene/cummingtonite-bearing SVC 2, 3 lavas; **Grain:** P = phenocryst; MC = microphenocryst; G = groundmass; C = core; INC = inclusion (mineral included within is stated in parentheses); **Position:** C = core; M = mantle, R = rim, osci. = oscillatory; UNZ = unzoned; **Other:** Dist. = distance from the core (μm); En = enstatite; Fs = forsterite; Wo = wollastonite; Mg# = 100*Mg / (Mg + Fe (ii)); Fe (ii) and Fe (iii) were calculated based on the minimum amount of Fe (iii) permissible in the structural formula.

Table G.4. Amphibole major element composition obtained by electron microprobe.

Group Sample	Opx-bearing SVC 2, 3 D SL-JL-83			Opx bearing SVC 2, 3 D SL-83-03					Opx-SVC 2, 3 D SL-JL-22	
	C1- Am1	C2- Am1	C3-Res 1	C1- Am1	C3- Am1	C3- Am2	C3- Am3	C4- Am2	C1- Am1	C5- Am1A
	MP	MP	MP	MP	MP	Res. P	MP	Res. P	MP	MP
Position:	C	C	C	C	C	R	C	M	C	C
SiO ₂	40.86	41.39	40.97	45.56	45.05	45.48	44.48	44.19	44.20	43.11
TiO ₂	1.79	1.66	1.70	1.62	1.38	1.48	1.67	1.46	1.81	2.00
Al ₂ O ₃	14.95	14.08	15.42	13.02	9.79	9.56	14.57	10.47	11.51	12.48
FeO	8.35	9.69	8.30	9.79	21.70	23.34	8.38	19.69	9.76	13.22
MnO	0.10	0.14	0.11	0.17	0.43	0.43	0.10	0.34	0.23	0.36
MgO	15.99	15.80	16.56	17.29	9.17	9.23	15.63	8.58	17.47	14.56
CaO	12.36	11.99	11.97	10.25	10.16	10.02	11.83	10.73	10.88	10.67
Na ₂ O	2.01	2.06	2.08	1.68	2.08	2.19	2.09	2.03	2.40	1.84
K ₂ O	0.44	0.34	0.39	0.34	0.36	0.23	0.40	0.37	0.29	0.22
Total	96.84	97.14	97.50	99.73	100.12	101.97	99.16	97.87	98.55	98.44
T sites										
Si	5.90	5.97	5.85	6.37	6.69	6.67	6.29	6.67	6.30	6.23
Al (iv)	2.10	2.03	2.15	1.63	1.31	1.33	1.71	1.33	1.70	1.77
Total	8.00	8.00	8.00	8.00	8.00	8.00	8.00	8.00	8.00	8.00
M1-3 sites										
Ti	0.19	0.18	0.18	0.17	0.15	0.16	0.18	0.17	0.19	0.22
Al (vi)	0.44	0.37	0.45	0.52	0.41	0.33	0.72	0.53	0.24	0.36
Fe (iii)	0.63	0.65	0.68	0.25	0.00	0.01	0.00	0.00	0.35	0.42
Fe (ii)	0.36	0.50	0.30	0.81	2.50	2.61	0.95	2.39	0.75	1.08
Ni	0.01	0.02	0.01	0.02	0.05	0.05	0.01	0.04	0.03	0.04
Mg	3.36	3.27	3.37	3.23	1.88	1.84	3.14	1.86	3.44	2.88
Total	5.00	5.00	5.00	5.00	5.00	5.00	5.00	5.00	5.00	5.00
M4 sites										
Fe(ii)	0.01	0.02	0.01	0.09	0.20	0.25	0.05	0.09	0.06	0.10
Mg	0.08	0.13	0.15	0.37	0.15	0.18	0.15	0.07	0.28	0.25
Mn	0.00	0.00	0.00	0.00	0.00	0.00	0.00	0.00	0.00	0.00
Ca	1.91	1.85	1.83	1.54	1.62	1.57	1.79	1.74	1.66	1.65
Na	0.00	0.00	0.00	0.00	0.04	0.00	0.01	0.10	0.00	0.00
Total	2.00	2.00	2.00	2.00	2.00	2.00	2.00	2.00	2.00	2.00
A sites										
Na	0.56	0.58	0.58	0.46	0.56	0.62	0.57	0.49	0.66	0.52
K	0.08	0.06	0.07	0.06	0.07	0.04	0.07	0.07	0.05	0.04
Total	0.64	0.64	0.65	0.52	0.63	0.67	0.64	0.56	0.72	0.56
Sum										
Mg#	15.64	15.64	15.65	15.52	15.63	15.67	15.64	15.56	15.72	15.56
Mg##	90.22	86.73	91.86	80.03	42.95	41.40	76.88	43.71	82.07	72.74
Mg##	77.34	74.41	78.05	75.88	42.95	41.32	76.88	43.71	76.14	66.23
Species										
	Mg- Hst	Tsch	Mg-Hst	Tsch	Mg-Hbl	Tsch	Tsch	Mg-Hbl	Tsch	Tsch
T (°C)	1044	1016	—	—	821	814	983	844	—	—
1 SE	22	22	—	—	22	22	56	56	—	—
P (MPa)	724	580	—	—	212	192	—	—	—	—
Max error	80	64	—	—	53	48	—	—	—	—
oceanic depth (km)	26	20	—	—	7	7	—	—	—	—
continental depth (km)	27	22	—	—	8	7	—	—	—	—
ΔNNO	1.42	1.51	—	—	0.01	0.09	—	—	—	—
logfO ₂	-8.0	-8.4	—	—	-13.4	-13.4	—	—	—	—
1 SE	0.4	0.4	—	—	0.4	0.4	—	—	—	—
H ₂ O melt (wt. %)	8.0	7.6	—	—	7.5	7.1	—	—	—	—
1 SE	1.2	1.1	—	—	0.4	1.1	—	—	—	—

Group: B = basalt; BA = basaltic andesite; A = andesite; D = dacite; R = rhyolite; Opx/Cgt-SVC 2, 3 = orthopyroxene/cummingtonite-bearing SVC 2, 3 lavas; **Grain:** P = phenocryst; MC = microphenocryst; G = groundmass; C = core; **Position:** C = core; M = mantle; R = rim; **Other:** Mg# = 100* Mg / (Mg + Fe (ii)); Mg ## = 100* Mg / (Mg + Fe (ii) + Fe (iii)); Res. = resorbed; Mg-Hst = magnesio-hastingsite; Tsch. = tschermakite; Hbl = hornblende; Mg-Hbl = Magnesio-hornblende; Cgt = cummingtonite; T = temperature; P = pressure; T, P, oxygen fugacity and water in the melt were calculated using the model of Ridolfi et al. (2009). Fe (ii) and Fe (iii) were calculated based on the minimum amount of Fe (iii) permissible in the structural formula.

Table G.4. (continued).

Group Sample	Opx-SVC 2, 3 D SL-JL-22		Opx-SVC 2, 3 D SL-83-24		Opx-SVC 2, 3 D SL-JL-79		Cgt-SVC 2, 3 D SL-83-08			
Name:	C5- Am1B	C5- Am2	C2- Am1A	C2- Am1B	C3- Am1	C4- Am1	C2- Am1	C1- Am1	C1- Am2	C4- Am1
Grain:	MP	MP	MP	MP	MP	MP	MP	MP	MP	P
Position:	R	M	C	R	C	R	C	R	C	M
SiO ₂	41.84	47.16	42.83	41.74	43.88	44.40	53.21	53.47	54.03	52.75
TiO ₂	1.92	1.54	1.71	1.61	1.31	1.33	0.34	0.39	0.31	0.42
Al ₂ O ₃	14.08	7.41	12.56	14.34	9.28	8.81	2.35	2.75	2.30	3.00
FeO	8.39	14.92	11.01	8.24	22.17	21.52	27.74	26.62	26.61	26.50
MnO	0.08	0.32	0.32	0.06	0.55	0.48	0.88	0.78	0.74	0.78
MgO	17.34	14.74	15.96	17.79	9.80	10.32	13.34	13.83	14.50	13.67
CaO	11.92	10.76	11.12	11.56	9.62	9.51	1.75	1.68	1.53	1.78
Na ₂ O	2.05	1.22	1.87	2.17	1.43	1.41	0.32	0.43	0.34	0.40
K ₂ O	0.26	0.30	0.31	0.37	0.51	0.50	0.02	0.02	0.01	0.02
Total	97.88	98.38	97.69	97.89	98.54	98.27	99.95	99.98	100.37	99.32
T sites										
Si	5.94	6.85	6.17	5.92	6.60	6.68	7.79	7.78	7.81	7.73
Al (iv)	2.06	1.15	1.83	2.08	1.40	1.32	0.21	0.22	0.19	0.27
Total	8.00	8.00	8.00	8.00	8.00	8.00	8.00	8.00	8.00	8.00
M1-3 sites										
Ti	0.20	0.17	0.18	0.17	0.15	0.15	0.04	0.04	0.03	0.05
Al (vi)	0.29	0.11	0.30	0.32	0.25	0.24	0.20	0.25	0.20	0.25
Fe (iii)	0.80	0.30	0.58	0.74	0.34	0.28	0.00	0.00	0.00	0.00
Fe (ii)	0.19	1.41	0.70	0.22	2.21	2.19	2.51	2.40	2.37	2.40
Ni	0.01	0.04	0.04	0.01	0.07	0.06	0.11	0.10	0.09	0.10
Mg	3.51	2.97	3.19	3.53	1.98	2.08	2.15	2.22	2.30	2.21
Total	5.00	5.00	5.00	5.00	5.00	5.00	5.00	5.00	5.00	5.00
M4 sites										
Fe(ii)	0.01	0.10	0.05	0.01	0.24	0.24	0.89	0.84	0.85	0.85
Mg	0.16	0.22	0.23	0.23	0.21	0.23	0.76	0.78	0.82	0.78
Mn	0.00	0.00	0.00	0.00	0.00	0.00	0.00	0.00	0.00	0.00
Ca	1.81	1.67	1.72	1.76	1.55	1.53	0.27	0.26	0.24	0.28
Na	0.02	0.00	0.00	0.00	0.00	0.00	0.08	0.12	0.09	0.10
Total	2.00	2.00	2.00	2.00	2.00	2.00	2.00	2.00	2.00	2.00
A sites										
Na	0.54	0.34	0.52	0.60	0.42	0.41	0.01	0.00	0.00	0.02
K	0.05	0.06	0.06	0.07	0.10	0.10	0.00	0.00	0.00	0.00
Total	0.59	0.40	0.58	0.66	0.52	0.51	0.02	0.01	0.01	0.02
Sum	15.59	15.40	15.58	15.66	15.52	15.51	15.02	15.01	15.01	15.02
Mg#	94.85	67.82	82.03	94.13	47.28	48.76	46.16	48.07	49.27	47.90
Mg##	78.65	63.77	72.09	79.38	44.06	46.07	46.16	48.07	49.27	47.90
Species	Mg-Hst	Mg-Hbl	Tsch	Mg-Hst	Tsch	Tsch	Cgt	Cgt	Cgt	Cgt
T (°C)	—	841	—	—	—	—	—	—	—	—
1 SE	—	22	—	—	—	—	—	—	—	—
P (MPa)	—	114	—	—	—	—	—	—	—	—
Max error	—	13	—	—	—	—	—	—	—	—
oceanic depth	—	—	—	—	—	—	—	—	—	—
(km)	—	4	—	—	—	—	—	—	—	—
continental depth	—	—	—	—	—	—	—	—	—	—
(km)	—	4	—	—	—	—	—	—	—	—
ΔNNO	—	1.94	—	—	—	—	—	—	—	—
logfO ₂	—	-11.1	—	—	—	—	—	—	—	—
1 SE	—	0.4	—	—	—	—	—	—	—	—
H₂O melt (wt. %)	—	5.4	—	—	—	—	—	—	—	—
1 SE	—	0.4	—	—	—	—	—	—	—	—

Group: B = basalt; BA = basaltic andesite; A = andesite; D = dacite; R = rhyolite; Opx/Cgt-SVC 2, 3 = orthopyroxene/cummingtonite-bearing SVC 2, 3 lavas; **Grain:** P = phenocryst; MC = microphenocryst; G = groundmass; C = core; **Position:** C = core; M = mantle; R = rim; **Other:** Mg# = 100* Mg / (Mg + Fe (ii)); Mg ## = 100* Mg / (Mg + Fe (ii) + Fe (iii)); Res. = resorbed; Mg-Hst = magnesio-hastingsite; Tsch. = tschermakite; Hbl = hornblende; Mg-Hbl = Magnesio-hornblende; Cgt = cummingtonite; T = temperature; P = pressure; T, P, oxygen fugacity and water in the melt were calculated using the model of Ridolfi et al. (2009). Fe (ii) and Fe (iii) were calculated based on the minimum amount of Fe (iii) permissible in the structural formula.

Table G.4. (continued).

Group Sample	Cgt-SVC 2, 3 D 11-01A		Cgt-SVC 2, 3 D SL-JL-33			
	C1- Am1	C3- Am1	C2- Am1	C3- Am1	C4- Am1A	C4- Am1B
Grain:	MP	MP	P	MP	P	P
Position:	C	C	M	C	C	R
SiO ₂	48.31	49.03	50.19	50.68	50.47	50.86
TiO ₂	0.49	0.41	0.44	0.28	0.38	0.31
Al ₂ O ₃	3.32	3.02	2.84	1.96	2.71	2.10
FeO	27.28	27.18	29.09	28.92	25.77	27.98
MnO	0.90	0.79	1.11	0.99	0.65	0.71
MgO	13.34	13.89	13.95	14.41	15.50	14.66
CaO	2.18	1.90	1.85	1.39	1.96	1.28
Na ₂ O	0.44	0.41	0.46	0.31	0.45	0.32
K ₂ O	0.04	0.03	0.02	0.00	0.05	0.02
Total	96.30	96.67	99.94	98.95	97.94	98.24
T sites						
Si	7.37	7.43	7.39	7.51	7.48	7.57
Al (iv)	0.63	0.57	0.61	0.49	0.52	0.43
Total	8.00	8.00	8.00	8.00	8.00	8.00
M1-3 sites						
Ti	0.06	0.05	0.05	0.03	0.04	0.03
Al (vi)	0.00	0.00	0.00	0.00	0.00	0.00
Fe (iii)	0.42	0.39	0.50	0.48	0.35	0.33
Fe (ii)	2.23	2.22	2.22	2.23	2.08	2.27
Ni	0.12	0.10	0.14	0.12	0.08	0.09
Mg	2.21	2.28	2.21	2.28	2.50	2.34
Total	5.00	5.00	5.00	5.00	5.00	5.00
M4 sites						
Fe(ii)	0.83	0.83	0.86	0.88	0.77	0.88
Mg	0.82	0.86	0.85	0.90	0.92	0.91
Mn	0.00	0.00	0.00	0.00	0.00	0.00
Ca	0.36	0.31	0.29	0.22	0.31	0.20
Na	0.00	0.00	0.00	0.00	0.00	0.00
Total	2.00	2.00	2.00	2.00	2.00	2.00
A sites						
Na	0.13	0.12	0.13	0.09	0.13	0.09
K	0.01	0.00	0.00	0.00	0.01	0.00
Total	0.14	0.13	0.13	0.09	0.14	0.09
Sum	15.14	15.13	15.13	15.09	15.14	15.09
Mg#	49.80	50.67	49.85	50.62	54.63	50.75
Mg##	46.58	47.67	46.09	47.03	51.73	48.29
Species	Cgt	Cgt	Cgt	Cgt	Cgt	Cgt
T (°C)	—	—	—	—	—	—
1 SE	—	—	—	—	—	—
P (MPa)	—	—	—	—	—	—
Max error	—	—	—	—	—	—
oceanic depth	—	—	—	—	—	—
(km)	—	—	—	—	—	—
continental depth	—	—	—	—	—	—
(km)	—	—	—	—	—	—
ΔNNO	—	—	—	—	—	—
logfO ₂	—	—	—	—	—	—
1 SE	—	—	—	—	—	—
H₂O melt (wt. %)	—	—	—	—	—	—
1 SE	—	—	—	—	—	—

Group: B = basalt; BA = basaltic andesite; A = andesite; D = dacite; R = rhyolite; Opx/Cgt-SVC 2, 3 = orthopyroxene/cummingtonite-bearing SVC 2, 3 lavas; **Grain:** P = phenocryst; MC = microphenocryst; G = groundmass; C = core; **Position:** C = core; M = mantle; R = rim; **Other:** Mg# = 100* Mg / (Mg + Fe (ii)); Mg ## = 100* Mg / (Mg + Fe (ii) + Fe (iii)); Res. = resorbed; Mg-Hst = magnesio-hastingsite; Tsch. = tschermakite; Hbl = hornblende; Mg-Hbl = Magnesio-hornblende; Cgt = cummingtonite; T = temperature; P = pressure; T, P, oxygen fugacity and water in the melt were calculated using the model of Ridolfi et al. (2009). Fe (ii) and Fe (iii) were calculated based on the minimum amount of Fe (iii) permissible in the structural formula.

Table G.5. Biotite major element composition obtained by electron microprobe.

Group: Sample:	Opx-SVC 2, 3 D SL-JL-22		Opx-SVC 2, 3 D SL-83-24		Opx-SVC 2, 3 D SL-JL-79		Cgt-SVC 2, 3 D SL-JL-33			Cgt-SVC 2, 3 D SL-83-08	
Name:	C1-Bi1	C2-Bi1	C1-Bi1	C4-Bi1	C1-Bi1	C2-Bi1	C2-Bi1	C2-Bi2	C1-Bi1	C2-Bi2	C1-Bi1
Grain:	P	Res. P	Res. P	Res. P	P	P	P	P	MP	MP	MP
Position:	C	C	C	C	C	C	C	C	C	C	C
SiO ₂	35.67	35.32	35.06	35.71	34.59	37.71	37.90	36.71	38.03	37.44	37.50
TiO ₂	4.54	4.50	4.58	4.36	4.38	4.55	4.72	4.78	4.78	4.35	4.44
Al ₂ O ₃	14.98	14.72	14.73	14.84	14.32	13.90	14.41	14.13	14.65	15.71	15.92
Cr ₂ O ₃	b.d.l	b.d.l	b.d.l	b.d.l	b.d.l	b.d.l	b.d.l	0.04	b.d.l	b.d.l	b.d.l
FeO	21.16	21.43	21.61	21.55	23.16	19.93	19.27	20.04	19.35	20.41	20.32
MnO	b.d.l	0.06	0.16	0.16	0.05	0.06	0.10	0.09	0.07	0.13	0.15
MgO	11.12	11.20	11.40	11.54	9.97	10.29	9.96	10.11	10.65	10.02	10.27
CaO	b.d.l	b.d.l	b.d.l	b.d.l	0.30	0.09	0.10	0.13	0.07	b.d.l	b.d.l
Na ₂ O	0.77	0.76	0.52	0.53	0.39	0.14	0.19	0.28	0.10	0.37	0.42
K ₂ O	8.77	8.63	8.80	8.85	7.74	7.92	7.93	7.75	8.43	8.14	8.13
P ₂ O ₅	b.d.l	b.d.l	b.d.l	b.d.l	b.d.l	b.d.l	b.d.l	b.d.l	b.d.l	b.d.l	b.d.l
NiO	0.04	b.d.l	b.d.l	b.d.l	b.d.l	b.d.l	b.d.l	b.d.l	b.d.l	b.d.l	b.d.l
Total	97.10	96.65	96.88	97.58	94.94	94.62	94.59	94.07	96.13	96.60	97.22
Si	5.40	5.38	5.34	5.39	5.40	5.75	5.76	5.65	5.70	5.61	5.58
Ti	0.52	0.52	0.53	0.50	0.51	0.52	0.54	0.55	0.54	0.49	0.50
Al (iv)	2.60	2.62	2.65	2.61	2.60	2.25	2.24	2.35	2.30	2.39	2.42
Al (vi)	0.07	0.03	0.00	0.03	0.03	0.25	0.34	0.22	0.29	0.38	0.37
Fe (iii)	0.00	0.00	0.00	0.00	0.00	0.00	0.00	0.00	0.00	0.00	0.00
Fe(ii)	2.68	2.73	2.75	2.72	3.02	2.54	2.45	2.58	2.43	2.56	2.53
Mn	b.d.l	0.01	0.02	0.02	0.01	0.01	0.01	0.01	0.01	0.02	0.02
Mg	2.51	2.54	2.59	2.60	2.32	2.34	2.26	2.32	2.38	2.24	2.28
Ca	b.d.l	b.d.l	b.d.l	b.d.l	0.05	0.01	0.02	0.02	0.01	b.d.l	b.d.l
Na	0.23	0.22	0.15	0.15	0.12	0.04	0.06	0.08	0.03	0.11	0.12
K	1.69	1.68	1.71	1.70	1.54	1.54	1.54	1.52	1.61	1.56	1.54
OH	4.00	4.00	4.00	4.00	4.00	4.00	4.00	4.00	4.00	4.00	4.00
Total	19.71	19.73	19.74	19.72	19.60	19.26	19.21	19.31	19.29	19.35	19.36
Mg#	48.37	48.23	48.46	48.83	43.40	47.93	47.95	47.34	49.52	46.66	47.40

Group: D = dacite; R = rhyolite; Opx/Cgt-SVC 2, 3 = orthopyroxene/cummingtonite-bearing SVC 2, 3 lavas; **Grain:** P = phenocryst; MC = microphenocryst; Res. = resorbed; **Position:** C = core; **Other:** Mg# = 100* Mg / (Mg + Fe (ii)); Fe (ii) and Fe (iii) were calculated based on the minimum amount of Fe (iii) permissible in the structural formula. OH was calculated following Tindle and Webb (1990).

Table G.6. Ilmenite major element compositions obtained by electron microprobe.

Group: Sample:	Pre-SVC1 B SL-83-44		Pre-SVC1 BA SL-83-25	Pre-SVC1 R SL-83-45							
Name:	C1- Ox1	C2- Ox1	C4-Ox1	C2- Ox1	C2- Ox2	C3- Ox1 INC (plag)	C3- Ox2	C4- Ox1	C5- Ox1 INC (opx)	C5- Ox2 INC (plag)	C5- Ox3 INC (plag)
Grain:	G	G	G	G	G	G	G	G	G	G	G
Position:	C	C	C	C	C	C	C	C	C	C	C
SiO ₂	0.25	0.17	1.46	0.09	0.11	0.09	0.10	0.19	0.13	0.17	1.03
TiO ₂	14.86	14.56	20.33	18.99	19.60	20.25	19.04	16.04	17.77	15.96	18.69
Al ₂ O ₃	1.98	2.16	2.21	0.86	1.04	1.20	0.87	0.97	0.66	0.83	1.12
FeO	74.16	74.46	65.55	74.19	73.59	72.25	73.40	75.89	75.56	76.26	72.08
MnO	0.38	0.36	0.06	1.06	1.04	1.12	1.10	1.03	0.82	0.77	1.13
MgO	0.72	0.88	0.05	0.35	0.39	0.39	0.39	0.24	0.37	0.32	0.33
CaO	0.11	0.10	0.09	b.d.l.	b.d.l.	0.06	0.06	0.06	0.05	0.06	0.08
Cr ₂ O ₄	b.d.l.	0.06	0.72	b.d.l.	b.d.l.	b.d.l.	b.d.l.	b.d.l.	b.d.l.	b.d.l.	b.d.l.
NiO	b.d.l.	b.d.l.	b.d.l.	b.d.l.	b.d.l.	b.d.l.	b.d.l.	b.d.l.	b.d.l.	b.d.l.	b.d.l.
P ₂ O ₅	b.d.l.	b.d.l.	0.05	b.d.l.	b.d.l.	b.d.l.	b.d.l.	b.d.l.	0.08	0.00	b.d.l.
Total	92.51	92.78	90.61	95.57	95.83	95.39	94.98	94.45	95.44	94.41	94.49
Si	0.01	0.01	0.08	0.00	0.01	0.00	0.01	0.01	0.01	0.01	0.05
Ti	0.58	0.56	0.82	0.72	0.75	0.77	0.73	0.62	0.68	0.61	0.72
Al	0.12	0.13	0.14	0.05	0.06	0.07	0.05	0.06	0.04	0.05	0.07
Fe(iii)	2.70	2.72	2.06	2.49	2.44	2.37	2.48	2.69	2.59	2.70	2.39
Fe (ii)	0.51	0.48	0.89	0.66	0.68	0.70	0.66	0.56	0.62	0.56	0.69
Mn	0.02	0.02	0.00	0.05	0.04	0.05	0.05	0.04	0.04	0.03	0.05
Mg	0.06	0.07	0.00	0.03	0.03	0.03	0.03	0.02	0.03	0.02	0.03
Ca	0.01	0.01	0.01	0.00	0.00	0.00	0.00	0.00	0.00	0.00	0.00
Total	4.00	4.00	4.00	4.00	4.00	4.00	4.00	4.00	4.00	4.00	4.00

Group: Sample:	Pre-SVC2 BA SL-83-26	SVC1 A SL-JL-02				SVC1 A SL-83-17				SVC1 D SL-JL-23	
Name:	C4-Ox1	C1-Ox1 INC (opx)	C1- Ox2 INC (opx)	C2- Ox1	C3- Ox1 INC (opx)	C1- Ox1	C1- Ox5	C2- Ox1 INC (opx)	C4- Ox1	C3- Ox1	C4- Ox1 INC (opx)
Grain:	MP	(opx)	(opx)	G	(opx)	G	G	(opx)	G	G	(opx)
Position:	C	C	C	C	C	C	C	C	C	C	C
SiO ₂	0.54	0.35	0.03	0.01	0.07	b.d.l.	b.d.l.	0.01	0.05	0.01	0.02
TiO ₂	19.64	21.84	46.01	41.36	47.00	48.94	48.78	48.64	48.10	47.26	45.41
Al ₂ O ₃	2.62	0.72	0.41	0.12	0.23	0.11	0.08	0.32	0.15	0.08	0.17
FeO	68.75	68.58	47.36	52.90	47.39	44.56	45.22	45.10	45.55	48.09	49.45
MnO	0.47	0.15	0.65	0.82	0.66	0.50	0.43	0.63	0.79	0.69	0.59
MgO	1.59	0.65	3.03	1.97	3.13	2.64	1.86	2.13	1.66	1.84	2.19
CaO	0.07	0.14	0.05	b.d.l.	b.d.l.	0.03	0.03	0.04	0.03	0.03	b.d.l.
Cr ₂ O ₄	0.04	b.d.l.	0.06	b.d.l.	0.05	0.07	b.d.l.	0.04	0.04	0.04	0.04
NiO	b.d.l.	b.d.l.	b.d.l.	b.d.l.	b.d.l.	0.04	0.04	b.d.l.	b.d.l.	b.d.l.	b.d.l.
P ₂ O ₅	0.13	b.d.l.	0.17	b.d.l.	0.25	b.d.l.	b.d.l.	b.d.l.	b.d.l.	b.d.l.	0.06
Total	93.89	92.49	97.81	97.26	98.83	96.90	96.47	96.92	96.35	98.05	97.94
Si	0.03	0.02	0.00	0.00	0.00	b.d.l.	b.d.l.	0.00	0.00	0.00	0.00
Ti	0.75	0.86	1.73	1.57	1.76	1.87	1.89	1.87	1.86	1.79	1.72
Al	0.16	0.04	0.02	0.01	0.01	0.01	0.00	0.02	0.01	0.00	0.01
Fe(iii)	2.29	2.19	0.51	0.85	0.47	0.25	0.22	0.25	0.26	0.40	0.55
Fe (ii)	0.63	0.82	1.48	1.39	1.50	1.65	1.72	1.67	1.70	1.63	1.53
Mn	0.02	0.01	0.03	0.04	0.03	0.02	0.02	0.03	0.03	0.03	0.03
Mg	0.12	0.05	0.23	0.15	0.23	0.20	0.14	0.16	0.13	0.14	0.16
Ca	0.00	0.01	0.00	0.00	0.00	0.00	0.00	0.00	0.00	0.00	0.00
Total	4.00	4.00	4.00	4.00	4.00	4.00	4.00	4.00	4.00	4.00	4.00

Group: B = basalt; BA = basaltic andesite; A = andesite; D = dacite; R = rhyolite; Opx/Cgt-SVC 2, 3 = orthopyroxene/cummingtonite-bearing SVC 2, 3 lavas; **Grain:** P = phenocryst; MC = microphenocryst; G = groundmass; INC = inclusion (mineral included within is stated in parentheses); **Position:** C = core; **Other:** Fe (ii) and Fe (iii) were calculated based on the minimum amount of Fe (iii) permissible in the structural formula.

Table G.6. (continued).

Group: Sample Name:	Opx-SVC2,3 D	Opx-SVC 2, 3 D	Opx-SVC 2, 3 D	Opx-SVC 2,3 D			Cgt-SVC 2, 3 D		
	SL-83-03 C1-Ox1	SL-JL-22 C5-Ox1	SL-83-24 C1-Ox1	C2-Ox1	SL-JL-79 C4-Ox1 INC	C4-Ox2	C1-Ox1	C2-Ox1 INC	C4-Ox1 INC
Grain:	G	G	G	INC (Bi)	(opx)	G	G	(cgt)	(cgt)
Position:	C	C	C	C	C	C	C	C	C
SiO ₂	0.02	b.d.l.	b.d.l.	0.04	0.02	0.00	b.d.l.	0.04	b.d.l.
TiO ₂	39.60	50.94	48.27	51.58	51.44	52.47	52.15	51.40	51.95
Al ₂ O ₃	0.13	b.d.l.	b.d.l.	b.d.l.	b.d.l.	b.d.l.	0.08	0.08	0.12
FeO	49.58	46.25	48.89	46.85	46.39	46.43	43.79	44.68	44.61
MnO	0.72	0.84	0.84	0.89	0.70	0.86	0.86	0.75	0.85
MgO	2.25	2.18	2.34	1.18	1.30	1.29	1.28	1.42	1.24
CaO	0.17	b.d.l.	b.d.l.	b.d.l.	0.03	b.d.l.	b.d.l.	0.05	b.d.l.
Cr ₂ O ₄	0.04	0.04	b.d.l.	b.d.l.	b.d.l.	0.06	b.d.l.	b.d.l.	b.d.l.
NiO	b.d.l.	b.d.l.	b.d.l.	b.d.l.	b.d.l.	b.d.l.	b.d.l.	0.04	b.d.l.
P ₂ O ₅	b.d.l.	b.d.l.	b.d.l.	b.d.l.	b.d.l.	b.d.l.	b.d.l.	b.d.l.	0.07
Total	92.58	100.27	100.39	100.82	99.90	101.15	98.20	98.51	98.89
Si	0.00	b.d.l.	b.d.l.	0.00	0.00	0.00	b.d.l.	0.00	b.d.l.
Ti	1.58	1.89	1.78	1.93	1.93	1.95	2.00	1.96	1.98
Al	0.01	0.00	0.00	0.00	0.00	0.00	0.00	0.00	0.01
Fe(iii)	0.84	0.21	0.43	0.14	0.13	0.10	0.00	0.07	0.04
Fe (ii)	1.36	1.70	1.58	1.80	1.81	1.82	1.86	1.82	1.85
Mn	0.03	0.04	0.03	0.04	0.03	0.04	0.04	0.03	0.04
Mg	0.18	0.16	0.17	0.09	0.10	0.09	0.10	0.11	0.09
Ca	0.01	0.00	0.00	0.00	0.00	0.00	0.00	0.00	0.00
Total	4.00	4.00	4.00	4.00	4.00	4.00	4.00	4.00	4.00

Group: B = basalt; BA = basaltic andesite; A = andesite; D = dacite; R = rhyolite; Opx/Cgt-SVC 2, 3 = orthopyroxene/cumingtonite-bearing SVC 2, 3 lavas; **Grain:** P = phenocryst; MC = microphenocryst; G = groundmass; INC = inclusion (mineral included within is stated in parentheses; **Position:** C = core; **Other:** Fe (ii) and Fe (iii) were calculated based on the minimum amount of Fe (iii) permissible in the structural formula.

Appendix H

Single plagioclase
trace element concentrations

Content

Table H.1. Details of all the composition of the international rock standards W-2, BHVO-1 and AGV-1 obtained during the analysis of the trace element concentrations of single plagioclases	409
Table H.2. Trace element concentrations of SVC single plagioclases analysed	410

Single plagioclase crystals analysed for $^{87}\text{Sr}/^{86}\text{Sr}$ at DGC were also investigated for selected trace element concentrations using aliquots of $\sim 10\%$ of the mass of each digested crystal, as described in section F6. However, the data were compromised by instrumental drifting during the analytical session and have not been discussed in any of the chapters of the thesis. Due to the very low trace element concentrations analysed, no internal standard solution was added to the sample solutions before analysis to avoid any contamination, and samples were analysed in a short run for 14 elements to minimise the impact of instrument drifting. Both concentrated and diluted international rock standard solutions (with similar concentrations to the sample solutions) were analysed regularly during the run to be able to monitor the occurrence of any major drifting. However, a positive drifting affected all the elements during the run and can be observed in the standard compositions. Below are presented the standard and sample concentrations obtained.

Table H.1. Details of all the composition of the international rock standards W-2, BHVO-1 and AGV-1 obtained during the analysis of the trace element concentrations of single plagioclases. The standard solutions were also diluted 10 times to be of similar concentration to the aliquots analysed.

	W-2			W2 diluted 10 times			BHVO-1		
	Accepted value	This study		Accepted value	This study		Accepted value	This study	
# in sequence:		3	40		6	43		4	41
Rb	21.00	21.71	26.09	2.10	2.17	2.57	9.11	9.92	12.00
Sr	196	207	239	19.60	20.56	25.69	396	395	479
Ba	172	186	207	17.20	18.07	20.84	131	142	158
La	10.80	11.67	11.73	1.08	1.15	1.22	15.20	16.57	17.14
Ce	23.40	24.25	25.33	2.34	2.41	2.63	37.50	40.16	41.35
Nd	13.00	13.28	14.20	1.30	1.30	1.24	24.50	25.17	27.00
Sm	3.30	3.37	3.68	0.33	0.34	0.39	6.07	6.19	6.85
Eu	1.08	1.11	1.24	0.11	0.11	0.13	2.07	2.07	2.26
Gd	3.66	3.86	4.26	0.37	0.38	0.46	6.24	6.27	7.17
Tb	0.62	0.63	0.70	0.06	0.06	0.08	0.92	0.95	1.09
Dy	3.79	3.75	4.18	0.38	0.38	0.44	5.31	5.17	5.76
Er	2.22	2.18	2.45	0.22	0.22	0.25	2.54	2.46	2.73
Yb	2.05	2.05	2.30	0.21	0.22	0.25	2.00	2.00	2.24
Lu	0.31	0.33	0.36	0.031	0.032	0.038	0.27	0.30	0.33

	BHVO-1 diluted 10 times			AGV-1				
	Accepted value	This study		Accepted value:	This study			
# in sequence:		7	44		5	20	30	42
Rb	0.91	1.01	1.10	66.6	66.4	70.4	76.7	90.0
Sr	39.60	42.84	51.47	660	610	639	679	805
Ba	13.10	14.00	15.84	1200	1217	1274	1319	1531
La	1.52	1.68	1.74	38.20	37.33	37.58	37.94	43.58
Ce	3.75	3.99	4.20	67.6	64.80	65.99	67.84	77.80
Nd	2.45	2.53	2.64	31.70	28.55	29.66	30.96	36.39
Sm	0.61	0.63	0.72	5.72	5.23	5.38	5.66	6.51
Eu	0.21	0.20	0.23	1.58	1.43	1.51	1.61	1.82
Gd	0.62	0.63	0.75	4.70	4.64	4.90	5.25	6.17
Tb	0.09	0.10	0.11	0.69	0.60	0.64	0.66	0.77
Dy	0.53	0.52	0.60	3.55	3.15	3.33	3.38	3.97
Er	0.25	0.25	0.29	1.82	1.61	1.66	1.71	2.05
Yb	0.20	0.21	0.23	1.63	1.54	1.57	1.60	1.89
Lu	0.027	0.031	0.035	0.24	0.23	0.25	0.25	0.30

	AGV-1 diluted 10 times					
	Accepted value:	This study				
# in sequence:		8	12	21	31	45
Rb	6.66	7.70	7.99	8.02	8.48	8.68
Sr	66	73	76	77	81	87
Ba	120	136	139	139	141	149
La	3.82	4.29	4.32	4.26	4.29	4.38
Ce	6.76	7.41	7.55	7.40	7.53	7.69
Nd	3.17	3.36	3.36	3.32	3.31	3.42
Sm	0.57	0.61	0.61	0.61	0.63	0.67
Eu	0.16	0.17	0.17	0.17	0.18	0.19
Gd	0.47	0.54	0.55	0.55	0.58	0.63
Tb	0.069	0.071	0.073	0.073	0.076	0.077
Dy	0.36	0.37	0.38	0.37	0.39	0.41
Er	0.18	0.19	0.19	0.19	0.19	0.20
Yb	0.16	0.18	0.18	0.19	0.18	0.19
Lu	0.024	0.026	0.028	0.028	0.030	0.030

Table H.2. Trace element concentrations of SVC single plagioclases analysed. The position of the sample in the analytical sequence (# in sequence) and the corresponding $^{87}\text{Sr}/^{86}\text{Sr}$ ratio are also shown.

	SL-83-17					SL-JL-24				
Name	8317PI1	8317PI2	8317PI3	8317PI4	8317PI5	JL24PI6	JL24PI7	JL24PI8	JL24PI9	JL24PI10
# in sequence	13	14	15	16	17	18	19	23	24	25
Rb	9.78	0.63	1.93	5.85	13.02	3.21	3.59	2.60	1.07	3.62
Sr	628	126	134	161	354	544	486	407	377	395
Ba	176	29	38	76	126	111	118	95	82	99
La	14.39	2.00	2.33	3.91	7.44	8.63	7.80	5.94	4.69	7.47
Ce	18.02	2.98	3.45	6.40	12.27	13.26	12.10	8.96	6.92	11.42
Nd	8.90	0.78	0.76	2.00	3.70	4.08	3.45	2.44	1.73	2.55
Sm	1.68	0.13	0.11	0.30	0.54	0.57	0.45	0.33	0.27	0.44
Eu	1.92	0.32	0.32	0.39	0.81	1.28	1.17	0.91	0.84	0.94
Gd	1.77	0.13	0.10	0.27	0.47	0.47	0.36	0.28	0.25	0.36
Tb	0.281	0.013	0.009	0.031	0.055	0.052	0.039	0.031	0.059	0.041
Dy	1.84	0.08	0.05	0.16	0.30	0.25	0.19	0.14	0.12	0.19
Er	1.32	0.05	0.03	0.09	0.18	0.11	0.09	0.06	0.07	0.09
Yb	1.71	0.06	0.02	0.09	0.19	0.10	0.08	0.06	0.07	0.09
Lu	0.276	0.008	0.003	0.014	0.030	0.014	0.012	0.009	0.047	0.012
$^{86}\text{Sr}/^{87}\text{Sr}$	0.709377	0.709107	0.708974	0.709071	0.709050	0.708482	0.708646	0.708478	0.708311	0.709143

	SL-JL-51					SL-JL-61				
Name	JL51PI11	JL51PI12	JL51PI13	JL51PI14	JL51PI15	JL61PI16	JL61PI17	JL61PI18	JL61PI19	JL61PI20
# in sequence	26	27	28	29	33	34	35	36	37	38
Rb	3.07	0.89	1.86	0.89	0.48	1.28	0.70	0.98	2.51	1.98
Sr	555	344	397	283	198	222	225	108	364	229
Ba	128	63	99	56	44	50	51	26	93	48
La	7.92	4.65	5.55	3.37	2.95	2.49	3.56	1.81	5.68	2.73
Ce	11.93	6.94	8.22	4.96	4.30	3.72	5.29	2.76	8.57	4.16
Nd	3.41	1.53	2.07	0.97	0.88	0.74	1.02	0.63	2.33	1.03
Sm	0.44	0.26	0.29	0.18	0.14	0.15	0.22	0.12	0.32	0.18
Eu	1.30	0.74	0.92	0.61	0.44	0.46	0.52	0.24	0.86	0.47
Gd	0.37	0.21	0.23	0.14	0.12	0.13	0.18	0.10	0.28	0.15
Tb	0.036	0.020	0.023	0.012	0.009	0.013	0.017	0.011	0.027	0.017
Dy	0.17	0.10	0.10	0.06	0.05	0.07	0.09	0.05	0.13	0.09
Er	0.07	0.03	0.04	0.03	0.02	0.03	0.03	0.02	0.06	0.04
Yb	0.06	0.03	0.03	0.02	0.01	0.03	0.03	0.02	0.06	0.04
Lu	0.009	0.005	0.006	0.003	0.002	0.004	0.004	0.004	0.008	0.006
$^{86}\text{Sr}/^{87}\text{Sr}$	0.708538	0.708501	0.708426	0.708400	0.708669	0.708352	0.708739	0.708901	0.708627	0.708691

